# Modèles et analyses mathématiques pour les mouvements collectifs de cellules

Vincent Calvez

**Université de Paris VI Pierre et Marie Curie**

**U.F.R. de Mathématiques**

# Modèles et analyses mathématiques pour les mouvements collectifs de cellules

## THÈSE

présentée et soutenue publiquement le 10 Octobre 2007

pour l'obtention du diplôme de

**Doctorat de l'université Paris VI Pierre et Marie Curie**

**(spécialité mathématiques)**

par

**Vincent Calvez**

sous la direction de Benoît Perthame

**devant le jury composé de**

| | |
|---|---|
| José Antonio CARRILLO | Examinateur |
| Jean DOLBEAULT | Rapporteur |
| Thierry GOUDON | Examinateur |
| Emmanuel GRENIER | Rapporteur |
| Benoît PERTHAME | Directeur de thèse |
| Laure SAINT-RAYMOND | Examinatrice |
| Cédric VILLANI | Examinateur |

**Département de Mathématiques et Applications** **Ecole Normale Supérieure**

Mis en page avec la classe thloria.

# Remerciements

Avant tout je voudrais exprimer toute ma gratitude à Benoît Perthame, qui a dirigé mes études et mes recherches dans le domaine des équations aux dérivées partielles appliquées à la biologie. Benoît aime à penser que non seulement la modélisation mathématique peut intervenir de manière cruciale en biologie et en médecine, mais aussi que ces nouveaux modèles apportent des problèmes déroutants et fascinants. Espérons qu'il sera comblé dans les années à venir. J'ai bénéficié au long de cette thèse de ses conseils précieux, de ses éclairages limpides. Sa disponibilité et sa clairvoyance ont fait de moi un thésard heureux et épanoui.

Je remercie Jean Dolbeault et Emmanuel Grenier, qui ont accepté de consacrer une portion de l'été à lire et commenter ce mémoire. Leurs remarques avisées ont amélioré le manuscrit à coup sûr. José Carrillo m'a fait le plaisir de prendre part au jury. Une partie de ce travail lui doit beaucoup, et j'espère que cette aventure se poursuivra à l'avenir, avec tous les résultats que l'on espère (ou presque). Je remercie Thierry Goudon, Laure Saint-Raymond et Cédric Villani qui m'ont fait l'honneur d'être membres du jury.

Je n'oublie pas Hatem Zaag, qui s'est beaucoup investi dans les maths-bio à l'ENS et à qui je dois beaucoup. J'ai eu la joie d'apprendre de très heureux événements pendant la période de ma thèse. Je lui souhaite beaucoup de bonheur. Philip Maini a également beaucoup compté dans mon apprentissage des maths-bio. Il m'a donné l'opportunité de passer un semestre à Oxford, ce qui fut une expérience très enrichissante. Je remercie toute l'équipe du CMB pour son accueil très chaleureux.

J'ai eu beaucoup d'intérêt à travailler avec Hossein Khonsari, pour la partie médicale de cette thèse. Hossein est une mine de problèmes et d'idées qui portent à la modélisation. Je lui souhaite beaucoup de réussite pour la suite dans ses projets. Collaborer avec Nikolaos Bournaveas est également un plaisir. Je le remercie de m'avoir invité à Edimbourg à l'hiver dernier. Je suis également très reconnaissant envers Lucilla Corrias. J'ai beaucoup appris de ses conseils pour mieux appréhender la recherche, et réussir la visite de Rio ! Enfin je garde un excellent souvenir d'avoir travaillé de concert avec Adrien Blanchet.

J'ai été très chaleureusement accueilli au sein du Département de Mathématiques et Applications de l'ENS. Je remercie Gilles, Patricia et Vincent pour l'organisation du groupe de travail maths-bio, toute l'équipe EDP, sans oublier l'équipe de choc avec Bénédicte, Zaïna, Lara et Laurence ! Merci à tous mes collègues et amis du bureau R3 où il fait bon travailler et discuter : Nejla, Philippe, Fadia, Susana, Mohsen, Abderrahman, Suman, Lin, Ye, Jiao, Hua, et Dietmar. Merci au groupe des thésards de Dauphine, en particulier Anne-Laure et Jean-Philippe.

J'ai eu pendant ces trois années des contacts privilégiés avec des personnes qui m'ont beaucoup marquées. Je pense en particulier à Jean Clairambault, à son enthousiasme et à sa curiosité très vive. Je suis très reconnaissant envers Francis Filbet qui m'a initié à l'analyse numérique pratique au cours du CEMRACS, dans une atmosphère très agréable. Je remercie Simone Séror et Barry Holland pour avoir piloté le projet MACBAC, Nicola Bellomo pour son investissement dans le projet MCRTN. Je remercie aussi Danielle Hilhorst, Angela Stevens, Jorge Zubelli et Marco Di Francesco pour m'avoir fait confiance et m'avoir invité à des conférences très enrichissantes.

Merci aussi à toutes mes amies, et tous mes amis, ceux que j'ai rencontrés à l'Ecole Normale, dans les Abers, à Brest et ailleurs. Une très grande pensée pour Merlin et Noureddine, avec qui j'ai partagé un toit pendant trois ans, en toute harmonie. Merci à Sylvain pour sa passion de la BD et de GP, à Cyril pour son amour du jazz qui nous a permis de garder un lien étroit et de partager des soirées mémorables. Merci à Mickael et Vanya, que j'espère revoir très souvent, autour d'un café ou au milieu de l'océan. Une grosse pensée pour Sylvain et sa guitare, pour Audrey, Philippe, Perrine, Federico et Céline, Isa et Julien, Pierre et Marion, Marianne et Florent, et bien d'autres encore... Merci à tous les coéquipiers de l'épopée des Black- et Yellow-Stars, jeunes et moins jeunes : Pierrot, Alex, Ana, Djé-Djé, Juj, Mat, Jo, Charlie le capitaine que l'histoire retiendra, et tous les autres... Merci à toute la bande de Porspo avec qui il est toujours aussi agréable de passer de merveilleux moments : Elsa et Philippe, Fabrice, Haude et John, Julien et Julie, Astrid. Merci à Tristan pour les récits qui transportent, et à Flo pour sa bonne humeur constante. Tonnerre de Brest ! Je n'oublierai pas Adrien et Sezny, Kalim, Simon, Pierre et Caro, Virginie, Benja, Fanch et Roma. Merci à Gégé.

Merci à Anne-Marie de m'accueillir toujours aussi chaleureusement chez elle, à Pierre et Virginie de m'avoir fait découvrir une région très séduisante, à Eve et Tanguy parce que cela ne saurait tarder.

Mes pensées les plus joyeuses vont à mes parents, ma sœur et mon frère. A ma Mamie et à ma Mammgozh, à mes cousines, mes cousins, mes oncles et tantes. Tous je les remercie du fond du cœur. Il n'y aura pas assez de mots pour dire tout le bien que je pense d'eux, alors je m'arrête...

Merci à Flore pour son sourire si grand.

*Pour Annick et Germaine,*

# Table des matières

# Introduction générale

**Organisation spatiale en biologie : problèmes et enjeux**

Le travail effectué durant cette thèse a pour fil directeur le phénomène de chimiotactisme (ou chémotaxie, nous adopterons la première dénomination). Le chimiotactisme, ou comment les cellules se déplacent en "traçant" un signal chimique, est fondamental pour la coopération des colonies bactériennes, en biologie du développement et plus généralement en morphogénèse. Il joue en effet un rôle clé lorsqu'il s'agit pour les cellules de s'organiser spatialement (et même de s'auto-organiser lorsque le signal chimique est émis par les cellules elles-même). Ce signal chimique est par nature complexe. Il existe des familles de chémokines qui entrainent une cascade de réactions à plusieurs centaines d'intermédiaires afin de transformer le signal en mouvement orienté. Nous occulterons cette complexité : le signal sera ici simplifié à l'extrême en une seule espèce (éventuellement deux).

Loin d'être exhaustifs, donnons deux exemples d'organismes où le chimiotactisme intervient de manière cruciale au cours du développement.

- **Le modèle cellulaire *Dictyostelium discoideum*.** Cet organisme unicellulaire vit à l'état individuel dans les premières phases de son développement, puis la population se structure en un organisme multicellulaire [248]. Les cellules se divisent tant que la nourriture disponible est abondante. En situation de stress nutritif, cette amibe sécrète un signal chimique, la molécule d'Adénosine MonoPhosphate cyclique (AMPc), qui attire les cellules voisines. On observe alors les individus s'agréger autour de centres d'émission des spirales d'AMPc. Cet amas d'environ cent milles cellules évolue en un organisme qui "porte" un spore de cellules en altitude. Ceci permet à certaines amibes d'échapper à la famine, aidées par le vent. Le phénomène de chimiotactisme est au cœur de cet exemple remarquable d'interactions cellulaires et de coopération entre individus.
- **Migrations cellulaires au cours de la gastrulation chez le poulet.** Au cours des premières étapes du développement de l'embryon des oiseaux (amniotes), la gastrulation marque la fin de la division cellulaire à un rythme effréné, et les cellules subissent alors une vague de réarrangement et de différentiation au sein de l'embryon [156, 89]. La symétrie axiale est mise en place, ainsi que la dissymétrie antéro-postérieure. Les cellules migrent dans le sillon primitif pour former trois feuillets cellulaires (ecto-, endo et mésoderme). Plus tard le sillon primitif régresse au profit de la croissance du tube notochordal. Il a été mis en évidence que ces vastes migrations sont le résultat d'une signalisation chimiotactique (attractive et répulsive) au sein de l'embryon [251, 204].

Il est d'autres situations où l'enjeu est important en biologie humaine. En particulier l'angiogénèse ou le développement du réseau de connexions neuronales. Lors de la phase primaire de la croissance tumorale, la tumeur sphéroïde "se nourrit" via l'interface avec le milieu extérieur, dont la taille grandit moins vite que le volume [213, 215, 41]. Il arrive une taille critique où la tumeur arrête sa croissance par manque d'oxygène. Elle émet à ce stade des facteurs de croissance de tumeur (TGF) qui agissent en dérivant des vaisseaux sanguins naissants à partir des vaisseaux établis environnants, afin d'irriguer la tumeur. Ce processus, appelé l'angiogénèse, est crucial pour deux raisons. Dans un premier temps la tumeur peut poursuivre son développement grâce à ce nouvel apport de nutriments. Par la suite elle pourra migrer au travers du réseau sanguin ainsi formé (après vasculogénèse). Notons qu'il existe une théorie alternative au stress nutritif pour justifier ce processus [111]. En effet les cellules tumorales sécrètent de hautes doses de poison qui diminuent le pH et favorisent les cellules anormales. Un effet secondaire de cet empoisonnement serait le recrutement des vaisseaux sanguins avoisinants pour pomper et évacuer ces substances acides. Par ailleurs les axones neuronaux sont célèbres pour leur capacité à parcourir une distance considérable

lors du développement du réseau de connexions dans le cerveau. Ces migrations sont faites d'une alchimie complexe de relais, de chimiotactisme attractif ou répulsif, local ou global [233].

Au-delà de ces motivations, le chimiotactisme joue un rôle prépondérant lors de la croissance de colonies de bactéries [44], et dans des modèles encore prospectifs où le couplage du chimiotactisme avec une instabilité chimique de Turing [236, 185] peut expliquer les motifs remarquables sur certaines peaux d'animaux (surtout chez les poissons tropicaux [203] – voir à ce sujet le paragraphe 1.3).

### Le phénomène de masse critique

Dans cette thèse nous nous sommes intéressés tout particulièrement à des phénomènes d'auto-organisation : les systèmes considérés sont fermés, *e.g.* une population de cellules qui produisent elles-même le signal chimique qui les attire. Nous nous sommes concentrés sur le modèle parabolique de chimiotactisme, le plus simple dirons-nous, qui rend compte du phénomène de masse critique, observé en réalité. Le principe est relativement simple à expliquer, et autrement plus délicat à analyser précisément ! Les cellules diffusent par agitation brownienne et s'attirent via un potentiel (un signal) chimique. Toutes choses étant égales par ailleurs, si les cellules sont suffisamment nombreuses elles vont sentir leurs présences respectives et s'attirer mutuellement en paquets (en agrégats). Autrement dit il existe une masse critique au-delà de laquelle une structure spatialement inhomogène émerge de la population.

### Hiérarchie des modèles

On peut distinguer trois échelles de modèles pour la description des interactions chimiotactiques d'une population de cellules [208, 209]. Les modèles paraboliques sont à l'échelle "macroscopique", et sont particulièrement mis en valeur dans cette thèse (le modèle de Keller-Segel). Ils mettent en jeu des flux qui déplacent la densité spatiale de la population. Nous avons mis l'accent sur ces modèles phénoménologiques car il nous a paru essentiel de maîtriser parfaitement le modèle le plus simple avant de l'insérer dans un système plus complexe, étape par étape. Mis en situation biologique, le modèle parabolique est pour nous la transcription du principe de masse critique avant tout.

Avec un niveau de description plus avancé, les modèles "mésoscopiques", ou cinétiques, prennent en compte une variable supplémentaire et permettent d'intégrer la distribution locale des cellules en vitesse. Il est possible de retrouver la classe des modèles paraboliques dans une certaine limite [134, 66, 65, 104] (voir aussi 1.2), ce qui fournit une interprétation des coefficients du modèle macroscopique basée sur des faits biologiques.

Les modèles "microscopiques" qui décrivent la population comme un grand système de particules en interaction [5, 199, 228, 90, 91] rejoignent les observations précédentes.

Bien que cela motive l'étude des équations cinétiques effectuée à l'aune de l'existence globale dans le chapitre 5, nous en sommes restés là, et nous nous sommes la plupart du temps contentés des modèles simples, macroscopiques, en situation de modélisation (voir la partie II).

### Quelques apports mathématiques

Cette thèse a été réalisée au sein d'une équipe d'Equations aux Dérivées Partielles, sous la direction d'un mathématicien qui croit que les applications à la biologie peuvent faire apparaître de nouveaux enjeux mathématiques, et qu'à tout le moins les mathématiques développées à ce jour n'expliquent pas suffisamment les observations issues de la biophysique. Nous voudrions énumérer ici quelques apports de cette thèse aux mathématiques. Ce qui nous a paru peut être le plus remarquable dans ce travail est la propension qu'a le système de Keller-Segel (KS) de flirter avec les inégalités fonctionnelles fines et optimales. Sorti de son contexte biologique, KS peut être vu comme la mise en balance d'une diffusion avec un potentiel d'interaction non-local. La compétition entre ces deux phénomènes aux tendances contraires est régie par l'inégalité d'Hardy-Littlewood-Sobolev à poids logarithmique (HLS log). Il a donc été nécessaire de pousser une étude détaillée et transversale de cette inégalité en vue de son utilisation optimale (voir à ce sujet l'annexe B).

Pour aller plus loin, KS peut être vu comme la réalisation du flot gradient d'une fonctionnelle entropie *moins* énergie d'interaction non-locale, la fonctionnelle n'étant pas convexe par déplacement. Nous

suggérons dans le chapitre 7 comment surmonter cette difficulté, au moins dans le cas 1D (la dimension $d \geq 2$ est en progression). Des applications numériques viennent conforter ces nouveaux résultats.

Dans le cadre des équations cinétiques de chimiotactisme enfin, l'absence de structure énergétique oblige à utiliser des inégalités de dispersion telles Strichartz. L'inégalité de Brascamp-Lieb a fait une apparition surprenante, cachée dans le chapitre 5. Ceci nous a suggéré un lien entre cette inégalité utilisée dans la théorie des corps convexes et le lemme de dispersion présent en cinétique des gaz (tout ceci est détaillé dans l'annexe C).

# 1 Les modèles de chimiotactisme : du macro au micro

## 1.1 Le modèle parabolique de Keller-Segel

Nous nous intéressons à une population de cellules en déplacement, qui interagissent via un signal chimique en remontant le gradient de potentiel. Si l'on ajoute à cela une diffusion (linéaire) pour les cellules, et pour les molécules du signal chimique, on obtient le système couplé suivant, dit modèle de Patlak-Keller-Segel (PKS ou KS) [206, 153, 154] :

$$\left\{ \begin{array}{rcl} \dfrac{\partial n}{\partial t} & = & \Delta n - \operatorname{div}\left(\chi n \nabla c\right), \quad t > 0,\ x \in \Omega \subset \mathbb{R}^2, \\ \varepsilon \dfrac{\partial c}{\partial t} & = & \Delta c + n - \alpha c\ . \end{array} \right. \tag{1}$$

Si le domaine $\Omega$ est borné régulier, les conditions au bord sont de type Neumann (flux nul) pour la densité de cellules (ce qui garantit la conservation de la masse totale), et de type Neumann ou Dirichlet pour la concentration de l'espèce chimique. Les paramètres du système sont la chemosensibilité $\chi > 0$, le coefficient inverse de diffusion $\varepsilon \geq 0$, le taux de dégradation $\alpha \geq 0$ et enfin la masse totale des cellules $M = \int n(t=0,x)\ dx$ qui est conservée au cours du temps.

Dans le cas $\varepsilon = 0$ (hypothèse quasi-stationnaire, voir [147]), $\alpha = 0$, et $\Omega$ borné avec conditions de Neumann au bord, $c$ est corrigé par sa moyenne spatiale, et résoud

$$-\Delta c = n - \langle n \rangle.$$

Dans le cas $\varepsilon = \alpha = 0$ et $\Omega = \mathbb{R}^2$ [86], $c$ est défini par la convolution avec la solution fondamentale de Poisson,

$$c(t,x) = -\frac{1}{2\pi} \int \log|x-y| n(t,y)\ dy. \tag{2}$$

Ce système non linéaire exhibe une boucle de rétro-action positive : les régions à haute densité cellulaire génèrent des concentrations chimiques fortes qui attirent de plus en plus de cellules... Ce processus est en fait contre-balancé par la diffusion pure qui tend à disperser les cellules. Le phénomène de masse critique évoqué plus haut est matérialisé par le théorème suivant [86, 35].

**Théorème 0.1** (Dolbeault et Perthame 2004)**.** *Dans l'espace tout entier $\Omega \subset \mathbb{R}^2$ avec $\alpha, \varepsilon = 0$, pour une donnée initiale $n_0\big(|\log n_0| + (1+|x|^2)\big) \in L^1$, nous avons l'alternative suivante : la solution est globale en temps si $\chi M < 8\pi$, alors qu'elle explose en temps fini si $\chi M > 8\pi$.*

Il existe des variantes antérieures à ce théorème pour le modèle (1) en domaine borné (voir [141] pour une revue). Nous pouvons remonter à Nanjundiah qui avait conjecturé le phénomène de masse critique [191, 71], qui a été démontré originalement par Jäger et Luckhaus [147] sans pour autant avoir obtenu le seuil optimal de $4\pi$ ou $8\pi$. La mise en relation avec l'inégalité de Trudinger-Moser et la constante optimale en domaine borné est due à Biler [32] et à Gajewski et Zacharias [107] qui se sont appuyés sur des méthodes d'énergie. Auparavant la constante optimale était déjà connue dans le cas radial ([187], voir annexe A). Le système est maintenant bien compris en domaine borné grâce aux contributions de Horstmann [140] et de Senba et Suzuki [221].

Le comportement asymptotique de (1), dans tout l'espace avec $\alpha, \varepsilon = 0$, est analysé précisément par Blanchet, Dolbeault et Perthame [35], et une compréhension fine de ces résultats a permis à Blanchet,

Carrillo et Masmoudi de traiter le cas de la masse critique $M = 8\pi/\chi$ [34]. Nous nous sommes attelés au chapitre 3 au système (1) sans hypothèse quasi-stationnaire ($\varepsilon, \alpha \geq 0$) dans tout l'espace $\mathbb{R}^2$. Nous avons obtenu un résultat de masse critique optimal tel que le théorème 0.1, mais le comportement asymptotique précis en variables auto-similaires (voir au paragraphe 3.1 par exemple) échoue par manque d'énergie sur le système renormalisé.

## 1.2 Le modèle cinétique

Le modèle cinétique (ou mésoscopique) d'Othmer, Dunbar et Alt [198] met en scène un bouillon de cellules. La densité $f(t,x,v)$ représente la densité de particules à la position $x \in \mathbb{R}^d$ (on traitera seulement $d = 3$ par la suite) en déplacement avec la vitesse $v \in V \subset\subset \mathbb{R}^d$ (voir annexe C). La moyenne en vitesse $\rho(t,x) = \int f(t,x,v)\ dv$ désigne la densité de cellules au point $x$ (c'est la même chose que $n(t,x)$ dans le paragraphe précédent). Comme dans le modèle au-dessus, les cellules créent un potentiel chimique $S$ de champ moyen

$$-\Delta S = \int f(t,x,v)\ dv\ , \quad \text{ou} \quad -\Delta S + \alpha S = \int f(t,x,v)\ dv.$$

L'équation cinétique qui régit l'évolution de la population $f$ exprime que les cellules (ou particules) se déplacent à la vitesse $v$ puis changent de direction ($v \to v'$) et réciproquement ($v' \to v$) avec un certain taux qui dépend du potentiel chimique $S$,

$$\partial_t f + v \cdot \nabla_x f = \int_{v' \in V} T[S] f(t,x,v')\ dv' - \lambda[S]\rho. \tag{3}$$

**Limite diffusive.** La limite diffusive s'obtient en introduisant un petit paramètre $\varepsilon > 0$ qui correspond au ratio entre le déplacement libre et la réorientation des cellules (phases 'run' et 'tumble' en anglais) [134, 66, 104]. Après changement d'échelles de temps $\tilde{t} = \varepsilon^2 t$ et d'espace $\tilde{x} = \varepsilon x$, la version adimensionnée de (3) devient

$$\varepsilon^2 \partial_t f + \varepsilon v \cdot \nabla_x f = \int_{v' \in V} T_\varepsilon[S] f(t,x,v')\ dv' - \lambda[S]\rho.$$

En pratique le noyau de changement de direction $T_\varepsilon[S]$ se développe en $T_0 + \varepsilon T_1[S] + O(\varepsilon^2)$ où $T_0$ (taux basal constant de réorientation) est responsable de la diffusion pure après passage à la limite $\varepsilon \to 0$. Par exemple un noyau

$$T_\varepsilon = \alpha_+ \psi\big(S(t,x+\varepsilon v)\big) + \alpha_- \psi\big(S(t,x-\varepsilon v')\big)\ ,$$

où $\psi$ est minorée $\psi \geq \psi_{\min} > 0$ et a une croissance au plus linéaire, donne l'expansion

$$T_0[S] = (\alpha_+ + \alpha_-)\psi\big(S(t,x)\big)\ , \quad T_1[S] = \psi'\big(S(t,x)\big)(\alpha_+ v - \alpha_- v') \cdot \nabla S\ .$$

La limite diffusive $\varepsilon \to 0$ donne l'équation suivante pour la densité macroscopique $\rho$

$$\partial_t \rho = \operatorname{div}\Big(D[S]\nabla\rho - \chi[S]\rho\nabla S\Big)\ ,$$

avec les expressions détaillées des coefficients

$$D[S] = \frac{1}{3|V|(\alpha_+ + \alpha_-)\psi(S)} \int_V |v|^2\ dv\ , \quad \chi[S] = \frac{\psi'(S)}{3\psi(S)} \int |v|^2\ dv\ .$$

**Effet de retard.** Le noyau $T[S]$ dépend en principe du potentiel chimique $S$ avec un effet de mémoire, par exemple

$$0 \leq T[S] \leq C\Big(1 + |S|(t,x+\varepsilon v) \text{ ou } |S|(t,x-\varepsilon v')\Big),$$

c'est-à-dire que les cellules peuvent mesurer la concentration chimique $S(x+\varepsilon v)$ dans un rayon d'action $\varepsilon V$ et s'orienter en fonction ; ou bien les cellules ont une certaine inertie du fait des réactions internes mises en jeu [96] et la "prise de décision" de changement de direction à la position $x$ découle de la mesure

en $x - \varepsilon v'$ (là est véritablement l'effet de mémoire). On peut également envisager une dépendance en les gradients de concentration [144],

$$0 \leq T[S] \leq C\Big(1 + |\nabla S|(t, x + \varepsilon v) \text{ ou } |\nabla S|(t, x - \varepsilon v')\Big).$$

Sur le plan de l'organisme, ceci nécessite une taille plus importante de la cellule et une machinerie interne plus complexe capable de mesurer les variations locales de concentration de $S$.

Des théorèmes d'existence globale pour des équations de type (3) ont été prouvés dans [66, 144], voir aussi le chapitre 5. La limite diffusive conduit au modèle parabolique KS localement en temps. Ceci n'est donc pas en contradiction avec l'explosion en temps fini observée avec KS lorsque la masse est sur-critique. A ce propos il n'y a pas de théorème d'explosion connu à ce jour pour des modèles cinétiques tels que (3). Soulignons qu'une échelle différente $\tilde{t} = \varepsilon t$ et $\tilde{x} = \varepsilon x$ (limite hydrodynamique) conduit à un modèle hyperbolique [104].

## 1.3 La marche aléatoire biaisée

Pour des modèles microscopiques, centrés sur les individus, il convient d'utiliser des équations différentielles stochastiques [228],

$$\frac{dp^k}{dt} = \chi(c)\nabla c \; dt + \sigma dB_t \; .$$

Sans rentrer dans ce formalisme par souci de simplicité, nous dressons le tableau de la marche aléatoire biaisée [199], approche microscopique dans cette hiérarchie des modèles de chimiotactisme (l'échelle "nanoscopique" serait alors une description individuelle du mouvement, voir à ce sujet les travaux de modélisation en mécanique intracellulaire [6, 195]). Nous reproduisons dans la suite du paragraphe des pans de [204], lui-même adapté de [5, 199].

On considère que l'espace est une grille régulière sur laquelle les cellules se déplacent par sauts de puce stochastiques. En dimension un d'espace pour simplifier, cette grille est $\mathbb{Z}dx$, où $dx > 0$ est le déplacement infinitésimal, et $dt$ représente l'intervalle de temps minimal entre deux sauts. La probabilité de transition entre les sites $x$ et $x \pm dx$ est fonction de la concentration chimique ambiante $(c_i)$. On note ces transitions à partir de la position $idx$ :

$$\mathbf{P}(x \to x \pm dx) = \mathcal{T}_i^{\pm}(c) \; , \quad \mathbf{P}(x \to x) = 1 - (\mathcal{T}_i^{+} + \mathcal{T}_i^{-}).$$

Il est de notoriété publique [185, 216] que l'asymptotique d'un tel processus à coefficients constants isotropiques $\mathcal{T}^+ = \mathcal{T}^- = 1/2$ dans la limite $dt \sim dx^2$ (échelle de diffusion) est l'équation de la chaleur $\partial_t n = \frac{1}{2}\partial^2_{xx} n$. Dans le cas d'une dépendance des transitions au signal chimique, on aboutit plus généralement à une équation de dérive-diffusion de type chimiotactisme :

$$\frac{\partial n}{\partial t} = \frac{\partial}{\partial x}\left(h(c)\frac{\partial n}{\partial x} - \chi(c) n \frac{\partial c}{\partial x}\right).$$

Afin de déterminer avec plus de précision la dépendance chimique des coefficients, il faut donner plus d'informations au cours de la modélisation.

**Modèles rigoureusement locaux.** Dans cette situation, les cellules sont capables de mesurer la concentration chimique à une position donnée et "prennent la décision" du déplacement selon : $\mathcal{T}_i^{\pm} = p(c_i)$. On obtient après passage à la limite diffusive,

$$\frac{\partial n}{\partial t} = \frac{\partial}{\partial x}\left(p(c)\frac{\partial n}{\partial x} + p'(c) n \frac{\partial c}{\partial x}\right).$$

Dans le cas d'un chimiotactisme attractif ($p'(c) \leq 0$ : le taux de transition diminue lorsque la concentration est grande), la chémosensibilité devient $\chi(c) = -p'(c) \geq 0$.

**Modèles à gradient.** Supposons que les cellules aient une taille supérieure et une machinerie interne plus élaborée, leur permettant d'évaluer les différences locales de concentration et de s'orienter en fonction : $\mathcal{T}_i^+ = 1/2 + 1/2\big(\tau(c_{i+1}) - \tau(c_i)\big)$ et $\mathcal{T}_i^- = 1/2 + 1/2\big(\tau(c_{i-1}) - \tau(c_i)\big)$. Ceci conduit à l'équation continue parabolique

$$\frac{\partial n}{\partial t} = \frac{1}{2}\frac{\partial^2 n}{\partial x^2} - \frac{\partial}{\partial x}\left(\tau'(c) n \frac{\partial c}{\partial x}\right),$$

et le coefficient de chémosensibilité est $\chi(c) = \tau'(c)$, positif si les cellules ont tendance à se diriger vers les régions de concentration chimique croissante.

**Dynamique des récepteurs.** On se focalise maintenant sur les interactions récepteurs-ligands qui précèdent la réponse chimiotactique de la cellule. On se restreint à des exemples très simples en jetant un flou sur la machinerie interne (pour plus de détails dans le contexte des équations cinétiques, voir Radek Erban and co.). Dans le cas d'une réponse linéaire, *i.e.* $\mathcal{T}_i^\pm = p(c_i) = p_0 - \chi_0 c_i$ pour le modèle local, ou encore $\tau(c_{i+1}) - \tau(c_i) = \chi_0(c_{i+1} - c_i)$ dans le modèle gradient, on obtient tout simplement des coefficients de chémosensibilité constants $\chi(c) \equiv \chi_0$.

Dans le cas d'une réponse saturée où le nombre de récepteurs membranaires est limitant, on peut par exemple choisir

$$\mathcal{T}_i^\pm = T_0 - \beta \frac{R_0 c}{K + c},$$

où $T_0$ est le taux basal de transition, dominant si la diffusion pure est le phénomène dominant, $R_0$ est le nombre total de récepteurs membranaires, et $K = k^-/k^+$ est le ratio entre la cinétique chimique de liaison récepteur-ligand ($k^-$) et la relaxation des récepteurs activés ($k^+$). Alors la chémosensibilité asymptotique du modèle local devient

$$\chi(c) = \frac{\beta R_0 K}{(K + c)^2}.$$

De la même façon, une fonction hypothétique $\tau(c) = \beta R_0 c/(K + c)$ conduit pour le modèle gradient à

$$\chi = \frac{\chi_0}{(1 + \gamma c)^2}.$$

**Formation de motifs : l'hypothèse de Turing.** Les considérations précédentes sont à la base des modèles retenus par l'école de Murray [185]. A titre d'exemple, on peut superposer (sans couplage en retour) cette équation parabolique de chimiotactisme à un système à deux espèces chimiques attracteur/répulseur. Ce système étant lui-même sujet à une instabilité spatiale de type activateur/inhibiteur (instabilité de Turing [236]).

$$\begin{cases} \dfrac{\partial u}{\partial t} &= D_u \Delta u + f(u, v), \\ \dfrac{\partial v}{\partial t} &= D_v \Delta v + g(u, v), \\ \dfrac{\partial n}{\partial t} &= \Delta n - \operatorname{div}\ \left(n\chi_1(u, v)\nabla u + n\chi_2(u, v)\nabla v\right). \end{cases}$$

Outre les bandes qui apparaissent sur la peau du poisson tropical *Pomacanthus* durant sa croissance, ce modèle à trois espèces permet d'expliquer la largeur affinée des bandes nouvellement formées, ce qui est en général impossible dans un scénario de Turing avec réactions chimiques seules, même si le domaine est croissant [158, 203].

## 2 Les méthodes paraboliques

Voici l'essence des méthodes paraboliques prépondérantes dans cette thèse. Pour ce qui est des méthodes liées au modèle cinétique, on renvoie à l'annexe C.

## 2.1 Les injections de Sobolev : une première approche

Un premier pas vers l'existence globale des systèmes assimilés à (1) consiste à contrôler l'évolution en temps des normes $L^p$ de la densité $n(t,x)$. Une intégration par parties directe donne

$$\frac{d}{dt}\int_\Omega n^p\ dx = -4\frac{p-1}{p}\int_\Omega |\nabla n^{p/2}|^2\ dx + \chi(p-1)\int_\Omega n^{p+1}. \tag{4}$$

On retrouve – c'est une constante dans toutes les estimations autour de KS – la compétition entre deux tendances opposées. La non-linéarité transparaît dans le terme $\int n^{p+1}$ dont l'homogénéité est trop forte pour pouvoir utiliser un lemme de Gronwall. Une solution adaptée ici est d'appliquer une inégalité de la famille Gagliardo-Nirenberg-Sobolev. Dans ce cas précis il faut choisir

$$\int n^{p+1} \le \mathcal{C}(p)\int |\nabla n^{p/2}|^2 \int n\ . \tag{5}$$

On voit en combinant (4) et (5) que la masse sous-critique $M \le 4/\chi p\ \mathcal{C}(p)$ entraîne immédiatement un contrôle global de la norme $L^p$ de la densité. On sait par ailleurs qu'une seule norme $L^p$ pour $p>1$ est suffisante. A la limite $p\to 1$, le calcul (4) devient

$$\frac{d}{dt}\int n\log n = -4\int |\nabla\sqrt{n}|^2 + \chi\int n^2,$$

et la quantité $\int n\log n$ reste bornée par au-dessus si $M \lesssim 1,86\times 4\pi/\chi$ grâce à (5). On sait *a posteriori* que ce seuil de masse est sous-optimal. Mais tout n'est pas perdu car le même calcul qu'en (4) en remplaçant $n$ par la densité tronquée $(n-k)_+$ conduit au résultat suivant [147], essentiel pour se fixer un objectif clair : *l'équi-intégrabilité est suffisante pour empêcher la formation de points singuliers et garantir l'existence de solutions régulières.* Dès lors nous sommes ramenés à chercher des bornes sur $\|n\|_{L^p}$ $(p>1)$ ou bien $\int n(\log n)_+$, ou n'importe quelle fonctionnelle sur-linéaire de la densité (mais c'est à $\int n\log n$ que l'on s'intéresse en général).

## 2.2 Hardy-Littlewood-Sobolev logarithmique et Trudinger-Moser : le nerf de la guerre

Le sésame pour mettre en évidence le seuil optimal de masse est l'énergie libre du modèle Keller-Segel. On peut factoriser le flux cellulaire,

$$\partial_t n = \text{div}\ \Big(n\nabla(\log n - \chi c)\Big),$$

ce qui suggère de tester l'équation contre $\log n - \chi c$. Dans le cas particulier $\varepsilon=\alpha=0$ et $\Omega=\mathbb{R}^2$ on trouve que l'énergie libre

$$\mathcal{E}(t) = \mathcal{F}[n(t)] = \int_{\mathbb{R}^2} n\log n\ dx + \frac{\chi}{4\pi}\iint_{\mathbb{R}^2\times\mathbb{R}^2} n(x)\log|x-y|n(y)\ dxdy, \tag{6}$$

est décroissante (on retrouve la compétition à nouveau). Il est alors judicieux d'appliquer l'inégalité de Hardy-Littlewood-Sobolev logarithmique [56, 23]

$$-\iint_{\mathbb{R}^2\times\mathbb{R}^2} n(x)\log|x-y|n(y)\ dxdy \le \frac{M}{2}\int_{\mathbb{R}^2} n\log n\ dx + C,$$

de laquelle on déduit que la fonctionnelle $\mathcal{F}$ est en quelque sorte coercitive si la masse $M$ est sous-critique :

$$\mathcal{F}[n] \ge \left(1-\frac{\chi M}{8\pi}\right)\int n\log n - C.$$

Dans tout l'espace, la partie négative $\int n(\log n)_-$ n'est pas nécessairement bornée (à cause de la fuite de masse à l'infini), ce qui amène des complications techniques inhérentes à l'équation de diffusion [35] (voir annexe D).

Dans le cas d'un domaine borné il était d'usage d'utiliser l'inégalité de Trudinger-Moser [184, 68] qui, fait intéressant au vu du paragraphe 2.1, est une limite d'injection de Sobolev [115] (voir aussi annexe B). L'énergie libre s'écrit ici

$$\mathcal{E}(t) = \int_\Omega n \log n - \chi \int_\Omega nc + \frac{\chi}{2} \int_\Omega |\nabla c|^2.$$

Il faut dans un premier temps minimiser la fonctionnelle d'énergie libre partiellement par rapport à $n$ :

$$\mathcal{F}[n,c] \geq -M \log \left( \int e^{\chi c} \right) + \frac{\chi}{2} \int |\nabla c|^2,$$

puis utiliser l'inégalité de Trudinger-Moser [107] (avec conditions de Neumann) valable pour un domaine borné régulier et $c \in H^1$ tel que $\int c = 0$,

$$\int_\Omega \exp(\chi c)\, dx \leq \mathcal{C}(\Omega) \exp\Big( \frac{\chi^2}{8\pi} \int_\Omega |\nabla c|^2\, dx \Big).$$

Là encore la fonctionnelle d'énergie libre est coercitive dans le cas sous-critique :

$$\mathcal{F}[n,c] \geq \left( \frac{\chi}{2} - \frac{M\chi^2}{8\pi} \right) \int |\nabla c|^2 - C.$$

Le seuil de masse dépend, en domaine borné, des conditions au bord pour l'espèce chimique (voir aussi l'annexe A). La version de l'inégalité Trudinger-Moser présentée ici correspond à des conditions de Neumann, ce qui donne $M_{\text{crit}} = 4\pi/\chi$. Les conditions de Dirichlet quant à elles garantissent la pseudo-coercitivité pour $M < 8\pi/\chi$ [32].

## 2.3 La convexité par déplacement

Les travaux de McCann [179] ont permis d'associer une notion de convexité aux fonctionnelles d'énergie de gaz en interaction du type

$$\mathcal{F}(n) = \int_{\mathbb{R}^d} U(n(x))\ dx + \int_{\mathbb{R}^d} n(x) V(x)\ dx + \iint_{\mathbb{R}^d \times \mathbb{R}^d} W(x-y) n(x) n(y)\ dxdy\ , \tag{7}$$

où $U$, $V$ et $W$ sont respectivement la fonctionnelle d'énergie interne (ou entropie), le potentiel de confinement des particules et le noyau d'interaction. Il ne s'agit plus d'interpoler les densités par des segments dans l'espace des densités : $n_t = (1-t)n_0 + tn_1$, mais par des segments dans l'espace des particules, ce qui s'écrit,

$$n_t = \Big( (1-t)\mathrm{Id} + t\nabla\varphi \Big) \# n_0, \tag{8}$$

où $T = \nabla\varphi$ est l'application qui transporte $n_0$ en $n_1$ de façon optimale [38, 244] (voir annexe D). En ce sens la fonctionnelle (7) est convexe (par déplacement) si les conditions suivantes sont réunies :

(i) La fonctionnelle d'énergie interne $U$ vérifie $U(0) = 0$ et la dilatation : $\Gamma :\ \lambda \to \lambda^d U(\lambda^{-d})$ est convexe décroissante pour $\lambda \in (0, \infty)$.

(ii) Les potentiels $V$ et $W$ sont convexes.

Disposer d'une structure convexe est bien entendu très enviable au vu des conséquences que cela implique (*e.g.* unicité du minimum, estimations de la vitesse de convergence du flot gradient). Par malheur le noyau d'interaction de notre énergie libre (6) est logarithmique et donc concave. Il est impossible d'appliquer directement la théorie issue de la convexité ou semi-convexité par déplacement [244].

Au lieu de développer dès l'introduction la théorie générale, décrivons la situation en une dimension d'espace, car les calculs sont simplifiés. On renvoie à l'annexe D pour une vision plus globale.

Dans le cas unidimensionnel, l'application de transport optimal $T = \varphi'$ entre deux densités de probabilité $\mu(x)$ et $\nu(y)$ est explicite. Si l'on note $F$ et $G$ les fonctions de répartition respectives, alors il s'agit

de $T = G \circ F^{-1}$, et la distance de Wasserstein associée au transport (égale au coût minimal du transport entre $\mu$ et $\nu$) est précisément

$$\mathcal{W}_2(\mu,\nu) = \|G^{-1} - F^{-1}\|_{L^2(0,1)} = \|\Psi - \Phi\|_{L^2} \ ,$$

où l'on a noté $\Phi$ et $\Psi$ les fonctions pseudo-inverses de $F$ et $G$ resp. La fonctionnelle d'énergie (7) se réécrit dans la variable $\rho = F(x)$ $(d\rho = n(x)dx)$,

$$\mathcal{G}[\Phi] = \int U\left(\frac{1}{\Phi'}\right)\Phi' \ d\rho + \int V\Big(\Phi(\rho)\Big) \ d\rho + \iint W\Big(\Phi(\rho) - \Phi(\eta)\Big) \ d\rho d\eta \ . \tag{9}$$

D'après les hypothèses faites sur $U,\ \Phi,\ \Psi$, on voit clairement que la fonctionnelle $\mathcal{G}$ est convexe pour l'interpolation $(1-t)\Phi + t\Psi$, ce qui correspond en fait à (8). Il est naturel d'étudier le flot gradient de $L^2$ de l'énergie (9),

$$\frac{\partial \Phi}{\partial t} = -\nabla \mathcal{G} \ ,$$

ce qui après retour aux variables originales est équivalent à

$$\frac{\partial n}{\partial t} = \frac{\partial}{\partial x}\left(n\frac{\partial}{\partial x}U'(n) + nV' + n\frac{\partial}{\partial x}(W * n)\right) \ .$$

En particulier si $V'' \geq \alpha > 0$ alors $\mathcal{G}$ est $\alpha-$convexe (d'après (9)), et il y a convergence exponentielle en distance de Wasserstein vers l'équilibre (l'équilibre existe ici par coercitivité).

# 3 Les résultats

## 3.1 Comprendre Keller-Segel par l'énergie, et le généraliser via l'énergie

L'énergie libre de KS étant au cœur du système, nous nous sommes concentrés sur cet outil pour définir et étudier des modèles plus généraux.

**Diffusion non linéaire [Chapitre 1].** Première avancée : nous avons déterminé un critère optimal d'existence globale pour des modèles paraboliques à coefficients de diffusion et de chémosensibilité non linéaires, dépendant de la densité cellulaire mais pas de la concentration chimique :

$$\left\{\begin{array}{rcl} \dfrac{\partial n}{\partial t} & = & \Delta f(n) - \text{div } (\chi(n) n \nabla c) \ , \quad t > 0, \ x \in \Omega \subset \mathbb{R}^2, \\ -\Delta c & = & n - \langle n \rangle \quad \text{ou} \quad c = -\dfrac{1}{2\pi}\displaystyle\int_{\mathbb{R}^2} \log|x-y| n(y) \ dy. \end{array}\right. \tag{10}$$

Les raisons biologiques qui motivent ce modèle sont multiples. En ce qui concerne la diffusion non linéaire, on part du constat que les cellules ont un volume minimal (une certaine rigidité) qui les empêche de s'interpénétrer[1]. La diffusion non linéaire de type puissance des milieux poreux $f(u) = u^m,\ m > 1$ agit donc comme effet de saturation dans les régions à haute densité cellulaire. Plusieurs approches micro et mésoscopiques ont abouti à ce modèle macro :

- dans [202], les taux de transition de la marche aléatoire biaisée décrite au paragraphe 1.3 sont pénalisés d'un facteur $q(n) \in [0,1],\ q(0) = 1,\ q(u) \to \infty$ qui agit pour les hautes densités. Ainsi les cellules ont une probabilité très faible de se déplacer lorsqu'elles sont empaquetées. Ceci aboutit à l'équation de chimiotactisme parabolique

$$\frac{\partial n}{\partial t} = \text{div } \Big(\big(q(n) - nq'(n)\big)\nabla n + \chi_0 q(n) n \nabla c\Big) = 0 \ ,$$

  avec coefficients de diffusion et de chimiotactisme densité-dépendants.

[1] En ce sens, les masses de Dirac obtenues avec KS sur-critique sont des idéalisations de la réalité. Si l'explosion est empêchée par la diffusion non linéaire, nous verrons que le phénomène de masse critique, essentiel pour la suite, lui n'a pas été écarté pour autant.

- Une modélisation analogue ajoutant au paragraphe 1.2 une saturation dans le noyau de changement de direction (si $\rho \geq \rho_{\max}$ le mouvement est purement aléatoire, sans biais), ainsi qu'un passage à la limite diffusive, ont été effectués au niveau cinétique par [67].
- Dans le modèle hyperbolique évoqué plus haut, Gamba et coll. ont introduit une fonction de pression $\phi(n)$ qui tient justement compte du fait que les cellules ne peuvent toutes s'accumuler au même point [108]. Dans le modèle hyperbolique, la population de cellules est décrite comme dans les équations d'Euler par la densité $n$ et la vitesse $v$.

$$\begin{cases} \dfrac{\partial n}{\partial t} + \operatorname{div}\,(nv) = 0 \\ \dfrac{\partial v}{\partial t} + v \cdot \nabla v = \mu \nabla c - \nabla h(n) \\ \dfrac{\partial c}{\partial t} = D\Delta c + \beta n - \alpha c\ . \end{cases}$$

  On trouvera dans [159] la justification qu'une telle fonction de pression aboutit après simplification à un modèle parabolique tel que (10). Dans ce même article un critère de non-explosion est mis en évidence par des calculs calqués sur (4).

Il existe des multitudes d'exemples, outre les équations de chimiotactisme, où la diffusion nonlinéaire cellulaire a son rôle à jouer [47, 112].

En s'appuyant sur les méthodes d'énergie, nous avons démontré un critère (optimal) d'existence globale pour le système (10).

**Théorème 0.2** (C. et Carrillo)**.** *On définit la fonction de pression*[2] *réduite $H$ par*

$$H'(u) = \frac{f'(u)}{\chi(u)u}, \quad H(1) = 0.$$

*Si la pression réduite $H$ est au-dessus de la pression critique en régime de hautes densités,*

$$\exists\, \mathcal{U},\ \delta > 0, \quad \forall u \geq \mathcal{U} \quad H(u) \geq \Big(\frac{\chi M}{8\pi \text{ ou } 4\pi} + \delta\Big) \log u$$

*alors les estimations* a priori *garantissent l'existence globale des solutions de* (10)*.*

Ecrivons dans un premier temps l'énergie associée au système. Dans ce but on définit la fonction d'énergie interne $\Phi$ par $\Phi'(u) = H(u)$ et $\Phi(0) = 0$.
Si

$$\mathcal{E}(t) = \int \Phi(n(x))\ dx - \frac{1}{2}\int nc,$$

alors

$$\frac{d}{dt}\mathcal{E}(t) = -\int \chi(n) n |\nabla(H(n) - c)|^2.$$

En comparant la pression (et par là même l'entropie réduite $\Phi$) avec la pression "classique" nous avons été capables d'obtenir des estimations sur $\int |\nabla c|^2$ en domaine borné, et sur $\int \Theta(n)\ dx$, où $\Theta$ est sur-linéaire, dans l'espace tout entier. Ensuite viennent dans ce chapitre des estimations de la régularité de $n$ en normes $L^p,\ p > 1$, jusqu'à $p = \infty$ grâce à la méthode itérative d'Alikakos-Moser [4].

Quelques applications numériques viennent illustrer ce théorème dans le chapitre 6 (voir aussi l'annexe A). A ce propos il nous paraît intéressant de souligner que le phénomène de masse critique n'a pas disparu de ce modèle à coefficients non linéaires, même si l'explosion n'a pas lieu, au travers des équilibres non homogènes spatialement. Nous n'avons pas effectué d'analyse asymptotique de la stabilité des équilibres. Ce travail existait déjà (voir entre autres [219, 250]) et nous avons trouvé dans ces références le principe d'émergence d'une structure spatialement non homogène lorsque la quantité de cellules dépasse un certain seuil.

[2] Dans le cas classique la fonction de pression est $h(u) = \log u$.

**Potentiel chimique à noyau logarithmique [Chapitre 2].** Telle qu'elle est écrite en (1), la dynamique du modèle de KS dépend fortement de la dimension. En dimension $d = 1$ l'explosion ne peut pas avoir lieu [187, 137]. En dimension $d = 3$ en revanche, l'explosion peut arriver pour des masses arbitrairement petites [130, 77]. Il est démontré dans [77] que pour $d \geq 2$ l'espace critique est $L^{d/2}$ (donc $L^1$ en dimension 2, c'est le phénomène de masse critique). D'autre part nous savons que l'inégalité de HLS log est au cœur de ce phénomène de masse critique, et qu'elle ne dépend pas vraiment de la dimension, quoique très légèrement au travers de la constante. Ceci nous a conduit à suggérer une variante du modèle de KS pour lequel la concentration chimique est donnée par la convolution avec le noyau critique logarithmique,

$$\left\{ \begin{array}{rcl} \dfrac{\partial n}{\partial t} & = & \Delta n - \operatorname{div}\left(\chi n \nabla c\right), \quad t > 0,\ x \in \Omega \subset \mathbb{R}^2, \\ c & = & -\dfrac{1}{d\pi} \log|z| * n. \end{array} \right. \tag{11}$$

En particulier, le gradient de concentration $\nabla c$ en dimension 1 est l'opposé de la transformée de Hilbert de $n$ : $\nabla c = -\mathcal{H} n$. Nous avons alors démontré, avec l'énergie libre cette fois-ci indépendante de la dimension, un phénomène de masse critique unifié tout à fait analogue à KS "classique" 2D.

**Théorème 0.3** (C., Perthame et Sharifi tabar)**.** *Si $\Omega$ est l'espace tout entier $\mathbb{R}^d$ et la donnée initiale vérifie $n_0\big(|\log n_0| + (1+|x|^2)\big) \in L^1$, alors la solution de* (11) *est globale si $\chi M < 2d^2\pi$, et il y a explosion en temps fini si $\chi M > 2d^2\pi$.*

Il est tout de même important de distinguer les dimensions lorsqu'il s'agit d'appliquer la méthode de la régularité $L^p$ de la densité. Quelques simulations numériques 1D en domaine borné viennent étayer ce résultat, et conforter l'idée que la dynamique est similaire à la dimension 2.

Ce chapitre 2, court et auto-contenu, est intéressant pour qui veut se faire une idée rapide et précise des méthodes mises en œuvre.

Avoir une version unidimensionnelle de Keller-Segel, partageant la même énergie libre, est intéressant du point de vue numérique. Les calculs 1D étant beaucoup moins coûteux, il est possible de faire une étude numérique fine du phénomène de masse critique, et de l'interaction entre plusieurs pics. Mais cela a également un intérêt théorique non négligeable. La formulation 1D nous a en effet suggéré de nouvelles pistes pour traiter les fonctionnelles d'énergie libre telles que (7) mais non convexes par déplacement, et les flots gradients associés pour la distance de Wasserstein (paragraphe 2.3). Ce travail ouvre des perspectives avec des extensions multidimensionnelles.

Notons pour conclure qu'il y a d'autres manières de construire une famille de modèles ayant comme espace critique $L^1$ en toute dimension. Citons à titre d'exemple le choix d'une diffusion fractionnaire [97], ou d'une diffusion non-linéaire (voir le chapitre 7), ou encore d'une chémosensibilité $\chi$ densité-dépendante (c'est-à-dire $\chi(n)n = n^{2/d}$, voir [142]).

**Défaut de convexité par déplacement : la méthode de factorisation de l'équilibre [Partie III].**

**Exemple de l'espace à trois points.** Après de nombreuses simplifications on peut se convaincre que l'exemple suivant est caractéristique des méthodes développées dans la partie III et en particulier dans les calculs liés au schéma numérique du chapitre 8. On introduit la fonctionnelle et la dynamique

$$F(u,v) = 2\log(u+v) - \log(u) - \log(v), \quad \dot{Y} = -\nabla F(Y). \tag{12}$$

Bien que la fonctionnelle $F$ ne soit aucunement convexe, nous pouvons montrer un résultat de convergence asymptotique. Les points critiques de la fonctionnelle vérifient $u = v$. Voyons ce que donne le calcul éculé

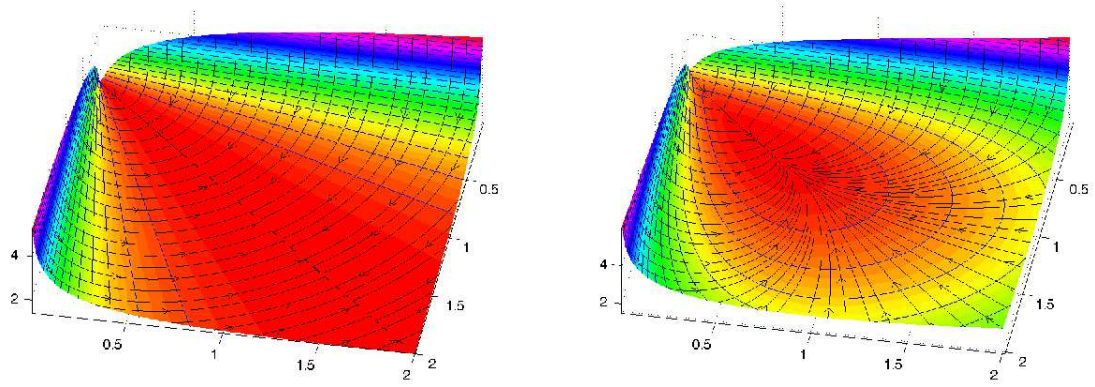


FIG. 1 – Un modèle caricatural pour illustrer la convergence du système gradient malgré le défaut de convexité par déplacement. (*gauche*) La dynamique associée à la fonctionnelle homogène F (12) est représentée par les lignes de niveau de $F$ ainsi que le champ de vecteur gradient. On observe la convergence vers la droite des points critiques $u = v$. (*droite*) L'homogénéité a été brisée et la fonctionnelle $F_\varepsilon$ (13) perturbée par un terme convexe qui garantit l'existence et l'unicité du point stationnaire. Il y a alors convergence vers cet équilibre à vitesse exponentielle.

de la distance à un point critique $X_0 = (a, b)$,

$$\begin{aligned}
\frac{d}{dt}\frac{1}{2}\|Y - X_0\|^2 &= -\langle Y - X_0 \mid \nabla F(Y) - \nabla F(X_0)\rangle \\
&= -(u-a)\left(\frac{2}{u+v} - \frac{1}{u} - \frac{2}{a+b} + \frac{1}{a}\right) - (v-b)\left(\frac{2}{u+v} - \frac{1}{v} - \frac{2}{a+b} + \frac{1}{b}\right) \\
&= -2\left(\frac{1}{u+v} - \frac{1}{a+b}\right)\Big((v-b) + (u-a)\Big) + \left(\frac{1}{u} - \frac{1}{a}\right)(u-a) + \left(\frac{1}{v} - \frac{1}{b}\right)(v-b) \\
&= -2\gamma\left(\frac{u+v}{a+b}\right) + \gamma\left(\frac{u}{a}\right) + \gamma\left(\frac{v}{b}\right),
\end{aligned}$$

où $\gamma(\lambda) = 2 - \lambda - 1/\lambda$ est concave et négative. Puisque $(a, b)$ est un point critique de $F$, nous avons $a = b$. Une simple inégalité de convexité donne finalement

$$\frac{d}{dt}\frac{1}{2}\|Y - X_0\|^2 \leq -2\gamma\left(\frac{u+v}{2a}\right) + \gamma\left(\frac{u}{a}\right) + \gamma\left(\frac{v}{a}\right) \leq 0,$$

avec cas d'égalité si et seulement si $(u, v) = (u, u)$ est un point critique.

L'exemple de la dynamique homogène (12) est dégénéré car il n'y a pas un unique état stationnaire, mais toute une droite par homogénéité (figure 1). En gardant toujours en tête le cas de la dimension infinie qui nous intéresse par la suite, on peut décider de briser cette homogénéité et d'ajouter un potentiel convexe :

$$F_\varepsilon(u, v) = k\log(u+v) - \log(u) - \log(v) + \frac{\varepsilon}{2}(u^2 + v^2)\ , \quad \dot{Y} = -\nabla F(Y), \tag{13}$$

avec $0 < k < 2$ et $\varepsilon > 0$. L'unique point d'équilibre $X_0 = (a, b)$ vérifie

$$\frac{k}{a+b} - \frac{1}{a} + \varepsilon a = \frac{k}{a+b} - \frac{1}{b} + \varepsilon b = 0.$$

L'évolution de la solution à ce point critique devient

$$\begin{aligned}\frac{d}{dt}\frac{1}{2}\|Y-X_0\|^2 &= -\langle Y-X_0 \mid \nabla F(Y)-\nabla F(X_0)\rangle \\ &= -(u-a)\left(\frac{k}{u+v}-\frac{1}{u}+\varepsilon u-\frac{k}{a+b}+\frac{1}{a}-\varepsilon a\right) \\ &\qquad -(v-b)\left(\frac{k}{u+v}-\frac{1}{v}+\varepsilon v-\frac{k}{a+b}+\frac{1}{b}-\varepsilon b\right) \\ &= -k\gamma\left(\frac{u+v}{a+b}\right)+\gamma\left(\frac{u}{a}\right)+\gamma\left(\frac{v}{b}\right)-\varepsilon\|Y-X_0\|^2, \end{aligned} \tag{14}$$

Utilisons une nouvelle fois la concavité de $\gamma$ :

$$-\gamma\left(\frac{a}{a+b}\frac{u}{a}+\frac{b}{a+b}\frac{v}{b}\right) \le -\frac{a}{a+b}\gamma\left(\frac{u}{a}\right)-\frac{b}{a+b}\gamma\left(\frac{v}{b}\right),$$

de sorte que

$$\frac{d}{dt}\frac{1}{2}\|Y-X_0\|^2 \le \left(1-\frac{ka}{a+b}\right)\gamma\left(\frac{u}{a}\right)+\left(1-\frac{kb}{a+b}\right)\gamma\left(\frac{v}{b}\right)-\varepsilon\|Y-X_0\|^2.$$

Pour conclure à la convergence exponentielle il suffit d'observer que, d'une part $\gamma$ est négative, d'autre part à l'équilibre on a $1-ka/(a+b)=\varepsilon a^2>0$ et *idem* pour $b$.

Malgré le défaut de convexité de $F$ (12), nous venons de mettre en évidence que la droite des points critiques attire les trajectoires. Nous ne sommes pas en mesure d'évaluer la vitesse de convergence, en revanche une perturbation avec un terme strictement convexe telle que $F_\varepsilon$ (13) garantit une convergence exponentielle vers l'unique état stationnaire (voir aussi la figure 1).

**Convergence de Keller-Segel 1D non linéaire.** Nous considérons par la suite une synthèse des deux extensions de KS précédentes (10) et (11) : diffusion non linéaire et synthèse chimique à noyau logarithmique. Le système est posé en dimension une dans tout l'espace :

$$\frac{\partial n}{\partial t}=\Delta n^m-\operatorname{div}\left(\chi n\nabla c\right), \quad \nabla c=-\mathcal{H}n\ , \tag{15}$$

où $\mathcal{H}$ désigne la transformée de Hilbert. On se restreint au cas $m\ge 1$ car nous allons soulever le problème de la convergence de $n(t,x)$ vers un unique état stationnaire. La masse totale est fixée à $M=1$ sans perte de généralité. Le centre de masse est conservé, disons que c'est $\int xn(t,x)\,dx=0$.

Dans le cas d'une diffusion linéaire $m=1$ nous savons par avance que l'énergie libre associée n'est pas bornée par en-dessous excepté pour le cas critique $\chi=2\pi$ [56]. Et même dans ce cas la situation est délicate car tous les états d'équilibres (il en existe une famille entière à un paramètre) sont de second moment infini, sauf la masse de Dirac en zéro, si l'on veut. Or comme nous le verrons, l'utilisation du second moment est cruciale ici car la convergence a lieu en distance de Wasserstein (voir paragraphe 2.3 et annexe D). Pour toutes ces raisons le cas $m=1$ est un cas dégénéré[3].

Une solution bien adaptée est d'effectuer un changement de variables auto-similaires (voir annexe D), ce qui amène à résoudre l'équation avec dérive

$$\frac{\partial u}{\partial t}=\Delta u+\operatorname{div}\left(\chi u(y-\nabla v)\right), \quad \nabla v=-Hu, \tag{16}$$

associée à l'énergie libre

$$\mathcal{E}(t)=\mathcal{F}(u)=\int u\log u\ dy+\frac{1}{2}\int |y|^2u(y)\ dy+\frac{\chi}{2\pi}\iint u(x)\log|x-y|u(y)\ dxdy. \tag{17}$$

[3]L'argument le plus convaincant est peut être de voir qu'une perturbation par diffusion non linéaire, ou plus légèrement en ajoutant un terme de dérive bien choisi, entraine l'unicité de l'état d'équilibre s'il existe. Ceci est réminiscent d'un phénomène d'effondrement des équilibres bien connu en systèmes dynamiques. Le système de Lotka-Volterra par exemple possède une famille de courbes invariantes concentriques. Si on lui ajoute une perturbation bien choisie, un cycle invariant unique attire toutes les trajectoires [149, Chap. 4.3 'Dynamical systems'].

Le potentiel de confinement $V(y) = \frac{1}{2}|y^2|$ va à l'encontre du phénomène d'évanouissement propre à l'équation de diffusion (la masse ne peut plus s'échapper à l'infini désormais). On démontre formellement les théorèmes suivants qui viennent approfondir le chapitre 2.

**Théorème 0.4** (C. et Carrillo)**.** *Si $\chi < 2\pi$, la fonctionnelle d'énergie libre* (17) *possède un unique minimiseur qui est l'unique état stationnaire du problème* (16)*.*

**Théorème 0.5** (C. et Carrillo)**.** *Si $\chi < 2\pi$ et si la donnée initiale possède un second moment fini, la solution du problème* (16) *converge vers l'unique état d'équilibre avec vitesse exponentielle en distance de Wasserstein.*

Donnons l'esquisse de démonstration du théorème (0.5), qui contient de fait une partie du théorème (0.4). Nous sommes en mesure d'estimer explicitement l'écart à l'équilibre de la solution en distance de Wasserstein :

$$\frac{d}{dt}\frac{1}{2}\mathcal{W}(u,\bar{u})^2 \leq \int_{\zeta=0}^{1} \gamma\Big(\frac{\partial_\rho \Phi}{\partial_\rho \Psi}\Big)(\zeta)\, d\zeta - \int_{\zeta=0}^{1} \gamma\Big(\frac{\partial_\rho \Phi}{\partial_\rho \Psi}\Big)(\zeta)\mathcal{J}[\Psi](\zeta)\, d\zeta - \mathcal{W}(u,\bar{u})^2 \ , \tag{18}$$

où $\Phi$ et $\Psi$ sont respectivement les fonctions inverses de répartition de $u$ et $\bar{u}$, où $\gamma(\lambda) = 2 - \lambda - 1/\lambda$ est négative et concave, et où enfin l'expression $\mathcal{J}[\Psi](\zeta)$ vaut uniformément 1 si et seulement si $\bar{u}$ est un état stationnaire du système (16). Cette inégalité cruciale est à rapprocher de (14).

Une réalisation numérique de ces idées a été accomplie (chapitre 8). Nous adaptons le schéma original qui "minimise le mouvement", introduit dans [148], au cas d'une fonctionnelle avec interaction quadratique non locale et non convexe par déplacement (voir aussi [200, 244, 7]).

Nous établissons dans un premier temps que le schéma discret en temps et continu en espace

$$u(t+dt) = \arg\min_w \left\{ \mathcal{F}[w] + \frac{1}{2dt}\mathcal{W}(u(t),w)^2 \right\} \ , \tag{19}$$

converge vers la solution faible du système continu lorsque le pas de temps $dt$ tend vers 0. Ceci utilise la méthode classique décrite simplement dans [244, Chap. 8], ainsi que les estimations *a priori* propres à KS (*e.g.* équi-intégrabilité et contrôle de la densité à l'infini par les moments).

Nous écrivons alors le schéma discret en temps et en espace correspondant à (19) qui n'est autre qu'un schéma d'Euler implicite portant sur la fonction de répartition $\Phi$. Par souci de simplicité le pas du maillage est constant égal à $h$.

$$-\frac{\Phi^i_{n+1} - \Phi^i_n}{dt} = \frac{1}{\Phi^{i+1}_{n+1} - \Phi^i_{n+1}} - \frac{1}{\Phi^i_{n+1} - \Phi^{i-1}_{n+1}} + \Phi^i_{n+1} + \frac{\chi}{\pi} \sum_{j:|\Phi^i_{n+1} - \Phi^j_{n+1}|>0} \frac{h}{\Phi^i_{n+1} - \Phi^j_{n+1}} \ .$$

Nous adaptons les calculs continus du chapitre 7 et décrivons la convergence en norme $L^2$ du système (19) (ici la norme $L^2$ entre les fonctions inverses de répartition est la distance de Wasserstein en variables originales).

**Théorème 0.6** (Blanchet, C. et Carrillo)**.** *Si $\chi(1-h) < 2\pi$ alors la solution discrète $\Phi_n$ converge vers l'unique équilibre $(\Psi^i)$ du schéma discret* (19) *avec vitesse exponentielle*

$$\|\Phi_n - \Psi\|^2 \leq \left(\frac{1}{1+2dt}\right)^n \|\Phi_0 - \Psi\|^2.$$

Le facteur $1-h$ est tout à fait naturel pour des raisons d'homogénéité dans l'énergie libre discrète (voir annexe B).

Le cas d'une diffusion non linéaire de type puissance $m > 1$ dans (15) a également été pris en compte (et même des situations plus générales d'une diffusion et d'une interaction non-locale en compétition, voir chapitre 7). Il n'est alors pas nécessaire d'ajouter un potentiel de confinement dans l'énergie car les effets se compensent à l'infini en faveur du confinement. On démontre à nouveau la convergence.

**Théorème 0.7** (C. et Carrillo). *Si $m > 1$, les solutions de* (15) *convergent vers l'unique état d'équilibre du système. Toutefois, sans potentiel de confinement nous n'avons pas d'estimation évidente de la vitesse de convergence.*

En conclusion, une étude fine autour de l'énergie libre permet de démontrer des résultats que l'on espère optimaux. Elle permet de surcroît de suggérer de nouveaux modèles, conduisant à des idées originales. Nous avons l'espoir d'arriver très prochainement à une version $d-$dimensionnelle des théorèmes 0.4 et 0.5, ce qui apporterait une pierre à l'édifice de la théorie des fonctionnelles de particules en interaction, vues sous l'angle du transport optimal.

**Le modèle parabolique/parabolique [Chapitre 3].** Nous avons étudié au chapitre 3 le modèle KS (1) posé dans tout l'espace $\mathbb{R}^2$. Les idées nouvelles de [86] pour $\alpha, \varepsilon = 0$ donnent l'espoir de réunir les conditions pour un théorème de masse critique optimal dans le cas parabolique / parabolique. Le schéma de preuve est le suivant, partant à nouveau de l'énergie libre

$$\mathcal{E} = \mathcal{F}[n,c] = \int n \log n - \chi \int nc + \frac{\chi}{2} \int |\nabla c|^2 + \frac{\chi\alpha}{2} \int c^2 \ .$$

Deux possibilités s'offrent à nous : si l'on minimise partiellement la fonctionnelle par rapport à $n$, on obtient

$$\mathcal{F}[n,c] \geq M \log M + \frac{\chi}{2}\Big(1 - M\frac{\chi}{8\pi}\Big) \int_{\mathbb{R}^2} |\nabla c(x)|^2 \ dx - \chi M \int_{\mathbb{R}^2} c(x) H(x) \ dx - 2 \int n(x) \log(1+|x|^2) \ ,$$

et une inégalité de Trudinger-Moser-Onofri (TMO) [23] est de bon augure :

$$\log\left( \int_{\mathbb{R}^2} e^{\chi c(x)} H(x) \ dx \right) \leq \frac{\chi^2}{16\pi} \int_{\mathbb{R}^2} |\nabla c(x)|^2 \ dx + \chi \int_{\mathbb{R}^2} c(x) H(x) \ dx \ , \tag{20}$$

où $H(x) = \dfrac{1}{\pi} \dfrac{1}{(1+|x|^2)^2}$ est le jacobien de la projection stéréographique inverse. Si en revanche on minimise partiellement $\mathcal{F}$ par rapport à $c$ (ce qui revient à faire une hypothèse quasi-stationnaire sur $c$), alors on est paré pour mettre en application l'inégalité d'HLS log (ou HLS log localisée si $\alpha > 0$, voir appendice du chapitre 3),

$$-\iint_{\mathbb{R}^2 \times \mathbb{R}^2} n(x) \log|x-y| n(y) \ dxdy \leq \frac{M}{2} \int_{\mathbb{R}^2} n \log n \ dx + C \ . \tag{21}$$

Ceci met en exergue la dualité des rôles joués par les quantités $n$ et $c$, qui transparaît dans la dualité entre HLS log et TMO. D'ailleurs la dualité était connue en domaine borné et sur la sphère [56, 23], et la dualité entre (20) et (21) "descend" de la sphère $\mathbb{S}^2$ (les détails sont dans l'annexe B).

Ces deux stratégies duales amènent bien sûr au même résultat d'existence globale sous-critique ($M < 8\pi/\chi$) que précédemment. En revanche nous n'avons pas déterminé le comportement asymptotique des solutions, pour la seule raison que nous n'avons pas pu trouver une énergie libre au problème renormalisé. De même nous n'avons pas de résultat d'explosion si $\varepsilon > 0$.

## 3.2 Des modèles sans énergie

Il semble naturel de ne pas avoir d'énergie dans les modèles biologiques car les mécanismes mis en œuvre sont le fruit de nombreuses simplifications d'un système où l'énergie est surabondante. Devant l'absence d'énergie il faut revenir à des estimations plus robustes.

**Un système à deux composantes chimiques [Chapitre 4].** Nous avons étudié dans un premier travail un modèle où l'équation parabolique de chimiotactisme est couplée à deux espèces chimiques :

$$\left\{ \begin{array}{rcl} \dfrac{\partial n}{\partial t} & = & \Delta n - \chi \mathrm{div}\ (n \nabla c) \quad t \geq 0 \ , \ x \in \Omega \subset \mathbb{R}^2, \\ -\Delta c & = & nf - \langle nf \rangle, \\ \dfrac{\partial f}{\partial t} & = & -nf. \end{array} \right. \tag{22}$$

C'est une simplification d'un modèle de colonies de bactéries en croissance où la réaction qui conduit à la synthèse du chémoattractant $c$ passe par un intermédiaire chimique : le succinate de concentration $f$ [40, 237, 185]. Présente au temps initial avec la concentration $f(t=0)$ elle est consommée au fur et à mesure par les cellules qui produisent le chémoattractant. A défaut d'une énergie nous avons trouvé une fonctionnelle de Lyapunov

$$\mathcal{W}(t) = \int n \log n + b \int n f^\gamma + \frac{a}{2} \int |\nabla f^\delta|^2,$$

décroissante le long des trajectoires pour des choix de paramètres $a$ et $b$, $\gamma$ et $\delta$ idoines, dès lors qu'une des inégalités de la famille

$$\chi \|f^0\|_\infty M^{1-\lambda} \leq C_\lambda, \quad \lambda \in [0, 1/4], \tag{23}$$

est vérifiée. La simple application de la méthode directe (4) due à Jäger et Luckhaus aboutit à la condition $\chi \|f^0\|_\infty M \leq C_0$, et nous voyons que l'approche fournie dans le chapitre 4, même si elle n'est peut-être pas optimale, exhibe une famille de relations (23) avec des homogénéités nouvelles.

**Le modèle cinétique [Chapitre 5].** Nous nous sommes intéressés au chapitre 5 au modèle cinétique de Othmer-Dunbar-Alt en dimension 3 d'espace [198],

$$\begin{cases} \partial_t f + v \cdot \nabla_x f = \displaystyle\int_{v' \in V} T[S] f(t,x,v')\, dv' - \lambda[S]\rho \\ -\Delta S = \rho \ , \quad \text{ou} \quad -\Delta S + \alpha S = \rho. \end{cases} \tag{24}$$

Les théorèmes d'existence, basés sur des estimations en normes $L^p$ de la densité $\|f(t)\|_{L^p_x L^p_v}$, sont dus à [66, 144], avec les hypothèses suivantes sur le noyau $T$ en dimension 3 :

$$0 \leq T[S](t,x,v,v') \leq C\Big(1 + S(t,x+v) + S(t,x-v')\Big),$$

ou bien

$$0 \leq T[S](t,x,v,v') \leq C\Big(1 + S(t,x+v) + |\nabla S(t,x+v)|\Big),$$

ou encore

$$0 \leq T[S](t,x,v,v') \leq C\Big(1 + S(t,x-v') + |\nabla S(t,x-v')|\Big).$$

Sans améliorer ces conditions de façon spectaculaire, nous avons affaibli cette série d'hypothèses en

$$0 \leq T[S](t,x,v,v') \leq C\Big(1 + S(t,x+v) + S(t,x-v') + |\nabla S(t,x+v)|\Big), \tag{25}$$

ou bien

$$0 \leq T[S](t,x,v,v') \leq C\Big(1 + S(t,x+v) + |\nabla S(t,x+v)| + |\nabla^2 S(t,x+v)|\Big). \tag{26}$$

**Théorème 0.8** (Bournaveas, C., Gutiérrez et Perthame)**.** *Si l'une des deux conditions* (25) *ou* (26) *ci-dessus est satisfaite, alors le modèle cinétique* (24) *admet des solutions globales en temps.*

Le point important est d'avoir réussi à obtenir des estimations en normes mixtes $\|f(t)\|_{L^p_x L^q_v}$ avec $1 \leq q \leq p$ bien choisis. Cela est possible en combinant l'effet de mémoire (voir annexe C) avec un lemme de dispersion [18, 64]. A l'origine nous avions fait intervenir une généralisation de l'inégalité de Young sur le mélange linéaire des variables : l'inégalité de Brascamp-Lieb [168]. Nous avons ensuite réalisé que le lemme de dispersion était bien adapté ici. Le lien entre ces deux inégalités est détaillé dans l'annexe, où une variante de Brascamp-Lieb avec des normes mixtes est proposée.

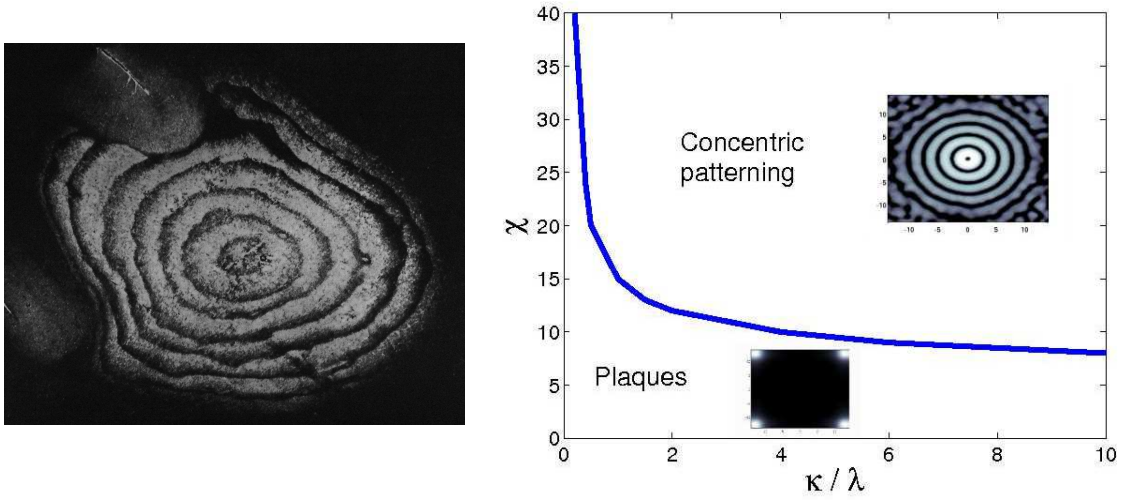


FIG. 2 – Modélisation de la sclérose concentrique de Baló. (*gauche*) Motif remarquable où des bandes concentriques de myéline endommagée remplacent les plaques que l'on observe en général pour la sclérose en plaques [17]. Le diamètre est d'environ $5cm$, donc le *pattern* est visible à l'œil nu. (*droite*) Diagramme de bifurcation pour le modèle (27). Il y a une alternative simple, réminiscente des résultats propres à KS tels que le théorème 0.1 : toutes choses étant égales par ailleurs, si la chémosensibilité dépasse un certain seuil, une organisation spatiale émerge en anneaux concentriques. Cette structure inhomogène est favorisée par l'augmentation des paramètres 'aggressifs' du modèle, la quantité de macrophages $\bar{m}$ et le taux de destruction des oligodendrocytes $\kappa$ par exemple. Les figures correspondent aux états finaux du système (27) avec perturbation stochastique de certains coefficients afin de mettre en évidence la robustesse du modèle.

## 3.3 Processus inflammatoire et auto-organisation dans le cerveau humain [Partie II]

La sclérose en plaques (SEP, *multiple sclerosis* en anglais), est une maladie auto-immune de la substance blanche du cerveau. Elle est dirigée contre la myéline et les cellules qui la produisent (les oligodendrocytes). La myéline est un matériau qui recouvre et isole les axones et garantit une transduction fiable du signal électrique entre les neurones. En termes précis, la SEP est une *maladie inflammatoire démyélinisante chronique du système nerveux central*. Elle doit son nom aux zones homogènes (plaques) de myéline endommagée dans la matière blanche. Les études, quoique très nombreuses, n'ont pas permis de comprendre les origines et les facteurs déclencheurs de la maladie. Concernant le déroulement de la maladie et le rôle du système immunitaire, plusieurs scénarii ont été décrits, et il faut concevoir la SEP comme une superposition de ces processus multiples. Une classification de ces mécanismes a été proposée récemment par Lassmann [162].

La sclérose concentrique de Baló, sujet de notre étude, est une variante de la SEP dont l'originalité réside dans la géométrie des régions démyélinisées. Ce sont des anneaux concentriques en coupe deux-dimensionnelle (motifs en cible de tir à l'arc, voir figure 2). Ces motifs, remarquablement robustes (la symétrie est rarement brisée), ont suscité notre intérêt de modélisateur.

Dans la classification de Lassmann, la sclérose concentrique de Baló est de type III : l'apoptose primitive des oligodendrocytes déclenche un processus inflammatoire secondaire. Ce mécanisme domine probablement aussi lors des phases les plus précoces de la SEP classique. Selon des travaux récents d'imagerie médicale, des anneaux concentriques ont été observés lors de phases préalables à la formation de plaques homogènes [19].

Face à un tel phénomène d'auto-organisation, manifestement robuste, nous avons cherché un scénario

simple permettant de décrire ce processus. Partant des modèles proposés auparavant – en particulier l'analogie avec les anneaux de Liesegang formés par précipitation lors de la croissance de cristaux, ou encore le mécanisme de préconditionnement qui protégerait les oligodendrocytes en aval d'un front de destruction [226] – nous avons confronté différentes hypothèses biologiques. Au vu des échelles de temps et d'espace nous suggérons de prendre en compte le principe de masse critique, décrit au-dessus, pour l'émergence d'une structure spatiale. D'après la classification de Lassmann, nous avons affaire principalement à une attaque de la microglie (les macrophages initialement répartis dans la matière blanche, inoffensifs à l'état ordinaire) envers les oligodendrocytes. Nous faisons dans le modèle de *recrutement local des macrophages* l'hypothèse d'un signal chimique attirant les macrophages sur les zones d'inflammation. De tels signaux sont dûment répertoriés, par exemple dans la famille des chémokines.

Des techniques récentes d'imagerie ont mis en évidence que les anneaux apparaissent successivement à partir du centre de la lésion, et non simultanément. De plus Chen et coll. [70] montrent qu'un front générant une légère anomalie de diffusion quasi-homogène précède l'apparition des anneaux. Par conséquent les motifs concentriques résulteraient d'une instabilité secondaire à l'arrière d'un front dont l'origine, la nature et l'action (ici activation des macrophages auto-immuns) sont sujets à controverse. Il est connu cependant qu'à l'origine de la SEP en général il y a un défaut d'imperméabilité locale des vaisseaux sanguins irriguant le cerveau, laissant des lymphocytes T CD4 ou CD8+, ainsi que des anticorps, pénétrer dans la matière blanche.

Ce scénario de recrutement local est décrit par le couplage d'un front d'activation (de type propagation, Fisher-KPP pour faire simple) avec un modèle de chimiotactisme :

$$\begin{cases} \dfrac{\partial m}{\partial t} = \underbrace{D\Delta m + \lambda m(\bar{m} - m)}_{\substack{\text{front d'activation} \\ \text{des macrophages}}} - \underbrace{\operatorname{div}\left(\chi m(\bar{m} - m)\nabla c\right)}_{\substack{\text{recrutement local} \\ \text{des macrophages}}}, \\ \dfrac{\partial d}{\partial t} = \underbrace{F(m)m(\bar{d} - d)}_{\text{destruction des oligodendrocytes}}, \\ \underbrace{-\varepsilon\Delta c + \alpha c = \mu d}_{\substack{\text{production et diffusion instantanée} \\ \text{du chémoattractant}}}. \end{cases} \tag{27}$$

On fait l'hypothèse réaliste que les oligodendrocytes détruits ($d$) libèrent un signal chimique ($c$) qui attire les macrophages activés auto-immuns ($m$) avoisinants. Non seulement ce modèle reproduit parfaitement les motifs et les échelles de la réalité, mais il permet quelques conclusions qualitatives non dénuées d'intérêt. Le coefficient réduit $\tilde{\chi} = \dfrac{\chi \bar{m} \mu \bar{d}}{D\alpha}$ joue le rôle d'un paramètre de bifurcation qui marque la transition entre des plaques et des anneaux concentriques (figure 2). Le modèle (27) est incroyablement robuste en ce qu'il exhibe soit des plaques, soit des anneaux, et pas d'autre pattern possible ; et qu'il résiste aux perturbations stochastiques. Par ailleurs nous avons mis en évidence une corrélation positive entre aggressivité de la maladie et émergence d'une structure inhomogène en espace (en jouant sur divers paramètres). Or il est bien connu chez les cliniciens que la sclérose concentrique de Baló est une variante de la SEP particulièrement aggressive et fulgurante.

Pas d'analyse mathématique menée à bien pour le modèle (27) à ce jour, mais nous projetons d'étudier plus avant un modèle plus simple d'interaction entre un front de progression (type Fisher) couplé avec un mécanisme d'agrégation (type KS).

# 4 Directions de recherches futures

**Défaut de convexité par déplacement en dimension $d \geq 2$.** Il s'agit d'étendre les résultats du chapitre 7 en dimension quelconque. Cela nécessite une bonne compréhension de la contraction des milieux poreux dans différentes formulations et des structures géométriques intervenant dans ces flots gradients du point de vue du transport optimal de masse.

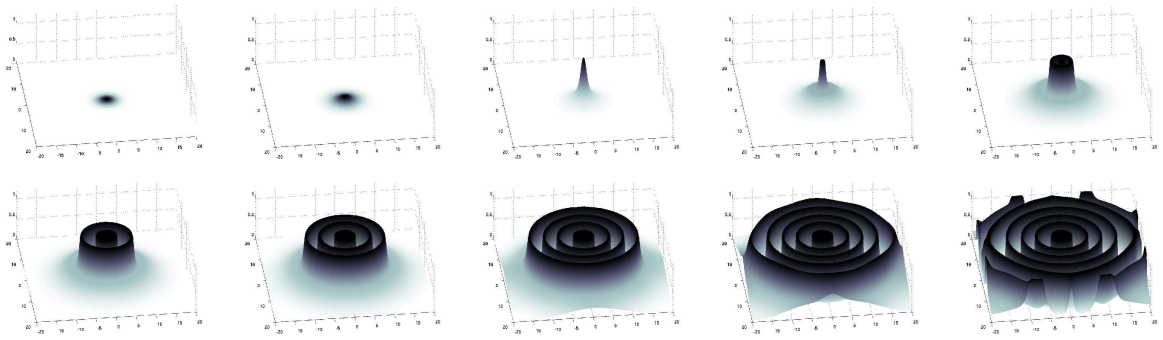

FIG. 3 – Evolution du couplage entre un front de Fisher (activation des macrophages auto-immuns ou bien prolifération cellulaire) et un processus de chimiotactisme de type Keller-Segel, selon le modèle (28). La densité de la population de cellules $n$ est figurée pour des temps successifs.

**Couplage Fisher/KS.** Afin de progresser dans la compréhension du système (27) nous voudrions étudier un couplage simple entre un front d'invasion cellulaire (Fisher-KPP) et un système de Keller-Segel saturé,

$$\begin{cases} \dfrac{\partial n}{\partial t} = \Delta n - \text{div}\left(\chi n(1-n)\nabla c\right) + \lambda n(1-n) \\ -\Delta c + \alpha c = n, \end{cases} \tag{28}$$

Il apparaît numériquement (figure 3) que ce système partage beaucoup de points communs qualitatifs avec le modèle précédent (27). Précisons que des modèles tels que (28) ont été pris en considération auparavant, par exemple dans [237], voir aussi [185]. A cela près que le coefficient de chemosensibilité n'est pas saturé dans ces références. Dans les modèles (28) et (27) nous avons à l'esprit une saturation qui, semblerait-il, sélectionne des anneaux plutôt que des amas localisés ('spots') et paraît plus robuste en ce sens. Signalons à ce propos qu'une étude des ondes solitaires pour le modèle sans saturation est en cours [186].

**Simulations sur des images de cerveau** Sur le plan numérique, l'étape faisant suite aux résultats présentés à la figure 2 ou 3 est la simulation en 3D sur une géométrie réaliste de matière blanche. C'est l'objet d'un projet réalisé par les numériciens Barbara Bouffandeau et Benoît Desjardins (voir figure 4).

**Lorsque $\chi$ dépend de $c$.** La question de l'existence globale sous la dépendance $\chi(c)$ (et non plus $\chi(n)$ comme c'est le cas dans (10)) est tout à fait ouverte.

$$\begin{cases} \dfrac{\partial n}{\partial t} = \Delta n - \text{div}\left(n\chi(c)\nabla c\right), \\ -\Delta c = n\ . \end{cases} \tag{29}$$

C'est pourtant une hypothèse naturelle provenant des différentes approches micro- ou mésoscopiques (*e.g.* marche aléatoire biaisée, modèle cinétique), et qui s'appuie sur des principes biophysiques simples (paragraphe 1.3). Il est notoire qu'aucune structure énergétique n'a été décelée dans ce cas. Nous suggérons de réécrire le système en changeant les variables de façon adéquate : $v = \phi(c)$, avec $\phi' = \chi$. Dans le cas

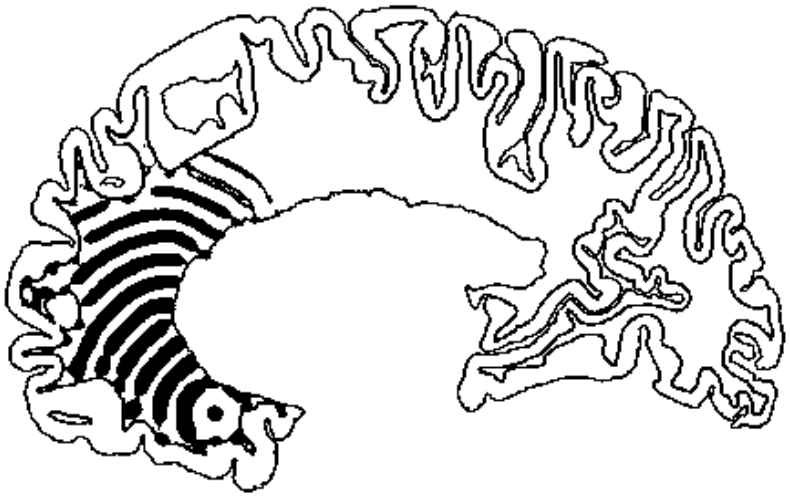

FIG. 4 – Simulations numériques du modèle (27) sur une géométrie deux dimensionnelle de cerveau (reproduit avec l'amabilité de Barbara Bouffandeau et Benoît Desjardins).

de $\chi(c) = \dfrac{\chi_0}{1+\gamma c}$ par exemple, l'équation de synthèse chimique pour $v$ dans (29) devient

$$\begin{cases} \dfrac{\partial n}{\partial t} = \Delta n - \text{div } (n\nabla v) \ , \\ -\Delta v - \frac{\gamma}{\chi_0}|\nabla v|^2 = n\chi_0 \exp\left(-\frac{\gamma}{\chi_0} v\right) \ . \end{cases}$$

Il nous faudrait alors utiliser des outils particuliers à l'équation de Hamilton-Jacobi pour la synthèse chimique.

**Le modèle de KS sur la sphère.** Il faut remarquer dans les calculs effectués au chapitre 3 la présence sous-jacente de la sphère. D'une part les inégalités à l'œuvre, Trudinger-Moser-Onofri et Hardy-Littlewood-Sobolev logarihmique sont des reliquats d'inégalités sur la sphère plus simples à écrire [56, 23],

$$\log \int_{\mathbb{S}^2} e^G \ d\xi \leq \frac{1}{4} \int_{\mathbb{S}^2} |\nabla G|^2 \ d\xi + \int_{\mathbb{S}^2} G \ d\xi \ ,$$

et

$$-\iint_{\mathbb{S}^2 \times \mathbb{S}^2} F(\xi) \log|\xi - \eta| F(\xi) \ d\xi d\eta \leq \frac{1}{2} \int F \log F \ d\xi - \int_{\mathbb{S}^2} \log|\xi - \eta| \ d\xi \ ,$$

avec $\int F d\xi = 1$. D'autre part le jacobien $H = \frac{1}{\pi}\left(\frac{1}{1+|x|^2}\right)^2$ de la projection stéréographique inverse joue un rôle prépondérant dans les estimations. Il serait donc intéressant d'écrire une EDP sur la sphère équivalente à KS pour $\mathbb{R}^2$ tout entier. Nous espérons ainsi pouvoir étudier un système intrinsèque qui contournerait les problèmes liés à la non-finitude de $\mathbb{R}^2$, et en particulier la condition de second moment fini qui n'est peut être qu'un artefact[4].

[4]Ceci est discutable car la condition du second moment fini paraît absolument nécessaire pour ce qui est de la convergence en distance de Wasserstein décrite dans la partie III.

# Première partie

# Extensions du modèle de Keller-Segel

# Chapitre 1

# Le modèle de Keller-Segel avec diffusion non linéaire

Cet article en collaboration avec José Carrillo adapte les méthodes d'énergie de [107] et [86] au modèle KS parabolique/elliptique avec une diffusion des cellules non-linéaire (et éventuellement un coefficient de chémosensitivité densité-dépendant [202, 159]), à la fois en domaine borné et dans tout l'espace $\mathbb{R}^2$. Les estimations *a priori* cruciales découlent des inégalités fonctionnelles très fines de Trudinger-Moser et de Hardy-Littlewood-Sobolev logarithmique. L'article est paru dans le Journal de Mathématiques Pures et Appliquées sous le titre *Volume effects in the Keller-Segel model : energy estimates preventing blow-up* [50].

## 1.1 Introduction

Chemotaxis is the movement of cells oriented by chemical cues. This phenomenon occurs for a large range of cells, of different sizes and from different backgrounds. Well-known examples are the bacteria *Escherichia Coli* [5], the amoeba *Dyctiostelium discoideum* [138] or endothelial cells of the human body which may respond to angiogenic factors secreted by a tumor [173]. Usually models for chemotaxis take into account at least two entities, namely the density of cells and the concentration of the chemical substance which is assumed to influence the movement of the population of cells.

The Patlak, Keller and Segel (PKS) model [206, 153, 154] has been introduced in order to explain chemotactic cell aggregation by means of a coupled system of two equations: a drift-diffusion type equation for the cell density $n$, and a reaction-diffusion equation for the chemoattractant concentration $c$:

$$\begin{cases} \partial_t n - \kappa \Delta n + \nabla \cdot \Big( \chi n \nabla c \Big) = 0 \quad t \geq 0 \, , \; x \in \Omega \subset \mathbb{R}^2, \\ -\Delta c = n - \langle n \rangle. \end{cases} \tag{1.1}$$

together with the initial condition $n(0,x) = n_0(x)$ and zero-flux boundary conditions both for $n$ and $c$, i.e.

$$\frac{\partial n}{\partial \eta} = \frac{\partial c}{\partial \eta} = 0 \quad t \geq 0 \, , \; x \in \partial\Omega, \tag{1.2}$$

being $\eta$ the outwards unit normal vector to the boundary $\partial\Omega$. Note that the system (1.1) is slightly different if the domain $\Omega$ is exactly the whole space (see [86] and Section 1.2). Parameters in this model are the diffusion coefficient $\kappa$, the chemosensitive coefficient $\chi$, and the total mass of cells, which is formally conserved through the evolution:

$$M = \int_\Omega n \, dx.$$

It is well-known that solutions of this system may blow up in finite time (see the review paper [141] and references therein). In fact there exists a threshold in the balance between the diffusion and the aggregation terms. Jäger and Luckhaus proved that there exists a constant $\mathcal{C}^*$ such that solutions are global in time whenever $\frac{\chi M}{\kappa} < \mathcal{C}^*$. They used direct *a priori* estimates based on a Gagliardo-Nirenberg-Sobolev inequality, what we will call "*Jäger & Luckhaus technique*" in the following [147]. It has also been shown that under an additional condition involving the second moment of $n$, the solution blows up in finite time if $\frac{\chi M}{\kappa} > \mathcal{C}^*_{opt}$, where

$$\mathcal{C}^*_{opt} = \begin{cases} 8\pi & \text{if } \Omega = \mathbb{R}^2, \\ 4\pi & \text{if } \Omega \text{ is a } C^2, \text{ bounded, connected domain.} \end{cases} \tag{1.3}$$

Note that in the radial case the threshold for blow-up is also $8\pi$ [187, 188, 214, 208]. In the following, we will restrict ourselves to $C^2$, bounded, connected domains (see [107] for results in the case of a piecewise $C^2$, bounded, connected domain).

Recently, improvements on the constant $\mathcal{C}^*$ given by Jäger and Luckhaus have been obtained both on a bounded domain by Gajewski and Zacharias [107] and Biler [29] (see also [32]), and in the whole space by Dolbeault and Perthame [86]. These improvements are based on fine estimates of the free energy using sharp variational inequalities. As a summary, in the linear diffusion classical PKS model one has the following result:

**Theorem 1.1** (Optimal constant for Linear Diffusion PKS)**.**
*Assume that* $\frac{\chi M}{\kappa} < \mathcal{C}^*_{opt}$.

*(i) Given a bounded initial data on a $C^2$, bounded, connected domain, there exists a weak solution globally defined on time.*

*(ii) Given an integrable initial data with second moment and entropy bounded, i.e., $(1+|x|^2)n_0 \in L^1(\mathbb{R}^2)$ and $n_0 \log n_0 \in L^1(\mathbb{R}^2)$, there exists a weak solution globally defined in time.*

Recent papers have pointed out the relevance of dealing with general nonlinear cell diffusion. For example Gamba *et al.* [108] introduced a pressure function $\phi(n)$ in their hyperbolic model, taking into account the fact that cells do not interpenetrate, that is, they are full bodies with nonzero volume. Kowalczyk [159] derived from this hyperbolic model a parabolic-elliptic system for chemotaxis where the first equation of (1.1) is replaced by

$$\partial_t n + \nabla \cdot \Big( - n\nabla h(n) + \chi n \nabla c \Big) = 0, \tag{1.4}$$

where $h$ is related to the pressure function. Due to its biological meaning, $h$ is an increasing function of the cell density $n$, which renders a saturation of the occupation number of cells. Note that the linear diffusion corresponds to $h(n) = \kappa \log n$.

On the other hand, Hillen and Painter [202] have included volume-filling in the model: in the context of biased random walks, they considered that the jumping probability depends on the amount of cells in the neighboring sites. Cells which are packed have less probability to move. If $q$ denotes the correcting decreasing function, authors derive the following continuous model

$$\partial_t n + \nabla \cdot \Big( - \kappa\big(q(n) - nq'(n)\big)\nabla n + \chi_0 q(n) n \nabla c \Big) = 0. \tag{1.5}$$

In another work, assuming the chemosensitivity $\chi$ vanishes for sufficiently large cell density, they proved that the blow-up of solutions is prevented [135], c.f. [164].

The aim of our work is to present a new derivation of *a priori* estimates which lead to equi-integrability and thus, $L^\infty$ bounds for the cell density. We do not attempt here to develop a complete existence theory for the nonlinear diffusion or chemosensitivity case. We refer to [107] and [86] for a complete proof in the linear case.

In this paper, we improve and extend to $\mathbb{R}^2$ Kowalczyk results [159] thanks to free energy methods. We show essentially that the assumption $h(u) \geq \kappa \log u$ for large $u$ with

$$\kappa > \frac{\chi M}{\mathcal{C}^*_{opt}} \tag{1.6}$$

is sufficient to prevent blow up. We will distinguish two cases: a bounded domain $\Omega$ (Section 1.4), and the whole space $\Omega = \mathbb{R}^2$ (Section 1.5). Main results are summarized in section 1.5.5. In Section 1.6 we extend our approach to the case of volume-filling type equations, i.e., a nonlinear chemosensitivity function, by connecting them to the nonlinear diffusion case, i.e., the nonlinear pressure model. In the next two sections, we will summarize the main ingredients and results of the PKS model (Section 2) and how to pass from equi-integrability bounds to $L^\infty$ bounds (Section 3).

## 1.2 Basics of the PKS model

We first clarify the basic assumption on the diffusion coefficient.

**Hypothesis H 1.2** (Basic Regularity on the Nonlinear Diffusion h)**.** *$h \in L^1_{loc}(0,\infty) \cap \mathcal{C}^1(0,\infty)$ is an increasing function with $h(1) = 0$.*

Now, we are entitled to define the functions $f$ and $\Phi$ by: $f'(u) = uh'(u)$ with $f(0) = 0$ and $\Phi'(u) = h(u)$ with $\Phi(0) = 0$, respectively.

The nonlinear diffusion PKS model in a bounded domain $\Omega \subset \mathbb{R}^2$ consists of:

$$\begin{cases} \partial_t n + \nabla \cdot \Big( - n\nabla h(n) + \chi n \nabla c \Big) = 0 \quad t \geq 0\,,\ x \in \Omega, \\ -\Delta c = n - \langle n \rangle. \end{cases} \tag{1.7}$$

together with the initial condition $n_0 \in L^1_+(\Omega) \cap L^\infty(\Omega)$ and the no-flux boundary conditions (1.2). Note that in (1.7) the equation on $c$ has to be understood modulo a constant, that is why we assign from now on

$$\int_\Omega c\, dx = 0, \tag{1.8}$$

when dealing with a bounded domain.

In the whole space $\mathbb{R}^2$ the equation $-\Delta c = n$ has to be understood in the sense of the Poisson kernel, and the system reads:

$$\begin{cases} \partial_t n + \nabla \cdot \Big( - n\nabla h(n) + \chi n \nabla c \Big) = 0 \quad t \geq 0\,,\ x \in \mathbb{R}^2, \\ c(t,x) = -\dfrac{1}{2\pi} \displaystyle\int_{\mathbb{R}^2} \log|x-y|\, n(t,y)\, dy. \end{cases} \tag{1.9}$$

**Hypothesis H 1.3** (The initial data $n_0$)**.** *$n_0 \in L^1_+(\Omega) \cap L^\infty(\Omega)$. Moreover, if $\Omega = \mathbb{R}^2$ we assume in addition that $n_0|x|^2 \in L^1_+(\mathbb{R}^2)$.*

**Remark 1.4.** *These assumptions are not the optimal ones, and blow up can be prevented starting from weaker conditions (see [86] for instance). However we plan to give uniform bounds, and for this purpose we impose $n_0 \in L^\infty(\Omega)$.*

In the following, we will derive results valid both for the bounded domain case and for the whole space case, and thus, we will not make explicit in the integrals the domain in which we work unless it is necessary. Both systems have a common Lyapunov functional which will be crucial in the rest.

**Lemma 1.5** (Free energy)**.** *Given a smooth solution of* (1.7) *and* (1.9)*, then the free energy functional [58]*

$$\mathcal{E}(t) = \int \Phi(n)\, dx - \frac{1}{2}\chi \int nc\, dx \tag{1.10}$$

*verifies*

$$\frac{d}{dt}\mathcal{E} = -\int n\, |\nabla(h(n) - \chi c)|^2\, dx \leq 0. \tag{1.11}$$

**Example 1.6** (Power Nonlinear Diffusion)**.** *In the case of a nonlinearity which behaves like a power : $f(u) = u^\alpha$ for some positive $\alpha$, then $h(u) = \frac{\alpha}{\alpha-1}u^{\alpha-1} - \frac{\alpha}{\alpha-1}$ and $\Phi(u) = \frac{1}{\alpha-1}u^\alpha - \frac{\alpha}{\alpha-1}u$.*

We will distinguish two cases, corresponding to the two possible behaviors of $h$ near the origin:

1. "Fast diffusion" case : $h(0^+) = -\infty$.
2. "Degenerate diffusion" case : $h(0^+) > -\infty$.

Let us recall that the optimal constant $\mathcal{C}^*_{opt}$ is given by (1.3). The main assumption of this paper is the following:

**Hypothesis H 1.7** (Superlinear at $\infty$ Nonlinear Diffusion)**.** *The nonlinear diffusion function $h$ grows faster than the critical one for large density levels, that is, there exists $\kappa > \dfrac{\chi M}{\mathcal{C}^*_{opt}}$ and $\mathcal{U} \in \mathbb{R}_+$ such that*

$$\forall u \geq \mathcal{U} \quad h(u) \geq \kappa \log u.$$

*Without loss of generality we assume that $\Phi(u) \geq 0$ for $u \geq \mathcal{U}$. Moreover, we assume that there exists $\delta > 0$ such that $uh'(u) \geq \delta$ for large $u$.*

This assumption means that the behaviour of the diffusion term has to be considered only at high levels of cell density. In the following we will see that, although this hypothesis is sufficient for our purpose when dealing with a bounded domain, it has to be completed by technical assumptions in the case of the whole space. Note that the assumption on the derivative on $h$ in (H1.7) implies the main hypothesis whenever $\delta = \kappa > \chi M/\mathcal{C}^*_{opt}$.

We will need the following easy consequence obtained by integrating hypothesis (H1.7) over $\{n \geq \mathcal{U}\}$.

**Lemma 1.8** (Internal Energy estimate from below)**.** *Given $R$ such that $h(u) = \kappa \log u + R(u)$, with $R \geq 0$ for $u \geq \mathcal{U}$, then*

$$\int_{\{n \geq \mathcal{U}\}} \Phi(n)\, dx \geq \kappa \int_{\{n \geq \mathcal{U}\}} n \log n\, dx + \int_{\{n \geq \mathcal{U}\}} \mathcal{R}(n)\, dx - C(\mathcal{U}, M, \kappa), \tag{1.12}$$

*where $\mathcal{R}' = R$ satisfying $\mathcal{R}(\mathcal{U}) = 0$.*

*Proof.* We integrate the relation $h(u) = \kappa \log u + R(u)$:

$$\Phi(u) - \Phi(\mathcal{U}) = \kappa(u \log u - u - \mathcal{U} \log \mathcal{U} + \mathcal{U}) + \mathcal{R}(u).$$

Consequently

$$\int_{\{n \geq \mathcal{U}\}} \Phi(n)\, dx = \kappa \int_{\{n \geq \mathcal{U}\}} n \log n\, dx + \int_{\{n \geq \mathcal{U}\}} \mathcal{R}(n)\, dx - \kappa \int_{\{n \geq \mathcal{U}\}} C(\mathcal{U})\, dx.$$

If $C(\mathcal{U}) > 0$, we use Markov's inequality to control the last term, obtaining

$$\int_{\{n \geq \mathcal{U}\}} \Phi(n)\, dx = \kappa \int_{\{n \geq \mathcal{U}\}} n \log n\, dx + \int_{\{n \geq \mathcal{U}\}} \mathcal{R}(n)\, dx - \kappa \frac{C(\mathcal{U})}{\mathcal{U}} M.$$

and thus (1.12). □

Whereas the formulation adopted here is well-adapted to the model (1.4) involving a pressure function $h$, it does not match with the volume filling model (1.5). We will present in section 1.6 an extension in which we consider both nonlinear diffusion and chemosensitivity. In particular, we show how to reduce the analysis to a nonlinear diffusion by means of introducing a natural quantity which plays the role of the nonlinear diffusion, namely $H$ defined by

$$H'(u) = \frac{f'(u)}{\chi(u)u}$$

and $H(1) = 0$ with a bounded chemosensitivity $\chi(u)$ positive for $u > 0$. This is obviously satisfied in the volume filling model since $\chi(u) = \chi_0 q(u)$ with $q$ decreasing for which

$$H'(u) = \kappa \frac{q(u) - uq'(u)}{\chi_0 q(u) u}.$$

In [202] authors choose $q(u) = \left(1 - \frac{u}{U_{max}}\right)\mathbf{1}_{\{u<U_{max}\}}$, which leads to

$$H'(u) = \begin{cases} \dfrac{\kappa}{\chi_0} \dfrac{1}{u - U_{max}} & \text{if } u < U_{max} \\ +\infty & \text{otherwise} \end{cases}.$$

They proved in [135] that a vanishing effect in the chemotactic response prevents blow up in the case of linear diffusion (in our formulation it consists of setting $H'(u) = +\infty$ for large $u$). This is an obvious consequence of the maximum principle using the constant steady states $n = U_{max}$ in (1.5). In our case we will consider positive decreasing chemotactic coefficient $\chi(u)$ asymptotically vanishing at $\infty$.

**Example 1.9** (Decreasing Nonlinear Chemotactic Coefficient)**.**

1. $q(u) = \frac{1}{1+u^\gamma}$, $\gamma > 0$, *leads to*

$$H'(u) = \frac{\kappa}{\chi_0} \frac{1 + (\gamma+1)u^\gamma}{u(1+u^\gamma)} \sim_\infty \frac{\kappa}{\chi_0} \frac{\gamma+1}{u},$$

*that is the diffusion corresponding to $H$ is asymptotically linear, with the coefficient $\frac{\kappa(1+\gamma)}{\chi_0}$.*

2. $q(u) = e^{-\beta u}$, $\beta > 0$, *leads to*

$$H'(u) = \frac{\kappa}{\chi_0} \frac{1 + \beta u}{u} \sim_\infty \frac{\kappa}{\chi_0} \beta,$$

*that is the associated free energy functional $F$ behaves like a square for large cell density.*

## 1.3 From equi-integrability to $L^\infty$ bound

Different approaches to get $L^\infty$ *a priori* estimates have been proposed in the literature [147, 159]. Here, we give a sketch of the argument to derive $L^\infty$ bounds of the cell density from equi-integrability estimates which is basically contained in the references above. In fact, the $L^\infty$ estimate will be obtained from equi-integrability, and this considerably reduces our effort to obtain equi-integrability for both the bounded domain (Section 1.4) and the whole space case (Section 1.5). We first prove a result which shows how to gain $L^p$ bound ($p > 2$) from equi-integrability.

The modulus of equi-integrability is denoted by

$$\omega(T, k) = \sup_{t\in[0,T]} \int (n - k)_+ \, dx.$$

**Lemma 1.10** ($L^p$ bound from equi-integrability)**.** [147] *Assume* (H1.2), (H1.3), (H1.7). *In addition given $T > 0$, assume the modulus of equi-integrability verifies*

$$\omega(T, k) \xrightarrow[k\to\infty]{} 0.$$

*Then $n \in L^\infty\big(0, T; L^p\big)$ for $p > 2$. Moreover, if equi-integrability does not depend on time $T$, i.e., the previous limit is uniform in $T$, then $n \in L^\infty\big(\mathbb{R}_+; L^p\big)$*

*Proof.* Let $p \geq 2$ and be $k$ large enough so we can use the assumption (H1.7) $uh'(u) \geq \delta$, then

$$\begin{aligned}\frac{d}{dt}\int (n-k)_+^p\,dx \leq & -4\frac{p-1}{p}\delta\int |\nabla (n-k)_+^{p/2}|^2\,dx + \chi(p-1)\int (n-k)_+^{p+1}\,dx \\ & + p\chi k\int (n-k)_+^p\,dx + p\chi k^2\int (n-k)_+^{p-1}\,dx.\end{aligned} \tag{1.13}$$

Because of the nonlinearity in the chemotactic term, we cannot apply directly a Gronwall lemma. However we can estimate the balance between the diffusion and the chemotactic contributions. Let us use the following Gagliardo-Nirenberg-Sobolev inequality [106, 193].

$$\int v^{p+1}\,dx \leq \mathcal{C}_{gns}(p)\int |\nabla v^{p/2}|^2\,dx\int v\,dx.$$

We estimate the diffusion part by the chemotactic part and the modulus of equi-integrability,

$$\begin{aligned}\frac{d}{dt}\int (n-k)_+^p\,dx \leq & (p-1)\left(-\frac{4\delta}{pC_p\int (n-k)_+\,dx}+\chi\right)\int (n-k)_+^{p+1}\,dx \\ & + p\chi k\int (n-k)_+^p\,dx + p\chi k^2\int (n-k)_+^{p-1}\,dx.\end{aligned}$$

We can interpolate $(n-k)_+^p$ and $(n-k)_+^{p-1}$ between $(n-k)_+^{p+1}$ and $(n-k)_+$, and we obtain the following estimate

$$\frac{d}{dt}\int (n-k)_+^p\,dx \leq (p-1)\left(-\frac{4\delta}{pC_p\,\omega(T,k)}+C(p,\chi)\right)\int (n-k)_+^{p+1}\,dx + C(p,\chi,k)\int (n-k)_+\,dx. \tag{1.14}$$

At this point, we choose $k$ large enough to ensure that not only (H1.7) is satisfied but also

$$-\frac{4\delta}{pC_p\,\omega(T,k)}+C(p,\chi)\leq -\frac{\delta}{p-1}.$$

We can interpolate once more in (1.14), and finally we have shown that there exists $\eta>0$ such that

$$\frac{d}{dt}\int (n-k)_+^p \leq -\eta\int (n-k)_+^p\,dx + C(p,\chi,k,\delta)\int (n-k)_+\,dx, \tag{1.15}$$

which guarantees that $\int (n-k)_+^p$ is bounded on $[0,T]$, and so that $n\in L^\infty\big(0,T;L^p\big)$ because of

$$\begin{aligned}\int n^p\,dx &\leq \int_{\{n<k\}} k^{p-1}n\,dx + \int_{\{n\geq k\}}(n-k)^p\,dx + C(p,k)\mathrm{meas}\Big\{n\geq k\Big\}\\ &\leq \int_{\{n\geq k\}}(n-k)^p\,dx + \Big(k^{p-1}+\frac{C(p,k)}{k}\Big)M.\end{aligned}$$

In addition, $\|n\|_p$ is bounded in time depending on $p$, $\chi$, $M$, $k$ and $\delta$. If the equi-integrability does not depend on time, then $k$ does not, and so the time $T$ does not appear in the estimate giving the last assertion of this lemma $n\in L^\infty\big(\mathbb{R}_+;L^p\big)$. □

As a consequence we get immediately that $n$ remains in $L^p$ for some $p>2$ as soon as $n$ is equi-integrable. We deduce from Morrey's embedding theorem that $\nabla c$ is in $L^\infty$, and moreover that $\nabla c\in L^\infty_{loc}\big(\mathbb{R}_+;L^\infty\big)$. Thanks to the following lemma, based on an iterative method due to J. Moser [4], we get that $n\in L^\infty_{loc}\big(\mathbb{R}_+;L^\infty\big)$. Let us point out that such a result was already obtained by Kowalczyk in the bounded domain case. Nevertheless, we are able to adapt his work for the whole space since all computations are led on the subset $\{n\geq k\}$ which has finite measure.

**Lemma 1.11** ($L^\infty$ bound by an iterative method)**.** [159] *Assume* (H1.2), (H1.3), (H1.7)*, and also that the chemotactic potential verifies $\nabla c\in L^\infty_{loc}\big(\mathbb{R}_+;L^\infty\big)$, then $n\in L^\infty_{loc}\big(\mathbb{R}_+;L^\infty\big)$ also. Moreover, if $\nabla c\in L^\infty\big(\mathbb{R}_+;L^\infty\big)$ then $n\in L^\infty\big(\mathbb{R}_+;L^\infty\big)$.*

*Proof.* We just describe in the following the main steps of the proof and refer to [159] for more details. The main idea is to use the $\|\nabla c\|_\infty$ estimate in order to decrease the homogeneity of the chemotactic term. Assume $p \geq 2$ and $k$ large enough to ensure the applicability of hypotheses (H1.7), then we deduce a similar estimate as in the lemma 1.10, except that the right-hand side term involves $\int (n-k)_+^{p/2}\,dx$.

$$\frac{d}{dt}\int (n-k)_+^p\,dx \leq -p^2C\|\nabla c\|_\infty^2 \int (n-k)_+^p\,dx + C^2p^4\frac{\|\nabla c\|_\infty^4}{\delta^2}\left(\int (n-k)_+^{p/2}dx\right)^2 + p^2C\|\nabla c\|_\infty^2,$$

where $C$ is a generic constant depending only on $\delta$, $\chi$, $M$ and $k$ ($C$ does not depend on $p$ !).

A refined study [159, Lemma 5.1] of this differential inequality is sufficient to propagate bounds for

$$\int (n-k)_+^{2^j}\,dx,$$

for $j \geq 0$, and to prove $L^\infty$ bound for $n$. We only highlight that $\|(n_0-k)_+\|_p^p \leq \mathrm{meas}\{n_0 \geq k\}\|n_0\|_\infty^p$. Consequently let us choose any $T > 0$ and define

$$K_j = \sup_{t\in[0,T]} \int (n-k)_+^{2^j}\,dx,$$

then

$$K_j \leq C\max\left(\|n_0\|_\infty^{2^j}\,,\ 2^{2j}K_{j-1}^2 + C\right). \tag{1.16}$$

Because $a+b \leq 2\max(a,b)$ we reduce to

$$L_j \leq C\max\left(1\,,\ 2^{2j}L_{j-1}^2\right),$$

where $K_j = L_j\|n_0\|_\infty^{2^j}$; furthermore we deal with the following recurrence,

$$\log_+ L_j \leq 2\log_+ L_{j-1} + j\log 4 + C.$$

Because $\sum j2^{-j}$ is convergent it ensures that $2^{-j}\log L_j$ is bounded, and finally we can pass to the limit $j \to \infty$. This proves that $n \in L^\infty\big(0,T;L^\infty(\Omega)\big)$.

□

Summarizing, these two previous lemmas imply that $n(t,\cdot)$ is in $L^\infty$ whenever $n$ is equi-integrable in the sense precised in Lemma 1.13. Moreover, the $L^\infty$ estimate is uniform or local in time whether equi-integrability is uniform or local in time.

## 1.4 *A priori* estimates on a bounded domain

Our aim is now to prove that the cell density $n(t,\cdot)$ is equi-integrable. In the linear case it is a common way to look for estimates like $\int n\log n$ or even any functional of $n$ growing faster than $n$. In this nonlinear context, $\Phi$ plays the role of this functional. First of all, if $\Omega$ is a bounded domain, we can prove directly that both terms of the energy are bounded and particularly that $n$ is equi-integrable.

**Theorem 1.12** (Equi-integrability in $\Omega$ bounded)**.** *Assume* (H1.2), (H1.3), (H1.7) *then*

$$\lim_{k\to\infty}\sup_{t\geq 0}\int_\Omega (n-k)_+\,dx = 0,$$

*and thus,* $n \in L^\infty\big(\mathbb{R}_+;L^\infty(\Omega)\big)$.

*Proof.* We first rewrite the free energy as

$$\mathcal{E}(t) = \int_\Omega \left\{\Phi(n) - \chi nc\right\} dx + \frac{\chi}{2}\int_\Omega |\nabla c|^2\, dx = J_c[n] + \frac{\chi}{2}\int_\Omega |\nabla c|^2\, dx \tag{1.17}$$

and we remind that due to Lemma 1.11 it is a non increasing function of time, that is, $\mathcal{E}(t) \le \mathcal{E}_0$.

**Step 1: Explicit estimate for $\nabla c \in L^2$.** Given $c \in W^{1,1}(\Omega)$, the convex functional $J_c[n]$ has a critical point $n^*$ which is solution of

$$h(n^*) - \chi c = \lambda, \tag{1.18}$$

whenever $n^* > 0$ and null otherwise. Here, $\lambda$ is the Lagrange multiplier associated to the constraint given by mass conservation $\int_\Omega n^* = M$ and fixed by this condition. We refer to [58, Proposition 5] for details. Therefore, we have

$$J_c[n] \ge \int_\Omega \left\{\Phi(n^*) - \chi n^* c\right\} dx = \int_{\{n^*>0\}} \left\{\Phi(n^*) - n^* h(n^*) + \lambda n^*\right\} dx.$$

In order to estimate precisely the right-hand side term, and particularly $\lambda$, we introduce the corrective term $R$ such that $h(n^*) = \kappa \log n^* + R(n^*)$, then

$$J_c[n] \ge \int_\Omega \left\{\Phi(n^*) - \kappa n^* \log n^*\right\} dx - \int_{\{n^*>0\}} n^* R(n^*)\, dx + \lambda M. \tag{1.19}$$

Moreover, (1.18) implies $\kappa \log n^* + R(n^*) = \lambda + \chi c$ whenever $n^* > 0$ and thus

$$\int_{\{n^*>0\}} \exp\left(\frac{R(n^*)}{\kappa}\right) n^*\, dx = e^{\lambda/\kappa} \int_{\{n^*>0\}} \exp\left(\frac{\chi}{\kappa}\, c\right)\, dx$$

and

$$\lambda = \kappa \log\left(\int_{\{n^*>0\}} e^{R/\kappa} n^*\, dx\right) - \kappa \log\left(\int_{\{n^*>0\}} e^{\chi c/\kappa}\, dx\right). \tag{1.20}$$

If we replace $\lambda$ by this expression in inequality (1.19), we conclude that

$$\begin{aligned} J_c[n] \ge \int_\Omega \left\{\Phi(n^*) - \kappa n^* \log n^*\right\} dx - \int_{\{n^*>0\}} n^* R(n^*)\, dx \\ + \kappa M \log\left(\int_{\{n^*>0\}} e^{R/\kappa} n^*\, dx\right) - \kappa M \log\left(\int_{\{n^*>0\}} e^{\chi c/\kappa}\, dx\right) \end{aligned} \tag{1.21}$$

On one hand, assumption (H1.7) and Lemma 1.8 tell us that

$$\int_{\{n^*\ge \mathcal{U}\}} \left\{\Phi(n^*) - \kappa n^* \log n^*\right\} dx \ge C,$$

by (1.12). On the other hand, we trivially have

$$\int_{\{n^*<\mathcal{U}\}} \left\{\Phi(n^*) - \kappa n^* \log n^*\right\} dx \ge -\Big(\sup_{[0,\mathcal{U})} \left(\Phi - \kappa n \log n\right)^-\Big)|\Omega|.$$

Therefore,

$$\int_\Omega \left\{\Phi(n^*) - \kappa n^* \log n^*\right\} dx$$

is bounded uniformly from below.

Now, the Jensen inequality for the probability density $n^*/M$ over the set where $n^* > 0$, gives us that

$$\exp\left(\int_{n^*>0} \frac{R(n^*)}{\kappa}\frac{n^*}{M}\, dx\right) \le \int_{n^*>0} e^{R/\kappa}\frac{n^*}{M}\, dx,$$

and thus,

$$\kappa M \log\left(\int_{n^*>0} e^{R/\kappa}\frac{n^*}{M}\,dx\right) - \int_{n^*>0} n^* R(n^*)\,dx \geq 0.$$

Finally, let us use the Trudinger-Moser inequality:

**Theorem 1.13** (Trudinger-Moser inequality)**.** [184, 68, 107] *Suppose that $\Omega \subset \mathbb{R}^2$ is a $C^2$, bounded, connected domain. It exists a constant $\mathcal{C}_\Omega$ such that for all $h \in H^1$ with $\int_\Omega h = 0$ we have*

$$\int_\Omega \exp(|h|)\,dx \leq \mathcal{C}_\Omega \exp\Big(\frac{1}{8\pi}\int_\Omega |\nabla h|^2\,dx\Big).$$

applied to $\chi c/\kappa$ to conclude

$$\int_{n^*>0} e^{\chi c/\kappa}\,dx \leq \int_\Omega e^{\chi c/\kappa}\,dx \leq C\exp\left(\frac{\chi^2}{8\pi\kappa^2}\int_\Omega |\nabla c|^2\,dx\right),$$

and thus,

$$-\kappa M \log\left(\int_{n^*>0} e^{\chi c/\kappa}\,dx\right) \geq -\frac{\chi^2}{8\pi\kappa} M \int_\Omega |\nabla c|^2\,dx.$$

Consequently, we have quite precisely estimated the free energy (1.10) in the case of a bounded domain, and if $C$ denotes a generic constant, combining (1.17) and (1.21) we get

$$\mathcal{E}_0 \geq \frac{\chi}{2}\left(1 - \frac{\chi M}{4\pi\kappa}\right)\int_\Omega |\nabla c|^2\,dx + C. \tag{1.22}$$

Finally, assumption (H1.7) implies that $\kappa > \dfrac{\chi M}{\mathcal{C}^*_{opt}}$, where $\mathcal{C}^*_{opt} = 4\pi$, *i.e.*, $1 - \dfrac{\chi M}{4\pi\kappa} > 0$ and thus $\displaystyle\int_\Omega |\nabla c|^2\,dx$ is uniformly bounded.

**Step 2: Equi-integrability of $n$.** Because we have started from

$$\mathcal{E}_0 \geq \mathcal{E}(t) = \int_\Omega \Phi(n)\,dx - \chi\int_\Omega |\nabla c|^2\,dx,$$

we get from (1.22) that $\displaystyle\int_\Omega \Phi(n)\,dx$ is also uniformly bounded. In addition, assumptions (H1.2) and (H1.7) implies that $\Phi$ is a continuous bounded from below function positive outside an interval $[0,\mathcal{U}]$, and thus

$$\int_\Omega \Phi^-(n)\,dx = \int_{0\leq n\leq \mathcal{U}} \Phi^-(n)\,dx \geq -\big(\sup \Phi^-\big)|\Omega|.$$

Therefore we are ensured that $\displaystyle\int_\Omega \Phi^+(n)\,dx$ is uniformly bounded in time being the function $\Phi^+(u)$ superlinear at infinity due again to assumption (H1.7). This condition is classically known to be sufficient for equi-integrability, i.e.,

$$\lim_{k\to\infty}\sup_{t\geq 0}\int_\Omega (n-k)_+\,dx = 0.$$

**Step 3: propagation of $L^p$ bounds.** Applying Lemmas 1.10 and 1.11 of Section 1.3, we know that not only $n \in L^\infty\big(\mathbb{R}_+; L^p(\Omega)\big)$ for all $1 \leq p < \infty$, but also $n \in L^\infty\big(\mathbb{R}_+; L^\infty(\Omega)\big)$. □

## 1.5 *A priori* estimates in the whole space

In the whole space the model analysis is more complicated because we require some control of the cell density $n$ for large values of $|x|$. We are looking for such additional information both to justify that we can pass to the limit in the approximation phase for existence; and to estimate $\int \Phi^-(n)$ when it is necessary (in the standard PKS model $\Phi(u) = u \log u$) since $n$ will decay somehow for large values of $|x|$. For this purpose the second moment of $n(t,\cdot)$, i.e.,

$$I\!I(t) = \frac{1}{2}\int_{\mathbf{R}^2} |x|^2 n(t,x)\,dx$$

will be our key quantity – see [86] and [77] for details in the linear PKS model.

Therefore, we need to distinguish several cases depending on the behavior of the diffusion for small values of the density $n$ or large values of $|x|$.

### 1.5.1 Equi-integrability: Degenerate diffusion

Let us first assume in this section that we deal with degenerate diffusion.

**Hypothesis H1.14.** *We assume that* $h(0^+) > -\infty$.

In the whole space case, the free energy (1.10)

$$\mathcal{E}(t) = \int_{\mathbb{R}^2} \Phi(n)\,dx - \frac{\chi}{2}\int_{\mathbb{R}^2} nc\,dx$$

can be rewritten as

$$\mathcal{E}(t) = \int_{\mathbb{R}^2} \Phi(n)\,dx + \frac{\chi}{4\pi}\int_{\mathbb{R}^2\times\mathbb{R}^2} \log|x-y| n(x) n(y)\,dx\,dy. \tag{1.23}$$

The second term in the right-hand side is well adapted to the Hardy-Littlewood-Sobolev inequality:

**Theorem 1.15** (The logarithmic Hardy-Littlewood-Sobolev inequality)**.** [56, 86] *Assume $f$ is a nonnegative function $\mathbb{R}^2 \to \mathbb{R}$ with total mass $M$ and $f(x)\log(1+|x|^2)$ integrable, then*

$$-\int_{\mathbb{R}^2\times\mathbb{R}^2} f(x)\log|x-y| f(y)\,dx\,dy \le \frac{M}{2}\int_{\mathbb{R}^2} f\log f\,dx + C$$

*where $C = M^2(1+\log\pi+\log M)/2$ is optimal.*

We deduce from this sharp estimate that

$$\mathcal{E}_0 \ge \mathcal{E}(t) \ge \int_{\mathbb{R}^2} \Phi(n)\,dx - \frac{\chi M}{8\pi}\int n\log n\,dx + C. \tag{1.24}$$

The assumption of degenerate diffusion (H1.14) is useful to control $\Phi$ near 0, since it implies that $\Phi(u) \ge Au$ with $A = h(0^+)$ for all $u \ge 0$. Now, denoting by $\Theta$ the functional

$$\Theta(u) = \Phi(u) - Au - \frac{\chi M}{8\pi} u\log u, \tag{1.25}$$

it is clear from (H1.7) and Lemma 1.8 that $\Theta$ is growing faster than linearly, that is

$$\lim_{u\to\infty} \frac{\Theta(u)}{u} = +\infty,$$

and that $\Theta$ is positive for large $u \ge r > 0$. Moreover, by (H1.14), $\Theta(u) \ge -\dfrac{\chi M}{8\pi} u\log u$, and thus,

$$\int_{\mathbb{R}^2} \Theta^-(n)\,dx = \int_{\{1\le n\le r\}} \Theta^-(n)\,dx \le \int_{\{1\le n\le r\}} \frac{\chi M}{8\pi} u\log u\,dx \le \frac{\chi M}{8\pi} M\log r. \tag{1.26}$$

Combining (1.24) and (1.26), we get consequently the estimate

$$\int_{\mathbb{R}^2} \Theta^+(n)\,dx \le C, \tag{1.27}$$

where $C$ does not depend on time and $\Theta^+(u)$ is growing faster than linearly. We deduce as previously the following statement.

**Theorem 1.16** (Equi-integrability for degenerate diffusion)**.** *Assume* (H1.2), (H1.3), (H1.7) *and* (H1.14)*, then*

$$\lim_{k\to\infty} \sup_{t\ge 0} \int (n-k)_+\,dx = 0,$$

*and therefore,* $n \in L^\infty(\mathbb{R}_+; L^\infty(\mathbb{R}^2))$*.*

### 1.5.2 Equi-integrability: a non optimal constant – The Jäger & Luckhaus' technique

Here we prove that if $uh'(u) \ge \mathcal{H}$ for large $u$, and sufficiently large $\mathcal{H}$ then we get equi-integrability for $n$ without any time dependance in the bounds.

**Hypothesis H1.17** (Kowalczyk)**.** *There exists A such that* $uh'(u) \ge \mathcal{H}$ *for* $u \ge A$*; where* $\mathcal{H} > \frac{3}{4}\chi M \mathcal{C}_{gns}$*.*

Here, $\mathcal{C}_{gns}$ refers to the optimal constant in a Gagliardo-Nirenberg-Sobolev inequality used below.

**Theorem 1.18** (Equi-integrability for a non optimal constant)**.** *Assume* (H1.2), (H1.3), (H1.7) *and* (H1.17)*, then*

$$\lim_{k\to\infty} \sup_{t\ge 0} \int_{\mathbb{R}^2} (n-k)_+\,dx = 0.$$

*Therefore* $n \in L^\infty\big(\mathbb{R}_+; L^\infty(\mathbb{R}^2)\big)$*.*

*Proof.* Here, we reproduce the Jäger and Luckhaus' arguments [147]:

$$\begin{aligned}
\frac{d}{dt}\int_{\{n\ge A\}} (n-A)^2\,dx =& -2\int_{\{n\ge A\}} \nabla(n-A)\cdot\nabla f(n)\,dx \\
&+ 2\chi \int_{\{n\ge A\}} \nabla(n-A)\cdot n\nabla c\,dx \\
=& -2\int_{\{n\ge A\}} nh'(n)|\nabla(n-A)|^2\,dx \\
&+ \chi\int_{\{n\ge A\}} \big\{(n-A)^2 + 2A(n-A)\big\} n\,dx,
\end{aligned}$$

and thus,

$$\begin{aligned}
\frac{d}{dt}\int_{\{n\ge A\}} (n-A)^2\,dx \le& -2\mathcal{H}\int_{\{n\ge A\}} |\nabla(n-A)|^2\,dx \\
&+\chi\int_{\{n\ge A\}} \big\{(n-A)^3 + 3A(n-A)^2 + 2A^2(n-A)\big\}\,dx.
\end{aligned} \tag{1.28}$$

We can easily bound the polynomial in the last integral using $2A(n-A)^2 \le (n-A)^3 + A^2(n-A)$ and we apply the following Gagliardo-Nirenberg-Sobolev inequality [106, 193]

$$\int_{\mathbb{R}^2} w^3\,dx \le \mathcal{C}_{gns}\int_{\mathbb{R}^2} |\nabla w|^2\,dx \int_{\mathbb{R}^2} w\,dx,$$

to conclude that

$$\frac{d}{dt}\int_{\mathbb{R}^2}(n-A)_+^2 dx \leq \left(-\frac{2\mathcal{H}}{M\mathcal{C}_{gns}}+\frac{3}{2}\chi\right)\int_{\mathbb{R}^2}(n-A)_+^3\,dx+\frac{7}{2}\chi A^2 M. \tag{1.29}$$

If $\mathcal{H}$ is chosen sufficiently large so that $\eta=\frac{2\mathcal{H}}{M\mathcal{C}_{gns}}-\frac{3}{2}\chi>0$ then we get immediately equi-integrability uniformly in time. Indeed $2(n-A)^2\leq(n-A)^3+(n-A)$, and a consequence of (1.29) is

$$\frac{d}{dt}\int_{\mathbb{R}^2}(n-A)_+^2\,dx\leq -2\eta\int_{\mathbb{R}^2}(n-A)_+^2\,dx+\eta M+\frac{7}{2}\chi A^2 M. \tag{1.30}$$

from which the theorem concludes. □

**Remark 1.19.** *The choice of the functional $\Psi(u)=(u-A)_+^2$ growing faster than linearly is almost arbitrary. Of course, another functional will lead to another constant, but our aim in this section is definitely not to exhibit a best constant. Here, we have shown that if we are not interested in an optimal growth of the nonlinearity, then equi-integrability is gained by assuming hypothesis* (H1.17).

### 1.5.3 Cell density control at $\infty$

We would like to get a control of $n$ near infinity to avoid a potential mass loss at $\infty$. We plan to reproduce the computation of the second moment $I\!I(t)$ [77, 208].

**Lemma 1.20** (Avoiding loss of mass at $\infty$: degenerate diffusion)**.** *Assume* (H1.2), (H1.14) *and that the solution satisfies $n\in L^\infty_{loc}\big(\mathbb{R}_+;L^\infty(\mathbb{R}^2)\big)$, then $I\!I(t)\in L^\infty_{loc}(\mathbb{R}_+)$. If the $L^\infty$ bound on the density is uniform, $n\in L^\infty\big(\mathbb{R}_+;L^\infty(\mathbb{R}^2)\big)$, then $I\!I(t)$ increases at most linearly in time.*

*Proof.* By computing formally the evolution of the second moment in (1.9), we get

$$\frac{d}{dt}I\!I(t)=2\int_{\mathbb{R}^2}f(n)\,dx-\frac{\chi}{4\pi}M^2. \tag{1.31}$$

The assumptions (H1.2) and (H1.14) ensures that $\frac{f(u)}{u}$ is bounded near zero. If the solution verifies $n\in L^\infty\big(\mathbb{R}_+;L^\infty(\mathbb{R}^2)\big)$, we deduce that

$$\frac{d}{dt}I\!I(t)\leq C\int_{\mathbb{R}^2}n\,dx=CM.$$

It is easy to conclude if $n\in L^\infty_{loc}\big(\mathbb{R}_+;L^\infty(\mathbb{R}^2)\big)$. □

Let us give an alternative hypothesis to get a substitute of Lemma 1.20 for non-degenerate diffusions. Indeed the assumption $f(u)\leq Cu$ is not generally met near zero and although $n\in L^\infty\big(\mathbb{R}_+;L^\infty(\mathbb{R}^2)\big)$, it is not easy to estimate directly the contribution of

$$\int_{\mathbb{R}^2}f(n)\,dx$$

in (1.31). Let us consider $\gamma(u)=\dfrac{f(u)}{u}$.

**Hypothesis H1.21.** *Given $h(0^+)=-\infty$, we assume that $\gamma$ is strictly decreasing on an interval $(0,\gamma^*)$, $\gamma(0^+)=\infty$ and that $f\circ\gamma^{-1}$ is integrable near infinity.*

**Remark 1.22.** *In the particular case of a power behavior near zero, $f(u)=\kappa u^\alpha\quad\forall u<a$ with $\alpha<1$, previous hypothesis (H1.21) is equivalent to $\alpha>\frac{1}{2}$. This excludes too fast diffusions near zero.*

**Lemma 1.23** (Avoiding loss of mass at $\infty$: fast diffusion)**.** *Assume* (H1.2), (H1.21) *and that the solution verifies $n\in L^\infty_{loc}\big(\mathbb{R}_+;L^\infty(\mathbb{R}^2)\big)$, then $I\!I(t)\in L^\infty_{loc}(\mathbb{R}_+)$.*

*Proof.* Given $T>0$, let us consider $U=\|n\|_{L^\infty((0,T);L^\infty(\mathbb{R}^2))}$. Now, we can fix any $0<a<\min(\gamma^*,U)$ to estimate

$$\int_{\{a\le n\le U\}} f(n)\,dx \le \Big(\max_{u\in[0,U]} f(u)\Big)\mathrm{meas}\Big\{n\ge a\Big\} \le \Big(\max_{u\in[0,U]} f(u)\Big)\frac{M}{a}.$$

Now, we can restrict to the set $\{n<a\}$ and split the integral as

$$\begin{aligned}\int_{\{n<a\}} f(n)\,dx &= \int_{\{n<a\}\bigcap\{\gamma(n)\le|x|^2\}} f(n)\,dx + \int_{\{n<a\}\bigcap\{\gamma(n)>|x|^2\}} f(n)\,dx\\ &\le \int_{\mathbb{R}^2}|x|^2 n\,dx + \int_{\{n<a\}\bigcap\{\gamma(n)>|x|^2\}} f(n)\,dx.\end{aligned}$$

We split again the last term into

$$\int_{\{n<a\}\bigcap\{\gamma(a)<|x|^2<\gamma(n)\}} f(n)\,dx + \int_{\{n<a\}\bigcap\{|x|^2\le\gamma(a)\}} f(n)\,dx. \tag{1.32}$$

The second term is easily controlled because we have reduced to a bounded domain, that is

$$\int_{\{n<a\}\bigcap\{|x|^2\le\gamma(a)\}} f(n)\,dx \le \pi\left(\max_{u\in[0,a]} f(u)\right)\gamma(a).$$

Dealing with the first term of (1.32) we can invert $\gamma$ and consequently

$$\begin{aligned}\int_{\{n<a\}\bigcap\{\gamma(a)<|x|^2<\gamma(n)\}} f(n)\,dx &\le \int_{\{|x|^2>\gamma(a)\}} |f\circ\gamma^{-1}(|x|^2)|\,dx\\ &= \int_{\gamma(a)}^{\infty} |f\circ\gamma^{-1}(r^2)|2\pi r\,dr\\ &= \pi\int_{\sqrt{\gamma(a)}}^{\infty} |f\circ\gamma^{-1}(s)|\,ds.\end{aligned}$$

Combining previous estimates, we deduce

$$\int_{\mathbb{R}^2} f(n)\,dx \le 2\mathit{\Pi}(t) + C_T, \tag{1.33}$$

for all $0\le t\le T$, that together with (1.31) implies the stated result. □

### 1.5.4 Equi-integrability: fast diffusion – An energy method

By using (H1.7), we can rewrite the energy estimate (1.24) as follows

$$\mathcal{E}_0 \ge \mathcal{E}(t) \ge \int_{\{n<\mathcal{U}\}} \Phi(n)\,dx + \int_{\{n\ge\mathcal{U}\}} \Phi(n)\,dx - \frac{\chi M}{8\pi}\int n\log n\,dx + C.$$

We split again the right-hand side term and we get thanks to (1.12)

$$\int_{\{n<\mathcal{U}\}} \Phi(n)\,dx + \int_{\{n\ge\mathcal{U}\}} \mathcal{R}(n)\,dx + (\kappa-\kappa^*)\int_{\{n\ge\mathcal{U}\}} n\log n\,dx + C \le \mathcal{E}_0,$$

and thus,

$$\int_{\{n<\mathcal{U}\}} \Phi(n)\,dx + \Big(1-\frac{\chi M}{\kappa 8\pi}\Big)\int_{\{n\ge\mathcal{U}\}} \Phi(n)\,dx + C \le \mathcal{E}_0. \tag{1.34}$$

Let us recall that $\Phi\ge 0$ for $u\ge\mathcal{U}$ (H1.7). Our problem now is to estimate the potential negative contribution arising from

$$\int_{\{n<\mathcal{U}\}} \Phi(n)\,dx \tag{1.35}$$

in the fast diffusion case. Let us remind that in the degenerate diffusion case, $|\Phi(u)|$ is dominated by $u$ near the origin giving a simple argument to control this negative contribution in section 1.5.1.

We propose to couple the evolution of the second moment of $n$ into the computations, more precisely, to couple the second moment evolution and the behaviour of (1.35). In fact, we will proceed analogously to Lemma 1.23 without the assumption of boundedness of $n$ since we will work on the set $\{n < \mathcal{U}\}$. Let us consider $\beta(u) = \dfrac{|\Phi(u)|}{u}$.

**Hypothesis H1.24.** *Given $h(0^+) = -\infty$, we assume that $\beta$ is strictly decreasing on an interval $(0, \beta^*)$, $\beta(0^+) = \infty$ and that $|\Phi| \circ \beta^{-1}$ is integrable near infinity.*

**Lemma 1.25** (Control of the negative contribution of the internal energy: fast diffusion)**.** *Assume* (H1.2) *and* (H1.24)*, then*

$$\int_{\{n<\mathcal{U}\}} |\Phi(n)|\, dx \le 2\mathit{\Pi}(t) + \pi \int_{\sqrt{\beta(a)}}^{\infty} |\Phi \circ \beta^{-1}(s)| ds + C_T, \tag{1.36}$$

*for any $0 \le t \le T$, and any $T > 0$.*

Previous lemma allows us to control the negative part of the internal energy once we know that the second moment is locally bounded in time.

Now, we still need to work on the differential equation [77, 208] verified by $\mathit{\Pi}(t)$ ,

$$\frac{d}{dt}\mathit{\Pi}(t) = 2\int f(n)\, dx - \frac{\chi M^2}{4\pi}. \tag{1.37}$$

In order to estimate the first term, we propose to compare $f$ and $\Phi$ near infinity to avoid the potential unboundedness of $n$ in contrast to Lemma 1.23.

**Hypothesis H1.26.** *There exists $\bar{\mathcal{U}}$ such that $f(u) \le C\Phi(u)$ for all $u \ge \bar{\mathcal{U}}$.*

We can now split the integral of $f(n)$ into three terms as

$$\frac{d}{dt}\mathit{\Pi}(t) \le 2\int_{\{n<a\}} f(n)\, dx + 2\int_{\{a\le n<\bar{\mathcal{U}}\}} f(n)\, dx + 2\int_{\{n\ge\bar{\mathcal{U}}\}} f(n)\, dx. \tag{1.38}$$

The first right-hand side term may be controlled as in the proof of Lemma 1.23 and thus, assuming hypothesis (H1.21), we deduce

$$\int_{\{n<a\}} f(n)\, dx \le A_T\mathit{\Pi}(t) + B_T, \tag{1.39}$$

for any $0 \le t \le T$ and any $T > 0$.

We have already seen in Lemma 1.23 that the second term of (1.38) is easily bounded. In addition, thanks to assumption (H1.26), the free energy estimate (1.34) and a simple estimate of the integral on the set $\{a < n < \mathcal{U}\}$ as in Lemma 1.23, we conclude

$$\int_{\{n\ge\bar{\mathcal{U}}\}} f(n)dx \le C\int_{\{n\ge\bar{\mathcal{U}}\}} \Phi(n)dx \le \mathcal{E}_0 + C + C\int_{\{n<a\}} |\Phi(n)|dx,$$

and finally combining with (1.36), we get a very simple Gronwall type inequality

$$\frac{d}{dt}\mathit{\Pi}(t) \le A_T + B_T\mathit{\Pi}(t), \tag{1.40}$$

for any $0 \le t \le T$ and any $T > 0$, which gives an *a priori* bound for the second moment of the cell density $n$.

Finally, coming back to the estimate (1.36) where we use that the second moment is locally in time bounded and going back to the free energy estimate (1.34), we finally conclude that

$$\int_{\mathbb{R}^2} \Phi^+(n)\, dx$$

is bounded for any $0 \le t \le T$ and any $T > 0$.

**Remark 1.27.** *The domination* (H1.26) *is valid as long as $h$ has a power behaviour for large $u$, but fails if $h(u) = e^u$ for instance. However this dramatic situation is contained obviously in the assumptions of the previous section* 1.5.2.

**Theorem 1.28** (Equi-integrability for the fast diffusion with an optimal constant)**.** *Assume* (H1.2), (H1.3), (H1.7), (H1.21), (H1.24) *and* (H1.26)*, then for all $T > 0$*

$$\lim_{k\to\infty} \sup_{t\in[0,T]} \int_{\mathbb{R}^2} (n-k)_+ \, dx = 0,$$

*and therefore, $n \in L^\infty_{loc}\big(\mathbb{R}_+; L^\infty(\mathbb{R}^2)\big)$.*

Note that in this proposition we only obtain local in time equi-integrability because of (1.36) and (1.40), on the contrary to theorems 1.16 and 1.18 where equi-integrability does not depend on time.

### 1.5.5 Conclusions of the *a priori* estimates

We remind the reader that we do not attempt here to make a complete existence theory for these models, but we remark that previous *a priori* estimates show that solutions obtained by suitable approximation procedures should satisfy uniform bounds on the cell density and then, the absence of blow-up in these models.

We can summarize the results of Sections 1.4 and 1.5, including Section 1.3 into the following main theorems:

**Theorem 1.29** (No Blow-up: Bounded domain)**.** *Assume* (H1.2) *and* (H1.7) *with $\Omega$ bounded, then any solution $n$ of* (1.7) *with initial data satisfying $n_0 \in L^1_+(\Omega) \cap L^\infty(\Omega)$ exists globally in time. Moreover, the cell density $n$ is globally bounded in $L^\infty$.*

**Theorem 1.30** (No Blow-up: $\mathbb{R}^2$)**.** *Assume* (H1.2) *and* (H1.7) *and take any initial data satisfying $n_0 \in L^1_+(\mathbb{R}^2) \cap L^\infty(\mathbb{R}^2)$ such that the second moment of $n_0$ is finite. Then, we have the following three independent statements:*

*(i) In addition, let us assume* (H1.14)*, then any solution of* (1.9) *exists globally in time and the cell density $n$ is uniformly bounded in time in $L^\infty$.*

*(ii) In addition, let us assume* (H1.17) *and* (H1.21)*, then any solution of* (1.9) *exists globally in time and the cell density $n$ is uniformly bounded in time in $L^\infty$.*

*(iii) In addition, let us assume* (H1.21)*,* (H1.24) *and* (H1.26)*, then any solution of* (1.9) *exists globally in time and the cell density $n$ is locally bounded in time in $L^\infty$.*

## 1.6 Extension to a nonlinear chemosensitivity

We plan to extend our previous results to both nonlinear diffusion and chemosensitivity $\chi(n)$. The first equation of our model is modified as following.

$$\partial_t n + \nabla \cdot \Big( -\nabla f(n) + \chi(n) n \nabla c \Big) = 0 \quad t \geq 0\,,\ x \in \Omega \subset \mathbb{R}^2. \tag{1.41}$$

First of all, we could keep all hypothesis made on $h$, and add some new hypothesis: basically $\chi$ is a positive bounded function. However, we point out that in [202], it comes from the derivation of the model that $h$ and $\chi$ are linked by an underlying function $q$ (1.5). Moreover, when we adapt previous arguments to this new system, it is natural to introduce a reduced diffusion term $H$, given by

$$H'(u) = \frac{f'(u)}{\chi(u)u} = \frac{h'(u)}{\chi(u)}, \tag{1.42}$$

which relates $h$ and $\chi$ and plays in fact the role of $h$.

Although it seems that we have already captured the feature of this nonlinear system, there is a difficulty hidden in this additional nonlinearity. Because we assume (H1.7) that $uh'(u) \geq \delta$ for large $u$ we reduce essentially to a linear diffusion in Section 1.3, and homogeneity is preserved in the calculations. But here $\chi$ may tend to zero: the diffusion is essentially nonlinear in the general case, and the Section 1.3 cannot be transposed exactly. That is why we will obtain by this method local in time estimates only (see section 1.6.2).

Let us now recall the hypothesis adapted to this new context.

**Hypothesis HN 1.31** (Basic Regularity on the Nonlinear Reduced Diffusion H)**.** *$H \in L^1_{loc}[0,\infty) \cap \mathcal{C}^1(0,\infty)$ is an increasing function with $H(1) = 0$.*

We define without any ambiguity $\Phi$ and $F$ corresponding to the functional $H$ as in Section 1.2: $F'(u) = uH'(u)$ and $F(0) = 0$; $\Phi'(u) = H(u)$ and $\Phi(0) = 0$.

**Hypothesis HN1.32** (The Nonlinear Chemosensitivity)**.** *$\chi \in L^\infty(\mathbb{R}_+)$ is a positive function. We denote by $\chi_0$ the bound $\|\chi\|_\infty$.*

**Hypothesis HN1.33** (Superlinear Reduced Diffusion at $\infty$)**.** *We assume that $H$ is growing faster than the critical diffusion function for large density levels, that is it exists $\kappa > \dfrac{M}{\mathcal{C}^*_{opt}}$ and $\mathcal{U} \in \mathbb{R}_+$ such that*

$$\forall u \geq \mathcal{U} \quad H(u) \geq \kappa \log u.$$

*Moreover we assume that it exists $\delta > 0$ such that $uH'(u) \geq \delta$ for large $u$.*

**Hypothesis HN1.34** (Degenerate Reduced Diffusion)**.** *We assume that $H(0^+) > -\infty$.*

**Hypothesis HN1.35** (Kowalczyk)**.** *It exists $A$ such that $uH'(u) \geq \mathcal{H}$ for $u \geq A$; where $\mathcal{H} > \frac{3}{4} M\mathcal{C}_{gns}$.*

In the case of non-degenerate diffusion, $\Gamma$ is defined as in section 1.5.3: $\Gamma(u) = \dfrac{F(u)}{u}$.

**Hypothesis HN1.36.** *We assume that $F \circ \Gamma^{-1}$ is integrable near infinity.*

We organize this section into three subsections. We firstly look at the free energy, and what can be deduced by an energy method. Secondly, we adapt the Jäger & Luckhaus computations. Finally, we check the evolution of the second moment, to avoid loss of mass at infinity.

### 1.6.1 The free energy estimate

Thanks to the reduction (1.42) we get a free energy similar to Section 1.2.

**Lemma 1.37** (Free energy)**.** *Given a smooth solution of* (1.41)*, then the free energy functional* [58]

$$\mathcal{E}(t) = \int \Phi(n)\, dx - \frac{1}{2} \int nc\, dx \tag{1.43}$$

*verifies*

$$\frac{d}{dt}\mathcal{E} = -\int n\chi(n) \left|\nabla(H(n) - c)\right|^2 dx \leq 0. \tag{1.44}$$

*Proof.* Indeed we can rewrite as following:

$$\partial_t n + \nabla \cdot \Big(\chi(n) n \big\{ - H'(n)\nabla n + \nabla c \big\}\Big) = 0.$$

We multiply by $H'\nabla n - \nabla c$, and we integrate by parts. Finally, we recover that the free energy

$$\mathcal{E}(t) = \int \Phi(n)\, dx - \frac{1}{2} \int nc\, dx,$$

is decreasing. □

At this stage, we could exactly reproduce the arguments in previous sections. However, we will see in the next subsections that this analogy is no longer valid for the whole analysis of (1.41).

Let us start by the simple cases which generalize to the present situation without any further difficulty. We can treat by the energy method the equi-integrability, both in the case of a bounded domain (Section 1.4), and a degenerate diffusion in the whole space (section 1.5.1).

**Proposition 1.38** (Equi-integrability in $\Omega$ bounded)**.** *Assume* (HN1.31), (H1.3), (HN1.32), (HN1.33) *then*

$$\lim_{K\to\infty}\sup_{t\geq 0}\int_\Omega (n-K)_+\,dx = 0,$$

**Proposition 1.39** (Equi-integrability for degenerate diffusion)**.** *Assume* (HN1.31), (H1.3), (HN1.32), (HN1.33) *and* (HN1.34)*, then*

$$\lim_{K\to\infty}\sup_{t\geq 0}\int_{\mathbb{R}^2} (n-K)_+\,dx = 0,$$

### 1.6.2 The Jäger & Luckhaus-type computation

We attempt here to reproduce and adapt the direct computation of $\frac{d}{dt}\int (n-K)_+^p\,dx$ as in sections 1.3 and 1.5.2. For this purpose, we fix a number $K$, and we deal with a convex functional $\varphi_K \in \mathcal{C}^2$ satisfying both $\varphi_K(K) = \varphi_K'(K) = 0$. Note that $\varphi_K$ stands for the additional nonlinearity and takes the place of $(n-K)_+^p$. Then, we have

$$\begin{aligned}\frac{d}{dt}\int_{\{n\geq K\}}\varphi_K(n)\,dx &= \int_{\{n\geq K\}}\varphi_K'(n)\partial_t n\,dx\\ &= -\int_{\{n\geq K\}}\varphi_K''(n)\nabla(n-K)\cdot\Big(\chi(n)n\big\{H'(n)\nabla n-\nabla c\big\}\Big)\,dx,\end{aligned}$$

and thus,

$$\begin{aligned}\frac{d}{dt}\int_{\{n\geq K\}}\varphi_K(n)\,dx = &-\int_{\{n\geq K\}}\varphi_K''(n)\chi(n)nH'(n)|\nabla(n-K)|^2\,dx\\ &+\int_{\{n\geq K\}}\varphi_K''(n)\chi(n)n\nabla c\cdot\nabla(n-K)\,dx.\end{aligned}\tag{1.45}$$

In order to recover the background of the Section 1.3 (namely, the Gagliardo-Nirenberg-Sobolev inequality), we define precisely $\varphi_K$ by

$$p(p-1)(v-K)_+^{p-2} = \varphi_K''(v)\chi(v),\tag{1.46}$$

in such a way that (1.45) becomes

$$\frac{d}{dt}\int_{\{n\geq K\}}\varphi_K(n)\,dx \leq -\eta\int (n-K)_+^p\,dx + O\Big(\int (n-K)_+\,dx\Big).\tag{1.47}$$

**Remark 1.40.** *Note that the calculations* (1.13)*,* (1.14) *and* (1.15) *involve only the right-hand sides of the inequalities. This justifies the validity of* (1.47)*, thanks to the choice* (1.46)*.*

We are now able to explicit the difficulty hidden in the nonlinear chemosensitivity. It is not possible to deduce strictly from (1.47) that $\int (n-K)_+^p\,dx$ is bounded uniformly in time, because $\varphi_K(v)$ and $(v-K)_+^p$ have not the same homogeneity. However, we get that $\int\varphi_K(n)\,dx$ grows at most linearly in time. Moreover, we integrate twice (1.46) and we find that $(v-K)_+^p \leq \chi_0\varphi_K(v)\ \forall v\geq K$. As a consequence, we deduce

$$\int (n-K)_+^p\,dx \leq \chi_0\int_{\{n\geq K\}}\varphi_K(n)\,dx.$$

**Lemma 1.41** ($L^p$ bound from equi-integrability)**.** *Assume* (HN1.31), (HN1.32), (H1.3), (HN1.33). *In addition given $T > 0$, assume the modulus of equi-integrability $\omega$ is such that*

$$\omega(T, K) \xrightarrow[K\to\infty]{} 0.$$

*Then $n \in L^\infty\big(0, T; L^p\big)$ for $p > 2$.*

**Remark 1.42.** *Suppose in addition that the equi-integrability modulus does not depend on time. We integrate* (1.47) *in time and we apply the Gronwall lemma resulting into*

$$\frac{1}{t}\int_0^t \int (n-K)_+^p \, dx\, ds \in L^\infty(\mathbb{R}_+),$$

*which is in a sense better than lemma* 1.41*, but weaker than lemma* 1.10*.*

**Remark 1.43.** *If the positive function $\chi$ is bounded from below by a positive constant, and if the equi-integrability modulus does not depend on time, then the bound we are looking for is also uniform in time. In fact, this situation is essentially similar to the case of $\chi$ being constant.*

Next we examine the validity of the corresponding lemma 1.11.

**Lemma 1.44** ($L^\infty$ bound)**.** *Assume* (HN1.31), (HN1.32), (H1.3), (HN1.33)*, and also that the chemotactic potential $\nabla c \in L^\infty_{loc}\big(\mathbb{R}_+; L^\infty\big)$, then the density satisfies $n \in L^\infty_{loc}\big(\mathbb{R}_+; L^\infty\big)$ too.*

*Proof.* We combine the proof of lemma 1.11 with (1.45) and (1.46) to obtain:

$$\frac{d}{dt}\int_{\{n\geq K\}} \varphi_K(n)\, dx \leq -p^2 C\|\nabla c\|_\infty^2 \int (n-k)_+^p \, dx + C^2 p^4 \frac{\|\nabla c\|_\infty^4}{\delta^2}\left(\int (n-k)_+^{p/2}\, dx\right)^2 + p^2 C\|\nabla c\|_\infty^2,$$

where the generic constant $C$ does not depend on $p$. We integrate in time for $p = 2^j$, and we use (HN1.32) to get

$$\int (n-K)_+^{2^j}\, dx \leq C_T 2^{4j} K_{j-1}^2 + 2^{2j} C_T,$$

with $K_j = \sup_{t\in[0,T]} \int (n-k)_+^{2^j}\, dx$. This ensures that $n \in L^\infty\big(0, T; L^\infty\big)$. □

On the other hand we check the validity of the theorem 1.18 in the case of a nonlinear chemosensitivity. By analogous arguments we obtain:

**Proposition 1.45** (Equi-integrability for a non optimal constant)**.** *Assume* (HN1.31), (HN1.32), (H1.3), (HN1.33) *and* (HN1.35)*, then*

$$\forall T > 0 \quad \lim_{K\to\infty} \sup_{t\in[0,T]} \int_{\mathbb{R}^2} (n-K)_+\, dx = 0.$$

### 1.6.3 Cell density control at $\infty$

When dealing with the model settled in the whole space, precise calculations of the second moment play a crucial role (see section 1.5.3).

**Lemma 1.46** (Avoiding loss of mass at $\infty$)**.** *Assume* (HN1.31), (HN1.32) *and that the solution satisfies both $\nabla c$ and $n \in L^\infty_{loc}\big(\mathbb{R}_+; L^\infty(\mathbb{R}^2)\big)$. Moreover, assume either* (HN1.34) *or* (HN1.36)*, then $I\!I(t) \in L^\infty_{loc}(\mathbb{R}_+)$.*

*Proof.* We reproduce both the proofs of section 1.5.3. First we recover an inequality similar to (1.31),

$$\begin{aligned}\frac{d}{dt}\int_{\mathbb{R}^2}\frac{|x|^2}{2}n(t,x)\,dx &= \int_{\mathbb{R}^2} f(n)\,dx + \int_{\mathbb{R}^2}\chi(n)n(x\cdot\nabla c)\,dx\\ &\leq \chi_0\int_{\mathbb{R}^2}F(n)\,dx + \chi_0\int_{\mathbb{R}^2} n|x||\nabla c|\,dx\\ &\leq \chi_0\int_{\mathbb{R}^2}F(n)\,dx + \chi_0\|\nabla c\|_\infty\Big(\int_{\mathbb{R}^2} n|x|^2\,dx\Big)^{1/2}\sqrt{M}\\ &\leq \chi_0\int_{\mathbb{R}^2}F(n)\,dx + \chi_0\|\nabla c\|_\infty\sqrt{2M}\big(I\!I(t)\big)^{1/2}.\end{aligned}$$

In the case of degenerate diffusion (HN1.34), we just control $\int F(n)$ as in lemma 1.20. In the case of fast diffusion together with (HN1.36) we get an estimate similar to (1.33), and we are able to conclude in the same way that $I\!I(t)\in L^\infty_{loc}(\mathbb{R}_+)$. □

**Remark 1.47.** *Theorem* 1.28 *cannot be generalized to this case. Due to the nonlinear chemoattractive feedback, we assumed a bound on* $\nabla c$ *which we are not able to combine with the calculations of section* 1.5.4.

### 1.6.4 Nonlinear diffusion and chemosensitivity results

We are now able to state the corresponding theorems to section 1.5.5, thanks to the combination of sections 1.6.1, 1.6.2 and 1.6.3. On a bounded domain, situation is quite similar, except the local in time estimate. Let us recall the equations we deal with:

$$\begin{cases}\partial_t n + \nabla\cdot\Big(-\nabla f(n) + \chi(n)n\nabla c\Big) = 0 \quad t\geq 0\,,\ x\in\Omega,\\ -\Delta c = n - \langle n\rangle,\end{cases}\tag{1.48}$$

together with Neumann boundary conditions.

**Theorem 1.48** (No finite-time Blow-up: Bounded domain)**.** *Assume* (HN1.31), (HN1.32) *and* (HN1.33) *with* $\Omega$ *bounded, then any solution* $n$ *of* (1.48) *with initial data satisfying* $n_0\in L^1_+(\Omega)\cap L^\infty(\Omega)$ *exists globally in time. Moreover, the cell density* $n$ *lies in* $L^\infty_{loc}\big(\mathbb{R}_+;L^\infty(\Omega)\big)$.

Concerning the whole space we generalize theorem 1.30, except the last item.

$$\begin{cases}\partial_t n + \nabla\cdot\Big(-\nabla f(n) + \chi(n)n\nabla c\Big) = 0 \quad t\geq 0\,,\ x\in\mathbb{R}^2,\\ c(t,x) = -\dfrac{1}{2\pi}\displaystyle\int_{\mathbb{R}^2}\log|x-y|\,n(t,y)\,dy.\end{cases}\tag{1.49}$$

**Theorem 1.49** (No finite-time Blow-up: $\mathbb{R}^2$)**.** *Assume* (HN1.31), (HN1.32) *and* (HN1.33)*. For any initial data satisfying* $n_0\in L^1_+(\mathbb{R}^2)\cap L^\infty(\mathbb{R}^2)$ *such that the second moment of* $n_0$ *is finite, then the following independent statements hold:*

*(i) In addition, we assume* (HN1.34)*, then the solution of* (1.49) *exists globally in time and the cell density* $n$ *is locally in time bounded in* $L^\infty(\mathbb{R}^2)$.

*(ii) In addition, we assume* (HN1.35) *and* (HN1.36)*, then the solution of* (1.49) *exists globally in time and the cell density* $n$ *is locally in time bounded in* $L^\infty(\mathbb{R}^2)$.

Please note that these results are well adapted to examples mentioned above in 1.9.

1. The choice $q(u)=\frac{1}{1+u^\gamma}$ in (1.5) leads essentially to the linear reduced diffusion with coefficient $\frac{\kappa(\gamma+1)}{\chi_0}$. Because it corresponds to fast diffusion we have to distinguish between a bounded domain and the whole space: the threshold we found is respectively optimal (HN1.33) and non optimal (HN1.35).

2. The choice $q(u) = \exp(-\beta u)$ leads to a superlinear reduced diffusion, and solution is global in time either on a bounded domain or in the whole space.

These theorems also hold for the regularized system proposed by Velázquez to understand what may happen after the blow-up time [240, 241].

# Chapitre 2

# Le modèle de Keller-Segel avec potentiel chimique à noyau logarithmique

---

A l'issue de cette collaboration avec Benoît Perthame et Mohsen Sharifi tabar, nous suggérons une formulation multi-dimensionnelle du modèle de Keller-Segel qui unifie la dynamique qualitative : du fait d'avoir choisi une singularité critique logarithmique pour la synthèse du potentiel chimique, on retrouve une masse critique pour l'explosion en toute dimension d'espace. Nous posons le système dans l'espace tout entier $\mathbb{R}^d$, puis dans un domaine borné pour lequel les conditions au bord singent les conditions de Neumann ou de Dirichlet (en quelque sorte). Cette approche est avantageuse autant pour les simulations numériques (plus efficaces en 1D) que pour une analyse plus avancée de KS (voir l'introduction et la partie III). Ceci est paru dans Contemporary Mathematics sous le titre *Modified Keller-Segel system and critical mass for the log interaction kernel* [55].

---

In biology, chemotaxis refers to collective cell movements directed by their interaction through an attractive chemical potential, the *chemoattractant*. This aggregation tendency is counter-balanced by diffusion of cells due to their brownian motion. Chemotaxis models generally couple an equation for the movement of cells ($n(t,x)$ denotes the cell density) together with the chemical constituent which is produced by the cells themselves ($c(t,x)$ denotes the concentration of the chemoattractant).

The mathematical question which arises in this class of models is to determine which contribution will dominate, either aggregation by directed chemoattraction or dispersion by stochastic diffusion. As we recall it below the answer depends highly upon the space dimension and makes the situation rather complex. Let us recall that in biology the experiments are carried out on a two dimensional dish and three dimensional effects are usually neglected. In astrophysics there is a similar model in three dimensions.

Here we introduce another form of the diffusion law for the chemoattractant which is aimed at providing properties that are dimension invariant. Namely we consider the Modified Keller-Segel system (MKS in short) set on an open subset $\Omega$ of $\mathbb{R}^d$, and for simplicity it is either a regular bounded domain or the

whole space $\mathbb{R}^d$,

$$\begin{cases} \dfrac{\partial n}{\partial t} = \Delta n - \chi \nabla \cdot \big(n \nabla c\big) & t > 0,\ x \in \Omega \subset \mathbb{R}^d, \\ c = K_d * n & t > 0,\ x \in \Omega \subset \mathbb{R}^d, \\ \dfrac{\partial n}{\partial \eta} - \chi n \dfrac{\partial c}{\partial \eta} = 0 & t > 0,\ x \in \partial\Omega, \\ n(t=0) = n_0 \geq 0, \end{cases} \tag{2.1}$$

where $\eta$ denotes the outward unit normal to $\Omega$ when it is a bounded domain. The critical kernel $K_d$ and mass $M_{\text{crit}}$ are defined as

$$K_d(z) = -\frac{1}{d\pi} \log |z|, \qquad M_{\text{crit}} = \frac{2d^2\pi}{\chi}. \tag{2.2}$$

Although the main interest is the better mathematical behavior of this system compared to the classical Keller-Segel system (see next section), there are several other motivations. Firstly we will see that even in one dimension, this system blows-up over a critical mass and this renders possible numerical studies of this highly subtle phenomena (see the non self-similarity of the explosion in [131, 132], and as pointed out in [177, 240] the continuation after blow-up depends upon the regularization). Even in one dimension, the numerical simulations are not easy. Secondly there is a recent interest on fractional diffusions in biology because the molecules undergo specific interactions with the overall medium.

The outline of the paper is as follows. We begin with a short presentation of the classical Keller-Segel system and its main properties. Then we study the MKS for both the whole space (section 2.2) and a bounded domain (section 2.3). We show the existence of a critical mass, based on the free energy and the second moment of $n$.

## 2.1 The classical framework and motivation for a log kernel

In any dimension the classical Keller–Segel model for chemotaxis is (see [153, 147, 141, 209])

$$\begin{cases} \dfrac{\partial n}{\partial t} = \Delta n - \chi \nabla \cdot \big(n \nabla c\big) & t > 0,\ x \in \Omega, \\ -\Delta c = n & t > 0,\ x \in \Omega. \end{cases} \tag{2.3}$$

We would like first to emphasize the role of boundary conditions. For the cell density we impose as usual zero-flux boundary conditions,

$$\frac{\partial n}{\partial \eta} - \chi n \frac{\partial c}{\partial \eta} = 0 \quad t \geq 0\,,\ x \in \partial\Omega, \tag{2.4}$$

whereas we distinguish between Neumann and Dirichlet boundary conditions (BC in short) for the chemical concentration,

$$\frac{\partial c}{\partial \eta} = 0 \quad \text{or} \quad c = 0 \quad t \geq 0\,,\ x \in \partial\Omega. \tag{2.5}$$

Notice that (2.4) and $n(t=0) = n_0 \geq 0$ guarantees nonnegative solutions $n(t,x) \geq 0$ and mass conservation

$$\int_\Omega n(t,x)dx = \int_\Omega n(t=0,x)dx := M. \tag{2.6}$$

**Remark 2.1.** *In case of Neumann BC, equation for c has to be replaced with*

$$-\Delta c = n - \langle n \rangle_\Omega.$$

*Therefore c is not interpreted as a concentration, but as a deviation to meanvalue.*

**Remark 2.2.** *We made the choice of a very simple description of the classical chemotaxis system. Note that the equation for the chemoattractant may be replaced with the more physical laws $-\Delta c + c = n$ or $\partial_t c - \Delta c = n$. But more elaborate models are used in practice, see [185, 54].*

In the particular case where $\Omega = \mathbb{R}^2$, the Poisson equation $-\Delta c = n$ becomes

$$c(t,x) = -\frac{1}{2\pi}\int_{\mathbb{R}^2} \log|x-y| n(t,y) dy. \tag{2.7}$$

The interesting feature of the model (2.3) is that solutions may become unbounded in finite time. We call *blow-up in finite time* such a behavior. Since the 70's and the seminal papers by Keller and Segel [153, 154], a great effort has been made in this direction, and these equations are now quite well understood. We propose to review the main results in this area. First of all, let us remark that the behavior of the system (2.3) highly depends on the dimension. In dimension $d = 1$ no solutions blow up [137] whereas in dimension $d \geq 3$ there exist blowing up solutions for any positive mass but the critical space is not scaled as mass in this case. The precise condition for existence involves small $L^{d/2}$ norm of $n_0$ and has been derived in [77] for the parabolic-elliptic and in [74] for the parabolic-parabolic KS systems. Always for $d > 2$, it is not known if blow-up follows from large $L^{d/2}$ norm of $n_0$ (only results involving a stronger norm that scales similarly are known). In the critical dimension $d = 2$ there is a threshold: solutions are global in time for small mass, and blow up for large mass.

This threshold phenomena is quite simple in the whole space $\mathbb{R}^2$, and is summarized in the following theorem [86, 35].

**Theorem 2.3** (Critical mass for the KS model in $\mathbb{R}^2$)**.**
*If $\Omega$ is the whole space $\mathbb{R}^2$ and $n_0\big(|\log n_0| + (1+|x|^2)\big) \in L^1$, then solutions are global in time if $\chi M < 8\pi$, or blow up in finite time if $\chi M > 8\pi$.*

Radial solutions show that the second moment might not be the most accurate additional criteria to the mass for existence and blow-up, but rather a comparison to the steady state solution (see [209]). On a bounded domain the analysis is more difficult because boundary effects play an important role. Concerning Dirichlet conditions, the situation is similar to the whole space: solutions are global in time if $\chi M < 8\pi$, and blow up in finite time if $\chi M > 8\pi$. On the other hand, there are several threshold values in the case of Neumann boundary conditions: if $\Omega$ is regular then solutions are global if $\chi M < 4\pi$, and may blow up above this threshold, either on the boundary or inside the domain. If $\Omega$ is piecewise $\mathcal{C}^2$ and $\Theta$ denotes the smallest angle then solutions are global if $\chi M < 4\Theta$, and may blow up above this threshold [141, 51]. On a disc, the situation is more clear and has been analyzed in [187, 30] and it turns out that, again, boundary conditions on $c$ play an important role.

Our goal in this paper is to study the Modified Keller-Segel system (2.1)–(2.2) and to generalize the phenomenon of blow-up to all dimensions. We start from the following remark: the dimension $d = 2$ is critical because the weight of the interacting kernel $K(z) = -\frac{1}{2\pi}\log|z|$ is itself critical. If we replace the equation for the chemical potential $-\Delta c = n$ by $c = K_d * n$, the corresponding behavior depends slightly on the dimension, namely through the threshold value.

There is some hidden subtlety in the formulation $c = K_d * n$ in the case of a bounded domain $\Omega$. For the convolution product $K_d * n$ to be well defined, it is necessary to extend $n$ outside $\Omega$. We distinguish two natural ways: the extension by 0, which corresponds in a certain sense to Dirichlet boundary conditions; and the extension by meanvalue which corresponds to Neumann boundary conditions (see Remark 2.8). The main difference is that constant densities are stationary solutions for Neumann BC in the KS model and for the extension by meanvalue in the MKS model. In other words we study in this paper two different models, namely one corresponding to $c = -\frac{1}{d\pi}\log|\cdot| * n$ (Sections 2.3.1 and 2.3.2) and the second one corresponding to $c = -\frac{1}{d\pi}\log|\cdot| * (n - \langle n\rangle)$ (Section 2.3.3). Of course these two approaches coincide in the whole space $\mathbb{R}^d$ where $\langle n\rangle = 0$ (Section 2.2).

## 2.2 MKS system in the whole space

There is a free energy naturally associated to the system (2.1), namely the Lyapunov functional [107, 32]

$$\mathcal{F}(n) = \int n\log n - \frac{\chi}{2}\int nc = \int n\log n - \frac{\chi}{2}\int n\ K_d * n, \tag{2.8}$$

satisfies $t \to \mathcal{F}\big(n(t)\big)$ is decreasing, more precisely

$$\frac{d}{dt}\mathcal{F}\big(n(t)\big) = -\int n|\nabla \log n - \chi \nabla c|^2 \leq 0. \tag{2.9}$$

Notice that it arises also in two dimensional vortices dynamics, [48]. From the *logarithmic Hardy-Littlewood-Sobolev inequality* [56] it comes that the functional (2.8) is bounded from below for small mass.

**Theorem 2.4** (Logarithmic Hardy-Littlewood-Sobolev inequality)**.**
*Assume $f$ is a nonnegative function $\mathbb{R}^d \to \mathbb{R}$ with total mass $M$ and $f(x)\log(1+|x|^2)$ integrable, then*

$$-\int_{\mathbb{R}^d}\int_{\mathbb{R}^d} f(x)\log|x-y|f(y)\,dx\,dy \leq \frac{M}{d}\int_{\mathbb{R}^d} f\log f\,dx + C(d,M).$$

As a consequence,

$$\begin{aligned}\mathcal{F}(n) &= \int n\log n + \frac{\chi}{2d\pi}\int n\ \log * n\\ &\geq \Big(1-\frac{\chi M}{2d^2\pi}\Big)\int n\log n + C\\ &= \Big(1-\frac{M}{M_{\rm crit}}\Big)\int n\log n + C.\end{aligned}$$

We deduce from this lower bound that the cell density $n$ is uniformly equi-integrable as soon as $M < M_{\rm crit}$ (see also [48]).

**Theorem 2.5** (Critical mass for a log kernel)**.**
*Let $\Omega$ be the whole space $\mathbb{R}^d$ and $n_0\big(|\log n_0| + 1 + |x|^2\big) \in L^1$. Assume $M > M_{\rm crit}$ then solutions to (2.1) blow-up in finite time and in fact become singular measures. If $M < M_{\rm crit}$, then the system (2.1) has a global weak solution and $L^p$ regularity is propagated; if additionally $n_0 \in L^p$ for some $p > d > 1$ then $n(t,x) \in L^\infty\big((\alpha,T)\times\mathbb{R}^d\big)$ for all $T > \alpha > 0$.*

One can check that $p > d/2$ is enough for the regularizing effect in $L^\infty$ (see [74]) but the argument is based on iterations that make it longer to present and we prefer to skip this technical issue.

The end of this section is devoted to the proof of these results. We shall mention noticeably that we only aim to give below *a priori* estimates which guarantee the apparition of singularities. A rigorous program based on those kind of estimates, followed by a regularization procedure, has been achieved by Blanchet and co-authors in [35].

**Blow-up and weak solutions.** To prove that solutions blow up in finite time we show, following [187], that the second moment of $n$ cannot remain positive for all time. It relies on the following computation in the case $d \geq 2$,

$$\begin{aligned}\frac{d}{dt}\int \frac{1}{2}|x|^2 n(x,t)\,dx &= \int \frac{|x|^2}{2}\frac{\partial}{\partial t}n\,dx\\ &= \int \frac{1}{2}|x|^2\nabla\cdot(\nabla n - \chi n\nabla c)\,dx\\ &= -\int x\cdot(\nabla n - \chi n\nabla c)\,dx\\ &= \int(\nabla\cdot x)n\,dx - \frac{\chi}{d\pi}\iint n(x)\frac{x\cdot(x-y)}{|x-y|^2}n(y)\,dy\,dx\\ &= M\Big(d - \frac{\chi}{2d\pi}M\Big)\\ &= dM\Big(1-\frac{M}{M_{\rm crit}}\Big).\end{aligned} \tag{2.10}$$

For $d = 1$ the computation is slightly different but the final result is the same. We have $\nabla c = -Hn$, where $H$ denotes the Hilbert transform [93]. We obtain therefore

$$\begin{aligned}\frac{d}{dt}\int \frac{1}{2}|x|^2 n(x,t)\,dx &= dM - \frac{\chi}{d\pi}\int n(x)\lim_{\varepsilon\to 0}\int_{|x-y|>\varepsilon}\frac{x}{x-y}n(y)dydx \\ &= dM - \frac{\chi}{2d\pi}\lim_{\varepsilon\to 0}\iint_{|x-y|>\varepsilon} n(x)n(y)dxdy \\ &= dM\Big(1-\frac{M}{M_{\rm crit}}\Big). \end{aligned} \tag{2.11}$$

For $M > M_{\rm crit}$, it proves that some singularity occurs that prevents this computation to be possible (otherwise there is a contradiction between the positivity of the second moment and its negative decay). The singularity can be further analyzed and we prove below (see also [35, 209]) that $n$ cannot remain an $L^1$ function. In order to do so, we need a concept of *weak solution to the Keller-Segel system* that can handle $L^1$ solutions and that was used in [222]. To do that, we use the usual definition of distributional solutions but take advantage of the symmetry in the drift term. Let $\psi \in \mathcal{D}(\mathbb{R}^d)$ a test function, and test it in (2.1), we arrive at

$$\frac{d}{dt}\int_{\mathbb{R}^d}\psi(x)n(t,x) = \int_{\mathbb{R}^d}\Delta\psi(x)n(t,x)dx - \frac{\chi}{d\pi}\int_{\mathbb{R}^d\times\mathbb{R}^d}\nabla\psi(x).\frac{x-y}{|x-y|^2}n(t,x)n(t,y)dx\,dy.$$

In this equation we still need to make sense of the singularity of order $1/|x-y|$. This can be avoided in defining solutions as uniformly bounded measures in $x$, and weakly continuous in time, such that

$$\frac{d}{dt}\int_{\mathbb{R}^d}\psi(x)n(t,x) = \int_{\mathbb{R}^d}\Delta\psi(x)n(t,x)dx - \frac{\chi}{2d\pi}\int_{\mathbb{R}^d\times\mathbb{R}^d}[\nabla\psi(x)-\nabla\psi(y)].\frac{x-y}{|x-y|^2}n(t,x)n(t,y)dx\,dy. \tag{2.12}$$

Because $[\nabla\psi(x)-\nabla\psi(y)].\frac{x-y}{|x-y|^2}$ is bounded by 1, this definition of weak solutions makes perfect sense for $n \in L^\infty(\mathbb{R}^+; L^1(\mathbb{R}^d))$.

Notice for instance that weak solutions are mass conservative. Indeed, we can choose a test function $\psi_R(x) = \psi(|x|/R)$ with $\psi$ a smooth function such that $\psi(r) = 1$ for $r \le 1/2$, $\psi(r) = 0$ for $r \ge 1$. Then

$$\left|\int_{\mathbb{R}^d}\Delta\psi_R(x)n(t,x)dx\right| \le \frac{C}{R^2}\int_{\mathbb{R}^d} n(t,x)dx \xrightarrow[R\to\infty]{} 0,$$

$$\left|\int_{\mathbb{R}^d\times\mathbb{R}^d}[\nabla\psi_R(x)-\nabla\psi_R(y)]\cdot\frac{x-y}{|x-y|^2}n(t,x)n(t,y)dx\,dy\right| \le \frac{C}{R^2}\int_{\mathbb{R}^d\times\mathbb{R}^d} n(t,y)n(t,x)dydx\,dy \xrightarrow[R\to\infty]{} 0.$$

Therefore, passing to the limit $R\to\infty$, we arrive (say test against a test function in time) at

$$\frac{d}{dt}\int_{\mathbb{R}^d} n(t,x)dx = 0.$$

With the help of this concept of weak solution, we can also prove the

**Lemma 2.6.** *A weak solution to* (2.1) *in the sense of (2.12) that satisfies* $\int_{\mathbb{R}^d}(1+|x|^2)n^0(x)\,dx < \infty$ *also satisfies, as long as it is a* $L^1(\mathbb{R}^d)$ *function,*

$$\frac{d}{dt}\int_{\mathbb{R}^d}|x|^2\,n(t,x)\,dx = 2dm^0\left(1-\frac{M}{M_{\rm crit}}\right). \tag{2.13}$$

To prove this lemma, we consider a family of functions $\psi_R(|x|) \in \mathcal{D}(\mathbb{R}^d)$ that grows nicely to $|x|^2$ as $R\to\infty$ as in the above argument for the total mass. Then, we compute, as before,

$$\begin{aligned}\frac{d}{dt}\int_{\mathbb{R}^d}\psi_R n dx &= \int_{\mathbb{R}^d}\Delta\psi_R\,n\,dx \\ &\quad -\frac{\chi}{2d\pi}\int_{\mathbb{R}^d}\frac{(\nabla\psi_R(x)-\nabla\psi_R(y))\cdot(x-y)}{|x-y|^2}\,n(t,x)\,n(t,y)\,dx\,dy.\end{aligned}$$

As before, both terms in the right hand side are bounded (because $\Delta\psi_R$ and $\frac{(\nabla\psi_R(x)-\nabla\psi_R(y))\cdot(x-y)}{|x-y|^2}$ are bounded. Therefore $\int_{\mathbb{R}^d}\psi_R\, n\ dx$ remains uniformly bounded and thus $\int_{\mathbb{R}^d}\psi_R\, n\ dx<\infty$. Finally, as $R\to\infty$, we may pass to the limit in each term using the Lebesgue monotone convergence theorem (as long as we can dominate the various terms by the $L^1$ function $n$). In this circumstance, we can pass to the limit and obtain equality (2.13).

**Second moment control for $M\le M_{\rm crit}$** For $M\le M_{\rm crit}$, the above argument gives a local in time control of the second moment which is important because it allows to use (see again [86, 35] for instance) the standard inequality for $n(x)\ge 0$,

$$\int n(x)\log_- n(x)dx\le C\Big(\int n(x)dx,\int |x|^2 n(x)dx\Big).$$

This provides a critical control, specific to the case $\Omega=\mathbb{R}^d$ which is enough, with the $L\log L$ bound, to prove the existence of weak solutions, see [86, 35].

**Stationary states.** One can look for steady states which are minimizers of the energy functional $\mathcal{F}$ (see section 2.3.2). In the case of the critical mass $M=M_{\rm crit}$ and the whole space $\mathbb{R}^d$ we know precisely the minimizers of $\mathcal{F}$ [48, 56]: they are given by the conformal images of the function

$$h(x)=|\mathbb{S}^d|^{-1}\left(\frac{2}{1+|x|^2}\right)^d.$$

**Propagation of $L^p$ bounds.** As soon as equi-integrability is gained, the remaining work is usually to propagate $L^p$ regularity for the cell density. This work was initiated by Jäger and Luckhaus [147] who pointed out that the Gagliardo–Nirenberg–Sobolev (GNS) inequality plays a key role within these estimates. Applying their method to model (2.1) we have to distinguish between dimension $d=1$, $d=2$ and $d\ge 3$. The case $d=2$ has already been well studied, because it is the classical KS model [147, 107, 29, 77, 50]. Nevertheless we explain briefly the strategy, based on the following computation,

$$\frac{d}{dt}\int n^p=-4\frac{p-1}{p}\int|\nabla n^{p/2}|^2+\chi(p-1)\int n^{p+1}. \tag{2.14}$$

We cannot apply a Gronwall lemma here, but the GNS inequality [106, 193] enables to compare the two opposite terms of the right-hand-side, namely

$$\int n^{p+1}\le C(p)\|\nabla n^{p/2}\|_2^2\int n. \tag{2.15}$$

Closing this computation requires a suboptimal mass condition which depends on $p$. In order to circumvent this difficulty, we still follow [147] and we can replace $n$ by $(n-k)_+$. We obtain finally for $p>1$:

$$\frac{d}{dt}\int(n-k)_+^p\le\left(-4\frac{p-1}{p}+C(p)\chi(p-1)\int(n-k)_+\right)\|\nabla(n-k)_+^{p/2}\|_2^2+O\left(\int(n-k)_+^p\right). \tag{2.16}$$

This proves $L^p$ regularity for all $p$ because the term $\int(n-k)_+$ is uniformly small for large $k$, just using the upper bound

$$\int(n-k)_+\le\int_{n\ge k}n\frac{\log n}{\log k}\le\int n\frac{\log_+ n}{\log k}\le\frac{C}{\log k}.$$

In the following we would like to apply the same strategy to the cases $d=1$ and $d\ge 3$. Although computations are more complex, they are precisely similar to $d=2$.

For $\mathbf{d \geq 3}$ the time derivative of the $L^p$ norm becomes

$$\frac{d}{dt}\int n^p = -4\frac{p-1}{p}\int |\nabla n^{p/2}|^2 + \chi(p-1)\int n^p\big(-\Delta c\big).$$

We focus on the last term,

$$\int n^p\big(-\Delta c\big) = \int n^p\Big(\big(-\Delta K_d\big) * n\Big).$$

In the sense of distributions we have $-\Delta K_d(z) = \dfrac{1}{d\pi}\dfrac{d-2}{|z|^2}$. In addition we propose to apply the Hardy-Littlewood-Sobolev inequality [168] together with a special case of the GNS inequality [106, 193],

$$\begin{aligned}
\left|\int_{\mathbb{R}^d}\int_{\mathbb{R}^d} f(x)|x-y|^{-\lambda}g(y)\,dx\,dy\right| &\leq C(d,\lambda,q)\|f\|_q\|g\|_r\ ,\\
q,r>1\ ,\ 0<\lambda<d\ ,\quad &\frac{1}{q}+\frac{\lambda}{d}+\frac{1}{r}=2\ ;\\
\int n^{p+2/d} \leq C(p)\|\nabla n^{p/2}\|_2^2\left(\int n\right)^{2/d}&. \qquad (2.17)
\end{aligned}$$

Finally it comes using interpolation inequality that

$$\begin{aligned}
\int n^p\big(-\Delta c\big) &= \frac{d-2}{d\pi}\iint n^p(x)|x-y|^{-2}n(y)\,dx\,dy,\\
&\leq C\|n^p\|_q\|n\|_r,\\
&\leq C\|n^p\|_q\|n\|_{p+2/d}^{\theta}\|n\|_1^{1-\theta},\\
&\leq C\left(\int n^{p+2/d}\right)^{\frac{1}{q}+\frac{\theta}{p+2/d}}\|n\|_1^{1-\theta},
\end{aligned}$$

where the numerology $q, r, \theta$ satisfies

$$pq = p+\frac{2}{d}\ ,\quad \frac{1}{q'}+\frac{1}{r'}=\frac{2}{d}\ ,\quad \theta=\frac{2}{d}\ ,\quad \frac{1}{q}+\frac{\theta}{p+2/d}=1.$$

We are now reduced to the case where GNS inequality (2.17) can be used. We can redo the computations with $(n-k)_+$ instead of $n$ to get an estimation corresponding to (2.16) in case $d=2$ and the conclusion is similar.

For $\mathbf{d=1}$ the term $-\Delta K_d$ becomes more complex. In the sense of distributions it is

$$\langle -\Delta K_d, \phi\rangle = -\frac{1}{\pi}\ \text{p.v.}\frac{1}{x}\Big(\frac{d\phi}{dx}\Big).$$

In other words, $Hf$ denoting the Hilbert transform of $f$ [93], we have $\nabla c = -Hn$. The Hilbert transform is strong $(p,p)$ for each $p>1$ (M. Riesz), that is $\|Hf\|_p \leq C(p)\|f\|_p$. We can rebuild the same argumentation as previously,

$$\begin{aligned}
\frac{d}{dt}\int n^p &= -4\frac{p-1}{p}\int|\nabla n^{p/2}|^2 + \chi(p-1)\int\nabla n^p\cdot\nabla c.\\
\int\nabla n^p\cdot\nabla c &\leq \|\nabla n^{p/2}\|_2\left(\int n^p|Hn|^2\right)^{1/2},\\
&\leq \|\nabla n^{p/2}\|_2\left(\int n^{pq}\right)^{\frac{1}{2q}}\|Hn\|_{2q'},\\
&\leq C\|\nabla n^{p/2}\|_2\left(\int n^{p+2}\right)^{1/2},
\end{aligned}$$

with the following definition of exponents: $pq = p+2 = 2q'$. We can apply the inequality (2.17) once again and replace $n$ by $(n-k)_+$. Then it is just the same as in dimension 2.

**$L^\infty$ bound.** The regularizing effect in $L^\infty$ can be obtained using the heat kernel $G(t,x)$. We have

$$n(t) = n_0 * G(t) - \int_0^t \nabla G(t-s) * (n\nabla c)(s) ds.$$

Since we know that $n \in L^\infty\big((0,T); L^p(\mathbb{R}^d)\big)$ (and $p > d'$), we also have $\nabla c = -\frac{1}{d\pi}\frac{x}{|x|^2} * n$ belongs to $L^\infty\big((0,T)\times\mathbb{R}^d\big)$. Therefore, we arrive at

$$\begin{aligned}\|n(t)\|_{L^\infty} &\leq \frac{C}{t^{d/2}}\|n_0\|_{L^1} + C\int_0^t \|\nabla G(t-s) * n(s)\|_{L^\infty} ds \\ &\leq \frac{C}{t^{d/2}}\|n_0\|_{L^1} + C\|n\|_{L^\infty\left((0,T);L^p(\mathbb{R}^d)\right)}\int_0^t \|\nabla G(s)\|_{L^{p'}}.\end{aligned}$$

And we conclude the bound since $\|\nabla G(s)\|_{L^{p'}} = Cs^{-\frac{1}{2}(1+\frac{d}{p})}$ and $\frac{1}{2}(1+\frac{d}{p}) < 1$ for $p > d$.

## 2.3 MKS system in a bounded domain.

From now on, we consider the model (2.1) set on a bounded domain $\Omega \subset \mathbb{R}^d$. First of all, we note that the model is homogeneous with respect to $\Omega$. More precisely, considering $\lambda\Omega$ as the new domain and letting $\tilde{n}(t,x) = \lambda^d n(t,\lambda x)$ (the total mass is unchanged), then we recover the equation in $\Omega$ with a $\lambda^2$ time scaling.

The definition of $c$ by a convolution forces us to extend $n$ outside the domain $\Omega$. We study separately two natural ways to perform this extension: by zero (section 2.3.1) and by meanvalue (section 2.3.3).

### 2.3.1 The cell density is extended by zero. Evolution

As mentioned earlier, this situation corresponds to Dirichlet BC on $c$, and is qualitatively similar to the whole space model. Starting from the main equation we get that this system is equipped with an energy functional,

$$\mathcal{F}(n) = \int_\Omega n\log n - \frac{\chi}{2}\int_\Omega nc\ , \quad c = K_d * n, \tag{2.18}$$

which satisfies, as in the case of the full space,

$$\frac{d}{dt}\mathcal{F}\big(n(t)\big) = -\int_\Omega n|\nabla\log n - \chi\nabla c|^2 \leq 0. \tag{2.19}$$

Because we can replace $\Omega$ by $\mathbb{R}^d$ in these formula, global existence under the critical mass follows the same structure as section 2.2: equi-integrability then $L^p$ bounds. Moreover computations are exactly the same because $n$ is well defined in whole $\mathbb{R}^d$.

**Blow up.** Again we follow [187] and the previous computation of the second moment of $n$,

$$J(t) = \int_\Omega \frac{1}{2}|x|^2 n(x,t)\ dx. \tag{2.20}$$

Its time derivative satisfies now (see above (2.10) and (2.11))

$$\begin{aligned}\frac{d}{dt}J &= -\int_\Omega x\cdot(\nabla n - \chi n\nabla c)\ dx \\ &= -\int_{\partial\Omega}(x\cdot\eta)n + \int_\Omega(\nabla\cdot x)n\ dx + \chi\int_\Omega x\cdot n\nabla c\ dx \\ &= -\int_{\partial\Omega}(x\cdot\eta)n + dM - \frac{\chi}{2d\pi}M^2,\end{aligned} \tag{2.21}$$

where $\eta$ still denotes the outside normal unit vector on the boundary. We may choose the origin to be the center of the star-shaped domain $\Omega$, ensuring that the first term in (2.21) is negative. Also the condition $\chi M > 2\pi d^2$ implies that $\frac{d}{dt}J \leq -\varepsilon < 0$. But $J$ should remain positive and this contradicts the global existence of solutions.

We summarize these properties in the following theorem.

**Theorem 2.7** (Critical mass; extension by zero)**.**
*Let $\Omega \subset \mathbb{R}^d$ be a bounded domain and $n_0 \in L\log L$. Assume $M < M_{\text{crit}}$, then the system (2.1) has a global weak solution. On the contrary assume $\Omega$ is a star-shaped domain and $M > M_{\text{crit}}$, then solutions to (2.1) blow-up in finite time.*

**Remark 2.8.** *The above Theorem 2.7 is similar to the case of Dirichlet boundary conditions for the chemical in the classical Keller-Segel setting in 2D. Namely it does not require any condition on the initial data, but on the domain's geometry. On the contrary, the Theorem 2.12 below does require such an assumption on the density's concentration measured by the second momentum. Intuitively, constant densities are stationary states when the extension is done by meanvalue. Those stationary states obviously do not blow-up, so that one requires more information on the initial density in general.*

**Remark 2.9.** *We may ask whether the assumption of a star-shaped domain is necessary or not. Consider the system (2.1) set on an annulus $a < r < b$ together with radial symmetry. One cannot expect any concentration point of cells from a radially symmetric initial data (it would break the symmetry which is conserved along time). See [48] for deeper considerations on the geomety of the domain.*

**Numerics.** We have performed numerical simulations for the system with extension by zero in dimension $d = 1$. The first point is to recover the critical mass from numerical experiments. Compared to the classical KS model there is an additional difficulty contained in the convolution term $c = K * n$. When it is discretized, the kernel $K$ is truncated relatively to the space step $\varepsilon$, namely $K^\varepsilon(z) = -\frac{1}{\pi}\log\varepsilon$ if $|z| < \varepsilon$. We have plotted in figures 2.1 and 2.2 the maxima of cell density for decreasing values of $\varepsilon$ together with the solution corresponding to the more accurate simulation, for $M < M_{\text{crit}}$ and $M > M_{\text{crit}}$ respectively. We note that these maxima depend sensitively upon on the space step. Consequently the notion of blow–up is difficult to track numerically in higher dimension. This illustrates one of the goals of the present model to also create a singularity in dimension 1.

As stated in the above theorem, the critical mass in this model is the same as in the whole space. The most remarkable property of the extension by zero is that constant distributions are not steady states because they do not satisfy the boundary conditions. Therefore it is of interest to study the possible steady distributions.

### 2.3.2 The cell density is extended by zero. Stationary states

From (2.19), we can deduce that the steady states are exactly the functions $n$ which satisfies $\nabla \log n = \chi \nabla c$ or $\log n = \chi c + \mu$, where $\mu$ is determined by mass conservation [58]. So we end up with the following equations for steady states:

$$n = M\frac{e^{\chi c}}{\int_\Omega e^{\chi c}}\ , \quad c = K_d * n. \tag{2.22}$$

This section will be continued by a proof of the following

**Theorem 2.10** (Steady states; extension by zero)**.**
*For $M < M_{\text{crit}}$ there is at least one solution to (2.22) with $c \in L^\infty$ and it is a minimizer for the energy functional $\mathcal{F}(n)$.*

We are not aware of a uniqueness result for this problem, e.g. using convexity along proper paths as in [179].

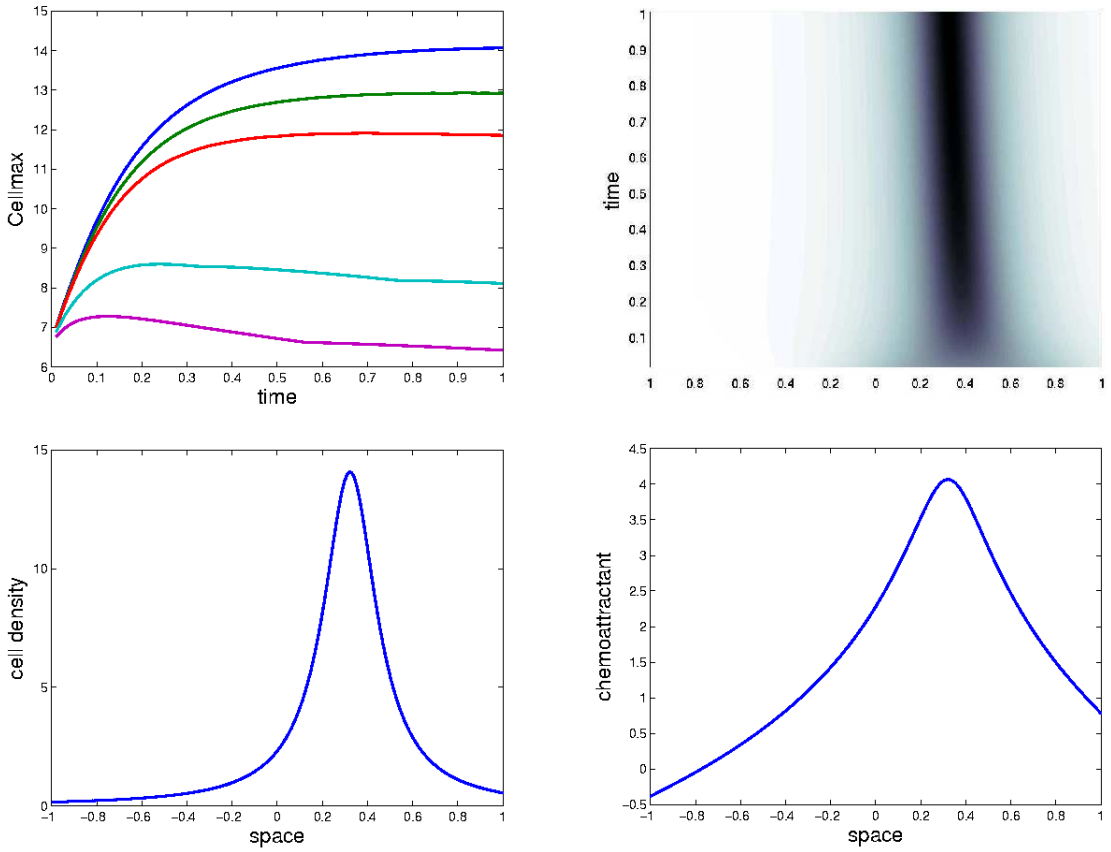


Figure 2.1: *(extension by zero)* In dimension 1, initially a gaussian with total mass $M = 1.8\pi < M_{\text{crit}}$ and chemosensitivity $\chi = 1$. (*up left*) The maximum value of the cell density is plotted for decreasing values of space step: $dx = [.001, .005, 0.01, 0.05, 0.1]$. (*up right*) The evolution of cell density corresponding to $dx = .001$. (*bottom*) Respectively the cell density and the chemical potential at the final time with $dx = .001$. See also figure 2.2.

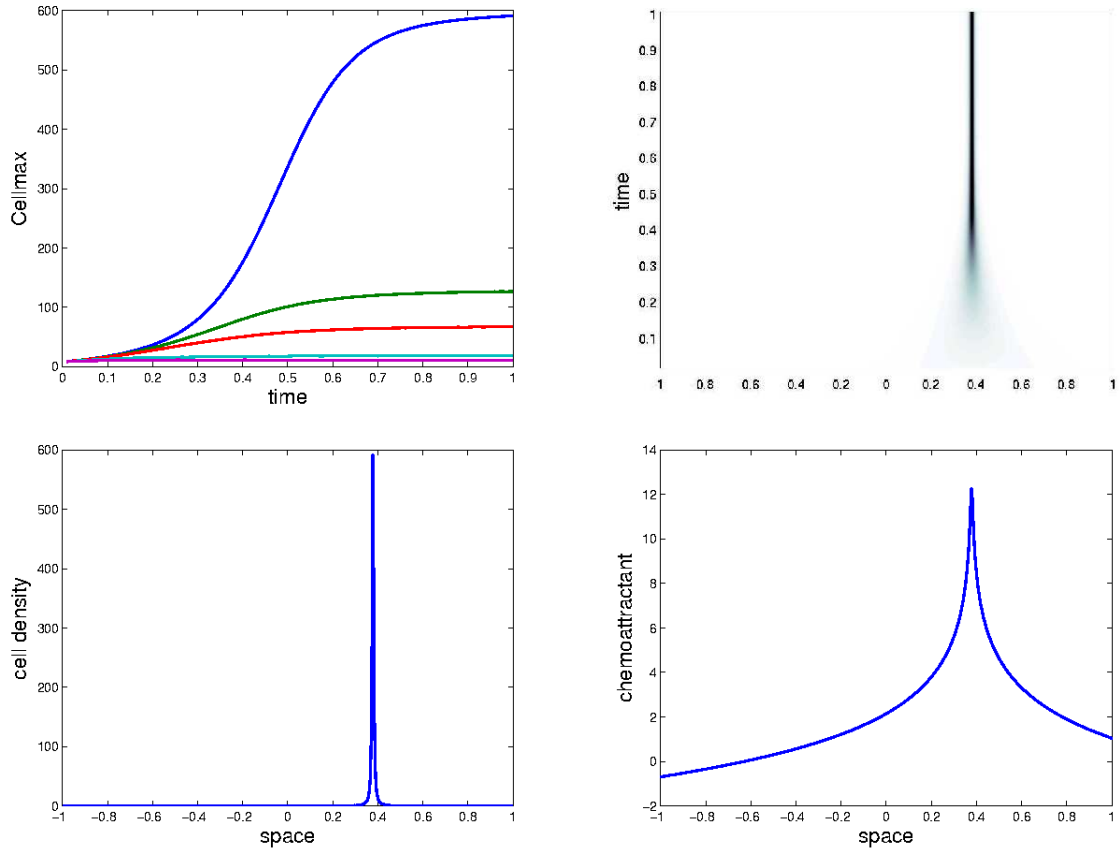


Figure 2.2: *(extension by zero)* Same as figure 2.1 with $M = 2.2\pi > M_{\text{crit}}$. Although we expect finite time blow-up in this situation from Theorem 2.7, we observe concentration of the density without singularities. This is due to the numerical scheme which regularizes the system: in the procedure the interaction kernel is given by $-\frac{1}{\pi}\log|z|$ if $|z| > dx$ and $-\frac{1}{\pi}\log|dx|$ otherwise. This explains also why we have to choose very small space steps to observe a significant concentration.

For proving the above theorem, we begin with the main estimate we get from logarithmic Hardy-Littlewood-Sobolev inequality (theorem 2.4),

$$\mathcal{F}(n) \geq C + \Big(1 - \frac{M}{M_{\text{crit}}}\Big) \int_\Omega n \log n \geq C - \Big(1 - \frac{M}{M_{\text{crit}}}\Big) e^{-1} |\Omega|.$$

In other words $\mathcal{F}$ is bounded from below, because $x \log x$ is bounded from below. In the following, we let $K = K_d$. Let $\{n_k\}$ be a minimizing sequence. From the above inequality, we deduce that $\int_\Omega n_k \big(\log n_k\big)_+$ is bounded. Therefore the family $\{n_k\}$ is equi-integrable and up to a subsequence we have $n_k \rightharpoonup n$ weakly in $L^1$. By convexity of the function $x\big(\log x\big)_+$, we can deduce that $n \in L \log L$ and more precisely

$$\int_\Omega n\big(\log n\big)_+ \leq \liminf \int_\Omega n_k \big(\log n_k\big)_+. \tag{2.23}$$

Using the duality inequality $ts \leq s \log s - s + e^t$, we show an $L^\infty$ estimate for $c_k := K * n_k$. Choose the parameter $\alpha < \pi d^2$ and compute

$$\begin{aligned} c_k(x) &= \int_\Omega K(x-y) n_k(y)\, dy \\ &\leq \int_\Omega \frac{n_k}{\alpha} \log \frac{n_k}{\alpha} + \int_\Omega e^{\alpha K(x-y)}\, dy \\ &\leq -\frac{\log \alpha}{\alpha} M + \frac{1}{\alpha} \int_\Omega n_k \log n_k + \int_\Omega |x-y|^{-\frac{\alpha}{d\pi}}\, dy \\ &\leq C. \end{aligned}$$

Thus $\{c_k\}$ is bounded in $L^\infty(\Omega)$. Now for any test function $\phi \in L \log L(\Omega)$, $\check{K} * \phi$ is bounded and thus

$$\int_\Omega c_k \phi = \int_\Omega (K * n_k)\phi = \int_\Omega n_k (\check{K} * \phi) \longrightarrow \int_\Omega n (\check{K} * \phi) = \int_\Omega (K * n)\phi = \int_\Omega c\phi.$$

This shows that $c_k \rightharpoonup c = K * n$, weakly in $L^q$ for all $q < \infty$.

In the following step we plan to deduce some compactness of $\{c_k\}$, say in $L^1$. First we remark that $\nabla K$ is integrable if $d \geq 2$, so that

$$\begin{cases} \nabla c_k = -H n_k\ , & d = 1, \\ \nabla c_k = \nabla K * n_k\ , & d \geq 2, \end{cases}$$

where $H$ is the Hilbert transform. On one hand, because $\int_\Omega n_k \big(\log n_k\big)_+$ is bounded we now that $\nabla c_k$ is bounded in $L^1$ in the case $d = 1$ [227, 49]. On the other hand $\nabla c_k$ is obviously bounded in $L^1$ for $d > 1$. Consequently $\{c_k\}$ is bounded in $W^{1,1}$ which is compactly embedded in $L^1$ for all dimensions. Up to a subsequence we have $c_k \to c$ strongly in $L^1$. In addition we can assume that $c_k \to c$ *a.e.* We invoke Egorov's theorem together with equi-integrability of $\{n_k\}$ and $L^\infty$ bound on $\{c_k\}$ to conclude that

$$\int_\Omega n_k c_k \longrightarrow \int_\Omega nc.$$

Combining this with (2.23) we get finally that

$$\mathcal{F}(n) = \int_\Omega n \log n - \frac{\chi}{2} \int_\Omega nc \leq \liminf \mathcal{F}(n_k) = \inf \mathcal{F}.$$

This proves that $n$ is a minimizer for $\mathcal{F}$.

**Remark 2.11.** *As $M \to M_{\text{crit}}$ one can check that, along subseqences, the corresponding behavior occurs, for some $x^* \in \overline{\Omega}$,*

$$n \to M_{\text{crit}} \delta(x - x^*) \ \textit{(weak sense of measures)},$$

$$c \to -\frac{2d}{\chi}\log|x-x^*| \ \ (\text{in } L^p,\ 1\le p<\infty), \qquad \nabla c \to -\frac{2d}{\chi}\frac{x-x^*}{|x-x^*|^2} \ \ (\text{in } L^p,\ 1\le p<d).$$

*Indeed, since $\nabla n = \chi n \nabla c$, after testing against $x$ and integration by parts, we obtain $\int_{\partial\Omega}(x\cdot\eta)n(x)\to 0$, in the case of a star-shaped domain $\Omega$. But the lower bound on $c$, and (2.22) show that this can occur only when $\int_\Omega e^{\chi c}\to\infty$, and thus $\int_\Omega n\log n\to\infty$. In order to go further and prove there is a single concentration point as stated above, more elaborate but standard arguments that we do not copy, are needed along the lines of [189, 114].*

### 2.3.3 Extension by mean value

The main drawback of the previous extension by zero is that constant densities are not steady states of the problem. To overcome this trouble we propose to extend $n$ outside the domain by its meanvalue $\langle n\rangle_\Omega$. For this purpose we have to redefine the chemical potentiel by

$$c = K_d * \Big(n - \langle n\rangle_\Omega\Big), \qquad n = \langle n\rangle_\Omega \ \text{ in } \ \Omega^C, \tag{2.24}$$

which is the exact analogue of the Neumann BC for the KS model [147]. For convenience we define $\bar n = n - \langle n\rangle_\Omega$ so that $c = K_d * \bar n$. The decreasing free energy related to this system is the following

$$\mathcal{F}(n) = \int_\Omega n\log n - \frac{\chi}{2}\int_\Omega \bar n c, \qquad \bar n = n - \langle n\rangle_\Omega, \quad c = K_d * \bar n. \tag{2.25}$$

We are now ready to state our global existence or blow up result as follows

**Theorem 2.12** (Critical mass; extension by meanvalue)**.**

*Let $\Omega\subset\mathbb{R}^d$ be a bounded domain and $n_0\in L\log L$. Assume $M<M_{\rm crit}$, then the system* (2.1) *with $c = K_d*\big(n-\langle n\rangle_\Omega\big)$ has a global weak solution. On the contrary assume $\Omega$ is a star-shaped domain and $d\ge 2$; if $M>M_{\rm crit}$ and the initial second moment $J(0)$ is small enough, then solutions to* (2.1) *blow-up in finite time.*

**Global existence.** There are some minor technical changes between this section and the previous one. The key idea is that we can modify $\bar n$ into the quadratic term in (2.25) up to some constant, to recover the extension by 0. We define the piecewise constant function $\zeta = \langle n\rangle_\Omega \mathbf{1}_\Omega$, such that $\bar n + \zeta$ is the extension by zero and

$$\int_\Omega n\log n - \frac{\chi}{2}\int_\Omega \big(\bar n+\zeta\big)K_d*\big(\bar n+\zeta\big) \quad = \quad \mathcal{F}(n) + \text{bounded terms.}$$

The remaining terms are bounded because the kernel $K_d$ is locally integrable. Keeping in mind this preliminary remark, the rest of the proof for existence is straightforward.

**Remark 2.13.** *Whereas in the classical KS model the critical masses differs between Dirichlet and Neumann BC (see section 2.1), in this new model they are the same. It seems surprising that the boundary curvature plays no effect on the mass threshold if the cell density is extended by its meanvalue. The reason is that we skip the boundary singularity of the Poisson kernel for a bounded domain in the logarithmic kernel $K_d(z) = -\frac{1}{d\pi}\log|z|$.*

**Blow up.** As in the previous sections we perform computations on the second moment of $n$ in the case $d\ge 2$ and a star-shaped domain $\Omega\subset\mathbb{R}^d$.

$$\begin{aligned}
\frac{d}{dt}J &= -\int_{\partial\Omega}(x\cdot\eta)n + dM - \frac{\chi}{2d\pi}M^2 + \frac{\chi}{d\pi}\langle n\rangle_\Omega\int_\Omega\int_\Omega n(x)\frac{x\cdot(x-y)}{|x-y|^2}\,dy\,dx\\
&\le dM - \frac{\chi}{2d\pi}M^2 + \frac{\chi}{d\pi}\langle n\rangle_\Omega\int_\Omega\int_\Omega |x|n(x)|x-y|^{-1}\,dy\,dx\\
&\le dM - \frac{\chi}{2d\pi}M^2 + \mathcal{C}\frac{\chi M}{d\pi|\Omega|}\int_\Omega |x|n(x)\,dx\\
&\le dM - \frac{\chi}{2d\pi}M^2 + \mathcal{C}\frac{\chi M}{d\pi|\Omega|}\sqrt{MJ}.
\end{aligned}$$

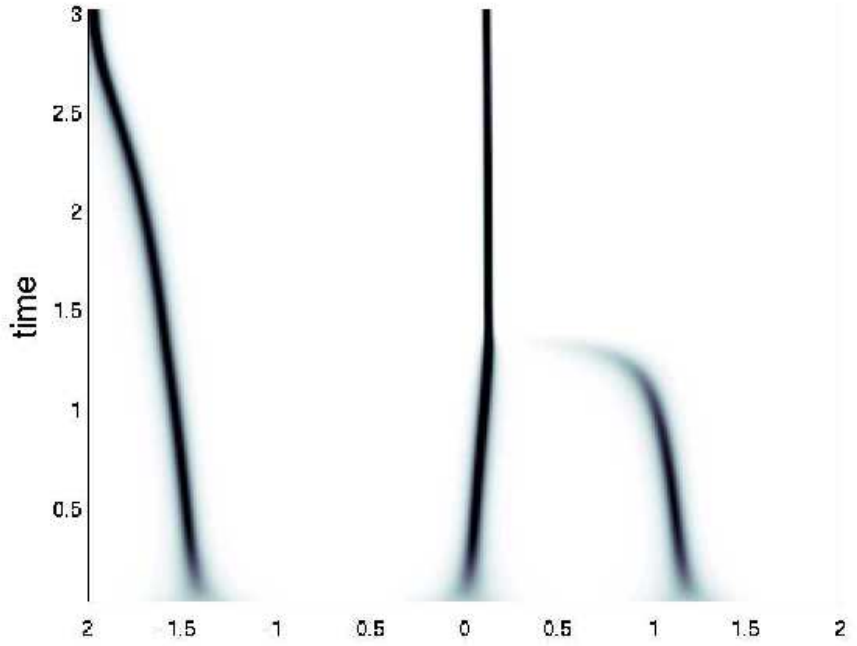


Figure 2.3: *(extension by meanvalue)* Initially 3 gaussian–like peaks with total mass $M = 7\pi > 3M_{\text{crit}}$ and chemosensitivity $\chi = 1$.

We can be more accurate on the constant $\mathcal{C}$, which is

$$\mathcal{C} = \sup_{x\in\Omega} \int_\Omega |x-y|^{-1}\, dy \leq \frac{d}{d-1}(\frac{1}{d}|\mathbb{S}^{d-1}||\Omega|^{d-1})^{\frac{1}{d}}.$$

which can be obtained by dividing the integral into $|x-y| \leq \lambda$ and $|x-y| > \lambda$ and optimizing the result with respect to $\lambda$. Finally we obtain that

$$\frac{d}{dt}J \leq dM - \frac{\chi}{2d\pi}M^2 + \frac{\chi}{\pi(d-1)}M^{\frac{3}{2}}\frac{\sqrt{J}}{R}\ , \tag{2.26}$$

with $|B(0,R)| = |\Omega|$. Consequently if $J(0)$ is small enough such that the right-hand-side of (2.26) is negative, then solutions blow up in finite time.

**Remark 2.14.** *$\frac{\sqrt{J}}{R}$ is homogeneous with respect to dilatations of $\Omega$ and this fact justifies the above calculations. Also one could not expect the blow up of solutions for large initial second moments; for example initial constant distribution. So it is necessary to have an upper bound for $J(0)$ to ensure blowing up of solutions.*

**Stationary states.** Obviously constant distributions of cells are steady states in this case. However unicity is not clear. Furthermore in dimension $d = 2$ with radial symmetry and the classical chemical potentiel $-\Delta c = n - \langle n\rangle$, the numerical computation of steady states are easier. Using a shooting method we can observe a non–trivial steady state appearing for $M > M_{\text{crit}}$ (*unpublished results*, see Annex A).

**Numerics.** We have performed simulations on a bounded domain with extension by meanvalue, in dimension $d = 1$. We have briefly tackled the problem of interaction between several peaks and the boundary. As it is the case in dimension two for Neumann boundary conditions, the boundary induces an

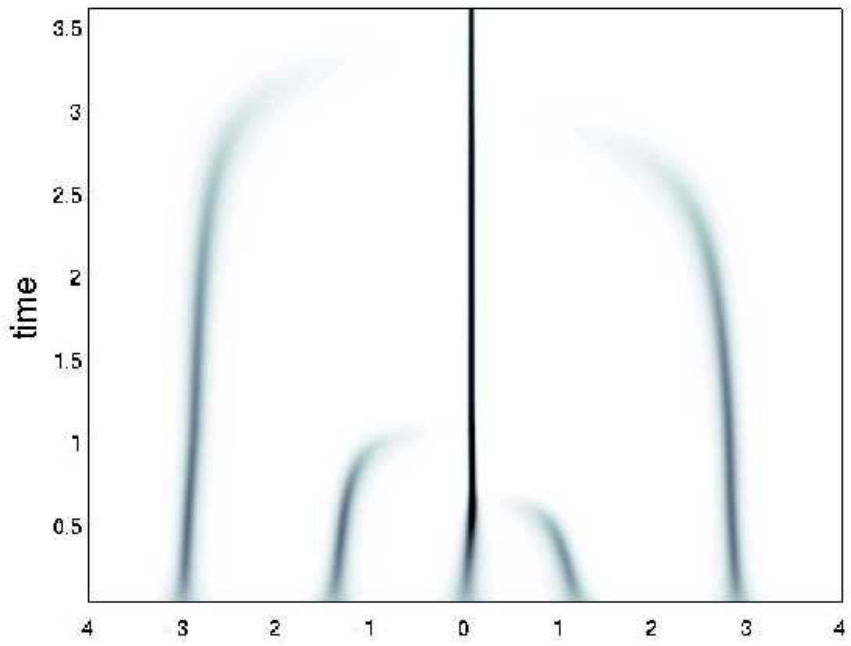


Figure 2.4: *(extension by meanvalue)* Initially 5 gaussian–like peaks with total mass $M = 12\pi > 5M_{\rm crit}$ and chemosensitivity $\chi = 1$.

attractive effect on peaks (Fig. 2.3). Furthermore, if we start initially from several gaussian–like peaks which are sufficiently far from each other, then they start to aggregate cells around independently, and finally they attract each other (Fig. 2.4).

The influence of the boundary can be viewed in 1D by computing the gradient of the potential $\nabla c$ subject to the usual ansatz [240, 87]

$$n(t,x) = \sum_{i=1}^{N} m_i(t)\delta(x = x_i(t)) + f(t,x) \ , \quad f \in L^1 \ .$$

Within this setting,

$$\begin{aligned}
\nabla c(x) &= -\frac{1}{\pi}\lim_{\varepsilon\to 0}\int_{|x-y|>\varepsilon} \frac{1}{x-y}\big(n(y) - \langle n\rangle\big)\ dy \\
&= -\frac{1}{\pi}\sum_{i=1}^{N}\frac{m_i}{x-x_i} - \frac{1}{\pi}\lim_{\varepsilon\to 0}\int_{|x-y|>\varepsilon}\frac{1}{x-y}f(y)\ dy - \frac{\langle n\rangle}{\pi}\lim_{\varepsilon\to 0}\left(\Big[\log(x-y)\Big]_a^{x-\varepsilon} + \Big[\log(y-x)\Big]_{x+\varepsilon}^{b}\right) \\
&= -\frac{1}{\pi}\sum_{i=1}^{N}\frac{m_i}{x-x_i} - \frac{1}{\pi}\lim_{\varepsilon\to 0}\int_{|x-y|>\varepsilon}\frac{1}{x-y}f(y)\ dy - \frac{M}{\pi(b-a)}\log\left(\frac{b-x}{x-a}\right) \ .
\end{aligned}$$

We recognize the vortex motion of the concentration regions [240], the $L^1$ remainder, plus an additional contribution, which is singular at the boundary with the attracting sign, but has only a logarithmic weight.

# Chapitre 3

# Le modèle de Keller-Segel parabolique/parabolique dans tout l'espace $\mathbb{R}^2$

---

Ce chapitre est une version préliminaire issue d'une collaboration avec Lucilla Corrias et Benoît Perthame. Il s'agit d'obtenir des estimations *a priori* suffisantes qui garantissent l'existence globale du système de KS parabolique/parabolique dans tout l'espace $\mathbb{R}^2$. La structure de ce système est plus compliquée que celle du système parabolique/elliptique parce que le problème renormalisé ne possède pas d'énergie évidente. On force cette renormalisation en introduisant certains 'moments' de la densité cellulaire et de la concentration chimique, dont on contrôle l'évolution parallèlement. Les étapes cruciales dans ces estimations découlent indépendamment des inégalités de Trudinger-Moser-Onofri, ou de Hardy-Littlewood-Sobolev logarithmique (voir aussi annexe B.4).

---

## 3.1 Introduction

Within living organisms, cells may communicate and therefore interact through chemical signals. This signaling pathway is of crucial importance for cell particles to move in the right direction or to organize themselves spatially. Biological challenges involving this phenomenon are numerous. It is known to be so actually in immunology and inflammatory processes, in bacterial growth colony and at some key stages of embryonic development for instance. Among mathematical models describing spatial organization of biological population through chemical signals ([209], [65], [96]) we highlight the following Patlak-Keller-Segel (PKS) model for chemotaxis ([152],[206])

$$\left\{\begin{array}{rcl} \dfrac{\partial n}{\partial t} & = & \kappa\Delta n - \chi\nabla\cdot(n\nabla c)\ , \quad t>0,\ x\in\Omega, \\ \varepsilon\dfrac{\partial c}{\partial t} & = & \eta\Delta c + \beta n - \alpha c\ , \quad t>0,\ x\in\Omega, \end{array}\right. \tag{PKS}$$

where $n$ denotes the density of a cell population and $c$ is the concentration of a chemical signal attracting the cells. The parameters $\kappa$, $\chi$ and $\beta$ are given positive constants, while $\varepsilon$, $\eta$ and $\alpha$ are given non-negative constants determining the type of evolution undergone by $c$. The set $\Omega$ is either a bounded domain in $\mathbb{R}^d$ or the whole space $\mathbb{R}^d$. In any case, boundary conditions or decay conditions at infinity have to be given for the densities $n$ and $c$ together with the initial conditions $n(\cdot,0)=n_0$ and $c(\cdot,0)=c_0$ if $\varepsilon>0$.

The modeling interest of such a system is to exhibit a phenomenon of "critical mass" in dimension $d = 2$. In a system like (PKS), the coupling between the cell equation and the chemical equation is a positive feedback: the more cells are aggregated, the more they produce a signal attracting other cells. This process is counter-balanced by pure diffusion of the cells, but if the amount of cells is sufficient this non-local chemical interaction dominates and cells attract themselves. Thus model (PKS) provides a simple phenomenological description of an instability broadly encountered in biology. The starvation stage of the slime mold amoebae *Dictyostelium discoideum* for instance is governed by this process, driving the population of unicellular organisms into a multicellular one ([248], [139]). More recently, a (PKS) type model has been suggested to solve a remarkable pattern formation issue in the human brain [157].

It is not overemphasize to say that system (PKS) has been the subject of a huge quantity of mathematical analysis over the last thirty years. The results of all these investigations can be simply summarized saying that the global existence or the blow-up of solutions of (PKS) is a space dimension dependent phenomenon. In particular, in dimension $d = 2$, the above biological instability has been precisely described mathematically at least when $\varepsilon = \alpha = 0$. Indeed, for the parabolic-elliptic system it has been shown that there exists a threshold for the initial mass $M = \int_\Omega n_0(x)\ dx$. For values of $M$ under this threshold the solution exists globally in time, while above this threshold the solution blow-up in finite time ([28],[35],[107],[190]). The modality of the blow-up has also been analyzed [131], as well as the critical case, i.e. when the initial mass $M$ equals the threshold value ([34], [31]).

Let us mention that in dimension $d \geq 3$ a similar critical phenomenon has been investigated. In this case, the $L^{\frac{d}{2}}$-norm of the initial density $n_0$ plays the same role as the initial mass $M$ in dimension $d = 2$. Indeed, in [74], [75], [77] the authors proved the global existence of weak solution of system (PKS) of parabolic-parabolic, parabolic-elliptic and parabolic degenerate type under a smallness condition on $\|n_0\|_{L^{d/2}}$. However, up to our knowledge, blow-up for large $\|n_0\|_{L^{d/2}}$ is still open and we conjecture that no critical threshold exists as in dimension 2.

Despite of all these results, mathematical open problems around (PKS) still subsist, especially for the full parabolic-parabolic system (PKS) ($\varepsilon > 0$). Let us observe that, whenever $\varepsilon = 0$ (quasi-stationary hypothesis for the chemical $c$), the system reduces to a single parabolic equation with a quadratic nonlocal nonlinearity, $c$ being expressed as a convolution between $n$ and the fundamental solution of the Laplace's equation. On the other hand, when $\varepsilon > 0$ the full parabolic-parabolic system is more difficult to handle with. We will see however that the densities $n$ and $c$ play dual roles in some sense (as it is highlighted by the dual inequalities used throughout this paper), providing some interesting features and structure to the system (PKS).

The goal of this paper is to tackle the global existence problem for the full parabolic-parabolic system (PKS) with $\varepsilon > 0$, $\eta > 0$, $\alpha \geq 0$ in dimension $d = 2$ and in the whole space $\mathbb{R}^2$. Indeed, for this problem the optimal threshold of $M$ for the global existence of solutions has not been found yet in the nonsymmetric case. A result exists in this direction in [188], but it does not give the exact critical mass. Here we obtain the optimal critical mass value using the energy method [107, 28, 35] and ad-hoc functional inequalities on $\mathbb{R}^2$. One more time, the free energy functional

$$\mathcal{E}(t) = \int_{\mathbb{R}^2} n(x,t) \log n(x,t)\ dx - \int_{\mathbb{R}^2} n(x,t)c(x,t)\ dx + \frac{1}{2}\int_{\mathbb{R}^2} |\nabla c(x,t)|^2\ dx + \frac{\alpha}{2}\int_{\mathbb{R}^2} c^2(x,t)\ dx$$

comes out to be the key ingredient leading to the global existence of solutions under the optimal smallness condition for the mass in dimension $d = 2$. Indeed, $\mathcal{E}(t)$ together with its evolution equation provide a gallery of *a priori* estimates on the solutions $(n, c)$ and we shall make use of each of them. For instance they allow to prove that the cellular flux in (3.1) $n\big(\nabla(\log n - c)\big) \in L^1(\mathbb{R}^+_{loc} \times \mathbb{R}^2)$. Therefore, the equation on $n$ holds in the distribution sense. Surprisingly, no specific restrictions on $c_0$ are required even for the fully parabolic-parabolic case under interest, except of course suitable regularity of the initial data.

It is convenient to adimensionalize system (PKS) through the following change of variables

$$t \to \tau = \kappa t\ , \quad n(x,t) \to \tilde{n}(x,\tau) = \frac{\beta\chi}{\eta\kappa}\ n\left(x, \frac{\tau}{\kappa}\right)\ , \quad c(x,t) \to \tilde{c}(x,\tau) = \frac{\chi}{\kappa}\ c\left(x, \frac{\tau}{\kappa}\right)\ .$$

Therefore, the system under consideration will be

$$\left\{\begin{array}{rcll} \partial_t \tilde{n} & = & \Delta \tilde{n} - \nabla \cdot (\tilde{n} \nabla \tilde{c}) \ , & t > 0, \ x \in \mathbb{R}^2, \\ \tilde{\varepsilon} \partial_t \tilde{c} & = & \Delta \tilde{c} + \tilde{n} - \tilde{\alpha} \tilde{c} \ , & t > 0, \ x \in \mathbb{R}^2, \\ \tilde{n}(\cdot, 0) & = & \tilde{n}_0(\cdot) = \frac{\beta_\chi}{\eta \kappa} \ n_0(\cdot) \ , & \tilde{c}(\cdot, 0) = \tilde{c}_0(\cdot) = \frac{\chi}{\kappa} \ c_0(\cdot), \quad x \in \mathbb{R}^2 \ . \end{array}\right. \tag{3.1}$$

with $\tilde{\varepsilon} = \frac{\varepsilon \kappa}{\eta} > 0$ and $\tilde{\alpha} = \frac{\alpha}{\eta} \geq 0$. The tilde sign will be removed in the sequel for clarity. Moreover, fast decay conditions at infinity for $n$ and $c$ have to be associated with (3.1). Concerning the cell density this decay will be expressed in terms of moments of $n$.

After this change of variables, the only parameters of the system to deal with are the total mass of cells $M = \int_{\mathbb{R}^2} n_0(x) \ dx$, which is conserved along time, the inverse diffusion rate of the chemical $\varepsilon$ and the chemical degradation rate $\alpha \geq 0$. The latter seems to play no essential role, unless it induces slightly technical difficulties in the estimates.

Our main results are the followings.

**Theorem 3.1** (Global existence)**.** . *Assume $\varepsilon > 0$ and $\alpha \geq 0$. Let $(n_0, c_0)$ be non-negative initial conditions for the parabolic-parabolic system (3.1) such that $n_0 \in L^1(\mathbb{R}^2) \cap L^1(\mathbb{R}^2, \log(1 + |x|^2) dx)$, $n_0 \log n_0 \in L^1(\mathbb{R}^2)$, $n_0 c_0 \in L^1(\mathbb{R}^2)$ and $c_0 \in H^1(\mathbb{R}^2)$ if $\alpha > 0$, while if $\alpha = 0$ $c_0 \in L^1(\mathbb{R}^2)$ and $|\nabla c_0| \in L^2(\mathbb{R}^2)$. Assume in addition that the mass is subcritical $M < 8\pi$, then there exists a global weak non-negative solution $(n, c)$ of (3.1) such that*

$$n \in L^\infty((0,\infty); L^1(\mathbb{R}^2)) \cap L^\infty_{loc}((0,\infty); L^1(\mathbb{R}^2, \log(1+|x|^2)dx)) \quad \text{and} \quad n \log n \in L^\infty_{loc}((0,\infty); L^1(\mathbb{R}^2)) \ ;$$

$$c \in L^\infty((0,\infty); L^1(\mathbb{R}^2)) \quad \text{for } \alpha > 0 \quad \text{and} \quad c \in L^\infty_{loc}((0,\infty); L^1(\mathbb{R}^2)) \quad \text{for } \alpha = 0 \ ;$$

$$c \in L^\infty_{loc}((0,\infty); H^1(\mathbb{R}^2)) \quad \text{and} \quad \partial_t c \in L^2_{loc}((0,\infty); L^2(\mathbb{R}^2)) \ ;$$

$$nc \in L^\infty_{loc}((0,\infty); L^1(\mathbb{R}^2)) \quad \text{and} \quad \int_0^t \int_{\mathbb{R}^2} n |\nabla(\log n - c)|^2 \ dxds < \infty \ ;$$

$$\mathcal{E}(t) + \int_0^t \int_{\mathbb{R}^2} n |\nabla(\log n - c)|^2 \ dxds + \varepsilon \int_0^t \int_{\mathbb{R}^2} |\partial_t c|^2 \ dxds \leq \mathcal{E}(0) \ .$$

*Moreover, $n \in L^\infty_{loc}((0,\infty); L^p(\mathbb{R}^2))$ for any $1 < p < \infty$ (regularizing effect).*

It is possible to weaken assumptions on the chmical concentration $c_0$ in case of $\alpha = 0$ (see Remarks 3.12 and 3.13 for a discussion).

**Theorem 3.2** (Blow-up)**.** *In addition to Theorem 3.1, assume $\varepsilon = 0$, $M > 8\pi$ and that the initial second momentum $\int |x|^2 n_0(x) \ dx$ is finite. There exists a universal constant $\mathcal{C}$ such that solutions blow-up if*

$$\alpha \int |x|^2 n_0(x) \ dx \leq \left( \frac{4(M/8 - \pi)}{\mathcal{C} M^{1/2}} \right)^2 \ .$$

Let us observe that we can adapt Theorem 3.1 and slightly improve the result in [35] (where $\varepsilon = \alpha = 0$) in the sense that we do not require finite second moment of $n_0$, i.e. $n_0 \in L^1(\mathbb{R}^2, |x|^2 dx)$, but the weaker and minimal condition $n_0 \in L^1(\mathbb{R}^2, \log(1+|x|^2)dx)$ for the global existence of weak solution (see Appendix 3.8.3).

The paper is organized as follows. In Section 3.2 we give a set of technical tools to be used in the sequel, and we describe briefly the two alternative strategies for obtaining the required *a priori* estimates. Namely we express the free energy, the dual minimization procedures and the evolution of some momentum of the cell density. In Section 3.3 we derive the key equi-integrability estimate and others from the so-called Onofri inequality on the whole space $\mathbb{R}^2$ in both cases $\alpha > 0$ and $\alpha = 0$. In section 3.4 we re-derive those estimates thanks to a dual strategy based on the logarithmic Hardy-Littlewood-Sobolev inequality. Section 3.5 is devoted to the proof of the regularizing effect acting on the solutions. Section 3.6 is a short description of the regularization procedure which leads to the rigorous proof of global existence

when combined with the *a priori* estimates derived in Sections 3.3 and 3.4. Blow-up of the solutions in the special case $\varepsilon = 0$ is shown for a super-critical mass in Section 3.7 under a smallness assumption on $\alpha \int |x|^2 n_0(x)\ dx$. Finally, several complementary results are given in the Appendix (Section 3.8).

In the sequel, we will denote by $C$ every positive constants that may vary from line to line in the computations. Only the dependence on crucial parameters will be written explicitly.

## 3.2 The free energy and the moments control

It is well known that system (3.1) is equipped with the following *free energy functional*

$$\mathcal{E}(t) = \int_{\mathbb{R}^2} n(x,t) \log n(x,t)\ dx - \int_{\mathbb{R}^2} n(x,t)c(x,t)\ dx + \frac{1}{2}\int_{\mathbb{R}^2} |\nabla c(x,t)|^2\ dx + \frac{\alpha}{2}\int_{\mathbb{R}^2} c^2(x,t)\ dx\ . \quad (3.2)$$

In the kinetic equation literature, the first term $\int_{\mathbb{R}^2} n(x,t)\log n(x,t)\ dx$ is usually referred to as the physical entropy. However, here it will be more convenient and natural to define the *entropy* in the line of [58] as

$$E(n;c)(t) = \int_{\mathbb{R}^2} (n(x,t)\log n(x,t) - n(x,t)c(x,t))\ dx\ , \quad (3.3)$$

including also the potential energy term $\int_{\mathbb{R}^2} n(x,t)c(x,t)dx$. On the other hand, the potential energy term has also to be included in the *chemical energy* associated to the elliptic equation $-\Delta c + \alpha c = n$, i.e.

$$F_\alpha(c;n)(t) = \frac{1}{2}\int_{\mathbb{R}^2} |\nabla c(x,t)|^2\ dx + \frac{\alpha}{2}\int_{\mathbb{R}^2} c^2(x,t)\ dx - \int_{\mathbb{R}^2} n(x,t)c(x,t)\ dx\ , \quad \alpha \geq 0\ . \quad (3.4)$$

Thereby, the free energy $\mathcal{E}(t)$ is a superposition of (3.3) and (3.4) thus reflecting the strongly coupled property of system (3.1). The quantity $\mathcal{E}(t)$ will play a fondamental role in the research of *a priori* estimates starting from the following proposition.

**Proposition 3.3.** *Let $(n,c)$ be any non-negative and sufficiently smooth solution of (3.1) with finite free energy (3.2). Then $\mathcal{E}(t)$ decreases along the trajectories of the dynamical system associated to (3.1), since*

$$\frac{d}{dt}\mathcal{E}(t) = -\int_{\mathbb{R}^2} n(x,t)|\nabla(\log n(x,t) - c(x,t))|^2\ dx - \varepsilon\int_{\mathbb{R}^2} |\partial_t c(x,t)|^2\ dx \leq 0\ . \quad (3.5)$$

*Proof.* The equation on $n$ can be written as $\partial_t n = \nabla\cdot\big(n\nabla(\log n - c)\big)$. Then, using the mass conservation, we obtain

$$\begin{aligned}\int_{\mathbb{R}^2} \partial_t n(x,t)\ (\log n(x,t) - c(x,t))\ dx &= \frac{d}{dt}\int_{\mathbb{R}^2} n(x,t)\log n(x,t)\ dx - \int_{\mathbb{R}^2} \partial_t n(x,t)\ c(x,t)\ dx \\ &= -\int_{\mathbb{R}^2} n(x,t)|\nabla(\log n(x,t) - c(x,t))|^2\ dx\ . \quad (3.6)\end{aligned}$$

On the other hand, testing the equation on $c$ against $\partial_t c$, we have

$$\varepsilon\int_{\mathbb{R}^2} |\partial_t c(x,t)|^2\ dx = -\frac{d}{dt}\int_{\mathbb{R}^2} \frac{|\nabla c(x,t)|^2}{2}\ dx + \int_{\mathbb{R}^2} n(x,t)\ \partial_t c(x,t)\ dx - \alpha\frac{d}{dt}\int_{\mathbb{R}^2} \frac{c^2(x,t)}{2}\ dx\ . \quad (3.7)$$

We conclude by summing (3.6) and (3.7). □

Equation (3.5) measures the dissipation of the free energy due to the *entropy production* term

$$I(t) = \int_{\mathbb{R}^2} n(x,t)|\nabla(\log n(x,t) - c(x,t))|^2\ dx\ , \quad (3.8)$$

and to the chemical production term $\varepsilon\int_{\mathbb{R}^2} |\partial_t c(x,t)|^2\ dx$. Let us observe however that any weak solution of (3.1) is not expected to satisfy (3.5) but the inequality

$$\mathcal{E}(t) + \int_0^t\int_{\mathbb{R}^2} n(x,s)|\nabla(\log n(x,s) - c(x,s))|^2\ dxds + \varepsilon\int_0^t\int_{\mathbb{R}^2} |\partial_t c(x,s)|^2\ dxds \leq \mathcal{E}(0)\ , \quad (3.9)$$

as it is under the quasi-stationary hypothesis $\varepsilon = \alpha = 0$ (see [35]).

The time-monotonicity of $\mathcal{E}(t)$ given by (3.5) provides us with an upper control of the entropy (3.3). But a control from below of the entropy is also needed in order to obtain *a priori* estimates on the solution and then the global existence result. In the case of the parabolic-parabolic system (3.1) on a bounded domain $\Omega \subset \mathbb{R}^2$, the strategy usually followed makes use essentially of two primary tools: a minimization principle with respect to $n$ of the entropy $E(n;c)$ and the Moser-Trudinger inequality. Moreover, their combination gives the *a priori* estimates under the exact critical mass value for $M$ (see [28], [50], [107], [190]).

Concerning system (3.1) in the whole space $\mathbb{R}^2$ under interest, the first result we give here is that the same method above can be followed. However, in order to do so, one has firstly to reinforce the space decay of $c$ as $|x| \to +\infty$ in order to minimize the entropy $E(n;c)$ with respect to $n$ and secondly to employ an ad-hoc Moser-Trudinger type inequality, i.e. the Onofri inequality [196].

The second result is that an alternative strategy, "dual" in some sense to the previous one, can be also adopted. The technical tools to be employed are: the minimization with respect to $c$ of the chemical energy $F_\alpha(c;n)$ (3.4) and the logarithmic Hardy-Littlewood-Sobolev inequality (HLS in the sequel, see Lemma 3.14 and [56]) if $\alpha = 0$, or a modified version of this inequality if $\alpha > 0$ (see Lemma 3.15). This method is new and it is somewhat the extension to the parabolic-parabolic system (3.1) of what was done in [35] for the parabolic-elliptic system (3.1) with $\varepsilon = \alpha = 0$. Indeed, in this case the free energy reads as

$$\mathcal{E}(t) = \int_{\mathbb{R}^2} n(x,t) \log n(x,t)\ dx - \frac{1}{2}\int_{\mathbb{R}^2} n(x,t)c(x,t)\ dx\ , \tag{3.10}$$

with the concentration of the chemical given by $c(x,t) = -\frac{1}{2\pi}\int_{\mathbb{R}^2} \log|x-y| n(y,t)\ dy$, and hence it is well adapted to apply the HLS inequality.

No matter of the method followed to obtain the necessary *a priori* estimates, we are in any case lead to consider the following modified free energy functional

$$\mathcal{E}_H(t) = \mathcal{E}(t) - \int_{\mathbb{R}^2} n(x,t)\log H(x)\ dx = E(n; c+\log H) + \frac{1}{2}\int_{\mathbb{R}^2} |\nabla c(x,t)|^2\ dx + \frac{\alpha}{2}\int_{\mathbb{R}^2} c^2(x,t)\ dx\ , \tag{3.11}$$

where

$$H(x) = \frac{1}{\pi}\frac{1}{(1+|x|^2)^2} \tag{3.12}$$

has been chosen so that $\mathcal{J}_{\mathcal{S}} := 4\pi H$ is the Jacobian of the usual stereographic projection on the sphere $\mathcal{S} : \mathbb{R}^2 \cup \{\infty\} \to \mathbb{S}^2$ and $\int_{\mathbb{R}^2} H(x)dx = 1$, (see [168]).

The introduction of the function $H$ will appear to the reader more natural in Sections 3.3 and 3.4 where the two methods will be developed respectively. Here, let us observe that, by opposition to $\mathcal{E}(t)$, the functional $\mathcal{E}_H(t)$ is not time decreasing. However, we can control its time-growth by the following computation. We have

$$\begin{aligned}
\frac{d}{dt}\int_{\mathbb{R}^2} n(x,t)\log H(x)\ dx &= -\int_{\mathbb{R}^2} n(x,t)\nabla \log H(x)\cdot\nabla(\log n(x,t) - c(x,t))\ dx \\
&= 2\int_{\mathbb{R}^2} n(x,t)\nabla\log(1+|x|^2)\cdot\nabla(\log n(x,t) - c(x,t))\ dx
\end{aligned}$$

and using equation (3.5), we easily obtain

$$\begin{aligned}
\frac{d}{dt}\mathcal{E}_H(t) &= -\int_{\mathbb{R}^2} n(x,t)|\nabla(\log n(x,t) - c(x,t))|^2\ dx - \varepsilon\int_{\mathbb{R}^2}|\partial_t c(x,t)|^2\ dx \\
&\qquad -2\int_{\mathbb{R}^2} n(x,t)\nabla\log(1+|x|^2)\cdot\nabla(\log n(x,t) - c(x,t)) \\
&= -\int_{\mathbb{R}^2} n(x,t)|\nabla(\log n(x,t) - c(x,t) + \log(1+|x|^2))|^2\ dx - \varepsilon\int_{\mathbb{R}^2}|\partial_t c(x,t)|^2\ dx \\
&\qquad +\int_{\mathbb{R}^2} n(x,t)|\nabla\log(1+|x|^2))|^2\ dx\ ,
\end{aligned}$$

where

$$\int_{\mathbb{R}^2} n(x,t)\left|\nabla \log(1+|x|^2)\right|^2\ dx = \int_{\mathbb{R}^2} \frac{4|x|^2}{(1+|x|^2)^2}\ n(x,t)\ dx \le M\ .$$

As a consequence, $\mathcal{E}_H(t)$ grows at most linearly in time.

Before concluding this preliminary section, we state the minimization lemmas for the entropy and the chemical energy respectively. Moreover, we derive also some bounds for the moments of the density $n$ in term of the entropy production (3.8) that is shown to be locally integrable in time in the sequel (see Theorem 3.8).

**Lemma 3.4** (The entropy minimization)**.** *Let $\psi$ be any function such that $e^\psi \in L^1(\mathbb{R}^2)$ and denote $\overline{n} = Me^\psi\Big(\int_{\mathbb{R}^2} e^\psi\ dx\Big)^{-1}$, with $M$ a positive arbitrary constant. Let $E\ :\ L^1_+(\mathbb{R}^2) \to \mathbb{R}\cup\{\infty\}$ be the entropy functional*

$$E(n;\psi) = \int_{\mathbb{R}^2} (n(x)\log n(x) - n(x)\psi(x))\ dx$$

*and $RE\ :\ L^1_+(\mathbb{R}^2) \to \mathbb{R}\cup\{\infty\}$*

$$RE(n|\overline{n}) = \int_{\mathbb{R}^2} n(x)\log\big(n(x)/\overline{n}(x)\big)\ dx$$

*the relative (to $\overline{n}$) entropy. Then, $E(n;\psi)$ and $RE(n|\overline{n})$ are finite or infinite in the same time and for all $n$ in the set $\mathcal{U} = \{n\in L^1_+(\mathbb{R}^2)\ ,\ \int_{\mathbb{R}^2} n(x)\ dx = M\}$ it holds true that*

$$E(n;\psi) - E(\overline{n};\psi) = RE(n|\overline{n}) \ge 0\ . \tag{3.13}$$

The entropy minimization Lemma 3.4 is now a classical lemma and the proof can be found for exemple in [58], where a more general class of entropy functionals including $E(n;\psi)$ is considered. Anyway, being this lemma of primary importance and for the sake of completeness, we will give the proof in the appendix 3.8.1.

**Lemma 3.5** (The chemical energy minimization)**.** *Assume $\alpha \ge 0$ and let $f\in L^1_+(\mathbb{R}^2)$ such that $f\log f \in L^1(\mathbb{R}^2)$ and $\int_{\mathbb{R}^2} f(x)\ dx = M$. In case of $\alpha = 0$, assume in addition that $f\in L^1(\mathbb{R}^2, \log(1+|x|^2)dx)$. Finally, let us denote*

$$\overline{c}(x) = \begin{cases} (B_\alpha * f)(x) & \text{if } \alpha > 0\ , \\ (E_2 * (f - MH))(x) & \text{if } \alpha = 0\ , \end{cases} \tag{3.14}$$

*where $*$ is the space convolution, $B_\alpha$ denotes the Bessel kernel $B_\alpha(z) = \frac{1}{4\pi}\int_0^{+\infty} \frac{1}{t}\ e^{-\frac{|z|^2}{4t} - \alpha t}\ dt$ and $E_2(z) = -\frac{1}{2\pi}\log|z|$ is the fundamental solution of the Laplace's equation in $\mathbb{R}^2$. Then, $\nabla\overline{c}\in L^2(\mathbb{R}^2)$ with*

$$\nabla\overline{c}(x) = \begin{cases} (\nabla B_\alpha * f)(x) & \text{if } \alpha > 0\ , \\ (\nabla E_2 * (f - MH))(x) & \text{if } \alpha = 0\ . \end{cases} \tag{3.15}$$

*Moreover, it holds true that*

$$F_\alpha(c;f) - F_\alpha(\overline{c};f) = \frac{1}{2}\int_{\mathbb{R}^2} |\nabla(c-\overline{c})(x)|^2\ dx + \frac{\alpha}{2}\int_{\mathbb{R}^2} (c-\overline{c})^2(x)\ dx \ge 0\ , \tag{3.16}$$

*if $\alpha > 0$ and*

$$F_\alpha(c;f-MH) - F_\alpha(\overline{c};f-MH) = \frac{1}{2}\int_{\mathbb{R}^2} |\nabla(c-\overline{c})(x)|^2\ dx \ge 0\ , \tag{3.17}$$

*if $\alpha = 0$.*

Let us observe that whenever $f\in L^2(\mathbb{R}^2)$ in (3.14) the chemical energy minimization Lemma 3.5 can be obtained easily applying the variational method, at least for $\alpha > 0$. However, we want to use here minimal hypotheses on $f$ and therefore the proof becomes a little more technical, expecially when $\alpha = 0$. Again, for the sake of completeness, the proof is given in appendix 3.8.2

**Lemma 3.6** (Moment Lemma)**.** *Let $c$ be a given smooth function. Let $n$ be any non-negative and sufficiently smooth solution of $\partial_t n = \Delta n - \nabla\cdot(n\nabla c)$, with fast decay at infinity and total mass $M$. Then, for any $\delta > 0$, we have the following bounds for the evolution of the moments of $n$:*

$$\int_{\mathbb{R}^2} n(x,t)\log(1+|x|^2)\,dx \le \int_{\mathbb{R}^2} n_0(x)\log(1+|x|^2)\,dx + \frac{M}{2\delta}t + \frac{\delta}{2}\int_0^t\int_{\mathbb{R}^2} n(x,s)|\nabla(\log n(x,s) - c(x,s))|^2\,dxds\ ; \tag{3.18}$$

$$\int_{\mathbb{R}^2} |x| n(x,t)\,dx \le \int_{\mathbb{R}^2} |x| n_0(x)\,dx + \frac{M}{2\delta}t + \frac{\delta}{2}\int_0^t\int_{\mathbb{R}^2} n(x,s)|\nabla(\log n(x,s) - c(x,s))|^2\,dxds\ ; \tag{3.19}$$

$$\int_{\mathbb{R}^2} |x|^2 n(x,t)\,dx \le 2\int_{\mathbb{R}^2} |x|^2 n_0(x)\,dx + 2\,t\int_0^t\int_{\mathbb{R}^2} n(x,s)|\nabla(\log n(x,s) - c(x,s))|^2\,dxds\ . \tag{3.20}$$

*Proof.* Writing the equation on $n$ as $\partial_t n = \nabla\cdot\big(n\nabla(\log n - c)\big)$, it follows that

$$\begin{aligned}\frac{d}{dt}\int_{\mathbb{R}^2} n(x,t)\phi(x)\,dx &= -\int_{\mathbb{R}^2} n(x,t)\nabla\phi(x)\cdot\nabla(\log n(x,t) - c(x,t))\,dx \\ &\le \frac{1}{2\delta}\int_{\mathbb{R}^2}\big|\nabla\phi(x)\big|^2 n(x,t)\,dx + \frac{\delta}{2}\int_{\mathbb{R}^2} n(x,t)|\nabla(\log n(x,t) - c(x,t))|^2\,dx\ ,\end{aligned}$$

with $\delta > 0$ arbitrary. Taking successively $\phi(x) = \log(1+|x|^2)$ and $\phi(x) = |x|$, observing that with the first choice of $\phi$ we have

$$|\nabla\phi(x)| = \left|\frac{2x}{1+|x|^2}\right| \le 1\ ,$$

and using the mass conservation property, inequlities (3.18) and (3.19) are proved. Inequality (3.20) follows in a similar way since for $\phi(x) = |x|^2$ it holds true that

$$\begin{aligned}\frac{d}{dt}\int_{\mathbb{R}^2} |x|^2 n(x,t)\,dx &= -2\int_{\mathbb{R}^2} n(x,t)\ x\cdot\nabla(\log n(x,t) - c(x,t))\,dx \\ &\le 2\left(\int_{\mathbb{R}^2} |x|^2 n(x,t)\,dx\right)^{1/2}\left(\int_{\mathbb{R}^2} n(x,t)|\nabla(\log n(x,t) - c(x,t))|^2\,dx\right)^{1/2}\ .\end{aligned} \tag{3.21}$$

Thereby, integrating (3.21), we obtain

$$\begin{aligned}\int_{\mathbb{R}^2} |x|^2 n(x,t)\,dx &\le \left[\left(\int_{\mathbb{R}^2} |x|^2 n_0(x)\,dx\right)^{1/2} + \int_0^t\left(\int_{\mathbb{R}^2} n(x,s)|\nabla(\log n(x,s) - c(x,s))|^2\,dx\right)^{1/2} ds\right]^2 \\ &\le 2\int_{\mathbb{R}^2} |x|^2 n_0(x)\,dx + 2\,t\int_0^t\int_{\mathbb{R}^2} n(x,s)|\nabla(\log n(x,s) - c(x,s))|^2\,dx\,ds\ ,\end{aligned}$$

and the lemma is proved.

□

The proof of the previous lemma is based uniquely on the equation on $n$ and on the specific expression of the weight function defining the moment. The evolution followed by $c$ doesn't play any role and the lemma holds true also for the (PKS) system with non-negative coefficients $\varepsilon$, $\eta$ and $\alpha$. Of course, one can estimate the evolution of other moments than those considered in the lemma. Here we have considered the most useful and used. In particular, the local in time bound of the weighted $L^1(\mathbb{R}^2, \log(1+|x|^2)dx)$ norm of $n$ will be of primary importance to obtain the key *a priori* bounds and the key equi-integrability of $n$ giving the global existence with a regularizing effect.

## 3.3 *A priori* estimates from the Moser-Trudinger-Onofri inequality

In [196] Onofri obtained the following sharp inequality on the sphere $\mathbb{S}^2$

$$\int_{\mathbb{S}^2} e^{v(s)}\, ds \leq \exp\left\{\int_{\mathbb{S}^2}\left(v(s)+\frac{1}{4}|\nabla_0 v(s)|^2\right)\, ds\right\}\,, \tag{3.22}$$

for all functions $v \in L^1(\mathbb{S}^2, ds)$ such that $|\nabla_0 v| \in L^2(\mathbb{S}^2, ds)$. Here, $ds$ is the uniform normalized surface measure on $\mathbb{S}^2$ so that $\int_{\mathbb{S}^2}\, ds = 1$. Moreover $\nabla_0$ is the covariant gradient with respect to the metric $ds_0^2 = d\theta^2 + \sin^2\theta\, d\phi^2$, $(\theta, \phi)$ being the polar coordinates, i.e.

$$|\nabla_0 v|^2 = \left(\frac{\partial v}{\partial \theta}\right)^2 + (\sin\theta)^{-2}\left(\frac{\partial v}{\partial \phi}\right)^2\,.$$

With the help of the stereographic projection $\mathcal{S}$, the same inequality can be stated equivalently on $\mathbb{R}^2$ as follows

**Lemma 3.7** (Onofri inequality in $\mathbb{R}^2$)**.** *Let $H$ be defined as in (3.12). Then*

$$\int_{\mathbb{R}^2} e^{u(x)}H(x)\, dx \leq \exp\left\{\int_{\mathbb{R}^2} u(x)H(x)\, dx + \frac{1}{16\pi}\int_{\mathbb{R}^2}|\nabla u(x)|^2\, dx\right\}\,, \tag{3.23}$$

*for all functions $u \in L^1(\mathbb{R}^2, H(x)dx)$ such that $|\nabla u(x)| \in L^2(\mathbb{R}^2, dx)$.*

*Proof.* It is sufficient to apply the Onofri inequality (3.22) to the function $e^{\tilde{u}}$ with $\tilde{u} = u \circ \mathcal{S}^{-1}$ and we get

$$\begin{aligned}\int_{\mathbb{R}^2} e^{u(x)}H(x)\, dx = \int_{\mathbb{S}^2} e^{\tilde{u}(s)}\, ds \quad &\leq \quad \exp\left\{\int_{\mathbb{S}^2}\left(\tilde{u}(s)+\frac{1}{4}|\nabla_0\tilde{u}(s)|^2\right)\, ds\right\}\\ &= \quad \exp\left\{\int_{\mathbb{R}^2} u(x)H(x)\, dx + \frac{1}{16\pi}\int_{\mathbb{R}^2}|\nabla u(x)|^2\, dx\right\}\,,\end{aligned}$$

since $|\nabla_0\tilde{u}(s)|^2 = (4\pi H(x))^{-1}|\nabla u(x)|^2$ and $ds = H(x)dx$.

□

Thanks to inequality (3.23), we are now able to follow the first strategy giving *a priori* estimates, namely the minimization of $\mathcal{E}(t)$ with respect to $n$. More precisely, first we apply the entropy minimization Lemma 3.4 with $\psi = c + \log H$ and then we make use of the Onofri inequality (3.23) with $u = c$. Working in this way, we are able to obtain the optimal threshold value, namely $8\pi$, for the mass $M$. Observe that this is the same threshold as the one obtained in [35] for the parabolic-elliptic (PKS) system with $\varepsilon = \alpha = 0$ over $\mathbb{R}^2$, as it would be expected. Moreover, we optimize the result given in [188], where the author obtained the global existence of non-negative solutions $(n, c)$ of (3.1) over $\mathbb{R}^2$ under the smallness condition $M < 4\pi$. This is due to the fact that in [188] the author use a Brezis-Merle type inequality for the heat equation on $\mathbb{R}^2$ instead of a Moser-Trudinger type inequality as (3.23).

We give the announced estimates first formally in the following Theorem. The procedure leading to the rigorous existence result will be given later in Section 3.6.

**Theorem 3.8.** *Under the same hypotheses as Theorem 3.1, we have that $n\log n \in L^\infty(0,T;L^1(\mathbb{R}^2))$, $n \in L^\infty(0,T;L^1(\mathbb{R}^2, \log(1+|x|^2)dx))$, for any $T > 0$, and the following a priori estimates hold true for all $t > 0$ :*

*(i)* $\int_{\mathbb{R}^2} n(x,t)(\log n(x,t))_+\, dx \leq C(1+t)$ ;

*(ii)* $\int_{\mathbb{R}^2} n(x,t)c(x,t)\, dx \leq C(1+t)$ ;

*(iii)* $\|c(t)\|^2_{H^1(\mathbb{R}^2)} \leq C(1+t)$ *if* $\alpha > 0$ , *and* $\|\nabla c(t)\|^2_{L^2(\mathbb{R}^2)} \leq C(1+t)$ *if* $\alpha = 0$ ;

*(iv)* $\mathcal{E}(t) \geq -C(1+t)$ ;
*(v)* $\mathcal{E}_H(t) \geq -C(M,\alpha)$ *if* $\alpha > 0$ *, and* $\mathcal{E}_H(t) \geq -C(1+t)$ *if* $\alpha = 0$ ;
*(vi)* $\int_0^t \int_{\mathbb{R}^2} n(x,s)|\nabla(\log n(x,s) - c(x,s))|^2 \, dxds \leq \mathcal{E}(0) + 2\int_{\mathbb{R}^2} n_0(x)\log(1+|x|^2)dx + C(1+t)$ ;
*(vii)* $\varepsilon \int_0^t \int_{\mathbb{R}^2} |\partial_t c(x,s)|^2 \, ds \leq C(1+t)$ .

*Proof.* Let us consider first the case $\alpha > 0$. Let $\delta > 0$ and $\tilde{\delta} > 0$ to be chosen later and let us define $\overline{n} = Me^{(1+\delta)c(x,t)}H(x)\left(\int_{\mathbb{R}^2} e^{(1+\delta)c(x,t)}H(x)\, dx\right)^{-1}$. We observe that, thanks to the Onofri inequality (3.23), it is sufficient to have $c(t) \in H^1(\mathbb{R}^2)$ in order to have $\overline{n}$ well defined and $\overline{n}(t) \in L^1(\mathbb{R}^2)$. Then, we can apply the Entropy Lemma 3.4 with $\psi = (1+\delta)c + \log H$ to obtain

$$E(n;(1+\delta)c+\log H) \geq E(\overline{n};(1+\delta)c+\log H) = M\log M - M\log\left(\int_{\mathbb{R}^2} e^{(1+\delta)c(x,t)}H(x)\, dx\right). \quad (3.24)$$

Furthermore, applying Lemma 3.7 with $u = (1+\delta)c$ to the last term in the right hand side of (3.24), we have for the modified free energy functional $\mathcal{E}_H(t)$ (3.11),

$$\begin{aligned}
\mathcal{E}_H(t) &= E(n;(1+\delta)c+\log H) + \delta\int_{\mathbb{R}^2} n(x,t)c(x,t)\, dx + \frac{1}{2}\int_{\mathbb{R}^2}|\nabla c(x,t)|^2\, dx + \frac{\alpha}{2}\int_{\mathbb{R}^2} c^2(x,t)\, dx \\
&\geq M\log M + \frac{1}{2}\left(1 - M\frac{(1+\delta)^2}{8\pi}\right)\int_{\mathbb{R}^2}|\nabla c(x,t)|^2\, dx - M(1+\delta)\int_{\mathbb{R}^2} c(x,t)H(x)\, dx \\
&\quad +\delta\int_{\mathbb{R}^2} n(x,t)c(x,t)\, dx + \frac{\alpha}{2}\int_{\mathbb{R}^2} c^2(x,t)\, dx \qquad (3.25) \\
&\geq \frac{1}{2}\left(1 - M\frac{(1+\delta)^2}{8\pi}\right)\int_{\mathbb{R}^2}|\nabla c(x,t)|^2\, dx + \left(\frac{\alpha}{2} - M(1+\delta)\frac{\tilde{\delta}}{2}\right)\int_{\mathbb{R}^2} c^2(x,t)\, dx + M\log M \\
&\quad +\delta\int_{\mathbb{R}^2} n(x,t)c(x,t)\, dx - M(1+\delta)\frac{1}{2\tilde{\delta}}\int_{\mathbb{R}^2} H^2(x)\, dx\ . \qquad (3.26)
\end{aligned}$$

Next, we choose $\delta > 0$ small enough such that $M < \dfrac{8\pi}{(1+\delta)^2}$ and $\tilde{\delta} > 0$ such that $\alpha > M(1+\delta)\tilde{\delta}$. This is possible because $M$ is less than the critical mass value $8\pi$. As a consequence, since $\mathcal{E}_H(t)$ grows at most linearly, (3.26) gives us (ii), (iii) and (v).

When $\alpha = 0$, we have to estimate differently $\int_{\mathbb{R}^2} c(x)H(x)\, dx$ in (3.25). That can be done using the following identity,

$$\int_{\mathbb{R}^2} c(x,t)\, dx = \frac{1}{\varepsilon}Mt + \int_{\mathbb{R}^2} c_0(x)\, dx \quad (3.27)$$

and the fact that $H$ is bounded.

From now on, let $\alpha \geq 0$. Proposition 3.3 , the Moment Lemma 3.6 and the definition (3.12) of $H$ give us the following estimate

$$\begin{aligned}
\int_0^t\int_{\mathbb{R}^2} n(x,s)|\nabla(\log n(x,s) - c(x,s))|^2\, dxds &\leq \mathcal{E}(0) - \mathcal{E}(t) = \mathcal{E}(0) - \mathcal{E}_H(t) - \int_{\mathbb{R}^2} n(x,t)\log H(x)\, dx \\
&= \mathcal{E}(0) - \mathcal{E}_H(t) + M\log\pi + 2\int_{\mathbb{R}^2} n(x,t)\log(1+|x|^2)\, dx \\
&\leq \mathcal{E}(0) - \mathcal{E}_H(t) + M\log\pi + 2\int_{\mathbb{R}^2} n_0(x)\log(1+|x|^2)\, dx + \frac{1}{\delta}Mt \\
&\quad +\delta\int_0^t\int_{\mathbb{R}^2} n(x,s)|\nabla(\log n(x,s) - c(x,s))|^2\, dxds\ .
\end{aligned}$$

Choosing $\delta < 1$ and using the lower bound (v) on $\mathcal{E}_H(t)$, we obtain (vi). As a consequence of (vi) and of the Moment Lemma 3.6 again, we have that $n \in L^\infty(0,T;L^1(\mathbb{R}^2,\log(1+|x|^2)dx))$.

In the same way, we obtain (vii) and the lower bound (iv) for the free energy $\mathcal{E}(t)$ since $\varepsilon \int_0^t \int_{\mathbb{R}^2} |\partial_t c(s)|^2 \, ds \leq \mathcal{E}(0) - \mathcal{E}(t)$ and $\mathcal{E}(t) = \mathcal{E}_H(t) + \int_{\mathbb{R}^2} n(x,t) \log H(x) \, dx$.

To conclude it remains to prove (i) and that $n \log n \in L^\infty(0,T;L^1(\mathbb{R}^2))$. This is a straightforward consequence of the following Lemma 3.9. Indeed, from the free energy definition (3.2) and the previous estimates it follows that

$$-C(1+t) \leq \int_{\mathbb{R}^2} n(x,t) \log n(x,t) \, dx \leq C(1+t) \; .$$

**Lemma 3.9** (The mass does not escape in finite time)**.** *Let $f \in L^1_+(\mathbb{R}^2)$, with total mass $\int f(x) \, dx = M$ such that $\int f(x) \log f(x) \, dx < \infty$. The negative contribution of $f \log f$ is controlled by the "logarithmic" momentum:*

$$\int f(x) (\log f(x))_- \, dx \leq (1+\delta) \int f(x) \log(1+|x|^2) \, dx + C \; , \tag{3.28}$$

*for any $\delta > 0$.*

*Proof.* Let us denote $v = f \, \mathbb{1}_{\{f \leq 1\}}$, $m = \int_{\mathbb{R}^2} f(x) \, dx \leq M$, $\psi(x) = -(1+\delta)\log(1+|x|^2)$ with arbitrary $\delta > 0$ such that $e^\psi \in L^1$, and $\overline{v}(x) = m e^{\psi(x)} (\int_{\mathbb{R}^2} e^{\psi(x)} \, dx)^{-1}$. Then, by the entropy minimization Lemma 3.4 we have

$$\begin{aligned} \int_{\mathbb{R}^2} (v(x) \log v(x) - v(x)\psi(x)) \, dx &\geq \int_{\mathbb{R}^2} (\overline{v}(x) \log \overline{v}(x) - \overline{v}(x)\psi(x)) \, dx \\ &= m \log m - m \log \left( \int_{\mathbb{R}^2} \frac{1}{(1+|x|^2)^{1+\delta}} \, dx \right) \; , \end{aligned}$$

which gives (3.28) thanks to

$$\int_{\{f \leq 1\}} f(x) \log(1+|x|^2) \, dx \leq \int_{\mathbb{R}^2} f(x) \log(1+|x|^2) \, dx \; .$$

□

Hence,

$$\begin{aligned} \int_{\mathbb{R}^2} n(x,t) (\log n(x,t))_+ \, dx &= \int_{\mathbb{R}^2} n(x,t) \log n(x,t) \, dx + \int_{\mathbb{R}^2} n(x,t) (\log n(x,t))_- \, dx \\ &\leq C(1+t) + (1+\delta) \int n(x,t) \log(1+|x|^2) \, dx + C \\ &\leq C(1+t) \; . \end{aligned}$$

and we have obtained (i). Finally, the identity

$$\int_{\mathbb{R}^2} |n \log n| \, dx = \int_{\mathbb{R}^2} n \log n \, dx + 2 \int_{\mathbb{R}^2} n(x,t) (\log n(x,t))_- \, dx \; ,$$

gives us, in the same way as before, that $n \log n \in L^\infty(0,T;L^1(\mathbb{R}^2))$.

□

**Remark 3.10.** *We cannot afford the critical mass value $M = 8\pi$ in the previous Theorem. Indeed this necessarily leads to $\delta = 0$ in (3.26). Then one can prove successively estimates (v), $\|c(t)\|^2_{L^2(\mathbb{R}^2)} \leq C(1+t)$ if $\alpha > 0$, (vi), $n \in L^\infty(0,T;L^1(\mathbb{R}^2, \log(1+|x|^2)dx))$, (iv), (vii), but we can't obtain the fundamental estimates (i), (ii) and (iii).*

In the following three remarks we discuss the assumptions that can be imposed to the initial chemical concentration $c_0$ when $\alpha = 0$.

**Remark 3.11.** *In the case $\alpha = 0$, under the stronger hypothesis $c_0 \in H^1(\mathbb{R}^2)$, Theorem 3.8 holds true with the additional estimate $\int_{\mathbb{R}^2} c^2(x,t)\ dx \leq C(1+t+t^2)$ that follows by*

$$\frac{\varepsilon}{2}\int_{\mathbb{R}^2} c^2(x,t)\ dx \leq \frac{\varepsilon}{2}\int_{\mathbb{R}^2} c_0^2(x)\ dx + \int_0^t \int_{\mathbb{R}^2} n(x,t)c(x,t)\ dx\ .$$

**Remark 3.12.** *When $\alpha = 0$, we can use weaker hypothesis on $c_0$ than Theorem 3.1 but strong enough to apply the Onofry inequality (3.23), i.e. $c_0 \in L^1(\mathbb{R}^2, H(x)dx)$. However, we can obtain only estimates exponentially increasing in time. Indeed, using the identity*

$$\varepsilon\frac{d}{dt}\int_{\mathbb{R}^2} c(x,t)H(x)\ dx = \int_{\mathbb{R}^2} c(x,t)\Delta H(x)\ dx + \int_{\mathbb{R}^2} n(x,t)H(x)\ dx$$

*and the computation $\Delta H(x) = \frac{8}{\pi}\left[\frac{2|x|^2-1}{(1+|x|^2)^4}\right]$, we easily have*

$$\varepsilon\frac{d}{dt}\int_{\mathbb{R}^2} c(x,t)H(x)\ dx \leq 4\int_{\mathbb{R}^2} c(x,t)H(x)\ dx + \frac{M}{\pi}\ .$$

*Then,*

$$\int_{\mathbb{R}^2} c(x,t)H(x)\ dx \leq e^{\frac{4}{\varepsilon}t}\left(\int_{\mathbb{R}^2} c_0(x)H(x)\ dx + \frac{M}{4\pi}\right)\ . \tag{3.29}$$

*Injecting (3.29) in (3.26) instead of (3.27), we have the assertion.*

**Remark 3.13.** *In the peculiar case $\alpha = 0$, one can develop another sort of solutions based on the following corrections. In fact it is sufficient to assume that initially $\nabla\left(c_0 + \frac{M}{4\pi}\log(1+|x|^2)\right)$ belongs to $L^2$, and $c_0$ belongs to $L^1(\mathbb{R}^2, H(x)dx)$. This hypothesis is hardly biologically relevant because it breaks the non-negativity assumption on $c_0$.*

*Define the chemical deviation $u(x,t) = c(x,t) - k\log H(x)$, where $k = \frac{M}{8\pi} < 1$ and $\log H$ satisfies the remarkable cancellation property:*

$$\begin{aligned} -\Delta\log H &= 2\Delta\log(1+|x|^2) \\ &= 8\left(\frac{1}{1+|x|^2} - \frac{|x|^2}{(1+|x|^2)^2}\right) \\ &= 8\pi H(x)\ . \end{aligned} \tag{3.30}$$

*The pair $(n,u)$ verifies the system*

$$\left\{\begin{array}{rcl} \partial_t n &=& \Delta n - \nabla\cdot(n\nabla(u + k\log H)) \\ \varepsilon\partial_t u &=& \Delta u + n - MH\ , \end{array}\right. \tag{3.31}$$

*which admits the following free energy:*

$$\begin{aligned} \mathcal{E}_{corr}(t) = \int_{\mathbb{R}^2} n(x,t)\log n(x,t)\ dx - \int_{\mathbb{R}^2} n(x,t)u(x,t)\ dx + \frac{1}{2}\int_{\mathbb{R}^2} |\nabla u(x,t)|^2\ dx \\ -k\int_{\mathbb{R}^2} n(x,t)\log H(x)\ dx + M\int_{\mathbb{R}^2} u(x,t)H(x)\ dx\ . \end{aligned} \tag{3.32}$$

*It is worth noticing that the free energy $\mathcal{E}_{corr}$ is exactly the original free energy $\mathcal{E}$: only the variables have changed and we shall highlight this point by modifying the notation.*

*We next apply the Onofri inequality, with some degree of freedom $\delta > 0$ to be chosen later:*

$$\begin{aligned} &(1-\delta)\int_{\mathbb{R}^2} n(x,t)\log n(x,t)\ dx - (1-\delta)\int_{\mathbb{R}^2} n(x,t)\left(\frac{u(x,t)}{1-\delta} + \log H(x)\right)\ dx \\ &\geq -(1-\delta)M\log\left(\int_{\mathbb{R}^2} e^{u(x,t)/(1-\delta)}H(x)\ dx\right) \\ &\geq -M(1-\delta)\left(\int_{\mathbb{R}^2}\frac{u(x,t)}{1-\delta}H(x)\ dx + \frac{1}{16\pi(1-\delta)^2}\int_{\mathbb{R}^2}|\nabla u(x,t)|^2\ dx\right)\ . \end{aligned}$$

*Plugging this estimate into the corrected free energy* (3.32)*, we deduce,*

$$\begin{aligned}\mathcal{E}_{corr}(t) \;\geq\; & \delta\int_{\mathbb{R}^2} n(x,t)\log n(x,t)\;dx + (1-k-\delta)\int_{\mathbb{R}^2} n(x,t)\log H(x)\;dx \\ & + \frac{1}{2}\left(1-\frac{M}{8\pi(1-\delta)}\right)\int_{\mathbb{R}^2}|\nabla u(x,t)|^2\;dx\;.\end{aligned}$$

*Note that we cannot have simultaneously* $1-k-\delta<0$ *and* $k<1-\delta$*, so that we eventually choose* $\delta>0$ *small enough to ensure both*

$$1-\frac{M}{8\pi(1-\delta)}>0\;,\quad 1-k-\delta>0\;.$$

*The bootstrap argument goes as previously: from Lemma 3.6 we obtain*

$$\begin{aligned}&\int_0^t\int_{\mathbb{R}^2} n(x,s)|\nabla(\log n(x,s)-c(x,s))|^2\;dxds\\ &\quad\le \mathcal{E}_{corr}(0)-\mathcal{E}_{corr}(t)\\ &\quad\le \mathcal{E}_{corr}(0)-\delta\int_{\mathbb{R}^2} n(x,t)\log n(x,t)\;dx-\frac{1}{2}\left(1-\frac{M}{8\pi(1-\delta)}\right)\int_{\mathbb{R}^2}|\nabla u(x,t)|^2\;dx\\ &\qquad+2(1-k-\delta)\int_{\mathbb{R}^2} n(x,t)\log(1+|x|^2)\;dx\\ &\quad\le \mathcal{E}_{corr}(0)-\delta\int_{\mathbb{R}^2} n(x,t)\log n(x,t)\;dx-\frac{1}{2}\left(1-\frac{M}{8\pi(1-\delta)}\right)\int_{\mathbb{R}^2}|\nabla u(x,t)|^2\;dx\\ &\qquad+2(1-k-\delta)\int_{\mathbb{R}^2} n_0(x,t)\log(1+|x|^2)\;dx+\frac{M2(1-k-\delta)}{2}t\\ &\qquad+(1-k-\delta)\int_0^t\int_{\mathbb{R}^2} n(x,s)|\nabla(\log n(x,s)-c(x,s))|^2\;dxds\;.\end{aligned}$$

*We can summarize the above computations into the following almost complete* a priori *bound*

$$\begin{aligned}&\delta\int_{\mathbb{R}^2} n(x,t)\log n(x,t)\;dx+\frac{1}{2}\left(1-\frac{M}{8\pi(1-\delta)}\right)\int_{\mathbb{R}^2}|\nabla u(x,t)|^2\;dx\\ &+(k+\delta)\int_0^t\int_{\mathbb{R}^2} n(x,s)|\nabla(\log n(x,s)-c(x,s))|^2\;dxds\\ &\qquad\le \mathcal{E}_{corr}(0)+2(1-k-\delta)\int_{\mathbb{R}^2} n_0(x,t)\log(1+|x|^2)\;dx+M(1-k-\delta)t\;.\end{aligned}$$

*In fact one should also take into account the negative contribution* $\int_{\mathbb{R}^2} n(x,t)(\log n(x,t))_-\;dx$ *when mass escapes to infinity. This can be done in the same time using the momentum* $\int_{\mathbb{R}^2} n(x,t)\log(1+|x|^2)\;dx$ *and Lemma 3.9, but we do not want to enter too much into technical details here.*

*Concluding this remark, let us emphasize that the technical difficulty arising from evaluating the integral* $\int_{\mathbb{R}^2} c(x,t)H(x)\;dx$ *in* (3.25) *– which can be resolved by playing with hypotheses on the initial data* $c_0$ *– can also be resolved by assuming that the deviation* $\nabla\left(c_0+\frac{M}{4\pi}\log(1+|x|^2)\right)$ *belongs to* $L^2$ *(as well as* $c_0$ *belongs to* $L^1(\mathbb{R}^2,H(x)dx)$*). This is motivated by the long time asymptotics. Indeed one expect at the limit to deal with* $\nabla\bar{u}=\nabla E_2*(n-MH)$ *which lies in* $L^2$ *thanks to the tails' correction (see Section 3.4).*

## 3.4 *A priori* estimates from the logarithmic HLS inequality

a strategy dual to the previous one, starting from minimizing the modified free energy functional $\mathcal{E}_H(t)$ with respect to $c$. The role of the Onofri inequality (3.23) will be played by the logarithmic HLS inequality below when $\alpha=0$ and its generalization to the Bessel kernel $B_\alpha$ when $\alpha>0$ (see Lemma 3.15). Therefore, the cases $\alpha>0$ and $\alpha=0$ have to be treated separately again.

**Lemma 3.14** (Logarithmic Hardy-Littlewood-Sobolev inequality in $\mathbb{R}^2$)**.** *For all non-negative functions $f \in L^1(\mathbb{R}^2)$ such that $\int_{\mathbb{R}^2} f(x)\,dx = M$, $f\log f \in L^1(\mathbb{R}^2)$ and $\int_{\mathbb{R}^2} f(x)\log(1+|x|^2)\,dx < \infty$, the following inequality holds true*

$$-\int_{\mathbb{R}^2}\int_{\mathbb{R}^2} f(x)\log|x-y|f(y)\,dxdy \le \frac{M}{2}\int_{\mathbb{R}^2} f(x)\log f(x)\,dx + C(M)\ . \tag{3.33}$$

The proof of Lemma 3.14 can be found for example in [56]. Let us observe here that inequality (3.33) can be written equivalently on $\mathbb{S}^2$. The logarithmic HLS inequality is dual to the Onofri inequality (3.22) in the sense that extremal functions for one inequality determine extremal functions for the other inequality (see [23], [56]). As an exemple of this kind of duality results, we show in the appendix 3.8.4 how one can obtain directly inequality (3.34) from the Onofri inequality on $\mathbb{R}^2$ (3.23).

The generalization of inequality (3.33) to the Bessel kernel $B_\alpha$ is the following. For other extensions of Lemma 3.14 see [23].

**Lemma 3.15.** *For all non-negative functions $f \in L^1(\mathbb{R}^2)$ such that $\int_{\mathbb{R}^2} f(x)\ dx = M$, $f\log f \in L^1(\mathbb{R}^2)$ and $\int_{\mathbb{R}^2} f(x)\log(1+|x|^2)\,dx < \infty$, the following inequality holds true*

$$\int_{\mathbb{R}^2}\int_{\mathbb{R}^2} f(x)B_\alpha(x-y)f(y)\,dx\,dy \le \frac{M}{4\pi}\int_{\mathbb{R}^2} f(x)\log f(x)\,dx + \frac{M}{2\pi}\int_{\mathbb{R}^2} f(x)\log(1+|x|^2)\,dx + C(M). \tag{3.34}$$

**Remark 3.16.** *The reason why the "logarithmic" momentum comes into the game in* (3.34) *is that the balance between the singularity at zero of the kernel and its tail arising in* (3.33) *has been broken by the Bessel potential $B_\alpha$, which is exponentially decreasing for large $|x|$. As a counterpart one has to control the decay of $f$ at infinity.*

*Proof.* The Bessel kernel $B_\alpha$ is a positive radial decreasing function such that $B_\alpha(z) \to +\infty$ when $|z| \to 0$ as $\frac{1}{2\pi}\log\left(\frac{1}{|z|}\right) + O(1)$. We only prove below the upper side of this asymptotic estimate, which is sufficient for our purpose. Indeed, following [88], $B_\alpha$ can be written as the sum of the three integrals $\int_0^{r^2} + \int_{r^2}^1 + \int_1^{+\infty}$ , with $r = |z| < 1$. For the first and third integrals we have respectively

$$\frac{1}{4\pi}\int_0^{r^2}\frac{1}{t}\ e^{-\frac{r^2}{4t}-\alpha t}\ dt \le \frac{1}{4\pi}\int_0^{r^2}\frac{1}{t}\ e^{-\frac{r^2}{4t}}\ dt = \frac{1}{4\pi}\int_{\frac14}^{+\infty}\frac{e^{-y}}{y}\ dy < \infty$$

and

$$\frac{1}{4\pi}\int_1^{+\infty}\frac{1}{t}\ e^{-\frac{r^2}{4t}-\alpha t}\ dt \le \frac{1}{4\pi}\int_1^{+\infty} e^{-\alpha t}\ dt < \infty\ .$$

The second integral satisfies

$$\frac{1}{4\pi}e^{-(\alpha+\frac14)}\log\left(\frac{1}{r^2}\right) \le \frac{1}{4\pi}\int_{r^2}^1\frac{1}{t}\ e^{-\frac{r^2}{4t}-\alpha t}\ dt \le \frac{1}{4\pi}e^{-r^2(\alpha+\frac14)}\log\left(\frac{1}{r^2}\right)\ . \tag{3.35}$$

As a consequence of (3.35), $\lim_{|z|\to 0} B_\alpha(z) = +\infty$ and

$$\begin{aligned}\int_{\mathbb{R}^2}\int_{\mathbb{R}^2} f(x)B_\alpha(x-y)f(y)\,dx\,dy \ &\le\ \int_{\mathbb{R}^2}\int_{|x-y|\le 1} f(x)\left(C - \frac{1}{2\pi}\log|x-y|\right)f(y)\,dx\,dy \\ &\quad + \int_{\mathbb{R}^2}\int_{|x-y|>1} f(x)B_\alpha(x-y)f(y)\,dx\,dy \\ &\le\ CM^2 - \frac{1}{2\pi}\int_{\mathbb{R}^2}\int_{\mathbb{R}^2} f(x)\log|x-y|f(y)\,dx\,dy \\ &\quad + \frac{1}{2\pi}\int_{\mathbb{R}^2}\int_{|x-y|>1} f(x)\log|x-y|f(y)\,dx\,dy\ .\end{aligned}$$

Using the inequality

$$\log|x-y| \le \frac{1}{2}\log 2 + \frac{1}{2}\log(1+|x|^2) + \frac{1}{2}\log(1+|y|^2)\ , \tag{3.36}$$

it follows that

$$\frac{1}{2\pi}\int_{\mathbb{R}^2}\int_{|x-y|>1} f(x)\log|x-y|f(y)\,dx\,dy \le CM^2 + \frac{M}{2\pi}\int_{\mathbb{R}^2} f(x)\log(1+|x|^2)\ dx\ .$$

Applying the logarithmic HLS inequality (3.33), we obtain (3.34).

□

*Proof of Theorem 3.8.* We first consider the case $\alpha > 0$. Let $0 < \delta < 1$ to be chosen later and let $\overline{c}$ be the quasi-stationary state (3.14) corresponding to $(1-\delta)^{-1}n$. Then, applying the minimization Lemma 3.5 the chemical energy (3.4) satisfies

$$F_\alpha\left(c;\frac{n}{1-\delta}\right) \ge F_\alpha\left(\overline{c};\frac{n}{1-\delta}\right) = -\frac{1}{2(1-\delta)}\int_{\mathbb{R}^2} n(x,t)\overline{c}(x,t)\ dx\ , \quad \alpha>0\ . \tag{3.37}$$

This is always possible whenever $c-\overline{c}$ belongs to $H^1(\mathbb{R}^2)$. Recall that $\overline{c}(t)$ is defined by $B_\alpha * n(t)/(1-\delta)$, so that $\nabla\overline{c}(t)\in L^2$ as soon as $n(t)\log n(t)\in L^1$ is finite (see also Appendix 3.8.2) . Next, from (3.37) and Lemma 3.15 we obtain

$$\begin{aligned}
\mathcal{E}(t) &= \int_{\mathbb{R}^2} n(x,t)\log n(x,t)\ dx + (1-\delta)F_\alpha\left(c;\frac{n}{1-\delta}\right) + \delta\left(\frac{1}{2}\int_{\mathbb{R}^2}|\nabla c(x,t)|^2\ dx + \frac{\alpha}{2}\int_{\mathbb{R}^2} c^2(x,t)\ dx\right)\\
&\ge \int_{\mathbb{R}^2} n(x,t)\log n(x,t)\ dx - \frac{1}{2(1-\delta)}\iint_{\mathbb{R}^2\times\mathbb{R}^2} n(x,t)B_\alpha(x-y)n(y,t)\ dx\ dy\\
&\qquad +\delta\left(\frac{1}{2}\int_{\mathbb{R}^2}|\nabla c(x,t)|^2\ dx + \frac{\alpha}{2}\int_{\mathbb{R}^2} c^2(x,t)\ dx\right)\\
&\ge \left(1-\frac{M}{8\pi(1-\delta)}\right)\int_{\mathbb{R}^2} n(x,t)\log n(x,t)\ dx - \frac{M}{4\pi(1-\delta)}\int_{\mathbb{R}^2} n(x,t)\log(1+|x|^2)\ dx - \frac{1}{1-\delta}C(M)\\
&\qquad +\delta\left(\frac{1}{2}\int_{\mathbb{R}^2}|\nabla c(x,t)|^2\ dx + \frac{\alpha}{2}\int_{\mathbb{R}^2} c^2(x,t)\ dx\right)\ .
\end{aligned}$$

Moreover, using the definition (3.12) of $H$ it follows that

$$\begin{aligned}
\mathcal{E}(t) &\ge \left(1-\frac{M}{8\pi(1-\delta)}\right)\int_{\mathbb{R}^2} n(x,t)\log n(x,t)\ dx + \frac{M}{8\pi(1-\delta)}\int_{\mathbb{R}^2} n(x,t)\log H(x)\ dx\\
&\qquad +\delta\left(\frac{1}{2}\int_{\mathbb{R}^2}|\nabla c(x,t)|^2\ dx + \frac{\alpha}{2}\int_{\mathbb{R}^2} c^2(x,t)\ dx\right) - \frac{1}{1-\delta}C(M)\ .
\end{aligned}$$

Therefore, the modified free energy $\mathcal{E}_H(t)$ verifies

$$\begin{aligned}
\mathcal{E}_H(t) &\ge \left(1-\frac{M}{8\pi(1-\delta)}\right)\int_{\mathbb{R}^2} n(x,t)\log\left(\frac{n(x,t)}{H(x)}\right)\ dx\\
&\qquad +\delta\left(\frac{1}{2}\int_{\mathbb{R}^2}|\nabla c(x,t)|^2\ dx + \frac{\alpha}{2}\int_{\mathbb{R}^2} c^2(x,t)\ dx\right) - \frac{1}{1-\delta}C(M)\ ,
\end{aligned}$$

and the Theorem follows from the above estimate. Indeed, since

$$\int_{\mathbb{R}^2} n(x,t)\log\left(\frac{n(x,t)}{H(x)}\right)\ dx = \int_{\mathbb{R}^2}\left(\frac{n(x,t)}{H(x)}\right)\log\left(\frac{n(x,t)}{H(x)}\right)H(x)\ dx \ge -e^{-1}\ ,$$

choosing $0<\delta<1$ such that $M < 8\pi(1-\delta)$ and using the facts that $\mathcal{E}_H(t)$ grows at most linearly, estimates (ii) of Theorem 3.8 follow as well as (iv) with $\alpha>0$. The remaining estimates of Theorem 3.8 follow exactly as in section §3.3.

To conclude, let us consider the case $\alpha = 0$. In this case, the minimization principle (3.37) does not hold true since the gradient of the partial minimum $\nabla\bar{c}(t) = \nabla E_2 * n(t)$ does not lie in $L^2$ in general. Nevertheless we can obtain the required estimates by considering the corrected quasi-stationary state $\bar{c} = E_2 * (n - MH)$, whose gradient does belong to $L^2$ (see Appendix 3.8.2 and Remark 3.13). Then, acting as before, we obtain for $0 < \delta < 1$

$$\begin{aligned}
\mathcal{E}(t) &= \int_{\mathbb{R}^2} n(x,t)\log n(x,t)\ dx + (1-\delta)F_0\left(c;(1-\delta)^{-1}(n-MH)\right) + \frac{1}{2}\delta\int_{\mathbb{R}^2}|\nabla c(x,t)|^2\ dx \\
&\qquad -M\int_{\mathbb{R}^2} c(x,t)H(x)\ dx \\
&\geq \int_{\mathbb{R}^2} n(x,t)\log n(x,t)\ dx - \frac{1}{2}\int_{\mathbb{R}^2}(n(x,t)-MH(x))\bar{c}(x,t)\ dx + \frac{1}{2}\delta\int_{\mathbb{R}^2}|\nabla c(x,t)|^2\ dx \\
&\qquad -M\int_{\mathbb{R}^2} c(x,t)H(x)\ dx \\
&= \int_{\mathbb{R}^2} n(x,t)\log n(x,t)\ dx + \frac{1}{4\pi(1-\delta)}\int_{\mathbb{R}^2\times\mathbb{R}^2}(n(x,t)-MH(x))\log|x-y|(n(y,t)-MH(y))\ dxdy \\
&\qquad +\frac{1}{2}\delta\int_{\mathbb{R}^2}|\nabla c(x,t)|^2\ dx - M\int_{\mathbb{R}^2} c(x,t)H(x)\ dx \\
&= \int_{\mathbb{R}^2} n(x,t)\log n(x,t)\ dx + \frac{1}{4\pi(1-\delta)}\int_{\mathbb{R}^2\times\mathbb{R}^2} n(x,t)\log|x-y|n(y,t)\ dxdy \\
&\qquad -\frac{M}{2\pi(1-\delta)}\int_{\mathbb{R}^2\times\mathbb{R}^2} H(x)\log|x-y|n(y,t)\ dxdy + \frac{M^2}{4\pi(1-\delta)}\int_{\mathbb{R}^2\times\mathbb{R}^2} H(x)\log|x-y|H(y)\ dxdy \\
&\qquad +\frac{1}{2}\delta\int_{\mathbb{R}^2}|\nabla c(x,t)|^2\ dx - M\int_{\mathbb{R}^2} c(x,t)H(x)\ dx\ .
\end{aligned}$$

Using inequality (3.36), it is straightforward to prove that

$$-\frac{M}{2\pi(1-\delta)}\int_{\mathbb{R}^2\times\mathbb{R}^2} H(x)\log|x-y|n(y,t)\ dxdy \geq -\frac{1}{1-\delta}C(M) - \frac{M}{4\pi(1-\delta)}\int_{\mathbb{R}^2} n(x,t)\log(1+|x|^2)\ dx\ .$$

Finally, applying the logarithmic HLS inequality (3.33) to $n$, we arrive exactly to the estimate

$$\begin{aligned}
\mathcal{E}(t) &\geq \left(1-\frac{M}{8\pi(1-\delta)}\right)\int_{\mathbb{R}^2} n(x,t)\log n(x,t)\ dx + \frac{M}{8\pi(1-\delta)}\int_{\mathbb{R}^2} n(x,t)\log H(x)\ dx \\
&\qquad +\frac{1}{2}\delta\int_{\mathbb{R}^2}|\nabla c(x,t)|^2\ dx - M\int_{\mathbb{R}^2} c(x,t)H(x)\ dx - \frac{1}{1-\delta}C(M)\ ,
\end{aligned}$$

as before and the proof follows as in the previous case.

□

**Remark 3.17.** *Again, we see here that the mass $M$ cannot equal the critical value $8\pi$, see the Remark 3.10.*

## 3.5 Regularizing effect

In the previous section it has been proved implicitly that under the hypothesis of Theorem 3.8, in particular for sub-critical mass $M$, the solution $n$ of system (3.1) is locally in time equi-integrable, i.e. there exists a modulus of equi-integrability $\omega$ such that for any $T > 0$ and any given real number $k > 0$,

$$\sup_{0\leq t\leq T}\int_{\mathbb{R}^2}\left(n(x,t)-k\right)_+\ dx \leq \omega(T;k) \quad \text{and} \quad \lim_{k\to+\infty}\omega(T;k) = 0\ , \tag{3.38}$$

Indeed, obviously $\int_{\mathbb{R}^2} \big(n(x,t)-k\big)_+ \, dx \le M$ for any $k>0$, while for $k>1$ we have

$$\int_{\mathbb{R}^2} \big(n(x,t)-k\big)_+ \, dx \le \frac{1}{\log k} \int_{\mathbb{R}^2} \big(n(x,t)-k\big)_+ \big(\log n(x,t)\big)_+ \, dx \le \frac{C(1+t)}{\log k} \ .$$

In this section, following a now classical idea initiated in [147], we will obtain *a priori* estimates for the $L^p$-norm of $n$, with the help of the equi-integrability property (3.38) and of the fact proved in Theorem 3.8 that $\partial_t c \in L^2(0,T;L^2(\mathbb{R}^2))$. Since the hypothesis $\|n_0\|_{L^p(\mathbb{R}^2)} < \infty$ is not required, the following result is an hypercontractivity type result.

**Theorem 3.18.** *Let $T>0$ and $1<p<\infty$. Under the hypothesis of Theorem 3.8, there exists a constant $C(T)$ not depending on $\|n_0\|_{L^p(\mathbb{R}^2)}$ such that*

$$\int_{\mathbb{R}^2} n^p(x,t) \, dx \le C(T) \big(1+t^{1-p}\big) \ , \quad \forall \ 0<t\le T \ , \tag{3.39}$$

*i.e. the cell density $n(\cdot,t)$ belongs to $L^p(\mathbb{R}^2)$ for any positive time $t$.*

*Proof.* Let $k>0$ to be chosen later. We derive a non-linear differential inequality for the quantity $Y_p(t) := \int_{\mathbb{R}^2} (n(x,t)-k)_+^p \, dx$, which guarantees that the $L^p$-norm of $n$ remains finite whatever $\|n_0\|_{L^p(\mathbb{R}^2)}$ is (possibly infinite).

*First step : the differential inequality.* Multiplying the equation on $n$ in (3.1) by $p(n-k)_+^{p-1}$ yields, after integration by parts,

$$\frac{d}{dt}\int_{\mathbb{R}^2} (n-k)_+^p \, dx = -4\frac{(p-1)}{p} \int_{\mathbb{R}^2} \big|\nabla (n-k)_+^{p/2}\big|^2 \, dx - (p-1)\int_{\mathbb{R}^2} (n-k)_+^p \Delta c \, dx - pk \int_{\mathbb{R}^2} (n-k)_+^{p-1} \Delta c \, dx \ . \tag{3.40}$$

There is some subtlety hidden here because we cannot use directly $-\Delta c = n - \alpha c$, as it is the case for the parabolic-elliptic system ($\varepsilon = 0$). However , using the equation on $c$, one obtains

$$\begin{aligned} \frac{d}{dt}\int_{\mathbb{R}^2} (n-k)_+^p \, dx \ &\le \ -4\frac{(p-1)}{p} \int_{\mathbb{R}^2} |\nabla (n-k)_+^{p/2}|^2 \, dx \\ &\quad + (p-1)\int_{\mathbb{R}^2} (n-k)_+^{p+1} \, dx + (2p-1)k \int_{\mathbb{R}^2} (n-k)_+^p \, dx + pk^2 \int_{\mathbb{R}^2} (n-k)_+^{p-1} \, dx \\ &\quad - \varepsilon(p-1)\int_{\mathbb{R}^2} (n-k)_+^p \partial_t c \, dx - \varepsilon pk \int_{\mathbb{R}^2} (n-k)_+^{p-1} \partial_t c \, dx \end{aligned} \tag{3.41}$$

and the additional non-linear terms $\int_{\mathbb{R}^2} (n-k)_+^p \partial_t c \, dx$ and $\int_{\mathbb{R}^2} (n-k)_+^{p-1} \partial_t c \, dx$ can be estimated in the following way.
Using the Gagliardo-Nirenberg inequality

$$\int_{\mathbb{R}^2} u^4(x) \, dx \le C \int_{\mathbb{R}^2} u^2(x) \, dx \int_{\mathbb{R}^2} |\nabla u(x)|^2 \, dx \ ,$$

with $u = (n-k)_+^{p/2}$, we obtain

$$\begin{aligned} \Big| \int_{\mathbb{R}^2} (n-k)_+^p \partial_t c \, dx \Big| \ &\le \ \Big( \int_{\mathbb{R}^2} (n-k)_+^{2p} \, dx \Big)^{1/2} \|\partial_t c\|_{L^2(\mathbb{R}^2)} \\ &\le \ C \Big( \int_{\mathbb{R}^2} (n-k)_+^p \, dx \Big)^{1/2} \Big( \int_{\mathbb{R}^2} \big|\nabla (n-k)_+^{p/2}\big|^2 \, dx \Big)^{1/2} \|\partial_t c\|_{L^2(\mathbb{R}^2)} \\ &\le \ \varepsilon C(p) \|\partial_t c\|_{L^2(\mathbb{R}^2)}^2 \int_{\mathbb{R}^2} (n-k)_+^p \, dx + \frac{2}{\varepsilon p} \int_{\mathbb{R}^2} \big|\nabla (n-k)_+^{p/2}\big|^2 \, dx. \end{aligned} \tag{3.42}$$

On the other hand, by interpolation and the above Gagliardo-Nirenberg-Sobolev inequality as before, we have for $p \geq \frac{3}{2}$

$$\begin{aligned}
\Big| \int_{\mathbb{R}^2} (n-k)_+^{p-1} \partial_t c \, dx \Big| &\leq \Big( \int_{\mathbb{R}^2} (n-k)_+^{2(p-1)} \, dx \Big)^{1/2} \|\partial_t c\|_{L^2(\mathbb{R}^2)} \\
&\leq \Big( C(M,p) + C(p) \int_{\mathbb{R}^2} (n-k)_+^{2p} \, dx \Big)^{1/2} \|\partial_t c\|_{L^2(\mathbb{R}^2)} \\
&\leq C(M,p) \|\partial_t c\|_{L^2(\mathbb{R}^2)} + \varepsilon C(p,k) \|\partial_t c\|^2_{L^2(\mathbb{R}^2)} \int_{\mathbb{R}^2} (n-k)_+^p \, dx \\
&\qquad + \frac{(p-1)}{\varepsilon p^2 k} \int_{\mathbb{R}^2} \big| \nabla (n-k)_+^{p/2} \big|^2 \, dx. \qquad (3.43)
\end{aligned}$$

Inserting (3.42) and (3.43) in (3.41) gives for $p \geq \frac{3}{2}$

$$\begin{aligned}
\frac{d}{dt} \int_{\mathbb{R}^2} (n-k)_+^p \, dx &\leq -\frac{(p-1)}{p} \int_{\mathbb{R}^2} |\nabla (n-k)_+^{p/2}|^2 \, dx \\
&\quad + (p-1) \int_{\mathbb{R}^2} (n-k)_+^{p+1} \, dx + (2p-1)k \int_{\mathbb{R}^2} (n-k)_+^p \, dx + pk^2 \int_{\mathbb{R}^2} (n-k)_+^{p-1} \, dx \\
&\quad + \varepsilon C \|\partial_t c\|^2_{L^2(\mathbb{R}^2)} \int_{\mathbb{R}^2} (n-k)_+^p \, dx + C \|\partial_t c\|_{L^2(\mathbb{R}^2)} \, . \qquad (3.44)
\end{aligned}$$

Next, we estimate the non-linear and negative contribution $-\frac{(p-1)}{p} \int_{\mathbb{R}^2} |\nabla (n-k)_+^{p/2}|^2 \, dx$ in term of $\int_{\mathbb{R}^2} (n-k)_+^{p+1} \, dx$ and of the modulus of equi-integrability $\omega(T;k)$, with the help of the Sobolev inequality. Indeed,

$$\begin{aligned}
\int_{\mathbb{R}^2} (n-k)_+^{p+1} \, dx &= \int_{\mathbb{R}^2} \left( (n-k)_+^{\frac{(p+1)}{2}} \right)^2 dx \leq C \left( \int_{\mathbb{R}^2} \left| \nabla (n-k)_+^{\frac{(p+1)}{2}} \right| dx \right)^2 \\
&= C(p) \left( \int_{\mathbb{R}^2} (n-k)_+^{\frac{1}{2}} |\nabla (n-k)_+^{\frac{p}{2}}| \, dx \right)^2 \\
&\leq C(p) \int_{\mathbb{R}^2} (n-k)_+ \, dx \int_{\mathbb{R}^2} |\nabla (n-k)_+^{p/2}|^2 \, dx \\
&\leq C(p) \omega(T;k) \int_{\mathbb{R}^2} |\nabla (n-k)_+^{p/2}|^2 \, dx \, , \quad \forall \, 0 < t \leq T \, . \qquad (3.45)
\end{aligned}$$

Moreover, since for $p \geq 2$ it holds true that

$$\int_{\mathbb{R}^2} (n-k)_+^{p-1} \, dx \leq \int_{\mathbb{R}^2} (n-k)_+ \, dx + \int_{\mathbb{R}^2} (n-k)_+^p \, dx \, , \qquad (3.46)$$

inserting (3.45) and (3.46) in (3.44) gives for $p \geq 2$ and $0 < t \leq T$

$$\begin{aligned}
\frac{d}{dt} \int_{\mathbb{R}^2} (n-k)_+^p \, dx &\leq (p-1) \left( 1 - \frac{1}{pC(p)\omega(T;k)} \right) \int_{\mathbb{R}^2} (n-k)_+^{p+1} \, dx \\
&\quad + C(1 + \varepsilon \|\partial_t c\|^2_{L^2(\mathbb{R}^2)}) \int_{\mathbb{R}^2} (n-k)_+^p \, dx + C \|\partial_t c\|_{L^2(\mathbb{R}^2)} + pk^2 M \, . \qquad (3.47)
\end{aligned}$$

Finally, for any fixed $p$ we choose $k = k(p,T)$ sufficiently large such that

$$\delta := \frac{1}{pC(p)\omega(T;k(p,T))} - 1 > 0 \, . \qquad (3.48)$$

This is clearly possible because $\omega(T;k) \to 0$ as $k \to +\infty$. For this $k$ and using the interpolation

$$\int_{\mathbb{R}^2} (n-k)_+^p \, dx \leq \left( \int_{\mathbb{R}^2} (n-k)_+ \, dx \right)^{\frac{1}{p}} \left( \int_{\mathbb{R}^2} (n-k)_+^{p+1} \, dx \right)^{(1-\frac{1}{p})} \leq M^{\frac{1}{p}} \left( \int_{\mathbb{R}^2} (n-k)_+^{p+1} \, dx \right)^{(1-\frac{1}{p})} \, ,$$

we end up with the following differential inequality for $Y_p(t)$, $p \geq 2$ fixed and $0 < t \leq T$

$$\frac{d}{dt}Y_p(t) \leq -(p-1)M^{-\frac{1}{p-1}}\,\delta\, Y_p^{\beta}(t) + C_1\left(1+\varepsilon\|\partial_t c(t)\|^2_{L^2(\mathbb{R}^2)}\right)Y_p(t) + C_2\left(1+\varepsilon\|\partial_t c(t)\|^2_{L^2(\mathbb{R}^2)}\right)\ , \quad (3.49)$$

where $\beta = \frac{p}{p-1} > 1$ .

*Second step : estimate on $Y_p$, $p \geq 2$.* Let us write the differential inequality (3.49) as follows for simplicity

$$\frac{d}{dt}Y_p(t) \leq -\gamma\, Y_p^{\beta}(t) + f(t)Y_p(t) + f(t)\ , \quad 0 < t \leq T\ , \quad (3.50)$$

where $\gamma = (p-1)M^{-\frac{1}{p-1}}\,\delta > 0$ and $f(t) = \overline{C}\left(1+\varepsilon\|\partial_t c(t)\|^2_{L^2(\mathbb{R}^2)}\right)$ with $\overline{C} = \max\{C_1, C_2\}$. Next we show that there exists a constant $C(T)$ not depending on $Y_p(0)$ such that

$$Y_p(t) \leq C(T)\frac{1}{t^{p-1}}\ , \quad 0 < t \leq T\ , \quad (3.51)$$

by comparison of $Y_p(t)$ with positive solutions of the differential equation

$$\frac{d}{dt}Z_p(t) = -\gamma\, Z_p^{\beta}(t) + f(t)Z_p(t) + f(t)\ , \quad 0 < t \leq T\ . \quad (3.52)$$

To do that, let $Z_p$ be a positive solution of (3.52) with $Z_p(0) \geq \left(\frac{\overline{C}}{\gamma}\right)^{1/(\beta-1)}$. By the definition of $f(t)$, $Z_p$ satisfies the differential inequality

$$\frac{d}{dt}Z_p(t) \geq -\gamma\, Z_p^{\beta}(t) + \overline{C}Z_p(t)\ , \quad 0 < t \leq T\ . \quad (3.53)$$

Therefore, since $\left(\frac{\overline{C}}{\gamma}\right)^{1/(\beta-1)}$ is a constant solution of $Z'(t) = -\gamma\, Z^{\beta}(t) + \overline{C}Z(t)$, by comparison in (3.53) we get $Z_p(t) \geq \left(\frac{\overline{C}}{\gamma}\right)^{1/(\beta-1)}$, $\forall\ 0 \leq t \leq T$. As a consequence, from (3.52) $Z_p$ satisfies also the differential inequality

$$\frac{d}{dt}Z_p(t) \leq -\gamma\, Z_p^{\beta}(t) + h(t)Z_p(t)\ , \quad 0 \leq t \leq T\ , \quad (3.54)$$

where $h(t) = \left(1+\left(\gamma\overline{C}^{-1}\right)^{1/(\beta-1)}\right)f(t)$. Integrating (3.54) over $(0,t)$, it is straightforward to prove that

$$Z_p^{1-\beta}(t) \geq Z_p^{1-\beta}(0)e^{(1-\beta)\int_0^t h(\tau)d\tau} + \gamma(\beta-1)\int_0^t e^{(1-\beta)\int_s^t h(\tau)d\tau}ds\ , \quad 0 \leq t \leq T\ .$$

Then, thanks to the estimate (vi) in Theorem 3.8 and by the definition of $h(t)$, it holds true that

$$\begin{aligned} Z_p^{1-\beta}(t) &\geq Z_p^{1-\beta}(0)e^{C(1-\beta)\varepsilon\int_0^T\|\partial_t c(s)\|^2_{L^2(\mathbb{R}^2)}ds}\ e^{C(1-\beta)t} + \frac{\gamma}{C}\ e^{C(1-\beta)\varepsilon\int_0^T\|\partial_t c(s)\|^2_{L^2(\mathbb{R}^2)}ds}(1-e^{C(1-\beta)t}) \\ &\geq \gamma(\beta-1)\ e^{C(1-\beta)(1+T)}e^{C(1-\beta)T}\ t = C(T)\ t\ , \quad 0 \leq t \leq T\ , \end{aligned}$$

and therefore

$$Z_p(t) \leq C(T)\frac{1}{t^{p-1}}\ , \quad 0 \leq t \leq T\ . \quad (3.55)$$

where $C(T)$ doesn't depend on $Z_p(0)$.

Finally, let $Z_p$ be a positive solution of (3.52) with $Z_p(0) = \max\left\{\left(\frac{\overline{C}}{\gamma}\right)^{1/(\beta-1)}, Y_p(0)\right\}$. Again by comparison, $Y_p(t) \leq Z_p(t)$, $\forall\ 0 < t \leq T$ and (3.51) follows by (3.55).

*Third step : $L^p$ regularity of $n$.* To conclude, it is sufficient to observe that for any $k > 0$ we have

$$\begin{aligned}\int_{\mathbb{R}^2} n^p(x,t)\ dx &= \int_{\{n\le 2k\}} n^p(x,t)\ dx + \int_{\{n>2k\}} n^p(x,t)\ dx \\ &\le (2k)^{p-1}M + 2^p \int_{\{n>2k\}} (n(x,t)-k)^p\ dx \\ &\le (2k)^{p-1}M + 2^p \int_{\mathbb{R}^2} (n(x,t)-k)_+^p\ dx\ , \end{aligned} \tag{3.56}$$

where the inequality $x^p \le 2^p(x-k)^p$, for $x \ge k2$, has been used. Therefore, estimate (3.39) follows for any $p \ge 2$ by (3.51) and (3.56) choosing $k = k(p,T)$ sufficiently large such that (3.48) holds true. For $1 < p < 2$, the Theorem follows by interpolation.

□

## 3.6 Global Existence

We are now able to prove Theorem 3.1 collecting all the results proved in the previous sections. In order to do that, we need first to regularize the chemotaxis system (3.1) and then to prove that the *a priori* estimates hold true and pass to the limit. Being this procedure quite technical and usual, we just sketch the proof. For the parabolic-elliptic case with $\alpha = 0$ one can consult for example [35], where the regularizing procedure has been written in full details.

The regularized system that we consider is

$$\begin{cases} \dfrac{\partial n^\sigma}{\partial t} &= \Delta n^\sigma - \nabla\cdot(n^\sigma \nabla c^\sigma)\ , \quad t>0,\ x\in\mathbb{R}^2, \\ \varepsilon\dfrac{\partial c^\sigma}{\partial t} &= \Delta c^\sigma + n^\sigma * \rho^\sigma - \alpha c^\sigma\ , \quad t>0,\ x\in\mathbb{R}^2, \\ n^\sigma(\cdot,0) &= n_0 * \rho^\sigma, \quad c^\sigma(\cdot,0) = c_0 * \rho^\sigma\ , \qquad x\in\mathbb{R}^2\ , \end{cases} \tag{3.57}$$

for some regularizing kernel $\rho^\sigma(x) = \frac{1}{\sigma^2}\rho(\frac{x}{\sigma})$ with $\rho \in \mathcal{D}^+(\mathbb{R}^2)$ and $\int_{\mathbb{R}^2}\rho(x)\ dx = 1$. The first step is to prove the local existence of a smooth solution $(n^\sigma, c^\sigma)$ of (3.57). This result can be obtained through a fixed-point method, writing $(n^\sigma, c^\sigma)$ as

$$n^\sigma(t) = G(t) * (n_0 * \rho^\sigma) - \int_0^t \nabla G(t-s) * (n^\sigma(s)\nabla c^\sigma(s))\ ds\ ,$$

$$c^\sigma(t) = e^{-\alpha t}G(t) * (c_0 * \rho^\sigma) + \int_0^t e^{\alpha(s-t)}G(t-s) * n^\sigma(s)\ ds\ ,$$

with $G(x,t) = \frac{1}{4\pi t}e^{-|x|^2/(4t)}$ the heat kernel in $\mathbb{R}^2$ (see [28]). The smoothness of $(n^\sigma, c^\sigma)$ follows by the regularizing property of the heat equation and by the smoothness of the initial data. The non-negativity of $(n^\sigma, c^\sigma)$ follows by the maximum principle. As a consequence, the *a priori* estimates in Theorem 3.8 hold true for the regularized solution $(n^\sigma, c^\sigma)$. These *a priori* bounds give a global in time control of the energy and energy dissipation, still uniform in $\sigma$. This gives space compactness on $c$ and $\nabla n$. The Lions-Aubin compactness method gives the required time compactness.

## 3.7 Blow-up

In this section we consider exceptionnally the case $\varepsilon = 0$. We shall prove Theorem 3.2 which states a blow-up result for the super-critical mass $M > 8\pi$ under a smallness assumption on the initial second momentum of the cell density.

Recall that when $\varepsilon = 0$, then the chemical potential is given by $c = B_\alpha * n$. Introduce $I(t) = \int_{\mathbb{R}^2} |x|^2 n(x,t)\ dx$. Then

$$\frac{d}{dt} I(t) = 4M + 2 \int_{\mathbb{R}^2} n(x,t)\ x \cdot (\nabla B_\alpha * n(t))(x)\ dt\ .$$

Moreover,

$$\nabla B_\alpha(z) = -\frac{z}{8\pi} \int_0^{+\infty} \frac{1}{t^2}\ e^{-\frac{|z|^2}{4t} - \alpha t}\ dt = -\frac{1}{2\pi} \frac{z}{|z|^2} \int_0^{+\infty} e^{-s - \alpha \frac{|z|^2}{4s}}\ ds\ .$$

Let denote $g_\alpha(z) = \int_0^{+\infty} e^{-s-\alpha\frac{|z|^2}{4s}}\ ds$. Then

$$\begin{aligned} \frac{d}{dt} I(t) &= 4M - \frac{1}{\pi} \iint_{\mathbb{R}^2 \times \mathbb{R}^2} n(x,t) \frac{x \cdot (x-y)}{|x-y|^2} g_\alpha(x-y) n(y,t)\ dydx \\ &= 4M - \frac{1}{2\pi} \iint_{\mathbb{R}^2 \times \mathbb{R}^2} n(x,t) g_\alpha(x-y) n(y,t)\ dydx\ . \end{aligned}$$

Since $g_\alpha$ is a positive radial decreasing function such that $g_\alpha(z) = g_1(\sqrt{\alpha} z)$, $g_\alpha(z) \leq 1$ and $g_\alpha(z) \to 1$ as $\alpha \to 0$ for all $z \in \mathbb{R}^2$, we recover from (3.58) the result in [35]. For $\alpha > 0$ we have

$$\frac{d}{dt} I(t) = 4M \left(1 - \frac{M}{8\pi}\right) + \frac{1}{2\pi} \int_{\mathbb{R}^2} \int_{\mathbb{R}^2} n(x,t)[1 - g_\alpha(x-y)] n(y,t)\ dydx \tag{3.58}$$

and one has to estimate the second term in the right hand side in term of $I(t)$. Denoting $r = |z|$ we have,

$$\frac{d}{dr}(1 - g_\alpha(r)) = -\sqrt{\alpha} \frac{dg_1}{dr}(\sqrt{\alpha} r)\ ,$$

where, reasoning as in Lemma 3.15 separately for $r < 1$, and for $r > 1$, we deduce

$$-\frac{dg_1}{dr}(r) = \frac{1}{2}\ r \int_0^{+\infty} \frac{1}{s} e^{-s - \frac{r^2}{4s}}\ ds \leq \mathcal{C}\ .$$

As a consequence we get for $z \in \mathbb{R}^2$,

$$0 \leq 1 - g_\alpha(z) \leq \sqrt{\alpha} \mathcal{C} |z|\ , \quad \mathcal{C} = \sup_{r \in (0,\infty)} \frac{1}{2}\ r \int_0^{+\infty} \frac{1}{s} e^{-s - \frac{r^2}{4s}}\ ds\ .$$

We plug this last bound into (3.58):

$$\begin{aligned} \frac{d}{dt} I(t) &\leq 4M \left(1 - \frac{M}{8\pi}\right) + \frac{\sqrt{\alpha}\mathcal{C}}{2\pi} \iint_{\mathbb{R}^2 \times \mathbb{R}^2} n(x,t) |x-y| n(y,t)\ dydx \\ &\leq 4M \left(1 - \frac{M}{8\pi}\right) + \frac{\sqrt{\alpha}\mathcal{C}}{\pi} M \int_{\mathbb{R}^2} |x| n(x,t)\ dx \\ &\leq 4M \left(1 - \frac{M}{8\pi}\right) + \frac{\sqrt{\alpha}\mathcal{C}}{\pi} M^{3/2} \sqrt{I(t)}\ . \end{aligned}$$

As a consequence, if $I(0)$ is small enough, given by

$$\alpha I(0) \leq \left(\frac{4(M/8 - \pi)}{\mathcal{C} M^{1/2}}\right)^2\ ,$$

then the second momentum becomes necessarily nonpositive in finite time, expressing the formation of a singularity before.

## 3.8 Appendix

### 3.8.1 The entropy minimization Lemma

The entropy minimization Lemma 3.4 is a classical lemma and one can prove it in several ways. For example, using the Jensen's inequality with respect to the probability measure $\frac{n}{M}dx$, $n \in \mathcal{U}$, we have

$$\frac{1}{M}\int_{\mathbb{R}^2}(n(x)\log n(x) - n(x)\psi(x))\,dx = -\int_{\mathbb{R}^2}\log\left(\frac{e^{\psi(x)}}{n(x)}\right)\frac{n(x)}{M}dx \geq -\log\left(\frac{1}{M}\int_{\mathbb{R}^2}e^{\psi(x)}\,dx\right) = \frac{1}{M}E(\overline{n};\psi)\,.$$

One can also appeal to the Legendre transform of the functional $\int_{\mathbb{R}^2} n(x)\log n(x)\,dx$ to find out (3.13). However, in these ways we loose the identity in (3.13). Therefore, the following proof, in the line of [58], is more complete.

*Proof of the entropy minimization Lemma 3.4.* First of all, by the definition of $\overline{n}$ we have that $\overline{n} \in \mathcal{U}$ and

$$\log\overline{n} = \psi + \log\left(M\Big/\int_{\mathbb{R}^2}e^{\psi}\,dx\right). \tag{3.59}$$

Therefore, the entropy functional $E$ is finite in $\overline{n}$ and it takes the value $E(\overline{n};\psi) = M\log\left(M/\int_{\mathbb{R}^2}e^{\psi}\,dx\right)$. Next, it is easy to see that for any $n$ in $\mathcal{U}$, $E(n;\psi)$ and $RE(n|\overline{n})$ are finite or infinite in the same time and that (3.13) holds true. Indeed, from (3.59) we deduce $n\log(n/\overline{n}) = n\log n - n\psi - n\log\left(M/\int_{\mathbb{R}^2}e^{\psi}\,dx\right)$. The non-negativity of $RE(n|\overline{n})$ over the set $\mathcal{U}$ follows by the computation

$$RE(n|\overline{n}) = \int_{\mathbb{R}^2}\left(n(x)\log n(x) - \overline{n}(x)\log\overline{n}(x) - (\log\overline{n}(x)+1)(n(x)-\overline{n}(x))\right)dx\,,$$

and the convexity of the function $u\log u$. □

### 3.8.2 The chemical energy minimization Lemma

*Proof of the chemical energy minimization Lemma 3.5.* Let us start with some basic regularity properties of $\overline{c}$ [168]. If $\alpha > 0$ then $\overline{c} \in L^p(\mathbb{R}^2)$, for all $p \in [1,\infty)$ since $f \in L^1(\mathbb{R}^2)$ by hypothesis. On the other hand, when $\alpha = 0$, $\overline{c} \in L^1_{loc}(\mathbb{R}^2)$ since $f \in L^1(\mathbb{R}^2) \cap L^1(\mathbb{R}^2, \log(1+|x|^2)dx)$. Thus (3.15) holds true in $\mathcal{D}'(\mathbb{R}^2)$ as well as $-\Delta\overline{c} + \alpha\overline{c} = f$ for $\alpha \geq 0$.

We aim to justify the integration by parts arising in (3.16). Assume first that $\alpha > 0$ and that we know *a priorily* that $\overline{c} \in H^1(\mathbb{R}^2)$. Then, for all $c \in H^1(\mathbb{R}^2)$, $c\Delta\overline{c} \in L^1(\mathbb{R}^2)$ and the following partial integration holds true

$$\int_{\mathbb{R}^2}\nabla c(x)\cdot\nabla\overline{c}(x)\,dx = -\int_{\mathbb{R}^2}c(x)\Delta\overline{c}(x)\,dx = \int_{\mathbb{R}^2}c(x)(f(x)-\alpha\overline{c}(x))\,dx\,. \tag{3.60}$$

Indeed, we have $-\Delta\overline{c} = h_1 + h_2$ with $h_1 := f + \alpha(\overline{c})_- \geq 0$, $h_1 \in L^1(\mathbb{R}^2)$ and $h_2 := -\alpha(\overline{c})_+ \in L^2(\mathbb{R}^2)$, (see [168]). Moreover, $F_\alpha(c;f)$ is finite for all $c \in H^1(\mathbb{R}^2)$. As a consequence of (3.60), we obtain easily (3.16). Indeed

$$\frac{1}{2}\int_{\mathbb{R}^2}|\nabla c - \nabla\overline{c}|^2 + \frac{\alpha}{2}\int_{\mathbb{R}^2}(c-\overline{c})^2\,dx = F_\alpha(c;f) + \frac{1}{2}\int_{\mathbb{R}^2}|\nabla\overline{c}|^2\,dx + \frac{\alpha}{2}\int_{\mathbb{R}^2}\overline{c}^2\,dx = F_\alpha(c;f) - F_\alpha(\overline{c};f)\,.$$

It remains to prove that $\nabla\overline{c} \in L^2(\mathbb{R}^2)$ ($\overline{c} \in H^1(\mathbb{R}^2)$ in case of $\alpha > 0$). Let us consider first the case $\alpha = 0$ that is much more complicated then the case $\alpha > 0$ because the fundamental solution $E_2$ does not lie in any $L^p(\mathbb{R}^2)$ spaces and $\nabla\overline{c} = \nabla E_2 * f$ in general does not lie in $L^2(\mathbb{R}^2)$ because of the critical fractional Sobolev embedding (see [168]). The case $\alpha > 0$ is considered subsequently.

The hypothesis $\int_{\mathbb{R}^2} f(x)\,dx = 0$ allows us to substract any function of $x$ to the integrand inside $\nabla\overline{c}$. Let us consider two radii $0 < r < 1 < R$ with $R^2 > e-1$ and let us denote $\mathcal{C}B(0,r) = \mathbb{R}^2 \setminus B(0,r)$. Then,

we split $\nabla \overline{c}$ in the following way

$$\begin{aligned}
\nabla \overline{c}(x) &= -\frac{1}{2\pi}\int_{\mathbb{R}^2}\left(\frac{x-y}{|x-y|^2}-\frac{x}{1+|x|^2}\ \mathbb{1}_{\mathcal{C}B(0,R)}(x)\right) f(y)\ dy \\
&= -\frac{1}{2\pi}\int_{\mathbb{R}^2}\left(\frac{x-y}{|x-y|^2}-\frac{x}{1+|x|^2}\ \mathbb{1}_{\mathcal{C}B(0,R)}(x)\right)\ \mathbb{1}_{B(0,r)}(x-y)f(y)\ dy \\
&\quad -\frac{1}{2\pi}\int_{\mathbb{R}^2}\left(\frac{x-y}{|x-y|^2}-\frac{x}{1+|x|^2}\ \mathbb{1}_{\mathcal{C}B(0,R)}(x)\right)\ \mathbb{1}_{\mathcal{C}B(0,r)}(x-y)f(y)\ dy \\
&=: I_1(x)+I_2(x) \qquad (3.61)
\end{aligned}$$

and we will show separately that $I_1$ and $I_2$ lie in $L^2(\mathbb{R}^2)$.

Concerning $I_1$ we have for all $x\in\mathbb{R}^2$,

$$|I_1(x)| \le \frac{1}{2\pi}\int_{\mathbb{R}^2}\frac{1}{|x-y|}\ \mathbb{1}_{B(0,r)}(x-y)|f(y)|\ dy + \frac{|x|\mathbb{1}_{\mathcal{C}B(0,R)}(x)}{2\pi(1+|x|^2)}\ \int_{\mathbb{R}^2}\mathbb{1}_{B(0,r)}(x-y)|f(y)|\ dy\ . \qquad (3.62)$$

Denoting $\Omega_x=\left\{y\in\mathbb{R}^2\ :\ |f(y)|>\frac{1}{|x-y|}\right\}$, the first integral in the right hand side of (3.62) can be split again in the following way

$$\begin{aligned}
\int_{\mathbb{R}^2}\frac{1}{|x-y|}\ \mathbb{1}_{B(0,r)}(x-y)|f(y)|\ dy &= \int_{\mathbb{R}^2}\frac{1}{|x-y|}\ \mathbb{1}_{B(0,r)}(x-y)|f(y)|\mathbb{1}_{\Omega_x}(y)\ dy \\
&\quad +\int_{\mathbb{R}^2}\frac{1}{|x-y|}\ \mathbb{1}_{B(0,r)}(x-y)|f(y)|\mathbb{1}_{\mathcal{C}\Omega_x}(y)\ dy \\
&=: I_{11}(x)+I_{12}(x)\ . \qquad (3.63)
\end{aligned}$$

Since for $y\in B(x,r)\cap\Omega_x$ it holds true that $|f(y)|>\frac{1}{|x-y|}>\frac{1}{r}>1$, we have

$$|I_{11}(x)| \le \frac{1}{2\pi}\int_{\mathbb{R}^2}\frac{1}{|x-y|}\frac{1}{\log\left(\frac{1}{|x-y|}\right)}\ \mathbb{1}_{B(0,r)}(x-y)|f(y)|\log|f(y)|\mathbb{1}_{\Omega_x}(y)\ dy\ . \qquad (3.64)$$

Therefore, since the right hand side of (3.64) belongs to $L^2(\mathbb{R}^2)$ thanks to the Young's inequality, $I_{11}\in L^2(\mathbb{R}^2)$. On the other hand, since for $y\in B(x,r)\cap\mathcal{C}\Omega_x$ it holds true that $|f(y)|\le\frac{1}{|x-y|}$, and we have

$$|I_{12}(x)| \le \int_{\mathbb{R}^2}\frac{1}{|x-y|^{3/2}}\ \mathbb{1}_{B(0,r)}(x-y)\sqrt{|f(y)|}\mathbb{1}_{\mathcal{C}\Omega_x}(y)\ dy\ . \qquad (3.65)$$

Again by the Young's inequality the right hand side of (3.65) belongs to $L^2(\mathbb{R}^2)$ and so $I_{12}$ too. Finally, since for $x\in\mathcal{C}B(0,R)$ and $y\in B(x,r)$ we have $|y|\ge|x|-r\ge R-r>0$, the second term in the right hand side of (3.62) can be dominated in the following way

$$\frac{|x|\mathbb{1}_{\mathcal{C}B(0,R)}(x)}{1+|x|^2}\ \int_{\mathbb{R}^2}\mathbb{1}_{B(0,r)}(x-y)|f(y)|\ dy \le \frac{|x|\mathbb{1}_{\mathcal{C}B(0,R)}(x)}{(1+|x|^2)\log(1+(|x|-r)^2)}\int_{\mathbb{R}^2}|f(y)|\log(1+|y|^2)\ dy\ . \qquad (3.66)$$

Therefore, it belongs to $L^2(\mathbb{R}^2)$. Collecting (3.62), (3.63), (3.64), (3.65) and (3.66), we obtain that $|I_1|\in L^2(\mathbb{R}^2)$.

Concerning $I_2$, it is enough to prove that $I_2\in L^2(\mathcal{C}B(0,R))$ since $I_2\in L^\infty(\mathbb{R}^2)$. Let $x\in\mathcal{C}B(0,R)$ and let us define $\Omega_x'=\left\{y\in\mathbb{R}^2\ :\ |y|<|x|/\log(1+|x|^2)\right\}$. Then,

$$\begin{aligned}
|I_2(x)| &\le \frac{1}{2\pi}\int_{\mathbb{R}^2}\left|\frac{x-y}{|x-y|^2}-\frac{x}{1+|x|^2}\right|\ \mathbb{1}_{\mathcal{C}B(0,r)}(x-y)|f(y)|\mathbb{1}_{\Omega_x'}(y)\ dy \\
&\quad +\frac{1}{2\pi}\int_{\mathbb{R}^2}\left|\frac{x-y}{|x-y|^2}-\frac{x}{1+|x|^2}\right|\ \mathbb{1}_{\mathcal{C}B(0,r)}(x-y)|f(y)|\mathbb{1}_{\mathcal{C}\Omega_x'}(y)\ dy \\
&=: I_{21}(x)+I_{22}(x)\ . \qquad (3.67)
\end{aligned}$$

For $x \in \mathcal{C}B(0,R)$ and $y \in \Omega_x'$ it holds true that $|x|-|y| > |x|\left(1-\frac{1}{\log(1+|x|^2)}\right) > 0$ since $R^2 > e-1$ and

$$\begin{aligned}\left|\frac{x-y}{|x-y|^2}-\frac{x}{1+|x|^2}\right| &\le \frac{|(x-y)(1+|x|^2)-x(|x|^2+|y|^2-2x\cdot y)|}{(|x|-|y|)^2(1+|x|^2)} \\ &\le \frac{|x|+|y|+3|y||x|^2+|x||y|^2}{(1+|x|^2)}\frac{\log^2(1+|x|^2)}{|x|^2(\log(1+|x|^2)-1)^2} \end{aligned} \tag{3.68}$$

The dominant contribution in (3.68) for $x \in \mathcal{C}B(0,R)$ and $y \in \Omega_x'$ is

$$\frac{3|x|^2}{1+|x|^2}\frac{\log(1+|x|^2)}{|x|(\log(1+|x|^2)-1)^2} := h(x)\ ,$$

which belongs to $L^2(\mathcal{C}B(0,R))$. Therefore $|I_{21}(x)| \le \frac{1}{2\pi}\|f\|_{L^1(\mathbb{R}^2)}h(x)$ implies that $I_{21} \in L^2(\mathcal{C}B(0,R))$ too. Finally, for all $x \in \mathcal{C}B(0,R)$ it holds true that

$$\begin{aligned}\log\left(1+\frac{\frac{1}{2}|x-y|^2}{\log^2(1+\frac{1}{2}|x-y|^2)}\right) &\le \max\left(\log\left(1+\frac{|x|^2}{\log^2(1+|x|^2)}\right),\log\left(1+\frac{|y|^2}{1+\log^2(1+|y|^2)}\right)\right) \\ &\le \log\left(1+|y|^2\right), \end{aligned} \tag{3.69}$$

because the left hand side is increasing with respect to $|x-y|$, and that both terms in the right hand side of (3.69) are smaller than $\log\left(1+|y|^2\right)$. We deduce the following bound which eventually proves that $I_{22} \in L^2(\mathcal{C}B(0,R))$:

$$\begin{aligned}|I_{22}(x)| &\le \frac{1}{2\pi}\int_{\mathbb{R}^2}\frac{1}{|x-y|}\ \mathbb{1}_{\mathcal{C}B(0,r)}(x-y)|f(y)|\mathbb{1}_{\mathcal{C}\Omega_x'}(y)\ dy \\ &\quad +\frac{|x|}{2\pi(1+|x|^2)}\ \int_{\mathbb{R}^2}\mathbb{1}_{\mathcal{C}B(0,r)}(x-y)|f(y)|\mathbb{1}_{\mathcal{C}\Omega_x'}(y)\ dy \\ &\le \int_{\mathbb{R}^2}\frac{1}{|x-y|}\frac{1}{\log\left(1+\frac{\frac{1}{2}|x-y|^2}{\log^2(1+\frac{1}{2}|x-y|^2)}\right)}\log\left(1+|y|^2\right)\ \mathbb{1}_{\mathcal{C}B(0,r)}(x-y)|f(y)|\mathbb{1}_{\mathcal{C}\Omega_x'}(y)\ dy \\ &\quad +\frac{|x|}{(1+|x|^2)\left(\log\left(1+\frac{|x|^2}{\log^2(1+|x|^2)}\right)\right)}\int\log(1+|y|^2)\ \mathbb{1}_{\mathcal{C}B(0,r)}(x-y)|f(y)|\mathbb{1}_{\mathcal{C}\Omega_x'}(y)\ dy\ , \end{aligned} \tag{3.70}$$

because $|y| > |x|/\log(1+|x|^2)$ on $\Omega_x'(y)$.

When $\alpha > 0$, we have that $|\nabla B_\alpha(z)| = \frac{1}{2\pi}\frac{1}{|z|}g_\alpha(z)$ with $g_\alpha(z) = \int_0^{+\infty} e^{-s-\alpha\frac{|z|^2}{4s}}\ ds$, (see Section 3.7). Therefore, $|\nabla B_\alpha(z)|$ has the same singularity as $|\nabla E_2(z)|$ in $z=0$ but $|\nabla B_\alpha(z)| \to 0$ exponentially as $|z| \to +\infty$. As a consequence, we can prove that $\nabla\overline{c} = \nabla B_\alpha * f \in L^2(\mathbb{R}^2)$ using the previous technique and without substracting any function of $x$ to the integrand in $\nabla\overline{c}$.

□

### 3.8.3 A remark on the case $\varepsilon = \alpha = 0$

As far as global existence is concerned, it is sufficient to assume that the cell density $n_0$ satifies both

$$\int_{\mathbb{R}^2} n_0(x)\log n_0(x)\ dx < \infty\ , \quad \text{and} \quad \int_{\mathbb{R}^2} n_0(x)\log(1+|x|^2)\ dx < \infty\ . \tag{3.71}$$

In fact, assumptions (3.71) are the optimal ones for several viewpoints. First, they are minimal for applying the logarithmic HLS inequality. Furthermore, the combination of these two ensures that the mass does not escape to infinity, and the balance is optimal again (see Lemma 3.28). Last but not least, it can be proved using free energy methods that conditions (3.71) are indeed propagated along the

solutions, with local in time bounds. Following the lines of computation (3.25) for instance, we are to estimate $\int_{\mathbb{R}^2} c(x,t)H(x)\ dx$ from above. This can be done with the following calculation,

$$\begin{aligned}\int_{\mathbb{R}^2} c(x,t)H(x)\ dx &= -\frac{1}{2\pi}\iint_{\mathbb{R}^2\times\mathbb{R}^2} n(t,y)\log|x-y|H(x)\ dydx \\ &= \frac{1}{8\pi}\int_{\mathbb{R}^2} n(y,t)\log H(y)\ dy + C\ ,\end{aligned}$$

which can be viewed as an integration by parts knowing (3.30) (see also [56] where the Euler-Lagrange equation for $H$ is clearly noticed). The latter is trivially bounded from above because $\int_{\mathbb{R}^2} n(y,t)\log H(y)\ dy$ is nonpositive.

Concerning the blow-up of solutions however, the assumption on the second momentum

$$\int_{\mathbb{R}^2} |x|^2 n_0(x)\ dx < \infty$$

seems to be crucial. For instance, there exist a family of stationary state for the critical mass $M = 8\pi$, with infinite second momentum but finite "logarithmic" momentum, for which blow-up does not occur, obviously [31, 34].

### 3.8.4 The duality

There is a true duality between the Onofri and the logarithmic Hardy-Littlewood-Sobolev inequalities [56, 23]. We followed this idea along this paper. In this appendix we give a formal proof of this duality in the whole space $\mathbb{R}^2$ for the sake of completeness, and we next derive another proof of Lemma 3.15.

First of all, let us write the Onofri inequality as

$$\frac{1}{8\pi}\log\left(\int_{\mathbb{R}^2} e^{8\pi u(x)}H(x)\ dx\right) \le \int_{\mathbb{R}^2} u(x)H(x)\ dx + \frac{1}{2}\int_{\mathbb{R}^2}|\nabla u(x)|^2\ dx\ . \tag{3.72}$$

Let $f$ be a function satisfying the hypotheses of Lemma 3.14, with $\int f(x)\ dx = 1$ without loss of generality. By the minimization procedure (see Appendix 3.8.2) we have

$$\begin{aligned}&-\frac{1}{2}\int_{\mathbb{R}^2}(f-H)(x)(E_2*(f-H))(x)\ dx \\ &\quad= \min_u\left\{\frac{1}{2}\int_{\mathbb{R}^2}|\nabla u(x)|^2\ dx - \int_{\mathbb{R}^2}(f-H)(x)u(x)\ dx\right\} \\ &\quad\ge \min_u\left\{\frac{1}{8\pi}\log\left(\int_{\mathbb{R}^2} e^{8\pi u(x)}H(x)\ dx\right) - \int_{\mathbb{R}^2} f(x)u(x)\ dx\right\} \\ &\quad\ge \min_u\left\{-\frac{1}{8\pi}\int_{\mathbb{R}^2} f(x)\log f(x) - f(x)\big(8\pi u(x)+\log H(x)\big)\ dx - \int_{\mathbb{R}^2} f(x)u(x)\ dx\right\} \\ &\quad\ge -\frac{1}{8\pi}\int_{\mathbb{R}^2} f(x)\log f(x)\ dx + \frac{1}{8\pi}\int_{\mathbb{R}^2} f(x)\log H(x)\ dx\ ,\end{aligned}$$

from the entropy minimization Lemma (see Appendix 3.8.1). On the other hand, the Euler-Lagrange formula for $H$ writes [56],

$$-\int_{\mathbb{R}^2}\log|x-y|H(y)\ dy = \frac{1}{4}\log H(x) + \frac{1}{4}\int_{\mathbb{R}^2} H(x)\log H(x)\ dx + C_0\ .$$

It is in fact the dual formulation of the cancellation property (3.30). We deduce that

$$\begin{aligned}&\frac{1}{4\pi}\iint_{\mathbb{R}^2\times\mathbb{R}^2} f(x)\log|x-y|f(y)\ dxdy + \frac{1}{4\pi}\iint_{\mathbb{R}^2\times\mathbb{R}^2} H(x)\log|x-y|H(y)\ dxdy \\ &\quad\ge \frac{1}{2\pi}\iint_{\mathbb{R}^2\times\mathbb{R}^2} f(x)\log|x-y|H(y)\ dxdy - \frac{1}{8\pi}\int_{\mathbb{R}^2} f(x)\log f(x)\ dx + \frac{1}{8\pi}\int_{\mathbb{R}^2} f(x)\log H(x)\ dx \\ &\quad\ge -\frac{1}{8\pi}\int_{\mathbb{R}^2} f(x)\log f(x)\ dx - \frac{1}{8\pi}\int_{\mathbb{R}^2} H(x)\log H(x)\ dx + \frac{C_0}{2\pi}\ .\end{aligned}$$

We have recovered the logarithmic Hardy-Littlewood-Sobolev inequality with the sharp constant.

Following the previous lines there is another way to derive the modified inequality for the kernel $B_\alpha$ (Lemma 3.15). We proceed as above, more directly because the Bessel kernel has nicer properties at infinity:

$$
\begin{aligned}
&-\frac{1}{2}\int_{\mathbb{R}^2} f(x)(B_\alpha * f)(x)\ dx \\
&\quad = \min_u \left\{ \frac{1}{2}\int_{\mathbb{R}^2} |\nabla u(x)|^2\ dx + \frac{\alpha}{2}\int_{\mathbb{R}^2} u^2(x)\ dx - \int_{\mathbb{R}^2} f(x)u(x)\ dx \right\} \\
&\quad \geq \min_u \left\{ \frac{1}{8\pi}\log\left(\int_{\mathbb{R}^2} e^{8\pi u(x)} H(x)\ dx\right) - \int_{\mathbb{R}^2} f(x)u(x)\ dx + \frac{\alpha}{2}\int_{\mathbb{R}^2} u^2(x)\ dx - \int_{\mathbb{R}^2} u(x)H(x)\ dx \right\} \\
&\quad \geq \min_u \left\{ -\frac{1}{8\pi}\int_{\mathbb{R}^2} f(x)\log f(x) - f(x)\big(8\pi u(x) + \log H(x)\big)\ dx - \int_{\mathbb{R}^2} f(x)u(x)\ dx \right. \\
&\qquad\qquad \left. + \frac{\alpha}{2}\int_{\mathbb{R}^2} u^2(x)\ dx - \int_{\mathbb{R}^2} u(x)H(x)\ dx \right\} \\
&\quad \geq -\frac{1}{8\pi}\int_{\mathbb{R}^2} f(x)\log f(x)\ dx + \frac{1}{8\pi}\int_{\mathbb{R}^2} f(x)\log H(x)\ dx + C(\alpha)\ ,
\end{aligned}
$$

because we have for $\alpha > 0$:

$$
\int_{\mathbb{R}^2} u(x)H(x)\ dx \leq \frac{\alpha}{2}\int_{\mathbb{R}^2} u^2(x)\ dx + \frac{1}{2\alpha}\int_{\mathbb{R}^2} H^2(x)\ dx\ .
$$

Let us mention to conclude this Appendix that there exists a third strategy to prove Lemma 3.15, which is based on a "weak logarithmic HLS inequality" (see [23, Theorem 3]).

# Chapitre 4

# Un exemple de système à deux espèces chimiques

Le système de Keller-Segel pour un couple densité cellulaire/potentiel chimique $(n, c)$ est maintenant bien connu, mais on sait peu de choses d'un système à deux espèces chimiques ou plus. Dans ce papier en collaboration avec Benoît Perthame, la synthèse chimique est modulée par un intermédiaire chimique, le succinate $f$ [237]. L'énergie fait défaut, mais nous exhibons tout de même une fonctionnelle de Lyapounov décroissante sous certaines conditions inédites $\chi\|f\|_{L^\infty} M^{1-\lambda} \leq C_\lambda$ avec $\lambda \in [0, 1/4]$. Ceci est paru dans BIT Numerical Mathematics sous le titre *A Lyapunov function for a two-chemical version of the chemotaxis model* [54].

## 4.1 Introduction – Statement of the problem

In the early 70's Keller and Segel have published seminal papers about the modeling of cell populations movements [153, 154] (see also [206]). They describe how chemotaxis may explain several features of cell movement. Chemotaxis means movement in response to a chemical cue, say for instance food, poison or any chemical signal. Various examples of such oriented movement can be found in bacterial motility (*Escherichia Coli* [5]), or in collective cell organization (the slime mold amoebae *Dictyostelium discoideum* and the cAMP molecule [138]). Chemotaxis is also involved, with more specific ingredients, in modelisation of pattern formation [205], vascular network formation [108, 223, 104] and angiogenesis [165, 173]. From a mathematical point of view, the interest of the Keller-Segel system stems from its nonlinear conservative structure which allows for blow-up, critical spaces, traveling waves...

In this paper we will focus on some variant of the classical Patlak, Keller and Segel model (see below for a brief overview of this model). It has been introduced by Brenner *et al.*, and promoted by Tyson *et al.* [40, 237] (see also [185]) in order to explain complex bacterial pattern formation in semi-solid medium [44]. The main additional feature is a second reactant, namely the stimulant $f$ which is consumed by the cells $n$ to produce $c$. We present here a simplified version which captures in a certain sense the main difficulties brought by the additional equation. Namely, we consider the system

$$\left\{ \begin{array}{rcl} \dfrac{\partial n}{\partial t} & = & \Delta n - \chi \nabla \cdot (n \nabla c) \quad t \geq 0\,,\ x \in \Omega \subset \mathbb{R}^2, \\ -\Delta c & = & nf - \langle nf \rangle, \\ \dfrac{\partial f}{\partial t} & = & -nf. \end{array} \right. \tag{4.1}$$

We complete this system with initial conditions $n^0$, $c^0$, $f^0$. Here $\Omega$ is a bounded domain, and we consider zero-flux boundary conditions for both $n$ and $c$.

**The Patlak, Keller and Segel (PKS) model.** The PKS system consists of two coupled equations for the evolution of the cell density $n(t,x)$ and the chemoattractant $c(t,x)$ respectively. Cell density is governed by a drift-diffusion equation

$$\frac{\partial n}{\partial t} + \nabla \cdot \Big( - \nabla n + \chi n \nabla c \Big) = 0 \,, \quad t \geq 0 \,,\ x \in \Omega \subset \mathbb{R}^2, \tag{4.2}$$

and the concentration of chemical satisfies a reaction-diffusion equation wich reads

$$- \Delta c = n - \langle n \rangle, \tag{4.3}$$

in the limiting case of fast diffusion [147]. Here $\langle n \rangle$ denotes the mean value of $n$ over the domain $\Omega$. Boundary conditions are zero-flux. The key parameters are $\chi$ the chemotactic sensitivity – which is assumed to be constant here – and $M$ the total mass of cells – which is formally conserved. The general behaviour of this system is now quite well understood, and main results are summarized in the following theorem [107, 29, 141, 77].

**Theorem 4.1** (Global existence for the PKS model)**.** *Assume $\Omega$ is a regular bounded domain and $n_0 \in L^\infty(\Omega)$. If $\chi M < 4\pi$ solutions are global in time. If $\chi M > 8\pi$ and the second moment of $n_0$ is large enough then the solution blows-up in finite time.*

*If $\Omega$ is the whole space $\mathbb{R}^2$ and both $n_0\big(|\log n_0| + (1+|x|^2)\big) \in L^1$, then solutions are global in time if $\chi M < 8\pi$, or blow up in finite time if $\chi M > 8\pi$.*

The existence parts of these results are based on two different strategies. The common feature is to prove equi-integrability for the cell density $n$ thanks to *a priori* estimates. These *a priori* estimates are of two types. Given a functional $\Phi$ growing faster than linearly (typically $\Phi(u) = u \log u$ or $\Phi(u) = u^p$), a direct computation of $\frac{d}{dt} \int \Phi(n)\, dx$ gives two terms of opposite signs. In general a Gagliardo-Nirenberg-Sobolev (GNS) inequality can be used to estimate the balance between the diffusion and the chemotactic contributions. The threshold condition coming from GNS inequality has the right homogeneity, but it is not optimal. On the other hand, the free energy for system (4.2), (4.3) writes

$$\mathcal{E}(t) = \int n \log n - \frac{\chi}{2} \int cn.$$

It is non increasing and therefore it is possible to estimate $\int n \log n$ if the two opposite contributions can be compared to each other, by means of fine inequalities (namely Trudinger-Moser or logarithmic Hardy-Littlewood-Sobolev inequalities).

There are several shortcomings to model (4.2), (4.3). Several biochemistry aspects are not taken into account, as well the type of physical support for the experiments [185, Vol. II chap. 5]. Also concentrations points do not move in usual numerical simulations [177] by opposition to experimental observations or numerical simulations of (4.1) as shown in Figure 4.1. The formulas for the aggregate motion in [240] confirm that different regularizations of (4.2), (4.3) give different dynamics.

**Statement of the main result.** As we mentioned above, a natural question arising among various studies of PKS models is whether solution blows up or not in finite time. Various modifications of the classical model (4.2), (4.3) have already been proposed to prevent formation of singularities. For instance, Kowalczyk analyzed a system including nonlinear cell diffusion [159]. On the other side Painter and Hillen considered a saturating effect on the chemotactic sensitivity [135]: $\chi(n)$ vanishes for large $n$ (see also [50] for a discussion concerning these volume effects). In the following we raise the question of any blow-up for the model (4.1), a question that we only partially answer here. Notice that (4.1) can be considered as an extension of some system arising to describe angiogenesis that has been studied in [77], and for which the question of blow up is also open.

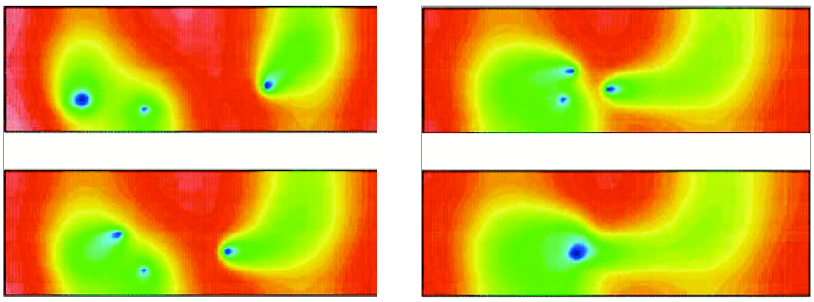

Figure 4.1: Motion of three aggregates in an extended Keller-Segel system as (4.1). Courtesy of A. Marrocco (work in preparation).

First let us present a method, directly inspired from [147]. It is based on the following Gagliardo-Nirenberg-Sobolev inequality [106, 193],

$$\int n^2 \leq \mathcal{C}_{gns} \int n \int |\nabla \sqrt{n}|^2. \tag{4.4}$$

This estimation appears naturally when computing the evolution of $\int n \log n$.

$$\begin{aligned} \frac{d}{dt} \int n \log n &\leq -4 \int |\nabla \sqrt{n}|^2 + \chi \int n^2 f \\ &\leq -4 \int |\nabla \sqrt{n}|^2 + \chi \|f\|_\infty \int n^2 \\ &\leq \big( -4 + \chi \|f\|_\infty M \mathcal{C}_{gns} \big) \int |\nabla \sqrt{n}|^2. \end{aligned}$$

Therefore, using this only ingredient, we can hope to conclude only under the condition

$$\chi \|f^0\|_\infty M < \mathcal{C}^*. \tag{4.5}$$

This condition is not satisfactory in the sense that it doesn't bring anything new by comparison to the classical Keller and Segel model, and because it doesn't capture the fine coupling with the additional equation $\partial_t f = -nf$.

Unfortunately we know no energy structure, wich makes this model dramatically different from (4.2), (4.3). However we derive in this paper a new class of conditions involving the parameters $\chi M$ and $\|f^0\|_\infty$ which guarantees *a priori* estimates.

**Theorem 4.2** (A priori estimates for the extended PKS model)**.** *Let $\Omega$ be a bounded domain. It exists a family of conditions*

$$\chi \|f^0\|_\infty M^{1-\lambda} \leq C_\lambda, \tag{4.6}$$

*indexed by $\lambda \in [0, \frac{1}{4}]$ such that: if at least one of these conditions is fulfilled, then the solution of* (4.1) *is* a priori *globally equi-integrable.*

From now on our strategy consists in studying the variations of a well-chosen functional $\mathcal{W}$ combining with homogeneity the standard energy of PKS equations and that of the angiogenesis model used in [77], namely

$$\mathcal{W}(t) = \int n \log n + b \int n f^\gamma + \frac{a}{2} \int |\nabla f^\delta|^2,$$

where $a$, $b$ are some constants depending on the parameters, and $\delta$, $\gamma$ are exponents without homogeneity.

At the end of this contribution we are concerned with the problem of global existence for the system (4.1), and we provide some discussion how to prove it based on theorem 4.2.

**Theorem 4.3** (Global existence for the extended model)**.** *Assume condition 4.6, $n^0 \in L^1 \cap L^p$ for some $p > 1$, and $\mathcal{W}(0)$ is finite, then there is a unique weak solution to* (4.1) *that satisfies $\mathcal{W}(t) \leq \mathcal{W}(0)$ and $n \in L^\infty\big(\mathbb{R}_+; L^1 \cap L^p\big)$.*

In section 4.2 we present some regularization estimates which justify the choice of the functional $\mathcal{W}$. In sections 4.3 and 4.4 we drive the calculation leading to $\frac{d}{dt}\mathcal{W} \leq 0$, and hence we prove theorem 4.2. Finally we prove theorem 4.3 in section 4.5.

## 4.2 Preliminaries: global existence for the chemotaxis and the angiogenesis models

In this section we review some basics of the existence theorems for the chemotaxis and the angiogenesis models respectively. The energy structure for the first one has already been described in introduction.

### 4.2.1 The chemotaxis model

We first highlight the following statement

$$\frac{d}{dt}\int n^p + 2\frac{p-1}{p}\int |\nabla n^{p/2}|^2 \leq \frac{\chi^2 p(p-1)}{2}\|\nabla c\|^2_{L^\infty_{t,x}}\int n^p, \tag{4.7}$$

which comes directly from (4.2). It means that some estimate on $\nabla c$ cancels the nonlinearity and provide any $L^p$ bound, $p < \infty$, for the cell density $n$. Unfortunately this $\nabla c$ estimate is not available *e.g.*, and the usual way is to start from equi-integrability, namely $\int n|\log n|\,dx \leq C$, which avoids the formation of Dirac masses; then to propagate $L^p$ bounds thanks to the following computation

$$\begin{aligned}\frac{d}{dt}\int (n-k)_+^p + 4\frac{p-1}{p}\int |\nabla (n-k)_+^{p/2}|^2 \\ \leq \chi(p-1)\int (n-k)_+^{p+1} + O\Big(\int (n-k)_+^p\Big).\end{aligned} \tag{4.8}$$

Indeed using the Gagliardo-Nirenberg-Sobolev inequality

$$\int (n-k)_+^{p+1}\,dx \leq \mathcal{C}_{gns}(p)\int |\nabla (n-k)_+^{p/2}|^2\,dx \int (n-k)_+\,dx,$$

and equi-integrability yelds the inequality

$$\frac{d}{dt}\int (n-k)_+^p \leq O\Big(\int (n-k)_+^p\Big),$$

which ensures that $\|n\|_{L^p}$ is controlled [147, 77]. This argumentation remains valid in the extended system (4.1), so we are to prove equi-integrability only.

### 4.2.2 The angiogenesis model

Following [9] a simplified model for angiogenesis has been proposed in [76]. It reads

$$\left\{\begin{array}{rcl}\dfrac{\partial n}{\partial t} &=& \Delta n - \chi\nabla\cdot(n\nabla f) \quad t \geq 0\,,\ x \in \Omega \subset \mathbb{R}^2, \\ \dfrac{\partial f}{\partial t} &=& -nf,\end{array}\right. \tag{4.9}$$

where $n$ denotes the endothelial cell density, and $f$ denotes some chemical angiogenic factor, secreted by a tumor for instance. Boundary conditions are zero-flux as well. Contrary to the chemotactic model PKS, this system admits a positive energy structure $\frac{d}{dt}\mathcal{E} \leq 0$ with

$$\mathcal{E}(t) = \int n\log n + 2\chi\int |\nabla\sqrt{f}|^2.$$

This energy structure provides us with global existence of weak solutions. It is also possible to derive $L^p$ bounds for the cell density similarly to (4.8) under smallness assumptions, but we won't enter into details here (see [77]).

## 4.3 Outline of the calculation

We consider a combination of the following type [107]

$$\mathcal{W}(t) = \int n\log n + b\int nf^\gamma + \frac{a}{2}\int |\nabla f^{\gamma-1}|^2. \tag{4.10}$$

Our goal is to show that it is decreasing for suitable values of $a$, $b$, which are proved to exist whenever $(\chi\|f^0\|_\infty)^\gamma M^{\gamma-1} \le C_\gamma$, $\gamma \ge 4$. Note that we will keep $\gamma$ along the paper, and we will introduce $\lambda = \gamma^{-1}$ in conclusion. We first compute each term of the derivative $\dfrac{d}{dt}\mathcal{W}$.

$$\frac{d}{dt}\int n\log n \;\le\; -4\int |\nabla\sqrt{n}|^2 + \chi\int n^2 f, \tag{4.11}$$

$$b\frac{d}{dt}\int nf^\gamma \;=\; -b\int \nabla n\cdot\nabla f^\gamma + \chi b\int n\nabla c\cdot\nabla f^\gamma - \gamma b\int n^2 f^\gamma, \tag{4.12}$$

$$\frac{a}{2}\frac{d}{dt}\int |\nabla f^{\gamma-1}|^2 \;=\; -\frac{\gamma-1}{2}a\int \nabla n\cdot\nabla f^{2\gamma-2} - (\gamma-1)a\int n|\nabla f^{\gamma-1}|^2. \tag{4.13}$$

In order to compensate the bad influence of the positive (*resp.* no-sign) terms in the right-hand side of (4.11) (*resp.* (4.12), (4.13)), we plan to associate them with the negative ones in two ways. The first group is made of

$$-4\int |\nabla\sqrt{n}|^2 - \left\{ \begin{array}{c} b\displaystyle\int \nabla n\cdot\nabla f^\gamma \\ \dfrac{\gamma-1}{2}a\displaystyle\int \nabla n\cdot\nabla f^{2\gamma-2} \end{array} \right\} - (\gamma-1)a\int n|\nabla f^{\gamma-1}|^2 \le 0. \tag{4.14}$$

The sign of this expression will be determined thanks to a recombination into a remarkable square. The second group is made of

$$\chi\int n^2 f - \gamma b\int n^2 f^\gamma.$$

The non-friendly term $\chi b\int n\nabla c\cdot\nabla f^\gamma$ plays an ambivalent role in this description, because it gives contributions to each group.

## 4.4 Details of the estimation

Our main objective is to preserve the homogeneity along computations. For this purpose we frequently introduce some homogeneity constant which has to be fixed later on.

### 4.4.1 The first group (4.14)

We force a remarkable square to appear thanks to the square terms. We are able to upperbound (4.14) by

$$-4\int |\nabla\sqrt{n}|^2 + 2b\frac{\gamma}{\gamma-1}\|f\|_\infty\int |\nabla\sqrt{n}|\cdot|\sqrt{n}\nabla f^{\gamma-1}| - (\gamma-1)a\int n|\nabla f^{\gamma-1}|^2 \le 0.$$

So a first condition concerning the homogeneity of $a$ and $b$ comes naturally for this expression to be non-positive: the discriminant is non-positive;

$$\left(2b\|f(t)\|_\infty\frac{\gamma}{\gamma-1}\right)^2 - 16a(\gamma-1) \le 0. \tag{4.15}$$

More precisely we choose the constants $a$, $b$ so that

$$\left(2b\|f^0\|_\infty \frac{\gamma}{\gamma-1}\right)^2 = a(\gamma-1), \quad \gamma > 1. \tag{4.16}$$

The same computation arises for the other expression of (4.14), namely

$$-4\int |\nabla\sqrt{n}|^2 + 2(\gamma-1)a\int |f|^{\gamma-1}|\nabla\sqrt{n}||\sqrt{n}\nabla f^{\gamma-1}| - (\gamma-1)a\int n|\nabla f^{\gamma-1}|^2 \le 0.$$

We get a similar condition on the discriminant of this expression, and we choose exactly the constant $a$ to be

$$4(\gamma-1)a\|f^0\|_\infty^{2\gamma-2} = 1, \tag{4.17}$$

and the combination of (4.16) and (4.17) gives in addition

$$4\left(b\|f^0\|_\infty^\gamma \frac{\gamma}{\gamma-1}\right) = 1. \tag{4.18}$$

In this subsection we have hidden the two terms $b\nabla n\cdot\nabla f^\gamma$ and $\frac{\gamma-1}{2}a\int \nabla n\cdot\nabla f^{2\gamma-2}$ in the negative contributions of

$$-2\int |\nabla\sqrt{n}|^2 \quad \text{and} \quad -\frac{1}{2}(\gamma-1)a\int n|\nabla f^{\gamma-1}|^2.$$

### 4.4.2 Estimating the ambivalent term $\int n\nabla c\cdot\nabla f^\gamma$

We can combine this no-sign term in a general way

$$\begin{aligned}\int n|\nabla c\cdot\nabla f^\gamma| &= \frac{\gamma}{\gamma-1}\int nf|\nabla c\cdot\nabla f^{\gamma-1}|,\\ &\le \left(\frac{\gamma}{\gamma-1}\right)^2\frac{K}{2}\int n|\nabla f^{\gamma-1}|^2 + \frac{1}{2K}\int nf^2|\nabla c|^2,\end{aligned} \tag{4.19}$$

with a homogeneity constant $K$ which has to be fixed. We would like to associate the first right-hand side term with $-(\gamma-1)a\int n|\nabla f^{\gamma-1}|^2$, that is

$$\chi\frac{K}{2}b\left(\frac{\gamma}{\gamma-1}\right)^2\int n|\nabla f^{\gamma-1}|^2 - \frac{1}{2}a(\gamma-1)\int n|\nabla f^{\gamma-1}|^2 \le 0.$$

In fact we choose

$$\chi b\left(\frac{\gamma}{\gamma-1}\right)^2 K = (\gamma-1)a, \quad \text{hence} \quad 4\chi b\left(\frac{\gamma}{\gamma-1}\right)^2\|f^0\|_\infty^{2(\gamma-1)}K = 1, \tag{4.20}$$

(after combination with (4.17)). The second right-hand side term of (4.19) will be eliminated thanks to the combination of a Sobolev inequality

$$\|\nabla c\|_4^4 \le \mathcal{C}_{\mathcal{S}}\|nf\|_{4/3}^4, \tag{4.21}$$

and a Gagliardo-Nirenberg-Sobolev inequality

$$\left(\int n^{4/3}\right)^3 \le \mathcal{C}_{gns}M^3\int |\nabla\sqrt{n}|^2.$$

Notice that this constant $\mathcal{C}_{gns}$ differs from (4.4): we just want to mention the origin of the constant in the following. It comes

$$\int nf^2|\nabla c|^2 \le \frac{L}{2}\int n^2f^4 + \frac{1}{2L}\int |\nabla c|^4, \tag{4.22}$$

and also

$$\int |\nabla c|^4 \leq \mathcal{C}^* \|f(t)\|_\infty^4 M^3 \int |\nabla \sqrt{n}|^2, \tag{4.23}$$

where $\mathcal{C}^* = \mathcal{C}_{\mathcal{S}} \mathcal{C}_{gns}$. To compare (4.23) with our available negative term $-4\int |\nabla\sqrt{n}|^2$ from (4.11), parameters should fulfill

$$\chi b K^{-1} L^{-1} \|f\|_\infty^4 M^3 \mathcal{C}^* \leq 16.$$

We choose precisely

$$\chi b K^{-1} L^{-1} \|f^0\|_\infty^4 M^3 \mathcal{C}^* = 4. \tag{4.24}$$

In this subsection we have consumed

$$-\int |\nabla\sqrt{n}|^2 \quad \text{and} \quad -\frac{1}{2}(\gamma-1)a\int n|\nabla f^{\gamma-1}|^2.$$

Finally we have to deal with the last remaining positive terms, namely $\int n^2 f$ in (4.11) and $\int n^2 f^4$ in (4.22).

At this stage we leave chosen the constants: $a$ by (4.17), $b$ by (4.18), $K$ by (4.20), and $L$ by (4.24).

### 4.4.3 The second group

In order to eliminate the two terms $\int n^2 f$ and $\int n^2 f^4$, we of course associate them with $\int n^2 f^\gamma$. That is why we impose $\gamma \geq 4$ in theorem 4.2. We use the following majorations which distinguish between high and low values of $f$.

$$Y \leq R^{-1}\mathcal{C}(\gamma) + R^{\gamma-1}Y^\gamma,$$

$$X^4 \leq S^{-4}\mathcal{C}(\nu) + S^{\gamma-4}X^\gamma\,, \quad 4\nu = \gamma,$$

with the constant $E(\nu) = \mathcal{C}(\nu)^{\nu-1} = \frac{(\nu-1)^{(\nu-1)}}{\nu^\nu}$. Then for each term $\int n^2 f^4$ and $\int n^2 f$ we get two new terms involving $\int n^2$ and $\int n^2 f^\gamma$:

$$\chi\int n^2 f \leq \chi\mathcal{C}(\gamma)R^{-1}\int n^2 + \chi R^{\gamma-1}\int n^2 f^\gamma,$$

$$\chi b\frac{K^{-1}L}{4}\int n^2 f^4 \leq \chi b\frac{K^{-1}L}{4}S^{-4}\mathcal{C}(\nu)\int n^2 + \chi b\frac{K^{-1}L}{4}S^{\gamma-4}\int n^2 f^\gamma.$$

At this stage we can use the first Gagliardo-Nirenberg-Sobolev inequality (4.4) to estimate $\int n^2$, and we deduce the following conditions

$$2\chi\mathcal{C}(\gamma)R^{-1}M\mathcal{C}_{gns} = 1, \quad 2\chi b\frac{K^{-1}L}{4}S^{-4}\mathcal{C}(\nu)M\mathcal{C}_{gns} = 1. \tag{4.25}$$

On the other hand we look for a cancellation of the last positive remaining terms involving both $\int n^2 f$, and therefore we impose

$$2\chi R^{\gamma-1} \leq \gamma b, \quad 2\chi b\frac{K^{-1}L}{4}S^{\gamma-4} \leq \gamma b. \tag{4.26}$$

Finally we have determined all the homogeneity constants introduced in the calculations, and we can restate (4.25), (4.26) as following:

$$2\chi\left(2\chi\mathcal{C}(\gamma)\mathcal{C}_{gns}M\right)^{\gamma-1} \leq \gamma b, \tag{4.27}$$

$$\chi b K^{-1}L\left(\chi b K^{-1}L\mathcal{C}(\nu)\mathcal{C}_{gns}M\right)^{\nu-1} \leq 2^\nu\gamma b, \quad \nu = \frac{\gamma}{4}, \tag{4.28}$$

and we recall that $b$, $K$, $L$ are already fixed. Notice that (4.27) and (4.28) are redundent thanks to the exponents involved.

### 4.4.4 Consequences of the homogeneity relations

Replacing $b$, $K$ and $L$ by their values (4.18), (4.20), (4.24), and because we have set $\gamma = 4\nu$, we find that the two redundent conditions (4.27) and (4.28) can summarize simply into the single inequality

$$E(\gamma)\chi^\gamma \|f\|_\infty^\gamma M^{\gamma-1} \leq C_\gamma^\gamma, \tag{4.29}$$

where the constants $C_\gamma$ are uniformly bounded. Consequently, taking the $\gamma$-root of (4.29) and because

$$E(\gamma)^{1/\gamma} = \frac{(1-1/\gamma)^{1-1/\gamma}}{(1/\gamma)^{1/\gamma}}$$

is bounded for $\gamma \geq 4$, we obtain the final condition, announced in theorem 4.2.

$$\chi\|f^0\|_\infty M^{1-\lambda} \leq C_\lambda, \quad \lambda \in [0, \frac{1}{4}],$$

with a bounded family of constants $(C_\lambda)$. Note that the special case $\lambda = 0$ corresponds to estimation (4.5).

## 4.5 Global existence for the system (4.1)

We prove theorem 4.3 and we proceed as usually in three steps.

**Step 1. Regularization of the system.** We propose to replace the second equation with

$$-\Delta c = T_K(nf) - \langle T_K(nf)\rangle, \tag{4.30}$$

where $T_K(u) = \min(u, K)$. The corresponding system together with regularized initial conditions is solved using Banach fixed point theorem. The truncature (4.30) ensures that the solution $(n_K, c_K, f_K)$ is global in time, because it avoids formation of any singularity; see section 4.2.1, and notice that $T_K(nf)$ is a priori bounded in $L^1 \cap L^\infty$, therefore $\nabla c \in W^{1,\infty}$ by Young's inequality.

**Step 2. Estimates for the regularized system.** *A priori* estimates which have been proved formally in section 4.4 can be adapted to the regularized system with minor modifications. First we compute the time derivative of $\mathcal{W}$ related to the regularized model.

$$\frac{d}{dt}\int n\log n \leq -4\int |\nabla\sqrt{n}|^2 + \chi\int nT_K(nf), \tag{4.31}$$

$$b\frac{d}{dt}\int nf^\gamma = -b\int \nabla n\cdot\nabla f^\gamma + \chi b\int n\nabla c\cdot\nabla f^\gamma - \gamma b\int n^2 f^\gamma, \tag{4.32}$$

$$\frac{a}{2}\frac{d}{dt}\int |\nabla f^{\gamma-1}|^2 = -\frac{\gamma-1}{2}a\int \nabla n\cdot\nabla f^{2\gamma-2} - (\gamma-1)a\int n|\nabla f^{\gamma-1}|^2. \tag{4.33}$$

Only the first part (4.31) is affected by the truncature. Consequently we are able to follow the consecutive steps of section 4.4, because the negative terms in (4.31), (4.32) and (4.33) necessary for cancellations remain unchanged.

**Step 3. Propagation of regularity.** Finally we can use the upperbound of $\int n\log n$ to prove $L^p$ bounds for the cell density (see [147, 77] and section 4.2). These estimations provide also time compactness in terms of

$$\int_0^\infty \|\nabla n^{p/2}\|_{L^2(\Omega)}^2 \leq C(\|n_0\|_{L^p(\Omega)}).$$

Passing to the limit, the main difficulty lies in the nonlinear term $\nabla\cdot(n\nabla c)$ and we need some compactness. It is provided by the Lions-Aubin lemma [14] which claims that the embedding

$$\left\{u \in L^2\big(0,T;H^1\big),\ \partial_t u \in L^2\big(0,T;L^2\big)\right\} \hookrightarrow \mathcal{C}\big(0,T;L^2\big)$$

is compact.

## 4.6 Conclusion

We have studied a priori bounds (and existence) for the variant (4.1) of the well-known Keller and Segel model. Because of the lack of energy structure we have introduced a new type of functional $\mathcal{W}$ which is decreasing under some condition involving the parameters. These new considerations may be extended to new kinds of models where several extracellular products are involved (angiogenesis for instance).

We have been able to find a new threshold condition (4.6) ensuring that $\int n \log n$ remains bounded and thus that $n$ is equi-integrable. But we have no certitude whether solutions may blow up or not above these thresholds. In fact we have not shown any existence of a blowing-up solution for this system, and the mechanism for such a blow-up is certainly more complex than for the Keller and Segel model.

# Chapitre 5

# Existence globale pour un modèle cinétique avec effet de mémoire

---

Dans ce travail en collaboration avec Nikolaos Bournaveas, Susana Gutiérrez et Benoît Perthame, nous abandonnons le modèle parabolique de Keller-Segel et ses multiples variantes, au profit du modèle cinétique d'Othmer, Dunbar et Alt [198]. Nous reprenons et poursuivons les travaux de [66] et [144] à l'aune de l'existence globale. Le jeu d'hypothèses sur le noyau de changement de direction est double : on peut légèrement affaiblir celles de [144] pour garantir l'existence globale des solutions pour tout masse (lemme de dispersion + effet de mémoire, voir aussi l'annexe C) ; d'autre part on peut prouver l'existence globale des solutions de masse petite sous des hypothèses encore plus faibles, à l'aide d'estimations de type Strichartz [64]. Ceci est à paraître dans Communications in Partial Differential Equations sous le titre *Global existence for a kinetic model of chemotaxis via dispersion and Strichartz estimates* [37].

---

## 5.1 Introduction

In this paper we study the Othmer-Dunbar-Alt kinetic model of chemotaxis and prove global existence of solutions under various assumptions on the turning kernel. This model was proposed in [5, 198] for the description of the chemotactic movement of cells in the presence of a chemical substance and it can be thought of as the mesoscopic analogue of the famous Keller-Segel model [152, 153, 154, 141]. It was proposed in the 80's, after the experimental observation that bacteria (*E. Coli* in the present case, but this is also true for other bacteria as *B. Subtilis* for instance) move by a series of 'run and tumble' corresponding to the clockwise or counterclockwise activations of their flagellas in response to chemoattractant substances and receptors saturation.

Denoting the cell density by $f(t,x,v)$ and the density of the chemoattractant by $S(t,x)$ the equations read as follows:

$$\partial_t f + v\cdot\nabla_x f = \int_V \left(T[S]f' - T^*[S]f\right) dv', \tag{5.1a}$$

$$f(0,x,v) = f_0(x,v), \tag{5.1b}$$

$$\beta S - \Delta S = \rho := \int_V f(t,x,v)dv,\ \beta = 0,1. \tag{5.1c}$$

We have used the abbreviations $T[S]f' = T[S](t,x,v,v')f(t,x,v')$ and $T^*[S]f = T[S](t,x,v',v)f(t,x,v)$. The velocity space $V$ is assumed to be a bounded three dimensional domain, typical examples being balls

$\{|v| \leq R\}$ and spherical shells $\{r \leq |v| \leq R\}$. As a consequence, if $f_0$ has compact support in $x$, this will be so for all later times, and many aspects of the present paper can be simplified or improved, but of course to the expense of generality. Therefore we do not go in that direction.

Several earlier works have been devoted to the mathematical study of this kinetic model of chemotaxis. In [134], the linear system has been studied (i.e. with a given field $S$) and in particular a major issue has been exhibited concerning the 'memory' effect present in the model through a time scale $\epsilon$ in expressions as $S(x-\epsilon v')$ or $S(x+\epsilon v)$. Not only this is a major experimental observation related to receptors saturation, but it also is responsible for an asymmetric kernel (in $v$, $v'$) which yields the drift term in the Keller-Segel model that is derived in the diffusion limit of equation (5.1). The meaning of $S(t, x-\epsilon v')$ is that cells measure the concentration of the chemical $S$ at position $x-\epsilon v'$ before changing their direction at position $x$, because of an internal memory effect. The other contribution $S(t, x+\epsilon v)$ is interpreted as follows: cells are able to measure the concentration at a location $x+\epsilon v$ thanks to sensorial protrusions. We set $\epsilon = 1$ in the following without loss of generality.

The nonlinear Initial Value Problem (5.1) was first studied in [66] where global existence was proved in $d = 3$ dimensions under the assumption that the turning kernel satisfies the condition

$$0 \leq T[S](t, x, v, v') \leq C\Big(1 + S(t, x+v) + S(t, x-v')\Big)$$

and the initial data satisfy $0 \leq f_0 \in L^1(\mathbb{R}^6) \cap L^\infty(\mathbb{R}^6)$. The proof starts with the fact that the $L^1_{x,v}$-norm of the solution $f$ is a-priori bounded thanks to conservation of mass

$$\iint_V f(t, x, v) dv dx = \iint_V f_0(x, v) dv dx =: M, \tag{5.2}$$

and then proceeds to bootstrap higher $L^p_{x,v}$-norms based on strong dispersion estimates (see [116, 208]).

The same method was used in the paper [144] which points out the difference in the dispersive arguments for terms involving both $S(t, x+v)$ and $S(t, x-v')$. The authors prove global existence in $d = 3$ dimensions under the assumption

$$0 \leq T[S](t, x, v, v') \leq C\Big(1 + S(t, x+v) + |\nabla S(t, x+v)|\Big)$$

or

$$0 \leq T[S](t, x, v, v') \leq C\Big(1 + S(t, x-v') + |\nabla S(t, x-v')|\Big),$$

and in $d = 2$ dimensions together with $\beta = 1$ under the assumption

$$0 \leq T[S](t, x, v, v') \leq C\Big(1 + S(t, x+v) + S(t, x-v') + |\nabla S(t, x+v)| + |\nabla S(t, x-v')|\Big).$$

The main difficulty appears: scattering terms involving $S(x-v')$ or $S(x+v)$ lead to use two different dispersion estimates, that lead to use a bootstrap with integrability exponents that are only compatible in dimensions less than four. The same dispersive method has been pushed forward in [144, 143], including more general biologically relevant turning kernels and pointing out several limitations.

For more results and models involving kinetic equations, see [104, 67, 136], for hyperbolic models [145, 95] and for surveys on the kinetic aspects [207, 208].

In this paper we use the dispersion and Strichartz estimates for solutions of the kinetic transport equation proved in [64] to extend the three dimensional results of [66] and [144] to more general turning kernels. Compared to [66] and [144] where $L^p_{x,v}$-spaces are used, the main feature of our present estimates is to work in $L^p_x L^q_v$-spaces for appropriate choices of $p$ and $q$ (see remark 5.8 for instance).

In our first result we combine the dispersion estimate of [64] with the well-known consequence of Calderón-Zygmund theory that any second derivative can be controlled in $L^p$ $(1 < p < \infty)$ by the Laplacian in $L^p$, to prove global existence for the IVP (5.1) under assumption (5.3) below. The latter assumption allows the turning kernel $T[S]$ to be controlled by second derivatives of the chemoattractant density $S$. Notice that this result is valid in all dimensions $d \geq 2$.

**Theorem 5.1.** *Let $d \geq 2$ and suppose that the (continuous) turning kernel satisfies*

$$0 \leq T[S](t,x,v,v') \leq C\left(1 + \sum_{|\alpha|\leq 2} |\partial^\alpha S(t,x+v)|\right). \tag{5.3}$$

*Fix $p \in \left(1, \frac{d}{d-1}\right)$. If the initial data $f_0 \in L^1(\mathbb{R}^{2d})$ is nonnegative and such that $\|f_0(x-tv,v)\|_{L^p(\mathbb{R}^d_x;L^1(\mathbb{R}^d_v))}$ is finite for all $t>0$ ([5]), then the Cauchy problem (5.1) with $\beta = 1$ has a global weak solution $f$ with $f(t) \in L^1(\mathbb{R}^{2d}) \cap L^p(\mathbb{R}^d_x; L^1(V))$ for all $t \geq 0$.*

As it was already commented in [66] and [144] it is difficult to mix terms involving $x+v$ with terms involving $x-v'$. In this direction we shall prove the following result.

**Theorem 5.2.** *Let $d = 3$ and suppose that the (continuous) turning kernel satisfies*

$$0 \leq T[S](t,x,v,v') \leq C\Big(1 + S(t,x+v) + S(t,x-v') + |\nabla S(t,x+v)|\Big). \tag{5.4}$$

*Let $q \in (1,3/2)$. Then there exists a $p \in (3/2,3)$ (depending on $q$) such that if the initial data $f_0 \in L^1(\mathbb{R}^6)$ is nonnegative and such that $\|f_0(x-tv,v)\|_{L^p(\mathbb{R}^3_x;L^q(\mathbb{R}^3_v))}$ is finite for all $t>0$, then the Cauchy problem (5.1) has a global weak solution $f$ with $f(t) \in L^1(\mathbb{R}^6) \cap L^p(\mathbb{R}^3_x; L^q(V))$ for all $t \geq 0$.*

Hypothesis (5.4) does not allow putting together the two gradients $\nabla S(t,x+v)$ and $\nabla S(t,x-v')$. However, our next result shows that if we add the assumption that the critical $L^{3/2}_{x,v}$-norm of the initial data is sufficiently small then we have global existence under a very general hypothesis on the turning kernel, see (5.5) and the even weaker (5.42). The proof uses the Strichartz estimates of [64] and can be made to work in $d = 2$ and 4 dimensions too, see Remark 5.10.

**Theorem 5.3.** *Let $d = 3$. Consider nonnegative initial data $f_0 \in L^1(\mathbb{R}^{2d}) \cap L^a(\mathbb{R}^{2d})$, where $\frac{3}{2} \leq a \leq 2$, and assume that $\|f_0\|_{L^a(\mathbb{R}^{2d})}$ is sufficiently small. Assume that the (continuous) turning kernel $T[S]$ satisfies the condition*

$$0 \leq T[S](t,x,v,v') \leq C\Big(1 + |S(t,x\pm v)| + |S(t,x\pm v')| + |\nabla S(t,x\pm v)| + |\nabla S(t,x\pm v')|\Big), \tag{5.5}$$

*where any combination of signs is allowed in the right hand side. Then the IVP (5.1) with $\beta = 1$ has a global weak solution $f \in L^3_t\left([0,\infty); L^p\left(\mathbb{R}^3_x; L^q(V)\right)\right)$, where $\frac{1}{p} = \frac{1}{a} - \frac{1}{9}$ and $\frac{1}{q} = \frac{1}{a} + \frac{1}{9}$. This result also holds if hypothesis (5.5) is replaced by the weaker (5.42) below.*

## 5.2 Dispersion and Strichartz estimates

In this section we collect the dispersion and Strichartz estimates we shall use later. We start with the dispersion estimate.

**Proposition 5.4.** *(Dispersion estimate, [64]) Let $f_0 \in L^q(\mathbb{R}^d_x; L^p(\mathbb{R}^d_v))$ where $1 \leq q \leq p \leq \infty$, and let $f$ solve*

$$\partial_t f + v \cdot \nabla_x f = 0 \tag{5.6}$$

*with initial data $f(0,x,v) = f_0(x,v)$. Then*

$$\|f(t)\|_{L^p(\mathbb{R}^d_x;L^q(\mathbb{R}^d_v))} \leq \frac{1}{|t|^{d\left(\frac{1}{q}-\frac{1}{p}\right)}} \|f_0\|_{L^q(\mathbb{R}^d_x;L^p(\mathbb{R}^d_v))}. \tag{5.7}$$

[5] This assumption means simply that the solution $f(t,x,v) = f_0(x-tv,v)$ of the linear homogeneous kinetic transport equation with initial data $f_0$ belongs to $L^p_x L^1_v$ for all times. This assumption is satisfied if for example $f_0$ is $L^1_x L^p_v$ (see proposition 5.4).

We are going to need the following two versions of the dispersion estimate. First of all observe that the solution of (5.6) with initial data $f_0(x,v)$ is simply $f(t,x,v) = f_0(x-tv,v)$. Therefore the dispersion estimate says that for any function $h \in L^q(\mathbb{R}^d_x; L^p(\mathbb{R}^d_v))$, where $1 \le q \le p \le \infty$, we have

$$\|h(x-tv,v)\|_{L^p(\mathbb{R}^d_x;L^q(\mathbb{R}^d_v))} \le \frac{1}{|t|^{d\left(\frac{1}{q}-\frac{1}{p}\right)}} \|h(x,v)\|_{L^q(\mathbb{R}^d_x;L^p(\mathbb{R}^d_v))}. \tag{5.8}$$

Replacing $h(x,v)$ by $h(x,v)\mathbb{1}_V(v)$ we get

$$\|h(x-tv,v)\|_{L^p(\mathbb{R}^d_x;L^q(V))} \le \frac{1}{|t|^{d\left(\frac{1}{q}-\frac{1}{p}\right)}} \|h(x,v)\|_{L^q(\mathbb{R}^d_x;L^p(V))}. \tag{5.9}$$

In the special case of a function $h(x)$ which is independent of $v$ we get

$$\|h(x-tv)\|_{L^p(\mathbb{R}^d_x;L^q(V))} \le \frac{C(|V|)}{|t|^{d\left(\frac{1}{q}-\frac{1}{p}\right)}} \|h(x)\|_{L^q(\mathbb{R}^d_x)}. \tag{5.10}$$

Next we recall the Strichartz estimates of [64].

**Proposition 5.5.** *(Strichartz estimates, [64]) Let $d \ge 2$ and let $r,p,q,a \in [1,\infty]$ satisfy the conditions*

$$p \ge q, \quad \frac{2}{r} = d\left(\frac{1}{q}-\frac{1}{p}\right) < 1, \quad a = HM(p,q) \le 2, \tag{5.11}$$

*where $HM$ denotes the harmonic mean.*

1. *If $f(t,x,v)$ solves*
$$\partial_t f + v\cdot\nabla_x f = g \quad , \quad f(0,x,v) = 0,$$
*then*
$$\|f\|_{L^r_t L^p_x L^q_v} \le C\|g\|_{L^{r'}_t L^q_x L^p_v}. \tag{5.12}$$

2. *If $f(t,x,v)$ solves*
$$\partial_t f + v\cdot\nabla_x f = 0 \quad , \quad f(0,x,v) = f_0(x,v),$$
*then*
$$\|f\|_{L^r_t L^p_x L^q_v} \le C\|f_0\|_{L^a_{x,v}}. \tag{5.13}$$

## 5.3 Global existence for arbitrarily large data

In this Section we prove Theorems 5.1 and 5.2. We start with Theorem 5.1. Using the dispersion estimate gives rise to two norms, $\|\partial^\alpha S\|_{L^p}$ and $\|\rho\|_{L^q}$, see (5.15). Of course each of them could be estimated in terms of $f$, but this would result in a quadratic term and would make the use of Gronwall's inequality impossible. However, thanks to conservation of mass, we can choose $q = 1$ (this corresponds to velocity averaging) and bound $\|\rho\|_{L^q}$ a-priori. The norm $\|\partial^\alpha S\|_{L^p}$ is then estimated using the well-known Calderón-Zygmund inequality if $|\alpha| = 2$, see (5.17) (see also Remark 5.9 at the end of this Section) and Young inequality if $|\alpha| \le 1$.

We use the standard abbreviations for mixed spaces, for example $L^p_x L^q_v$ stands for $L^p(\mathbb{R}^d_x; L^q_v(V))$. In all cases $x$ varies in the whole space $\mathbb{R}^d$ while $v$ and $v'$ are restricted in the bounded velocity space $V$.

*Proof of Theorem 5.1.* Fix $p$ and $q$ with $1 \le q \le p \le \infty$. Arguing as in [66] we have

$$\begin{aligned} f(t,x,v) \le f_0(x-tv,v) &+ C\int_0^t \rho(t-s,x-sv)dv \\ &+ C\sum_{|\alpha|\le 2}\int_0^t |\partial^\alpha S(t-s,x-sv+v)|\,\rho(t-s,x-sv)ds \end{aligned} \tag{5.14}$$

therefore, using the dispersion estimate (5.8), we have

$$\begin{aligned}
\|f(t,x,v)\|_{L^p_x L^q_v} &\le \|f_0(x-tv,v)\|_{L^p_x L^q_v} + C(|V|)\int_0^t \frac{1}{s^{d\left(\frac{1}{q}-\frac{1}{p}\right)}}\,\|\rho(t-s,\cdot)\|_{L^q}\,ds \\
&+ C\sum_{|\alpha|\le 2}\int_0^t \frac{1}{s^{d\left(\frac{1}{q}-\frac{1}{p}\right)}}\,\|\partial^\alpha S(t-s,x+v)\rho(t-s,x)\|_{L^q_x L^p_v}\,ds \\
&\le C_0(t) + C(|V|)\int_0^t \frac{1}{s^{d\left(\frac{1}{q}-\frac{1}{p}\right)}}\,\|\rho(t-s,\cdot)\|_{L^q}\,ds \\
&+ C\sum_{|\alpha|\le 2}\int_0^t \frac{1}{s^{d\left(\frac{1}{q}-\frac{1}{p}\right)}}\,\|\partial^\alpha S(t-s,\cdot)\|_{L^p}\,\|\rho(t-s,\cdot)\|_{L^q}\,ds
\end{aligned} \tag{5.15}$$

where we have set $C_0(t) = \|f_0(x-tv,v)\|_{L^p_x L^q_v}$. Choose $q=1$ and $p \in (1, \frac{d}{d-1})$. Then by conservation of mass $\|\rho(t-s,\cdot)\|_{L^q} = M$. Using Young's inequality and conservation of mass for the derivatives of order one, we have

$$\|\nabla S(t-s,\cdot)\|_{L^p} = C\,\|\rho(t-s,\cdot) * \nabla G\|_{L^p} \le \|\rho(t-s,\cdot)\|_{L^1}\,\|\nabla G\|_{L^p} = CM \tag{5.16}$$

where $G(x) = \frac{1}{4\pi}\int_0^\infty e^{-\pi\frac{|x|^2}{4s}-\frac{s}{4\pi}} s^{\frac{-d+2}{2}}\frac{ds}{s}$ is the Bessel potential, and we get a similar estimate for $S$. For the derivatives of order two we have ([227], p. 59, Proposition 3)

$$\begin{aligned}
\|\partial_{ij} S(t-s)\|_{L^p} \le C(d,p)\,\|\Delta S(t-s)\|_{L^p} &\le C(d,p)\,\|\rho(t-s)\|_{L^p} + C\,\|S(t-s)\|_{L^p} \\
&\le C(d,p)\,\|\rho(t-s)\|_{L^p} + CM.
\end{aligned} \tag{5.17}$$

Therefore (5.15) gives

$$\|\rho(t)\|_{L^p} \le C_1(t) + C(d,p,M)\int_0^t \frac{1}{s^{d/p'}}\,\|\rho(t-s)\|_{L^p}\,ds.$$

Since $d/p' < 1$, we can use Gronwall's inequality to get

$$\|\rho(t)\|_{L^p} \le C(d,p,t,f_0).$$

This completes the a-priori estimates. See remark 5.11. □

**Remark 5.6.** *We have chosen $\beta = 1$ so that our $S$ decays sufficiently fast in order to apply the Calderón-Zygmund inequality. If $\beta = 0$ we have $S = S^s + S^l \in L^p + L^\infty$ and we have no decay for $S^l$.*

The proof of Theorem 5.2 uses the dispersion estimate of Proposition 5.4 as well as Young's convolution inequality and the Hardy-Littlewood-Sobolev inequality. The dispersion estimate is used to handle functions of $x - sv$ and $v$ which arise when we integrate the kinetic equation (5.1a), see (5.19) and (5.20) below. Each term in the right hand side of hypothesis (5.4) requires an estimate in $L^p_x L^q_v$ for a certain range of $p$ and $q$. Terms involving $x+v$ usually require small $p$ while terms involving $x-v'$ require large $p$. The main difficulty then is to find one set of parameters that makes both estimates work. To deal with this we will view the term $\nabla S(t-s, x-sv+v)\rho(t-s,x-sv)$ as $\nabla S(t-s, x-(s-1)v)\rho(t-s, x-(s-1)v-v)$. This shifting of the singularity from $s=0$ to $s=1$ (see (5.22)) results in a redistribution of norms that allows us to estimate the terms involving $\nabla S(x+v)$ and $S(x+v)$ without any restrictions on the parameter $p$, and it creates enough freedom so that, when we come to the more complicated estimates for $S(x-v')$, we are able to find a pair $(p,q)$ that works for both.

*Proof of Theorem 5.2.* We shall only present a-priori estimates via a bootstrap argument for the solution $f$ of (5.1) in the space $L^p(\mathbb{R}^3_x; L^q_v(V))$. The existence part of Theorem 5.2 then follows by well-known methods, see Remark 5.11. We present the proof in the more difficult case $\beta = 0$.

Observe that $S = S^s + S^l$ where $S^s(t) = \frac{1}{4\pi}\rho(t) * \frac{\mathbb{1}_{|x|\leq 1}}{|x|}$ and $S^l(t) = \frac{1}{4\pi}\rho(t) * \frac{\mathbb{1}_{|x|\geq 1}}{|x|}$. The long part $S^l(t)$ is a-priori bounded thanks to conservation of mass:

$$\left|S^l(t,x)\right| \leq C\left\|\rho(t)\right\|_{L^1}\left\|\frac{\mathbb{1}_{|x|\geq 1}}{|x|}\right\|_{L^\infty} \leq CM.$$

Similarly we split $\nabla S$ as $\nabla S = (\nabla S)^s + (\nabla S)^l$ where $(\nabla S)^s(t) = \frac{1}{4\pi}\rho(t) * \frac{\mathbb{1}_{|x|\leq 1}}{|x|^2}$ and $(\nabla S)^l(t) = \frac{1}{4\pi}\rho(t) * \frac{\mathbb{1}_{|x|\geq 1}}{|x|^2}$ and show that $(\nabla S)^l$ is a-priori bounded. It follows that we may replace hypothesis (5.4) by

$$0 \leq T[S](t,x,v,v') \leq C\Big(1 + S^s(t,x+v) + S(t,x-v') + \left|(\nabla S)^s(t,x+v)\right|\Big) \tag{5.18}$$

where the new constant $C$ depends on the mass $M$. For technical reasons it is more convenient not to split $S(t,x-v')$. Following the reasoning in [66] we estimate $f$ as follows:

$$f(t,x,v) \leq Cf_0(x-tv,v) + C\int_0^t \rho(t-s,x-sv)ds + C\sum_{j=1}^3 f_j(t,x,v) \tag{5.19}$$

where

$$\begin{aligned} f_1(t,x,v) &= \int_0^t\int_V S^s(t-s,x-sv+v)f(t-s,x-sv,v')dv'ds \\ &= \int_0^t S^s(t-s,x-sv+v)\rho(t-s,x-sv)ds \end{aligned} \tag{5.20a}$$

$$f_2(t,x,v) = \int_0^t\int_V S(t-s,x-sv-v')f(t-s,x-sv,v')dv'ds \tag{5.20b}$$

$$f_3(t,x,v) = \int_0^t \left|(\nabla S)^s(t-s,x-sv+v)\right|\rho(t-s,x-sv)ds \tag{5.20c}$$

Fix $p$ and $q$ with $q \in [1,3/2)$ such that

$$\lambda := 3\left(\frac{1}{q} - \frac{1}{p}\right) < 1,\ 1 \leq q \leq p \leq \infty \tag{5.21}$$

These restrictions on $p$ and $q$ will be enough for all estimates involving $f_1$ and $f_3$ but more restrictions will be imposed later when we estimate $f_2$ and we will want to know that there is a pair $(p,q)$ that satisfies all of them ([6]). We start our estimates with $f_3$. We have

$$\begin{aligned} \left\|f_3(t,x,v)\right\|_{L^p_xL^q_v} &\leq \int_0^t \left\|\left(\nabla S\right)^s(t-s,x-sv+v)\,\rho(t-s,x-sv)\right\|_{L^p_xL^q_v}ds \\ &= \int_0^t \left\|\left(\nabla S\right)^s(t-s,x-(s-1)v)\,\rho(t-s,x-(s-1)v-v)\right\|_{L^p_xL^q_v}ds. \end{aligned}$$

For fixed $t \geq 0$ and $s \in (0,t)$ we use the dispersion estimate (5.9) with $t$ replaced by $s-1$ and $h(x,v) = \left|(\nabla S)^s(t-s,x)\right|\rho(t-s,x-v)$ to get

$$\left\|f_3(t,x,v)\right\|_{L^p_xL^q_v} \leq \int_0^t \frac{1}{|s-1|^\lambda}\left\|\left(\nabla S\right)^s(t-s,x)\,\rho(t-s,x-v)\right\|_{L^q_xL^p_v}ds \tag{5.22}$$

$$\leq \int_0^t \frac{1}{|s-1|^\lambda}\left\|(\nabla S)^s(t-s,\cdot)\right\|_{L^q}\left\|\rho(t-s,\cdot)\right\|_{L^p}ds. \tag{5.23}$$

Because $q < 3/2$ the quantity $\left\|(\nabla S)^s(t-s,\cdot)\right\|_{L^q}$ is uniformly bounded. Indeed, using Young's inequality we have

$$\left\|(\nabla S)^s(t-s,\cdot)\right\|_{L^q} \leq C\left\|\rho(t-s,\cdot)\right\|_{L^1}\left\|\frac{\mathbb{1}_{|x|\leq 1}}{|x|^2}\right\|_{L^q(\mathbb{R}^3)} \leq C(q)M. \tag{5.24}$$

[6] One choice of parameters that works is: $p = \frac{9}{5}$, $q = \frac{9}{7}$.

On the other hand, since the velocity space is bounded, we have

$$\|\rho(t-s,\cdot)\|_{L^p} = \|f(t-s,x,v)\|_{L^p_x L^1_v} \leq C(|V|,q)\,\|f(t-s,x,v)\|_{L^p_x L^q_v}\,.$$

We conclude that

$$\|f_3(t,x,v)\|_{L^p_x L^q_v} \leq C(|V|,q)M \int_0^t \frac{1}{|s-1|^\lambda}\,\|f(t-s,x,v)\|_{L^p_x L^q_v}\,ds. \tag{5.25}$$

The estimate for $f_1$ is almost exactly the same. The only difference is that in the a-priori estimate (5.24) the norm $\left\|\frac{\mathbb{1}_{|x|\leq 1}}{|x|^2}\right\|_{L^q(\mathbb{R}^3)}$ is replaced by $\left\|\frac{\mathbb{1}_{|x|\leq 1}}{|x|}\right\|_{L^q(\mathbb{R}^3)}$ which is again finite because $q < 3/2 < 3$. We get:

$$\|f_1(t,x,v)\|_{L^p_x L^q_v} \leq C(|V|,q)M \int_0^t \frac{1}{|s-1|^\lambda}\,\|f(t-s,x,v)\|_{L^p_x L^q_v}\,ds. \tag{5.26}$$

**Remark 5.7.** *Splitting in addition between small and long times ($s \gtrless 1/2$ for example) we end up with a priori estimates without any restriction on the exponent $p$. But this technical improvement is not relevant in this proof.*

Next we estimate $f_2$. We start with some numerology which we explain later. Fix $q \in (1, 3/2)$. There exists a $p \in (3/2, 3)$ such that

$$3\left(\frac{1}{q} - \frac{1}{p}\right) = 1 - \frac{3p'}{(q')^2}. \tag{5.27}$$

To see this write (5.27) as $\delta(p) := 1 - \frac{3p'}{(q')^2} - 3\left(\frac{1}{q} - \frac{1}{p}\right) = 0$ and think of this expression as a continuous function of the variable $p \in [3/2, 3]$. For $p = 3/2$ we have $\delta(3/2) = 1 - \frac{9}{(q')^2} - 3\left(\frac{1}{q} - \frac{2}{3}\right) = \frac{3(q'-3)}{(q')^2} > 0$. On the other hand for $p = 3$ we have $\delta(3) = 1 - \frac{9}{2(q')^2} - 3\left(\frac{1}{q} - \frac{1}{3}\right) < -\frac{9}{2(q')^2} < 0$. The existence of $p$ follows. Notice that with this choice of $p$ and $q$ we still have $1 \leq q \leq p \leq \infty$ and moreover the integrability condition $\lambda < 1$ is satisfied thanks to (5.27).

**Remark 5.8.** *In fact we are allowed to choose $q$ and $p$ to be in the following set of exponents*

$$\mathcal{A} = \Big\{p' \geq 1,\ q' \geq 1 \;\Big|\; q' > p'\ ,\ 3\left(\frac{1}{q} - \frac{1}{p}\right) + \frac{3p'}{(q')^2} \leq 1\ ,\ \frac{1}{q} - \frac{1}{p} < \frac{1}{3}\Big\}. \tag{5.28}$$

*This set of admissible exponents for the estimate of $\|f_2(t,x,v)\|_{L^p_x L^q_v}$ is plotted in figure 5.1a in the coordinates $(q', p')$. The key point is that it intersects the constrain $\{q' > 3\}$ which comes from the estimates on $f_1$ and $f_3$. This can be done only by decoupling $p$ and $q$.*
*Assuming some linear contribution of $\nabla S(x - v')$ in the turning kernel bound (5.4) would have lead to the set represented in figure 5.1b. The latter does not intersect the half-plane $\{q' > 3\}$.*

Finally we define $\theta \in (0,1)$, $c \in (1,q)$ and $b \in (1,c')$ by the following relations:

$$\frac{1}{q} = 1 - \theta + \frac{\theta}{p}\ ,\ \frac{1}{c} = 1 - \theta + \frac{\theta}{q}\ ,\ \frac{1}{b} + \frac{1}{c} = \frac{5}{3}. \tag{5.29}$$

Proceeding with the estimates we have

$$\|f_2(t,x,v)\|_{L^p_x L^q_v} \leq \int_0^t \left\| \int_V S(t-s, x-sv-v')\, f(t-s, x-sv, v')\, dv' \right\|_{L^p_x L^q_v} ds. \tag{5.30}$$

For fixed $t \geq 0$ and $s \in (0,t)$ use the dispersion estimate (5.10) with

$$h(x) = \int_V S(t-s, x-v') f(t-s,x,v') dv'$$

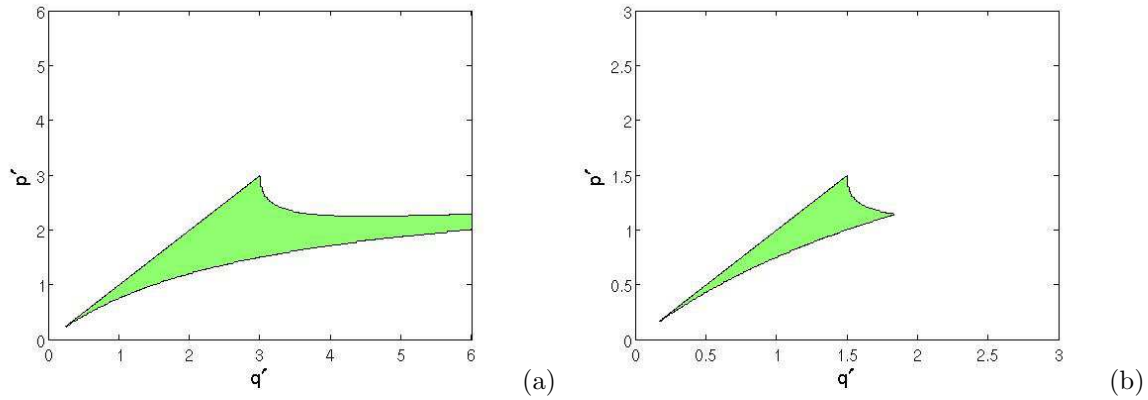


Figure 5.1: Set of admissible exponents $(q', p')$ for the estimate of $\|f_2(t,x,v)\|_{L^p_x L^q_v}$, corresponding to $S(x-v')$ (a) and $\nabla S(x-v')$ (b) respectively.

to get

$$\left\| \int_V S(t-s, x-sv-v')\, f(t-s, x-sv, v')\, dv' \right\|_{L^p_x L^q_v} \leq \frac{1}{s^\lambda} \left\| \int_V S(t-s, x-v') f(t-s, x, v') dv' \right\|_{L^q_x} . \tag{5.31}$$

By Hölder's inequality

$$\int_V S(t-s, x-v') f(t-s, x, v') dv' \leq \|S(t-s,\cdot)\|_{L^{c'}_x} \|f(t-s, x, v')\|_{L^c_{v'}} . \tag{5.32}$$

Since $1 < b < c' < \infty$ and $\frac{1}{b} - \frac{1}{c'} = \frac{2}{3}$ we can apply the Hardy-Littlewood-Sobolev inequality (see for instance [227], Theorem 1, page 199) to get

$$\|S(t-s,\cdot)\|_{L^{c'}} = C \left\| \rho(t-s,\cdot) * \frac{1}{|x|} \right\|_{L^{c'}(\mathbb{R}^3)} \leq C \|\rho(t-s,\cdot)\|_{L^b} . \tag{5.33}$$

It is easy to check that $1 < b < p$ ([7]), therefore if we define $\epsilon \in (0,1)$ by

$$\frac{1}{b} = 1 - \epsilon + \frac{\epsilon}{p} \tag{5.34}$$

we can use interpolation and conservation of mass to obtain

$$\|\rho(t-s)\|_{L^b} \leq \|\rho(t-s)\|^{1-\epsilon}_{L^1} \|\rho(t-s)\|^{\epsilon}_{L^p} \leq M^{1-\epsilon} \|\rho(t-s)\|^{\epsilon}_{L^p} .$$

We have shown that

$$\int_V S(t-s, x-v') f(t-s, x, v') dv' \leq C M^{1-\epsilon} \|\rho(t-s,\cdot)\|^{\epsilon}_{L^p} \|f(t-s, x, v')\|_{L^c_{v'}} ,$$

and as a product we obtain

$$\left\| \int_V S(t-s, x-v') f(t-s, x, v') dv' \right\|_{L^q_x} \leq C M^{1-\epsilon} \|\rho(t-s,\cdot)\|^{\epsilon}_{L^p} \|f(t-s, x, v)\|_{L^q_x L^c_v} . \tag{5.35}$$

We aim to interpolate the $L^q_x L^c_v$-norm between $L^1 L^1$ and $L^p L^q$ in order to conclude with a Gronwall lemma. This is achieved thanks to the first two relations in (5.29).

$$\begin{aligned} \|f(t-s,x,v)\|_{L^q_x L^c_v} &\leq \|f(t-s,x,v)\|^{1-\theta}_{L^1_x L^1_v} \|f(t-s,x,v)\|^{\theta}_{L^p_x L^q_v} \\ &\leq M^{1-\theta} \|f(t-s,x,v)\|^{\theta}_{L^p_x L^q_v} . \end{aligned} \tag{5.36}$$

[7] $\frac{1}{b} - \frac{1}{p} = \frac{5}{3} - \frac{1}{c} - \frac{1}{p} = \frac{5}{3} - 1 + \theta - \frac{\theta}{q} - \frac{1}{p} = \left(\frac{2}{3} - \frac{1}{p}\right) + \frac{\theta}{q'} > 0.$

Using this estimate together with $\|\rho(t-s,\cdot)\|_{L^p} \leq C(|V|,q)\,\|f(t-s,x,v)\|_{L^p_x L^q_v}$ into (5.35), we get

$$\left\| \int_V S(t-s,x-v')f(t-s,x,v')dv' \right\|_{L^q_x} \leq C(|V|,q)M^{2-(\epsilon+\theta)}\,\|f(t-s,x,v)\|^{\epsilon+\theta}_{L^p_x L^q_v}\,. \tag{5.37}$$

We can now argue that we opted for (5.27) to ensure that $\epsilon+\theta=1$ ([8]). Therefore

$$\left\| \int_V S(t-s,x-v')f(t-s,x,v')dv' \right\|_{L^q_x} \leq C(|V|,q)M\,\|f(t-s,x,v)\|_{L^p_x L^q_v}\,. \tag{5.38}$$

From (5.30), (5.31) and (5.38), we conclude that

$$\|f_2(t,x,v)\|_{L^p_x L^q_v} \leq C(|V|,q)M\int_0^t \frac{1}{s^\lambda}\,\|f(t-s,x,v)\|_{L^p_x L^q_v}\,ds. \tag{5.39}$$

This completes the estimate of $f_2$. Finally we have to estimate the first two terms in the right hand side of (5.19). For the first term we have by our hypothesis on the initial data that $\|f_0(x-tv,v)\|_{L^p_x L^q_v} =: C_0(t) < \infty$ for all $t$. We can use dispersion and interpolation for the second term, leading to

$$\left\| \int_0^t \rho(t-s,x-sv)ds \right\|_{L^p_x L^q_v} \leq \int_0^t s^{-\lambda}\,\|\rho(t-s)\|_{L^q_x}\,ds \leq C\int_0^t s^{-\lambda}\,\|\rho(t-s)\|^\theta_{L^p_x}\,ds,$$

where $\theta$ has already been defined in (5.29).

Putting everything together we conclude that

$$\|f(t,x,v)\|_{L^p_x L^q_v} \leq C_0(t) + C(|V|,q)M\int_0^t K(s)\,\|f(t-s,x,v)\|_{L^p_x L^q_v}\,ds \\ + C\int_0^t s^{-\lambda}\,\|f(t-s)\|^\theta_{L^p_x L^q_v}\,ds, \tag{5.40}$$

where $K(s) = 1 + \frac{1}{s^\lambda} + \frac{1}{|s-1|^\lambda}$. Since $\lambda < 1$ we can apply Gronwall's inequality to obtain

$$\|f(t,x,v)\|_{L^p_x L^q_v} \leq C(|V|,q,t,f_0). \tag{5.41}$$

□

**Remark 5.9.** *It would be interesting to know whether, in the case $\beta = 1$, the hypotheses* (5.4) *and* (5.3) *can be combined into the single assumption:*

$$0 \leq T[S](t,x,v,v') \leq C\left(1 + S(t,x+v) + S(t,x-v') + |\nabla S(t,x+v)|\right) + C\sum_{i,j=1}^{3} |\partial_{ij}S(t,x+v)|\,.$$

*The obstruction in our estimates is that the proof of Theorem 5.1 requires $q=1$, so that the norm $\|\rho\|_{L^q}$ in* (5.15) *can be estimated a-priori, while the estimates for $f_2$ in the proof of Theorem 5.2 do not work with $q=1$ because it gives $b=3/2$, $c=1$ which is not allowed in the HLS inequality in* (5.33).

[8] We have $\theta = \frac{p'}{q'}$ and $\epsilon = \frac{p'}{b'}$ therefore $\epsilon+\theta=1$ is equivalent to $\frac{1}{q'}+\frac{1}{b'} = \frac{1}{p'}$. We calculate $\frac{1}{p'} - \frac{1}{q'} - \frac{1}{b'} = \left(\frac{1}{q} - \frac{1}{p}\right) - 1 + \frac{1}{b}$. Now $-1 + \frac{1}{b} = -1 + \frac{5}{3} - \frac{1}{c} = \frac{2}{3} - \left(1 - \theta + \frac{\theta}{q}\right) = -\frac{1}{3} + \frac{\theta}{q'} = -\frac{1}{3} + \frac{p'}{(q')^2}$, therefore $\frac{1}{p'} - \frac{1}{q'} - \frac{1}{b'} = \left(\frac{1}{q} - \frac{1}{p}\right) - \frac{1}{3} + \frac{p'}{(q')^2}$ which is equal to zero thanks to (5.27).

## 5.4 Global existence for small data in the critical norm

Strichartz estimates have been very successful in dealing with many classes of nonlinear Schrödinger, wave and other dispersive equations. Typically they are used to show either local existence of solutions with low regularity data or global existence under an additional smallness assumption on the initial data, see [230].

*Proof of Theorem 5.3.* To simplify the notation we use again the standard abbreviations for mixed spaces, for example $L^r_t L^p_x L^q_v$. In all cases the space variable $x$ runs through all of $\mathbb{R}^3$ and the velocity variables $v$ and $v'$ always vary in the velocity space $V$.

Observe first that hypothesis (5.5) implies that for all $p_1, p_2, p_3 \in [1, \infty]$ with $p_1 \geq p_2, p_3$ we have

$$\|T[S](t,x,v,v')\|_{L^{p_1}_x L^{p_2}_v L^{p_3}_{v'}} \leq C(|V|, p_2, p_3)\,[\|S(t,\cdot)\|_{L^{p_1}} + \|\nabla S(t,\cdot)\|_{L^{p_1}}]\,. \tag{5.42}$$

Indeed, since $p_1 \geq p_2, p_3$, we can use Minkowski's inequality to obtain

$$\|S(t,x+v)\|_{L^{p_1}_x L^{p_2}_v L^{p_3}_{v'}} \leq \|S(t,x+v)\|_{L^{p_2}_v L^{p_3}_{v'} L^{p_1}_x} = C(|V|)\,\|S(t,\cdot)\|_{L^{p_1}}$$

with similar estimates for all other terms in the right hand side of (5.5). From now on the proof will use estimate (5.42) instead of hypothesis (5.5). We present a bootstrap argument for the solution $f$ in the space $L^3_t L^p_x L^q_v$. The existence result of Theorem 5.3 then follows by standard methods.

As usual we have:

$$f(t,x,v) \leq f_1(t,x,v) + f_2(t,x,v)$$

where $f_1(t,x,v)$ solves

$$\partial_t f_1 + v \cdot \nabla_x f_1 = 0 \quad , \quad f_1(0,x,v) = f_0(x,v)$$

and $f_2(t,x,v)$ solves

$$\partial_t f_2 + v \cdot \nabla_x f_2 = \int_V T[S] f' dv' \quad , \quad f_2(0,x,v) = 0.$$

Recall that $a \in [3/2, 2]$. Choose $r = 3$ and define $p \in [9/5, 18/7]$ and $q \in [9/7, 18/11]$ by $\frac{1}{p} = \frac{1}{a} - \frac{1}{9}$ and $\frac{1}{q} = \frac{1}{a} + \frac{1}{9}$. It is easy to verify that the quadruplet $(r,p,q,a)$ satisfies the conditions (5.11) required for applying the Strichartz estimates. Apply estimate (5.12) to $f_1(t,x,v)$ and estimate (5.13) to $f_2(t,x,v)$ to get:

$$\|f\|_{L^3_t L^p_x L^q_v} \leq \|f_1\|_{L^3_t L^p_x L^q_v} + \|f_2\|_{L^3_t L^p_x L^q_v} \tag{5.43}$$

$$\leq C\,\|f_0\|_{L^a_{x,v}} + C\left\|\int_V T[S] f' dv'\right\|_{L^{3/2}_t L^q_x L^p_v}. \tag{5.44}$$

To estimate the last term in (5.44), apply first Hölder's inequality to get:

$$\int_V T[S](t,x,v,v') f(t,x,v') dv' \leq \|T[S](t,x,v,v')\|_{L^{q'}_{v'}}\,\|f(t,x,v')\|_{L^q_{v'}}\,.$$

Taking the $L^p_v$-norm of both sides we find:

$$\left\|\int_V T[S] f' dv'\right\|_{L^p_v} \leq \|T[S](t,x,v,v')\|_{L^p_v L^{q'}_{v'}}\,\|f(t,x,v')\|_{L^q_{v'}}\,.$$

Taking next the $L^q_x$-norm of both sides and using Hölder's inequality with $\frac{1}{q} = \frac{1}{p} + \frac{2}{9}$ we find:

$$\left\|\int_V T[S] f' dv'\right\|_{L^q_x L^p_v} \leq \|T[S](t,x,v,v')\|_{L^{9/2}_x L^p_v L^{q'}_{v'}}\,\|f(t,x,v')\|_{L^p_x L^q_{v'}}\,. \tag{5.45}$$

It is easy to check that $\frac{9}{2} \geq p$ and $\frac{9}{2} \geq q'$, therefore we can use (5.42) to get

$$\begin{aligned}\|T[S](t,x,v,v')\|_{L_x^{9/2}(L_v^p(L_{v'}^{q'}))} &\leq C(|V|,p,q')\left[\|S(t,x)\|_{L_x^{9/2}} + \|\nabla S(t,x)\|_{L_x^{9/2}}\right] \\ &= C(|V|,p,q')\left[\|G*\rho(t)\|_{L_x^{9/2}} + \|\nabla G*\rho(t)\|_{L_x^{9/2}}\right]\end{aligned}$$

where $G$ is the Bessel potential (see the proof of theorem 5.1).

If $\frac{9}{5} < p$ we proceed by using Young's inequality. One can show that $G \in L^b$ for all $b < 3$ and that $\nabla G \in L^b$ for all $b < \frac{3}{2}$. Define $b$ by $1 + \frac{2}{9} = \frac{1}{b} + \frac{1}{p}$. Then $\frac{6}{5} \leq b < \frac{3}{2}$. We get

$$\begin{aligned}\|G*\rho\|_{L_x^{9/2}} + \|\nabla G*\rho\|_{L_x^{9/2}} &\leq \|G\|_{L^b}\|\rho\|_{L_x^p} + \|\nabla G\|_{L^b}\|\rho\|_{L_x^p} \\ &\leq C(b)\|\rho(t,x)\|_{L_x^p} \\ &\leq C(b,q,|V|)\|f(t,x,v)\|_{L_x^pL_v^q}.\end{aligned}$$

If $\frac{9}{5} = p$ we use Young's inequality for the $G$-term and the HLS inequality for the $\nabla G$-term. Defining $b$ as above now gives $b = \frac{3}{2} < 3$ therefore

$$\|G*\rho\|_{L_x^{9/2}} \leq \|G\|_{L^{3/2}}\|\rho\|_{L_x^p} \leq C\|\rho\|_{L_x^p} \leq C(q,|V|)\|f(t,x,v)\|_{L_x^pL_v^q}. \tag{5.46}$$

One can show that $|\nabla G(x)| \leq \frac{C}{|x|^2}$ for all $x$. Therefore, by HLS,

$$\|\nabla G*\rho\|_{L_x^{9/2}} \leq \left\|\frac{C}{|x|^2}*\rho\right\|_{L_x^{9/2}} \leq C\|\rho\|_{L_x^{9/5}} = C\|\rho\|_{L_x^p} \leq C(q,|V|)\|f(t,x,v)\|_{L_x^pL_v^q}.$$

The above argument shows that

$$\|T[S](t,x,v,v')\|_{L_x^{9/2}L_v^pL_{v'}^{q'}} \leq C(a,|V|)\|f(t,x,v)\|_{L_x^pL_v^q}. \tag{5.47}$$

Using (5.47) into (5.45) we get:

$$\left\|\int_V T[S]f'dv'\right\|_{L_x^qL_v^p} \leq C(a,|V|)\|f(t,x,v)\|^2_{L_x^pL_v^q}. \tag{5.48}$$

Taking the $L_t^{3/2}$-norm of both sides we obtain:

$$\left\|\int_V T[S]f'dv'\right\|_{L_t^{3/2}L_x^qL_v^p} \leq \left\|\|f(t,x,v)\|^2_{L_x^p(L_v^q)}\right\|_{L_t^{3/2}} = \|f(t,x,v)\|^2_{L_t^3L_x^pL_v^q}. \tag{5.49}$$

Using this in (5.44) we find

$$\|f\|_{L_t^3L_x^pL_v^q} \leq C\|f_0\|_{L^a(\mathbb{R}^6)} + C\|f(t,x,v)\|^2_{L_t^3L_x^pL_v^q}. \tag{5.50}$$

This completes the a-priori estimates which enable to bootstrap for small initial data. See remark 5.11. □

**Remark 5.10.** *The proof of Theorem 5.3 works in $d = 4$ dimensions too. One may choose for instance $(q,p,r,a) = (3,12/5,12/7,2)$. Notice that $a = \frac{d}{2}$. It also works in dimension $d = 2$, however, in this case a better result (global existence without a smallness assumption) is available in [144].*
*Using the same method we can prove local existence for large data.*

**Remark 5.11.** *We have proved a priori estimates for the IVP* (5.1)*. We can prove the existence of weak solutions using regularization and compactness. In particular the compactness can be gained using averaging lemmas (see [207] for instance) provided we get some a priori estimate on the $L^pL^q$-norm of $f$ with $q > 1$. This has been obtained in the proofs of theorems 5.2 and 5.3, whereas in theorem 5.1 an additional bootstrap step is needed. Of course continuity of $T[S]$ in spaces $L^p_{loc}$ is needed for passing to the limit in all cases.*

## Conclusions and perspectives

In this paper we have considered a number of classes of turning kernels in the kinetic model of chemotaxis. We have proved global existence for arbitrarily large data using dispersion estimates for several of them, and, using Strichartz estimates, we have obtained global existence for small solutions in the most difficult case of a turning kernel that involves $|\nabla S(t, x + v)| + |\nabla S(t, x - v')|$ (Theorem 3). The de-localization induced by $v$ or $v'$ in these formula is fundamental both for mathematical theory and biophysical interpretation. However, several questions remain that show that the present theory still needs to be improved. We would like to mention a few of them.

At first, obviously is the case of large initial data in Theorem 5.3 which remains open. Notice that the time integrability in the Strichartz estimates implies some decay to zero at infinity which is only possible for small initial data, as we know from the Keller-Segel system [35, 77].

A second question is to include some of these examples in a more general assumption such as

$$\|T[S](t, x, v', v)\|_{L^\infty_{loc}} \leq C\Big(1 + \|S\|_{L^\infty_{loc}}\Big).$$

Because this does not include directly de-localization, the methods used here do not apply for global existence.

More related to biophysical interpretation there is a third question: unlike in the Keller-Segel model – where having turning kernels of the form $S(t, x + v')$ and $\nabla S(t, x + v')$ gives a repellent drift [66] and then there is no blow-up, and the existence theory is much simpler – in the arguments carried out in the proof of the results we do not see why it should be better to have turning kernels of the latter form.

## Deuxième partie

# Application à la génération de patterns : la sclérose concentrique de Baló

# Chapitre 6

# La sclérose concentrique : une instabilité de nature chimiotactique ?

La sclérose concentrique décrite par Baló en 1927 est une forme rare et tout à fait remarquable de sclérose en plaques. Par l'allure des zones endommagées (en cible de tir à l'arc), par leur taille caractéristique (visibles à l'œil nu) et par leur robustesse, elle présente un enjeu pour la modélisation des interactions cellulaires dans le cerveau. Dans ce travail, fruit d'une collaboration avec Hossein Khonsari et Benoît Perthame, nous proposons un scénario plausible, à base de réponse inflammatoire (sur le plan biologique) et d'instabilité de Keller-Segel (sur le plan mathématique), qui répond à de multiples interrogations de manière satisfaisante. Ceci est à paraître dans Mathematical and Computer Modelling sous le titre *Mathematical description of concentric demyelination in the human brain : self-organization models, from Liesegang rings to chemotaxis*. Une version courte avec une discussion médicale plus étoffée est parue dans PLoS ONE sous le titre *The origins of concentric demyelination : self-organization in the human brain* (annexe E et [157]).

## 6.1 Introduction

Spatial cellular self-organization is a challenging area at the interface of mathematics and biology [84]. Biological phenomena involving self-organization are as different as bacterial colony growth [25, 44, 150], embryology [185], wound healing [80] and cancer growth [213, 47]. The importance of chemical species in morphogenesis was first suggested by Alan Turing [236], who introduced the so-called diffusion-driven instability. Our personal approach is based on chemotaxis, which provides basic instabilities for collective aggregation [208]. It is probably one of the main phenomena explaining cellular spatial organization. When dealing with a large number of cells, the models mainly involve parabolic PDEs [65], as it is for the Patlak, Keller & Segel model [206, 153, 154].

The biological phenomenon we study in this paper is the concentric demyelination occuring in a particular form of multiple sclerosis (MS), namely the Baló's concentric sclerosis (BCS). The pathogeny of BCS has been a neuropathologic enigma for many years. We suggested in a previous paper [157] that the robust patterns appearing in this disease may result from a chemotactic mechanism, involving three

species.

$$\begin{aligned}
\frac{\partial m}{\partial t} &= \underbrace{D\Delta m + \lambda m(\bar{m}-m)}_{\substack{\text{front of macrophages}\\ \text{activation}}} - \underbrace{\nabla\cdot\Big(\chi m(\bar{m}-m)\nabla c\Big)}_{\substack{\text{local recruitment}\\ \text{of macrophages}}} \\
\frac{\partial d}{\partial t} &= \underbrace{F(m)m(\bar{d}-d)}_{\text{destruction of myelin}} \\
&\underbrace{-\varepsilon\Delta c + \alpha c = \mu d}_{\substack{\text{production and fast diffusion}\\ \text{of the attracting signal}}} \quad ,
\end{aligned} \tag{6.1}$$

The combined effects of the activating front propagation and aggregation lead to the formation of robust concentric bands of destroyed myelin (see section 6.5.2). Furthermore, as a consequence of the mathematical properties of our chemotaxis-based model, the striking patterns observed in BCS may be the result of the peculiar aggressivity of this pathology [157].

Interesting analogies between BCS and LR have been raised early in the literature [127]. In the following we present models inspired from these analogies, but adapted to the current discoveries on the cellular mechanisms of demyelination. The paper is organized as follows. We first introduce the basics of aggregation modeling and survey the state of the art in the Patlak, Keller & Segel model [206, 153] (section 6.2). We then briefly describe the neuropathology of BCS (section 6.3, we refer to [157] for a more in-depth presentation). Section 6.4 introduces the Ostwald supersaturation scenario for the formation of Liesegang rings and the preconditioning model proposed by Stadelman et al. [226] for BCS. Finally, section 6.5 presents more refined models for concentric patterning by self-organization, namely the post-nucleation scenario for Liesegang rings and our local macrophage recruitment model.

## 6.2 Cellular self-organization and chemotaxis

Chemotaxis is the motion of cells in response to a chemical signal. It occurs for instance in tumoral angiogenesis [8, 108, 173] and in avian gastrulation during the formation of the primitive streak [251]. In the brain, chemotaxis is known to play a role in the neural migration that leads to cortical development [233]. Furthermore, cellular motion in immunologic response is directed by chemokines like TGF$\beta$ or INF$\gamma$. Chemotaxis may also be involved in the genesis of pigmentation patterns [203] (see also [110]).

When cells themselves are involved in the production of cell-attracting chemical signals, self-organization may occur. The simplest non-linear chemotaxis-based model is the Patlak, Keller & Segel (PKS) model for collective cellular aggregation. Many exciting research topics have emerged from this theory. This model involves only two variables: the cell density and the chemoattractant concentration. The core of PKS is the following nonlinear coupling: the amount of chemoattractant produced by the cells increases with the number of cells. Other models involving more realistic and complex kinetics have been proposed. For instance, in order to describe the aggregation phase in the amoebae *Dictyostelium discoideum*'s life cycle, the chemotaxis master equation has been coupled with a system of two reaction-diffusion equations involving traveling pulses in an excitable medium [139]. Related results have been obtained in [54] where a one-parameter family of smallness conditions is derived for existence of global solutions.

In the following subsection, we review classical PKS from a mathematical viewpoint. We aim to describe the chemotaxis aggregation principle involving, among other parameters, the total mass of cells. Next, we present recent theoretical developments taking into account density-dependent saturation effects on cellular movements (nonlinear diffusion and/or saturation of the chemotactic response).

### 6.2.1 The classical PKS model – A brief overview

The PKS model has been introduced to describe the aggregation phase of a cellular population viewed as a continuum (bacterial colonies, aggregation phase in the life cycle of *Dictyostelium*). Depending on

the modeling goals, several PKS variants have been proposed, involving for instance blow-up or traveling waves. Here, we only consider two species, namely the cell density $n(t,x)$ and the chemoattractant concentration $c(t,x)$, in dimension two. From Jäger and Luckhaus [147] we write, in the fast chemical diffusion case,

$$\left\{ \begin{array}{rcl} \dfrac{\partial n}{\partial t} & = & D\Delta n - \nabla \cdot \big(\chi n \nabla c\big) \quad \text{ in } \mathbb{R}^+ \times \Omega, \\ -\Delta c & = & \mu\Big(n - \langle n \rangle\Big), \end{array} \right. \tag{6.2}$$

$\Omega \subset \mathbb{R}^2$ being the domain under consideration, which can be a bounded domain or the full space $\mathbb{R}^2$. In the former case, boundary conditions are zero flux,

$$\left\{ \begin{array}{l} D\dfrac{\partial n}{\partial \eta} - \chi n \dfrac{\partial c}{\partial \eta} = 0 \qquad \text{on } \partial\Omega, \\ \qquad\qquad \dfrac{\partial c}{\partial \eta} = 0, \end{array} \right.$$

$\eta$ being the outwards unit normal vector to the domain boundary $\partial\Omega$. The compatibility correction $\langle n \rangle$ is the mean value of the cell density over the domain; it corresponds to Neumann boundary conditions for $c$ in a bounded domain $\Omega$ and has zero value if $\Omega$ is the full space. In the full space, the Poisson equation $-\Delta c = \mu n$ has to be understood with $c$ being

$$c = -\frac{\mu}{2\pi} \int_{\mathbb{R}^2} \log|x-y| \; n(t,y) \; dy. \tag{6.3}$$

We can adimensionalize the system (6.2) and we end up with only one reduced parameter,

$$\tilde{\chi} = \frac{\mu \chi M}{D}, \tag{6.4}$$

where $M$ is the total mass of cells, conserved along time.

The qualitative behaviour of this model results from the balance between two opposite tendencies. The following alternative arises: either cells spread (when interactions are negligible), or they aggregate, that is the cell density blows up (cell-to-cell attraction dominates). The principle of mass constrain can be stated as follows: the reduced parameter $\tilde{\chi}$ drives the structure of the cellular population. If all the parameters of the dimensionalized model (6.2) are fixed, the amount of cells determines whether self-organization takes place or not.

**Theorem 6.1** (Full space, [86])**.** *If $\Omega$ is the whole space $\mathbb{R}^2$ and the initial data satisfies $n_0\big(|\log n_0| + (1+|x|^2)\big) \in L^1$, then solutions are global in time if $\mu\chi M/D < 8\pi$, or blow up in finite time if $\mu\chi M/D > 8\pi$.*

This theorem and its variants are due to several contributions, among which Jäger and Luckhaus [147], Biler and Nadzieja [32], Nagai [187], Gajewski and Zacharias [107], Dolbeault and Perthame [86].

**Remark 6.2.** *The alternative in the full space is simple because there is a single threshold. On a bounded domain, the boundary conditions imposed to the chemical species are crucial. For instance, Neumann boundary conditions lead to global existence under the condition $\mu\chi M/D < 4\pi$ because of boundary effects [32, 107, 141, 51].*

The method for proving global existence in theorem 6.1 is based on the free energy associated with the system (6.4). In the adimensional form, the following quantity is time decreasing,

$$\mathcal{E}(t) = \int \tilde{n} \log \tilde{n} - \frac{\tilde{\chi}}{2} \int \tilde{n}\tilde{c}. \tag{6.5}$$

The proof involves the logarithmic Hardy-Littlewood-Sobolev inequality [56], which compares the opposite contributions of diffusion and chemical potential to cellular motion.

**Remark 6.3** (PKS model in dimension $d \neq 2$)**.** *At least two ways of generalizing the PKS model in dimensions other than two are possible, depending on the spatial law for chemical diffusion.*

- *First, one may keep the equation $-\Delta c = n$. The qualitative behaviour thus depends on the dimension: for $d = 1$, blow-up never occurs [187], but may happen in higher dimensions. In this case, the $L^{d/2}$-norm is critical instead of the mass [77].*
- *Following* (6.3)*, one may use the logarithmic interaction kernel and state $c = -\frac{1}{d\pi} \log|x| * n$. In this case, the qualitative picture is the same for every dimension $d$ and the threshold is $2d^2\pi$ [55].*

### 6.2.2 Volume effects – Recent issues

Several approaches lead to volume effects in the chemotaxis equation. It is mathematically relevant to include nonlinear density-dependent coefficients in order to avoid non-realistic blow-up. From a modeling point of view, the pressure function may be overvaluated for high cell-density levels [108, 159]. Another possibility is to come back to the biased random walk framework [5] and introduce a nonincreasing function $q$. This function takes into account that cellular motion is slowed down when cells are packed [202]. All these saturating effects are included in the following master equation,

$$\frac{\partial n}{\partial t} + \nabla \cdot \Big( - n\nabla h(n) + \chi(n) n \nabla c \Big) = 0, \tag{6.6}$$

$h(u)$ being the pressure function and $\chi(u)$ the density–dependent chemosensitivity. In addition we introduce the nonlinear reduced pressure function, defined by

$$H'(u) = \frac{h'(u)}{\chi(u)}, \quad H(1) = 0. \tag{6.7}$$

**Theorem 6.4** (Volume effects, [50])**.** *Let $\Omega \subset \mathbb{R}^2$ be a bounded domain. We assume that $H$ is growing to infinity faster than $\frac{\mu M}{4\pi} \log u$ for large $u$, that is there exists $\delta > 0$ and $\mathcal{U} \in \mathbb{R}_+$ such that*

$$\forall u \geq \mathcal{U}, \quad H(u) \geq \Big( \frac{\mu M}{4\pi} + \delta \Big) \log u. \tag{6.8}$$

*Then, there are global solutions under suitable initial conditions.*

**Remark 6.5.** *The criterion for blow-up prevention is the non–linear analogue of theorem 6.1. The non–linear reduced pressure* (6.7) *is involved in the balance between spread (high pressure) and cell-to-cell attraction (low pressure), instead of the reduced coefficient $\mu\chi M/D$. In fact theorem 6.4 reduces to theorem 6.1 because $h(u) = D \log u$ in the "linear case".*

The proof of theorem 6.4 also relies on refined estimations of the free energy,

$$\mathcal{E}(t) = \int \Phi(n)\, dx - \frac{\mu}{2} \int nc\, dx, \quad \text{with } \Phi \text{ defined as } \quad \Phi'(u) = H(u),\ \Phi(0) = 0.$$

#### Examples and numerics

In the biased random walk approach, the density dependent transition rate $q$ represents the saturation effects [202]. The relation between $q$ and the nonlinear pressure and chemosensitivity functions in (6.6) is given by

$$\begin{cases} uh'(u) = D\Big(q(u) - uq'(u)\Big), \\ \chi(u) = \chi_0 q(u), \end{cases} \qquad H'(u) = \frac{D}{\chi_0}\ \frac{q(u) - uq'(u)}{q(u)u}. \tag{6.9}$$

The overcrowding effect is illustrated by the following two generic examples (see also figure 6.1).

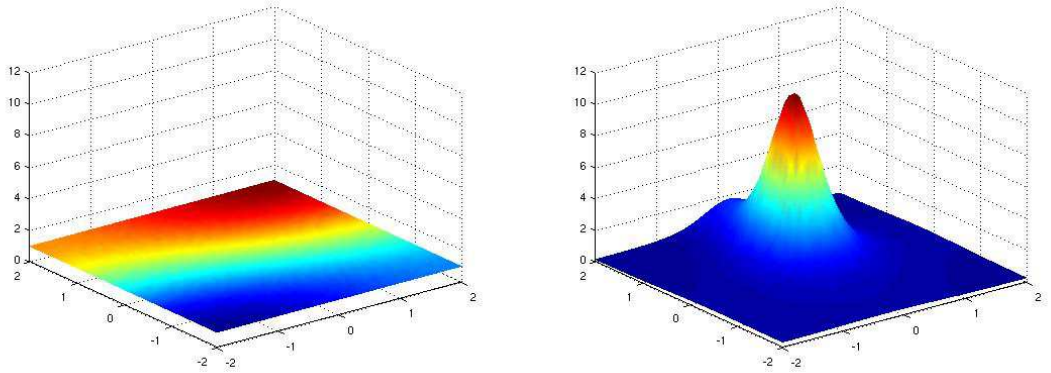

(a)

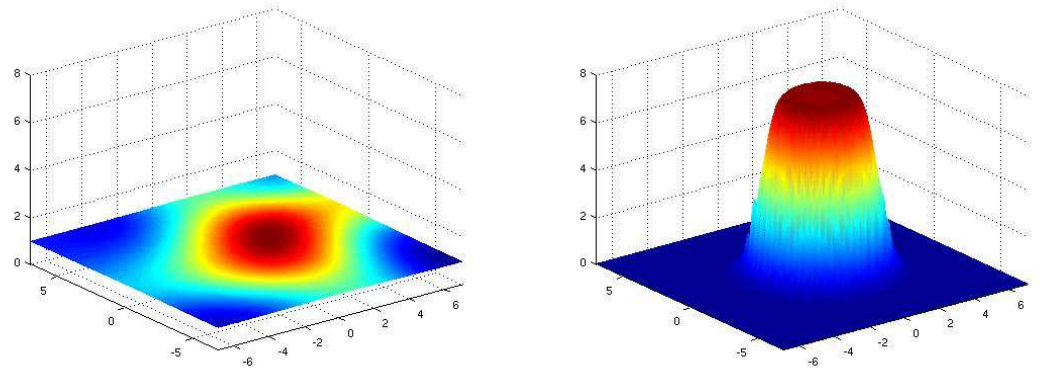

(b)

Figure 6.1: Illustration of the chemotaxis principle with volume effects: each figure corresponds to the final equilibrium state of the cell density (except in *top-right*, where blow-up occurs). Simulations are performed on a square regular grid using the discretization (6.12). (a) The transition rate is $q(u) = \frac{1}{1+u}$. The initial condition is a perturbation of a homogeneous cell population with density 1 and total mass $M = 16$. Other parameters are $D = 1$, $\mu = 1$ and (*left*) $\chi_0 = 2$, (*right*) $\chi_0 = 10$. For convenience, the right figure is an intermediate state: all the mass is finally concentrated at one point (blow-up). The situation is qualitatively close to the classical model, where blow-up occurs if $\mu\chi_0 M/D$ is sufficiently large. (b) We set $q(u) = e^{-u}$. The initial condition is a perturbation of a homogeneous cell population with density 1 and total mass $M = 200$. Other parameters are $D = 1$, $\mu = 1$ and (*left*) $\chi_0 = 2.6$, (*right*) $\chi_0 = 3$. Although the solutions do not blow-up, there is a transition in equilibria between the spread of cells and aggregation, where cell density is highly localized.

(a) If $q$ has a polynomial decay, $q(u) = \frac{1}{1+u^\gamma}$, $\gamma > 0$, then we get

$$H'(u) = \frac{D}{\chi_0}\,\frac{1+(\gamma+1)u^\gamma}{u(1+u^\gamma)} \sim_\infty \frac{D}{\chi_0}\,\frac{\gamma+1}{u}. \tag{6.10}$$

In this case, the corresponding diffusion law is asymptotically linear, and blow-up is avoided if $D(1+\gamma)/\chi_0 > \mu M/4\pi$.

(b) If $q$ is exponentially decreasing as $q(u) = e^{-\beta u}$, $\beta > 0$, then we obtain

$$H'(u) = \frac{D}{\chi_0}\,\frac{1+\beta u}{u} \sim_\infty \frac{D}{\chi_0}\,\beta. \tag{6.11}$$

Here, the reduced diffusion is asymptotically quadratic for large cell density and blow-up never occurs because the condition (6.8) is always verified.

Filbet [103] provided theoretical results on PKS numerics based on discrete functional inequalities. Here we adopt the Scharfetter & Gummel [220] factorization method for our numerical scheme. This method is common in the theory of semi-conductor devices, and gives a key role to the reduced pressure function. We rewrite the flux term of (6.6) as follows,

$$\frac{\partial n}{\partial t} = \nabla\cdot\Big(Dq(n)^2 e^{\frac{\chi_0}{D}c}\nabla\big(\frac{n}{q(n)}e^{-\frac{\chi_0}{D}c}\big)\Big). \tag{6.12}$$

**Remark 6.6.** *Note that* (6.12) *is a particular case of the following computation*

$$\begin{aligned}\frac{\partial n}{\partial t} &= \nabla\cdot\Big(n\chi(n)\nabla\big(H(n)-c\big)\Big)\\ &= \nabla\cdot\Big(Dn\frac{\chi(n)}{\chi_0}e^{\frac{\chi_0}{D}c-\frac{\chi_0}{D}H(n)}\nabla\big(e^{\frac{\chi_0}{D}H(n)-\frac{\chi_0}{D}c}\big)\Big),\end{aligned}$$

*because* (6.9) *implies*

$$\frac{\chi_0}{D}H(u) = \log u - \log\Big(q(u)/q(1)\Big).$$

Our aim is now to use a semi-implicit scheme to solve the time-space discrete version of (6.12) on a square regular grid. For convenience we only present the method in dimension $d = 1$. We first solve the Poisson equation for the chemical potential implicitely: $n(t) \longrightarrow c(t+dt)$. Then we discretize (6.12),

$$n_i(t+dt) - n_i(t) = dt\left(\frac{\mathcal{F}_{i+\frac12} - \mathcal{F}_{i-\frac12}}{dx}\right),$$

where the discrete flux $\mathcal{F}_{i\pm\frac12}$ is defined by

$$\mathcal{F}_{i+\frac12} = \frac{1}{dx}D\Big[q(n)^2(t)\Big]_{i+\frac12}\exp\Big(\frac{\chi_0}{D}\frac{c_{i+1}+c_i}{2}\Big)\times\left(\frac{n_{i+1}(t+dt)}{q(n_{i+1}(t))}e^{-\frac{\chi_0}{D}c_{i+1}} - \frac{n_i(t+dt)}{q(n_i(t))}e^{-\frac{\chi_0}{D}c_i}\right).$$

For the explicit nonlinear contribution, we choose the geometric mean

$$\Big[q(n)^2\Big]_{i+\frac12} = q(n_{i+1})q(n_i).$$

In figure 6.1, we have plotted long time evolution corresponding to $q(u) = 1/(1+u^\gamma)$ and $q(u) = e^{-\beta u}$. The chemotaxis principle is also valid in the nonlinear case: depending on the parameters (among which high amount of cells and high chemosensitivity favour structure emergence), we observe either cellular aggregation or spread.

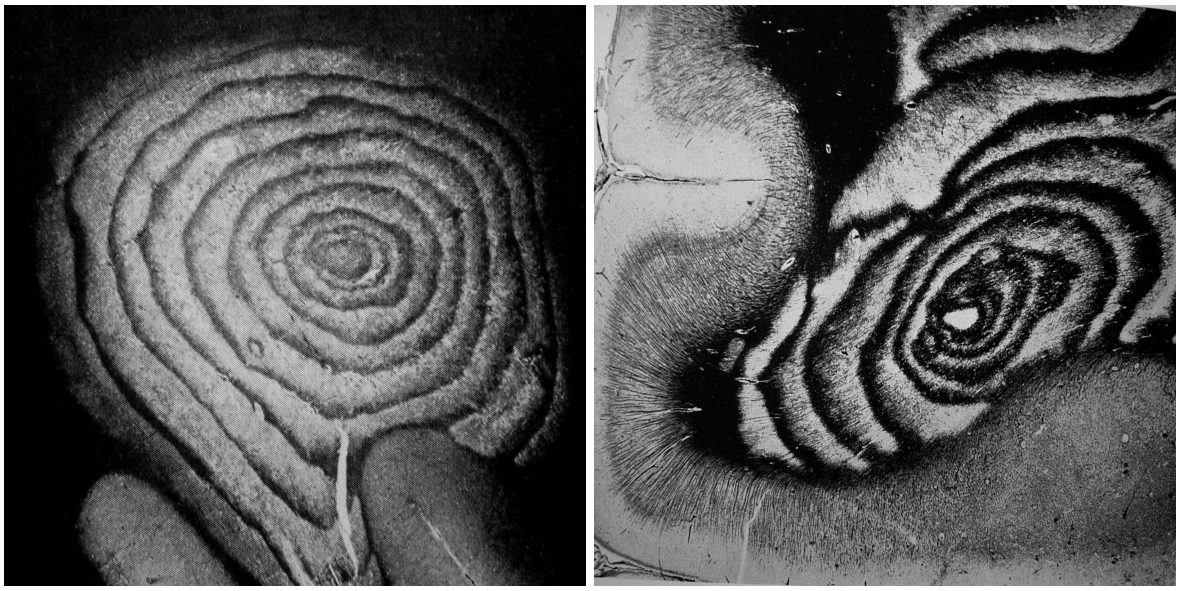

Figure 6.2: Neuropathology of Baló's concentric sclerosis from (*left*) Baló 1928 [17] and (*right*) Hallervorden et al. 1933 [127]. The lesional process is remarkably robust, even in constrained areas (*right*). The analysis of these pictures provides morphometric data on the lesions and helps to establish space laws for the pattern.

**Stationary states**

Asymptotic behaviours of the linear or non-linear PKS systems (6.2) and (6.6) have been thoroughly analysed by Keller & Segel (1970), Nanjundiah (1973), Childress and Percus (1981) and Schaaf (1985) (see [141]). From these authors' viewpoint, the aggregation principle is related to the instability of the homogeneous steady-state (emergence of spatial structure). More recently, the volume-filling model with the particular saturating function $q(u) = (1 - u/u_{max})_+$ has been studied in dimension one and others [135]. This saturating function corresponds to an infinite valued pressure for large $u$ and can therefore be viewed as a caricatural variant of a more general equation as (6.6). In this case, the formation of plateaus occurs in a fast time scale, then these plateaus merge on a slow time scale [85]. It is proved in [250] that the aggregation principle also holds in this situation: the uniform steady state becomes unstable under some condition similar to $\mu\chi M/D > 8\pi$.

## 6.3 Baló's concentric sclerosis: a modeling challenge

The white matter contains the axons of neurons connecting together the cortex, the basal ganglia, the brain stem and the spinal chord. Multiple sclerosis is a chronic demyelinating disease that affects the brain's white matter, and more precisely myelin. Myelin is a fatty substance that surrounds the axons and is necessary for a proper nervous signal transmission. In the central nervous system, myelin is produced by specialized cells, the oligodendrocytes. Several interdependant cellular and molecular processes are involved in demyelination and oligodendrocyte destruction. The neuropathological lesions of MS are plaques (in 2D sections) of demyelinated areas, generally centered on a blood vessel [163].

Baló's concentric sclerosis is a rare and aggressive variant of MS where demyelination regions consists of concentric bands centered by a blood vessel. The process that leads to the formation of such patterns is extremely robust (see figure 6.2).

The study of BCS may shed some light on the pathogeny of the usual forms of MS. In fact, recent neuropathological studies have pointed out that concentric patterning may occur during the very early

stages of most MS cases [19]. Furthermore, epidemiology of Baló's concentric sclerosis shows a clear predominance of this disease in South-East Asia, indicating that concentric demyelination may be caused by some specific genetic predisposition [70]. BCS may thus be an extreme form of MS sharing some common underlying mechanisms with the more usual types of demyelination. In the last section of this paper, we underline the fact that there may exist some positive correlation between cellular aggressitivity and spatial organization (as a consequence of the aggregation principle described in section 6.2). In this context, Baló's sclerosis may be a subtype of multiple sclerosis in which the cellular agressivity of demyelinating effectors is unsually increased.

We are convinced that a simple mathematical principle underlies such a robust process. In the next sections, we analyse several models sharing a set of common fundamental hypotheses. One hypothesis is the presence of a propagating front of activation in the brain. The origins of this *leading reaction front* are unknown and its shape varies from one model to another. The link between BCS and LR is based on the presence of this front. In fact, this interesting analogy was suggested and thoroughly studied early in the litterature, first by Hallervorden et al. [127]. We reconsider these analogies in the light of the recent discoveries on LR and use this fruitful comparison for the construction of our model.

## 6.4 Direct concentric patterning

In this section, we present direct pattern processes that do not involve secondary rearrangement scenarios but immediate pattern emergence as the leading reaction front interacts with the medium. The cases in which the pattern is the result of secondary non-linear rearrangements at the back of the propagating front will be studied in the next section.

### 6.4.1 Liesegang rings and Ostwald's supersaturation scenario

Liesegang rings, first described by Liesegang in 1896 [169], occur both in chemical processes [129] and in geology [161]. Precipitate rings are the result of chemical interactions between a propagating front and a motionless species. The fact that rings commonly appear in gels, where the viscosity is high, accounts for the necessary reduced mobility of one of the species.

Several scenarios have been proposed to explain periodic precipitation. One of the earliest theories, the so-called *supersaturation* scenario, was formulated by Ostwald in 1897 [197]. Ostwald's supersaturation (OS) involves a single precipitation reaction with an intermediate compound $C = AB$,

$$A + B \longrightarrow C \longrightarrow D \quad \text{(precipitation)}.$$

The reaction kinetics are based on the existence of two different precipitation thresholds.
Initially, $B$ is uniformly distributed in the gel and $A$ propagates in the domain. Precipitation occurs whenever the concentration of the compound $C = AB$ exceeds the supersaturation threshold $q^*$ and takes place as long as $[AB] > q$ (q being the saturation threshold, with $q < q^*$). Each precipitated band of $D$ depletes the surrounding gel from $B$ by acting as a sink. The presence of two distinct thresholds in the kinetic term ensures that the reaction goes on even when the concentration $[AB]$ is locally below $q^*$.

Since the early 80's, a lot of works have been dedicated to OS. One of the most intuitive models is probably the one proposed by Keller & Rubinow [155],

$$\left\{ \begin{array}{lcl} \partial_t a &=& D_1 a - kab, \\ \partial_t b &=& D_2 b - kab, \\ \partial_t c &=& D_3 c + kab - P, \\ \partial_t d &=& P, \end{array} \right. \tag{6.13}$$

where the precipitation rate is given by

$$\left\{ \begin{array}{ll} P = (c-q)_+ & \text{if } d > 0 \text{ or } c \geq q^*, \\ P = 0 & \text{otherwise.} \end{array} \right.$$

Recently, Hilhorst et al. [133] have derived a simplification of system (6.13) for large reaction rate $k \to \infty$. In addition they have equivalently reformulated the precipitation rate $P$ as follows,

$$P = (c-q)_+ \; H\left( \int_0^t \left( c(s,x) - q^* \right)_+ ds \right), \tag{6.14}$$

where $H$ denotes the Heaviside function. In other words, as soon as the concentration $c$ is over $q^*$ for some time $t_0$, it goes on for $t \geq t_0$ (because $\int_0^t \left( c(s,x) - q^* \right)_+ ds > 0$) unless $c$ becomes less than $q$.

**Model 1** (Ostwald's supersaturation scenario)**.** *In the limit of a fast precipitation reaction between the two species $A$ and $B$, the concentration compound $C$ satisfies a singular equation,*

$$\frac{\partial c}{\partial t} = \Delta c + \delta(x = \beta t) - P, \tag{6.15}$$

*where the precipitation rate $P$ is given by* (6.14)*. The adimensionalized parameters are the speed of the front $\beta$ and the supersaturation threshold $q^*$.*

We should mention that numerical simulations of equations (6.13) and (6.15) turn out to be difficult (see also [242]). In fact this model belongs to the class of free boundary problems (as the Stefan problem). Recurrent precipitation can be exhibited, however the wavelength of the pattern strongly depends on the space step.

### Prenucleation

The Ostwald's supersaturation scenario is a limiting case of the so-called prenucleation theory where precipitate particles grow in size after their formation (by 'ripening'), independently from each other [242]. Accordingly, the precipitation rate writes

$$P = \frac{\partial d}{\partial t}\ , \quad \text{with } d \propto \int_0^t J(s) r(t', t; x) dt', \tag{6.16}$$

the nucleation rate $J$ being function of the supersaturation $s(t,x) = c(t,x)/c_0$. Numerical evidence that such a mechanism eventually leads to recurrent precipitation is given by [82] and [161, 160] for example.

**Remark 6.7.** *Liesegang rings verify several experimental quantitative space and time laws. The* time law *states that the position of the nth band $x_n$ is proportional to $\sqrt{t_n}$, where $t_n$ is the time elapsed before the precipitation starts. The* spacing law *indicates that the ratio between the position of two successive bands converges towards a finite value 1+p, where $p > 0$. However, these laws are not biologically relevant in the study of BCS [157]. In the following models, the quantitative space and time laws will always depend on the nature of the propagating front.*

## 6.4.2 The preconditioning model

The preconditioning hypothesis has been first proposed by Stadelmann et al. [226]. Preconditioning is a theory formulated by biologists interested in ischemia. Cells that find themselves in an ischaemic environnement are supposed to produce *preconditioning molecules* (for example heat shock proteins) that protect their neighbouring cells from the deleterious effects of oxygen deficiency. In the scenario of Stadelman et al., a propagating front of oligodendrocyte apoptosis triggers the production and diffusion of molecular signals that protect surrounding oligodendrocytes at the edge of front (see figure 6.3). The following three-species continuous model is inspired by the qualitative description of [226]. A leading front of a molecular signal $u(t,x)$ activates the microglia and induces the apoptosis of the oligodendrocytes. The density of the damaged cells is $d(t,x)$, whereas the total cell density is a constant denoted by $\bar{d}$. Attacked cells produce a preconditioning potential $\phi(t,x)$, which diffuses rapidly and protects the cells that have not be damaged yet. The preconditioning potential is active over a range of action compatible with the free diffusion ability of molecules in the brain.

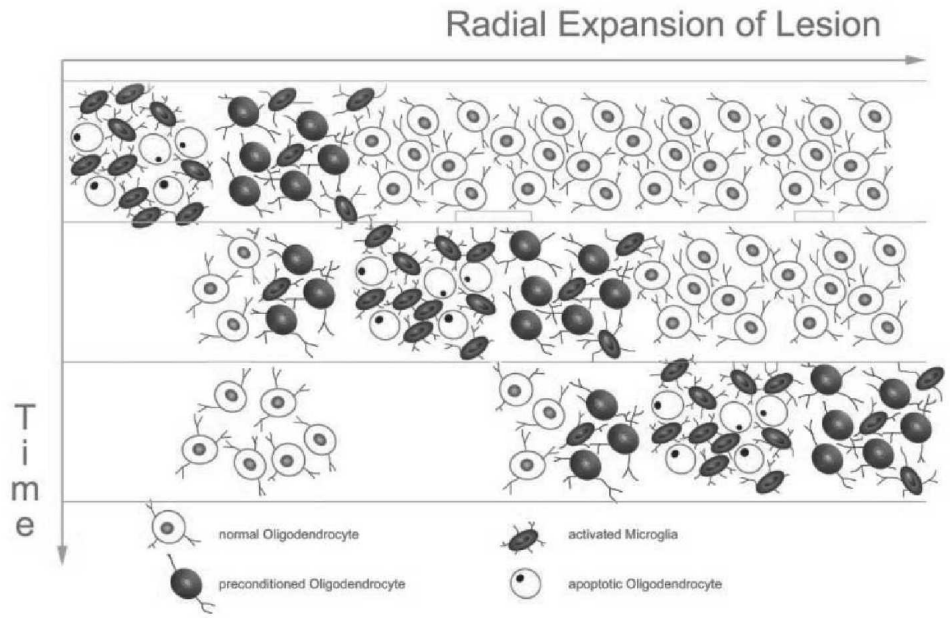


Figure 6.3: Qualitative description of the preconditioning scenario. The preconditioned oligodendrocytes are not destroyed by the activated microglia (from Stadelmann et al. 2005 [226]).

**Model 2** (Preconditioning model)**.** *Let $u$ denote the leading reaction front, $d$ the density of destroyed oligodendrocytes and $\phi$ the protection potential.*

$$\begin{aligned} &\frac{\partial d}{\partial t} = A(u)P(\phi)\ (\bar{d} - d), \\ &-\varepsilon\Delta\phi + \alpha\phi = \mu d. \end{aligned} \tag{6.17}$$

*The evolution of the outer variable $u$ is not specified (it is a basic traveling front in figure 6.4).*

The protection is expressed by the cut-off function $P(\phi) = (q - \phi)_+$, with a fixed threshold $q$: if the preconditioning potential is sufficiently high, aptotosis does not occur. The activation term $A(u)$ is typically $H(u - q')$, corresponding to some level set of the leading reaction front. Neither regeneration of oligodendrocytes nor remyelination are taken into account, therefore $d$ can only increase. The potential equation (linear production, natural decay and linear fast diffusion) is chosen to be consistent with our other models. It is still unclear whether preconditioning with this choice for $\phi$ can lead to the emergence of concentric rings. As a matter of fact, we have numerical evidence that it does not in 1D and in 2D, but this point still requires investigation.

Within system (6.17), an equilibrium is reached at the tip of the moving front (see also [242]). Concentric bands only appear for some formulations of the potential $\phi$ (see figure 6.4) which have no biological meaning.

It is worth mentioning that the width of the bands is entirely determined by the range of action of the potential $\phi$. However, the wavelength of the BCS patterns (figure 6.2) is considerably larger than any molecular signal diffusion range known in the brain (see [157] for discussion). It seems thus unlikely that the preconditioning potential could be, as stated by Stadelman et al. [226], the simple resultant of the diffusion of a protective molecule produced by the attacked oligodendrocytes.

The precipitation term in preconditioning is very different from the one used in OS. Indeed, in system (6.13), this rate is notably discontinuous between $d > 0$ and $d = 0$ (this discontinuity is due to the presence of two distinct thresholds, $q$ and $q^*$). Moreover, in preconditionning, concentric patterns may arise from a temporal discontinuity in the progession of the front: the front may progress, stop, allow the protection to be effective and then start progressing again. The clinical evolution of MS is characterized

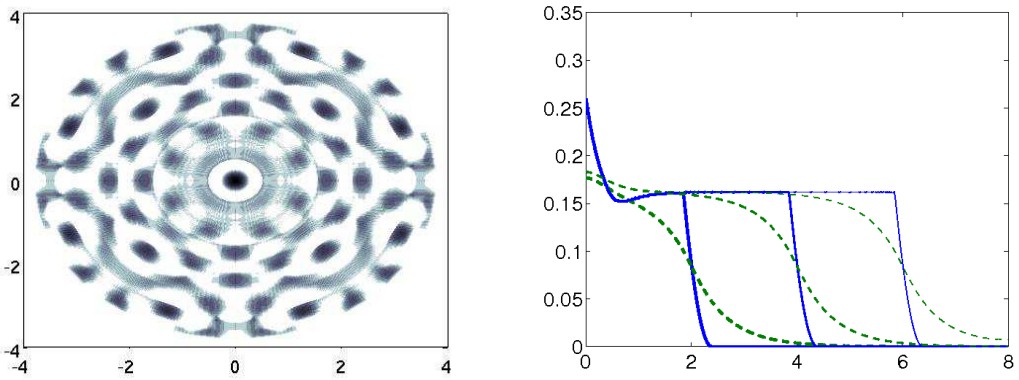


Figure 6.4: Pattern formation in the preconditioning model 2. (*left*) We replace the potential production in (6.17) by $\phi = K * d$, the kernel $K$ being a stiff Hill function with a range of action equal to $\sqrt{\varepsilon}$: $K(z) = \mathbf{1}_{|z|\leq\sqrt{\varepsilon}}$. Interestingly, the radial symmetry is not preserved. In addition, the pattern wavelength is close to the range $\sqrt{\varepsilon}$. The front speed is $v = 0.1$ and other parameters are $\varepsilon = 0.4$, $q = 0.1$. Very strong preconditioning with $\phi(x) = \max_{|z|\leq\sqrt{\varepsilon}} d(x+z)$ leads to recurrent ring formation where symmetry is conserved. However, the wavelength of such a pattern is not compatible with the biological data. (*right*) In the one-dimensional case, an equilibrium is reached at the front tip. The potential production is driven by $-\varepsilon\Delta\phi + \phi = d$, and parameters are the same as above.

by the occurence of attacks, corresponding to demyelination episodes, which could correspond to such temporal discontinuities. However, several MS attacks occuring successively in a few hours period would be necessary to induce concentric demyelination in accordance with pathology's time scales. Such an evolution has never been clinically described.

A concept derived from the prenucleation model (6.16) for LR may help to improve the preconditioning model. By introducing a "maturation in death" effect, damaged oligodendrocytes would die progressively and induce a differential secretion of the signal $\phi$. Nevertheless, this new model will not solve the molecular range of action paradox.

## 6.5 Secondary rearrangement at the back of the front

The two models described in this section share the common characteristic of producing patterns behind the leading reaction front. The first one, the competitive coarsening model was first formulated to improve the theoretical description of LR by using a degenerated bistability process. We have already described the second model based on self-attraction of immune cells in our earlier study of BCS [157].

### 6.5.1 Postnucleation – The theory of competitive coarsening

Pre- and postnucleation scenarios are extensions of OS based on physical arguments. They both assume that the particles produced by the precipitation reaction have the ability to modify their size at the back of the front. These two theories differ by the supposed nature of the particles (*resp.* solid precipitate and colloid) and the competition mechanism that occurs between growing particles. Postnucleation states that ring formation may be the result of an instability mechanism at the macroscopic level [105]. A more recent model, which will be described below, initially proposed by Feinn et al. [101], involves a two-species instability, namely the growing potential and the local mean radius of particles.

One of the main objections to the direct application of OS to LR formation or concentric demyelination is that in both cases, an area of homogeneous turpitude appears before periodic patterning. In the postnucleation theory, this area corresponds to a non periodic field of colloidal particles and in BCS, to a diffusion anomaly observed with MRI in the white matter before concentric demyelinization [249].

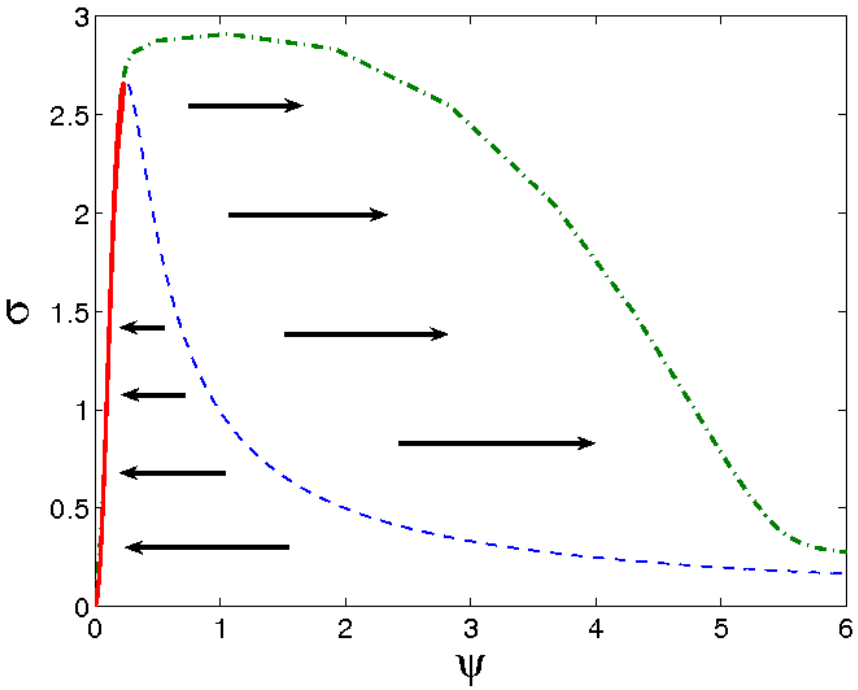


Figure 6.5: Post-nucleation instability mechanism: the *relaxation* function $g(\psi)$ is plotted in dashed line. In addition, two trajectories in the phase diagram $(\psi, \sigma)$ are represented in full and dot-dashed lines, corresponding respectively to the black and white arrows in figure 6.6.

The chemical basis of the postnucleation theory is the same as in OS (section 6.4.1), namely

$$A + B \longrightarrow C \longrightarrow D.$$

In addition however, the reaction front induces the formation of colloidal particles (intermediate state between a molecule and a precipitate) by aggregation of the compound $C = AB$ [101]. A colloid is in fact a compound made out of a small number of aggregated molecules, where the surface tension plays a non-negligible role. Spatial structure emerges because large colloids grow faster at the expense of small ones. It is worth noticing that self-organization is driven by the constrain of mass conservation.

The model combines a reaction-diffusion equation for the growing potential with an ODE for the size of the particles. The time and space laws are not taken into account, as mentioned before (remark 6.7). Accordingly, we build an abstract propagating front with unspecified shape and speed. The concentration of the hypothetical propagating species $U$ is denoted by $u = [U]$. The front forms colloidal particles which are described by a growing potential $\sigma$, also called *supersaturation*. The mean colloidal particle size $\psi$ evolves according to a two-sided relaxation towards bistable equilibria (figure 6.5),

$$\sigma^* = g(\psi) = \frac{2\psi^3}{2\psi^3 + \psi_c^3}.$$

**Model 3** (Post-nucleation)**.** *Let $u$ denote the leading reaction front. The post-nucleation instability writes*

$$\begin{aligned} \frac{\partial u}{\partial t} &= \beta \Delta u + G u (A - u), \\ \frac{1}{\beta} \frac{\partial \sigma}{\partial t} &= \Delta \sigma - \psi^2 \left[ \sigma - g(\psi) \right] + u, \\ \frac{\partial \psi}{\partial t} &= \sigma - g(\psi). \end{aligned} \tag{6.18}$$

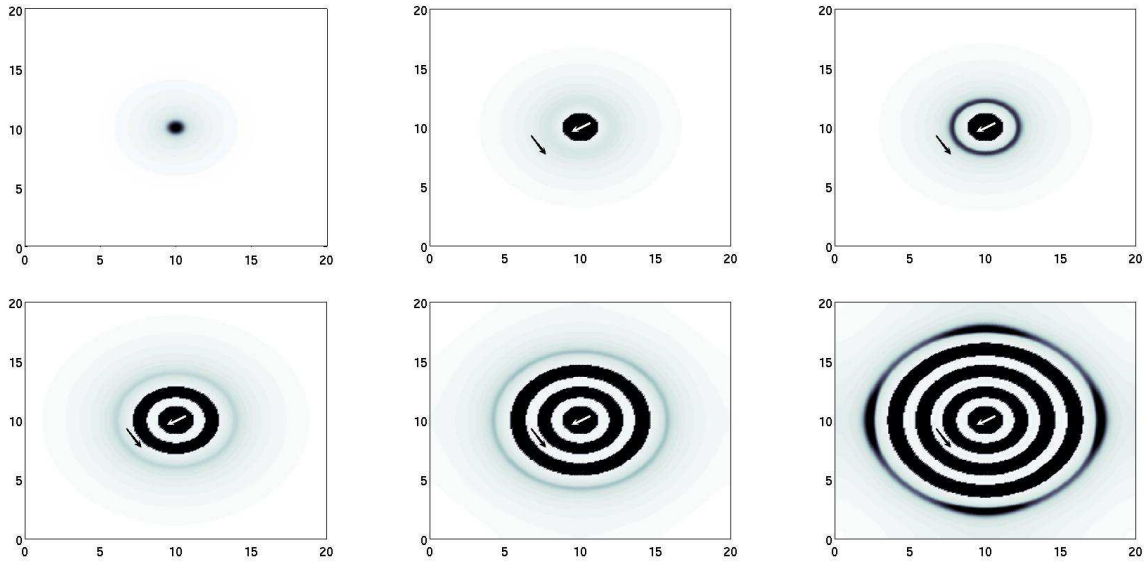

Figure 6.6: Postnucleation model on a square regular grid: the mean colloidal particle size $\psi$ is successively represented for $t = 22,\ 30,\ 32,\ 42,\ 53,\ 64$. The front is Fisher–type, with speed 0.2 and amplitude $A = 10$. Other parameters are $\beta = 0.1$ and $\psi_c = 0.25$ (from Krug et al. [161]). For the black and white arrows, see figure 6.5.

*where $\psi$ denotes the mean particle radius at position $x$ and time $t$, and $\sigma$ is the growing potential.*

For the sake of coherence with the other models 2 and 4, we have opted for a Fisher reaction-diffusion equation driving the outer activation variable $u$. We are interested in its amplitude $A$ and its speed $2\sqrt{\beta G A}$. Figure 6.6 illustrates the evolution of the mean particle size $\psi$. Note that the rings appear far from the leading front, as a result of the bistable mechanism described in figure 6.5.

The secondary rearrangement of growing colloids at the back of the front inspired our model for BCS. In this case however, the instability mechanism is driven by chemotaxis.

### 6.5.2 Chemotaxis hypothesis for Baló's concentric sclerosis

The mathematical models for morphogenesis were originally based on chemical reactions involving only hypothetical morphogens [236, 110]. Such reaction-diffusion mechanisms could occur in BCS but we focus our study on self-organization processes due to chemotaxis. The main idea of our model is that organization arises from chemotactic movements in a population of macrophages. The chemical signals attracting the macrophages – supposedly pro-inflammatory molecules – are produced by damaged oligodendrocytes. By recruiting the surrounding macrophages, these oligodendrocytes indirectly protect neighbouring zones.

**Model 4** (Local recruitment of macrophages [157])**.** *Let $m$ be the density of activated macrophages, $c$ the concentration of the attractive signal and $d$ the density of the destroyed oligodendrocytes. The system writes*

$$\frac{\partial m}{\partial t} = D\Delta m + \lambda m(\bar{m} - m) - \nabla \cdot \Big(\chi m(\bar{m} - m)\nabla c\Big) \tag{6.19}$$

$$\frac{\partial d}{\partial t} = F(m)m(\bar{d} - d) \tag{6.20}$$

$$-\varepsilon\Delta c + \alpha c = \mu d, \tag{6.21}$$

*where $\bar{m}$, $\bar{d}$ are characteristic macrophage and oligodendrocyte densities. The damaging function $F$ can be chosen almost arbitrarily as long as it is both positive and increasing. We set $F(m) = \kappa\ m/(\bar{m} + m)$.*

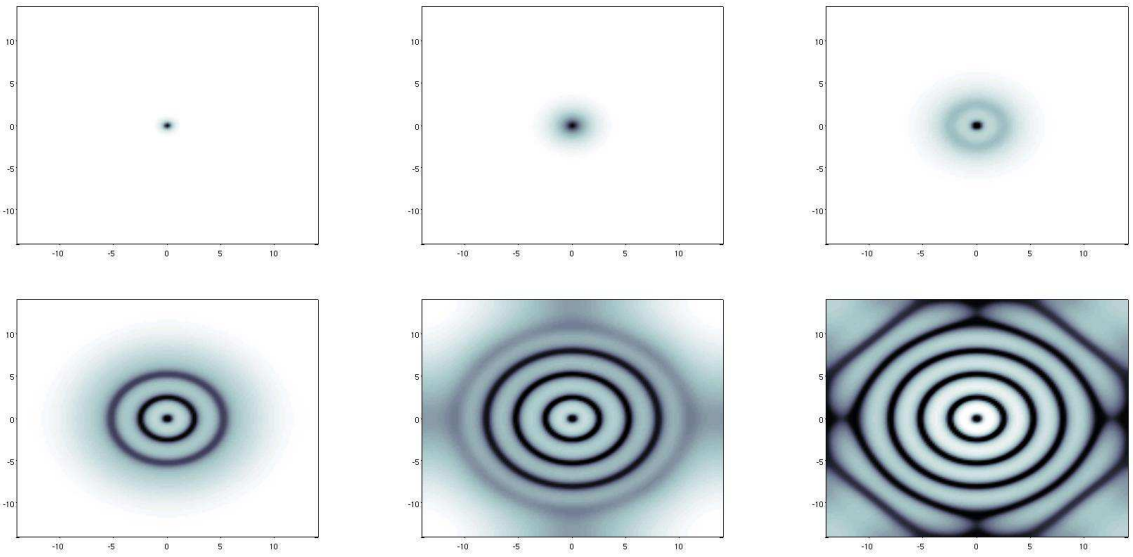

Figure 6.7: Local recruitment of macrophages: evolution of $d$ (damaged oligodendrocytes) for $t = 1h,\ 4h,\ 7h,\ 10h,\ 13h,\ 16h$, from numerical simulations of model 4. Parameters are $r = 2,\ \varepsilon = 0.2$ and $\chi = 30$. The unit length is $L = 1mm$, and the domain width is thus approximately $3cm$. Numerical values for simulations were extracted from [192] and [171]. Destroyed oligodendrocytes are figured in black. Interestingly, successive bands appear behind the edge of the front.

The system reads as follows: macrophages are activated through a Fisher equation and organize chemotactically (6.19), oligodendrocytes are destroyed by activated macrophages (6.20) and produce a chemoattracting signal (6.21). This mechanism leads to concentric band formation at the back of a turpitude area for a wide range of parameters (figure 6.7). In fact, this model only produces two patterns : concentric bands, as in BCS, and homogeneous plaques of destroyed oligodendrocytes, as in MS (figure 6.9).

We have opted for a Fisher-type front in (6.19), but the final pattern is independent of this particular choice. Instead we could have used the heat equation accounting for the diffusion of a molecule, or a traveling pulse corresponding to the transduction of some molecular signal (typically cAMP in the modeling of *Dictyostelium*'s aggregation phase [139]). Nevertheless there are quantitative differences between these alternatives (numerical results are shown in figure 6.8). Furthermore, the analysis of those quantitative differences can provide a suitable test fot the selection of the true underlying mechanism which drives macrophages activation (reaction-diffusion, pure diffusion or transduction). The activation front hypothesis raises a controversial point. In fact, one of the main arguments we produced against the preconditioning theory was that the hypothesis of a protective molecule diffusing on centimetric distances was not biologically realistic. In our model the activation front also involves molecular movements on long distances. Nevertheless, no hypothesis is necessary on the nature of this molecule, or on its interactions with the cerebral tissue. There is no particular reason to believe that the propagation of the activation front should be driven by pure diffusion alone. On the other hand, preconditioning involves well characterized molecules which are not known to be involved in specific interactions that would help them to travel through the white matter by any other way than diffusion.

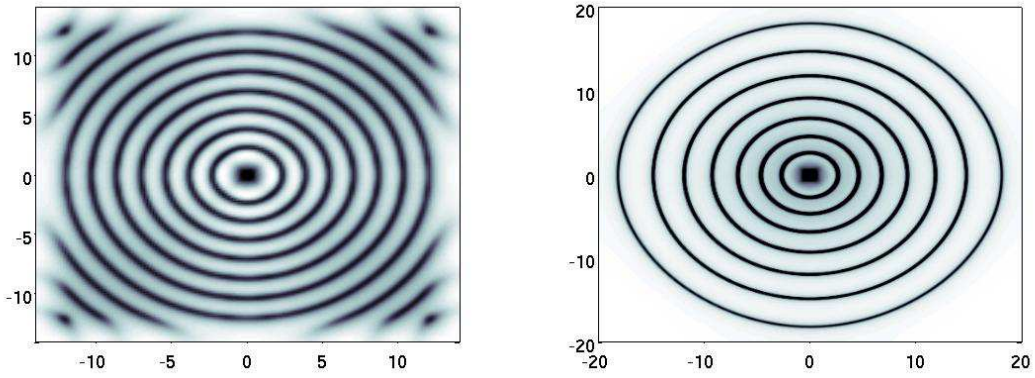


Figure 6.8: Pattern formation with two different front propagation types: (*left*) the front is a traveling pulse with constant speed, and (*right*) a diffusing molecule activates the macrophages. Note that space and time laws depends on the specific nature of this leading front.

**Adimensionalized equations.** We set the reduced variables and parameters as follows,

$$\tilde{m} = \frac{m}{\bar{m}}, \quad \tilde{d} = \frac{d}{\bar{d}}, \quad \tilde{c} = \frac{\alpha}{\mu \bar{d}}, \quad \tau = \lambda \bar{m} t, \quad y = \sqrt{\frac{\lambda \bar{m}}{D}} x,$$
$$\tilde{\chi} = \frac{\chi \bar{m} \mu \bar{d}}{D\alpha}, \quad \tilde{F}(\tilde{m}) = \frac{\kappa}{\lambda} \frac{\tilde{m}}{1+\tilde{m}}, \quad \tilde{\varepsilon} = \frac{\varepsilon \lambda \bar{m}}{D\alpha}. \quad (6.22)$$

In particular, the speed of the front and the destructive strenght of the macrophages are balanced by the ratio $r = \kappa/\lambda$. We obtain the following adimensionalized system,

$$\begin{cases} \dfrac{\partial \tilde{m}}{\partial \tau} = \Delta \tilde{m} + \tilde{m}(1-\tilde{m}) - \nabla \cdot \Big( \tilde{\chi} \tilde{m}(1-\tilde{m}) \nabla \tilde{c} \Big), \\ \dfrac{\partial \tilde{d}}{\partial \tau} = \tilde{F}(\tilde{m}) \tilde{m}(1-\tilde{d}), \\ -\tilde{\varepsilon} \Delta \tilde{c} + \tilde{c} = \tilde{d}. \end{cases} \quad (6.23)$$

Only three parameters remain, namely the reduced chemosensitivity $\tilde{\chi}$, the reduced chemical diffusivity $\tilde{\varepsilon}$ and the damaging ratio $r = \kappa/\lambda$.

## Some qualitative properties of the local macrophages recruitment model

Several qualitative properties are *a posteriori* confirmations of the validity of our model. Local macrophages recruitment model creates concentric patterning, is very robust and allows to draw links between BCS and MS.

The first interesting point is that here, the wavelength of the pattern is not directly related to the range of action of the chemical potential $c$, as opposed to the preconditioning model 2 (see [157]).

**Spatial structuration as a result of aggressivity.** The reduced parameter $\tilde{\chi}$ defined in (6.4) drives the spatial organization of cells in the basic PKS model (6.2), and is also a major parameter in model 4. Consequently, according to the chemotaxis principle (section 6.2), we expect qualitatively the corresponding $\tilde{\chi}$ in (6.22) to play a similar role. As a matter of fact, by increasing $\tilde{\chi}$, we induce a transition between homogeneous density of damaged oligodendrocytes and concentric patterns (figure 6.9).

Furthermore, there exists a positive correlation between the aggressivity of the disease and the emergence of structure. The underlying reduced parameter $\tilde{\chi} = \chi \bar{m} \mu \bar{d} / D\alpha$ increases with the aggressivity. Indeed, $\bar{m}$ stands for the amount of immune cells and is in the numerator (note that $\bar{m}$ also appears in

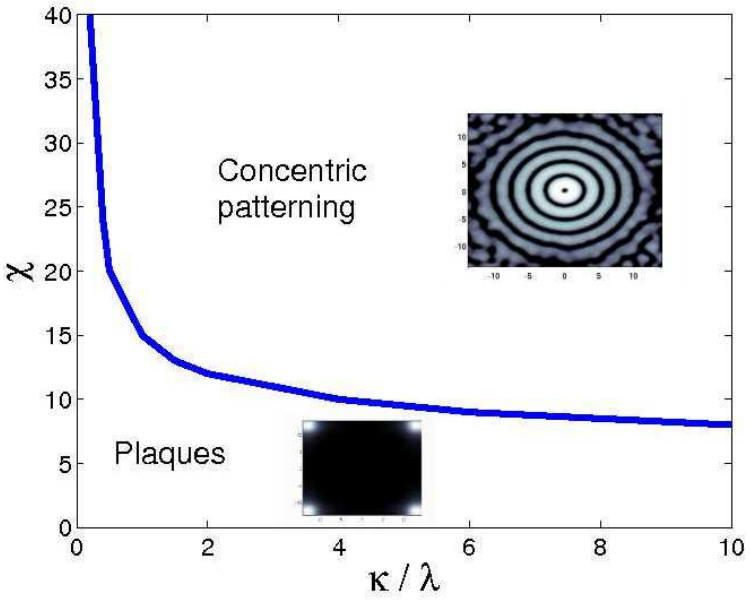


Figure 6.9: Bifurcation diagram for model 4, with a fixed reduced parameter $\tilde{\varepsilon} = 0.1$. Two situations appear: concentric patterning (structure) or plaques (no structure). Transition between these two states is driven by the structural parameters $\tilde{\chi}$ and $r$ for fixed $\tilde{\varepsilon}$. Concentric patterning is favoured for increasing parameter values: aggressivity is thus positively correlated to spatial structure. The figure in top-right is performed under random perturbation of the chemical diffusivity, showing robustness of the model.

the reduced parameter $\tilde{\varepsilon}$, but only because of its role in front speed). As $\tilde{\chi}$ drives the bifurcation between plaques (no structure) and concentric bands (structure), this parameter makes the junction between aggressivity and spatial structure. This assertion is also true for the damaging parameter $r = \kappa/\lambda$, which is related to the macrophages ability to destroy the oligodendrocytes (see figure 6.9).

**Model robustness.** The chemotactic scenario for BCS is highly robust. In fact, our model only produces plaques (no structure) or concentric bands (spatial organization). This simple alternative contrasts with the results of other types of pattern formation models. For instance, in Turing systems, many different patterns can emerge, such as spots or labyrinthic patterns [185, 110], depending on the parameters. In models of bacterial colony growth, chemotaxis can lead to localized cellular aggregates [40, 238]. Furthermore, another argument that accounts for the robustness of our model is that radial symmetry is well-conserved under different perturbations (see [157] and figure 6.9).

**Short-time assumption.** A major hypothesis of model 4 is that the chemoattractant $c$ is produced by the damaged oligodendrocytes $d$. This is obviously irrelevant for long evolution times, because the damaged oligodendrocytes are digested by the macrophages. However, we suggest that the relaxation time for macrophages before they re-attack the preserved area is longer than the time scale of concentric demyelination (approximately a few days, BCS is typically aggressive). The macrophages need a "digestion time" before being effective again. This assumption may explain why concentric patterns are observed in very early MS cases [19]. The temporal transition from rings to plaques may first be the result of self-organization (local recruitment), followed by the relaxation of macrophages that spread again in the domain and destroy the pattern to form plaques.

## 6.6 Conclusion

Liesegang ring formation and Baló's concentric sclerosis both involve the interaction between a propagating front (whose origin is unknown in BCS) and non-moving molecules or cells. The postnucleation instability in Liesegang rings led us to propose chemotaxis as a self-organization mechanism. The model we built, namely the local macrophages recruitment model, is very robust and closely fits biological data. Three characteristics of our model need further investigations. First, the space and time laws of the pathological process highly depends on the nature of the underlying front. The study of this dependance may help to understand the mechanism of propagation. Secondly, the wavelength of the pattern decreases when the density of macrophages increases. This intuitive statement, based on a refined analysis of chemotaxis-based models, has been numerically verified but still needs theoretical confirmation. Finally, the aggressivity of the disease may account for its structuring ability. BCS may then be a variant of MS where the same general pathogenic mechanisms occur with particular intensity.

## Troisième partie

# Keller-Segel 1D : le point de vue du transport optimal

# Chapitre 7

# Défaut de convexité par déplacement : l'exemple de Keller-Segel 1D

---

Ce chapitre est une rédaction (très) préliminaire d'un travail en commun avec José Carrillo. Le système Keller-Segel 1D (chapitre 2) est interprété comme un flot gradient généralisé pour la distance de Wasserstein. Pratiquement, cela consiste en 1D à écrire l'évolution de la fonction inverse de répartition de la densité cellulaire. Les techniques analytiques qui contournent le défaut de convexité (par déplacement), par des arguments d'homogénéité, sont décrites ici. Elles sont adaptées telles quelles dans le contexte discret au chapitre 8. Un système dynamique (EDO) épuré, qui possède ces propriétés remarquables d'homogénéité, est présenté dans l'introduction (page 11). Les méthodes développées ici en dimension infinie sont rigoureusement identiques.

---

## 7.1 Introduction and motivations

McCann's displacement convexity theory was a deep contribution to the theory of interacting particles [179] (see [244] for a very user-friendly textbook). He introduced a new concept of interpolation between probability densities, making some functionals being convex along the displacement pathways. Those functionals typically belong to the following class

$$\mathcal{F}(n) = \int U(n(x)) + \int n(x)V(x)\ dx + \iint W(x-y)n(x)n(y)\ dxdy, \tag{7.1}$$

for suitable internal energy $U$, confinement potential $V$ and interaction kernel $W$. In particular, the latter is required to be a nondecreasing convex function. However in the simplest formulation of the Keller-Segel model that we will describe below [55], the last assumption fails: the interaction kernel is $W = \log|\cdot|$. In this case the balance between two opposite trends (diffusion against cell-to-cell attraction) plays a major role and one need to have a refined understanding of this competition to describe the long time behaviour of the model.

So, the original motivation of the present work arised from biology models (even very simple ones). However it comes out that our method of *equilibrium factorization* can be applied to a wider range of functionals of the type (7.1) which are not displacement convex. We will present our results in a progressive way, starting with the most simple and original model, namely the Keller-Segel system (which

turns out to be degenerate in some sense actually) and we will conclude with a more general form under appropriate assumptions. All the argumentations in the sequel are one-dimensional (the higher dimension is in progress) and it requires the same two ingredients:

1. some discrete inequality adapted to each situation (it is simply the Jensen inequality in the degenerate Keller-Segel case),

2. an equilibrium state, solution of the corresponding Euler-Lagrange equation.

As soon as these two have been stated, and some sort of homogeneity holds for the functional, we can prove uniqueness of the functional's minimizer which is unsurprisingly the stationary state of item 2. Note that item 2 will come from previous existence proofs, and nothing is new in this work.

The plan of this chapter goes as follows: in section 7.2 we present briefly the Keller-Segel in its various formulations (classical, rescaled, or with non-linear diffusion). In section 7.3 we prove the logarithmic Hardy-Littlewood-Sobolev inequality in this new 1D setting, and we generalize it, involving non-linear diffusion or a quadratic confinement potential. In section 7.4 we investigate how this 'equilibrium factorization' trick can help to measure the trend to equilibrium in term of the quadratic Wasserstein distance. Finally in section 7.5 we depict briefly which assumptions can be made in general for the coupling diffusion/interaction in (7.1) to ensure the same kind of results.

### Notations

We review now the list of notations for the sake of coherence and clarity.

**Variables.** $x$ denotes the space variable, $\rho$ is the 'transport' variable, $\rho$ lies in $(0,1)$ in 1D.

**Functions.** $n(t,x)$ or $\underline{n}(t,x)$ usually denote the cell densities, whereas $\Phi(t,\rho)$ and $\Psi(t,\rho)$ are the pseudo-inverse distribution functions. We denote by $d_W(n,\underline{n})$ the Wasserstein distance, which corresponds to the $L^2-$norm of $\Phi-\Psi$. Also, $H, K$ results from doubling the variables: for instance $H = \Phi(\rho)-\Phi(\eta)$.

**Functionals.** $f(u)$ is the (non-linear) diffusion, usually homogeneous: $f(u)=u^m$ (say $m\geq 1$ for the moment). $U$ stands for the internal energy of the system; $V(x)$ and $W(x)$ are respectively the confinement potential and the interaction potential. The pressure function $h$ is given by $f'(u) = uh'(u)$ and verifies also $U'(u)=h(u)$. If the diffusion is linear, then $U = u\log u - u$ and $h(u)=\log u$. In the case $f(u)=u^m$, $m\neq 1$, then $U=\frac{1}{m-1}(u^m-mu)$ and $h(u)=\frac{m}{m-1}(u^{m-1}-1)$. Finally $A$ is the corresponding internal energy in the transport variables, defined as $A(\omega)=\omega U(1/\omega)$.

**Energy functionals.** In the classical framework, we have

$$\mathcal{F}(n)=\int U(n(x))\ dx+\int V(x)n(x)\ dx+\iint W(x-y)n(x)n(y)\ dxdy.$$

From the new point of view we have equivalently

$$\mathcal{G}(\Phi)=\int A(\Phi')\ d\rho+\int V(\rho)\ d\rho+\iint W\Big(\Phi(\rho)-\Phi(\eta)\Big)\ d\rho d\eta,$$

and of course $\mathcal{F}(n)=\mathcal{G}(\Phi)$.

## 7.2 Chemotaxis and Optimal transportation

The Keller-Segel system [153, 154] for chemotaxis-like interacting cells in the whole space $\mathbb{R}^d$ reads

$$\begin{cases} \dfrac{\partial n}{\partial t}=\Delta n-\operatorname{div}\ (\chi n\nabla c)\ , \quad t>0,\ x\in\Omega\subset\mathbb{R}^d, \\ -\Delta c=n\ , \end{cases} \tag{7.2}$$

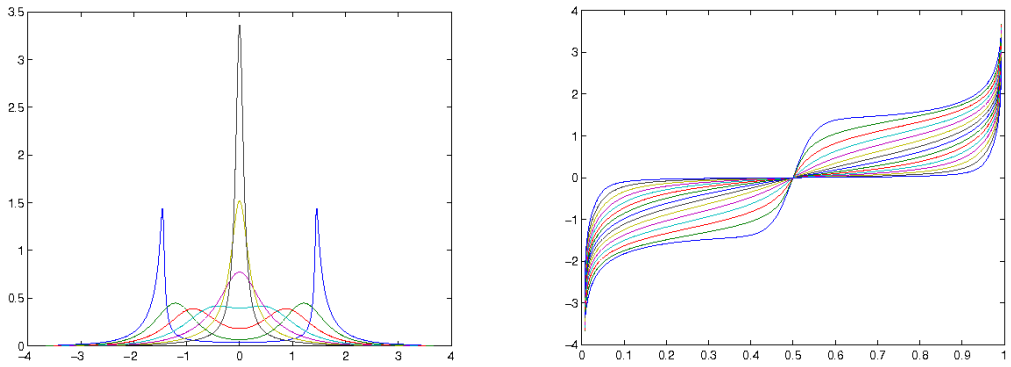

Figure 7.1: Illustration of the pseudo-inverse distribution function (from the work [33]). Respectively the cell density $n(t,x)$ and the inverse distribution function $\Phi(t,\rho)$. Initial condition is a 2-peaks cell distributions, where each of the peak contain not enough mass to blow-up by itself. Blow-up occurs in the upper-critical case $\chi = 2.2\pi > \chi_c$.

together with the decreasing free energy

$$\mathcal{E}(t) = \mathcal{F}(n(t)) = \int n \log n - \frac{1}{2}\int nc.$$

This system is subject to a critical mass phenomenon in dimension $d = 2$: if $\int n_0 > 8\pi/\chi$ then blow-up occurs in finite time, otherwise there is global existence [86, 34]. In [55] authors propose a new way of generalizing the KS model in other dimensions than two, keeping the space $L^1$ to be critical (leading to an interesting critical mass phenomenon). This comes from the following statement: *there exists a critical mass in dimension two because the interaction kernel* $W(z) = \log|z|$ *has a critical weight.* Therefore replacing the chemical potential equation $-\Delta c = n$ with $c = -\frac{1}{d\pi}\log|\cdot| * n$, for every dimension $d$, enhances the existence of a mass threshold, which is given by $M^* = 2d^2\pi/\chi$ (within this particular choice of constant in front of the logaritmic kernel).

### Notations and change of variables

In the sequel we adimensionalize the system, and we reduce to only one parameter, namely the chemosensitivity $\chi$. Without loss of generality the total mass of cells is always assumed to be $M = 1$. Therefore the 'critical mass' becomes a critical chemosensitivity for the paramater value in dimension one:

$$\chi_c = 2\pi \ .$$

Note that the center of mass is also conserved through evolution in system (7.2), so that we can always assume $\int xn(t,x) = 0$.

First we will care about the KS model in its classical setting,

$$\begin{cases} \dfrac{\partial n}{\partial t} = \dfrac{\partial^2 n}{\partial x^2} - \chi \dfrac{\partial}{\partial x}\left(n\dfrac{\partial c}{\partial x}\right) & t > 0\ ,\ x \in \mathbb{R}\ , \\ c = -\dfrac{1}{\pi}\log|z| * n, \quad \longleftrightarrow \quad \dfrac{\partial c}{\partial x} = -\mathcal{H}n\ , \end{cases} \tag{7.3}$$

where $\mathcal{H}$ denotes the Hilbert transform [227]. We introduce the distribution function of the cell density $n$ and its pseudo–inverse,

$$N(t,x) = \int_{-\infty}^{x} n(t,y)\ dy, \quad \Phi(t,\rho) = \inf\{x : N(x) > \rho\}.$$

We can formally derive the equation for $\Phi$ when $n$ is regular, performing the change of variables $\rho = N(x)$,

$$\begin{aligned} \frac{\partial N}{\partial t} &= \frac{\partial n}{\partial x} + \chi(n\mathcal{H}n) \\ -\frac{\partial \Phi}{\partial t} &= \frac{\partial}{\partial \rho}\Big(\Big(\frac{\partial \Phi}{\partial \rho}\Big)^{-1}\Big) + \chi\Omega[\Phi], \end{aligned}$$

where the nonlinear functional $\Omega$ is given by

$$\begin{aligned} \Omega[\Phi](\rho) &= \mathcal{H}n \qquad (7.4) \\ &= \lim_{\varepsilon\to 0}\frac{1}{\pi}\int_{|x-y|>\varepsilon}\frac{1}{x-y}n(y)dy\ , \\ &= \lim_{\varepsilon\to 0}\frac{1}{\pi}\int_{|\Phi(\rho)-\Phi(\eta)|>\varepsilon}\frac{1}{\Phi(\rho)-\Phi(\eta)}d\eta\ . \qquad (7.5) \end{aligned}$$

It is worth noticing that this transformation $n \longrightarrow \Phi$ is related to optimal transportation in the sense that $N$ is the natural transport map from $\mu = n(x)dx$ onto the Lebesgue measure $\lambda(0,1) = \mathbf{1}_{\rho\in(0,1)}d\rho$ [244] (see also [20]).

**The Keller-Segel system with nonlinear diffusion**

We perform the same change of variables when dealing with nonlinear diffusion, namely

$$\begin{cases} \dfrac{\partial n}{\partial t} = \dfrac{\partial^2 f(n)}{\partial x^2} - 2\pi\dfrac{\partial}{\partial x}\left(n\dfrac{\partial c}{\partial x}\right) & t>0,\ x\in\mathbb{R}, \\ c = -\dfrac{1}{\pi}\log|z| * n, \quad \longleftrightarrow \quad \nabla c = -\mathcal{H}n, \end{cases} \tag{7.6}$$

with the same notations as previously. Note that we are now reduced to $\chi = 2\pi$ because the nonlinear diffusion $f$ contains all the parameters. Following [50] we introduce the pressure and the entropy functionals,

$$f'(u) = uh'(u), \quad \text{and} \quad U'(u) = h(u),$$

together with $h(1) = 0$ and $U(0) = 0$, respectively.

Within the new variable $\rho = N(x)$, the system (7.6) reads

$$-\frac{\partial \Phi}{\partial t} = \Big(f\Big(\frac{1}{\Phi'}\Big)\Big)' + 2\pi\Omega[\Phi]. \tag{7.7}$$

**The rescaled Keller-Segel system**

Back to the linear diffusion case, it is known that system (7.3) admits (non unique) equilibria only for the critical parameter $\chi = \chi_{crit} = 2\pi$ [56]. Therefore one should not expect any convergence in the subcritical case $\chi < \chi_{crit}$. However Blanchet *et al.* [35] proved convergence towards a unique equilibrium in the self-similar variables $(\tau, y)$,

$$\frac{\partial u}{\partial t} = \frac{\partial^2 u}{\partial x^2} + \frac{\partial}{\partial x}\left(\chi u\left(y - \frac{\partial v}{\partial x}\right)\right)\ , \quad \nabla v = -\mathcal{H}u\ , \tag{7.8}$$

In our setting the rescaled problem becomes

$$-\frac{\partial \Phi}{\partial t} = \frac{\partial}{\partial \rho}\Big(\Big(\frac{\partial \Phi}{\partial \rho}\Big)^{-1}\Big) + \chi\Omega[\Phi] + \Phi,$$

where the additional drift term is transcripted in the last contribution.

## 7.3 The log HLS inequality revisited and its consequences

### 7.3.1 Alternative proof of the log HLS inequality in 1D

In this section we recover the logarithmic Hardy-Littlewood-Sobolev inequality[9] [56, 23] with the help of the Jensen inequality. Recall from section 7.2 that $\Phi$ denotes the pseudo-inverse of the distribution function $N$.

**Theorem 7.1** (Log HLS inequality in the new variables)**.** *Let $n$ be any function $n : \mathbb{R} \to \mathbb{R}_+$ with total mass 1, and satisfying both $\int n \log n$ and $\int n(x) \log(1 + |x|^2) dx$ are finite. Then it holds true that*

$$\int n \log n \; dx \geq - \iint n(x) \log |x - y| n(y) \; dxdy + C,$$

*and the optimal constant $C$ is known from the extremal functions.*

After the change of variables $\rho = N(x)$, this inequality becomes

$$\int_0^1 \int_0^1 \log \big|\Phi(\eta) - \Phi(\rho)\big| \; d\eta \; d\rho \geq \int_0^1 \log \Phi'(\zeta) \; d\zeta + C. \tag{7.9}$$

We shall now prove the statement (7.9) using the Jensen inequality combined with a particular weight which we know in advance to be a minimizer of the associated functional

$$\mathcal{F}(n) = \int n \log n + \iint n(x) \log |x - y| n(y) \; dxdy. \tag{7.10}$$

First we use the symmetry on the left-hand-side of (7.9) and the non-decreasing property of $\Phi$ to remove the absolute value. This shows that (7.9) is equivalent to:

$$\begin{aligned} 2 \iint_{\eta \geq \rho} \log \Big( \Phi(\eta) - \Phi(\rho) \Big) \; d\eta \; d\rho &\geq \int_0^1 \log \Phi'(\zeta) \; d\zeta + C \\ 2 \iint_{\eta \geq \rho} \log \left( \int_\rho^\eta \Phi'(\zeta) \; d\zeta \right) &\geq \int_0^1 \log \Phi'(\zeta) \; d\zeta + C \end{aligned}$$

We then invoke a discrete inequality (and its continuous version), which will be in fact the sharp key estimate in each of the three proofs inside this section. In this first situation it is fairly easy and degenerated in some sense (just compare the equilibrium cases as opposed to the next lemmas 7.6 and 7.13).

**Lemma 7.2** (A discrete Jensen inequality)**.** *Let $\alpha, \beta$ be two positive real numbers. Then for all positive $p, q$ we have*

$$\log(p + q) \geq \frac{1}{\alpha + \beta} \Big( \alpha \log p + \beta \log q \Big) + C(\alpha, \beta), \tag{7.11}$$

*where equality occurs if, and only if $\dfrac{p}{\alpha} = \dfrac{q}{\beta}$.*

*Proof.* This is nothing but the Jensen inequality applied to $(p/\alpha, q/\beta)$ with weights $\left(\frac{\alpha}{\alpha+\beta}, \frac{\beta}{\alpha+\beta}\right)$ using that log is concave. □

The infinitesimal version of (7.11) to be used in the sequel is

$$\log \int \phi \geq \frac{1}{\int \psi} \int (\log \phi) \psi + C(\psi).$$

[9] Voir aussi l'annexe B.

*Alternative proof of the log HLS inequality.* We introduce a weight function $\psi$ to be chosen later, and we denote by $\Psi$ a primitive of $\psi$. We apply our trivial lemma 7.2 (weighted Jensen inequality), then we invert the order of integration

$$\begin{aligned} 2\iint_{\eta\geq\rho} \log\left(\int_\rho^\eta \Phi'(\zeta)\,d\zeta\right) &\geq 2\iint_{\eta\geq\rho} \frac{1}{\Psi(\eta)-\Psi(\rho)}\int_\rho^\eta \Big(\log\Phi'(\zeta)\Big)\psi(\zeta)+C(\psi) \\ &= \int_{\zeta=0}^1 d\zeta\,\big(\log\Phi'(\zeta)\big)\left\{2\psi(\zeta)\int_{\rho=0}^\zeta d\rho\int_{\eta=\zeta}^1 d\eta\,\frac{1}{\Psi(\eta)-\Psi(\rho)}\right\}+C(\psi). \end{aligned}$$

We are led to the following problem: *find a weight* $\psi:(0,1)\to\mathbb{R}$ *solving*

$$\forall\zeta\quad 2\psi(\zeta)\int_0^\zeta d\rho\int_\zeta^1 d\eta\,\frac{1}{\Psi(\eta)-\Psi(\rho)}=1.$$

Note that the right-hand-side 1 is precisely the meanvalue of the left-hand-side. Differentiating this relation, we shall solve

$$\Big(\frac{1}{\psi}\Big)' = 2\lim_{\varepsilon\to0}\int_{|\rho-\zeta|>\varepsilon}\frac{d\rho}{\Psi(\rho)-\Psi(\zeta)}\,d\rho\ . \tag{7.12}$$

A good way to solve this problem is to know the solution in advance. We are in a good shape here because the corresponding problem is very well known: we are in fact looking for the stationary problem,

$$\frac{\partial^2 n}{\partial x^2}+2\pi\frac{\partial}{\partial x}(n\mathcal{H}n)=0\ , \tag{7.13}$$

with $\mathcal{H}n$ being the Hilbert transform of $n$. Its variational formulation involves precisely the functional associated to the log HLS inequality (7.10). The minimizers are conformal images of the Cauchy distribution [56]:

$$h(x)=\frac{1}{\pi}\frac{1}{1+x^2}.$$

This leads to

$$\Psi(\rho)=\tan\Big(\pi\Big(\rho-\frac{1}{2}\Big)\Big).$$

We can verify by hand that such a $\Psi$ indeed solves the problem (7.12). □

As a first consequence of this alternative proof, we obtain for free the following corollary concerned with the equilibrium states.

**Corollary 7.3** (Stationary states are minimizers of the functional)**.** *There is a unique stationary state solution of* (7.13) *(up to basic transformations = conformal changes).*

*Proof.* In fact we are able to describe the equality cases in the previous lines of calculations. Equality arises (in the Jensen inequality) if the derivative $\Phi'(\zeta)$ is proportional to the equilibrium state $\psi(\zeta)$. For a given equilibrium $\psi$ solving (7.12) we obtain a log HLS inequality with constant $C$ depending on $\psi$:

$$\iint\log\big|\Phi(\eta)-\Phi(\rho)\big|\,d\eta\,d\rho\geq\int_0^1\log\Phi'(\zeta)\,d\zeta+C(\psi). \tag{7.14}$$

In particular (resulting from the equality case) we have

$$\iint\log\big|\Psi(\eta)-\Psi(\rho)\big|\,d\eta\,d\rho-\int_0^1\log\psi(\zeta)\,d\zeta=C(\psi)=\mathcal{G}(\Psi)\ .$$

We can inject some absolute minimizer $\varpi$ in (7.14) and we obtain $\mathcal{G}(\varpi)\geq C(\psi)$. Therefore the constant $C(\psi)$ is optimal and $\psi$ minimizes the functional (7.10). □

As a second consequence, we introduce a new weak formulation for the Keller-Segel system (different from what can be found in [222]), factorizing in a certain sense the flux, and making the equation for equilibrium appear.

**Definition 7.4** (Weak formulation of the 1D KS model)**.** *We consider the KS system in 1D in the transport variables $\rho = N(x)$. For any test function $\varphi \in \mathcal{D}(0,1)$ we have the following weak formulation*

$$\frac{d}{dt}\int \varphi\Phi \; d\rho = \int \frac{\varphi'}{\Phi'}\Big(1 - \frac{\chi}{2\pi}\mathcal{J}[\Phi]\Big), \tag{7.15}$$

*where $\mathcal{J}[\Phi]$ is strongly related to the equilibrium states:*

$$\mathcal{J}[\Phi](\zeta) = 2\Phi'(\zeta)\int_0^\zeta d\rho \int_\zeta^1 d\eta \; \frac{1}{\Phi(\eta)-\Phi(\rho)}$$

*statisfies $\Big\langle \mathcal{J}[\Phi]\Big\rangle_{MV} = 1$ and $\mathcal{J}[\Psi] \equiv 1$ if $\Psi$ is an equilibrium state of the system.*

*Proof.* Testing equation (7.5) against $\varphi$ yields

$$\begin{aligned}
-\frac{d}{dt}\int \varphi\partial_t\Phi &= -\int \frac{\varphi'}{\Phi'} + \frac{\chi}{\pi}\int \varphi(\zeta)\int \frac{1}{\Phi(\zeta)-\Phi(\rho)}\; d\rho d\zeta \\
&= -\int \frac{\varphi'}{\Phi'} - \frac{\chi}{\pi}\int \varphi'(\zeta)\int_0^\zeta\int_\zeta^1 \frac{1}{\Phi(\rho)-\Phi(\eta)}\; d\eta d\rho d\zeta \\
&= -\int \frac{\varphi'}{\Phi'} + \frac{\chi}{2\pi}\int \frac{\varphi'(\zeta)}{\Phi'(\zeta)}\left\{2\Phi'(\rho)\int_0^\zeta\int_\zeta^1 \frac{1}{\Phi(\eta)-\Phi(\rho)}\; d\eta d\rho\right\} d\zeta\ .
\end{aligned}$$

□

Note that the weak formulation comes from the symmetrization trick involved when computing the second momentum evolution of the cell density [209]. In fact this computation is contained in (7.15) replacing $\varphi$ with $\Phi$ (the second momentum of $n$ is precisely the $L^2-$norm of $\Phi$).

**Remark 7.5.** *We also observe that $\mathcal{J}[\Phi]$ is homogeneous in the following sense. Let $n_\varepsilon$ be the mass-preserving rescaling $\frac{1}{\varepsilon}n(\frac{x}{\varepsilon})$, and $\Phi_\varepsilon$ be the corresponding pseudo-inverse distribution function. Then we have $\Phi_\varepsilon = \varepsilon\Phi$ and $\mathcal{J}[\Phi_\varepsilon] = \mathcal{J}[\Phi]$. Facing the issue of defining $\mathcal{J}$ on a Dirac mass, we observe that it strongly depends on the "regularization" (what is expected after Velázquez' work [240, 87]). Therefore we heuristically find that the profile $n$ has to be somehow in the equilibrium shape in order to give sense to $\mathcal{J}[\Phi]$ after blow-up in the weak formulation* (7.15)*.*

### 7.3.2 The log HLS inequality adapted to NL diffusion

We now focus on the KS model with non-linear diffusion (7.6). We are to adapt the previous log HLS inequality to more general internal energies of the porous medium type. We again pay attention to make the equation for the equilibrium state appear. For this purpose we need some sharp inequality in place of the Jensen inequality crucially involved in section 7.3.1.

For convenience we only deal with a power diffusion: $f(u) = \kappa u^m,\ m > 1$. Recall that the entropy $U$ is defined by $U' = h$, where $h$ is the pressure function. We also denote $A(\omega) = \omega U(1/\omega)$. The free energy associated to our issue writes

$$\int U(n(x))\; dx + \iint n(x)\log|x-y|n(y)\; dxdy = \int A\Big(\Phi'\Big)\; d\rho + \iint \log\big|\Phi(\rho)-\Phi(\eta)\big|\; d\rho d\eta.$$

**Lemma 7.6** (A non-linear Jensen inequality)**.** *Let $\alpha, \beta$ be two positive real numbers. Then for all $p, q > 0$ we have*

$$\log(p+q) \geq -\frac{1}{\alpha+\beta}\left(\frac{A(p)}{f(1/\alpha)} + \frac{A(q)}{f(1/\beta)}\right) + C(\alpha,\beta), \tag{7.16}$$

*where equality occurs if, and only if,* $(p,q)=(\alpha,\beta)$. *This inequality is truly motivated by the equilibrium state equation. Finally let us remark that the inequality* (7.16) *degenerates into the Jensen inequality when* $m \to 1$.

*Sketch of proof of lemma 7.16.* This is a straightforward proof, and it will be proved later under more general assumptions. But let's do it at first glance for a better understanding.

First we have to do some algebra in order to rearrange the inequality in a more convenient shape. First we claim that $-A'(\omega) = f(1/\omega)$. To see this we use the relations between $f$, $U$ and $A$:

$$f(u) = uU' - U = u(uA(1/u))' - uA(1/u) = -A'(1/u).$$

Secondly we focus on the function

$$(p,q) \longmapsto \log(p+q) + \frac{1}{\alpha+\beta}\left(\frac{A(p)}{f(1/\alpha)} + \frac{A(q)}{f(1/\beta)}\right),$$

and look at its critical points. We differentiate and obtain the following system,

$$\frac{1}{p+q} - \frac{1}{\alpha+\beta}\frac{1}{p^2}\frac{A'(p)}{f(1/\alpha)} = 0\ ,$$
$$\frac{1}{p+q} - \frac{1}{\alpha+\beta}\frac{1}{q^2}\frac{A'(q)}{f(1/\beta)} = 0\ .$$

Therefore we obtain

$$\frac{1}{p+q} - \frac{1}{\alpha+\beta}\frac{f(1/p)}{f(1/\alpha)} = 0\ ,$$
$$\frac{1}{p+q} - \frac{1}{\alpha+\beta}\frac{f(1/q)}{f(1/\beta)} = 0\ .$$

Consequently we get the following key relation at the critical point:

$$\frac{f(1/p)}{f(1/\alpha)} = \frac{\alpha+\beta}{p+q} = \frac{f(1/q)}{f(1/\beta)}. \tag{7.17}$$

In the case of a porous medium diffusion, (7.17) rewrites

$$\left(\frac{p}{\alpha}\right)^m = \frac{\alpha\dfrac{p}{\alpha} + \beta\dfrac{q}{\beta}}{\alpha+\beta} = \left(\frac{q}{\beta}\right)^m.$$

Together with

$$\frac{p}{\alpha} \le \frac{\alpha\dfrac{p}{\alpha} + \beta\dfrac{q}{\beta}}{\alpha+\beta} \le \frac{q}{\beta},$$

this in turn implies $(p,q)=(\alpha,\beta)$ in the case $m>1$. □

**Remark 7.7.** *More general property of the non-linear diffusion* $f$ *should have been pointed out to ensure lemma 7.6. The elasticity of* $f$ *seems to be the right notion here actually, rather than homogeneity.*

The infinitesimal version of (7.16) to be used in the following reads

$$\log \int \phi \ge \frac{1}{\int \psi} \int \frac{-A(\phi)}{f(1/\psi)} + C(\psi).$$

**Proposition 7.8** (Log HLS inequality with "non-linear" internal energy)**.** *The free energy functional*

$$\mathcal{F}(n) = \int U(n) + \iint \log|x-y| n(x) n(y)\ dxdy\ ,$$

*is bounded from below if, and only if, there exists a solution to the corresponding stationary problem in* (7.6). *If so, the stationary states are exactly the minimizers and are unique up to some basic transformation (here any translation).*

*Proof.* The proof is absolutely similar to section 7.3.1, using lemma 7.6 instead of the weighted Jensen inequality.

$$\begin{aligned} 2\iint_{\eta\geq\rho} \log\Big(\Phi(\eta)-\Phi(\rho)\Big)\,d\eta\,d\rho &= 2\iint_{\eta\geq\rho} \log\left(\int_\eta^\rho \Phi'(\zeta)\,d\zeta\right) \\ &\geq 2\iint_{\eta\geq\rho}\int_{\zeta=\rho}^{\eta} \frac{-A\big(\Phi'(\zeta)\big)}{f\big(1/\psi(\zeta)\big)}\frac{1}{\int_\zeta w(\zeta)} + C(\psi) \\ &= \int_{\zeta=0}^1 -A\big(\Phi'(\zeta)\big)\times\left\{\frac{2}{f\big(1/\psi(\zeta)\big)}\int_{\rho=0}^{\zeta}\int_{\eta=\zeta}^1 \frac{1}{\Psi(\eta)-\Psi(\rho)}\right\} + C(\psi). \end{aligned}$$

If $\psi$ is a stationary state described by

$$\frac{2}{f\big(1/\psi(\zeta)\big)}\int_{\rho=0}^{\zeta}\int_{\eta=\zeta}^1 \frac{1}{\Psi(\eta)-\Psi(\rho)} \equiv 1\ ,$$

then we obtain a log HLS type inequality. Moreover we can describe the equality cases and this gives uniqueness. □

**Remark 7.9.** *This proposition does not prove any inequality* ab nihilo. *We claim that given some stationary state we deduce such an inequality, and uniqueness of the stationary state comes afterwards. We refer to [50] for some existence condition related to the original log HLS inequality (supercritical growth of the pressure function for large $u$).*

For the sake of completeness we give such an existence proof. The following proposition states the existence of a stationary solution to the system (7.6).

**Proposition 7.10** (A priori estimates for a porous medium diffusion: $f(u)=u^m,\ m>1$)**.** *Let $(n_i)$ be a minimizing sequence of probability densities with respect to $\mathcal{F}$. We have the following* a priori *estimates:*

**No Dirac mass:** $\int \Theta(n_i)\,dx \leq C$, *where $\Theta$ is positive and grows superlinearly at infinity.*

**Mass confinement:** $\displaystyle\int_{|x|\geq R} n_i(x)\,dx \leq \frac{C}{\log R}$.

*Proof.* We wish to transform the energy estimate

$$C \geq \frac{1}{m-1}\int n_i^m + \iint n_i(x)\log|x-y|n_i(y)\,dxdy,$$

into useful *a priori* estimates for the family $(n_i)$. We shall proceed in several steps, following [50] and [179].

- For all $i$ we have, using the classical log HLS inequality (theorem 7.1),

$$C \geq \int \frac{n_i^m}{m-1} - \int n_i\log n_i + C.$$

  The functional $\Theta(u)=\left(\frac{1}{m-1}u^m - u\log u\right)_+$ satisfies a superlinear growth. The remaining part has a sign and can be easily bounded because it is nonzero for $\{0<a\leq u\leq b\}$ only, which is of finite measure. As a consequence, $(n_i)$ is bounded in $L^m$.

- Using the $L^m$ estimate we are able to bound the short-range part of the interaction kernel:

$$\int_{|x-y|\leq 1}\Big|\log|x-y|\Big|n_i(y)\,dy \leq \left(\int_{|x-y|\leq 1}\Big|\log|x-y|\Big|^{m'}\right)^{1/m'}\left(\int n_i^m\right)^{1/m} \leq C\|n_i\|_{L^m}.$$

  Therefore

$$\iint_{|x-y|\leq 1}\Big|\log|x-y|\Big|n_i(y)n_i(x)\,dydx \leq C\|n_i\|_{L^m}.$$

- (Following [179, Th. 3.1]) Because of the Riesz's rearrangement inequality [168, 56] we can reduce to a minimizing sequence of symmetric functions: $n(-x) = n(x)$. For all $|x| \geq 1$ we have

$$\begin{aligned}\int_{|x-y|\geq 1} \log|x-y| n_i(y)\ dy &\geq \int_{\langle x,y\rangle \leq 0} \log|x-y| n_i(y)\ dy \\ &\geq \frac{1}{2}\log|x|.\end{aligned}$$

  Indeed $\langle x, y\rangle \leq 0$ implies $|x-y| \geq 1$, and on the other hand, half of the mass is contained on each half-space by symmetry. We then integrate against $n_i(x)$ over $|x| \geq R > 1$, and we obtain

$$\begin{aligned}\iint_{|x-y|\geq 1} \log|x-y| n_i(y) n_i(x)\ dxdy &\geq \iint_{|x-y|\geq 1,\ |x|\geq R} \log|x-y| n_i(y) n_i(x)\ dxdy \\ &\geq \frac{\log R}{2}\int_{|x|\geq R} n_i(x)\ dx.\end{aligned}$$

□

Combining propositions 7.8 and 7.10 we deduce the following theorem

**Theorem 7.11.** *For a power diffusion with superlinear growth at infinity ($f(u) = u^m$) there exists a unique stationary state to the system* (7.6)*, which is the minimizer of $\mathcal{F}$.*

### 7.3.3 The rescaled problem for subcritical parameter

We first recall the rescaled KS equation and the corresponding free energy,

$$-\frac{\partial \Phi}{\partial t} = \frac{\partial}{\partial \rho}\left(\left(\frac{\partial \Phi}{\partial \rho}\right)^{-1}\right) + \chi\Omega[\Phi] + \Phi. \tag{7.18}$$

$$\mathcal{G} = -\int \log \Phi' + \frac{1}{2}\int |\Phi|^2 + \frac{\chi}{2\pi}\iint \log\left|\Phi(\eta) - \Phi(\rho)\right| d\rho d\eta. \tag{7.19}$$

**Doubling the variables.** In this section we recall the following assumption,

$$\int \Phi = 0,$$

from which we claim that

$$\int |\Phi|^2 = \frac{1}{2}\iint |\Phi(\eta) - \Phi(\rho)|^2 d\rho d\eta.$$

**Theorem 7.12** (Rescaled variables)**.** *Assume $\chi < 2\pi$. Then the KS system with rescaled variables admits a unique stationary state which is the unique minimizer of the associated free energy.*

*Proof.* We proceed as in section 7.3.2, that is we distinguish clearly between existence (nothing is new, note the assumption $\chi < 2\pi$ is crucial) and uniqueness (need for a factorization method). For existence we claim that proposition 7.10 remains true for the rescaled problem, even if the diffusion is now linear. In fact we can avoid loss of mass at infinity thanks to the additional drift term in the free energy (see [35, 33]).

For uniqueness we need a discrete lemma, analogous to lemmas 7.2 and 7.6.

**Lemma 7.13.** *Let $\alpha, \beta$ be two positive real numbers. Then for all $p, q > 0$ we have*

$$\frac{\chi}{2\pi}\log(p+q) + \frac{1}{4}(p+q)^2 \geq \left(\frac{\chi/2\pi}{\alpha+\beta} + \frac{1}{2}(\alpha+\beta)\right)\left(\alpha\log p + \beta\log q\right) + C(\alpha,\beta). \tag{7.20}$$

*proof of lemma 7.13.* We differentiate as usual (7.20) with respect to $(p, q)$ and try to identify the critical points. Uniqueness of those critical points is crucial here. We obtain the following nonlinear but symmetric system,

$$\frac{1}{2}(p+q) + \frac{\chi}{2\pi(p+q)} - \Big(\frac{\chi}{2\pi(\alpha+\beta)} + \frac{1}{2}(\alpha+\beta)\Big)\frac{\alpha}{p} = 0 \ ,$$
$$\frac{1}{2}(p+q) + \frac{\chi}{2\pi(p+q)} - \Big(\frac{\chi}{2\pi(\alpha+\beta)} + \frac{1}{2}(\alpha+\beta)\Big)\frac{\beta}{q} = 0 \ .$$

Necessarily we have $\frac{p}{\alpha} = \frac{q}{\beta}$. Therefore we get

$$\frac{1}{2}\Big(\frac{\beta}{\alpha}+1\Big)p + \frac{\chi}{2\pi\Big(\frac{\beta}{\alpha}+1\Big)p} = \frac{\chi}{2\pi\Big(\frac{\beta}{\alpha}+1\Big)p} + \frac{1}{2}\Big(1+\frac{\beta}{\alpha}\Big)\frac{\alpha^2}{p},$$

from which we deduce $p^2 = \alpha^2$.

□

The infinitesimal version of (7.20) to be used in the sequel writes

$$\frac{\chi}{2\pi}\log\int\phi + \frac{1}{4}\int|\phi|^2 \geq \Big(\frac{\chi}{2\pi\int\psi} + \frac{1}{2}\int\psi\Big)\Big(\int(\log\phi)\psi\Big) + C(\psi).$$

We shall now apply this sharp inequality to bound the free energy from below:

$$\begin{aligned}
&\frac{2\chi}{2\pi}\iint_{\eta\geq\rho}\log\Big(\Phi(\eta)-\Phi(\rho)\Big) + \frac{1}{4}\Big(\Phi(\eta)-\Phi(\rho)\Big)^2\,d\eta d\rho \\
&\quad\geq 2\iint_{\eta\geq\rho}\left(\frac{\chi}{2\pi\int\psi} + \frac{1}{2}\int\psi\right)\int_\rho^\eta\Big(\log\Phi'(\zeta)\Big)\psi(\zeta)\,d\zeta + C(\psi) \\
&\quad\geq \int_{\zeta=0}^1\Big(\log\Phi'\Big)\left\{2\psi(\zeta)\int_0^\zeta\int_\zeta^1\frac{\chi/2\pi}{\Psi(\eta)-\Psi(\rho)} + \frac{1}{2}\big(\Psi(\eta)-\Psi(\rho)\big)\right\} + C(\psi), \\
&\quad\geq \int_{\zeta=0}^1\Big(\log\Phi'\Big)\mathcal{J}[\Psi](\zeta)d\zeta + C(\psi).
\end{aligned}$$

To conclude the proof it remains to recognize the equation for the stationary solution in the new variables $\mathcal{J}[\Psi]\equiv 1$. We can transform it by integration in the following steps,

$$\begin{aligned}
&\left(\frac{1}{\Psi'}\right)' + \chi\Omega[\Psi] + \Psi = 0, \\
&\frac{1}{\Psi'} + 2\int_0^\zeta\int_\zeta^1\frac{\chi/2\pi}{\Psi(\rho)-\Psi(\eta)}\,d\rho d\eta + \int_0^\zeta\Psi(\rho)\,d\eta =, 0 \\
&2\psi\left(\int_0^\zeta\int_\zeta^1\frac{\chi/2\pi}{\Psi(\eta)-\Psi(\rho)}\,d\rho d\eta + \frac{1}{2}\int_0^\zeta\int_\zeta^1\big(\Psi(\eta)-\Psi(\rho)\big)d\rho\,d\eta\right) = 1.
\end{aligned}$$

In fact we have the following identity (related to the doubling of variables made above),

$$\int_0^\zeta\int_\zeta^1\big(\Psi(\eta)-\Psi(\rho)\big)d\eta d\rho = \zeta\int_\zeta^1\Psi(\eta)d\eta - (1-\zeta)\int_0^\zeta\Psi(\rho)d\rho = -\int_0^\zeta\Psi(\rho)\,d\rho \ ,$$

thanks to $\int\Psi = 0$. □

## 7.4 Trend to equilibrium

### 7.4.1 The linear "degenerate" case

We presumably have the tools to tackle the computation of the 2-Wasserstein distance between two solutions of the 1D Keller-Segel model [59]. We denote these two solutions by $n(t,x)$ and $\underline{n}(t,x)$ (we think of $\underline{n}(t,x)=\underline{n}(x)$ as being a stationary state). We denote also by $\Phi$ and $\Psi$ the respective pseudo–inverse distribution functions. Because we are in a one-dimensional setting, the expression of this distance is particularly tractable [244],

$$d_W[n,\underline{n}]^2=\int_0^1\Big(\Phi(\rho)-\Psi(\rho)\Big)^2d\rho.$$

We formally compute the time derivative of $d_W[n,\underline{n}]$:

$$\begin{aligned}
-\frac{d}{dt}\frac{1}{2}\int_0^1\Big(\Phi(\rho)-\Psi(\rho)\Big)^2 &= \int_0^1\Big(\Phi(\rho)-\Psi(\rho)\Big)\Big(-\frac{\partial\Phi}{\partial t}+\frac{\partial\Psi}{\partial t}\Big)\\
&= \int_0^1(\Phi-\Psi)\left[\frac{\partial}{\partial\rho}\Big(\Big(\frac{\partial\Phi}{\partial\rho}\Big)^{-1}\Big)-\frac{\partial}{\partial\rho}\Big(\Big(\frac{\partial\Psi}{\partial\rho}\Big)^{-1}\Big)+\chi\Omega\Phi(\rho)-\chi\Omega\Psi(\rho)\right]\\
&= -\int_0^1\Big(\partial_\rho\Phi-\partial_\rho\Psi\Big)\Big(\frac{1}{\partial_\rho\Phi}-\frac{1}{\partial_\rho\Psi}\Big)+\chi\int_0^1\Big(\Phi-\Psi\Big)\Big(\Omega[\Phi](\rho)-\Omega[\Psi](\rho)\Big).
\end{aligned}$$

We artificially double the variables (see 1D granular flows' models for details [166, 61]) and we introduce the notation $H=\Phi(\eta)-\Phi(\rho)$, $K=\Psi(\eta)-\Psi(\rho)$. We eventually obtain

$$\int_0^1\Big(\Phi-\Psi\Big)\Big(\Omega[\Phi](\rho)-\Omega[\Psi](\rho)\Big)=\frac{1}{2\pi}\iint\Big(H-K\Big)\Big(\frac{1}{H}-\frac{1}{K}\Big)\,d\rho d\eta.$$

At this stage we can state the following intermediate proposition.

**Proposition 7.14.** *Let $n,\underline{n}$ be two solutions of the Keller–Segel system in 1D. Then we have formally*

$$\frac{d}{dt}\frac{1}{2}d_W[n,\underline{n}]^2=\int_0^1\Gamma[\partial_\rho\Phi,\partial_\rho\Psi]-\frac{\chi}{2\pi}\iint\Gamma[H,K],\tag{7.21}$$

*the function $\Gamma$ being $\Gamma(x,y)=(x-y)(1/x-1/y)\le 0$.*

We recognize in proposition 7.14 the balance between the diffusion (cells' spread) and the chemotactic contribution (cell-to-cell attraction) usualy established in this sort of models. The challenge of the KS estimations [147, 86] is to compare the relative influence of each. The function $\Gamma$ is not concave whereas it is concave in each variable. It is an homogeneous function, thus it can be written as $\Gamma(x,y)=\gamma(x/y)$, where $\gamma(\lambda)=2-\lambda-1/\lambda$ is concave and non-positive.

Then we perform in (7.21) the change of variables $q=\Psi(\eta),\ p=\Psi(\rho)$,

$$\begin{aligned}
\iint d\rho\ d\eta\ \gamma\Big(\frac{H}{K}\Big) &= 2\iint_{\eta\ge\rho}(\partial_\rho\Psi)^{-1}dp\ (\partial_\rho\Psi)^{-1}dq\ \gamma\Big(\frac{\Phi\Psi^{-1}q-\Phi\Psi^{-1}p}{q-p}\Big)\\
&= 2\iint(\partial_\rho\Psi)^{-1}dp\ (\partial_\rho\Psi)^{-1}dq\ \gamma\left(\int_{s=p}^q\partial_p(\Phi\Psi^{-1})(s)\frac{ds}{q-p}\right)\\
&\ge 2\iint(\partial_\rho\Psi)^{-1}dp\ (\partial_\rho\Phi)^{-1}dq\ \int_{s=p}^q\gamma\Big(\partial_p(\Phi\Psi^{-1})(s)\Big)\frac{ds}{q-p}\quad\text{by Jensen}\\
&= 2\iint d\rho\ d\eta\ \int_{\zeta=\rho}^\eta\gamma\Big(\frac{\partial_\rho\Phi}{\partial_\rho\Psi}\Big)(\zeta)\frac{\partial_\rho\Psi(\zeta)\ d\zeta}{\Psi(\eta)-\Psi(\rho)}\\
&= \int_{\zeta=0}^1 d\zeta\ \gamma\Big(\frac{\partial_\rho\Phi}{\partial_\rho\Psi}\Big)(\zeta)\left\{2\partial_\rho\Psi(\zeta)\int_0^\zeta d\rho\int_\zeta^1 d\eta\frac{1}{\Psi(\eta)-\Psi(\rho)}\right\}.
\end{aligned}$$

We recognize in the right-hand-side the stationary characterization that we have already encountered in section 7.3.1:

$$\frac{d}{dt}\frac{1}{2}d_W[n,\underline{n}]^2 \leq \int_0^1 \Gamma[\partial_\rho\Phi,\partial_\rho\Psi] - \frac{\chi}{2\pi}\int_{\zeta=0}^1 \Gamma[\partial_\rho\Phi,\partial_\rho\Psi](\zeta)\ \mathcal{J}[\Psi](\zeta)\ d\zeta\ .$$

As we know, such a $\Psi$ solving $\mathcal{J}[\Psi]\equiv 1$ exists for the critical parameter $\chi = 2\pi$. We deduce $\frac{d}{dt}d_W \leq 0$, and we keep in mind that we are able to describe the equality cases.

**Remark 7.15.** *This situation (linear diffusion without rescaling) is degenerate in the following sense: an equilibrium exists only for the critical parameter $\chi = 2\pi$. Therefore we can simplify the above expression involving a stationary state $\mathcal{J}[\Psi]\equiv 1$ only if $\chi = 2\pi$. In this case however all the possible equilibria $\underline{n}$ – except maybe the Dirac mass – have an infinite second momentum, that is their inverse distribution functions do not lie in $L^2$. So the Wasserstein distance $d_W[n,\underline{n}]$ does make sense only if $n$ has itself an infinite second momentum, being somehow close to some equilibrium $\underline{n}$ 'at infinity'. This has to be related to recent work of Biler et al. [31] where the authors observe that the equilibria have basins of attraction made of solutions having infinite second momentum.*

### 7.4.2 The nonlinear diffusion case

Although the previous result is somehow meaningless (see remark 7.15), it really helps to generalize, taking into account the nonlinear diffusion case for instance (and below the rescaled problem).

We still consider only porous medium diffusion law: $f(u) = u^m,\ m > 1$. Keeping the same notations as above, the evolution of the Wasserstein distance reads as following,

$$\begin{aligned}\frac{d}{dt}\frac{1}{2}d_W^2 &= \int(\Phi'-\Psi')\Big(f\Big(\frac{1}{\Phi'}\Big)-f\Big(\frac{1}{\Psi'}\Big)\Big) - 2\pi\int_0^1\Big(\Phi-\Psi\Big)\Big(\Omega[\Phi](\rho)-\Omega[\Psi](\rho)\Big)\\ &= \int\Gamma_m[\Phi',\Psi'] - \iint\Gamma[H,K]\ d\rho\ d\eta,\end{aligned}$$

the new functional $\Gamma_m$ being $(1-m)-$homogeneous:

$$\Gamma_m(x,y) = \frac{1}{y^{m-1}}\gamma_m\Big(\frac{x}{y}\Big),\quad \gamma_m(\lambda) = (\lambda-1)(\lambda^{-m}-1).$$

On the one hand we re-arrange the second term in the right-hand side as previously, namely

$$\begin{aligned}\iint\Gamma[H,K]\ d\rho\ d\eta &\geq \int_{\zeta=0}^1 d\zeta\ \gamma\Big(\frac{\partial_\rho\Phi}{\partial_\rho\Psi}\Big)(\zeta)\ 2\partial_\rho\Psi(\zeta)\int_0^\zeta d\rho\int_\zeta^1 d\eta\frac{1}{\Psi(\eta)-\Psi(\rho)}\\ &= \int_{\zeta=0}^1 d\zeta\ \frac{1}{(\Psi')^{m-1}}\gamma\Big(\frac{\Phi'}{\Psi'}\Big)(\zeta)\ \left\{2(\Psi')^m(\zeta)\int_0^\zeta d\rho\int_\zeta^1 d\eta\frac{1}{\Psi(\eta)-\Psi(\rho)}\right\}.\end{aligned}$$

On the other hand we observe that $\gamma_m(\lambda)\leq\gamma(\lambda)$, with equality at $\lambda = 1$. Subsequently we have

$$\frac{d}{dt}d_W^2[n,\underline{n}] \leq 0,$$

whenever $\underline{n}$ is the stationary state, satisfying the characterization

$$2(\Psi')^m(\zeta)\int_0^\zeta d\rho\int_\zeta^1 d\eta\frac{1}{\Psi(\eta)-\Psi(\rho)} \equiv 1\ .$$

**Remark 7.16.** *It looks like this is another proof of the equilibrium uniqueness, because the dissipation of entropy is strictly negative unless $n$ is equal to $\underline{n}$ (up to translation). In fact we could start from another equilibrium state as initial condition, and prove that necessarily they are equal.*

### 7.4.3 The linear diffusion problem in rescaled variables

We proceed as in the original case, with an additional term due to the drift, and obtain formally

$$\frac{d}{dt}\frac{1}{2}d_W[n,m]^2 = \int_0^1 d\rho\ \Gamma[\partial_\rho\Phi,\partial_\rho\Psi] - \frac{\chi}{2\pi}\iint d\rho\ d\eta\ \Gamma[H,K] - \int|\Psi-\Phi|^2. \tag{7.22}$$

**Proposition 7.17.** *In the rescaled variables, the 1D Keller-Segel system converges to the unique steady state with exponential rate in Wasserstein distance.*

*Proof.* We make the equilibrium appear (7.22). This has already been partly done in section 7.4.1.

$$\begin{aligned}\iint d\rho\ d\eta\ \gamma\Big(\frac{H}{K}\Big) &\geq \int_{\zeta=0}^1 d\zeta\ \gamma\Big(\frac{\partial_\rho\Phi}{\partial_\rho\Psi}\Big)(\zeta)\left\{2\partial_\rho\Psi(\zeta)\int_0^\zeta d\rho\int_\zeta^1 d\eta\frac{1}{\Psi(\eta)-\Psi(\rho)}\right\}\\ &\geq \int_{\zeta=0}^1 d\zeta\ \gamma\Big(\frac{\partial_\rho\Phi}{\partial_\rho\Psi}\Big)(\zeta)\ \partial_\rho\Psi(\zeta)\left\{2\int_0^\zeta d\rho\int_\zeta^1 d\eta\frac{1}{\Psi(\eta)-\Psi(\rho)} - \int_0^\zeta\Psi(\rho)d\rho\right\},\end{aligned}$$

where we justify the last inequality arguing that $\int_0^\zeta\Psi$ and $\gamma$ are both nonpositive, and $\partial_\rho\Psi$ is nonnegative. To see the former, just observe that the map $\zeta\mapsto\int_0^\zeta\Psi$ is convex, being 0 at $\zeta=0$ and $\zeta=1$ (because the center of mass is assumed to be 0). Therefore we obtain

$$\frac{d}{dt}\frac{1}{2}d_W[n,m]^2 \leq \int_{\zeta=0}^1 d\zeta\ \gamma\Big(\frac{\partial_\rho\Phi}{\partial_\rho\Psi}\Big)(\zeta) - \int_{\zeta=0}^1 d\zeta\ \gamma\Big(\frac{\partial_\rho\Phi}{\partial_\rho\Psi}\Big)(\zeta)\mathcal{J}[\Psi](\zeta) - \int|\Psi-\Phi|^2.$$

If we set $\Psi$ being the stationary state, then we immediately obtain exponential trend to equilibrium because $\mathcal{J}[\Psi]\equiv 1$:

$$d_W[n,\underline{n}]\leq Ce^{-t}.$$

□

**Numerics.** We have transcripted those 'continuous' computations down to a discrete setting for numerical purpose (see chapter 8 and [33]).

## 7.5 Formal extension to more general functionals

In this section we shall extend previous methods formally to a wider class of free energy functionals (8.12). We will focus on homogeneity cases for the sake of simplicity. We assume basically the following:

- the confinement potential is convex (if quadratic, $|x|^2/2$ say, it gives a good convergence rate, but it is not required here),
- diffusion and interaction's homogeneities (elasticity would be the right notion by the way) are comparable in a sense we will give later on.

We first recall the free energy in the transport variables,

$$\mathcal{G}(\Phi) = \int A(\Phi') + \int V(\Phi)\ d\rho + \iint W\big(\Phi(\rho)-\Phi(\eta)\big)\ d\rho d\eta.$$

### 7.5.1 Uniqueness of the ground state

McCann's proof of minimizer uniqueness is based on the notion of displacement convexity. To summarize, a new way of interpolating between two probability measures is introduced in [179], for which the functional (8.12) is convex along the interpolation trajectories under suitable assumptions (among which the convexity of $W$). It is worth noticing that displacement convexity is strongly related to optimal

transportation of measures, which is also the underlying concept here (even if it does not clearly come out because we restrict ourselves to the one dimensional case).

We will first prove uniqueness of a minimizer for (8.12) under weaker assumptions than convexity. Roughly speaking, McCann proved that each term of the free energy is displacement convex, ensuring that the whole functional is displacement convex. In our setting however we will balance the contributions of each term (as it is in the chemotaxis aggregation model), using the equilibrium itself. The principle is the following: as soon as there exists an equilibrium, it is unique under competing assumptions. As far as we know, the only previous combination of opposite trends between diffusion and interaction has been investigated in [60].

**Theorem 7.18.** *Assume no confinement potential ($V \equiv 0$), and that the other contributions are homogeneous, namely $f(u) = u^m$, with $m > 0$, and $W(\xi) = |\xi|^k/k$, with $-1 \le k \le 1$ (and $W(\xi) = \log|\xi|$ if $k = 0$). If $m + k > 1$ the free energy is bounded from below as soon as some stationary state do exist.*

*Sketch of proof.* First we have to identify the equation characterizing the equilibrium state. One possible expression is

$$f\Big(\frac{1}{\Phi'}\Big) \equiv 2\int^{\zeta}\int_{\zeta} W'(\Phi(\eta) - \Phi(\rho))\, d\rho d\eta.$$

The second step consists of associating it with a key inequality. Here this inequality reads

$$W\Big(\int \phi\Big) \ge W'\Big(\int \psi\Big)\int -\frac{A(\phi)}{f(1/\psi)} + C(\psi). \tag{7.23}$$

In a discrete setting, inequality (7.23) becomes

$$W(p+q) \ge W'(\alpha+\beta)\Big(\frac{-A(p)}{f(1/\alpha)} + \frac{-A(q)}{f(1/\beta)}\Big) + C(\alpha,\beta),$$

where equality arises if, and only if $(p,q) = (\alpha,\beta)$. For this purpose derive with respect to $p$ and $q$, and obtain the following system of equations for the critical points,

$$\begin{cases} W'(p+q) = W'(\alpha+\beta)\dfrac{f(1/p)}{f(1/\alpha)}\ , \\ W'(p+q) = W'(\alpha+\beta)\dfrac{f(1/q)}{f(1/\beta)}\ . \end{cases}$$

This yields

$$\frac{f(1/p)}{f(1/\alpha)} = \frac{W'(p+q)}{W'(\alpha+\beta)} = \frac{f(1/q)}{f(1/\beta)}.$$

Therefore, assuming $f(u) = u^m$ and $W(\xi) = |\xi|^k$ we have

$$\left(\frac{p}{\alpha}\right)^{m/(1-k)} = \frac{p+q}{\alpha+\beta} = \left(\frac{q}{\beta}\right)^{m/(1-k)}.$$

If $k > 1$, then the interacting contribution to the energy is convex and McCann's theorem applies, so we ignore it. Otherwise $m + k > 1$ enhances $\dfrac{m}{1-k} > 1$ and necessarily $(p,q) = (\alpha,\beta)$. □

### 7.5.2 Trend to equilibrium

In addition to the ground state uniqueness, we prove in the following convergence towards this equilibrium in the so-called gradient flow equation. As a matter of fact, the link between the evolution equation

$$\frac{\partial n}{\partial t} = \frac{\partial}{\partial x}\left(n\frac{\partial h(n)}{\partial x} + nV'(x) + 2nW' * n\right)\ , \tag{7.24}$$

and the free energy functional (8.12) has been pointed out by Otto [200]. The former can be viewed as the gradient flow equation of the energy under the Wasserstein induced metric where constant speed geodesic are the trajectories of McCann's interpolation [244, 7].

**Remark 7.19.** *Another motivation for this work can be enlightened by this point of view. Geodesics in Otto's interpretation are given by* $\rho^0 \xrightarrow{\lambda} \rho^1$ *:*

$$\rho^\lambda = \Big((1-\lambda)Id + \lambda\nabla\varphi\Big)\#\rho^0,$$

*where* $T = \nabla\varphi$ *is the optimal static transport map pushing* $\rho^0$ *onto* $\rho^1$*. Therefore, in the transport variables, geodesics are in fact straight lines, because the metric structure becomes euclidean.*

In the transport variables, (7.24) reads

$$-\frac{\partial\Phi}{\partial t} = \left(f\Big(\frac{1}{\Phi'}\Big)\right)' + V'(\Phi) + 2\Omega[\Phi], \tag{7.25}$$

where the interaction term $\Omega$ is defined as

$$\Omega[\Phi] = \int W'\Big(\Phi(\rho) - \Phi(\eta)\Big)\, d\eta.$$

We formally compute the evolution of the Wasserstein distance $d_W = \|\Phi - \Psi\|_{L^2(0,1)}$ between two solutions of (7.25).

$$\frac{d}{dt}\frac{1}{2}d_W^2 = \int(\Phi'-\Psi')\left(f\Big(\frac{1}{\Phi'}\Big) - f\Big(\frac{1}{\Psi'}\Big)\right) - \int(\Phi-\Psi)\Big(V'(\Phi)-V'(\Psi)\Big) - 2\int_0^1 \Big(\Phi-\Psi\Big)\Big(\Omega[\Phi]-\Omega[\Psi]\Big). \tag{7.26}$$

**Remark 7.20** (The drift term)**.** *The previous computation* (7.26) *clearly motivates the convexity assumption imposed to the confinement potential* $V$*. Indeed ensuring* $V'$ *being nondecreasing makes things easier. Furthermore, the case where* $V = \frac{1}{2}|x|^2$ *(and analogs) leads to a coercive inequality*

$$\int(\Phi-\Psi)\Big(V'(\Phi)-V'(\Psi)\Big) \geq d_W^2,$$

*which is even better and eventually enhances an exponential trend to equilibrium.*

We double the variables in the interaction term and obtain

$$\Gamma[H,K] = \iint(H-K)\Big(W'(H)-W'(K)\Big) = 2\int(\Phi-\Psi)\Big(\Omega[\Phi]-\Omega[\Psi]\Big),$$

provided that $W'$ is an odd function.

**Remark 7.21** (The interaction term)**.** *If we assume that* $W$ *is convex then we thoroughly have* $\Gamma[H,K] \geq 0$ *and consequently*

$$\frac{d}{dt}\frac{1}{2}d_W^2 \leq \int(\Phi'-\Psi')\left(f\Big(\frac{1}{\Phi'}\Big) - f\Big(\frac{1}{\Psi'}\Big)\right).$$

*Since* $f$ *is traditionnally assumed to be nondecreasing in the 1D case [179] then we immediately gain the contraction in Wasserstein distance. The case where* $W$ *is concave is more interesting because we loose the contraction principle. However we have to balance the competing contributions of opposite signs coming from diffusion and interaction (see above and below).*

**Theorem 7.22.** *Suppose* $f$ *and* $W$ *are homogeneous functions of respective degrees* $m$ *and* $k$*, and* $V = 0$*. If* $m+k > 1$ *then solutions to the evolution equation* (7.25) *converge to the unique stationary state in* $L^2$*.*

*Sketch of proof.* We proceed as in section 7.4.2:

$$\frac{d}{dt}\frac{1}{2}d_W^2 = \int\Gamma_m[\Phi',\Psi'] - \iint\Gamma_{1-k}[H,K]\, d\rho\, d\eta\ .$$

Recall that the functional $\Gamma_{1-k}$ is $k-$homogeneous:

$$\Gamma_{1-k}(x,y) = y^k \gamma_{1-k}\Big(\frac{x}{y}\Big), \quad \gamma_{1-k}(\lambda) = (\lambda-1)(\lambda^{k-1}-1).$$

The function $\gamma_{1-k}$ is concave providing that $0 \leq k \leq 1$ (as a sum of concave functions). Therefore we have, using the Jensen inequality,

$$\begin{aligned}\frac{d}{dt}\frac{1}{2}d_W^2 &\leq \int_0^1 \frac{1}{(\Psi')^{m-1}}\gamma_m\Big(\frac{\Phi'}{\Psi'}\Big) - \int_{\zeta=0}^1 \frac{1}{(\Psi')^{m-1}}\gamma_{1-k}\Big(\frac{\Phi'}{\Psi'}\Big)(\zeta)\ \left\{2(\Psi')^m \int_0^\zeta \int_\zeta^1 W'\big(\Psi(\eta)-\Psi(\rho)\big)\right\} \\ &\leq \int_0^1 \frac{1}{(\Psi')^{m-1}}\gamma_m\Big(\frac{\Phi'}{\Psi'}\Big) - \int_{\zeta=0}^1 \frac{1}{(\Psi')^{m-1}}\gamma_{1-k}\Big(\frac{\Phi'}{\Psi'}\Big)(\zeta)\ \mathcal{J}[\Psi](\zeta)\ d\zeta\ .\end{aligned}$$

On the other hand we recall that the family of functions $(\gamma_i)$ is ordered, so that $\gamma_m(\lambda) \leq \gamma_{1-k}(\lambda)$, with equality at $\lambda = 1$, thanks to the hypothesis $m + k > 1$. We are exactly in a similar shape as in section 7.4.2. □

As we already mentioned, we should prove independently the existence of such a minimizer. For instance we simply give an intuitive way to see that the condition $m + k > 1$ ensures that the free energy is bounded from below (this is a preliminary step towards a minimizer existence). Under the action of mass-preserving dilations: $u_\lambda(z) = \lambda u(\lambda z)$, the energy functional behaves like

$$\mathcal{F}(u_\lambda) = \frac{\lambda^{m-1}}{m-1}\int u(x)^m\ dx + \lambda^{-k}\iint u(x)|x-y|^k u(y)\ dxdy\ ,$$

If $m > 1$ the energy functional (7.1) is clearly nonnegative. If $0 < m < 1$ we see that it is bounded from below as $\lambda \to 0$ provided that $k > 1 - m$.

# Chapitre 8

# Un schéma numérique qui "minimise le mouvement"

Ce travail, fruit d'une collaboration avec Adrien Blanchet et José Carrillo, est la réalisation numérique de l'interprétation 'flot gradient généralisé' de Keller-Segel. Nous montrons la consistance du schéma qui minimise le mouvement [148] pour KS. Ceci fait appel aux estimations *a priori* usuelles. Nous adaptons également les idées nouvelles du chapitre 7 au schéma discret 1D, afin de démontrer la convergence vers un unique équilibre à vitesse exponentielle. L'annexe B (paragraphe B.3) montre le volet 'existence' de cet équilibre discret et vient ainsi compléter la proposition 8.15 de ce chapitre. Cet article a été soumis à publication sous le titre *Convergence of the mass-transport steepest descent scheme for the sub-critical Patlak-Keller-Segel model.*

## 8.1 Introduction

The Patlak-Keller-Segel (PKS) equation is widely used in mathematical biology to model the collective motion of cells which are attracted by a self-emitted chemical substance, being the slime mold amoebae *Dictyostelium discoideum* a prototype organism for this behaviour. Moreover, the PKS equation has become a paradigmatic mathematical problem since it shows a concentration-collapse dichotomy: for masses larger than a critical value solutions aggregate their mass, as Delta Diracs, in finite time while solutions exist globally and disperse collapsing down to zero below this critical mass threshold. This coexistence of phenomena in this simple-looking mathematical model makes appealing and difficult to develop numerical schemes capable of dealing with both situations.

Historically, the first mathematical models in chemotaxis were introduced in 1953 by C. S. Patlak in [206] and E. F. Keller and L. A. Segel in [152] in 1970. Here, we focus on the modified Patlak-Keller-Segel system for the log interaction kernel introduced by B. Perthame, the second author and M. Sharifi tabar in [55]

$$\begin{cases} \dfrac{\partial n}{\partial t}(t,x) = \Delta n(t,x) - \chi \nabla \cdot [n(t,x) \nabla c(t,x)] & t>0\,,\ x \in \mathbb{R}^d\,, \\ c(t,x) = -\dfrac{1}{d\pi} \displaystyle\int_{\mathbb{R}^d} \log|x-y|\, n(t,y)\, \mathrm{d}y\,, & t>0\,,\ x \in \mathbb{R}^d\,, \\ n(0,x) = n_0 \geq 0 & x \in \mathbb{R}^d\,. \end{cases} \tag{8.1}$$

Here $(t,x) \mapsto n(t,x)$ represents the cell density, and $(t,x) \mapsto c(t,x)$ is the concentration of chemo-attractant. The constant $\chi > 0$ is the *sensitivity* of the bacteria to the chemo-attractant. Mathematically,

it measures the interaction force between cells, and hence, the strength of the non-linear coupling. Note that, only in dimension 2, the logarithmic kernel is the Poisson kernel and the system (8.1) corresponds to the variant of the Patlak-Keller-Segel model in the simplified version introduced by W. Jäger and S. Luckhaus in [147]. In other dimension the log kernel has no physical interpretation. However, as we will see below, this is a good "toy model" to study the competition blow-up phenomenon *versus* global existence. Initial data are assumed to verify

$$(1+|x|^2)\, n_0 \in L^1_+(\mathbb{R}^d) \quad \text{and} \quad n_0 \log n_0 \in L^1(\mathbb{R}^d)\,. \tag{8.2}$$

The solutions satisfy the formal conservation of the total mass of the system

$$\int_{\mathbb{R}^d} n_0(x)\,\mathrm{d}x = \int_{\mathbb{R}^d} n(t,x)\,\mathrm{d}x.$$

Without loss of generality we assume that the total mass is 1, such that all the parameters of the system are contained in the reduced parameter $\chi$. The centre of mass is also conserved as time evolves, and thus, we fix it to be zero for the sake of simplicity,

$$\int_{\mathbb{R}^d} x\, n(t,x)\,\mathrm{d}x = \int_{\mathbb{R}^d} x\, n_0(x)\,\mathrm{d}x = 0.$$

We first remind that a notion of weak solution $n$ in the space $C^0\big([0,T);L^1_{\text{weak}}(\mathbb{R}^d)\big)$, with fixed $T>0$, using the symmetry in $x$, $y$ for the concentration gradient, was introduced in [222] able to handle measure solutions, see also [212] for an alternative theory. We shall say that $n$ is a weak solution to the system (8.1) if for all test functions $\zeta \in \mathcal{D}(\mathbb{R}^d)$,

$$\begin{aligned}\frac{\mathrm{d}}{\mathrm{dt}}\int_{\mathbb{R}^d}\zeta(x)\,n(t,x)\,\mathrm{d}x = \int_{\mathbb{R}^d}\Delta\zeta(x)\,n(t,x)\,\mathrm{d}x \\ - \frac{\chi}{2\,d\,\pi}\iint_{\mathbb{R}^d\times\mathbb{R}^d}[\nabla\zeta(x)-\nabla\zeta(y)]\cdot\frac{x-y}{|x-y|^2}\,n(t,s)\,n(t,y)\,\mathrm{d}x\,\mathrm{d}y\end{aligned} \tag{8.3}$$

together with $n(t=0)=n_0$ in the distributional sense in $(0,T)$.

As proved in [46, 35, 55], this problem presents the following dichotomy: either solutions blow-up in finite time for the super-critical case $\chi > 2d^2\pi$ or rather solutions exist globally in time and spread in space decaying towards a stationary solution in rescaled variables as $t\to\infty$ in the sub-critical case $\chi < 2d^2\pi$.

Global improved weak solutions have been constructed for the system (8.1) in the sub-critical case, $\chi<2d^2\pi$, for $d=2$ [86, 35] and $d\neq 2$ in [55]; and in the critical case for $d=2$ in [34]. Very recently, in [87], J. Dolbeault and C. Schmeiser investigate the super-critical case in dimension 2. Accordingly, the regularisation of the logarithmic kernel produces a defect measure when passing to the limit, accounting for a blow-up phenomenon. In the sub-critical case, the proof of global existence of the improved weak solutions relies on the decreasing character of a free energy functional for the PKS equation given by:

$$t \mapsto \mathcal{F}[n](t) := \mathcal{S}[n](t) + \mathcal{W}[n](t) \tag{8.4}$$

where $\mathcal{S}[n]$ is the standard Boltzmann's entropy and $\mathcal{W}[n]$ is the interaction energy defined by

$$\mathcal{S}[n](t) := \int_{\mathbb{R}^d} n(t,x)\log n(t,x)\,\mathrm{d}x \quad \text{and} \quad \mathcal{W}[n](t) := \frac{\chi}{2d\pi}\iint_{\mathbb{R}^d} n(t,x)\,n(t,y)\,\log|x-y|\,\mathrm{d}x\,\mathrm{d}y.$$

The free energy $\mathcal{F}[n]$ is related to its time derivative, the corresponding Fisher information, in the following way: consider a non-negative solution $n\in\mathcal{C}^0([0,T),L^1(\mathbb{R}^d))$ of the Patlak-Keller-Segel system (8.1) such that $n(1+|x|^2)$, $n\log n$ are bounded in $L^\infty((0,T),L^1(\mathbb{R}^d))$, $\nabla\sqrt{n}\in L^1((0,T),L^2(\mathbb{R}^d))$ and $\nabla c\in L^\infty((0,T)\times\mathbb{R}^d)$, then

$$\frac{\mathrm{d}}{\mathrm{dt}}\mathcal{F}[n](t) = -\int_{\mathbb{R}^d} n(t,x)\,|\nabla\log n(t,x) - \chi\nabla c(t,x)|^2\;\mathrm{d}x. \tag{8.5}$$

The functional $\mathcal{F}$ structurally belongs to the general class of free energies for interacting particles introduced in [179, 59, 60] and further analysed in [73, 3]. The functionals treated in those references are of the general form:

$$\mathcal{E}[n] := \int_{\mathbb{R}^d} U[n(x)]\,\mathrm{d}x + \int_{\mathbb{R}^d} n(x)\,V(x)\,\mathrm{d}x + \frac{1}{2}\iint_{\mathbb{R}^d\times\mathbb{R}^d} W(x-y)\,n(x)\,n(y)\,\mathrm{d}x\,\mathrm{d}y \tag{8.6}$$

under the basic assumptions $U : \mathbb{R}^+ \to \mathbb{R}$ is a density of internal energy, $V : \mathbb{R}^d \to \mathbb{R}$ is a convex confinement potential and $W : \mathbb{R}^d \to \mathbb{R}$ is a symmetric convex interaction potential. The internal energy $U$ should satisfy the following dilation condition, introduced in McCann [179]

$$\lambda \longmapsto \lambda^d U(\lambda^{-d}) \qquad \text{is convex non-increasing on } \mathbb{R}^+. \tag{8.7}$$

The most important case of application, as it is for our case, is $U(s) = s\log s$, which identifies the internal energy with Boltzmann's entropy.

Continuity equations where the velocity field is formally derived from the variational derivative of free energy functionals of the type (8.6), given by

$$\frac{\partial\rho}{\partial t} = \mathrm{div}\,\left(\rho\nabla\frac{\delta\mathcal{E}}{\delta\rho}\right), \qquad \text{in} \qquad (0,+\infty)\times\mathbb{R}^d, \tag{8.8}$$

appear in various contexts: the interest for a convex interaction potential energy arose from its use in the modelling of granular flows: see the works of D. Benedetto, E. Caglioti, the last author, M. Pulvirenti, G. Toscani and C. Villani [27, 26, 235, 245] and the references therein for the physical background and related mathematical analysis. Nice mathematical and physical reviews are provided in [244, Chapter 5] and [245].

A very powerful theory has been developed in the past decade starting from the seminal paper by R. McCann [179] where the notion of displacement convexity for a functional acting on probability measures was introduced. This notion provides functionals of the form (8.6) with a natural convexity structure. However, the interacting kernel $W$ is itself required to be convex. Later, F. Otto [200] introduced a formal Riemaniann structure giving sense to this family of equations (8.8) as the gradient flow of the convex free-energy functional (8.8) with respect to a metric that induces the euclidean Wasserstein distance for measures. Geodesics in Otto's interpretation correspond to optimal transportation pathways (or *displacement interpolation*),

$$\rho^t = \Big((1-t)\mathrm{Id} + t\nabla\varphi\Big)\#\rho^0,$$

where $T = \nabla\varphi$ is the optimal static transport map between the endpoints $\rho^0$ and $\rho^1$.

On the other hand, a steepest descent scheme based on optimal transport of measures was introduced in [148] for the linear Fokker-Planck equation, exhibiting very nice properties. This scheme is now well understood and has been formalised for a large class of degenerate parabolic equations in [2], and in a more abstract setting, by L. Ambrosio, N. Gigli and G. Savaré [7] with the name of 'minimising movement scheme'. The idea corresponds to a discrete version of the gradient flow or steepest descent of the free energy under the Wasserstein metric structure, see Section 2 below for precise definitions.

In our case, the free-energy functional shows a non convex interaction potential, characteristic also of other models in mathematical biology [36, 46] and swarming [234]. To weaken the convexity assumption on the interaction kernel and to find under which conditions stationary states continue to be global attractors of the dynamics are issues of great interest for applications in mathematical biology.

The main results of this work, Theorem 8.8 and Proposition 8.15, show the convergence of the Jordan-Kinderlehrer-Otto steepest descent discrete method [148] using Otto's interpretation of the PKS equation (8.1) as the gradient flow of the free-energy functional for the sub-critical case and the exponential convergence towards a unique stationary profile in scaled variables for the sub-critical one-dimensional case. The first result recovers the available global existence results in the sub-critical cases for the PKS equation in [46, 35, 55]. Moreover, we solve numerically this scheme in the one-dimensional case showing its abilities on capturing the blow-up for super-critical cases without the need of mesh-refinement.

The plan of this paper is the following: we first recall in Section 8.2.1 some recent results on free energies and rescaled variables which allows to obtain *a priori* estimates. We remind in Section 8.2.2

notions on optimal transport and on the Wasserstein distance that we will use in Section 8.3 to prove the convergence of the scheme (8.17). The exponential convergence towards a unique equilibrium is shown in the scaled one-dimensional setting in Subsection 8.4.1. Finally, one-dimensional numerical simulations are given in Subsection 8.4.2.

## 8.2 Preliminaries

### 8.2.1 *A priori* estimates in the sub-critical case

Here, we review some aspects of the PKS model that were already used in [46, 35, 55, 34] as the main tools for the proof of global existence of weak solutions in the sub-critical and critical cases, respectively.

We will make a fundamental use of the Logarithmic Hardy-Littlewood-Sobolev inequality [23, 56]: let $f$ be a non-negative function in $L^1(\mathbb{R}^d)$ such that $f\log f$ and $f\log(1+|x|^2)$ belong to $L^1(\mathbb{R}^d)$. If

$$\int_{\mathbb{R}^d} f(x)\,\mathrm{d}x = 1$$

then

$$\int_{\mathbb{R}^d} f(x)\log f(x)\,\mathrm{d}x + d\iint_{\mathbb{R}^d\times\mathbb{R}^d} f(x)f(y)\log|x-y|\,\mathrm{d}x\,\mathrm{d}y \geq -\,C(d) \tag{8.9}$$

with $C(d) := (1/2)\log\pi + (1/d)\log[\Gamma(d/2)/\Gamma(d)] + (1/2)[\psi(d) - \psi(d/2)]$ where $\psi$ is the logarithmic derivative of the $\Gamma$-function. The Logarithmic Hardy-Littlewood-Sobolev inequality (8.9) implies that the functional energy (8.4) is bounded from below if $\chi = \chi_c := 2\,d^2\pi$.

Since we will work mainly in the sub-critical case $\chi < \chi_c$, it is clearer, although not necessary, to solve the equation in rescaled variables. Let us define the rescaled functions $\rho$ and $v$ by:

$$n(t,x) = \frac{1}{R^d(t)}\,\rho\left(\tau(t), \frac{x}{R(t)}\right) \quad \text{and} \quad c(x,t) = v\left(\tau(t), \frac{x}{R(t)}\right) \tag{8.10}$$

with

$$R(t) = \sqrt{1+2t} \quad \text{and} \quad \tau(t) = \log R(t)\,.$$

The rescaled system is

$$\begin{cases} \dfrac{\partial\rho}{\partial t}(t,x) = \Delta\rho(t,x) + \nabla\cdot\{\rho(t,x)\,[x - \chi\nabla v(t,x)]\} & t>0\,,\ x\in\mathbb{R}^d\,, \\ v(t,x) = -\dfrac{1}{d\,\pi}\,\log|\cdot| * \rho(t,x) - \dfrac{1}{d\,\pi}\,\tau(t) & t>0\,,\ x\in\mathbb{R}^d\,, \\ \rho(0,x) = \rho^0 = n_0 \geq 0 & x\in\mathbb{R}^d\,. \end{cases} \tag{8.11}$$

In the rescaled variables, the confinement potential $V(x) = \frac{1}{2}|x|^2$ is added and the free energy becomes

$$\mathcal{G}[\rho] = \int_{\mathbb{R}^d} \rho(x)\log\rho(x)\,\mathrm{d}x + \frac{1}{2}\int_{\mathbb{R}^d} |x|^2\,\rho(x)\,\mathrm{d}x + \frac{\chi}{2\,d\,\pi}\iint_{\mathbb{R}^d\times\mathbb{R}^d} \log|x-y|\,\rho(x)\,\rho(y)\,\mathrm{d}x\,\mathrm{d}y \tag{8.12}$$

With the definition (8.3) we shall say that $\rho$ is a weak solution to the system (8.11) if for all test functions $\zeta\in\mathcal{D}(\mathbb{R}^d)$,

$$\begin{aligned}\frac{\mathrm{d}}{\mathrm{dt}}\int_{\mathbb{R}^d}\zeta(x)\,\rho(t,x)\,\mathrm{d}x = \int_{\mathbb{R}^d}\Delta\zeta(x)\,\rho(t,x)\,\mathrm{d}x - \int_{\mathbb{R}^d}\nabla\zeta(x)\cdot x\,\rho(t,x)\,\mathrm{d}x \\ - \frac{\chi}{2\,d\,\pi}\iint_{\mathbb{R}^d\times\mathbb{R}^d}[\nabla\zeta(x)-\nabla\zeta(y)]\cdot\frac{x-y}{|x-y|^2}\,\rho(t,x)\,\rho(t,y)\,\mathrm{d}x\,\mathrm{d}y\end{aligned} \tag{8.13}$$

together with $\rho(t=0) = \rho^0$ in the distributional sense in $(0,T)$. The following Lemma extracts enough information from this decreasing free energy to proceed.

**Lemma 8.1** (*A priori* estimates)**.** *The functional $\mathcal{G}$ is bounded from below on the set*

$$\mathcal{K} := \left\{ \rho \in L^1_+(\mathbb{R}^d) \ : \ \int_{\mathbb{R}^d} \rho(t,x) = 1,\ |x|^2\,\rho \in L^1(\mathbb{R}^d),\ \int_{\mathbb{R}^d} \rho(t,x)\,|\log \rho(t,x)|\ \mathrm{d}x < \infty \right\}$$

*if and only if $\chi \le \chi_c$. In addition, if $\chi < \chi_c$ we have on every subset $\{\mathcal{G} \le C\}$,*

*i)* no concentration: $\displaystyle\int_{\mathbb{R}^d} \rho |\log \rho| \le C$,

*ii)* mass confinement: $\displaystyle\int_{\mathbb{R}^d} |x|^2 \rho \le C$,

*As a consequence, every level subset $\{\mathcal{G} \le C\}$ is equi-integrable.*

*Proof.* The first use of the Logarithmic Hardy-Littlewood-Sobolev inequality (8.9) to bound from below the free energy $\mathcal{G}$ is due to [86]. Rewrite

$$\begin{aligned} \mathcal{G}[\rho](t) &= (1-\theta) \int_{\mathbb{R}^d} \rho(t,x)\,\log \rho(t,x)\ \mathrm{d}x + \frac{1}{2}\int_{\mathbb{R}^d} |x|^2\,\rho(t,x)\ \mathrm{d}x \\ &+ \theta d \left[ \frac{1}{d}\int_{\mathbb{R}^d} \rho(t,x)\,\log \rho(t,x)\ \mathrm{d}x + \frac{\chi}{2\,d^2\,\pi\,\theta} \iint_{\mathbb{R}^d\times\mathbb{R}^d} \rho(t,x)\,\rho(t,y)\,\log|x-y|\ \mathrm{d}x\ \mathrm{d}y \right]. \end{aligned} \tag{8.14}$$

The Logarithmic Hardy-Littlewood-Sobolev inequality (8.9) controls the third term if we choose $\theta = \chi/\chi_c$. Because the function $\rho\log\rho$ is negative for small $\rho$, we need to control somehow the density for large $x$. We use in fact the confinement potential, i.e., the second momentum of $\rho$.

**Lemma 8.2** (Carleman's estimates)**.** *For any probability density $u \in L^1_+(\mathbb{R}^d)$, if the second moment $\int_{\mathbb{R}^d} |x|^2\,u(x)\ \mathrm{d}x$ and the entropy $\int_{\mathbb{R}^d} u\log u\ \mathrm{d}x$ are bounded from above, then $u\log u$ is uniformly bounded in $L^1(\mathbb{R}^d)$ and we have*

$$\int_{\mathbb{R}^d} u(x)\,|\log u(x)|\ \mathrm{d}x \le \int_{\mathbb{R}^d} u(x)\left(\log u(x) + \frac{1}{2}|x|^2\right)\mathrm{d}x + d\log(4\pi) + \frac{2}{e}\,.$$

*Proof.* The proof goes as follows. Let $\bar u := u\,\mathbb{1}_{\{u\le 1\}}$ and $m = \int_{\mathbb{R}^d} \bar u(x)\ \mathrm{d}x \le \int_{\mathbb{R}^d} u(x)\ \mathrm{d}x = 1$. Then

$$\int_{\mathbb{R}^d} \bar u(x)\,\left(\log \bar u(x) + \frac{1}{4}|x|^2\right)\ \mathrm{d}x = \int_{\mathbb{R}^d} U(x)\log U(x)\ \mathrm{d}\mu - m\frac{d}{2}\log(4\pi)$$

where $U := \bar u/\mu$, $d\mu(x) = (4\pi)^{-d/2}e^{-|x|^2/4}\ \mathrm{d}x$. The Jensen inequality yields

$$\int_{\mathbb{R}^d} U(x)\,\log U(x)\ \mathrm{d}\mu \ge \left(\int_{\mathbb{R}^d} U(x)\ \mathrm{d}\mu\right)\,\log\left(\int_{\mathbb{R}^d} U(x)\ \mathrm{d}\mu\right) = m\,\log m$$

and

$$\begin{aligned} \int_{\mathbb{R}^d} \bar u(x)\,\log \bar u(x)\ \mathrm{d}x &\ge m\log m - m\frac{d}{2}\log 4\pi - \frac{1}{4}\int_{\mathbb{R}^d} |x|^2\,\bar u(x)\ \mathrm{d}x \\ &\ge -\frac{1}{e} - \frac{d}{2}\log(4\pi) - \frac{1}{4}\int_{\mathbb{R}^d} |x|^2\,u(x)\ \mathrm{d}x\,. \end{aligned}$$

Using

$$\int_{\mathbb{R}^d} u(x)\,|\log u(x)|\ \mathrm{d}x = \int_{\mathbb{R}^d} u(x)\,\log u(x)\ \mathrm{d}x - 2\int_{\mathbb{R}^d} \bar u(x)\,\log \bar u(x)\ \mathrm{d}x\,,$$

this completes the proof. □

We apply this lemma to obtain the first part of the result from (8.14):

$$\mathcal{G}[\rho](t) \geq (1-\theta) \int_{\mathbb{R}^d} \rho(t,x) \,|\log \rho(t,x)|\, \mathrm{d}x + \frac{\theta}{2} \int_{\mathbb{R}^d} |x|^2 \,\rho(t,x)\, \mathrm{d}x + C.$$

On the other hand, the functional $\mathcal{G}[\rho]$ has an interesting scaling property. For a given $\rho$, let $\rho_\lambda(x) = \lambda^d \rho(\lambda x)$. It is straightforward to check that $\|\rho_\lambda\|_{L^1(\mathbb{R}^d)} = 1$ and

$$\mathcal{G}[\rho_\lambda] = \mathcal{G}[\rho] + d\left(1 - \frac{\chi}{\chi_c}\right) \log\lambda + \frac{\lambda^{-2}-1}{2} \int_{\mathbb{R}^d} |x|^2 \,\rho \,\mathrm{d}x\,.$$

Since $\lambda \mapsto \mathcal{G}[\rho_\lambda]$ is clearly not bounded from below if $\chi > \chi_c$, the proof concludes. □

We shall also state another technical Lemma, which will plays a major role when passing to the limit in the quadratic interaction contribution.

**Lemma 8.3** (Doubling of variables)**.** *Assume $f_i \rightharpoonup f$ in $L^1$ and the family $\{f_i\}$ is equi-integrable in the sense of Lemma* 8.1*, then $f_i \otimes f_i \rightharpoonup f \otimes f$ in $L^1(\mathbb{R}^d \times \mathbb{R}^d)$.*

*Proof.* Let $\psi(x,y)$ denote any test function in $L^\infty(\mathbb{R}^d \times \mathbb{R}^d)$. For almost every $x \in \mathbb{R}^d$ define

$$\lim \Psi^i(x) := \lim \int_{\mathbb{R}^d} f_i(y)\,\psi(x,y)\,\mathrm{d}y = \int_{\mathbb{R}^d} f(y)\,\psi(x,y)\,\mathrm{d}y =: \Psi(x)$$

Note that for any $x$, $|\Psi^i(x)|$ and $|\Psi(x)|$ are bounded by $\|\psi\|_{L^\infty}$.

By Egorov's theorem for any $R > 0$ and $\delta > 0$, there exists a measurable set $X_\delta$ such that $|X_\delta| < \delta$ and $\Psi^i$ uniformly converges to $\Psi$ in $B_R \setminus X_\delta$. We have

$$\begin{aligned}
&\left| \int_{\mathbb{R}^d} \left[\Psi^i(x)\, f_i(x) - \Psi(x)\, f(x)\right] \,\mathrm{d}x \right| \\
&\quad \leq \int_{B_R \setminus X_\delta} \left|\Psi^i(x)\, f_i(x) - \Psi(x)\, f(x)\right| \,\mathrm{d}x + \int_{X_\delta} \left|\Psi^i(x)\, f_i(x) - \Psi(x)\, f(x)\right| \,\mathrm{d}x \\
&\qquad + \int_{B_R^c} \left|\Psi^i(x)\, f_i(x) - \Psi(x)\, f(x)\right| \,\mathrm{d}x \\
&\quad \leq \int_{B_R \setminus X_\delta} \left|\Psi^i(x)\, f_i(x) - \Psi(x)\, f(x)\right| \,\mathrm{d}x + \|\psi\| \int_{X_\delta} f_i(x) + f(x) \,\mathrm{d}x \\
&\qquad + \|\psi\| \,\frac{1}{R^2} \int_{B_R^c} |x|^2 \,[f_i(x) + f(x)] \,\mathrm{d}x\,.
\end{aligned}$$

Egorov's theorem and the weak-$L^1$ convergence of $f_i$ towards $f$ ensures that the first term is as small as desired by choosing $i$ large enough. By the *a priori* estimates in Lemma 8.1, $\int_{X_\delta} f_i(x)\,\mathrm{d}x$ and $\int_{X_\delta} f(x)\,\mathrm{d}x$ can me made as small as desired by choosing $\delta$ small enough, as well as the third term can be made as small as desired by choosing $R$ large enough. □

### 8.2.2 Optimal transport and the Wasserstein distance

We recall some standard results related to optimal transportation and Wasserstein distance that we will use in the sequel of this paper. The interested reader can refer to the books of C. Villani [244, 246] and the book of L. Ambrosio, N. Gigli and G. Savaré [7]. A short summary of properties of the Wasserstein distance can be seen in [62].

Let $\mu$ and $\nu$ be in $\mathcal{P}(\mathbb{R}^d)$ the space of probability measure in $\mathbb{R}^d$, $\mathcal{P}_2(\mathbb{R}^d)$ the subset of probability measures with finite second-momentum, $\mathcal{P}_2^{\mathrm{ac}}(\mathbb{R}^d)$ its subset formed by the absolutely continuous measures with respect to Lebesgue and $T$ be a measurable map $\mathbb{R}^d \to \mathbb{R}^d$. We say that $T$ *transports* $\mu$ onto $\nu$ and we note $\nu = T\#\mu$ if for any measurable set $B \subset \mathbb{R}^d$, $\nu(B) = \mu \circ T^{-1}(B)$. We also say $\nu$ is the *push-forward* or *the image measure* of $\mu$ by $T$ *i.e.*

$$\int_{\mathbb{R}^d} \zeta \circ T(x)\, \mathrm{d}\mu(x) = \int_{\mathbb{R}^d} \zeta(y)\, \mathrm{d}\nu(y) \quad \forall \zeta \in \mathcal{C}_b^0(\mathbb{R}^d)\ . \tag{8.15}$$

The Wasserstein distance between $\mu$ and $\nu$, $d_W$ can be defined by

$$d_W^2(\mu,\nu) := \inf_{T:\ \nu = T\#\mu} \int_{\mathbb{R}^d} |x - T(x)|^2\, \mathrm{d}\mu(x)\ .$$

By Brenier's theorem [38, 178, 180], see [244, Theorem 2.32, p.85] for a review, if $\mu$ is absolutely continuous with respect to Lebesgue measure, then there is one measurable plan $T$ such that $\nu = T\#\mu$ and $T = \nabla\varphi$ for some convex function $\varphi$. As a consequence,

$$d_W^2(\mu,\nu) = \int_{\mathbb{R}^d} |x - \nabla\varphi(x)|^2\, \mathrm{d}\mu(x)\ . \tag{8.16}$$

The variational problem leading to the definition of the Wasserstein distance can be relaxed to the linear program

$$d_W^2(\mu,\nu) = \inf_{\Pi\in\Gamma} \left\{ \int_{\mathbb{R}^d\times\mathbb{R}^d} |x-y|^2\, \mathrm{d}\Pi(x,y) \right\},$$

where $\Pi$ runs over the set of transference plans $\Gamma$, that is, the set of joint probability measures on $\mathbb{R}^d \times \mathbb{R}^d$ with marginals $\mu$ and $\nu$. In fact, the infimum above is a minimum by Kantorovich duality theorems [244, Chapter 1]. The optimal transference plan, in case Brenier's theorem applies, is given by $\Pi_o = (\mathrm{id}_{\mathbb{R}^d} \otimes \nabla\varphi)\#\mu$.

Let us remind a simple consequence of the definition of the Wasserstein distance for controlling averages [62, Corollary 2.4].

**Lemma 8.4** (Convergence of averages with $d_W$)**.** *Given $\zeta$ a Lipschitz function with Lipschitz constant $L$ and $\mu,\nu \in \mathcal{P}_2(\mathbb{R}^d)$, then we have*

$$\left| \int_{\mathbb{R}^d} \zeta(x)\, \mathrm{d}\mu - \int_{\mathbb{R}^d} \zeta(x)\, \mathrm{d}\nu \right| \le L\, d_W(\mu,\nu).$$

*Proof.* Let $\Pi_o$ the optimal plan between $\mu$ and $\nu \in \mathcal{P}_2(\mathbb{R}^d)$ for $d_W$. Then

$$\int_{\mathbb{R}^d\times\mathbb{R}^d} |x-y|^2\, \mathrm{d}\Pi_o(x,y) = d_W^2(\mu,\nu),$$

and we can write

$$\int_{\mathbb{R}^d} \zeta(x)\, \mathrm{d}\mu - \int_{\mathbb{R}^d} \zeta(x)\, \mathrm{d}\nu = \int_{\mathbb{R}^d\times\mathbb{R}^d} (\zeta(x) - \zeta(y))\ \mathrm{d}\Pi_o(x,y).$$

Using that $\zeta$ is Lipschitz with constant $L$ and estimating by Hölder's inequality, we get

$$\begin{aligned}\left| \int_{\mathbb{R}^d} \zeta(x)\, \mathrm{d}\mu - \int_{\mathbb{R}^d} \zeta(x)\, \mathrm{d}\nu \right| &\le \int_{\mathbb{R}^d\times\mathbb{R}^d} |\zeta(x) - \zeta(y)|\ \mathrm{d}\Pi_o(x,y) \\ &\le L \int_{\mathbb{R}^d\times\mathbb{R}^d} |x-y|\ \mathrm{d}\Pi_o(x,y) \le L\, d_W(\mu,\nu),\end{aligned}$$

giving the assertion. □

## 8.3 Time discretisation

We consider a time-step $\tau > 0$, an initial datum $\rho^0 \in \mathcal{P}_2^{\mathrm{ac}}(\mathbb{R}^d)$. We introduce the sequence $(\rho_\tau^n)_{n\in\mathbb{N}}$ recursively defined by $\rho_\tau^0 = \rho^0$ and

$$\rho_\tau^{n+1} \in \arg\inf_{\rho\in\mathcal{K}} \left\{ \mathcal{G}[\rho] + \frac{1}{2\,\tau} d_W^2(\rho_\tau^n, \rho) \right\} . \tag{8.17}$$

The Jordan-Kinderlehrer-Otto (JoKinOt98) steepest descent scheme can be viewed formally as a time discretisation of the abstract gradient flow equation,

$$\frac{\partial \rho}{\partial t} = -"\nabla_W" \mathcal{G}[\rho] ,$$

where the space $\mathcal{K} \subset \mathcal{P}_2^{\mathrm{ac}}(\mathbb{R}^d)$ is endowed with a formal riemannian structure compatible with the Wasserstein $d_W$ distance [200]. We refer to [200, 244, 7, 60] for a deeper discussion and the rigorous sense of the "$\nabla_W$" definition. Next lemma ensures that this discrete scheme is well defined.

**Lemma 8.5** (Existence of minimisers)**.** *Let $\rho_0$ satisfies* (8.2) *and $\chi < \chi_c$, then there recursively exists a minimiser to* (8.17)*.*

*Proof.* Introduce the function

$$\mathcal{K} \ni \xi \mapsto \mathcal{G}[\xi] + \frac{1}{2\,\tau} d_W^2(\rho_\tau^n, \xi) . \tag{8.18}$$

By the *a priori* estimates in Lemma 8.1, this function is bounded from below. Consider $(\xi_k)_{k\in\mathbb{N}}$ a minimising sequence, without loss of generality, we can assume that it satisfies $\mathcal{G}[\xi_k] \leq \mathcal{G}[\rho_\tau^n]$ for all $k \in \mathbb{N}$. Proceeding as in Lemma 8.1, we get

$$(1-\theta) \int_{\mathbb{R}^d} \xi_k(x) \,|\log \xi_k(x)|\, \mathrm{d}x + \frac{\theta}{2} \int |x|^2 \xi_k(x) \leq \mathcal{G}[\rho_\tau^n] + \theta\, C(d) .$$

If $\chi < \chi_c$, then $\theta = \dfrac{\chi}{\chi_c} < 1$ and this shows that $\xi_k \log \xi_k$ is bounded in $L^1(\mathbb{R}^d)$.

The bound on the second momentum avoid vanishing, while the $L^1(\mathbb{R}^d)$-bound on $\xi_k \log \xi_k$ avoid concentration: indeed,

$$\int_{\{\xi_k \geq Q\}} \xi_k \,\mathrm{d}x \leq \frac{1}{\log Q} \int_{\{\xi_k \geq Q\}} \xi_k \log \xi_k \,\mathrm{d}x \leq \frac{1}{\log Q} \int_{\mathbb{R}^d} \xi_k \,|\log \xi_k|\, \mathrm{d}x ,$$

can be made as small as desired for $Q > 1$ large enough. Hence the family $\{\xi_k\}_{k\in\mathbb{N}}$ verifies the hypotheses in Dunford-Pettis theorem, and thus, there exists a sub-sequence still denoted $(\xi_k)_{k\in\mathbb{N}}$ which converges weakly $L^1$ to a density $\xi_*$.

It remains to prove that this candidate $\xi_*$ realises in fact a minimum of (8.18). The weak-$L^1$ lower semi-continuity of the entropy $\mathcal{S}$, the second momentum and the Wasserstein distance are well known, see [148, 7] and references therein. We will prove that the quadratic interaction term is continuous for the weak-$L^1$ convergence in our situation. We split it into

$$\iint_{\mathbb{R}^d\times\mathbb{R}^d} \xi_k(x)\,\xi_k(y)\, \log|x-y| \,\mathrm{d}x\,\mathrm{d}y = \mathrm{A} + \mathrm{B} + \mathrm{C},$$

with

$$\mathrm{A} := \iint_{|x-y|<\varepsilon} \xi_k(x)\,\xi_k(y)\, \log|x-y| \,\mathrm{d}x\,\mathrm{d}y,$$

$$\mathrm{B} := \iint_{\varepsilon\leq|x-y|\leq R} \xi_k(x)\,\xi_k(y)\, \log|x-y| \,\mathrm{d}x\,\mathrm{d}y$$

$$\text{and} \quad \mathrm{C} := \iint_{|x-y|>R} \xi_k(x)\,\xi_k(y)\, \log|x-y| \,\mathrm{d}x\,\mathrm{d}y ,$$

where $\varepsilon < 1$ and $R > \sqrt{e}$.

**Control of** A$(t)$**.** We use the duality inequality, $ab \le e^a + b\log b - b$.

$$\begin{aligned}
|\mathrm{A}| &\le \iint_{|x-y|<\varepsilon} \xi_k(x)\xi_k(y)\log\frac{1}{|x-y|}\,\mathrm{d}x\,\mathrm{d}y \\
&\le \int\Big\{\xi_k(x)\int_{|x-y|<\varepsilon}\alpha^{-1}\xi_k(y)\log(\alpha^{-1}\xi_k(y)) - \alpha^{-1}\xi_k(y) + \exp\Big(\alpha\log\frac{1}{|x-y|}\Big)\Big\} \\
&\le \alpha^{-1}\int \xi_k(y)\log(\alpha^{-1}\xi_k(y))\int_{|x-y|<\varepsilon}\xi_k(x)\,\mathrm{d}x\,\mathrm{d}y + \int\xi_k(x)\,\mathrm{d}x\int_{|z|<\varepsilon}\frac{1}{|z|^\alpha}\,\mathrm{d}z.
\end{aligned}$$

By the $L^1(\mathbb{R}^d)$-bound on $\xi_k\,\log\xi_k$, $\int_{X_\varepsilon}\xi_k$ is uniformly small on small sets $X_\varepsilon$, and therefore the last term can be made as small as desired uniformly in $k$ by choosing $\varepsilon$ small enough and $\alpha < d$.

**Control of** B**.** We shall use the Lemma 8.3 because $\log|x-y|$ is bounded on the set $\{\varepsilon < |x-y| < R\}$

**Control of** C**.** For $R > \sqrt{e}$, $R \mapsto R^2/\log R$ is an increasing function, so that

$$0 \le \mathrm{C} \le \frac{2\,\log R}{R^2}\int_{\mathbb{R}^2}|x|^2\,\xi_k(t,x)\,\mathrm{d}x\,.$$

Because we uniformly bound the second momentum, this can be made as small as desired while choosing $R$ large enough.

Finally, collecting terms we get that the difference

$$\left|\iint_{\mathbb{R}^d\times\mathbb{R}^d}\xi_k(x)\,\xi_k(y)\log|x-y|\,\mathrm{d}x\,\mathrm{d}y - \iint_{\mathbb{R}^d\times\mathbb{R}^d}\xi_*(x)\,\xi_*(y)\log|x-y|\,\mathrm{d}x\,\mathrm{d}y\right|$$

can be made as small as desired by choosing $\varepsilon$ and $\delta$ small enough, and $r$, $R$ and $k$ large enough. □

**Remark 8.6** (Uniqueness of Minimisers)**.** *Since the functional $\mathcal{G}[n]$ is not convex, we cannot conclude the uniqueness of minimisers for the discrete scheme, and thus, the scheme* (8.17) *is defined by choosing any element realising the infimum as $\rho_\tau^{n+1}$. Each choice might in principle give rise to a solution in the limit $\tau \to 0$. It is an open problem to deal with the uniqueness of solutions in the sub-critical case.*

Now, we define the time interpolation of the discrete scheme as a family of Lipschitz curves $(\rho_\tau)_{\tau>0}$ connecting every pair $\{\rho_\tau^n, \rho_\tau^{n+1}\}$ with a constant speed geodesic in the interval $[n\,\tau, (n+1)\,\tau)$. Accordingly for any $t \in [n\,\tau, (n+1)\,\tau)$ we have,

$$d_W\left(\rho_\tau^n, \rho_\tau(t)\right) = \frac{t-n\tau}{\tau}\,d_W\left(\rho_\tau^n, \rho_\tau^{n+1}\right)\,.$$

Obviously $\rho_\tau(n\tau) = \rho_\tau^n$. This is possible due to Brenier theorem by defining the displacement interpolant

$$\rho_\tau(t) = \left(\frac{(n+1)\tau - t}{\tau}\mathrm{Id} + \frac{t-n\tau}{\tau}\nabla\varphi^n\right)\#\rho_\tau^n$$

with $\nabla\varphi^n$ being the optimal map transporting $\rho_\tau^n$ onto $\rho_\tau^{n+1}$.

**Remark 8.7** (Comparison to Literature)**.** *Let us point out that once the free energy $\mathcal{G}[n]$ is bounded from below (Lemma* 8.1*) and the approximation scheme is well-defined (Lemma* 8.5*), then* [7, Theorem 11.1.6, pp. 288-289] *applies. For the convenience of the reader we give a shorter proof adapted to our problem. Our proof is based on the founding idea of* [148] *proving the convergence of the ad-hoc scheme for the linear Fokker-Planck equation. A nice sketch of the proof of* [148] *can be found in* [244, Section 8.4,pp. 256-262].

**Theorem 8.8** (Convergence of the scheme as $\tau \to 0$)**.** *Under assumption* (8.2)*, if* $\chi < \chi_c$ *then the family* $(\rho_\tau)_{\tau>0}$ *admits a sub-sequence converging weakly in* $L^1(\mathbb{R}^d)$ *to a weak solution of* (8.13)*.*

*Proof.* We proceed in three steps:
**Step 1.-** ***A priori*** **estimates in space and time**: Since $\rho_\tau^{n+1}$ minimises (8.17) we obviously have

$$\mathcal{G}[\rho_\tau^{n+1}] + \frac{1}{2\,\tau} d_W^2(\rho_\tau^n, \rho_\tau^{n+1}) \leq \mathcal{G}[\rho_\tau^n] \,.$$

As a consequence we obtain an *energy estimate*

$$\sup_{n\in\mathbb{N}} \mathcal{G}[\rho_\tau^n] \leq \mathcal{G}[\rho_\tau^0], \tag{8.19}$$

and a *total square estimate*

$$\frac{1}{2\,\tau} \sum_{n\in\mathbb{N}} d_W^2(\rho_\tau^n, \rho_\tau^{n+1}) \leq \mathcal{G}[\rho_\tau^0] - \inf_{n\in\mathbb{N}} \mathcal{G}[\rho_\tau^n] \,. \tag{8.20}$$

The right-hand side is bounded thanks to Lemma 8.1.

From the total square estimate (8.20) we deduce a $\frac{1}{2}$-*Hölder-estimate* in time of $(\rho_\tau)_{\tau\geq 0}$: indeed, for any $0 \leq m \leq n$,

$$d_W(\rho_\tau^m, \rho_\tau^n) \leq \sqrt{2\,\tau} \sum_{k=m}^{n-1} \frac{1}{\sqrt{2\,\tau}} d_W(\rho_\tau^k, \rho_\tau^{k+1}) \leq \sqrt{2\,\tau}\,\sqrt{(n-m)} \sqrt{\mathcal{G}[\rho_\tau^0] - \inf_{n\in\mathbb{N}} \mathcal{G}[\rho_\tau^n]} \,.$$

As a consequence for any $0 \leq s \leq t$

$$\begin{aligned}
d_W(\rho_\tau(s), \rho_\tau(t)) &\leq d_W\Big(\rho_\tau(s), \rho_\tau^{\left[\frac{s}{\tau}+1\right]\tau}\Big) + d_W\Big(\rho_\tau^{\left[\frac{s}{\tau}+1\right]\tau}, \rho_\tau^{\left[\frac{t}{\tau}\right]\tau}\Big) + d_W\Big(\rho_\tau^{\left[\frac{t}{\tau}\right]\tau}, \rho_\tau(t)\Big) \\
&\leq \left(\left[\frac{s}{\tau}+1\right] - \frac{s}{\tau}\right) d_W\Big(\rho_\tau^{\left[\frac{s}{\tau}\right]\tau}, \rho_\tau^{\left[\frac{s}{\tau}+1\right]\tau}\Big) \\
&\quad + \sqrt{2\,\tau\left(\left[\frac{t}{\tau}\right] - \left[\frac{s}{\tau}+1\right]\right)\Big(\mathcal{G}(\rho_\tau^0) - \inf_{n\in\mathbb{N}} \mathcal{G}(\rho_\tau^n)\Big)} \\
&\quad + \left(\frac{t}{\tau} - \left[\frac{t}{\tau}\right]\right) d_W\Big(\rho_\tau^{\left[\frac{t}{\tau}\right]\tau}, \rho_\tau^{\left[\frac{t}{\tau}+1\right]\tau}\Big) \\
&\leq \sqrt{6\,\Big(\mathcal{G}(\rho^0) - \inf_{n\in\mathbb{N}} \mathcal{G}(\rho^n)\Big)}\,(t-s)^{\frac{1}{2}} \,.
\end{aligned} \tag{8.21}$$

**Step 2.- Compactness**: By the $\frac{1}{2}$-Hölder-estimate (8.21), $\rho_\tau$ is bounded in $\mathcal{P}_2(\mathbb{R}^d)$ so the family $\{\rho_\tau\}_{\tau>0}$ is tight. By the *a priori* estimates (Lemma 8.1), the family $\{\rho_\tau(t)\}_{\tau>0}$ can neither concentrate nor vanish and the family $\{\rho_\tau(t)\}_{\tau>0}$ is equi-integrable. In the other hand by the estimate (8.21) the curves $\rho_\tau(t,\cdot)$ are $\frac{1}{2}$-Hölder continuous in time. Ascoli-Arzéla's theorems yield the relative compactness of the family $(\rho_\tau(t,\cdot))_{\tau>0}$.

Finally $\{\rho_\tau\}_{\tau>0}$ is relatively compact in $\mathcal{C}^0([0,T], L^1_{\text{weak}}(\mathbb{R}^d))$ for any $T>0$. As a consequence, for any $T>0$, there exists a sub-sequence still denoted $(\rho_\tau)_{\tau>0}$, such that $(\rho_\tau)_{\tau>0}$ converges in $\mathcal{C}^0([0,T], L^1_{\text{weak}}(\mathbb{R}^d))$ to a function $\rho$ when $\tau$ goes to 0.

**Step 3.- Approximate Euler-Lagrange equation in weak formulation**:
*Weak space derivative.-* Let $\zeta$ be a test function and $\nabla\zeta$ be a smooth vector field with compact support.

Let us define $\nabla\varphi_\varepsilon$ with $\varphi_\varepsilon(x) := \frac{|x|^2}{2} + \varepsilon\,\zeta$. For $\varepsilon$ small enough $\nabla\varphi_\varepsilon$ is a $\mathcal{C}^\infty$-diffeomorphism and $\mathrm{Det}\, D^2\varphi_\varepsilon = \mathrm{Det}\,(\mathrm{Id} + \varepsilon\, D^2\zeta) > 0$. We define $\overline{\rho_\varepsilon}$ the push-forward perturbation of $\rho_\tau^{n+1}$ by $\nabla\varphi_\varepsilon$:

$$\overline{\rho_\varepsilon} = \nabla\varphi_\varepsilon \# \rho_\tau^{n+1}\ .$$

Changing variables and using (8.15), we have

$$\mathcal{G}[\overline{\rho_\varepsilon}](t) = \int_{\mathbb{R}^d} \log \frac{\rho_\tau^{n+1}(x)}{\mathrm{Det}\, D^2\varphi_\varepsilon} \rho_\tau^{n+1}(x)\,\mathrm{d}x + \int_{\mathbb{R}^d} \frac{1}{2}|x - \varepsilon\,\nabla\zeta(x)|^2 \rho_\tau^{n+1}(x)\,\mathrm{d}x \\ + \iint_{\mathbb{R}^d\times\mathbb{R}^d} \frac{\chi}{2\,d\,\pi} \log|\nabla\varphi_\varepsilon(x) - \nabla\varphi_\varepsilon(y)|\, \rho_\tau^{n+1}(x)\, \rho_\tau^{n+1}(y)\,\mathrm{d}x\,\mathrm{d}y\ .$$

Alternatively we introduce the optimal map $\nabla\varphi^n$ which transports $\rho_\tau^n$ onto $\rho_\tau^{n+1}$. By (8.16)

$$d_W^2(\rho_\tau^n, \rho_\tau^{n+1}) = \int_{\mathbb{R}^d} |x - \nabla\varphi^n(x)|^2 \rho_\tau^n(x)\,\mathrm{d}x\ . \tag{8.22}$$

The map $\nabla\varphi_\varepsilon \circ \nabla\varphi^n$ transports $\rho_\tau^n$ on $\overline{\rho_\varepsilon}$. We do not know if this is the optimal map however by definition of the Wasserstein distance

$$d_W^2(\rho_\tau^n, \overline{\rho_\varepsilon}) \le \int_{\mathbb{R}^d} \left|x - \nabla\varphi_\varepsilon \circ \nabla\varphi^n(x)\right|^2 \rho_\tau^n(x)\,\mathrm{d}x\ . \tag{8.23}$$

Using the minimising property of the scheme (8.17), and combining (8.22) and (8.23) we obtain

$$\begin{aligned} 0 &\le \frac{1}{2\,\tau} d_W^2(\rho_\tau^n, \overline{\rho_\varepsilon}) + \mathcal{G}[\overline{\rho_\varepsilon}] - \frac{1}{2\,\tau} d_W^2(\rho_\tau^{n+1}, \rho_\tau^n) - \mathcal{G}[\rho_\tau^{n+1}] \\ &\le \frac{1}{2\,\tau} \int_{\mathbb{R}^d} \Big( |x - \nabla\varphi^n(x) - \varepsilon\,\nabla\zeta\circ\nabla\varphi^n(x)|^2 - |x - \nabla\varphi^n(x)|^2 \Big) \rho_\tau^n(x)\,\mathrm{d}x \\ &\quad + \frac{1}{2} \int_{\mathbb{R}^d} \left( \left(|x - \varepsilon\nabla\zeta(x)|^2 - |x|^2\right) - \log\left[\mathrm{Det}\,(\mathrm{Id} + \varepsilon\, D^2\zeta)\right] \right) \rho_\tau^{n+1}(x)\,\mathrm{d}x \\ &\quad + \frac{\chi}{2\,d\,\pi} \iint \left( \log\left|x - y + \varepsilon(\nabla\zeta(x) - \nabla\zeta(y))\right| - \log|x-y| \right) \rho_\tau^{n+1}(x)\, \rho_\tau^{n+1}(y)\,\mathrm{d}x\,\mathrm{d}y. \end{aligned}$$

Dividing by $\varepsilon$ and letting $\varepsilon > 0$ going to zero we find

$$0 \le \frac{1}{\tau} \int_{\mathbb{R}^d} \left\langle \nabla\varphi^n(x) - x, \nabla\zeta\circ\nabla\varphi^n(x) \right\rangle \rho_\tau^n(x)\,\mathrm{d}x + \int_{\mathbb{R}^d} [-\Delta\zeta(x) - x\cdot\nabla\zeta(x)]\, \rho_\tau^{n+1}(x)\,\mathrm{d}x \\ + \frac{\chi}{2\,d\,\pi} \iint_{\mathbb{R}^d\times\mathbb{R}^d} \frac{[\nabla\zeta(x) - \nabla\zeta(y)]\cdot(x-y)}{|x-y|^2} \rho_\tau^{n+1}(x)\, \rho_\tau^{n+1}(y)\,\mathrm{d}x\,\mathrm{d}y\ .$$

Since we can change $\varepsilon$ in $-\varepsilon$ we have in fact

$$\frac{1}{\tau} \int_{\mathbb{R}^d} \left\langle \nabla\varphi^n(x) - x, \nabla\zeta\circ\nabla\varphi^n(x) \right\rangle \rho_\tau^n(x)\,\mathrm{d}x = \int_{\mathbb{R}^d} [\Delta\zeta(x) + x\cdot\nabla\zeta(x)]\, \rho_\tau^{n+1}(x)\,\mathrm{d}x \\ - \frac{\chi}{2\,d\,\pi} \iint_{\mathbb{R}^d\times\mathbb{R}^d} \frac{[\nabla\zeta(x) - \nabla\zeta(y)]\cdot(x-y)}{|x-y|^2} \rho_\tau^{n+1}(x)\, \rho_\tau^{n+1}(y)\,\mathrm{d}x\,\mathrm{d}y\ . \tag{8.24}$$

*Weak time derivative.*- Using the Taylor's expansion

$$\zeta(\nabla\varphi^n(x)) - \zeta(x) = \left\langle \nabla\varphi^n(x) - x, \nabla\zeta\circ\nabla\varphi^n(x) \right\rangle + O\Big(|x - \nabla\varphi^n(x)|^2\Big)$$

we can recast the left-hand side of (8.24) as

$$\frac{1}{\tau} \int_{\mathbb{R}^d} [\zeta\circ\nabla\varphi^n(x) - \zeta(x)]\, \rho_\tau^n(x)\,\mathrm{d}x + O\left( \frac{1}{\tau} \int_{\mathbb{R}^d} |x - \nabla\varphi^n(x)|^2\, \rho_\tau^n(t)\,\mathrm{d}x \right) \\ = \frac{1}{\tau} \left( \int_{\mathbb{R}^d} \zeta(x) \rho_\tau^{n+1}(x)\,\mathrm{d}x - \int_{\mathbb{R}^d} \zeta(x) \rho_\tau^n(x)\,\mathrm{d}x \right) + O\left( \frac{1}{\tau} d_W^2\left(\rho_\tau^n, \rho_\tau^{n+1}\right) \right)\ .$$

We multiply (8.24) by $\tau$ and eventually obtain

$$\int_{\mathbb{R}^d} \zeta(x)\left[\rho_\tau^{n+1}(x)-\rho_\tau^n(x)\right]\,\mathrm{d}x + O\big(d_W^2\left(\rho_\tau^n,\rho_\tau^{n+1}\right)\big) \tag{8.25}$$
$$=\tau\int_{\mathbb{R}^d}\left[\Delta\zeta(x)+x\cdot\nabla\zeta(x)-\frac{\chi}{2\,d\,\pi}\int_{\mathbb{R}^d}\frac{[\nabla\zeta(x)-\nabla\zeta(y)]\cdot(x-y)}{|x-y|^2}\rho_\tau^{n+1}(y)\,\mathrm{d}y\right]\rho_\tau^{n+1}(x)\,\mathrm{d}x.$$

Let $0\le t_1<t_2$ be fixed times, $m=[t_1/\tau]+1$ and $n=[t_2/\tau]$. By summing equation (8.25) we have thanks to the total square estimate (8.20),

$$\int_{\mathbb{R}^d}\zeta(x)\left[\rho_\tau^n(x)-\rho_\tau^m(x)\right]\,\mathrm{d}x+O(\tau)=\sum_{k=m}^{n-1}\tau\int_{\mathbb{R}^d}[\Delta\zeta(x)+x\cdot\nabla\zeta(x)]\,\rho_\tau^{k+1}(x)\,\mathrm{d}x$$
$$-\frac{\chi}{2\,d\,\pi}\sum_{k=m}^{n-1}\tau\iint_{\mathbb{R}^d\times\mathbb{R}^d}\frac{[\nabla\zeta(x)-\nabla\zeta(y)]\cdot(x-y)}{|x-y|^2}\rho_\tau^{k+1}(x)\rho_\tau^{k+1}(y)\,\mathrm{d}x\,\mathrm{d}y, \tag{8.26}$$

On the other hand, we can split

$$\int_{\mathbb{R}^d}\zeta(x)\left[\rho_\tau(t_2,x)-\rho_\tau(t_1,x)\right]\,\mathrm{d}x=\int_{\mathbb{R}^d}\zeta(x)\left[\rho_\tau(t_2,x)-\rho_\tau^n(x)\right]\,\mathrm{d}x$$
$$+\int_{\mathbb{R}^d}\zeta(x)\left[\rho_\tau^n(x)-\rho_\tau^m(x)\right]\,\mathrm{d}x+\int_{\mathbb{R}^d}\zeta(x)\left[\rho_\tau^m(x)-\rho_\tau(t_1,x)\right]\,\mathrm{d}x\,.$$

By Lemma 8.4, we control the bordering averages,

$$\int_{\mathbb{R}^d}\zeta(x)\left|\rho_\tau^m(x)-\rho_\tau(t_1,x)\right|\,\mathrm{d}x\le C\,d_W(\rho_\tau^m,\rho_\tau(t_1,x))\le C\,d_W(\rho_\tau^m,\rho_\tau^{m-1})\le O(\tau^{1/2})\,.$$

In addition, integrating in time Lemma 8.4 implies for all integer $k$, $m\le k\le n-1$,

$$\tau\int_{\mathbb{R}^d}\psi(x)\rho_\tau^{k+1}(x)\,\mathrm{d}x=\int_{k\tau}^{(k+1)\tau}\int_{\mathbb{R}^d}\psi(x)\rho_\tau(s,x)\,\mathrm{d}x\,\mathrm{d}s+O(\tau\;d_W(\rho_\tau^k,\rho_\tau^{k+1}))\,,$$

where $\psi$ denotes any bounded test function. Hence we can transform the discrete in time sum (8.26) into a continuous time integration. Finally, the test contributions are bounded in $L^\infty((0,T)\times\mathbb{R}^d)$ so that the bordering time integrands are negligible,

$$\int_{t_1}^{m\tau}\int_{\mathbb{R}^d}[\Delta\zeta(x)+x\cdot\nabla\zeta(x)]\,\rho_\tau(s,x)\mathrm{d}x\,\mathrm{d}s$$
$$-\frac{\chi}{2\,d\,\pi}\int_{t_1}^{m\tau}\iint_{\mathbb{R}^d\times\mathbb{R}^d}\frac{[\nabla\zeta(x)-\nabla\zeta(y)]\cdot(x-y)}{|x-y|^2}\rho_\tau(s,y)\rho_\tau(s,x)\,\mathrm{d}y\,\mathrm{d}x\,\mathrm{d}s=O(\tau)\,.$$

Collecting all the terms we end up with

$$\int_{\mathbb{R}^d}\zeta(x)\left[\rho_\tau(t_2,x)-\rho_\tau(t_1,x)\right]\,\mathrm{d}x=\int_{t_1}^{t_2}\int_{\mathbb{R}^d}[\Delta\zeta(x)+x\cdot\nabla\zeta(x)]\,\rho_\tau(s,x)\,\mathrm{d}x\,\mathrm{d}s \tag{8.27}$$
$$-\frac{\chi}{2\,d\,\pi}\int_{t_1}^{t_2}\iint_{\mathbb{R}^d\times\mathbb{R}^d}\frac{[\nabla\zeta(x)-\nabla\zeta(y)]\cdot(x-y)}{|x-y|^2}\rho_\tau(s,y)\,\rho_\tau(s,x)\,\mathrm{d}y\,\mathrm{d}x\,\mathrm{d}s+O(\tau^{1/2}).$$

**Step 4.- Passing to the limit**: The relative compactness of the family of curves $\{\rho_\tau\}_{\tau>0}$ in $\mathcal{C}^0([0,T],L^1_{\mathrm{weak}}(\mathbb{R}^d))$ for any $T>0$, allows to pass to the limit in the linear parts of (8.27) because $\nabla\zeta$ and $\Delta\zeta$ are bounded in $L^\infty(\mathbb{R}^d)$. The quadratic last term of (8.27), coming from the concave interaction energy, is more difficult to handle with. Actually, we shall make another use of the doubling of variables' trick: $\rho_\tau\otimes\rho_\tau\rightharpoonup\rho\otimes\rho$

thanks to the equi-integrability, obtained in Lemma 8.3. In addition, recall that the convergence is uniform in time thanks to Ascoli-Arzéla's theorems, and that equi-integrability bounds are also uniform with respect to $\tau$. We can thus pass to the limit when $\tau$ goes to zero in (8.27) to obtain for any $t_1$, $t_2$

$$\int_{\mathbb{R}^d} \zeta(x)\left[\rho(t_2,x)-\rho(t_1,x)\right]\,\mathrm{d}x = \int_{t_1}^{t_2}\int_{\mathbb{R}^d}\left[\Delta\zeta(x)+x\cdot\nabla\zeta(x)\right]\rho(s,x)\,\mathrm{d}x\,\mathrm{d}s \\ -\frac{\chi}{2\,d\,\pi}\int_{t_1}^{t_2}\int_{\mathbb{R}^d\times\mathbb{R}^d}\frac{[\nabla\zeta(x)-\nabla\zeta(y)]\cdot(x-y)}{|x-y|^2}\rho(s,y)\rho(s,x)\,\mathrm{d}y\,\mathrm{d}x\,\mathrm{d}s\ ,$$

which is a formulation of the weak solution as defined in (8.13). □

**Remark 8.9** (Original variables)**.** *This theorem is true in original variables* (8.1) *locally in time, when we consider the free energy* (8.4) *with minor changes, see also* [148]*. However, the long time asymptotics are better understood in scaled variables (see the numerical results, Section* 8.4.2*).*

**Remark 8.10** (Comparison to Literature)**.** *Rigorous convergence of numerical schemes were first obtained by F. Filbet in* [103] *in the non-radial case. His approach relies on the entropy and the Gagliardo-Nirenberg-Sobolev's inequality. However, in our case as we crucially use the free energy functional we are able to prove in Theorem* 8.8 *the convergence of the JKO scheme for all values $\chi < \chi_c$, where $\chi_c$ is known to be optimal. It is worth noticing that the 'minimising movement' scheme is very expensive numerically in dimension greater than one, at least as a direct implicit discretisation detailed in Section* 8.4.2*. Whereas the two-dimensional PKS model is much more manageable following* [103]*.*

*Beyond the optimal threshold, there is another result arguing on this alternative scheme's behalf. Namely for a given $\tau$ the solution $\{\rho_\tau^n\}_n$ is shown to converge towards the unique stationary state, with explicit exponential rate in the one-dimensional case, see next section Proposition* 8.15*.*

**Remark 8.11** (Non-linear diffusions)**.** *The ongoing work extends to non-linear diffusions, under suitable assumptions, $\Delta f(n)$ without deeper difficulty. The main points is that the free energy should be bounded from below – this results from a balance between diffusion at high density level (diffusion must be super-linear at infinity above the optimal threshold) and at low density level (basically $f(u) \gtrsim u^\alpha$ where $\alpha > \max(1/2, 1-2/d)$ preventing mass to escape too fast towards infinity), see* [50] *and* [58]*.*

**Remark 8.12** (Radial case)**.** *In the two-dimensional radial case, one can write a closed equation for the mass inside a ball, see* [187]*. The equation for this radially cumulative function is a local one-dimensional parabolic equation of Burger's type which can be solved in a standard way. As we shall see, we also deal, in dimension 1, with the cumulative distribution functions but leads to a non-local equation. The radial case has already been treated by several authors, see for instance* [39]*. Let us also note that in radial coordinates we loose the gradient flow structure of the equation which is the basis of the JKO scheme.*

## 8.4 One-dimensional Case

In the case of the real line, consider $\mu$ and $\nu$ two absolutely continuous measures with respect to the Lebesgue measure, of respective densities $f$ and $g$. Let $\nabla\varphi$ be the optimal map which transports $\mu$ onto $\nu$. In dimension bigger than one the optimal map is the solution of the following so-called Monge-Ampére equation

$$f = g\circ\nabla\varphi\ \mathrm{Det}\,D^2\varphi\ .$$

which is fully non-linear and cannot be solved in general. However in dimension one, it is a increasing rearrangement as we will discuss below. Let $F$ and $G$ be the cumulative functions of $f$ and $g$. As the cumulative distribution function is non-decreasing we can define the pseudo-inverse function by

$$V(z) = F^{-1}(z) := \inf\{x \,:\, F(x) \geq z\} \,.$$

By Brenier's theorem and the definition of the image measure (8.15), we have

$$F(x) = \int_{-\infty}^{x} f(y)\,\mathrm{d}y = \int_{-\infty}^{\varphi'(x)} g(y)\,\mathrm{d}y = G\circ\varphi'(x) \,.$$

Hence, the transport map can be stated explicitly $\varphi' = G^{-1}\circ F$ and the Wasserstein distance can be expressed in the following more tractable way

$$d_W^2(\mu,\nu) = \int_0^1 |F^{-1}(w) - G^{-1}(w)|^2\,\mathrm{d}w \,. \tag{8.28}$$

In fact, $G^{-1}\circ F$ is the optimal map for all convex costs in dimension one [244, Theorem 2.18].

This expression of the one-dimensional Wasserstein distance has been used for non-linear diffusions and non-linear non-local friction equations in granular media [61, 166, 57] to analyse the long-time asymptotics and the contraction properties with respect to Wasserstein distances of those equations. Moreover, these ideas have first been used in [119, 120] for numerical purposes. Explicit in time numerical schemes for the equations of the inverse distribution function are proposed keeping the contraction of the Wasserstein distance at the discrete level. Here, we prefer to solve it by an implicit in time Euler scheme since it coincides with the JKO scheme through the representation (8.28) and moreover, the contraction property of the Wasserstein distance is not true due to the lack of convexity of the functional $\mathcal{G}$.

More precisely, let $F_n$ and $F_{n+1}$ be the cumulative distribution functions associated respectively to $\rho_\tau^n$ and $\rho_\tau^{n+1}$. By the expression (8.28) of the Wasserstein distance on the real line, the scheme (8.17) can be rewritten in terms of $V_n = F_n^{-1}$ and $V_{n+1} = F_{n+1}^{-1}$ as the gradient flow of the inverse distribution function subject to $L^2-$metric structure:

$$V_{n+1} \in \arg\inf_{\{W\,:\,(W^{-1})'\in\mathcal{K}\}} \left[\tilde{\mathcal{G}}[W] + \frac{1}{2\,\tau}\|W - V_n\|^2_{L^2(0,1)}\right]$$

where

$$\tilde{\mathcal{G}}[W] := -\int_0^1 \log W'(w)\,\mathrm{d}w + \int_0^1 |W(w)|^2\,\mathrm{d}w + \frac{\chi}{\pi}\int_0^1 \log|W(w) - W(z)|\;\mathrm{d}w\,\mathrm{d}z \,.$$

Here the metric is Euclidean, hence the Euler-Lagrange equation associated to this minimisation problem is

$$\frac{V_{n+1} - V_n}{\tau} = -\nabla\tilde{\mathcal{G}}[V_{n+1}] \,,$$

where $\nabla$ is the usual gradient operator in $L^2(\mathbb{R})$. This Euler-Lagrange equation can be rewritten

$$-\frac{V_{n+1}(w) - V_n(w)}{\tau} = \frac{\partial}{\partial w}\left[\left(\frac{\partial V_{n+1}(w)}{\partial w}\right)^{-1}\right] + V_{n+1}(w) + \chi H[V_{n+1}] \tag{8.29}$$

where $\tilde{H}$ is related to the Hilbert transform and is defined by

$$\tilde{H}[V](w) := \frac{1}{\pi}\lim_{\varepsilon\to 0}\int_{|V(w)-V(z)|\geq\varepsilon} \frac{1}{V(w) - V(z)}\,\mathrm{d}z \,.$$

For sake of simplicity we assume that the space step is constant, equal to $h$. If we set $V_n^i := V_n(ih)$, for any $i = 0\cdots N$, and $Nh = 1$, the finite difference discretisation in space of (8.29) is the following implicit Euler scheme in rescaled variables,

$$-\frac{V_{n+1}^i - V_n^i}{\tau} = \frac{1}{V_{n+1}^{i+1} - V_{n+1}^i} - \frac{1}{V_{n+1}^i - V_{n+1}^{i-1}} + V_{n+1}^i + \frac{\chi h}{\pi}\lim_{\varepsilon\to 0}\sum_{j:|V_{n+1}^i - V_{n+1}^j|\geq\varepsilon} \frac{1}{V_{n+1}^i - V_{n+1}^j} \,. \tag{8.30}$$

with initial condition $V_0 = \rho_0$. We impose Neumann boundary conditions in the $\rho-$problem (8.11), *i.e.* for any $n$, $\frac{1}{V_n^N - V_n^{N-1}} = 0$ and $\frac{1}{V_n^1 - V_n^0} = 0$, so that the 'centre of mass' is conserved:

$$\forall n \ \sum_{i=0}^{N} V_n^i = 0.$$

The solution at each time step of the non-linear system of equations is obtained by an iterative Newton-Raphson procedure.

**Remark 8.13** (Higher dimensions)**.** *A way to extend the previous numerical scheme to higher dimensions is to solve an equivalent $L^2$ gradient flow for diffeomorphisms proposed in* [100]*. The price to pay is that one needs to solve a fully non-linear coupled system of $d$ partial differential equations.*

### 8.4.1 Exponential Convergence in 1-D

Here comes the second main improvement and motivation for this numerical scheme. In addition to convergence as the time step goes to zero, we are able to show that for a fixed $\tau > 0$, the discrete solution converges to a unique steady state as time goes to infinity. First we prove existence of this steady state equilibrium, see Proposition 8.14. Uniqueness and convergence follow from Proposition 8.15.

**Proposition 8.14.** *Let $(V^i)_i$ be an increasing sequence. The discrete free energy functional defined as*

$$\tilde{\mathcal{G}}_h[V] = -\sum_{i=1}^{N-1} h \log\left(\frac{V^{i+1} - V^i}{h}\right) + \frac{1}{2}\sum_{i=1}^{N} h|V^i|^2 + \frac{\chi}{2\pi}\sum_{i=1}^{N}\sum_{j=1,\ j\neq i}^{N} h^2 \log|V^j - V^i|,$$

*is coercive and bounded from below if $\chi(1-h) < \chi_c = 2\,\pi$.*

*Proof.* We shall adapt to the discrete setting the so-called Logarithmic Hardy-Littlewood-Sobolev (8.9) and Carleman inequalities, see Lemma 8.2.

**Step 1: A discrete Logarithmic Hardy-Littlewood-Sobolev inequality**. We will prove the following discrete Logarithmic Hardy-Littlewood-Sobolev inequality

$$\sum_{i=1}^{N}\sum_{j=1, j\neq i}^{N} h^2 \log|V^j - V^i| \geq (1-h)\sum_{i=1}^{N-1} h \log\left(\frac{V^{i+1} - V^i}{h}\right) + C_h. \tag{8.31}$$

Observe that the space step $h$ modifies the apparent space dimension: the factor $d_h := 1 - h$ replaces $d = 1$ in front of the entropy term. Observe also that the correcting factor $d_h$ is the only admissible one for homogeneity reasons. In fact, when $V$ is multiplied by $\lambda > 0$ (think of $\lambda \to 0$ or $\lambda \to \infty$), then inequality (8.31) is violated if $d_h \neq 1 - h$: the additional term $h(N-1)\big(hN - (1-h)\big)\log\lambda$ comes out, and $hN = d_h$.

The left-hand-side in (8.31) can be reorganised as following, where the increasingness of $(V^i)_i$ is

crucially used:

$$\begin{aligned}
\sum_{i=1}^{N}\sum_{j=1,j\neq i}^{N} h^2\log|V^j-V^i| &= \sum_{i=1}^{N}\sum_{j=i+1}^{N} h^2\log(V^j-V^i)+\sum_{i=1}^{N}\sum_{j=1}^{i-1} h^2\log(V^i-V^j)\\
&\geq \sum_{i=1}^{N-1}\sum_{j=i+1}^{N} h^2\log(V^{i+1}-V^i)+\sum_{k=1}^{N-1}\sum_{j=1}^{k} h^2\log(V^{k+1}-V^j)\\
&\geq \sum_{i=1}^{N-1} h^2(N-i)\log(V^{i+1}-V^i)+\sum_{k=1}^{N-1} h^2k\log(V^{k+1}-V^k)\\
&= \sum_{i=1}^{N-1} h(hN)\log(V^{i+1}-V^i)\\
&= d_h\sum_{i=1}^{N-1} h\log\left(\frac{V^{i+1}-V^i}{h}\right)+C_h\ ,
\end{aligned}$$

which proves the discrete Logarithmic Hardy-Littlewood-Sobolev inequality (8.31).
**Step 2: A discrete Carleman inequality**. We shall prove next the following inequality:

$$-\sum_{i=1}^{N-1} h\log\left(\frac{V^{i+1}-V^i}{h}\right)+\frac{1}{2}\sum_{i=1}^{N} h|V_i|^2\geq C_h. \tag{8.32}$$

Introduce the median of the sequence $(V^i)_i$, that is select $k^0$ such that $|V^{k_0}|=\min|V^k|$. Within this choice we have in particular: $V^k\leq 0$ for $k<k_0$ and $V^k\geq 0$ for $k>k_0$. Thus we obtain

$$\begin{aligned}
&-\sum_{i=1}^{N-1} h\log\left(\frac{V^{i+1}-V^i}{h}\right)+\frac{1}{2}\sum_{i=1}^{N} h|V^i|^2\\
&\geq -\sum_{i=1}^{N-1} h\log\Big(\frac{V^{i+1}-V^i}{h}\Big)+\frac{1}{2}\sum_{i=1,i\neq k_0}^{N} h|V^i|^2\\
&= -h(N-1)\sum_{i=1}^{k_0-1}\frac{1}{N-1}\log\Big((V^{i+1}-V^i)\mathrm{e}^{-\frac{1}{2}|V^i|^2}\Big)\\
&\qquad -h(N-1)\sum_{i=k_0}^{N-1}\frac{1}{N-1}\log\Big((V^{i+1}-V^i)\mathrm{e}^{-\frac{1}{2}|V^{i+1}|^2}\Big)+C_h\\
&\geq -h(N-1)\log\left[\frac{1}{N-1}\left(\sum_{i=1}^{k_0-1}(V^{i+1}-V^i)\mathrm{e}^{-\frac{1}{2}|V^i|^2}+\sum_{i=k_0}^{N-1}(V^{i+1}-V^i)\mathrm{e}^{-\frac{1}{2}|V^{i+1}|^2}\right)\right]+C_h\\
&\geq C_h\ ,
\end{aligned}$$

thanks to Jensen inequality, and the peculiar choice of $k_0$. The last minoration step comes from:

$$\begin{aligned}
&\sum_{i=1}^{k_0-1}\mathrm{e}^{-\frac{1}{2}|V^i|^2}(V^{i+1}-V^i)+\sum_{i=k_0}^{N-1}\mathrm{e}^{-\frac{1}{2}|V^{i+1}|^2}(V^{i+1}-V^i)\\
&\leq \sum_{i=1}^{k_0-1}\mathrm{e}^{-\frac{1}{2}|V^i|^2}|V^i|+\mathrm{e}^{-\frac{1}{2}|V^{k_0-1}|^2}|V^{k_0}|+\mathrm{e}^{-\frac{1}{2}|V^{k_0+1}|^2}|V^{k_0}|+\sum_{i=k_0}^{N-1}\mathrm{e}^{-\frac{1}{2}|V^{i+1}|^2}|V^{i+1}|\\
&\leq C_h\ ,
\end{aligned}$$

because the function $\mathrm{e}^{-\frac{1}{2}|X|^2}|X|$ is uniformly bounded and $|V^{k_0}|\leq\min\{|V^{k_0-1}|,|V^{k_0+1}|\}$.

**Step 3: Coercivity of the discrete free energy**. As a by-product of discrete Logarithmic Hardy-Littlewood-Sobolev and Carleman inequalities we obtain the following coercivity *a priori* estimate ensuring the existence of a minimiser (which is the stationary state we are looking for). Define $\theta = \dfrac{\chi(1-h)}{2\pi} < 1$ and deduce from the discrete Logarithmic Hardy-Littlewood-Sobolev inequality (8.31) that

$$\tilde{\mathcal{G}}_h[V] \geq (1-\theta)\left( -\sum_{i=1}^{N-1} h \log\Big(\frac{V^{i+1}-V^i}{h}\Big)\right) + \frac{1}{2}\sum_{i=1}^{N} h|V^i|^2 + C_h \ . \tag{8.33}$$

Then apply the discrete Carleman inequality (8.32) to eventually obtain

$$\tilde{\mathcal{G}}_h[V] \geq \frac{\theta}{2}\sum_{i=1}^{N} h|V^i|^2 + C_h,$$

□

As a by-product we obtain existence of a stationary state realised as a minimiser of the free energy functional. Indeed, it remains to show that a minimising sequence cannot "blow-up" in the sense that $V_{i+1}-V_i$ is prevented to vanish. If so, this would contradict the upper-bounded obtained above in (8.33).

**Proposition 8.15** (Convergence in the sub-critical case)**.** *Assume that $\chi(1-h) < \chi_c$. Then the solution of the numerical scheme* (8.30) *converges to the unique steady-state of the problem with exponential rate.*

*Proof.* First we need the following two characterisations of the unique equilibrium state. The uniqueness will in fact follow from the convergence proof, as we shall see later (Remark 8.16). The discrete function $(V_*^i)_i$ is an equilibrium if and only if

$$\forall i \quad 0 = \frac{1}{V_*^{i+1}-V_*^i} - \frac{1}{V_*^i - V_*^{i-1}} + V_*^i + \frac{\chi}{\pi}\sum_{j\neq i} h\frac{1}{V_*^i - V_*^j}, \tag{8.34}$$

or equivalently

$$\forall k \quad (V_*^{k+1}-V_*^k)\left\{\frac{\chi}{\pi}\sum_{j=0}^{k}\sum_{i=k+1}^{N} h\frac{1}{V_*^i-V_*^j} - \sum_{i=0}^{k} V_*^i\right\} = 1. \tag{8.35}$$

To see that (8.34) and (8.35) are equivalent, rewrite the latter as

$$\forall k \quad \frac{1}{V_*^{k+1}-V_*^k} = \frac{\chi}{\pi}\sum_{j=0}^{k}\sum_{i=k+1}^{N} h\frac{1}{V_*^i-V_*^j} - \sum_{i=0}^{k} V_*^i,$$

then 'derive' the ongoing expression in a discrete way,

$$\begin{aligned}\frac{1}{V_*^{k+1}-V_*^k} - \frac{1}{V_*^k - V_*^{k-1}} &= \frac{\chi}{\pi}\sum_{j=0}^{k}\sum_{i=k+1}^{N} h\frac{1}{V_*^i-V_*^j} - \frac{\chi}{\pi}\sum_{j=0}^{k-1}\sum_{i=k}^{N} h\frac{1}{V_*^i-V_*^j} - V_*^k \\ &= \frac{\chi}{\pi}\sum_{i=k+1}^{N} h\frac{1}{V_*^i-V_*^k} - \frac{\chi}{\pi}\sum_{j=0}^{k-1} h\frac{1}{V_*^k-V_*^j} - V_*^k.\end{aligned}$$

We proceed as computing the time evolution of the $L^2-$distance between $V_n$ and the stationary state $V_*$.

$$\begin{aligned}\frac{1}{2\tau}\Big(\|V_{n+1}-V_*\|^2 - \|V_n - V_*\|^2\Big) &= \frac{1}{2\tau}\sum_i h(V_{n+1}^i - V_n^i)(V_{n+1}^i + V_n^i - 2V_*^i) \\ &= \sum_i h\frac{V_{n+1}^i - V_n^i}{\tau}(V_{n+1}^i - V_*^i) - \frac{1}{2\tau}\sum_i h(V_{n+1}^i - V_n^i)^2.\end{aligned}$$

We then input the evolution equation for $V_{n+1} - V_n$, and obtain thanks to (8.34),

$$\begin{aligned}\frac{1}{2\tau}\Big(\|V_{n+1}-V_*\|^2 - \|V_n - V_*\|^2\Big) &\leq -\sum_i h\Big(\frac{1}{V^{i+1}-V^i} - \frac{1}{V^i - V^{i-1}} - \frac{1}{V_*^{i+1}-V_*^i} \\ &\quad + \frac{1}{V_*^i - V_*^{i-1}} + V^i - V_*^i + \frac{\chi}{\pi}\sum_{j\neq i} h\frac{1}{V^i - V^j} \\ &\quad - \frac{\chi}{\pi}\sum_{j\neq i} h\frac{1}{V_*^i - V_*^j}\Big)(V^i - V_*^i) \\ &= A_n + B_n + C_n,\end{aligned}$$

where $V$ stands for $V_{n+1}$ without any ambiguity. We integrate by part the first (diffusion) contribution,

$$\begin{aligned}A &= -\sum_i h\Big(\frac{1}{V^{i+1}-V^i} - \frac{1}{V^i - V^{i-1}} - \frac{1}{V_*^{i+1}-V_*^i} + \frac{1}{V_*^i - V_*^{i-1}}\Big)(V^i - V_*^i) \\ &= \sum_i h\Big(\frac{1}{V^{i+1}-V^i} - \frac{1}{V_*^{i+1}-V_*^i}\Big)(V^{i+1} - V_*^{i+1} - V^i + V_*^i).\end{aligned}$$

We have carefully used the boundary conditions $\frac{1}{V^N - V^{N-1}} = 0$ and $\frac{1}{V^1 - V^0} = 0$. We can rewrite $A$ using zero-homogeneity of the last expression, namely

$$A = \sum_i h\gamma\Big(\frac{V^{i+1}-V^i}{V_*^{i+1}-V_*^i}\Big),$$

where $\gamma(\lambda) = 2 - \lambda - \lambda^{-1}$ is concave and non-positive. The second contribution coming from variables rescaling is obvious but crucial, namely

$$B = -\sum_i h(V^i - V_*^i)^2 = -\|V_{n+1} - V_*\|^2.$$

The last (interaction) contribution is more tricky to handle with, and involves variables doubling, as it is known from granular media, see [61]. We have

$$\begin{aligned}C &= -\frac{\chi}{\pi}\sum_i h\Big(\sum_{j\neq i} h\frac{1}{V^i - V^j} - \sum_{j\neq i} h\frac{1}{V_*^i - V_*^j}\Big)(V^i - V_*^i) \\ &= -\frac{\chi}{2\pi}\sum_{i,j,i\neq j} h^2\Big(\frac{1}{V^i - V^j} - \frac{1}{V_*^i - V_*^j}\Big)(V^i - V^j - V_*^i + V_*^j) \\ &= -\frac{\chi}{2\pi}\sum_{i,j,i\neq j} h^2\gamma\Big(\frac{V^i - V^j}{V_*^i - V_*^j}\Big).\end{aligned}$$

Notice that the above expression is symmetric between the two possible choices $i < j$ and $j < i$. We shall also make use of the concavity property of $\gamma$ as following,

$$\begin{aligned}C &= -2\frac{\chi}{2\pi}\sum_{j<i} h^2\gamma\Big(\sum_{j\leq k<i}\frac{V^{k+1}-V^k}{V_*^{k+1}-V_*^k}\cdot\frac{V_*^{k+1}-V_*^k}{V_*^i - V_*^j}\Big) \\ &\leq -\frac{\chi}{\pi}\sum_{i<j} h^2\sum_{j\leq k<i}\gamma\Big(\frac{V^{k+1}-V^k}{V_*^{k+1}-V_*^k}\Big)\frac{V_*^{k+1}-V_*^k}{V_*^i - V_*^j} \\ &= -\frac{\chi}{\pi}\sum_k h\gamma\Big(\frac{V^{k+1}-V^k}{V_*^{k+1}-V_*^k}\Big)(V_*^{k+1} - V_*^k)\sum_{j=0}^{k}\sum_{i=k+1}^{N} h\frac{1}{V_*^i - V_*^j} \\ &\leq -\sum_k h\gamma\Big(\frac{V^{k+1}-V^k}{V_*^{k+1}-V_*^k}\Big)(V_*^{k+1} - V_*^k)\left\{\frac{\chi}{\pi}\sum_{j=0}^{k}\sum_{i=k+1}^{N} h\frac{1}{V_*^i - V_*^j} - \sum_{i=0}^{k} V_*^i\right\},\end{aligned}$$

where we have used the fact that $D_k := \sum_{i=0}^{k} V_*^i$ is a non-positive quantity for all $k$.

Let us prove this last claim. Indeed, $D_{k+1} - D_{k-1} - 2\,D_k = V_*^{k+1} - V_*^k \geq 0$. Hence, $D_{k+1} - D_k \geq D_{k-1} - D_k$. Since $D_N = 0$ and $D_0 = V_*^0 \leq 0$, there exists $k_0$ such that $(D_k)_{1\leq k\leq k_0}$ is non-decreasing and $(D_k)_{k_0\leq k\leq N}$ is non-increasing. As a consequence $D_k \leq D_0 \leq 0$ for any integer $k$, $1 \leq k \leq k_0$ and $D_k \leq D_N = 0$ for any integer $k$, $k_0 + 1 \leq k \leq N$ which proves the assertion.

At this stage we bring in the alternative representation of the stationary solution (8.35), so that $A + C \leq 0$. As a consequence we obtain

$$\frac{1}{2\tau}\Big(\|V_{n+1} - V_*\|^2 - \|V_n - V_*\|^2\Big) \leq -\|V_{n+1} - V_*\|^2. \tag{8.36}$$

We finally get the exponential convergence rate,

$$\|V_n - V_*\|^2 \leq \Big(\frac{1}{1+2\tau}\Big)^n \|V^0 - V_*\|^2.$$

If $\tau$ is small, we can thus approximate $\log(1+2\tau) \approx 2\tau$ and $\left(\frac{1}{1+2\tau}\right)^n \approx \exp(-2n\tau) \approx \exp(-2t)$. Thus, the bound on the rate, we find, does not depend on the parameter $\chi < \chi_c$. □

**Remark 8.16** (Uniqueness of Stationary Solution)**.** *We can deduce* a posteriori *the uniqueness of the equilibrium. As a matter of fact let consider another equilibrium state $\tilde{V}_*$ and set $V_{n+1} = V_n = \tilde{V}_*$ in the above computations. We eventually obtain $\|\tilde{V}_* - V_*\| \leq 0$ from* (8.36)*, which proves the uniqueness.*

To complete the picture, we shall prove here that the discrete approximation (8.30) (without the drift term) "blows-up" in finite time in the supercritical case $(1-h)\chi > \chi_c$, in the sense that the iterations cannot be recursively handled forever. In fact at some point some increment $V_n^{i+1} - V_n^i$ may vanish, breaking the scheme. We proceed as for the continuous viriel method, by computing the evolution of the "second momentum", that is the $L^2-$norm of $(V_n)$ in this context. It is shown to vanish eventually in finite time, which is an obstruction.

**Proposition 8.17** (Blow-up of the discrete solution)**.** *Assume we are in the supercritical case $\chi(1-h) > \chi_c$ then the Keller-Segel steepest-descent scheme (without a drift term) blows-up in finite time.*

*Proof.* We follow exactly the proof of Proposition 8.15, where integration by parts and symmetrisation of the "kernel" were already performed.

$$\begin{aligned}
\frac{1}{2\tau}\left(\|V_{n+1}\|^2 - \|V_n\|^2\right) &= \frac{1}{2\tau}\sum_i h(V_{n+1}^i - V_n^i)\left(V_{n+1}^i + V_n^i\right)\\
&= \sum_i h\frac{V_{n+1}^i - V_n^i}{\tau}V_{n+1}^i - \frac{1}{2\tau}\sum_i h\left(V_{n+1}^i - V_n^i\right)^2\\
&\leq \sum_i h\frac{V_{n+1}^i - V_n^i}{\tau}V_{n+1}^i\\
&\leq \sum_i h\left(\frac{1}{V^{i+1} - V^i} - \frac{1}{V^i - V^{i-1}} + \frac{\chi}{\pi}\sum_{j\neq i} h\frac{1}{V^i - V^j}\right)V^i\\
&= A + B\ ,
\end{aligned}$$

where $V$ stands for $V_{n+1}$ without any ambiguity. In fact

$$A = \sum_i h\,\frac{V^{i+1} - V^i}{V^{i+1} - V^i} = 1\ ,$$

and, doubling the sum,

$$\begin{aligned} C &= -\frac{\chi}{2\pi}\sum_{i,j,i\neq j} h^2 \frac{V^i - V^j}{V^i - V^j} \\ &= -\frac{\chi h^2}{2\pi} N\,(N+1) = -\frac{\chi(1-h)}{2\pi}\ . \end{aligned}$$

Thus, in case of $(1-h)\chi > \chi_c$ the second momentum decreases at least linearly in time, ensuring "blow-up" after a finite time. □

**Remark 8.18** (Original Variables)**.** *When coming back in the continuous setting to the original variables $n(t,x)$ by* (8.10)*, we are not able to show even that*

$$n(t,x) = n^\infty(t,x) + O_W(1),$$

*where $n^\infty$ is the dilatation of the stationary state,*

$$n^\infty(t,x) = \frac{1}{1+2t} V_*\left(\frac{x}{\sqrt{1+2t}}\right),$$

*and $O_W$ means infinitesimal in the $d_W$ sense. The reason is that the found estimate on the speed of convergence does not depend on the reduced parameter $\chi$, but only on the variables rescaling, and the change of variables restores back exactly the factor $e^t$ due to the scaling properties of $d_W$* [244, 62]*. This result should be improved as seen from the numerical experiments below and it is an open problem how to get a faster speed of convergence in the scaled equation leading to a polynomial decay in original variables. In fact, we conjecture that if we fix the centre of mass then the rate on convergence of the solution to the stationary solution in rescaled variables is of order $\mathrm{e}^{-2t}$. This fact coincides with other situations as in nonlinear diffusions in which fixing certain invariants of the equation improves the rate of convergence* [83]*. Certainly the situation is close to the heat equation for small mass solutions* [94]*.*

In the next subsections, we will show some numerical experiments for the PKS equation using the scheme (8.30). We begin with the sub-critical case $\chi = \pi$ (remind that in dimension one the critical parameter is $\chi_c = 2\,\pi$) for the not rescaled (Section 8.4.2) as opposed to the rescaled system (Section 8.4.2). We next approach the critical parameter plugging $\chi = 1.8\pi$, and initialise the scheme with a two-peaks density $n_0$ (*resp.* Sections 8.4.2 and 8.4.2). We then investigate the upper-critical case starting with respectively a single peak (Section 8.4.3), two symmetric peaks attracting each other (Section 8.4.3) and two asymmetric peaks (Section 8.4.4).

In the following, we assume a uniform in space discretisation $w_i = ih,\ i = 0\ldots N$, and $Nh = 1$.

### 8.4.2 Sub-critical case

#### Not rescaled case

Starting with the centred initial data,

$$V_0^i = 2\,\frac{w_i - 0.5}{\left[(w_i + 0.01)\,(1.01 - w_i)\right]^{1/4}}\ ,$$

corresponding to a compact supported density $n_0$, we numerically solve the PKS equation on the time interval $[0, 400]$ with $\chi = \pi$. Figures 8.1 and 8.2 show the evolution of the solution both for the density (Fig. 8.2) and its inverse distribution function (Fig. 8.1).

Observe in Figure 8.1 that the branches of the inverse cumulative function $V$ goes eventually to $\pm\infty$. This is expected because the support of the cell density spreads as time goes on, and therefore the distribution tails are wider. Remind that in the sub-critical regime, the diffusion process dominates. The

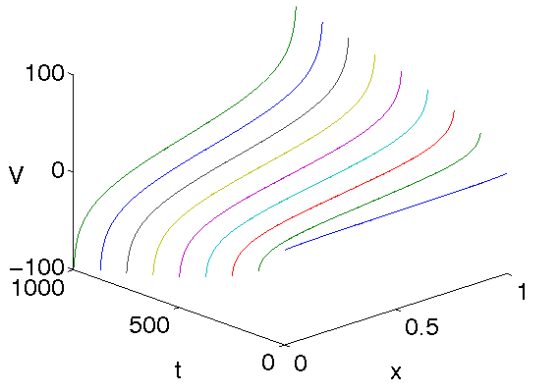


Figure 8.1: Inverse cumulative distribution function for $\chi = \pi$. Note that the initial data seems to be flat relatively to the very large scale on the $V-$axis, as opposed to Figure 8.5.

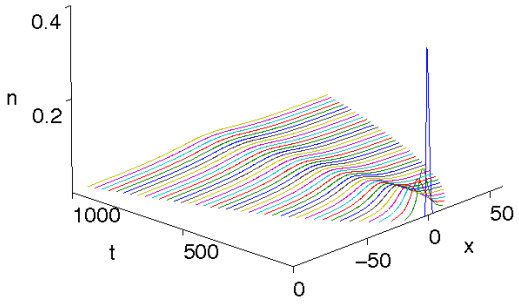


Figure 8.2: Cell density $n$ as time evolves, obtained from its inverse cumulative distribution function. Accordingly to Figure 8.1, the space scale is also very large, and therefore the density seems highly concentrated at $t = 0$.

scheme captures well the collapse down to zero of the cell density and the spreading of the solution. Interestingly, this scheme handles easily with moving density's support (note that finite speed of propagation is a numerical artifact) whereas the reference domain $[0, 1]$ is fixed because we deal with probability densities (mass is conserved).

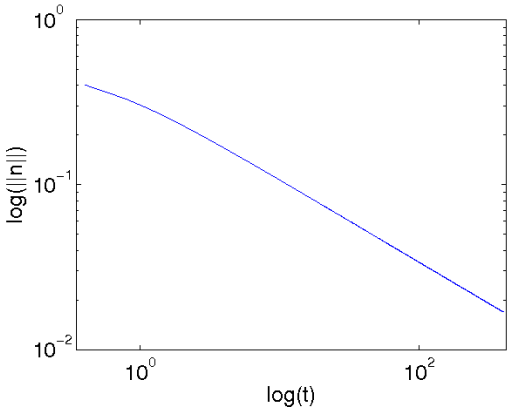


Figure 8.3: $L^2$-norm's evolution for the cell density $n$, in a $\log - \log$ scale. The decay appears to be polynomial.

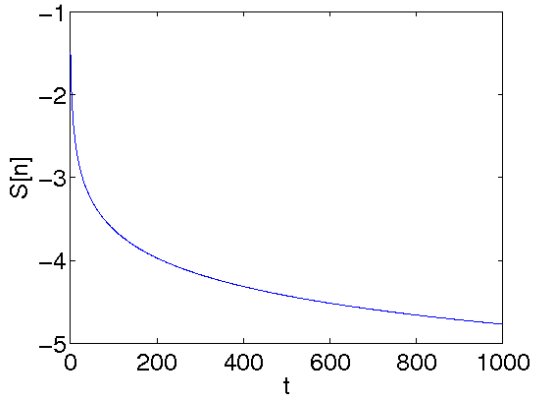


Figure 8.4: Evolution of the entropy $\mathcal{S}[n]$ showing slow decay.

Moreover, the spreading towards zero seems to be polynomial from Figure 8.3 showing the evolution of the $L^2$-norm of the cell density in log-log scale. The entropy decay is plotted in Figure 8.4.

**Rescaled variables:** $\chi = \pi$

Given the compactly supported initial data,

$$V_0^i = 2\,\frac{w_i - 0.5}{\left[(w_i + 0.01)\,(1.01 - w_i)\right]^{1/4}}\,,$$

we numerically solve the PKS equation in rescaled variables on the time interval $[0, 5]$ with $\chi = \pi$ (corresponding results are shown in figures 8.5 and 8.6, 8.7 and 8.8).

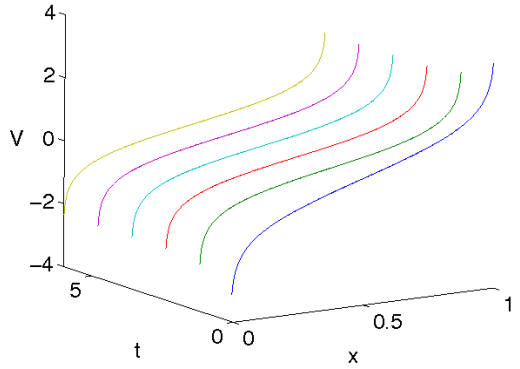


Figure 8.5: Fast convergence towards the stationary solution for $\chi = \pi$ and rescaled variables.

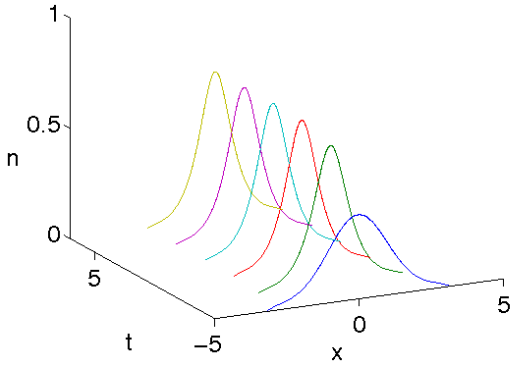


Figure 8.6: Evolution of the corresponding cell density $n$.

Contrary to previous Section 8.4.2, we observe an exponential convergence towards the stationary solution (see Figures 8.5 and 8.7). When computing the Wasserstein distance between the density at time $t$ and the expected stationary solution (last computed time), we find out that the convergence is faster than $e^{-t}$ (Figure 8.7) obtained in Proposition 8.15. This confirms the open problem of trying to find a better decay rate in scaled variables that will eventually lead to a polynomial decay rate towards self-similarity in original variables for sub-critical masses.

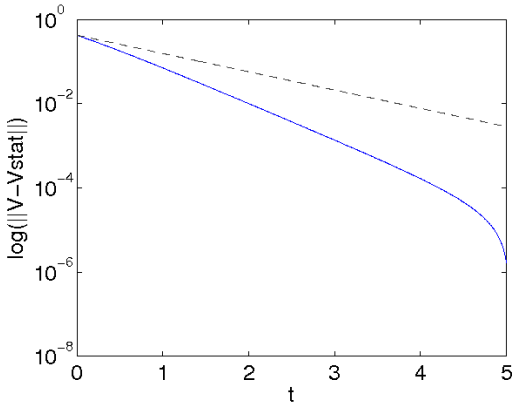


Figure 8.7: Wasserstein distance between the density at time $t$ and the final computed density assumed to be almost the stationary solution. Dashline: decay rate proved in Proposition 8.15.

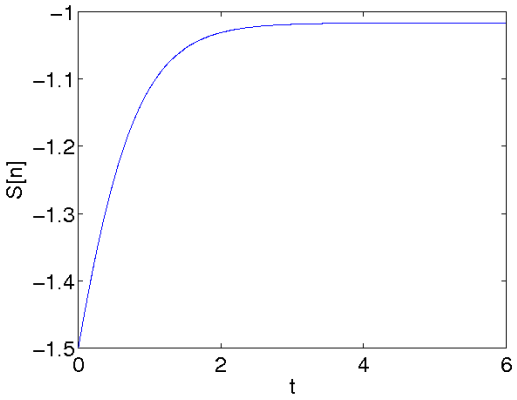


Figure 8.8: Evolution of the entropy.

**Rescaled variables:** $\chi = 1.8\pi$

Given the compactly supported initial data,

$$V_0^i = 2\,\frac{w_i - 0.5}{\left[(w_i + 0.01)\,(1.01 - w_i)\right]^{1/4}}\,,$$

we numerically solve the PKS equation in rescaled variables on the time interval $[0, 5.5]$ with $\chi = 1.8\pi$. Figures 8.9 and 8.10 show the evolution of the solution.

The initial data is the same as in Section 8.4.2 but $\chi$ is closer to the critical parameter $\chi_c$. The solution again converges exponentially to the stationary solution (see Figures 8.9 and 8.10). According

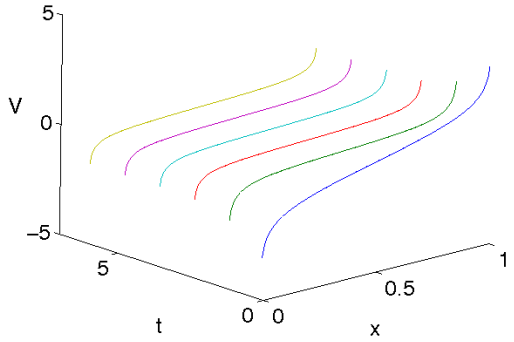


Figure 8.9: Cumulative distribution function $V$ for the sub-critical case $\chi = 1.8\pi < \chi_c$.

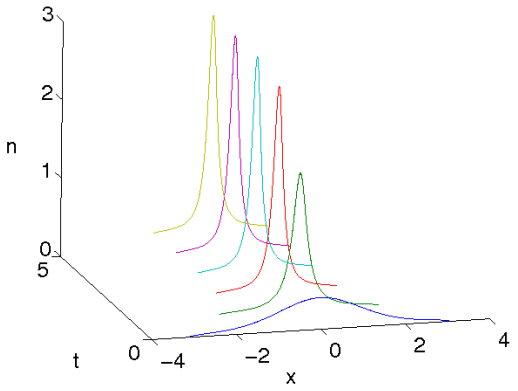


Figure 8.10: Evolution of the cell density $n$.

to Proposition 8.15, the rate of convergence is at least the same as in Section 8.4.2, compare Fig. 8.11 to Fig. 8.7 and the slope are the same (of order $e^{-2t}$). On the other hand, the equilibrium state is more concentrated (Fig. 8.10), corresponding to a flat plateau in Fig. 8.9, as we expect it converges to a Dirac mass.

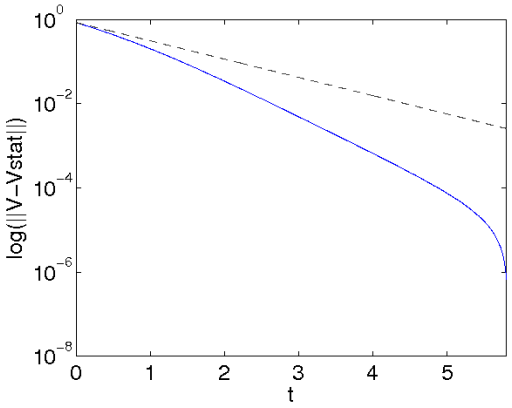


Figure 8.11: Wasserstein distance between the density at time $t$ and the final computed density assumed to be almost the stationary solution. Dashline: decay rate proved in Proposition 8.15.

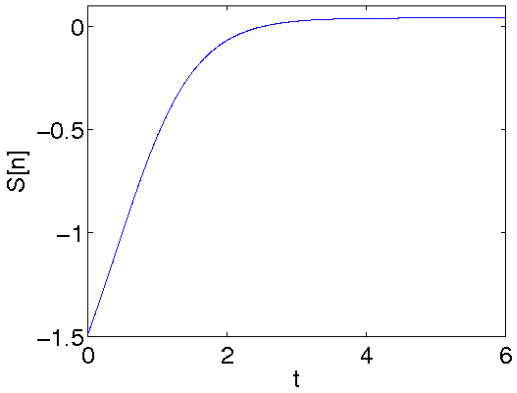


Figure 8.12: Evolution of the entropy.

### Two peaks initial data

Initialise with the centred cumulative distribution function,

$$V_0^i = \frac{\exp\left[10\ (w_i - 0.5)\right] - 1}{\left[(w_i + 0.01)\,(1.01 - w_i)\right]^{1/4}}\ ,$$

corresponding to a two-peaks like density with compact support. We numerically solve the PKS equation in rescaled variables on the time interval $[0, 5]$ with $\chi = \pi$.

Whereas the parameter $\chi$ is the same as in Section 8.4.2, the initial data is qualitatively different. The two peaks diffuse, eventually merging and finally converging to the stationary solution with exponential speed (see Figures 8.13 and 8.14). Let us finally mention that the numerical scheme does not preserve

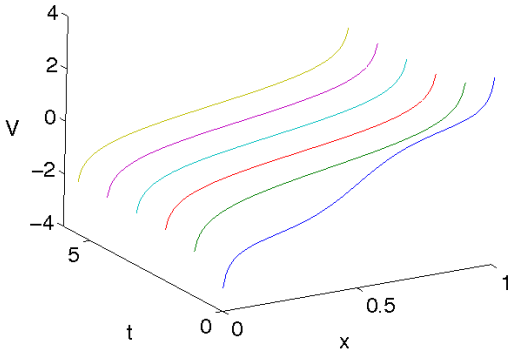


Figure 8.13: Cumulative distribution function $V$ for $\chi = \pi$ and a two-peaks initial condition.

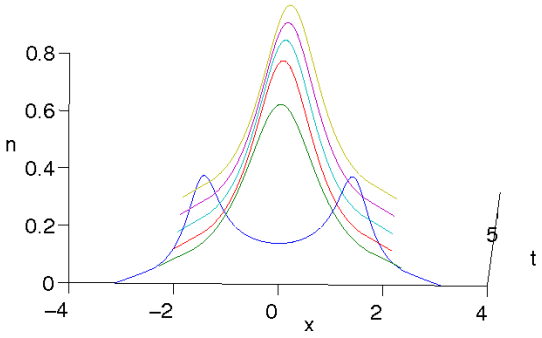


Figure 8.14: Cell density $n$.

the exact value of the critical mass. The scheme does not preserve the law of evolution of the second moment. However, with the same initial data as in the first two subsections, the numerical critical mass is situated between $1.973\pi$ and $1.974\pi$.

### 8.4.3 Super-critical case

#### Single peak initial data

Given the compactly supported initial data,

$$V_0^i = 2\,\frac{w_i - 0.5}{\left[(w_i + 0.01)\,(1.01 - w_i)\right]^{1/4}}\,,$$

we numerically solve the PKS equation in original variables on the time interval $[0, 0.32]$ with $\chi = (5/2)\,\pi$. Note that in the upper-critical case, the variables' rescaling seems to play no role.

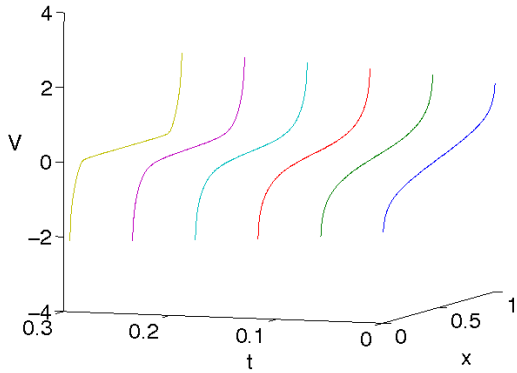


Figure 8.15: Cumulative distribution function $V$ for $\chi > \chi_c$. The solution blows-up exhibiting a plateau in finite time.

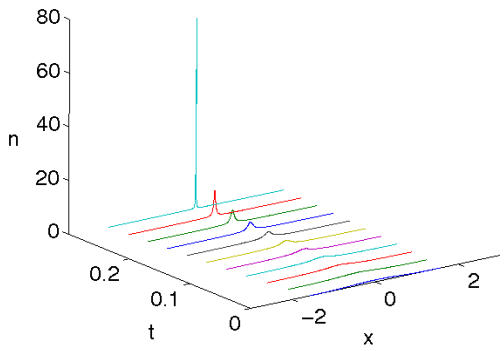


Figure 8.16: Cell density $n$. We observe blow-up in finite time.

The solution blows-up in finite time (either a flat portion or a highly concentrated region appears, *resp.* Figure 8.15 and Figure 8.16). Visualised in Wasserstein distance (namely the square root of the second momentum), the convergence to the Dirac mass located at zero seems to be linear in time (see Figure 8.17) as it should be from the theoretical viewpoint. However the computed distance does not

reach zero in finite time. This is not surprising, because when blow-up occurs, part of the mass is still away from the blow-up point (here, zero). In order to see some vanishing distance, one can normalise the process in the following away: localise the Wasserstein distance in the transport variable ($L^2-$distance for the cumulative distribution function), to capture only the final plateau. This plateau is *a priorily* known from the beginning because it is entirely determined by the ratio $\chi_c/\chi$. However this does not provide any new insight of what happens after blow-up, and it is known from theoretical works that the behaviour highly depends upon the regularisation procedure [240, 241, 87].

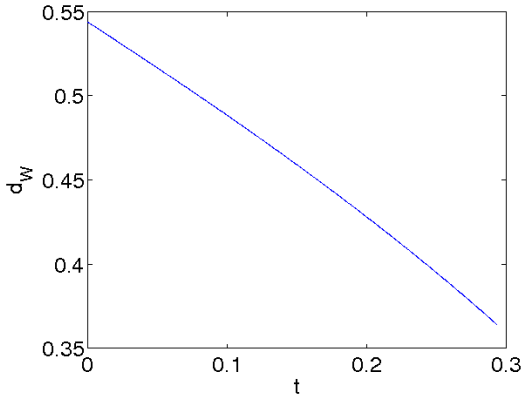


Figure 8.17: Wasserstein distance to the Dirac mass at zero $\delta_0$. Blow-up occurs previously, and part of the mass has not yet reached zero at this time.

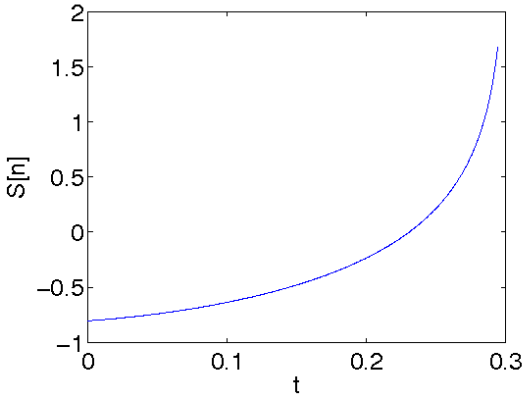


Figure 8.18: The variation of the entropy $\mathcal{S}[n]$ seems to blow-up.

Interestingly, numerics are able to track the blow-up phenomenon quite precisely, without mesh refinement. Indeed, if the space step is even uniform, the number of space points at the density level adapt to the highly concentrated (blow-up) regions, corresponding to plateaus (compare Figure 8.15 and Figure 8.16). This is the counterpart of the 'moving support' observed in Section 8.4.2.

**Two symmetric peaks: case $\chi = 3\,\pi$**

Given the compactly supported initial data,

$$V_0^i = \frac{\exp\left[10\ (w_i - 0.5)\right] - 1}{\left[(w_i + 0.01)\,(1.01 - w_i)\right]^{1/4}}\ ,$$

we numerically solve the PKS equation in original variables on the time interval $[0, 1.3]$ with $\chi = 3\,\pi$.

The factor $\chi$ is super-critical but is less than $2\,\chi_c$. Then, according to the conjectures in [239, 240, 241] there should be only one blow-up point. The density first diffuses (see Figure 8.20) and then concentrates in a delta Dirac (see Figures 8.19 and 8.21).

**Two symmetric peaks: case $\chi = 5\,\pi$**

Starting with the centred cumulative distribution function,

$$V_0^i = \frac{\exp\left[10\ (w_i - 0.5)\right] - 1}{\left[(w_i + 0.01)\,(1.01 - w_i)\right]^{1/4}}\ ,$$

corresponding to a two-peaks like initial density, we numerically solve the PKS equation in original variables on the time interval $[0, 0.45]$ with $\chi = 5\,\pi$.

The initial condition is the same as in Section 8.4.3 but $\chi$ is now bigger than $2\,\chi_c$. The blow-up occurs in two different points (see Figures 8.23 and 8.24).

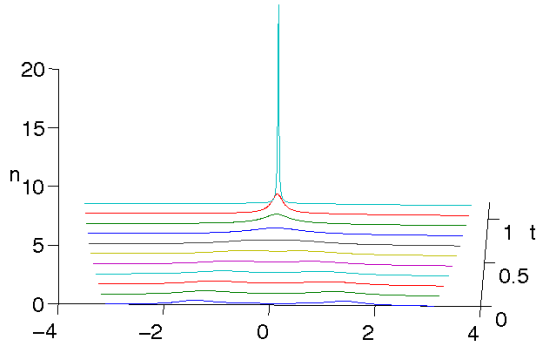


Figure 8.19: Cell density $n$ for $\chi = 3\pi$ and two initial peaks.

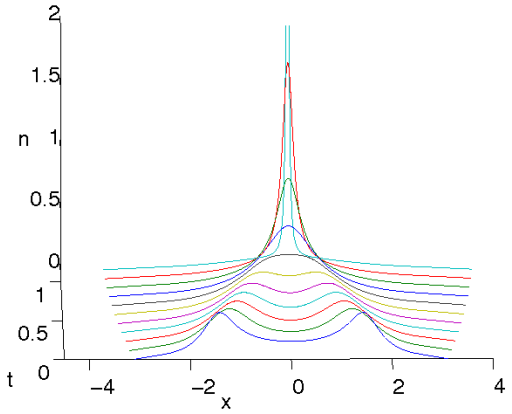


Figure 8.20: Zoom of Figure 8.19. Because both two peaks do not contain enough mass to blow-up far from each other, they first merge, then the solution blows-up.

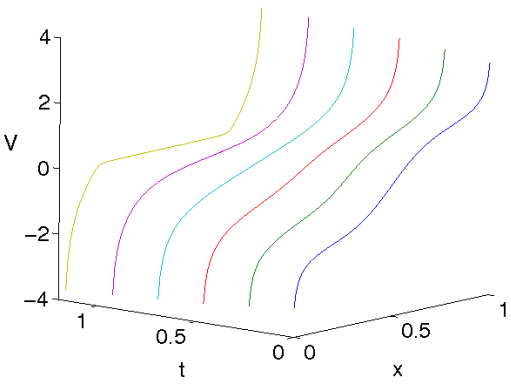


Figure 8.21: Cumulative function distribution function $V$ for $\chi = 3\pi$ and two initial plateaus (that is, density peaks). The solution flattens into a single plateau.

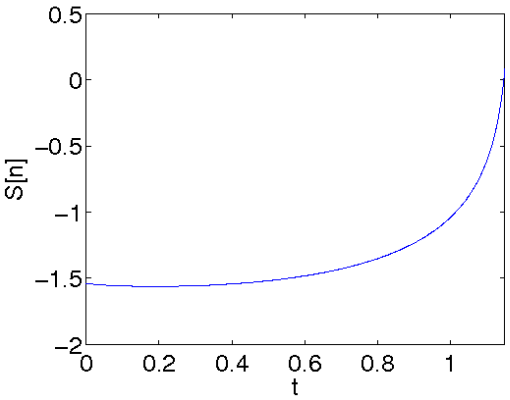


Figure 8.22: Evolution of the entropy.

### 8.4.4 Two asymmetric peaks

Given the compactly supported initial data,

$$V_0^i = \frac{\exp\left[10\ (w_i - 0.45)\right] - 1}{\left[(w_i + 0.01)\,(1.01 - w_i)\right]^{1/4}}\ ,$$

we numerically solve the PKS equation in original variables on the time interval $[0, 1.1]$ with $\chi = 3\,\pi$. Note that the initial density is not centred, but it has no effect because proposition 8.15 does not hold in this case.

When the parameter is between the critical parameter $\chi_c$ and twice the critical parameter $2\,\chi_c$, if the peaks are asymmetric the blowup occurs at the centre of mass which is closer to the highest peak. The peaks diffuses and then the density blows-up at the centre of mass (see Figures 8.25 and 8.26).

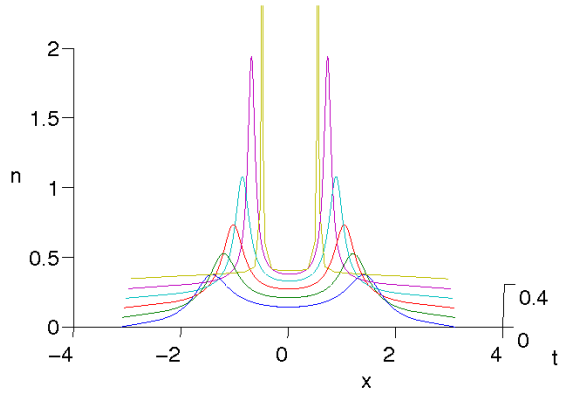


Figure 8.23: Cell density $n$ for two initial peaks and $\chi = 5\pi$. As opposed to the previous Section 8.4.3, each peak contains enough mass to blow-up itself.

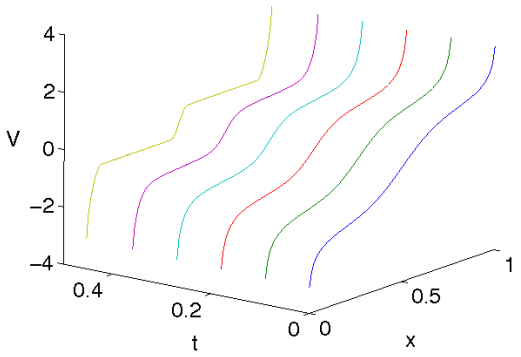


Figure 8.24: Cumulative distribution function $V$. Two distinct plateaus may appear when $\chi$ is above twice the critical parameters $\chi_c$.

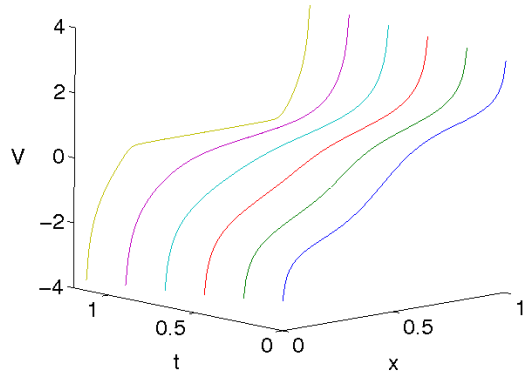


Figure 8.25: Cumulative distribution function $V$ when $\chi \in (\chi_c, 2\,\chi_c)$, and initial data is a two-peaks like density.

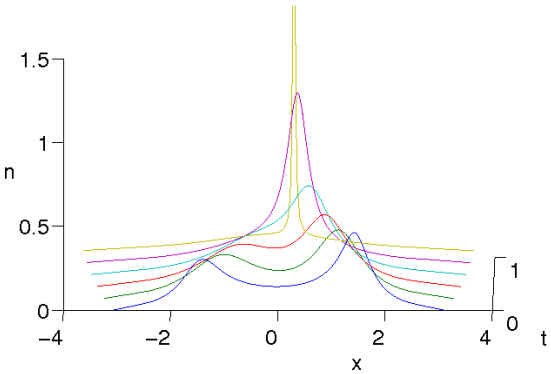


Figure 8.26: Evolution of the cell density $n$.

# Annexes

# Annexe A

# Numérique autour de KS

Dans cette première annexe nous regroupons et développons l'aspect numérique de cette thèse. Nous présentons successivement, par ordre d'originalité croissante, le modèle de KS radial à deux dimensions, puis le modèle KS 2D sans symétrie particulière, éventuellement avec effets volumiques (voir chapitre 1). Vient ensuite le modèle à 3 espèces de recrutement local des macrophages (partie II) qui exhibe une transition entre plaques homogènes et anneaux concentriques, suite au phénomène de masse critique. Cette annexe s'achève avec des illustrations du schéma discret de flot gradient pour la distance de Wasserstein appliqué à KS 1D (avec, là encore, des effets de volume). Ces dernières figures viennent compléter celles déjà obtenues au chapitre 8.

Le but de cette partie n'est pas d'apporter des réponses tranchées à des problèmes théoriques, mais plutôt de fournir des illustrations aussi précises que possible (du phénomène d'explosion, de la masse critique de cellules nécessaire à l'explosion dans le cas linéaire ou non-linéaire, des différentes hypothèses adéquates).

## A.1 Le cas de la symétrie radiale

La symétrie radiale présente un avantage décisif : elle permet de se ramener à une seule équation, locale qui plus est, après élimination de l'équation de la variable chimique $c$, au prix bien entendu de coefficients singuliers à l'origine.

### A.1.1 Le modèle radial 2D

On considère un domaine $\Omega = \mathcal{B}(0,R) \subset \mathbb{R}^2$ (éventuellement $R = \infty$). Dans le cas d'une donnée initiale $n_0$ à symétrie radiale, le modèle est plus simple à étudier. On réécrit le modèle à symétrie radiale : $n(t,x) = n(t,r),\ r \in (0,R)$ par abus de notation.

$$\left\{ \begin{array}{rcl} \dfrac{\partial n}{\partial t} & = & \dfrac{1}{r}\dfrac{\partial}{\partial r}\Big(r\dfrac{\partial n}{\partial r}\Big) - \dfrac{1}{r}\dfrac{\partial}{\partial r}\Big(r\chi n\dfrac{\partial c}{\partial r}\Big) \\ -\dfrac{1}{r}\dfrac{\partial}{\partial r}\Big(r\dfrac{\partial c}{\partial r}\Big) & = & n - \dfrac{M}{|\Omega|} \end{array} \right. \tag{A.1}$$

On peut alors se ramener à une seule équation sur la masse de cellules contenues dans une boule de rayon $r$ :

$$N(t,r) = 2\pi \int_0^r \rho n(t,\rho) d\rho \ ,$$

qui vérifie des conditions aux bords de type Dirichlet : $N(t,0) = 0$ et $N(t,R) = M$. En intégrant la seconde équation dans (A.1)

$$-r\frac{\partial c}{\partial r} = \frac{1}{2\pi}\left( N(t,r) - M\Big(\frac{r}{R}\Big)^2 \right) \ ,$$

et par là même (A.1) se réduit à une seule équation aux dérivées partielles

$$\frac{\partial N}{\partial t} = r\frac{\partial}{\partial r}\Big(\frac{1}{r}\frac{\partial N}{\partial r}\Big) + \frac{\chi}{2\pi r}\frac{\partial N}{\partial r}\left(N - M\Big(\frac{r}{R}\Big)^2\right) \ . \tag{A.2}$$

Une précieuse conséquence de cette unique équation est de disposer maintenant d'un principe de comparaison entre les solutions (ce qui était inenvisageable jusque là). Il s'agit du principe de comparaison pour une équation de Burgers à coefficients non constants [224, 79].

**Proposition A.1** (Principe de comparaison)**.** *Si $N_1$ et $N_2$ sont deux solutions définies sur $[0,T]$ telles que $\forall r\ N_1(0,r) \le N_2(0,r)$ ; alors*

$$\forall t < T\ \forall r \in [0,R] \quad N_1(t,r) \le N_2(t,r)$$

En radial, le comportement des solutions est plus simple que dans un domaine sans symétrie particulière, et se rapproche dans un sens du cas où $\Omega = \mathbb{R}^2$ [187, 141].

**Théorème A.2** (Nagai)**.** *Si $\Omega = \mathcal{B}(0,R)$ et si $n_0$ est à symétrie radiale,*

*(i) si $\chi M < 8\pi$ il y a existence globale*[10]*,*

*(ii) si $\chi M > 8\pi$ et si le moment d'ordre 2 est suffisamment petit, alors il y a explosion en temps fini, au centre de la boule. Si $R = \infty$, on demande à ce que le second moment soit fini [208, 209].*

Il existe des versions plus récentes et beaucoup plus fines de ce résultat grâce aux travaux récents de Laurençot et collaborateurs. En particulier l'asymptotique de l'explosion en temps infini est décrite précisément pour la masse critique $M = 8\pi/\chi$ [30, 31], et un théorème optimal d'existence est énoncé pour des coefficients de diffusion et de chémosensitivité non-linéaires (toujours dans le cas radial) [164]. Il est à noter que l'équation choisie pour la synthèse chimique évince alors la condition de petitesse du second moment sur un disque borné (voir aussi le chapitre 2).

*Démonstration.* On va démontrer assez rapidement le point (i) grâce à un argument de comparaison. On va s'appuyer sur les états stationnaires du problème dans tout l'espace et sur un principe de sur-solution [208]. Un état stationnaire dans tout l'espace vérifie donc d'après (A.2), après le changement de variable $s = r^2$,

$$\begin{aligned} 2\partial_s\big(s\partial_s \mathbf{N}_\lambda\big) - 2\partial_s \mathbf{N}_\lambda + \frac{\chi}{4\pi}\big(\mathbf{N}_\lambda^2\big) &= 0 \\ s\partial_s \mathbf{N}_\lambda - \mathbf{N}_\lambda\Big(1 - \frac{\chi}{8\pi}\mathbf{N}_\lambda\Big) &= 0 \end{aligned}$$

Les solutions de cette équation avec les conditions aux limites de Dirichlet adéquates forment une famille paramétrée par $\lambda > 0$ caractérisée par

$$M = M_{\text{crit}} = \frac{8\pi}{\chi}\,, \quad \mathbf{N}_\lambda(r) = \frac{8\pi}{\chi}\frac{r^2}{\lambda + r^2}\ .$$

Un calcul rapide montre que $\mathbf{N}_\lambda$ est une sur-solution de l'équation sur $[0,R]$. En effet

$$\partial_t \mathbf{N} - 2s\partial_{ss}^2 \mathbf{N} - \frac{\chi}{2\pi}\partial_s \mathbf{N}\left(\mathbf{N} - M\frac{s}{S}\right) = \frac{\chi}{2\pi}\partial_s \mathbf{N}\left(M\frac{s}{S}\right) \ge 0\ .$$

Si $\chi M < 8\pi$, on obtient finalement par comparaison $N(t,\cdot) \le \mathbf{N}_\lambda$ à condition d'avoir initialement $\forall r\ N(0,r) \le \mathbf{N}_\lambda(r)$ et en particulier $M < \dfrac{8\pi}{\chi}\dfrac{R^2}{\lambda + R^2}$. On voit que l'on peut choisir $\lambda > 0$ aussi petit que l'on veut, ce qui ne garantit pas $N(0) \le \mathbf{N}_\lambda$ pour autant. Pour y remédier, Perthame introduit une dépendance temporelle $\lambda(t)$ qui permet de prendre en compte le degré de liberté en $\lambda$ de manière 'optimale' [208]. □

Par ailleurs, on peut se demander si la condition de petitesse du second moment est nécessaire dans (ii), ou si c'est un artefact de démonstration[11]. C'est le but de la section A.1.3. Mais présentons auparavant quelques résultats numériques pour le système (A.1).

[10] il n'y a pas d'effet de bord en quelque sorte.

[11] en effet, si le domaine est l'espace $\mathbb{R}^2$ tout entier, et que le second moment est fini, il y a explosion en temps fini.

### A.1.2 Explosion auto-similaire

Comme nous venons de le voir, le théorème de Nagai précise les conditions de l'explosion. Notamment lorsque la masse est supérieure à la masse critique $8\pi/\chi$, il y a éventuellement explosion en temps fini au centre du disque. Une question subséquente est le comportement asymptotique de la solution à l'approche du temps d'explosion (voir [130, 39] pour la dimension $d \geq 3$). Dans un article désormais célèbre, Herrero et Velázquez [131] ont construit formellement une solution qui explose en temps fini et possède une invariance d'échelle auto-similaire au voisinage du point d'explosion :

$$n(t,r) \approx \frac{1}{R(t)^2}\varphi\big(\frac{r}{R(t)}\big) \ ,$$

lorsque $r \leq KR(t)$. La méthode est celle des 'matched asymptotic expansions' (voir aussi [247]). Il s'agit de découper le domaine en une zone proche 'inner' et une zone éloignée 'outer' du point d'explosion, puis de résoudre indépendamment l'équation dans ces zones, et enfin de recoller les deux solutions grâce à certaine condition de compatibilité. Cette solution a le profil d'équilibre $\varphi(r) = \dfrac{8\pi}{\chi}\dfrac{1}{\pi(1+r^2)^2}$, ainsi que le taux d'explosion

$$R(t) \sim C\exp\Big(-\frac{1}{2}\tau - \frac{1}{\sqrt{2}}\sqrt{\tau} + \big(\frac{1}{4\sqrt{\tau}} - \frac{1}{4}\big)\log\tau\Big)$$

où $\tau = log(T-t)^{-1}$, autrement dit $R(t) \approx C\sqrt{T-t} \times$ (correction).

Un tel comportement auto-similaire a été mis en évidence numériquement dans [43] par exemple. De notre côté nous nous sommes attachés à retrouver cette dynamique dans un premier exercice de confrontation numérique avec KS.

Une premier choix pour résoudre KS radial est d'introduire le changement de variable $r = \exp(\zeta)$, $\zeta \in (-\infty, \log R)$, tel que $r\dfrac{\partial}{\partial r} = \dfrac{\partial}{\partial \zeta}$. Alors (A.1) devient

$$\left\{\begin{array}{rcl} e^{2\zeta}\dfrac{\partial n}{\partial t} & = & \dfrac{\partial^2 n}{\partial \zeta^2} - \dfrac{\partial}{\partial \zeta}\Big(\chi n \dfrac{\partial c}{\partial \zeta}\Big) \ , \\ -\dfrac{\partial^2 c}{\partial \zeta^2} & = & e^{2\zeta}\big(n - \langle n\rangle\big) \ . \end{array}\right.$$

Ceci a au moins deux avantages notables : premièrement le nouveau système a une forme plus sympathique car la diffusion et l'advection sont homogènes en espace, deuxièmement une grille régulière en $\zeta$ signifie une accumulation de points à l'origine, ce qui est intéressant pour suivre l'explosion. A chaque étape en temps, on calcule successivement $c(t+dt)$ à partir de $n(t)$ ; puis $n(t+dt)$ à partir de $c(t+dt)$ grâce à un schéma aux différences finies implicite en temps.

Afin de suivre l'explosion de manière précise il est également envisageable d'effectuer le changement de variables auto-similaire

$$y = \frac{r}{\sqrt{T-t}} \ , \quad \tau = \log(T-t)^{-1}$$

et la renormalisation

$$n = (T-t)^{-1}u(\tau, y) \ , \quad c = v(\tau, y) \ .$$

Les équations pour $u$ et $v$ deviennent respectivement :

$$\left\{\begin{array}{l} \partial_\tau(yu) + \partial_y\big(\dfrac{1}{2}y^2 u\big) = \partial_y\big(y\partial_y u - \chi yu\partial_y v\big) \ , \\ \partial_\tau(yv) + \dfrac{1}{2}y^2\partial_y v = \partial_y\big(y\partial_y v\big) + yu \ . \end{array}\right. \tag{A.3}$$

Un terme de dérive apparaît pour retenir en quelque sorte la densité cellulaire loin de l'origine.

**Remarque A.3.** *Deux difficultés au moins sont soulevées par le système renormalisé* (A.3) *:*

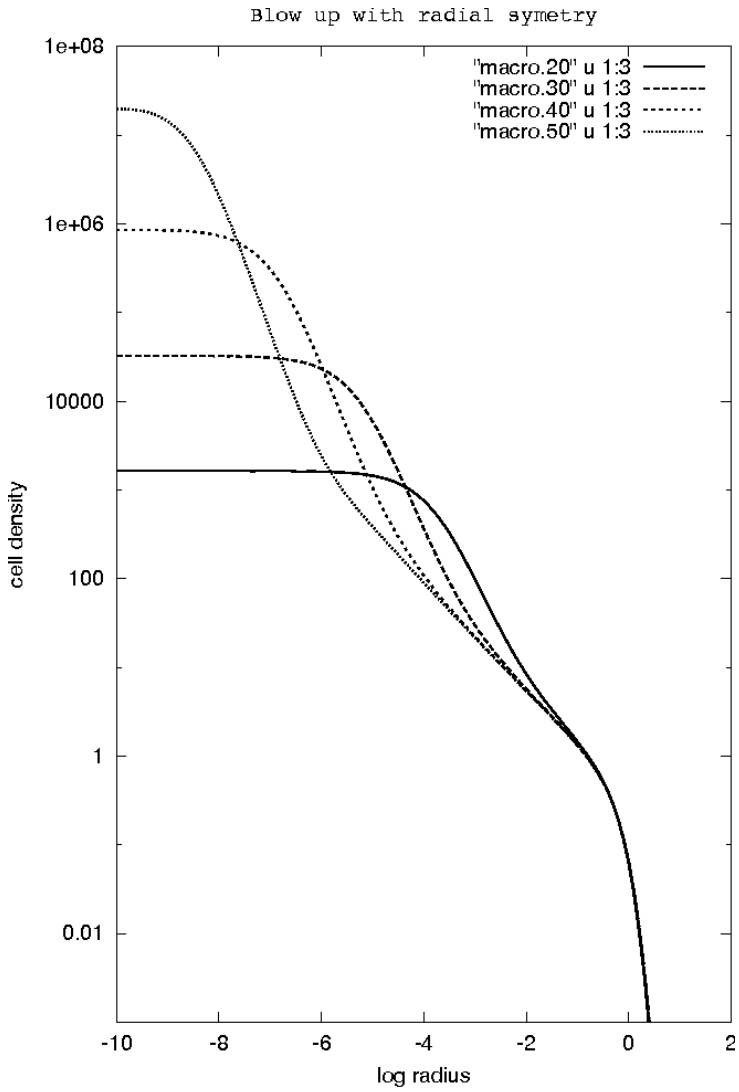


FIG. A.1 – Explosion en temps fini d'une solution à symétrie radiale (l'échelle est logarithmique en abscisse et en ordonnée). Le comportement auto-similaire' de la solution au voisinage du point et du temps d'explosion est à rapprocher des travaux d'Herrero & Velázquez [131] qui ont construit théoriquement une solution avec un profil auto-similaire dans une région voisine du point d'explosion (*the inner region* tout à fait repérable ici). On appelle solution auto-similaire une solution qui reproduit un profil par changements d'échelle au cours du temps, par exemple dans le cas présent (la masse est conservée) $n(t,r) \approx R(t)^{-2}\varphi\big(rR(t)^{-1}\big)$.

– *les conditions au bord : le domaine étant maintenant de taille variable, comment adapter les conditions au bord ? En réalité, plusieurs indices laissent à penser que cela n'a aucune importance si le domaine initial est assez grand (idéalement $\mathcal{I} = \mathbb{R}_+$). Pour être plus exact, il faudrait étudier les flux au voisinage du bord à droite pour voir si beaucoup de masse se créé/disparaît à droite en $y = R\,(T-t)^{-1/2}$.*
– *la donnée initiale : le temps d'explosion $T$ a disparu des équations, mais il est contenu dans la donnée initiale qui se doit de subir le changement de variables. Il faudrait donc estimer au préalable le temps d'explosion à l'aide de la méthode directe, puis injecter la donnée initiale correspondante dans le nouveau système.*

### A.1.3 La condition portant sur le second moment est-elle nécessaire ?

Au regard du théorème A.2(ii) on peut ouvertement s'interroger quant à la nécessité de la condition de petitesse du second moment sur un disque borné. Y a-t'il explosion dès que la masse est supérieure à $8\pi$, ou bien faut-il que les cellules soient initialement suffisamment concentrées ? Dans la suite nous proposons deux réponses relativement simples à cette question. Il apparaît que les cellules doivent effectivement être suffisamment concentrées (en domaine borné) pour que l'explosion ait lieu. Mieux, cette concentration initiale requise est de plus en plus accentuée lorsque $M$ est proche de la masse critique.

**Première réponse.** $\mathcal{N}^u(t,r) = M\Big(\dfrac{r}{R}\Big)^2$ est un état stationnaire de (A.2) (correspondant à la distribution uniforme de cellules).

**Corollaire A.4.** *Si initialemment $N(0,r) \le M\Big(\dfrac{r}{R}\Big)^2$ alors il y a existence globale et*

$$\forall t \ge 0\ \forall r \quad N(t,r) \le M\Big(\frac{r}{R}\Big)^2 .$$

**Remarque A.5.** *Ceci montre déjà que si à $t = 0$ les cellules sont 'moins concentrées' que la distribution uniforme, il ne peut y avoir explosion. Mais cette comparaison n'est pas très intéressante, car cela ne règle pas le problème de la donnée initiale d'un amas de cellules localisé (des données initiales 'moins concentrées' que la distribution uniforme font plutôt penser à des anneaux, des couronnes de cellules).*

**Deuxième réponse.**

**Résultat numérique A.6.** *Si $\chi M > 8\pi$, l'équation admet un état stationnaire supplémentaire. Cet état d'équilibre correspond à une répartition de plus en plus concentrée lorsque $\chi M \to 8\pi+$ : si l'on note $\mathcal{N}^{nu}$ ce nouvel état, $\mathcal{N}^{nu}(r, \chi M)$ est une fonction décroissante de $\chi M$.*

*Démonstration.* Sans perte de généralité, on choisit par commodité $\chi = 1$ et $R = 1$ (voir plus loin). On cherche à résoudre l'équation stationnaire

$$r\frac{d}{dr}\left(\frac{1}{r}\frac{dN}{dr}\right) + \frac{1}{2\pi r}\frac{dN}{dr}\big(N - Mr^2\big) = 0 .$$

On pose $A(r) = \dfrac{1}{2\pi}\big(N - Mr^2\big)$ et $B(r) = \dfrac{M}{\pi} - \dfrac{1}{2\pi r}\dfrac{dN}{dr}$, c'est-à-dire que $A(r)$ est la différence avec l'état stationnaire trivial, et $B(r) = \langle n\rangle - n$ en termes de densité. Alors

$$\left\{\begin{array}{rcl} \dfrac{dA}{dr} & = & -rB\ , \\ \dfrac{dB}{dr} & = & \dfrac{A}{r}\big(-B + \dfrac{M}{\pi}\big)\ . \end{array}\right.$$

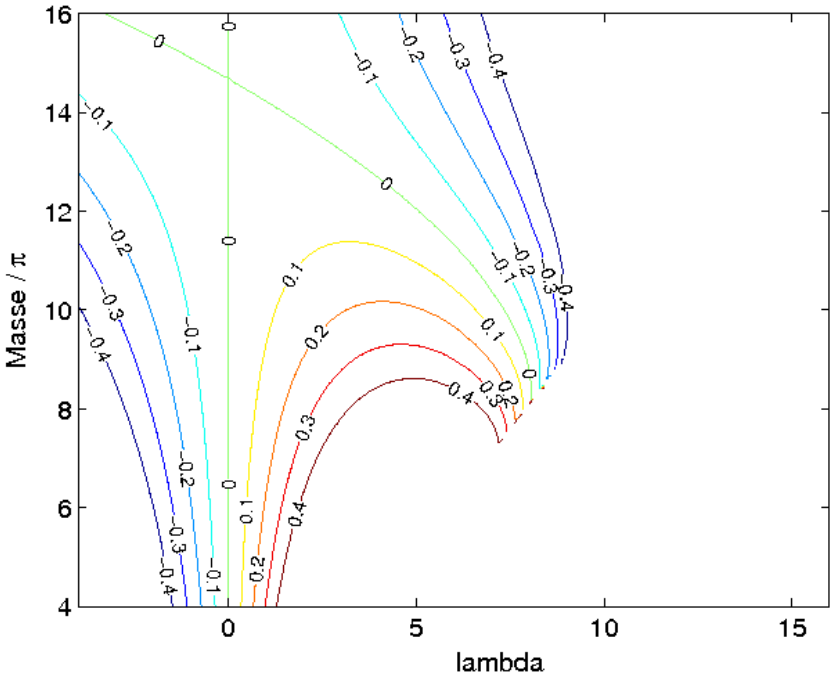


FIG. A.2 – Isoclines de la fonction $(\lambda, M/\pi) \to A(\infty)$. Un nouvel état stationnaire pour (A.2) (*i.e.* $A(\infty) = 0$) apparaît dès que $M > 8\pi/\chi$.

Pour résoudre ce système différentiel, on renverse le domaine $[0;1]$ puis on envoye la singularité $r = 0$ en $+\infty$ grâce au changement de variable $r = \exp(-\xi)$.

$$\left\{ \begin{array}{rcl} \dfrac{dA}{d\xi} & = & \exp(-2\xi)B \ , \\ \dfrac{dB}{d\xi} & = & A\big(B - \dfrac{M}{\pi}\big) \ . \end{array} \right. \tag{A.4}$$

Il est nécessaire de transcrire également les données au bord dans la nouvelle variable. Les conditions de Dirichlet étaient $N(r=0) = 0\,,\ N(r=1) = M$. Elles deviennent $A(\xi = 0) = 0\,,\ A(\xi = +\infty) = 0$. Afin de détecter un nouvel état stationnaire différent de l'état stationnaire trivial (qui correspond à $A(u) \equiv 0$), on résout le problème de Cauchy (A.4) avec les conditions initiales $A(0) = 0\,,\ B(0) = \lambda$ pour différents $\lambda \leq \dfrac{M}{\pi}$, et on traque une solution qui vérifie $A(+\infty) = 0$ ('méthode de tir'). On se convainc aisément que si $\lambda > \dfrac{M}{\pi}$ alors la condition $A(+\infty) = 0$ est impossible (dans ce cas $A$ est croissant !). Ceci correspond d'ailleurs à une condition initiale $n_0(r=1) < 0$.

On a tracé à la figure A.2 les isoclines de l'application *numérique* qui à $\lambda$ et $M/\pi$ associe $A(+\infty)$. On constate qu'une nouvelle ligne de niveau $A(+\infty) = 0$ surgit pour $M/\pi > 8$, c'est à dire pour $\chi M > 8\pi$. On remarque de plus que ce nouvel état stationnaire coïncide avec l'état trivial pour $\chi M$ aux alentours de $15\pi$. □

**Corollaire A.7.** *(Voir figure A.3) Si $\chi M \gtrsim 8\pi$ alors la solution doit être très concentrée initialement pour qu'il y ait explosion.*

**Remarque A.8.** *Il semble que pour $\chi M \lesssim 15\pi$ ce nouvel état d'équilibre soit instable. On a tracé pour $\chi M = 10\pi$ l'évolution de deux perturbations au dessus et en dessous de ce nouvel état stationnaire*

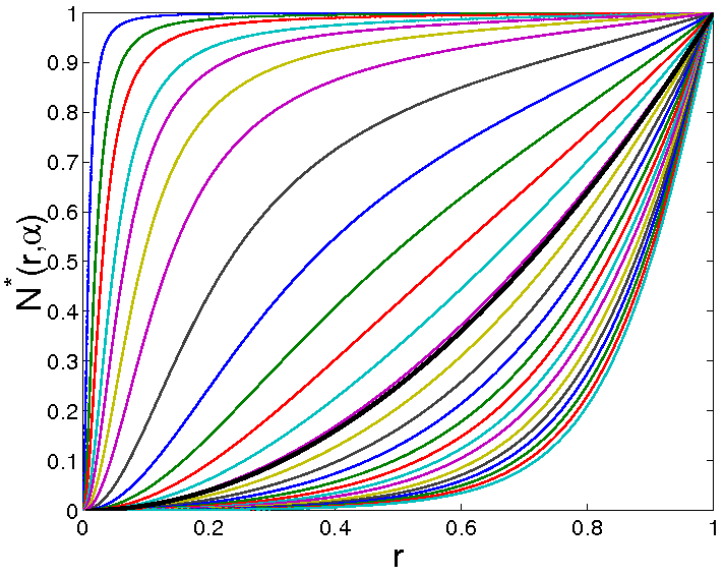


FIG. A.3 – Graphe du nouvel état stationnaire pour l'intervalle $[0;1]$ et pour différentes valeurs de $\alpha = \chi M$. Contrairement à la description du texte, on a renormalisé toutes les fonctions pour avoir une masse totale $M = 1$. Lorsque $\chi M \to 8\pi+$ cet état tend vers la fonction partout égale à 1, tandis que lorsque $\chi M \to \infty$ ce nouvel état s'écrase en zéro. On a tracé en gras l'état d'équilibre trivial qui correspond à une répartition uniforme de cellules. Les valeurs de $\chi M/\pi$ sont (du haut vers le bas) 8,01 ; 8,05 ; 8,1 ; 8,2 ; 8,3 ; 8,5 ; 8,8 ; 9,5 ; 10,5 ; 11,5 ... 27,5.

*(respectivement figures A.4 (a) et (b)). Cependant il reste du travail à faire pour étudier le comportement d'une perturbation qui ne satisfait pas à la comparaison.*

**Echelle de l'équation et des états stationnaires.** On présente rapidement l'adimensionnement de l'équation qui justifie *a posteriori* que l'on puisse poser $R = 1$ et disposer d'un seul paramètre ($\chi$ ou $M$, c'est selon). Rappelons qu'un état stationnaire sur $[0;R]$ vérifie l'équation

$$r\frac{\partial}{\partial r}\Big(\frac{1}{r}\frac{\partial N}{\partial r}\Big) + \frac{\chi}{2\pi r}\frac{\partial N}{\partial r}\left(N - M\Big(\frac{r}{R}\Big)^2\right) = 0 \ .$$

On peut tout d'abord renormaliser la masse en posant $\tilde{N} = \dfrac{N}{M}$. L'équation devient

$$r\frac{\partial}{\partial r}\Big(\frac{1}{r}\frac{\partial \tilde{N}}{\partial r}\Big) + \frac{\chi M}{2\pi r}\frac{\partial \tilde{N}}{\partial r}\left(\tilde{N} - \Big(\frac{r}{R}\Big)^2\right) = 0 \ .$$

Puis on se ramène à l'intervalle $[0;1]$ grâce au changement $u = \dfrac{r}{R}$. Le rayon $R$ disparaît de l'équation qui devient

$$u\frac{\partial}{\partial u}\Big(\frac{1}{u}\frac{\partial \tilde{N}}{\partial u}\Big) + \frac{\alpha}{2\pi u}\frac{\partial \tilde{N}}{\partial u}\big(\tilde{N} - u^2\big) = 0 \ .$$

On a ainsi fait apparaître le paramètre important $\alpha = \chi M$ qui détermine principalement la dynamique du problème et on constate que pour le nouvel état d'équilibre qui nous intéresse :

$$\mathcal{N}^{nu}_{[0;R]}(r,\alpha) = \mathcal{N}^{nu}_{[0;1]}(\frac{r}{R},\alpha) \ .$$

**Remarque A.9.** *Ceci me semble cohérent avec le modèle radial dans tout l'espace où le seul état d'équilibre non trivial existe pour $\chi M = 8\pi$. En effet si $\alpha$ est fixe et que l'on fait tendre $R \to \infty$, on aura pour $r \in O(1)$*

$$\mathcal{N}^{nu}_{[0;R]}(r,\alpha) \to \mathcal{N}^{nu}_{[0;1]}(0,\alpha) \ ,$$

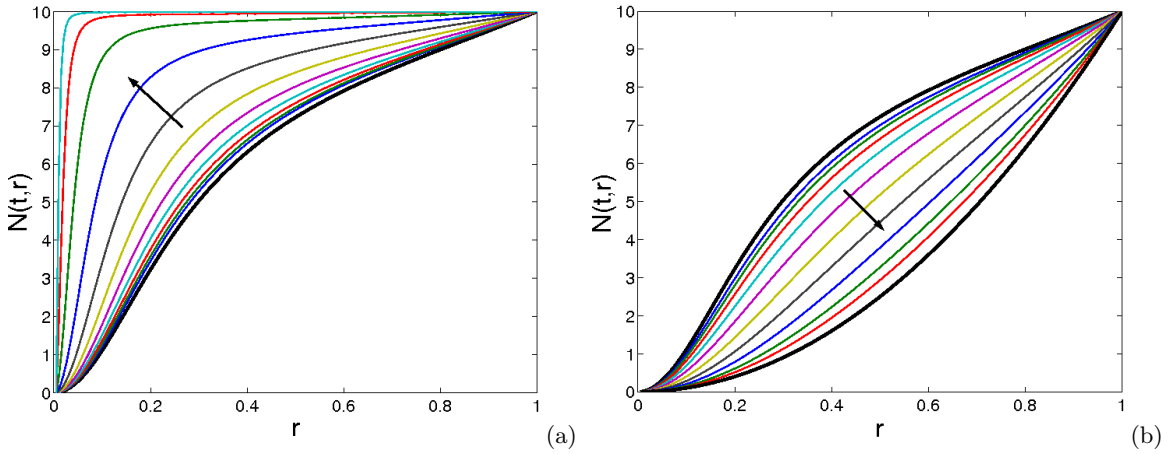


FIG. A.4 – Perturbations du nouvel état stationnaire $\mathcal{N}^{nu}(r, 10\pi)$ qui préservent la comparaison. On constate dans ce cas que l'état d'équilibre paraît instable : (a) il y a explosion (toute la masse se concentre en 0) ; (b) il y a convergence vers l'état uniforme. Les états stationnaires sont tracés en gras et la flèche indique le sens du temps.

*qui vaut 0 grosso modo sauf lorsque* $\alpha = 8\pi$.

**Remarque A.10.** *D'autre part si on fixe une concentration initiale (*un profil*) et un* $\alpha$*, et que l'on fait tendre* $R \to \infty$*, il y aura certainement explosion tout comme pour le modèle dans tout l'espace. Ceci permet de tronquer le domaine pour les simulations dans tout l'espace. En effet, lorsqu'on dilate suffisamment ce nouvel état stationnaire, il n'a plus d'effet dominant sur la donnée initiale, et il faut un second moment de plus en plus grand pour éviter l'explosion.*

## A.2 Le modèle KS asymétrique en 2D

### A.2.1 Simulations comparées en domaine borné

Nous présentons dans un premier temps des simulations en domaine borné, carré, du modèle de Keller-Segel 'classique', c'est-à-dire avec des coefficients de chémosensitivité et de diffusion constants, ce que l'on reprend ici en

$$\begin{cases} \dfrac{\partial n}{\partial t} = D\Delta n - \text{div}\ (n\nabla c)\ , \quad t > 0,\ x \in \Omega \subset \mathbb{R}^2, \\ -\Delta c = n - \langle n \rangle\ . \end{cases} \tag{A.5}$$

Ces simulations mettent en évidence l'importance jouée par les conditions au bord portant sur l'équation elliptique pour la synthèse chimique. Par là même des conditions de Neumann entrainent une masse critique de $4\Theta D$, où $\Theta$ est l'angle minimal à la frontière du domaine ($\Theta = \pi$ si $\Omega$ est régulier). En revanche des conditions de Dirichlet assurent l'existence globale sans explosion dès que $M < 8\pi D$. L'explosion au bord du domaine lorsque $4\Theta D < M < 8\Theta D$ distingue ces deux situations : cela ne peut arriver avec des conditions de Dirichlet qui imposent un gradient chimique orienté vers l'intérieur du domaine, et par conséquent 'repoussent' les cellules loin du bord. Il est bon de noter que le modèle 1D proposé au chapitre 2 est assujetti à un phénomène tout à fait analogue sur un intervalle borné.

Une manière simple de contrecarrer ce qui peut parfois être pressenti comme un artefact numérique est de simuler KS sur un domaine avec conditions périodiques (ce que nous avons mis en œuvre, simulations non présentées pour le modèle 'classique').

**Protocole numérique.** Afin de résoudre le système (A.5), nous avons utilisé un schéma très classique aux différences finies sur une grille rectangulaire régulière. Nous nous sommes inspirés d'une méthode

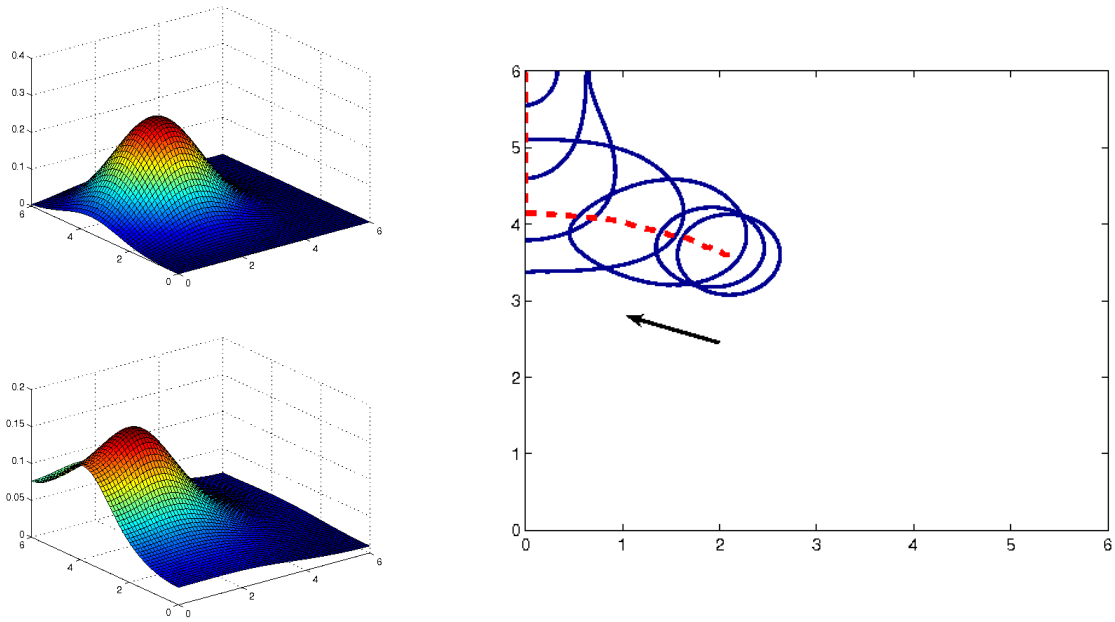

FIG. A.5 – Le modèle KS 'classique' (A.5) assujetti aux conditions de Neumann pour $c$. (*gauche*) La densité cellulaire aux temps $t = 0$ et $t = 60$. (*droite*) Lignes de niveau successives de la densité cellulaire $n$ entre les temps $t = 0$ et $t = 144$ correspondant à un niveau $5/6\ n_{\max}$. La trajectoire du pic (visualisé en son maximum) est suivie par le trait haché. La condition initiale est une gaussienne centrée en $(x_0, y_0) = (2.1, 3.6)$, avec une masse totale $M = 2$. Le coefficient de diffusion est $D = 0.05$, de sorte que $M_{\text{crit}} = 4\pi \times D \approx 0.63 < M$. L'explosion a lieu approximativement au temps $T_{bu} = 160$.

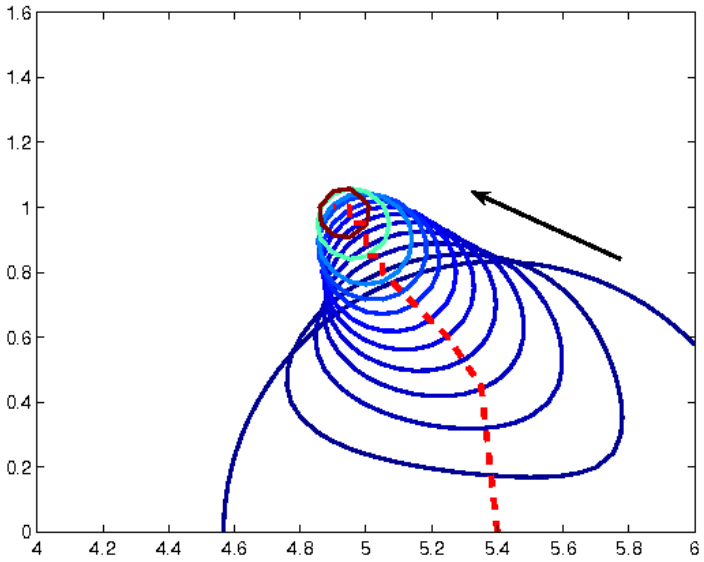

FIG. A.6 – Le modèle KS 'classique' (A.5) assujetti aux conditions de Dirichlet pour $c$. Des lignes de niveau successives sont représentées entre les temps $t = 0$ et $t = 20$ correspondant au niveau de troncature $1/2\ n_{\max}$. La condition initiale est une gaussienne centrée sur la frontière. La masse totale est $M = 1.6$, et $D = 0.05$, de sorte que $8\pi \times D \approx 1.26 < M$. L'explosion a lieu approximativement au temps $T_{bu} = 25$.

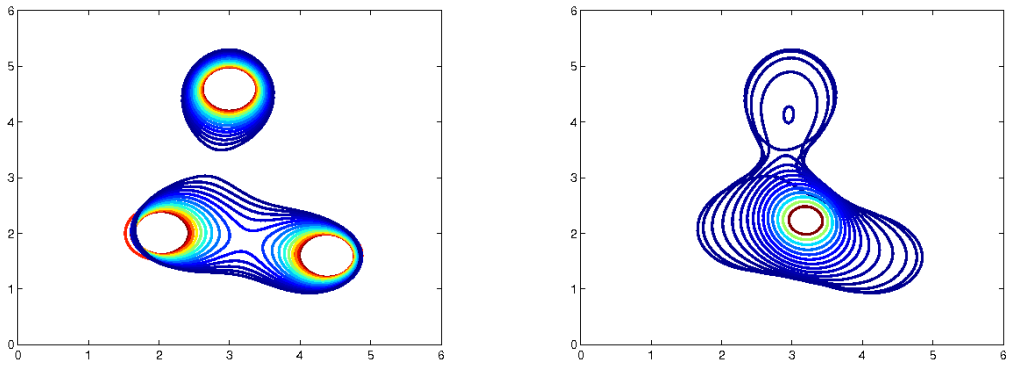

FIG. A.7 – Interactions entre plusieurs pics pour le modèle KS 'classique' (A.5), avec des conditions de Neumann au bord du domaine pour $c$. Des lignes de niveau successives sont représentées entre les temps (*à gauche*) $t = 0$ et $t = 16$, (*à droite*) $t = 16$ et $t = 44$, pour un niveau de troncature $2/5\ n_{\max}$. La condition initiale est une somme de trois pics gaussiens dont la masse totale est $M = 3.6$, le coefficient de diffusion est $D = 0.05$. Le temps d'explosion est à peu près $T_{bu} = 50$.

due à Scharfetter et Gummel [220] proposée à l'origine pour des modèles de semi-conducteurs [176]. A cet effet on factorise le flux de l'équation pour la densité cellulaire comme suit,

$$\frac{\partial n}{\partial t} = D \text{ div } \left( e^{c/D} \nabla n e^{-c/D} \right).$$

La discrétisation du flux est calquée sur cette réécriture. Nous procédons alors successivement par résoudre l'équation de Poisson discrète pour le potentiel chimique $c$ :

$$Ac(t + dt) = n(t) - \langle n(t) \rangle \ ,$$

où $A$ est la matrice de Poisson avec conditions de Neumann ou de Dirichlet au bord ; puis l'équation d'advection-diffusion pour $n$, semi-implicite en temps. Par souci de simplicité on présente la discrétisation en dimension un d'espace :

$$n_i(t + dt) - n_i(t) = dt \left( \frac{\mathcal{F}_{i+\frac{1}{2}} - \mathcal{F}_{i-\frac{1}{2}}}{dx} \right) \ ,$$

$$\mathcal{F}_{i+\frac{1}{2}} = \frac{D}{dx} \exp\left( \frac{c_{i+1} + c_i}{2D} \right) \times \left( n_{i+1}(t + dt) e^{-c_{i+1}/D} - n_i(t + dt) e^{-c_i(t)/D} \right) \ .$$

Les grandes matrices, non symétriques par le biais de l'advection sont inversées itérativement en utilisant une routine de descente le long du gradient, GMRES ou le double gradient conjugué, enfin celle qui apporte le meilleur compromis entre robustesse et rapidité, selon les situations.

On renvoie également à [177, 103] pour la résolution numérique du modèle KS.

Lorsqu'on calcule des solutions approchées avec conditions de Neumann on relève immédiatement l'attraction qu'exerce la frontière du domaine sur la densité et en particulier les points où l'angle minimal $\Theta$ est atteint (voir figure A.5).

**Simulations comparées.** Cette situation est à mettre en perspective avec des modèles KS plus généraux, et en particulier pour des modèles 2D avec effets de volumes, *i.e.* où les coefficients de diffusion et de chémosensitivité sont non-linéaires. Lors d'une collaboration avec div YASMIN DOLAK-STRUSS qui a fait l'objet d'un acte de la conférence ECMTB, Dresden, 2005 [51], nous avons fait le point sur quelques propriétés qualitatives entre le modèle KS 'classique' (A.5) et le modèle avec saturation de la réponse chimiotactique [HiPai01, DoSchm05,BuDoSchm07] (figure A.8) :

$$\frac{\partial n}{\partial t} = D\Delta n - \text{div } (n(1 - n)\nabla c) \ . \tag{A.6}$$

Il apparaît que l'influence du bord du domaine est inhérente au systèmes de type KS, ce qui est tout à fait intuitif par ailleurs. Dans les figures A.5&A.9, A.6&A.10, et A.7&A.11, sont illustrées respectivement le mouvement net vers la frontière du domaine avec conditions au bord chimiques de type Neumann, le mouvement vers l'intérieur du domaine avec conditions de Dirichlet, et le mouvement conjoint de plusieurs pics, dont les interactions ont été décrites formellement par Velázquez [240], et plus récemment par Dolbeault et Schmeiser [87].

### A.2.2 Le phénomène de masse critique

Le phénomène de masse critique, dans sa plus grande généralité, exprime que des cellules, sujettes à un phénomène de chimiotactisme auto-alimenté se structurent spatialement si elles sont suffisamment nombreuses. Dans le contexte 'classique', cela se traduit simplement par l'explosion lorsque la masse est sur-critique (ici la structure correspond à l'apparition de points d'agrégation cellulaire). Dans le cas de coefficients de diffusion ou de chémosensitivité non linéaires, l'alternative est moins triviale car il arrive que le phénomène d'explosion soit écarté mais qu'un équilibre stable non homogène le remplace. Une illustration simple est disponible dans [250].

Ce phénomène de masse critique est réellement au cœur du modèle de recrutement local des macrophages proposé à la partie II. Nous reprenons ici l'essence de ce qui a été présenté dans la partie préliminaire du chapitre 6.

Dans l'approche par marche aléatoire biaisée (voir introduction), Painter et Hillen ont introduit une pénalisation densité-dépendante $q(n)$ qui traduit une saturation due au non empiètement des cellules [202]. L'expression de la pression non linéaire et de la chémosensitivité macroscopiques dans

$$\frac{\partial n}{\partial t} = \operatorname{div}\Big(n\nabla h(n) - n\chi(n)\nabla c\Big)\,, \tag{A.7}$$

est reliée à $q$ via

$$\begin{cases} uh'(u) = D\Big(q(u) - uq'(u)\Big), \\ \chi(u) = \chi_0 q(u), \end{cases} \qquad H'(u) = \frac{D}{\chi_0}\,\frac{q(u) - uq'(u)}{q(u)u}. \tag{A.8}$$

Rappelons que la pression réduite $H$ contient l'information asymptotique qui détermine si l'explosion de la densité va avoir lieu ou non. Il faut pour cela comparer $H$ avec la pression critique $\frac{\mu M}{4\pi}\log u$ en régime de hautes densités. On illustre ce phénomène de saturation par les deux exemples génériques suivants (voir figure A.12).

- Si $q$ a une décroissance polynômiale : $q(u) = \frac{1}{1+u^\gamma}$, $\gamma > 0$, alors la pression réduite devient

$$H'(u) = \frac{D}{\chi_0}\,\frac{1 + (\gamma+1)u^\gamma}{u(1+u^\gamma)} \sim_\infty \frac{D}{\chi_0}\,\frac{\gamma+1}{u}.$$

  Dans ce cas la pression réduite est asymptotiquement 'classique', donc il faut comparer les coefficients, et l'on trouve finalement que l'explosion est évitée si $D(1+\gamma)/\chi_0 > \mu M/4\pi$. Notons que l'on observe numériquement l'explosion au-delà d'un certain seuil.
- Si $q$ a une décroissance exponentielle : $q(u) = e^{-\beta u}$, $\beta > 0$, alors la pression réduite est

$$H'(u) = \frac{D}{\chi_0}\,\frac{1+\beta u}{u} \sim_\infty \frac{D}{\chi_0}\,\beta.$$

  Donc la pression réduite est asymptotiquement linéaire (diffusion quadratique) et l'emporte à coup sûr contre la pression 'critique'. L'explosion n'a pas lieu.

Nous adoptons à nouveau la méthode de factorisation du flux de Scharfetter et Gummel, usuelle en théorie des semi-conducteurs, et qui laisse apparaître ici la pénalisation $q$. On réécrit tout d'abord (A.7) comme suit,

$$\frac{\partial n}{\partial t} = \nabla\cdot\left(Dq(n)^2 e^{\frac{\chi_0}{D}c}\nabla\Big(\frac{n}{q(n)}e^{-\frac{\chi_0}{D}c}\Big)\right). \tag{A.9}$$

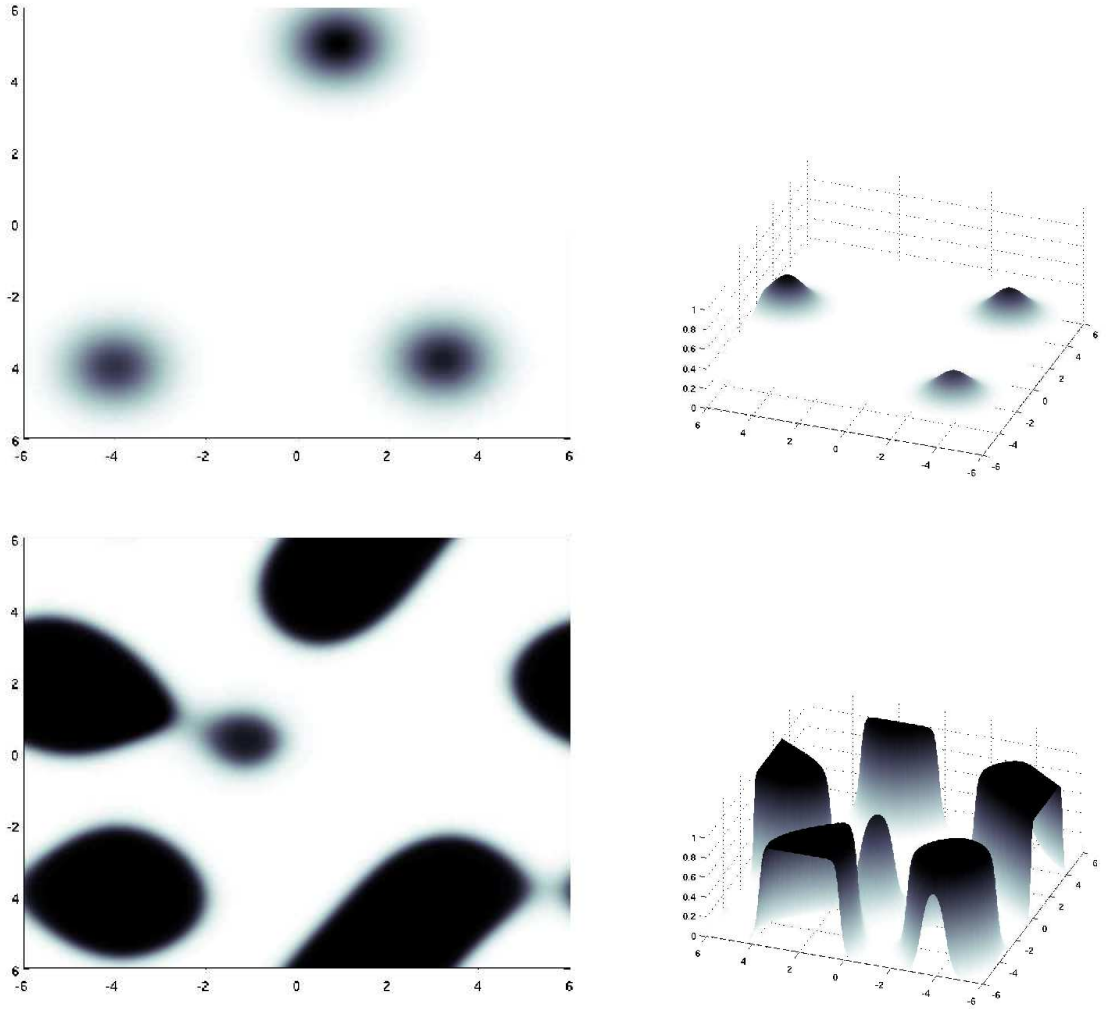

FIG. A.8 – Des plateaux pour le modèle (A.6) où la réponse chimiotactique est saturée : (*en haut*) la condition initiale, (*en bas*) évolution de la densité cellulaire et apparition d'agrégats intermédiaires (la densité est à peu près nulle en dehors des agrégats). La donnée initiale est une perturbation par trois petits amas d'une densité uniforme $\approx 0.55$. Le domaine est un tore. Les paramètres sont $\chi = 26$, $D = 1$ et $M = 80$. La partie advection dans (A.6) est traitée par un schéma classique 'upwind' (voir le paragraphe A.2.2). La densité figurée en bas n'est pas l'état stationnaire du système. On observe de fait un lent mouvement des plateaux qui se rejoignent et s'agglutinent [85, 45].

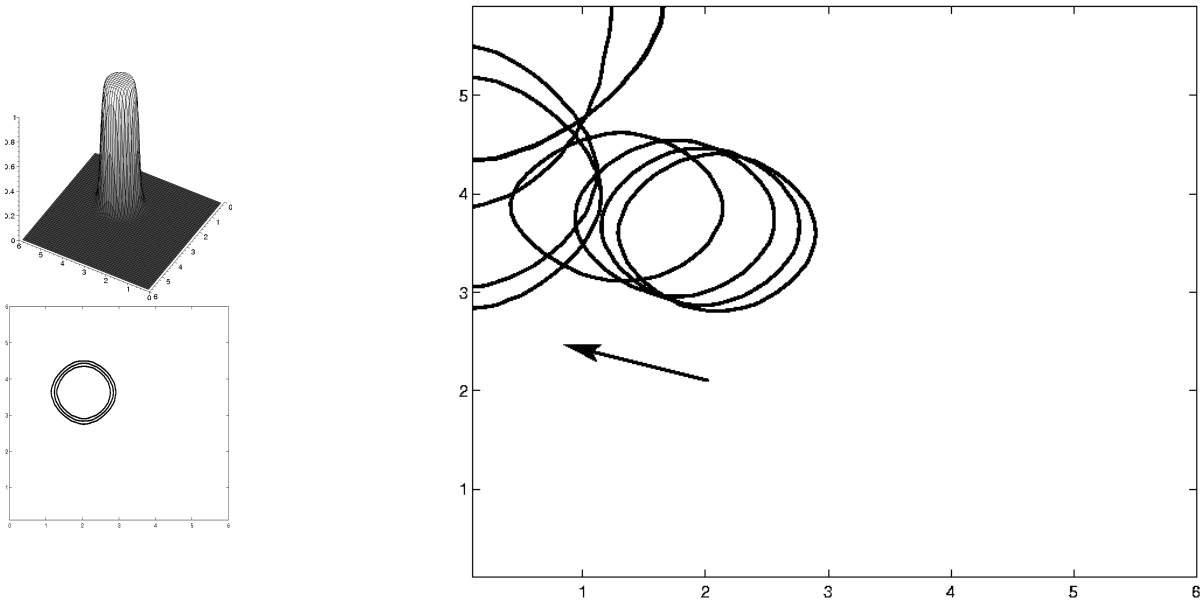

FIG. A.9 – (Y. Dolak-Struß) Le modèle KS avec chémosensitivité densité-dépendante et conditions de Neumann au bord pour $c$. (*gauche*) Vue en plongée et lignes de contour de la densité cellulaire où l'on voit le plateau déjà mis en place au temps $t = 25$. (*droite*) Mouvement lent de ce plateau entre les temps $t = 0$ et $t = 3500$. La condition initiale est elle-même un plateau centré en $(x_0, y_0) = (3.6, 2.1)$, avec la masse totale $M = 2$. Le coefficient de diffusion est $D = 0.01$.

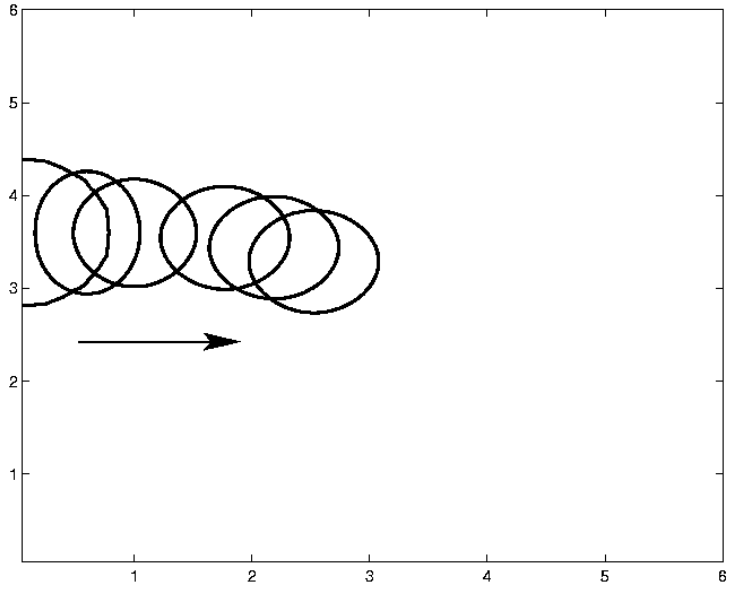

FIG. A.10 – (Y. Dolak-Struß) Le modèle KS avec chémosensitivité densité-dépendante et conditions de Dirichlet au bord pour $c$. Mouvement lent de la densité cellulaire vers l'intérieur du domaine entre les temps $t = 0$ et $t = 12500$. On reprend les mêmes paramètres qu'à la figure A.9.

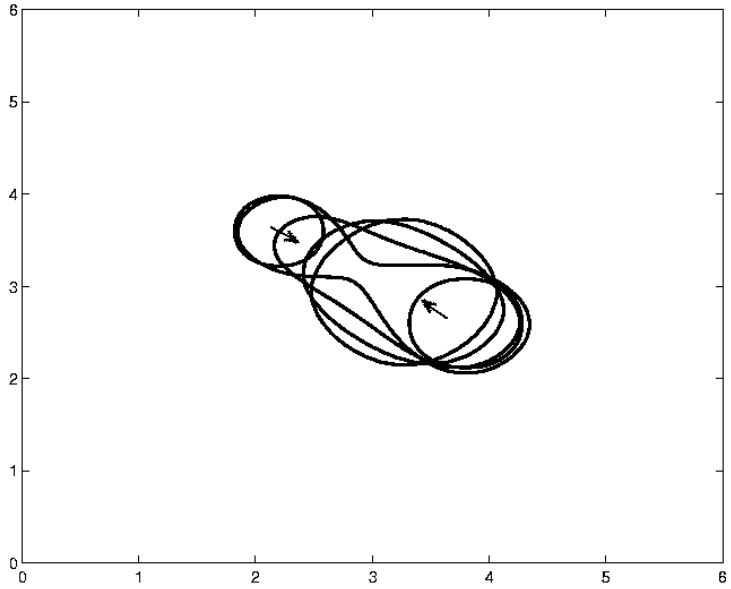


FIG. A.11 – (Y. Dolak-Struß) Le modèle KS avec chémosensitivité densité-dépendante et conditions de Neumann au bord pour $c$. Interaction entre deux plateaux s'agrégeant (les lignes de niveau $1/2$ sont représentées entre $t = 0$ et $t = 500$). Comme condition initiale nous avons deux plateaux centrés en $(x_0, y_0) = (3.6, 2.2)$ et $(x_0, y_0) = (2.6, 3.8)$. La masse totale est là encore $M = 2$, et $D = 0.005$.

On résout alors le système comme d'habitude, c'est-à-dire qu'on calcule dans un premier temps le potentiel $c$ ($n(t) \longrightarrow c(t + dt)$) avant de déterminer $n$ grâce à un schéma semi-implicite ($c(t + dt) \longrightarrow n(t + dt)$). Par souci de simplicité, on présente ici la méthode en dimension d'espace $d = 1$ à nouveau.

$$n_i(t + dt) - n_i(t) = dt\left(\frac{\mathcal{F}_{i+\frac{1}{2}} - \mathcal{F}_{i-\frac{1}{2}}}{dx}\right) ,$$

$$\mathcal{F}_{i+\frac{1}{2}} = \frac{1}{dx} D\Big[q(n)^2(t)\Big]_{i+\frac{1}{2}} \exp\left(\frac{\chi_0}{D}\frac{c_{i+1} + c_i}{2}\right) \times \left(\frac{n_{i+1}(t + dt)}{q(n_{i+1}(t))} e^{-\frac{\chi_0}{D}c_{i+1}} - \frac{n_i(t + dt)}{q(n_i(t))} e^{-\frac{\chi_0}{D}c_i}\right) .$$

Pour ce qui est de la contribution non linéaire, nous avons tenté la moyenne géométrique

$$\Big[q(n)^2\Big]_{i+\frac{1}{2}} = q(n_{i+1})q(n_i) ,$$

qui présente l'avantage de simplifier les dénominateurs.

Lorsque $q(u) = (1 - u)_+$, le schéma ci-dessus est instable en pratique, et on préfère revenir à une méthode standard 'upwind' pour le terme d'advection dans (A.6). Les résultats présentés à la figure A.8 ont été obtenus de la sorte.

## A.3 Recrutement local des macrophages

### A.3.1 Les calculs de la partie II

Le protocole numérique du modèle de recrutement local des macrophages

$$\begin{cases} \dfrac{\partial m}{\partial t} = D\Delta m + \lambda m(\bar{m} - m) - \text{div}\left(\chi m(\bar{m} - m)\nabla c\right) \\ \dfrac{\partial d}{\partial t} = F(m)m(\bar{d} - d) \\ -\varepsilon\Delta c + \alpha c = \mu d , \end{cases} \tag{A.10}$$

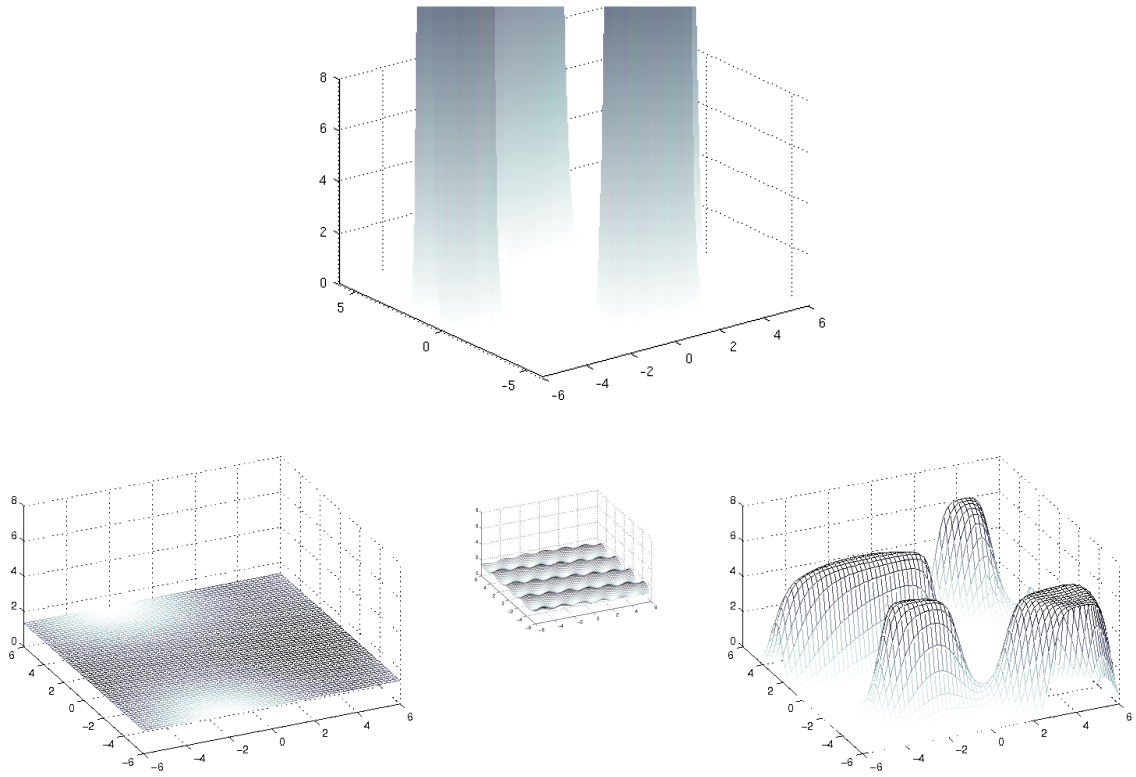

FIG. A.12 – Illustration numérique du principe de masse critique dans le cadre des effets de volume. Les calculs sont effectués sur une grille régulière avec conditions périodiques au bord, à l'aide d'une discrétisation de type Scharfetter-Gummel (6.12). (*au centre*) Voici la condition initiale : une perturbation de la densité uniforme $\approx 1.4$. (*en haut*) Ici la pénalisation du taux de transition est $q(u) = \frac{1}{1+u^2}$. Les autres paramètres du système sont $M = 200$, $D = 1$, $\mu = 1$ et $\chi = 6$. Il y a apparemment explosion en temps fini (un état intermédiaire est montré), c'est-à-dire émergence d'une structure spatiale non homogène pour ce qui nous concerne. La situation est qualitativement proche du modèle 'classique', où il y a explosion si $\mu\chi_0 M/D$ dépasse un certain seuil. (*à gauche*) Il y a retour à l'équilibre si $\chi_0$ descend sous un certain seuil, toutes choses étant égales par ailleurs. Ici $\chi_0 = 2$, et $q$ est indifféremment $1/(1+u^2)$ ou $e^{-u}$. (*à droite*) Ici la pénalisation vaut $q(u) = e^{-u}$ et $\chi_0 = 6$ à nouveau. La densité n'explose en aucun cas, conformément à la théorie, mais on observe tout de même un phénomène d'agrégation (état où la densité de cellules est très localisée).

est sans surprise au vu des paragraphes précédents. On résout successivement les trois équations en adoptant un schéma de Scharfetter-Gummel pour le flux de cellules :

$$\partial_t m = \nabla \cdot \left( e^{\chi c}(1-m)^2 \nabla\Big(\frac{m}{1-m} e^{-\chi c}\Big)\right) + m(1-m) \ .$$

Le terme de réaction est explicite en temps, et le flux est semi-implicite,

$$m_i(t+dt) - m_i(t) = dt\left(\frac{\mathcal{F}_{i+\frac{1}{2}} - \mathcal{F}_{i-\frac{1}{2}}}{dx}\right) + dt\ m_i(t)(1-m_i(t)),$$
$$\mathcal{F}_{i+\frac{1}{2}} = \frac{1}{dx}\exp\Big(\chi\frac{c_{i+1}(t)+c_i(t)}{2}\Big)(1-m)^2_{i+\frac{1}{2}} \times \left(\frac{m_{i+1}(t+dt)}{1-m_{i+1}(t)} e^{-\chi c_{i+1}(t)} - \frac{m_i(t+dt)}{1-m_i(t)} e^{-\chi c_i(t)}\right).$$

Une difficulté apparaît ici qui n'était pas dans le paragraphe précédent : c'est la division par $1-m_i(t)$ qui peut devenir très proche de 0. Nous avons tenté le choix de la moyenne géométrique $(1-m)^2_{i+\frac{1}{2}} = (1-m_{i+1})(1-m_i)$, mais ce choix induit quelque instabilité (oscillations locales inattendues). Par conséquent on s'accommode de

$$\mathcal{F}_{i+\frac{1}{2}} = \frac{1}{dx}\left( m_{i+1}(t+dt)(1-m_i(t))\exp\Big(\chi\frac{-c_{i+1}+c_i}{2}\Big) - m_i(t+dt)(1-m_i(t))\exp\Big(\chi\frac{c_{i+1}-c_i}{2}\Big)\right) ,$$

qui se trouve être beaucoup plus stable.

Insistons sur le fait que le front cellulaire de réaction-diffusion (Fisher-KPP) n'est pas nécessaire pour obtenir une structure concentrique en anneaux. Ce choix a été mis en avant pour disposer d'un système fermé à trois équations, mais un front extérieur $u(t)$ bien choisi :

$$\frac{\partial m}{\partial t} = D\Delta m + u(t) - \text{div}\ \Big(\chi m(\bar{m}-m)\nabla c\Big) \ ,$$

exhibe également des anneaux. En revanche les lois d'espacement des anneaux dépendent bien entendu de la nature du front (voir chapitre 6).

Afin d'obtenir un 'diagramme' de bifurcation entre plaques et anneaux (voir l'introduction et le chapitre 6) nous avons criblé l'espace des paramètres à diffusion $\varepsilon$ constante, et relevé la courbe de transition 'à la main'.

Pour une analyse d'échelle et des conclusions qualitatives, on renvoie au chapitre 6.

### A.3.2 Perspectives : un couplage entre un front de Fisher et KS

Une prolongation naturelle du paragraphe précédent consiste à tenter de réduire le nombre d'équations tout en préservant la dynamique du système (A.10). Si on isole les deux phénomènes principaux : propagation d'un front et chimiotactisme, on est confronté au système suivant à deux espèces :

$$\begin{cases} \dfrac{\partial n}{\partial t} = \Delta n - \text{div}\ \Big(\chi n(1-n)\nabla c\Big) + \lambda n(1-n) \ , \\ -\Delta c + \alpha c = n, \end{cases} \tag{A.11}$$

dont les simulations sont semblables au modèle de recrutement local des macrophages (voir figure A.13).

## A.4 Le point de vue du transport optimal

Nous avons introduit au chapitre 8 un schéma numérique à base de transport optimal de mesures qui permet des estimations optimales de convergence, pour l'instant en une dimension d'espace. En 1D

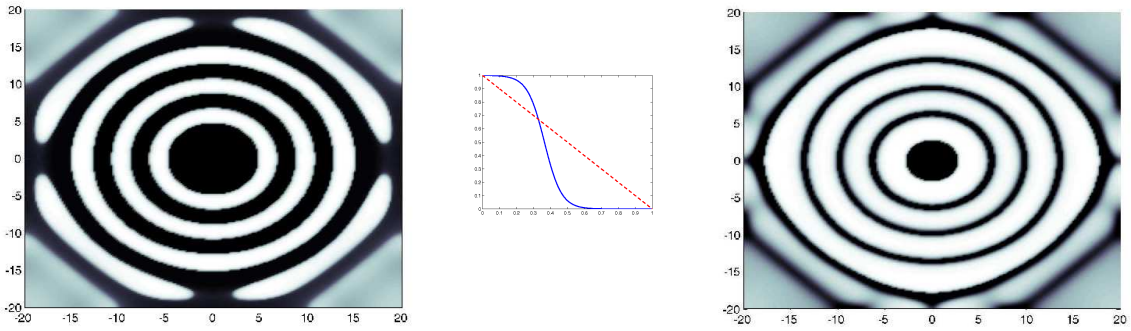

FIG. A.13 – Couplage entre un front de réaction-diffusion de type Fisher KPP et un modèle de chimiotactisme (KS) exhibant un phénomène de masse critique (A.11). La propagation du front structure l'organisation spatiale des cellules. Le modèle de KS est saturé par une fonction sous-jacente $q$ (voir dans l'introduction la pénalisation de la marche aléatoire biaisée). A gauche est figurée l'émergence d'anneaux pour $q$ une fonction de seuil proche de Heaviside (ligne pleine). A droite $q(u) = \max(1-u, 0)$ (ligne hachée).

donc, le modèle KS défini préalablement au chapitre 2, auquel s'ajoute une dérive pour capturer le profil asymptotique auto-similaire (annexe D), se résume en une seule équation non locale

$$\frac{\partial u}{\partial t} = \Delta u + \operatorname{div}\left(yu + \chi u H u\right) . \tag{A.12}$$

La masse totale est fixée à $M = 1$ dans la suite, de sorte que le seul paramètre libre est $\chi$. Ainsi on peut disposer directement des théories s'appliquant aux densités de probabilités. Le système dynamique (A.12) peut se concevoir comme le flot gradient généralisé associé à la fonctionnelle d'énergie libre

$$\mathcal{F}[u] = \int u \log u + \frac{1}{2}\int |y|^2 u \; dy + \frac{1}{2\pi}\iint n(x)\log|x-y| n(y) \; dxdy \; , \tag{A.13}$$

pour la structure métrique de Wasserstein [148, 200, 7]. Voilà une manière bien sophistiquée d'exprimer que KS devient un flot $L^2$ s'il est transposé à la fonction de répartition inverse de la densité cellulaire $\Phi = U^{-1}$, où $U(t,x) = \int_{-\infty}^{x} u(t,x)\; dx$ (voir aussi l'introduction et le chapitre D). Avec le changement de variables $\rho = U(t,x)$, $\rho \in (0,1)$ ($d\rho = u\; dx$), la fonctionnelle d'énergie libre se réécrit

$$\mathcal{G}[\Phi] = -\int \log \Phi' \; d\rho + \frac{1}{2}\int |\Phi|^2 \; d\rho + \frac{\chi}{2\pi}\iint \log\left|\Phi(\eta) - \Phi(\rho)\right| \; d\rho d\eta \; .$$

Si l'on se focalise sur la discrétisation en temps du flot, le schéma itératif

$$u(t+dt) = \arg\min_w \left\{ \mathcal{F}[w] + \frac{1}{2dt} W\left(u(t), w\right)^2 \right\} \; ,$$

devient

$$\Phi(t+dt) = \arg\min_\Omega \left\{ \mathcal{G}[\Omega] + \frac{1}{2dt}\left\|\Phi(t) - \Omega\right\|^2 \right\} \; ,$$

qui n'est autre que le flot $L^2$ de $\mathcal{G}$ implicite en temps :

$$\frac{\Phi(t+dt) - \Phi(t)}{dt} = -\nabla_{L^2}\mathcal{G}[\Phi(t+dt)] \; .$$

De ce point de vue, le schéma discret en temps préserve les estimations d'énergie cruciales pour l'optimalité des résultats. Il n'y a qu'une étape vers la discrétisation en espace et la résolution numérique. On définit

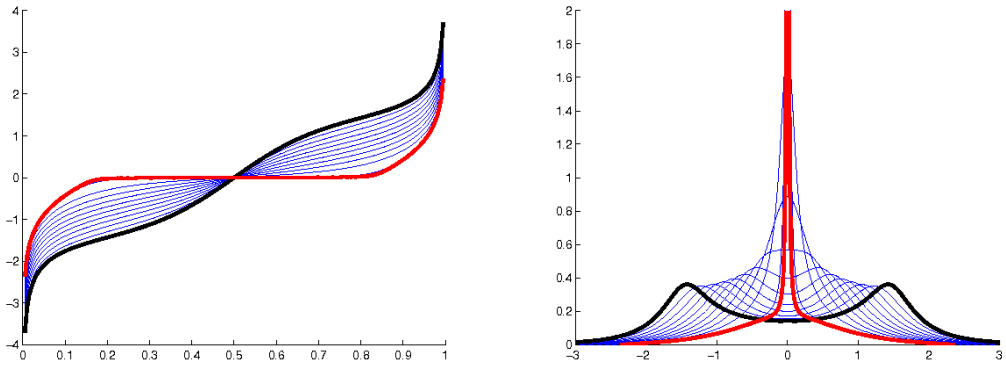

FIG. A.14 – Illustration du phénomène d'explosion pour le modèle KS 1D résolu numériquement par l'algorithme de flot gradient généralisé (A.14). La chémosensitivité est $\chi = 3\pi$ (et la masse totale est $M = 1$). (*gauche*) Graphes successifs de la fonction inverse de répartition $\Phi$. Le plateau correspond à l'apparition d'une masse de Dirac pour la densité (*à droite*).

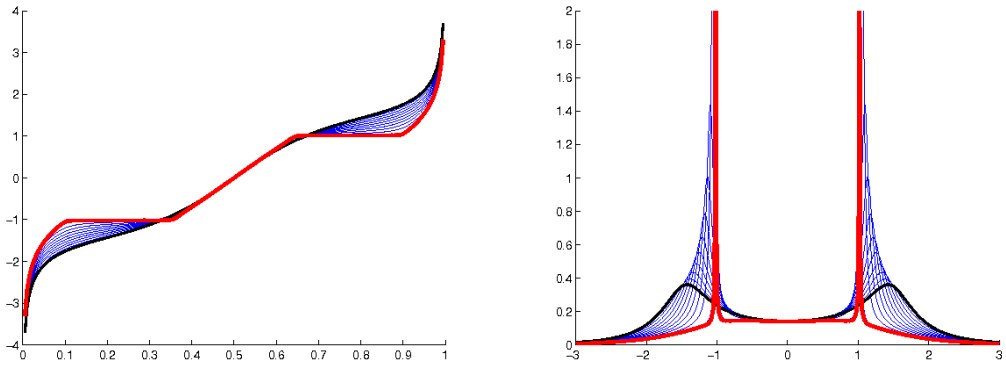

FIG. A.15 – Illustration du phénomène d'explosion comme à la figure A.14. Le paramètre $\chi = 8\pi$ est plus grand, ce qui explique pourquoi deux masses de Dirac apparaissent (l'explosion est accentuée).

donc la fonction inverse de répartition discrète de la densité cellulaire : $(\Phi_i)$ sur un maillage régulier de pas $h > 0$. L'énergie libre devient

$$\mathcal{G}_h[\Phi] = -\sum_{i=1}^{N-1} h \log\left(\frac{\Phi^{i+1}-\Phi^i}{h}\right) + \frac{1}{2}\sum_{i=1}^{N} h|\Phi^i|^2 + \frac{\chi}{2\pi}\sum_{i=1}^{N}\sum_{j=1,\ j\neq i}^{N} h^2 \log|\Phi^j - \Phi^i| \ ,$$

et le flot $L^2$ discret correspondant est :

$$-\frac{\Phi^i_{n+1}-\Phi^i_n}{\tau} = \frac{1}{\Phi^{i+1}_{n+1}-\Phi^i_{n+1}} - \frac{1}{\Phi^i_{n+1}-\Phi^{i-1}_{n+1}} + \Phi^i_{n+1} + \frac{\chi}{\pi}\sum_{j:|\Phi^i_{n+1}-\Phi^j_{n+1}|>0} h\frac{1}{\Phi^i_{n+1}-\Phi^j_{n+1}} \ . \quad \text{(A.14)}$$

La théorie prédit l'existence d'un équilibre unique et la convergence à vitesse exponentielle dès que $\chi(1-h) < 2\pi$. Dans le cas d'un terme de diffusion non linéaire de type milieu poreux $\Delta n^m$, $m > 1$, il y a convergence vers l'unique équilibre quelque soit le coefficient de chémosensitivité $\chi$, et ce sans estimation évidente de la vitesse de convergence (par ailleurs il n'est pas nécessaire de renormaliser la solution).

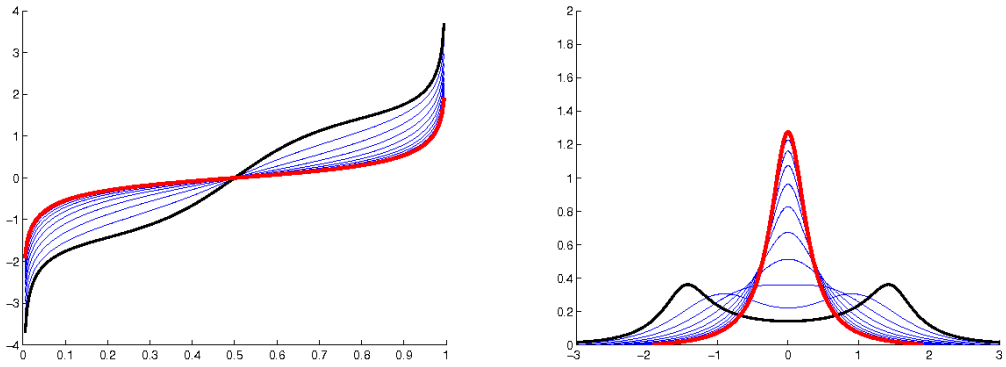

FIG. A.16 – Convergence vers l'état stationnaire du problème de KS 1D après changement d'échelle auto-similaire (A.12). La convergence a lieu à vitesse exponentielle.

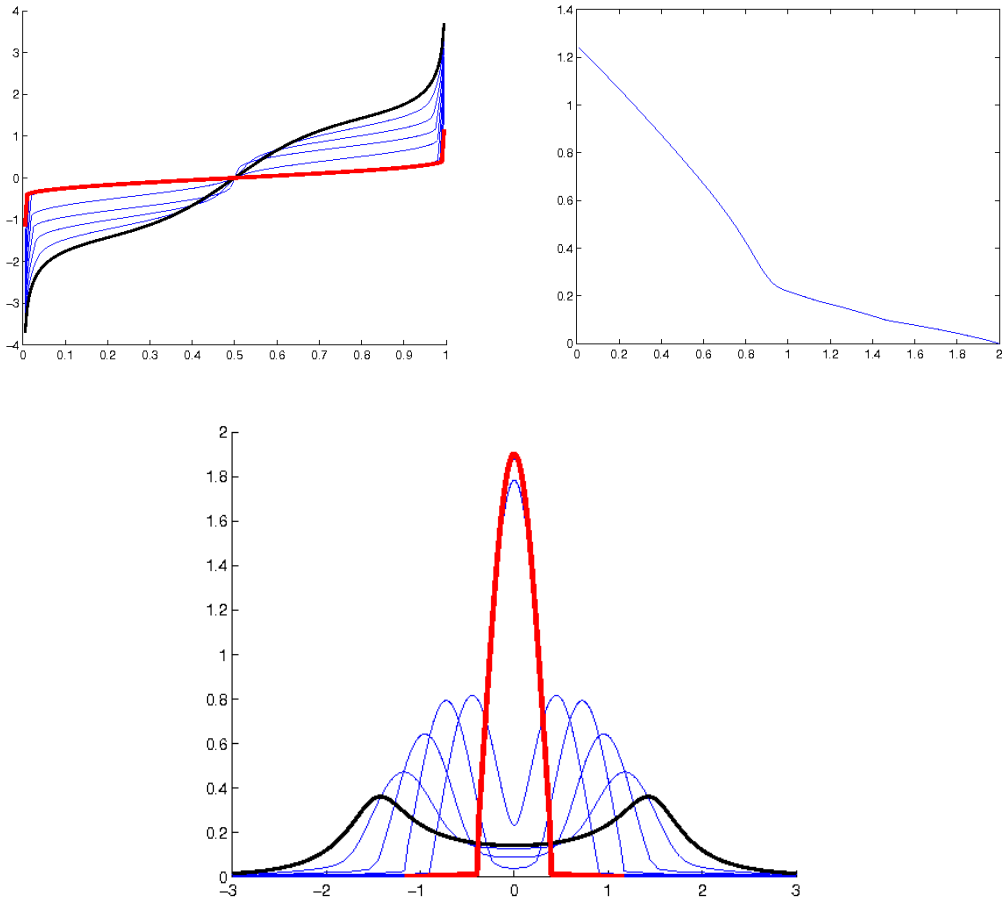

FIG. A.17 – Modèle de KS 1D avec diffusion non linéaire de type milieu poreux (avec exposant $m = 2$) et $\chi = 3$. Il y a convergence vers l'unique état d'équilibre du système sans avoir recours à un changement d'échelle auto-similaire. La vitesse de convergence en norme de Wasserstein (norme $L^2$ pour ce qui concerne $\Phi$) vers l'état stationnaire (dernier résultat du calcul) est montrée, ce qui laisse sceptique.

Mentionnons finalement deux avantages que présente cette méthode numérique outre les estimations d'énergie qui rendent les résultats optimaux. Tout d'abord, en cas d'explosion dans le cas 'classique' sans changement d'échelle (autrement dit sans terme de dérive), un maillage régulier pour $(\Phi_i)$ permet d'accumuler les points autour des régions de haute concentration (ce sont les plateaux pour $\Phi$) lorsqu'on revient au tracé de la densité (figure A.14). Deuxièmement nous avons ramené la droite réelle à un intervalle fixe $(0, 1)$, ce qui permet de s'affranchir d'une nécessaire troncature si nous avions souhaité simuler directement la densité cellulaire dans tout l'espace. En pratique, une donnée initiale à support compact va se propager à vitesse finie (en raison du schéma discret), sans pour autant que notre domaine de calcul soit modifié (figure 8.2).

# Annexe B

# Autour de l'inégalité de Hardy-Littlewood-Sobolev logarithmique

Cette annexe est consacrée aux multiples facettes de l'inégalité de Hardy-Littlewood-Sobolev logarithmique, sortie du contexte de Keller-Segel. Nous apportons différentes preuves (dont deux sont originales et ne résultent pas d'un passage à la limite), puis nous faisons le point sur la dualité qui existe entre Hardy-Littlewood-Sobolev logarithmique et l'inégalité de Trudinger-Moser en dimension deux.

Commençons par rappeler l'inégalité fonctionnelle de Hardy-Littlewood-Sobolev à poids logarithmique [56, 23]. Nous parlerons dans la suite d'inégalité HLS logarithmique, ou HLS log. Il ne faut pas la confondre avec l'inégalité de Sobolev logarithmique (ou log Sobolev), voir annexe D [11].

**Théorème B.1.** *Soit $f$ une fonction positive : $\mathbb{R}^d \to \mathbb{R}$ de masse totale $\int f(x)\ dx = 1$ telle que $f(x)\log(1+|x|^2)$ est intégrable. Alors*

$$-\iint_{\mathbb{R}^d\times\mathbb{R}^d} f(x)\log|x-y|f(y)\,dx\,dy \leq \frac{1}{d}\int_{\mathbb{R}^d} f\log f\,dx + C(d). \tag{B.1}$$

L'inégalité HLS logarithmique est au cœur de l'analyse des systèmes de Keller-Segel à deux dimensions d'espace (ainsi que les modèles étendus où le potentiel chimique est donné par la convolution avec un poids logarithmique, voir chapitre 2). En résumé l'énergie libre de Keller-Segel s'écrit – dans le cas simple – comme suit,

$$\mathcal{E}(0) \geq \mathcal{E}(t) = \int n\log n\ dx + \frac{\chi}{4\pi}\iint n(x)\log|x-y|n(y)\ dxdy. \tag{B.2}$$

En général on ne peut pas conclure instantanément car les deux termes n'ont pas de signe, et expriment des tendances opposées (resp. dispersion des cellules et agrégation). L'inégalité d'HLS log permet de comparer ces deux contributions et d'énoncer un théorème de masse critique optimale (nous restons volontairement vague pour ne retenir que l'essentiel, pour des détails voir les différents contextes dans l'introduction).

**Théorème B.2** (Dolbeault et Perthame)**.** *Soit $M = \int n_0$ la masse de cellules conservée au cours du temps. Si $\chi M < 8\pi$, le système de Keller-Segel 2D admet une solution définie et régulière pour tout temps positif.*

Nous verrons dans cet appendice plusieurs approches qui aboutissent à l'inégalité (B.1) (approche originale par limite de la famille HLS, approche unidimensionnelle par le transport de masse, ainsi qu'une

version discrète élémentaire, toujours en 1D). Avant de présenter l'approche originale de Carlen & Loss [56] et de Beckner [23], rappelons deux ou trois observations quant à cette inégalité.

– L'inégalité est vraie si la fonctionnelle

$$\mathcal{F}(f) = \frac{1}{d}\int f\log f + \iint f(x)\log|x-y|f(y)\ dxdy, \tag{B.3}$$

est bornée par en-dessous pour les fonctions positives de masse totale 1.

– La fonctionnelle $\mathcal{F}$ est homogène de degré 0 au sens ci-dessous. Elle est quasi-homogène si la masse totale est différente de 1. Si $n_\lambda(x) = \lambda^d n(\lambda x)$ alors

$$\begin{aligned}\mathcal{F}(n_\lambda) &= \frac{1}{d}\int n\log(\lambda^d n(x))\ dx + \iint n(x)\log\lambda^{-1}|x-y|n(y)\ dxdy\\ &= \mathcal{F}(n) + (M-M^2)\log\lambda.\end{aligned}$$

Par cet argument on voit également que le seul facteur envisageable au-devant de $\int f\log f$ dans (B.1) est précisement $1/d$ (ou $M/d$ si la masse est différente de 1).

– Les minimiseurs de $\mathcal{F}$ sont connus (ce sont également les états stationnaires de Keller-Segel dans tout l'espace). Il s'agit des images par transformation conforme de

$$h(x) = \frac{1}{|\mathbb{S}^d|}\left(\frac{2}{1+|x|^2}\right)^d, \tag{B.4}$$

qui n'est autre que le jacobien de la projection stéréographique (voir Carlen & Loss et le calcul de la constante additive optimale $C(d)$ dans (B.1)).

– Il existe un version de (B.1) sur la sphère ainsi que des variantes après réarrangement décroissant du noyau de potentiel (voir [23] et l'appendice du chapitre 3).

## B.1 L'approche originale

Dans cette approche, l'inégalité HLS log s'obtient par passage à la limite de l'injection de Sobolev fractionnaire (ou Hardy-Littlewood-Sobolev, ou Young faible, voir Lieb&Loss),

$$\iint f(x)|x-y|^{-\lambda}f(y)\ dxdy \le \mathcal{C}(d,\lambda)\|f\|_p\|f\|_p, \tag{B.5}$$

avec la relation d'homogénéité $2/p + \lambda/d = 2$. La constante optimale et les cas d'égalités (fonctions extrémales) sont connus. A transformation conforme près, il s'agit de

$$\mathcal{C}(d,\lambda) = \pi^{\lambda/2}\frac{\Gamma(\frac{d}{2}-\frac{\lambda}{2})}{\Gamma(d-\frac{\lambda}{2})}\left(\frac{\Gamma(\frac{d}{2})}{\Gamma(d)}\right)^{-1+\frac{\lambda}{d}}, \quad h_p(x) \propto h(x)^{1/p} \propto \left(\frac{2}{1+|x|^2}\right)^{d/p}. \tag{B.6}$$

Par convention, dans la suite on suppose $\int h_p = 1$.

*Preuve formelle de HLS log.* L'inégalité HLS (B.5) peut se réécrire sur la sphère $\mathbb{S}^d$, où elle apparaît plus naturelle [167, 23] :

$$\iint_{\mathbb{S}^d\times\mathbb{S}^d} F(\xi)|\xi-\eta|^{-\lambda}F(\eta)\ d\xi d\eta \le \left(\int|\xi-\eta|^{-\lambda}\ d\xi\right)\|F\|^2_{L^p(\mathbb{S}^d)},$$

où $d\xi$ est la mesure normalisée à un sur la sphère. Sans perte de généralité on suppose $\int F = 1$. Alors on a clairement [23] :

$$\iint \Big(F(\xi)-1\Big)\Big(|\xi-\eta|^{-\lambda}-1\Big)\Big(F(\eta)-1\Big)\ d\xi d\eta \le \left(\int|\xi-\eta|^{-\lambda}\ d\xi\right)(\|F\|_p^2-1).$$

En divisant par $\lambda = 2d(p-1)/p$ et en faisant tendre $\lambda$ vers 0 (équivalent à $p \to 1$), on obtient l'inégalité de HLS log sur la sphère :

$$\iint_{\mathbb{S}^d \times \mathbb{S}^d} \Big(F(\xi) - 1\Big) \log|\xi - \eta|^{-1} \Big(F(\eta) - 1\Big)\ d\xi d\eta \leq \frac{1}{d} \int F(\xi) \log F(\xi)\ d\xi\ ,$$

grâce à

$$\lim_{\lambda \to 0} \frac{|\xi - \eta|^{-\lambda} - 1}{\lambda} = \log|\xi - \eta|^{-1}\ ,$$
$$\lim_{\lambda \to 0} \frac{1}{d} \left( \int |\xi - \eta|^{-\lambda}\ d\xi \right) = \frac{1}{d}\ ,$$
$$\lim_{\lambda \to 0} \frac{1}{2} \frac{\|F\|_p^2 - 1}{p - 1} = \int F \log F\ dx.$$

Pour retrouver l'inégalité HLS log sur $\mathbb{R}^d$, on utilise la transformation qui préserve la masse : $F(\xi) = (f/h) \circ \mathcal{S}$, où $\mathcal{S}$ est la projection stéréographique, et $h$ est donné par (B.4).

Observons pour conclure que la constante additive optimale dans HLS log est connue d'après les minimiseurs. La caractérisation complète des minimiseurs, elle, est plus délicate à obtenir [56]. □

On parle 'd'information au bord' en $L^1$ car cette inégalité est obtenue comme développement limité d'une famille d'inégalités lorsque l'exposant $p \to 1$. Un autre exemple de passage à la limite est donné par l'inégalité de Trudinger en dimension 2, qui apparaît comme la limite des injections de Sobolev

$$\|f\|_{q\star} \leq C \|\nabla f\|_q\ , \quad q\star = \frac{2q}{2 - q}\ ,$$

en domaine borné, lorsque l'exposant $q\star$ tend vers l'infini [115] :

$$\int_\Omega \exp\left( \frac{|v|}{c\|\nabla v\|_2} \right)^2 \leq C|\Omega|\ . \tag{B.7}$$

Une version optimale de (B.7) due à Moser [184], et qui s'applique au système KS en domaine borné, est présentée au paragraphe B.4.

## B.2 Une preuve unidimensionelle de HLS log

Dans le chapitre 7 nous avons présenté une preuve tout à fait différente de celle qui précède, connaissant *a priori* les minimiseurs de la fonctionnelle (B.3). Cette nouvelle approche se base tout à fait sur une interprétation type flot gradient du système de Keller-Segel 1D (tel qu'il est défini au chapitre 2) :

$$\frac{\partial n}{\partial t} = \frac{\partial^2 n}{\partial x^2} + \chi \frac{\partial}{\partial x}(n \mathcal{H} n)\ , \tag{B.8}$$

où $\mathcal{H}n$ désigne la transformée de Hilbert de $n$ (cette interprétation de KS comme le flot gradient de la fonctionnelle d'énergie libre (B.2) pour la distance de Wasserstein est dépeinte brièvement dans l'introduction). Pour faire court, nous trouvons l'estimation pour toute densité de probabilité $f$,

$$-\iint f(x) \log|x - y| f(y)\ dxdy \leq \int f(x) \log f(x) \Big( \mathcal{J}[h](x) \Big)\ dx + C(h)\ , \tag{B.9}$$

avec $\mathcal{J}[h] \equiv 1$ si et seulement si $h$ est la distribution de Cauchy

$$h(x) = \frac{1}{\pi} \frac{1}{1 + x^2}, \tag{B.10}$$

(éventuellement après une transformation conforme). Il y égalité dans (B.9) si et seulement si $f$ est une transformation conforme de $h$.

**Théorème B.3.** *L'inégalité HLS logarithmique est conséquence de l'inégalité de Jensen. Par ailleurs les solutions stationnaires de* (B.8) *ne sont ni plus ni moins que les minimiseurs de la fonctionnelle associée* (B.3)*, bien qu'elle ne soit pas convexe par déplacement.*

*Démonstration.* D'après le théorème de Brenier [244], il existe une fonction convexe $\varphi$ qui transporte la densité $f(x)\ dx$ vers la densité d'équilibre $h(x)$ de manière optimale. On désigne la fonction convexe conjuguée par $\psi(x)$, de sorte que l'énergie d'interaction se réécrit :

$$\iint \log|y-x| f(x)f(y)\ dxdy = \iint \log|\psi'(v)-\psi'(u)| h(u)h(v)\ dudv\ .$$

En dimension un notamment, la fonction de transport $\psi$ est explicite, mais nous ne l'utilisons pas ici. On réécrit tout d'abord la partie d'interaction en utilisant la monotonie de $\psi'$,

$$\log|\psi'(v)-\psi'(u)| = \log\Big(\big(\psi'(v)-\psi'(u)\big)\cdot\big(v-u\big)\Big) - \log|v-u|\ ,$$

Nous avons successivement, en utilisant l'inégalité de Jensen,

$$\begin{aligned}
\iint \log|\psi'(v)-\psi'(u)| h(u)h(v)\ dudv &\geq \iint \log\left(\int_{t=0}^1 \psi''(\zeta)(v-u)^2\ dt\right) h(u)h(v)\ dudv - C \\
&\geq \iint\int_{t=0}^1 \log\big(\psi''(\zeta)\big) h(u)h(v)\ dtdudv - C \\
&= \int_\zeta \log\big(\psi''(\zeta)\big) \int_{\xi\in\mathbb{R}}\int_{t=0}^1 h(\zeta-t\xi)h(\zeta-t\xi+\xi)\ dtd\xi d\zeta - C\ ,
\end{aligned}$$

avec $\zeta = (1-t)u+tv$ et $\xi = v-u$. On peut vérifier que la quantité

$$\int_{\xi\in\mathbb{R}}\int_{t=0}^1 h(\zeta-t\xi)h(\zeta-t\xi+\xi)\ dtd\xi\ ,$$

est partout égale à $h(\zeta)$ lorsque $h$ est précisémenent la densité à l'équilibre, donnée par (B.10). Lorsqu'on effectue le changement de variable inverse $x=\psi'(\zeta)$, on retrouve l'inégalité de Hardy-Littlewood-Sobolev logarithmique avec la constante optimale (on contrôle parfaitement les cas d'égalité dans l'inégalité de Jensen). □

Cette approche se généralise parfaitement aux diffusions de type puissance dès lors qu'un équilibre existe. En ce sens l'inégalité HLS log est un cas dégénéré car une famille d'équilibre existe uniquement avec la masse critique (voir la discussion dans l'introduction). Dans le cas d'une diffusion type milieux poreux $\frac{\partial^2 n^m}{\partial x^2}$, $m>1$, un équilibre unique existe pour toute masse. Le cas de la dimension 2 et supérieure est en cours de prospection.

## B.3 Une preuve élémentaire de l'inégalité HLS log discrète et application au schéma numérique

Dans le chapitre 8, le besoin s'est fait sentir d'une version discrète de HLS log (B.13) adaptée au schéma numérique, en vue de démontrer un théorème discret à partir des idées nouvelles du chapitre 7 (voir aussi l'introduction pour un aperçu rapide). Ce qui suit vient compléter et achever le théorème numérique 8.15 du chapitre 8.

**Contexte numérique.** Soit $h=\frac{1}{N+1}$ un pas de maillage constant. On discrétise la fonction inverse de répartition $\Phi=(\Phi^i)_{\{i=1\dots N\}}$ croissante définie sur le maillage $[h,2h,\dots,1-h]$. Le but de ce paragraphe est de démontrer qu'à la condition nécessaire et suffisante $\chi(1-h)<2\pi$, il existe une unique solution au système

$$\forall k\in[\![1,N]\!]\quad 0 = \frac{1}{\Phi^{k+1}-\Phi^k} - \frac{1}{\Phi^k-\Phi^{k-1}} + \Phi^k + \frac{\chi}{\pi}\sum_{i\neq k} h\frac{1}{\Phi^i-\Phi^k}\ , \tag{B.11}$$

avec conditions de bord $\frac{1}{\Phi^{N+1}-\Phi^N} = \frac{1}{\Phi^1-\Phi^0} = 0$. Ceci est une conséquence de la formulation variationnelle suivante :

**Proposition B.4.** *Soit $(\Phi^i)$ une fonction discrète croissante. La fonctionnelle discrète d'énergie, définie par*

$$\mathcal{G}_h[\Phi] = -\sum_{i=1}^{N-1} h \log\Big(\frac{\Phi^{i+1}-\Phi^i}{h}\Big) + \frac{1}{2}\sum_{i=1}^{N} h|\Phi^i|^2 + \frac{\chi}{2\pi}\sum_{i=1}^{N}\sum_{j=1,\ j\neq i}^{N} h^2 \log|\Phi^j-\Phi^i|, \tag{B.12}$$

*est minorée et coercitive si $\chi(1-h) < 2\pi$. Par conséquent il existe une solution au problème d'équilibre* (B.11).

Calquant les méthodes continues, il s'agit de démontrer des variantes discrètes des inégalités de HLS logarithmique et de Carleman (voir le chapitre 8).

**Une inégalité de HLS log discrète.** Dans le cas d'un maillage discret, le facteur 'dimensionnel' $d_h = 1-h$ vient corriger la dimension $d = 1$ dans le cas continu.

$$\sum_{i=1}^{N}\sum_{j=1,\ j\neq i}^{N} h^2 \log|\Phi^j-\Phi^i| \geq (1-h)\sum_{i=1}^{N-1} h \log\Big(\frac{\Phi^{i+1}-\Phi^i}{h}\Big) + C_h. \tag{B.13}$$

Cette estimation entraîne naturellement l'existence d'un état stationnaire comme minimiseur de l'énergie lorsque $\chi(1-h) < 2\pi$. Ce coefficient correcteur $1-h$ est le seul envisageable pour une raisons d'homogénéité (si $\Phi$ est multipliée par un facteur $\lambda > 0$, $\lambda \to 0$ ou bien $\lambda \to \infty$, alors cette inégalité est violée si $d_h \neq 1-h$ car on fait ressortir le facteur $h(N-1)\big(hN-(1-h)\big)\log\lambda$). D'autre part, observons que $hN = d_h$.

Le membre gauche de (B.13) peut se réorganiser comme suit, en utilisant seulement la croissance de $(\Phi^i)$,

$$\begin{aligned}
\sum_{i=1}^{N}\sum_{j=1,\ j\neq i}^{N} h^2 \log|\Phi^j-\Phi^i| &= \sum_{i=1}^{N}\sum_{j=i+1}^{N} h^2\log(\Phi^j-\Phi^i) + \sum_{i=1}^{N}\sum_{j=1}^{i-1} h^2\log(\Phi^i-\Phi^j)\\
&\geq \sum_{i=1}^{N-1}\sum_{j=i+1}^{N} h^2\log(\Phi^{i+1}-\Phi^i) + \sum_{k=1}^{N-1}\sum_{j=1}^{k} h^2\log(\Phi^{k+1}-\Phi^j)\\
&\geq \sum_{i=1}^{N-1} h^2(N-i)\log(\Phi^{i+1}-\Phi^i) + \sum_{k=1}^{N-1} h^2 k\log(\Phi^{k+1}-\Phi^k)\\
&= \sum_{i=1}^{N-1} h(hN)\log(\Phi^{i+1}-\Phi^i)\\
&= d_h\sum_{i=1}^{N-1} h\log\Big(\frac{\Phi^{i+1}-\Phi^i}{h}\Big) + C_h\ ,
\end{aligned}$$

ce qui achève la preuve de la proposition B.4.

**Une inégalité de Carleman discrète.** Venons en au deuxième point de l'existence de l'état stationnaire (la compacité en quelque sorte). L'inégalité de Carleman est au centre de ces pérégrinations. Rappelons que dans un contexte continu, l'inégalité de Carleman utilisée au chapitre 8 s'écrit

$$\int n(x)\Big(\log n(x) + \frac{1}{2}|x|^2\Big)\,\mathrm{d}x \geq \int n(x)\,|\log n(x)|\,\mathrm{d}x + C\ .$$

En voici une version discrète adaptée à notre sujet :

$$-\sum_{i=1}^{N-1} h\log\Big(\frac{\Phi^{i+1}-\Phi^i}{h}\Big) + \frac{1}{2}\sum_{i=1}^{N} h|\Phi_i|^2 \geq C_h. \tag{B.14}$$

Introduisons la 'médiane' de $\Phi$ : il existe $k_0$ tel que $|\Phi^{k_0}| = \min|\Phi^k|$. Avec ce choix nous avons en particulier : $\Phi^k \leq 0$ pour $k < k_0$ et $\Phi^k \geq 0$ pour $k > k_0$. Ainsi

$$
\begin{aligned}
&- \sum_{i=1}^{N-1} h \log\Big(\frac{\Phi^{i+1}-\Phi^i}{h}\Big) + \frac{1}{2}\sum_{i=1}^{N} h|\Phi^i|^2 \\
&\geq - \sum_{i=1}^{N-1} h \log\Big(\frac{\Phi^{i+1}-\Phi^i}{h}\Big) + \frac{1}{2}\sum_{i=1,\ i\neq k_0}^{N} h|\Phi^i|^2 \\
&= -h(N-1)\sum_{i=1}^{k_0-1}\frac{1}{N-1}\log\Big((\Phi^{i+1}-\Phi^i)e^{-\frac{1}{2}|\Phi^i|^2}\Big) - h(N-1)\sum_{i=k_0}^{N-1}\frac{1}{N-1}\log\Big((\Phi^{i+1}-\Phi^i)e^{-\frac{1}{2}|\Phi^{i+1}|^2}\Big) + C_h \\
&\geq -h(N-1)\log\left(\frac{1}{N-1}\sum_{i=1}^{k_0-1}(\Phi^{i+1}-\Phi^i)e^{-\frac{1}{2}|\Phi^i|^2} + \frac{1}{N-1}\sum_{i=k_0}^{N-1}(\Phi^{i+1}-\Phi^i)e^{-\frac{1}{2}|\Phi^{i+1}|^2}\right) + C_h \\
&\geq C_h\ ,
\end{aligned}
$$

par l'inégalité de Jensen, et grâce au choix de la médiane $\Phi^{k_0}$. La dernière minoration provient de :

$$
\begin{aligned}
&\sum_{i=1}^{k_0-1} e^{-\frac{1}{2}|\Phi^i|^2}(\Phi^{i+1}-\Phi^i) + \sum_{i=k_0}^{N-1} e^{-\frac{1}{2}|\Phi^{i+1}|^2}(\Phi^{i+1}-\Phi^i) \\
&\leq \sum_{i=1}^{k_0-1} e^{-\frac{1}{2}|\Phi^i|^2}|\Phi^i| + e^{-\frac{1}{2}|\Phi^{k_0-1}|^2}|\Phi^{k_0}| + e^{-\frac{1}{2}|\Phi^{k_0+1}|^2}|\Phi^{k_0}| + \sum_{i=k_0}^{N-1} e^{-\frac{1}{2}|\Phi^{i+1}|^2}|\Phi^{i+1}| \\
&\leq C_h\ ,
\end{aligned}
$$

car la fonction $e^{-\frac{1}{2}|X|^2}|X|$ est bornée, et $k_0$ est précisément la médiane de $\Phi$, de sorte que $|\Phi^{k_0}| \leq \min(|\Phi^{k_0-1}|, |\Phi^{k_0+1}|)$.

Un produit dérivé des deux inégalités précédentes (HLS log et Carleman) est l'estimation *a priori* de coercitivité qui prélude généralement à l'existence d'un état d'équilibre. On définit le facteur $\theta = \dfrac{\chi(1-h)}{2\pi} < 1$ tel que l'inégalité HLS log (B.13) donne,

$$
\mathcal{G}_h[\Phi] \geq (1-\theta)\left(-\sum_{i=1}^{N-1} h\log\Big(\frac{\Phi^{i+1}-\Phi^i}{h}\Big)\right) + \frac{1}{2}\sum_{i=1}^{N} h|\Phi^i|^2 + C_h\ . \tag{B.15}
$$

Ceci combiné avec l'estimation de Carleman (B.14) garantit

$$
\mathcal{G}_h[\Phi] \geq \frac{\theta}{2}\sum_{i=1}^{N} h|\Phi^i|^2 + C_h,
$$

de sorte que la fonctionnelle d'énergie libre est coercitive. Pour conclure il reste à vérifier qu'une suite minimisante ne peut en aucun cas 'exploser', ici que $\Phi_{i+1}-\Phi_i$ ne peut pas s'écraser en zéro. En l'occurrence cela contredirait le caractère minimisant des suites dans (B.15).

## B.4 Dualité Trudinger-Moser/HLS log

La dualité entre ces deux inégalités en dimension 2 est évoquée dans [48] et esquissée dans [23]. Nous donnons ici plus de détails. Si l'on se replace dans le contexte des modèles de Keller-Segel, l'inégalité de Trudinger-Moser, adaptée aux conditions de Neumann [68, 107],

$$
\forall c \in H^1 \text{ t.q. } \int_\Omega c = 0\ ,\quad \int_\Omega \exp(\chi c)\,dx \leq C(\Omega)\exp\Big(\frac{\chi^2}{8\pi}\int_\Omega |\nabla c|^2\,dx\Big). \tag{B.16}
$$

est utilisée pour démontrer l'existence globale en domaine borné. L'inégalité HLS log (B.1) pour sa part est utilisée lorsque le problème est posé dans l'espace $\mathbb{R}^2$ tout entier. Ces deux approches ont été unifiées dans le chapitre 3 pour le système de KS à coefficients linéaires dans tout l'espace.

D'après [23], la dualité entre HLS log et TM peut se concevoir dans le cadre très abstrait suivant,

**Proposition B.5.** *Soient $K, \Lambda$ deux opérateurs auto-adjoints positifs définis sur un espace mesuré $\sigma-$fini, et qui satisfont $\Lambda K = K\Lambda = 1$. Alors les deux inégalités suivantes sont équivalentes :*

$$\int f(Kf) \leq \int f \log f + C \quad \textit{quelque soit } f \geq 0, \int f = 1, \tag{B.17}$$

$$\log \int e^{2g} \leq \int |\Lambda^{1/2} g|^2 + C \quad \textit{quelque soit } g \in D(\Lambda). \tag{B.18}$$

**Dualité en domaine borné.** Dans ce paragraphe nous avons à cœur de développer autour de la proposition B.5 pour un domaine borné régulier $\Omega \subset \mathbb{R}^2$.

Tout d'abord on définit la fonction auxiliaire constante $h_\Omega = 1/|\Omega|$. On introduit $\Lambda_0 g = -\Delta g$, avec la convention que $\int g = 0$, ainsi que le problème inverse $K_0(f-h) = B_0 * (f-h)$, où $B_0$ est la fonction de Green correspondant à l'opérateur $-\Delta$ associé aux conditions de Neumann sur $\partial\Omega$. On rajoute par convention que $\int K_0(f-h) = 0$. Le poids de la singularité de $B_0(x,a)$ est $\frac{1}{2\pi}\log|x-a|^{-1}$ si $a \in \Omega$, et $\frac{1}{\pi}\log|x-a|^{-1}$ si $a$ est localisé sur $\partial\Omega$, à cause de la réflexion sur la frontière. Par conséquent on a en toute généralité $B_0 \leq \frac{1}{\pi}\log|x-a|^{-1} + C$.

**Proposition B.6** (Dualité en domaine borné)**.** *L'inégalité de Trudinger-Moser*

$$\forall g \in H^1 \ \text{ t.q.} \int g = 0 \ , \quad \int_\Omega \exp(4\pi g)\, dx \leq C(\Omega) \exp\left(2\pi \int_\Omega |\nabla g|^2\, dx\right) \ ,$$

*et l'inégalité de HLS log 'en domaine borné'*

$$\forall f \in L\log L \ \text{ t.q.} \int f = 1 \ , \quad \iint_{\Omega\times\Omega} f(x) B_0(x,y) f(y) \leq \frac{1}{2\pi}\int_\Omega f\log f + C(\Omega) \ ,$$

*sont duales.*

Il est bon de noter que cette proposition ne démontre aucune des deux inégalités ci-dessus indépendamment l'une de l'autre. A titre d'exemple, l'inégalité de HLS log en domaine borné se déduit de l'inégalité dans tout l'espace (B.1) :

$$\begin{aligned} \iint_{\Omega\times\Omega} f(x) B_0(x,y) f(y) &\leq \frac{1}{\pi}\iint_{\mathbb{R}^2\times\mathbb{R}^2} f(x)\mathbf{1}_{x\in\Omega}\log|x-y|^{-1} f(y)\mathbf{1}_{y\in\Omega} + C(\Omega) \\ &\leq \frac{1}{2\pi}\int f\log f + C, \end{aligned}$$

où l'on a aussi utilisé que $|x-y|$ reste borné lorsque $x$ et $y$ sont dans $\Omega$.

*Démonstration.* On ne détaille qu'un seul sens de la dualité. La réciproque s'obtient de la même manière (à titre d'exemple, le sens inverse est présenté dans tout l'espace, voir ci-dessous).

Soit $g$ une fonction dans le domaine de définition de $\Lambda_0$. On cherche à maximiser la fonctionnelle quadratique

$$\mathcal{H}_0(f) = \int (f-h)g - \frac{1}{2}\int (f-h)K_0(f-h),$$

sous la contrainte $\int f = 1$. La contrainte induit un multiplicateur de Lagrange constant $\mu : K_0(\underline{f}-h) - g = \mu = 0$ car les fonctions sont de moyenne nulle. Par conséquent le maximum est réalisé pour $\underline{f}$ tel que

$-\Delta g = \underline{f} - h$. La valeur maximale de $\mathcal{H}_0$ vaut alors $\frac{1}{2}\int(\underline{f}-h)K_0(\underline{f}-h) = \frac{1}{2}\int|\nabla g|^2$. Il vient

$$\begin{aligned}\frac{1}{2}\int|\nabla g|^2 &\geq \sup\left\{\int(f-h)g - \frac{1}{2}\int(f-h)K_0(f-h)\ \Big|\ \int f = 1\right\}\\ &\geq \sup\left\{\int fg - \frac{1}{2}\iint f(x)B_0(x,y)f(y)\ \Big|\ \int f = 1\right\} + C(\Omega)\\ &\geq \frac{1}{4\pi}\sup\left\{4\pi\int fg - \int f(x)\log f(x)\ dx\ \Big|\ \int f = 1\right\} + C\ .\end{aligned}$$

On reconnaît la transformée de Legendre de la fonction $4\pi g$, ce qui amène à conclure :

$$\frac{1}{2}\int|\nabla g|^2 \geq \frac{1}{4\pi}\log\left(\int\exp(4\pi g)\right) + C\ .$$

De fait, si on redéfinit $c = 4\pi g/\chi$, on retrouve (B.16). □

**Dualité dans tout l'espace.** Enonçons tout d'abord l'inégalité de Trudinger-Moser-Onofri [196, 23] que nous avons pour l'espace $\mathbb{R}^2$ tout entier. Nous la ramenons de la sphère (voir le paragraphe 3), c'est pourquoi il est judicieux de définir à nouveau le jacobien de la projection stéréographique inverse,

$$h_{\mathbb{R}^2}(x) = \frac{1}{\pi}\frac{1}{(1+|x|^2)^2}\ ,$$

**Théorème B.7** (L'inégalité de Trudinger-Moser dans tout l'espace $\mathbb{R}^2$)**.** *Soit $g$ un potentiel appartenant à $H^1(\mathbb{R}^2)$. Alors $e^{8\pi g}\in L^1(h(x)dx)$ avec l'estimation*

$$\frac{1}{8\pi}\log\left(\int_{\mathbb{R}^2}e^{8\pi g(x)}h(x)\ dx\right) \leq \frac{1}{2}\int_{\mathbb{R}^2}|\nabla g(x)|^2\ dx + \int_{\mathbb{R}^2}g(x)h(x)\ dx\ . \tag{B.19}$$

*Il est remarquable qu'il n'y ait pas de constante additive supplémentaire.*

A l'inverse du paragraphe précédent nous détaillons ici la réciproque de la dualité. Soit une densité $f$ dans $L^1_+(\mathbb{R}^2)$ de masse 1. On suppose de plus que $f\in L\log L\cap L^1\big(\log(1+|x|^2)\big)$. Nous avons vu au-dessus que le passage d'une inégalité à l'autre s'appuie essentiellement sur la résolution de $-\Delta\underline{g} = f$. Seulement une telle solution, définie comme

$$\underline{g}(x) = -\frac{1}{2\pi}\int\log|x-y|f(y)\ dy\ ,$$

ne vérifie pas $\nabla\underline{g}\in L^2$ en général. Pour corriger ce défaut on introduit le potentiel négatif $\phi(x) = -\frac{1}{4\pi}\log(1+|x|^2)$ qui vérifie $-\Delta\phi = h$ et $e^{8\pi\phi} = \pi h$ ; et on définit $\tilde{g}$ par la déviation $g = \tilde{g}+\phi$, ce qui revient à résoudre $-\Delta\tilde{g} = f-h$.

On cherche à maximiser la fonctionnelle quadratique

$$\mathcal{H}_0(g) = \int\tilde{g}(f-h) - \frac{1}{2}\int|\nabla\tilde{g}|^2.$$

Le maximum est atteint pour $\underline{\tilde{g}}$ tel que $-\Delta\underline{\tilde{g}} = f-h$, qui vérifie $\nabla\underline{\tilde{g}}\in L^2$ par compensation (voir l'appendice du chapitre 3). Ce maximum vaut

$$\begin{aligned}\sup\mathcal{H}_0 &= \frac{1}{2}\int|\nabla\underline{\tilde{g}}|^2\ dx = \frac{1}{2}\int\underline{\tilde{g}}(-\Delta\underline{\tilde{g}})\\ &= \frac{1}{2}\int(\underline{g}-\phi)(f-h) = \frac{1}{2}\int\underline{g}f + \frac{1}{2}\int\phi h - \frac{1}{2}\int\underline{g}h - \frac{1}{2}\int\phi f\\ &= \frac{1}{2}\int\underline{g}f + \frac{1}{2}\int\phi h - \int\phi f,\end{aligned}$$

après avoir intégré par parties : $\int \underline{g}(-\Delta\phi) = \int (-\Delta \underline{g})\phi$.

D'autre part, d'après le théorème B.7 nous avons

$$\begin{aligned}\int \tilde{g}(f-h) - \frac{1}{2}\int |\nabla \tilde{g}|^2 &\leq \int \tilde{g}(f-h) + \int \tilde{g}h - \frac{1}{8\pi}\log\left(\int e^{8\pi(g-\phi)}h(x)\ dx\right)\\ &= \int gf - \int \phi f - \frac{1}{8\pi}\log\left(\frac{1}{\pi}\int e^{8\pi g}\ dx\right) + C.\end{aligned}$$

Si on passe au maximum à gauche puis à droite, on obtient

$$\frac{1}{2}\int \underline{g}f + \frac{1}{2}\int \phi h - \int \phi f \leq \frac{1}{8\pi}\sup_g\left\{\int gf - \log\left(\int e^{8\pi g}\ dx\right)\right\} - \int \phi f + \frac{1}{8\pi}\log\pi,$$

où l'on reconnaît une transformée de Legendre dans le membre de droite. En conclusion,

$$-\frac{1}{4\pi}\iint f(x)\log|x-y|f(y)\ dxdy \leq \frac{1}{8\pi}\int f(x)\log f(x)\ dx - \frac{1}{2}\int \phi(x)h(x)\ dx + \frac{1}{8\pi}\log\pi.$$

Nous venons ainsi de démontrer la moitié d'un théorème de dualité : HLS log (B.1) se déduit de Trudinger-Moser-Onofri dans tout l'espace $\mathbb{R}^2$ par une méthode similaire au domaine borné, à ceci près qu'il convient de prendre en compte un poids $h$ non constant. Remarquons que tous ces calculs sont en fait adaptés de la dualité sur la sphère [56, 23].

# Annexe C

# Equations cinétiques : Vlasov-Poisson, Brascamp-Lieb et le lemme de dispersion

## C.1 De la particule à Vlasov-Poisson

Dans ce premier paragraphe nous présentons très rapidement les considérations qui aboutissent aux modèles cinétiques très généraux tels qu'étudiés au chapitre 5. Pour (beaucoup) plus d'informations, on renvoie à [207, 209, 175].

Les lois de la physique newtonienne décrivent le mouvement d'une particule soumise à un champ de forces $F$ :

$$\left\{ \begin{array}{ll} \dot{x} = v & x(t=0) = x_0 \\ \dot{v} = \frac{1}{m} F & v(t=0) = v_0 \ . \end{array} \right.$$

En physique statistique la 'population' de particules est décrite par sa densité dans l'espace position/vitesse $f(t,x,v)$ : le nombre de particules dans la portion $A \subset \mathbb{R}^3 \times \mathbb{R}^3$ est $\iint_A f(t,x,v)\ dxdv$. La dynamique de $f$ est régie, dans un tel cadre hamiltonien, par une équation aux dérivées partielles qui exprime que l'évolution de la densité le long de la trajectoire de chaque particule est nulle :

$$\begin{aligned} &\frac{d}{dt} f\big(t, x(t), v(t)\big) = 0 \ , \\ &\frac{\partial f}{\partial t} + v \cdot \nabla_x f + \frac{1}{m} F(x) \cdot \nabla_v f = 0 \ , \end{aligned}$$

avec la donnée initiale $f(0,\cdot,\cdot) = f_0$. C'est l'équation de Liouville (ou de Vlasov). En particulier si le champ de force $F$ est nul, on retrouve l'équation de transport libre,

$$\frac{\partial f}{\partial t} + v \cdot \nabla_x f = 0 \ .$$

Dans bon nombre de situations, le champ de forces découle d'un potentiel : $F = m\nabla\phi$ qui est produit par les particules elles-même : on parle d'interactions à longue portée (*e.g.* forces gravitationnelles, électrostatiques, forces chimiotactiques avec hypothèse de remontée le long du gradient chimique). On obtient alors le système de Vlasov-Poisson

$$\left\{ \begin{array}{l} \dfrac{\partial f}{\partial t} + v \cdot \nabla_x f + \nabla\phi \cdot \nabla_v f = 0 \\ -\Delta\phi = \displaystyle\int f \ dv \ . \end{array} \right.$$

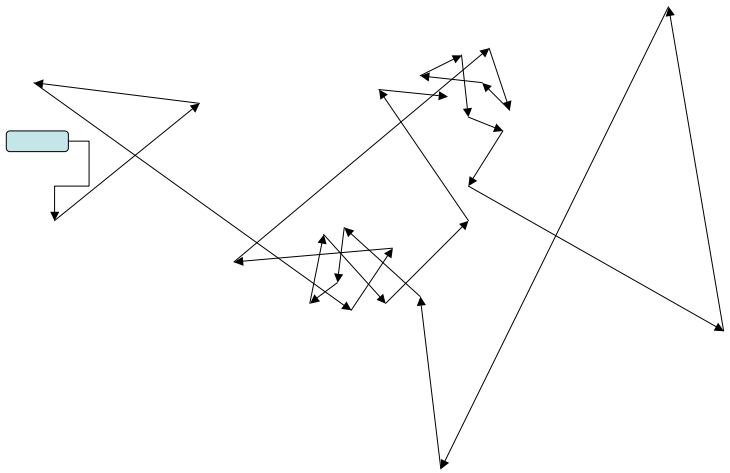

FIG. C.1 – La course d'une bactérie entrecoupée de changements de direction. On distingue nettement les zones de forte concentration en signal chimique.

On peut ajouter à cela des interactions locales entre les particules. L'équation de Boltzmann [243] en est l'exemple le plus fameux, qui rend compte des collisions entre des particules en course libre. Dans le contexte du chimiotactisme, on s'intéresse plutôt à des réorientations individuelles des bactéries assujetties à un champ de signalisation. La trajectoire des bactéries est grossièrement rectiligne par morceaux (voir figure C.1). Au cours du temps, la cellule subit des événements très courts de réorientation ('tumble phase'), dont la fréquence dépend de la concentration chimique. Lorsque cette concentration s'accroît, les changements de direction deviennent monnaie courante, ce qui a pour effet de confiner les bactéries dans ces régions où le signal est très fort.

Dans le processus de modélisation [198] on ajoute un terme de changement de direction à l'équation de transport libre. Le potentiel chimique $S$ est produit par les cellules elles-même.

$$\frac{\partial f}{\partial t} + v \cdot \nabla_x f = \mathcal{T}[S]f - \lambda[S]\rho \ ,$$
$$-\Delta S = \rho = \int f \ dv \ ,$$

où l'opérateur $\mathcal{T}$ est linéaire en la densité $f$, mais induit une non-linéarité quadratique au travers de sa dépendance en $S$ (voir paragraphe C.2.2).

## C.2 L'inégalité de Brascamp-Lieb : extension aux normes mixtes en position/vitesse

L'inégalité de Brascamp-Lieb [168] fait partie des inégalités géométriques qui ont connu un regain d'intérêt avec les récentes avancées obtenues grâce aux techniques de transport optimal et tout particulièrement les travaux de McCann ou Barthe [179, 21, 22]. De façon surprenante, cette inégalité apparaît également de manière cachée dans les estimations d'existence globale pour le modèle cinétique de chimiotactisme (chapitre 5), en raison du mélange des variables du à l'effet de mémoire. Dans la suite, nous

faisons un rapide survol des inégalités géométriques qui conduisent à l'inégalité de Brascamp-Lieb générale démontrée par Barthe. Puis nous montrons le lien avec le problème cinétique, et nous en déduisons par interpolation une inégalité de Brascamp-Lieb qui autorise des normes mixtes $L^p_x L^q_v$ en position/vitesse.

### C.2.1 Inégalités géométriques autour des inégalités de Brunn-Minkowsky et de Young

**Brunn-Minkowsky : une preuve d'après McCann.** Commençons avec l'inégalité de Brunn-Minkowsky qui certifie une propriété de concavité pour une certaine longueur caractéristique des ensembles compacts de $\mathbb{R}^n$. On renvoie à [109] pour un état de l'art très complet autour de cette inégalité.

**Théorème C.1** (Inégalité de Brunn-Minkowsky)**.** *Soient $X$, $Y$ deux compacts de $\mathbb{R}^d$. Alors pour tout $t \in (0,1)$ on a*

$$|(1-t)X + tY|^{1/d} \geq (1-t)|X|^{1/d} + t|Y|^{1/d}.$$

*Démonstration.* Un résultat fondamental issue de la théorie du transport optimal de masse (annexe D) est la convexité par déplacement de la fonctionnelle de la densité $\rho$,

$$\mathcal{U}(\rho) = -\int \rho(x)^{1-1/d}\, dx\ ,$$

où l'exposant $1 - 1/d$ est critique [179]. Ceci découle de l'inégalité arithmético-géométrique pour les matrices symétriques positives. L'inégalité de Brunn-Minkowsky s'en déduit en appliquant cette inégalité de convexité aux densités caractéristiques des ensembles $X$ et $Y$.

On introduit $\rho_0 = \dfrac{\mathbf{1}_X}{|X|}$ et $\rho_1 = \dfrac{\mathbf{1}_Y}{|Y|}$. Alors $\mathcal{U}(\rho_0) = -|X||X|^{1/d-1} = -|X|^{1/d}$, et de même pour $|Y|$. On définit l'interpolant par déplacement (annexe D) $\rho_t = [\rho_0, \rho_1]_t$ pour $t \in (0,1)$, et on note $S_t = \text{Supp}\ \rho_t$. On ne sait pas en général si $\rho_t$ est une densité caractéristique, en revanche

$$\begin{aligned}
\mathcal{U}(\rho_t) &= -|S_t| \int \rho_t(x)^{1-1/d} \frac{dx}{|S_t|} \\
&\geq -|S_t| \left( \int \rho_t(x) \frac{dx}{|S_t|} \right)^{1-1/d} \\
&= -|S_t|^{1/d}.
\end{aligned}$$

Au final, l'inégalité de convexité

$$\mathcal{U}(\rho_t) \leq (1-t)\mathcal{U}(\rho_0) + t\mathcal{U}(\rho_1),$$

se réécrit

$$|S_t|^{1/d} \geq (1-t)|X|^{1/d} + t|Y|^{1/d}.$$

Il reste à vérifier que $S_t \subset (1-t)X + tY$, ce qui découle de la définition de $\rho_t$ :

$$\rho_t = \Big[(1-t)Id + t\nabla\varphi\Big] \# \rho_0,$$

avec $\nabla\varphi : X \to Y$. Il semblerait que l'on perde beaucoup de 'volume' dans cette dernière estimation, mais le fait est que $S_t = (1-t)X + tY$ si $X$ et $Y$ sont convexes. □

Les implications de cette inégalité sont nombreuses. Rappelons ici :

(i) elle est équivalente à une inégalité isopérimétrique régulière dans $\mathbb{R}^d$,

$$\left(\frac{S(X)}{S(B)}\right)^{1/(d-1)} \geq \left(\frac{|X|}{|B|}\right)^{1/d}\ . \tag{C.1}$$

(ii) elle est à la base de la théorie des corps convexes [22],

(iii) l'inégalité de Sobolev optimale

$$\|f\|_{L^{d/(d-1)}} \leq \frac{1}{d|B|^{1/d}} \|\nabla f\|_{L^1},$$

est une version fonctionnelle de l'inégalité isopérimétrique (C.1).

**Une version fonctionnelle de BM : l'inégalité de Prékopa-Leindler.**

**Théorème C.2.** *Soient $f$, $g$, $h$ des fonctions positives intégrables, telles que $h\big((1-t)x+ty\big) \geq f(x)^{1-t}g(y)^t$. Alors*

$$\int_{\mathbb{R}^n} h(z)\ dz \geq \left(\int f(x)\ dx\right)^{1-t} \left(\int g(y)\right)^t .$$

Il existe plusieurs preuves à base de transport optimal et d'inégalité arithmético-géométrique pour les matrices symétriques. Nous nous contenterons ici de quelques remarques :

(i) L'inégalité PL entraine BM à l'aide des fonctions caractéristiques.

(ii) PL est une forme renversée de l'inégalité de Hölder. Avec $t = 1/q$, $1-t = 1/p$, et $f = f_0^p$, $g = g_0^q$, Hölder s'écrit

$$\int f(x)^{1-t}g(x)^t\ dx \leq \left(\int f(x)\ dx\right)^{1-t} \left(\int g(y)\right)^t ,$$

ce qui montre bien que la fonction $h$ dans PL doit être bornée inférieurement d'une façon ou d'une autre, ce qui justifie *a posteriori* l'hypothèse sur $h$ dans le théorème C.2.

**L'inégalité de Brascamp-Lieb.** Voici une généralisation englobant les inégalités précédentes. Elle met en jeu un 'mélange linéaire des variables'. Mais auparavant, un exemple.

**Exemple C.3.** *L'inégalité de Young pour les produits de convolution exprime la chose suivante :*

$$\|f*g\|_{L^{r'}} \leq A\|f\|_{L^p}\|g\|_{L^q}\ , \quad 1+\frac{1}{r'} = \frac{1}{p}+\frac{1}{q}.$$

*Il existe une formulation de cette inégalité par dualité [168], qui fait jouer des rôles symétriques aux exposants,*

$$\iint f(x)g(x-y)h(y)\,dxdy \leq A\|f\|_{L^p}\|g\|_{L^q}\|h\|_{L^r}\ ,$$
$$\frac{1}{p}+\frac{1}{q}+\frac{1}{r} = 2\ ,\ A = (A_pA_qA_r)^d\ ,\ A_p = \sqrt{\frac{p^{1/p}}{p'^{1/p'}}}.$$

**Théorème C.4** (Inégalité de Brascamp-Lieb)**.** *Soient $N \in \mathbb{N}$, $d_i \in \mathbb{N}$ et $p_i \in [0,\infty)$ tels que*

$$\sum_{i=1}^m \frac{d_i}{p_i} = N.$$

*Soient $B_i : \mathbb{R}^N \to \mathbb{R}^{d_i}$ des applications linéaires surjectives. Alors*

$$\int_{\mathbb{R}^N} \prod_{i=1}^m f_i(B_ix)\ dx \leq \frac{1}{\sqrt{D}} \prod_{i=1}^m \|f_i\|_{L^{p_i}}. \tag{C.2}$$

*Pour l'instant rien n'est dit car la constante $D$ est éventuellement nulle. Il est remarquable que la constante optimale puisse être évaluée parmi les fonctions gaussiennes centrées, autrement dit,*

$$D = \inf\left\{ \frac{\det\left(\sum \frac{1}{p_i}B_i^*A_iB_i\right)}{\prod(\det A_i)^{1/p_i}}\ ;\quad A_i \in \mathcal{S}_{d_i}^+ \right\}. \tag{C.3}$$

**Exemple C.5.** *Avec $N = 2d$ et $d_1 = d_2 = d_3 = d$, avec*

$$B_1(x,y) = x\ ,\quad B_2(x,y) = x-y\ ,\quad B_3(x,y) = y$$

*on retrouve l'inégalité de Young.*

Pour la preuve nous renvoyons à [22] (voir aussi [244]). Le lien entre PL et BL vient de ce que Barthe a en fait démontré une forme renversée de BL qui généralise PL (non présentée ici, voir [21]). Précisons que la technique du transport optimal de masse permet de 'transporter' l'inégalité fonctionnelle (C.2) vers une inégalité matricielle (C.3) tout comme l'inégalité de Brunn-Minkowski devient, après transport, une simple inégalité arithmético-géométrique (voir aussi annexe D). Cette idée de reformuler le problème en une inégalité plus simple (tout simplement AG en 1D par exemple), a éte mise à l'œuvre au chapitre 7, dans lequel des inégalités ponctuelles 1D telles que Jensen impliquent des inégalités fonctionnelles telles que l'inégalité de Hardy-Littlewood-Sobolev à poids logarithmique, avec des variantes correspondant à des diffusions non linéaires.

### C.2.2 L'effet de mémoire et l'inégalité de Brascamp–Lieb généralisée

Après cette courte introduction à l'inégalité de Brascamp-Lieb et consorts, motivons l'inégalité (C.2) dans le cadre du modèle cinétique de Keller-Segel [198, 66, 96].

**Notations.** Par convention dans les modèles cinétiques, $f(t,x,v)$ et $\rho(t,x) = \int f(t,x,v)\ dv$ décrivent la densité cellulaire, et $S$ désigne la concentration chimique, donnée par une équation de champ moyen :

$$-\Delta S = \rho\ , \quad \text{ou} \quad -\Delta S + \alpha S = \rho.$$

On s'intéresse à un modèle cinétique avec effet de mémoire (ou d'inertie réactionnelle, voir l'interprétation ci-dessous),

$$\partial_t f + v\cdot\nabla_x f = \int_{v'\in V} T f(t,x,v')\ dv' - \lambda\rho. \tag{C.4}$$

Le noyau de changement de direction des cellules est bien sûr fonction de $S$ (voir le chapitre 5), mais c'est surtout sa dépendance en les variables $v$ ou $v'$ qui nous intéresse ici. On fait l'hypothèse que $T$ dépend d'une position antérieure (resp. ultérieure) des cellules :

$$0 \le T(t, x-\varepsilon v') \quad \text{ou} \quad 0 \le T(t, x+\varepsilon v),$$

où $\varepsilon$ est un paramètre temporel d'inertie (positif ou négatif), que nous fixerons à 1 par souci de simplicité, sans changer les résultats d'un iota.

**Interprétation.** Dans [96] la cinétique interne à la cellule en déplacement est considérée. Un effet de mémoire 'antérieur' $T(t,x-\varepsilon v')$ modélise par exemple un organisme dont la 'prise de décision stochastique' du changement de direction est retardée du fait de la chaîne de réactions complexes mise en œuvre à l'intérieur de la cellule. Durant ce temps, l'organisme a parcouru une certaine distance $\varepsilon v'$ (ceci est le cas d'une cellule de petite taille, disons la bactérie *E. Coli* par exemple). Un effet de mémoire 'ultérieur' $T(t,x+\varepsilon v)$ peut modéliser des organismes de plus grande taille qui envoient des protrusions (*lamellipodium*) 'en reconnaissance' dans un rayon d'action $\varepsilon V$. Ils privilégient alors le mouvement dans les directions $x+\varepsilon v$ où la concentration est la plus élevée (c'est le cas par exemple de *D. discoideum*).

La solution de (C.4) s'exprime en fonction de l'historique de la trajectoire des bactéries :

$$f(t,x,v) = f_0(x,v) + \int_0^t \int_{v'} T(t-s, x-sv-v') f(t-s, x-sv, v')\ dv' ds$$
$$\text{ou} \quad \int_0^t \int_{v'} T(t-s, x-sv+v) f(t-s, x-sv, v')\ dv' ds\ .$$

La partie délicate à évaluer dans la solution du problème (C.4) est la contribution

$$f^-(t,x,v) = \int_0^t \int_{v'} T(t-s, x-sv-v') f(t-s, x-sv, v')\ dv' \tag{C.5}$$

pour l'effet antérieur, et

$$f^+(t,x,v) = \int_0^t \int_{v'} T(t-s, x-sv+v) f(t-s, x-sv, v')\ dv'\ ds \tag{C.6}$$

pour l'effet ultérieur. Pour des raisons techniques, nous valorisons la dépendance ultérieure $T(t, x+v)$. Une des avancées du chapitre 5 est l'estimation

$$\|f^+(t,x,v)\|_{L^p_x L^q_v} \leq \int_s \frac{1}{(1-s)^{3(1/q-1/p)}} \|\rho(t-s)\|_{L^p}\ \|T(t-s)\|_{L^q}, \quad 1 \leq q \leq p\ , \tag{C.7}$$

ce qui permet des estimations fines grâce aux normes mixtes en position/vitesse. Dans la suite nous faisons le lien entre un cas particulier de (C.7) et l'inégalité de Brascamp-Lieb. La forme générale de (C.7) est une conséquence simple du lemme de dispersion [18, 64] qui s'obtient lui-même par interpolation. Ce parallèle conduit à une forme légèrement plus affinée de BL incluant des normes mixtes.

**L'inégalité de dispersion 1D et BL.** Pour (C.7) dans le cas $q = 1$, nous avons

$$\|\rho^+(t,x)\|_{L^p_x} \leq \int_s \frac{1}{(1-s)^{3(1-1/p)}} \|\rho(t-s)\|_{L^p}\ \|T(t-s)\|_{L^1}, \tag{C.8}$$

et un lemme de Gronwall peut être appliqué en général. Pour réaliser (C.7) ou (C.8) on peut tester $f^+$ contre une fonction $\varphi(x,v)$,

$$\iint_{\mathbb{R}^d \times \mathbb{R}^d} f^+(t,x,v)\ \varphi(x,v)\ dv\ dx = \int_{s=0}^t \int_{x\in\mathbb{R}^d} \int_{v\in\mathbb{R}^d} T(x-sv+v)\ \rho(x-sv)\ \varphi(x,v). \tag{C.9}$$

Si l'on veut $q = 1$ on se doit de sortir dans le membre de droite $\|\varphi(x,v)\|_{L^\infty_v}$, ce qui amène à considérer des fonctions tests $\varphi$ indépendantes de la vitesse $v$ :

$$\int_{\mathbb{R}^d} \rho^+(t,x)\ \varphi(x)\ dx = \int_{s=0}^t \int_x \int_v T(x-sv+v)\ \rho(x-sv)\ \varphi(x). \tag{C.10}$$

On reconnaît une forme d'application de l'inégalité de Brascamp-Lieb (mélange linéaire des variables), plus sophistiquée que l'inégalité de Young (exemple C.3). Les détails sont présentés ci-dessous en une dimension.

**Corollaire C.6** (Exemple 1D)**.** *Soient $p \geq 1$ et $p'$ son exposant conjugué. L'inégalité suivante de type Young est valide pour tout $0 \leq s < 1$,*

$$\int_x \int_v g_1(x-vs+v) g_2(x-vs) g_3(x) dv dx \leq \frac{1}{(1-s)^{1-1/p}} \|g_1\|_{L^1} \|g_2\|_{L^p} \|g_3\|_{L^{p'}}. \tag{C.11}$$

*Démonstration.* On commence par mettre en place le matériel nécessaire à l'application de l'inégalité de Brascamp-Lieb,

$$\begin{aligned} B_1 &= (1 \ \ 1-s) & B_1^* B_1 &= \begin{pmatrix} 1 & 1-s \\ 1-s & (1-s)^2 \end{pmatrix} \\ B_2 &= (1 \ \ -s) & B_2^* B_2 &= \begin{pmatrix} 1 & -s \\ -s & s^2 \end{pmatrix} \\ B_3 &= (1 \ \ 0) & B_3^* B_3 &= \begin{pmatrix} 1 & 0 \\ 0 & 0 \end{pmatrix} \end{aligned}$$

Nous souhaitons montrer l'inégalité matricielle suivante,

$$\det\left( a_1 \begin{pmatrix} 1 & 1-s \\ 1-s & (1-s)^2 \end{pmatrix} + \frac{a_2}{p} \begin{pmatrix} 1 & -s \\ -s & s^2 \end{pmatrix} + \frac{a_3}{p'} \begin{pmatrix} 1 & 0 \\ 0 & 0 \end{pmatrix} \right) \geq C a_1 a_2^{1/p} a_3^{1/p'}.$$

Après quelques remaniements, on trouve que le déterminant se réduit à

$$\frac{a_1a_2}{p}+\frac{a_1a_3}{p'}(1-s)^2+\frac{a_2a_3}{pp'}s^2\geq a_1\Big(\frac{a_2}{p}+\frac{a_3}{p'}(1-s)^2\Big).$$

L'inégalité de Young nous informe que ce dernier terme est finalement supérieur à

$$(1-s)^{2/p'}a_1a_2^{1/p}a_3^{1/p'}\ .$$

Autrement dit, avec les notations du théorème C.4, $D\geq(1-s)^{2/p'}$ et par conséquent $1/\sqrt{D}\leq(1-s)^{-(1-1/p)}$, d'où l'on déduit (C.6). □

Si maintenant $g_3=\varphi$ est une fonction test, on déduit de (C.11) que

$$\Big\|g_1(x-sv+v)g_2(x-sv)\Big\|_{L^p_xL^1_v}\leq\frac{1}{(1-s)^{1-1/p}}\|g_1\|_{L^1}\|g_2\|_{L^p}.$$

Par ailleurs nous soulignons que cette dernière estimation est une conséquence immédiate du lemme de dispersion [18, 64] dont la preuve s'appuie sur la théorie de l'interpolation des opérateurs linéaires.

**Lemme C.7** (Lemme de dispersion)**.** *La solution de l'équation de transport libre $f^0(x-tv,v)$ vérifie les estimations en normes mixtes,*

$$\|f^0(x-tv,v)\|_{L^p_xL^q_v}\leq t^{-3(1/q-1/p)}\|f^0(x,v)\|_{L^q_xL^p_v},\quad\forall\ 1\leq q\leq p\leq\infty.$$

*Preuve alternative du corollaire C.6.* On réécrit

$$g_1(x-sv+v)g_2(x-sv)=g_1(x+(1-s)v)g_2(x-v+(1-s)v),$$

où l'on reconnaît la solution de l'équation de transport libre prise au temps $1-s$ à partir de la donnée initiale $g_1(x)g_2(x-v)$. Si l'on applique le lemme de dispersion on obtient :

$$\begin{aligned}\Big\|g_1(x-sv+v)g_2(x-sv))\Big\|_{L^pL^1}&\leq\frac{1}{(1-s)^{d/p'}}\|g_1(x)g_2(x-v)\|_{L^1_xL^p_v}\\&\leq\frac{1}{(1-s)^{d/p'}}\|g_1\|_{L^1}\|g_2\|_{L^p}.\end{aligned}$$

□

Sans aucune difficulté supplémentaire, le lemme de dispersion a également pour conséquence le résultat énoncé au début de ce paragraphe,

**Proposition C.8** (Estimation *a priori* pour la dépendance ultérieure)**.** *Soit $f^+$ la contribution* (C.6) *à l'équation cinétique* (C.4)*. Alors l'estimation suivante permet de contrôler les temps petits sans restriction sur $\lambda=3(1/q-1/p)$,*

$$\|f^+(t,x,v)\|_{L^p_xL^q_v}\leq\int_{s=0}^t\frac{1}{(1-s)^{3(1/q-1/p)}}\|\rho(x)\|_{L^p}\ \|\nabla S(x)\|_{L^q}.$$

Par conséquent, si jamais $q<3/2$, alors les injections classiques de Sobolev nous apprennent que $\|\nabla S\|_{L^q}\leq C\|\rho\|_{L^1}$, ce qui garantit un contrôle de $\|f^+(t,x,v)\|_{L^p_xL^q_v}$ dans (C.4) grâce à un lemme de Gronwall idoine.

**L'inégalité de Brascamp-Lieb généralisée.** Partons du constant négatif suivant : « nous n'avons pas idée comment démontrer une estimation telle que (C.7) à l'aide de l'inégalité BL ». Une raison est que la fonction test $\varphi$ dans (C.9) dépend à la fois de $x$ et $v$ et que nous ne savons pas comment séparer ces deux variables. A l'exception du cas $q = 1$ où cette difficulté est contournée car on prend le supremum en $v$ dans la norme duale, éliminant ainsi la variable $v$.

Si l'on se tourne vers le lemme de dispersion, on retient l'importance du rôle joué par l'interpolation. A l'aide de cette comparaison, nous suggérons la généralisation suivante de l'inégalité de Brascamp-Lieb, qui permet une plus grande liberté dans le choix des exposants.

Par souci de simplicité, on se focalise ici sur le cas de deux variables $(x, v) \in \mathbb{R}^d \times \mathbb{R}^d$. Soient $B_1, B_2 : \mathbb{R}^{2d} \to \mathbb{R}^d$ deux applications surjectives qui 'mélangent' linéairement les variables $x$ et $v$. On suppose $\ker B_1 \bigcap \ker B_2 = \{0\}$, ou de manière équivalente que la matrice $2d \times 2d : B = \begin{pmatrix} B_1 \\ B_2 \end{pmatrix}$ est inversible.

**Théorème C.9.** *Soit $1 \leq q \leq p$ et $\alpha = p'/q' \in [0, 1]$. Quelles que soient les fonctions $F, G : \mathbb{R}^d \to \mathbb{R}$, on a*

$$\Big\| F\big(B_1(x,v)\big) G\big(B_2(x,v)\big) \Big\|_{L^p_x L^q_v} \leq D^{-(1-\alpha)/2} |\det B|^{-\alpha/p} \|F\|_{L^q} \|G\|_{L^p}.$$

*Démonstration.* On commence par le cas $p = q$, qui se traite aisément par le découplage des variables $\begin{pmatrix} y \\ u \end{pmatrix} = B \begin{pmatrix} x \\ v \end{pmatrix}$. on obtient alors

$$\begin{aligned} \Big\| F\big(B_1(x,v)\big) G\big(B_2(x,v)\big) \Big\|_{L^p_x L^p_v} &= \left( \int_{x,v} \Big( F(y) G(u) \Big)^p |\det B|^{-1} \, dydu \right)^{1/p} \\ &= |\det B|^{-1/p} \|F\|_{L^p} \|G\|_{L^p}. \end{aligned}$$

Le cas $q = 1$ quant à lui provient de l'inégalité classique de Brascamp-Lieb. A partir de la formulation duale on obtient

$$\begin{aligned} \Big\| F\big(B_1(x,v)\big) G\big(B_2(x,v)\big) \Big\|_{L^p_x L^1_v} &= \sup_{\|\varphi\|_{L^{p'}} = 1} \int F\big(B_1(x,v)\big) G\big(B_2(x,v)\big) \varphi(x) \, dxdv \\ &\leq \frac{1}{\sqrt{D}} \|F\|_{L^1} \|G\|_{L^p}, \end{aligned}$$

où la constante $D$ (éventuellement nulle) est donnée, d'après Brascamp-Lieb, par les gaussiennes centrées :

$$D = \inf \left\{ \frac{\det \left( B_1^* A_1 B_1 + \frac{1}{p} B_2^* A_2 B_2 + \frac{1}{p'} \begin{pmatrix} 1 \\ 0 \end{pmatrix} A_3 \begin{pmatrix} 1 & 0 \end{pmatrix} \right)}{\det A_1 (\det A_2)^{1/p} (\det A_3)^{1/p'}} \right\}$$

On conclut par interpolation des opérateurs linéaires (pour un certain $G$ fixé disons),

$$\Big\| F\big(B_1(x,v)\big) G\big(B_2(x,v)\big) \Big\|_{L^p_x L^q_v} \leq \left( \frac{1}{\sqrt{D}} \right)^{1-\alpha} |\det B|^{-\alpha/p} \|F\|_{L^q} \|G\|_{L^p},$$

où l'interpolant $\alpha$ est donné par $1/q = 1 - \alpha + \alpha/p$.

□

## C.3 L'effet de mémoire et le lemme de dispersion : estimations duales

Nous avons vu rapidement au paragraphe précédent comment le lemme de dispersion permet d'estimer la contribution à la réorientation des cellules qualifiée d'ultérieure.

$$f^+(t,x,v) = \int_0^t \int_{v'} T(t-s, x-sv+v) f(t-s, x-sv, v') \, dv' \, ds$$

L'avantage de cette estimation est d'être faite de normes mixtes en position et vitesse :

$$\|f^+(t,x,v)\|_{L^p_x L^q_v} \leq \int_s \frac{1}{(1-s)^{3(1/q-1/p)}} \|\rho(t-s)\|_{L^p} \, \|T(t-s)\|_{L^q} \ . \tag{C.12}$$

Si l'on se focalise maintenant sur l'autre contribution dite 'antérieure',

$$f^-(t,x,v) = \int_0^t \int_{v'} T(t-s, x-sv-v') f(t-s, x-sv, v') \ dv' \tag{C.13}$$

nous observons sans mal qu'une estimation en quelque sorte duale de (C.12) est possible :

$$\|f^-(t,x,v)\|_{L^\infty_x L^p_v} \leq |V|^{1/q'} \int_s \frac{1}{s^{3/p}} \|f(t-s)\|_{L^p L^q} \, \|T(t-s)\|_{L^{q'}}, \tag{C.14}$$

pour un exposant $q$ quelconque.

*Démonstration.* En testant (C.13) contre $\varphi(x,v)$ quelconque et en posant $y = x - sv$, on obtient la succession d'inégalités suivantes,

$$\begin{aligned}
\iint_{x,v} f^- \varphi \ dxdv &= \int_{s=0}^t \int_y \int_v \int_{v'} T(t-s, y-v') f(t-s, y, v') \varphi(y+sv, v) \ dv' dv dy ds \\
&\leq \int_{s=0}^t \|f(t-s)\|_{L^p L^q} \left\| T(t-s, y-v') \int_v \varphi(y+sv, v) \ dv \right\|_{L^{p'} L^{q'}} \\
&\leq |V|^{1/q'} \int_{s=0}^t \|f(t-s)\|_{L^p L^q} \|T(t-s)\|_{L^{q'}} \|\varphi(y+sv, v) \ dv\|_{L^{p'} L^1} \\
&\leq \left( |V|^{1/q'} \int_{s=0}^t \frac{1}{s^{3/p}} \|f(t-s)\|_{L^p L^q} \|T(t-s)\|_{L^{q'}} \right) \|\varphi\|_{L^1 L^{p'}} \ ,
\end{aligned}$$

grâce au lemme de dispersion judicieusement appliqué à $\|\varphi(y+sv, v) \ dv\|_{L^{p'} L^1}$. On en déduit (C.12) par dualité. □

**Remarque C.10.** *Replacé dans le contexte du modèle cinétique pour le chimiotactisme (chapitre 5), cette estimation nécessite $q' < 3/2$ afin de 'tuer' la non linéarité quadratique et appliquer un lemme de Gronwall. En effet, la dépendance en le gradient $T[S] \leq C(1 + \nabla S(x-v'))$ est estimée par $\|\nabla S\|_{L^{q'}} \leq C\|\rho\|_{L^1}$ à condition d'avoir $q' < 3/2$ par les injections de Sobolev. Si l'on revient à* (C.12) *on observe que $q < 3/2$ est requis, ce qui montre bien l'incompatibilité de ces deux approches.*

# Annexe D

# Méthodes d'énergie pour l'équation de Fokker-Planck

Nous nous intéressons dans cette annexe à l'équation linéaire de Fokker-Planck, et illustrons certaines manipulations sur ce cas-là, similaires aux méthodes employées pour le modèle de KS 'lorsque la masse s'échappe à l'infini' par exemple. D'une certaine façon l'équation bien connue de Fokker-Planck peut être vue comme une équation de chimiotactisme linéaire, pour des modèles où le potentiel chimique qui attire les cellules est externe à la population. L'originalité de KS étant de coupler la synthèse du signal à la densité cellulaire. En ce sens cette annexe est tout à fait indépendante des estimations *a priori* inhérentes à KS (estimation $\int n \log n$ ou calcul d'explosion en général), mais se focalise sur des phénomènes propres aux équations de diffusion.

C'est également l'occasion pour nous d'introduire brièvement quelques aspects de la théorie récente du transport optimal appliqué aux EDPs [244]. Des résultats énoncés précédemment seront démontrés ici, rendant ce mémoire plus complet. Le fil directeur de ces différentes approches est la fonctionnelle d'énergie libre qui, comme nous l'avons vu à maintes reprises, est également au cœur du système de KS (voir l'introduction).

## D.1 Renormalisation de l'équation de la chaleur

L'équation de la chaleur $\partial_t n = \Delta n$ n'a plus de secrets dès lors que l'on connaît la solution de manière très précise : $n = G(t) * n_0$, où $G(t)$ est le noyau de la chaleur [99]. En particulier $n(t)$ tend vers 0 dans tous les espaces $L^p$ avec $p > 1$. ce résultat ne s'étend cependant pas à $L^1$ car la masse est conservée pour une donnée initiale $n_0 \in L^1$. Dans la suite nous nous intéressons à une méthode entropique, qui ne fait pas appel à l'analyse de Fourier, pour glaner de l'information sur le comportement asymptotique dans un cadre entropique.

Premier constat : puisque la solution s'écrase en zéro, il est judicieux d'effectuer un changement d'échelle afin de capturer le comportement asymptotique. Une renormalisation adéquate est fournie par le changement de variables auto-similaire qui préserve la masse,

$$n(t,x) = \frac{1}{R(t)^d}\, u\left(\tau, \frac{x}{R(t)}\right) \quad R(t) = \sqrt{1+2t}\ , \quad \tau = \log R(t)\ ,$$

qui conduit à l'équation de Fokker-Planck particulière,

$$\frac{\partial u}{\partial t} = \Delta u + \operatorname{div}\,(uy)\ , \tag{D.1}$$

que l'on peut réécrire en factorisant le flux,

$$\frac{\partial u}{\partial t} = \operatorname{div}\,\Big(u\nabla(\log u - y)\Big)\ . \tag{D.2}$$

Cette formulation suggère de multiplier l'équation par $\log u - y$, ce qui donne en cascade la définition et les estimations suivantes.

**Définition D.1.** *Soient $\mu$ et $\nu$ deux densités de probabilité. L'entropie relative (ou information de Kullback) est définie comme*

$$\mathbf{Ent}(\mu|\nu) = \int \mu(y) \log\left(\frac{\mu(y)}{\nu(y)}\right)\ dy\ .$$

*L'information de Fisher quant à elle, est définie par*

$$\mathbf{I}(\mu|\nu) = \int \mu(y) \left|\nabla \log\left(\frac{\mu(y)}{\nu(y)}\right)\right|^2\ dy\ .$$

**Proposition D.2** (Dissipation de l'entropie)**.** *Soit $u_0$ une donnée initiale positive de masse 1 et $\gamma(y) = \frac{1}{Z}e^{-|y|^2/2}$ la mesure gaussienne. Alors le long des trajectoires solutions de* (D.1) *nous avons*

$$\frac{d}{dt}\mathbf{Ent}(u|\gamma) = -\mathbf{I}(u|\gamma)\ .$$

Le théorème-clé suivant exhibe une relation entre l'entropie et la dissipation d'entropie, c'est-à-dire l'information de Fisher [121, 11].

**Théorème D.3** (Inégalité de Sobolev logarithmique)**.** *Soit $\gamma$ la mesure gaussienne et $h \in L^2_+(\gamma(y)dy)$. Nous avons l'inégalité suivante qui ne dépend pas de la dimension $d$,*

$$\int h^2 \log h^2\ d\gamma \le 2\int |\nabla h|^2\ d\gamma + \left(\int h^2\ d\gamma\right)\log\left(\int h^2\ d\gamma\right)\ .$$

*Cette estimation est équivalente à l'inégalité entropie/dissipation de l'entropie :*

$$\mathbf{Ent}(u|\gamma) \le \frac{1}{2}\mathbf{I}(u|\gamma)\ .$$

A ce stade il découle des deux inégalités précédentes que l'entropie relative $\mathbf{Ent}(u|\gamma)$ converge exponentiellement vite vers zéro. Donc la solution de la chaleur renormalisée converge vers la mesure gaussienne au sens de l'entropie. Ceci entraine en fin de compte la convergence au sens $L^1$, grâce à l'inégalité de Csiszár-Kullback valable pour deux densités de probabilité $\mu$ et $\nu$

$$\|\mu - \nu\|_{L^1} \le \mathbf{Ent}(\mu|\nu)\ .$$

De retour aux variables originales $(t, x)$, on retrouve que $n$ se rapproche asymptotiquement de la mesure gaussienne auto-similaire (c'est-à-dire le noyau de la chaleur).

## D.2 Fokker-Planck et inégalités de Sobolev logarithmique

Tournons nous maintenant vers l'équation de Fokker-Planck associée à un potentiel $V$ plus général :

$$\frac{\partial u}{\partial t} = \Delta u + \text{div}\ (u\nabla V)\ . \tag{D.3}$$

A condition d'avoir $e^{-V} \in L^1$, on introduit la mesure stationnaire

$$\nu_V(y) = \frac{1}{Z}e^{-V(y)}\ , \quad Z = \int e^{-V(y)}\ dy\ ,$$

qui réalise le minimum de l'énergie libre

$$\mathcal{F} = \int u\log u + \int uV = \mathbf{Ent}(u|\nu_V) + C\ .$$

Nous avons vu que le point crucial de la preuve de convergence (au sens de l'entropie relative) est l'existence d'une inégalité de Sobolev logarithmique pour la mesure stationnaire $\nu_V$. Nous retiendrons ici un critère simple pour l'existence d'une inégalité de Sobolev logarithmique [15].

**Théorème D.4** (Bakry-Emery)**.** *Si $V$ est $\alpha-$convexe, c'est-à-dire $D^2V \geq \alpha \mathrm{Id}$, alors $\nu_V$ satisfait une inégalité de Sobolev logarithmique :*

$$\mathbf{Ent}(\mu|\nu_V) \leq \frac{1}{2\alpha}\mathbf{I}(\mu|\nu_V) \ .$$

Cette inégalité garantit comme dans le paragraphe précédent la convergence de $u(t)$, solution de (D.3), vers la densité stationnaire, avec vitesse exponentielle.

L'entropie telle qu'elle est définie ici est bien adaptée aux équations d'advection-diffusion linéaire. Il existe également des variantes non-linéaires de l'entropie relative, avec une théorie analogue des estimations entropie/dissipation d'entropie [58].

## D.3 Un point de vue de transport optimal

Nous dressons rapidement le tableau d'une théorie alternative, basée sur les travaux de McCann [179], dont le théorème de Brenier [38] fut la pierre d'achoppement. Le cadre métrique de cette théorie est donné par la distance de Wasserstein, et tous les résultats sont donnés dans ce contexte [244].

**Définition D.5.** *Soient $(X, \mu)$ un espace de probabilité et $T$ une application mesurable de $X$ vers $Y$. L'image de $\mu$ par $T$, que l'on note $\nu = T\#\mu$ est donnée par son action sur les ensembles mesurables : $\nu(B) = \mu[T^{-1}(B)]$.*

**Le théorème de Brenier.** Etant données deux densités de probabilité $\mu(x)$ et $\nu(y)$, le problème du transport de Monge est de déplacer $\mu$ en $\nu$ à l'aide d'une application $T : X \to Y$ telle que $T\#\mu = \nu$. Si $T$ est un difféomorphisme, on a par le théorème de changement de variables

$$\mu(x) = \nu(T(x))|\det DT(x)| \ . \tag{D.4}$$

Il y a bien évidemment un vaste choix pour $T$. Illustrons ceci sur l'exemple précédent, qui n'est pas sans rapport avec les événements du chapitre 7.

Il y a bien sûr un vaste choix pour l'application $T$. En revanche, si l'on plaque sur l'espace produit $X \times Y$ une fonction de coût $c(x, y)$, cela restreint les possibilités pour l'application $T$. En pratique on considère par la suite la distance au carré $c(x, y) = |x - y|^2$, qui est satisfaisante à bien des égards [98].

La question naturelle à ce stade est de savoir caractériser les 'meilleures' applications de transport $T : X \to Y$ qui réalisent le coût minimal

$$\min_{T:\ T\#\mu=\nu} \int_X |x - T(x)|^2 \ \mu(x)dx \ . \tag{D.5}$$

Nous passons sous silence la technique de relaxation de Kantorovitch, qui permet de se ramener à un problème linéaire plus faible que (D.5), mâtinée de dualité, et qui permet de montrer que le problème (D.5) est bien posé. D'autre part le théorème de Brenier caractérise cette application dans le cas où $\mu(x)$ et $\nu(y)$ sont des densités de probabilité.

**Théorème D.6** (Brenier)**.** *Soient $\mu(x)$ et $\nu(y)$ deux densités de probabilité telles que le second moment de $\nu$ est fini. L'application optimale dans* (D.5) *est l'unique gradient de fonction convexe $T = \nabla\varphi$ qui transporte $\mu$ en $\nu$ : $\nabla\varphi\#\mu = \nu$.*

Le théorème de Brenier est intimement lié au coût quadratique, ce qui justifie ce choix là *a posteriori*. Une caractérisation plus générale existe pour des coûts $c$ strictement convexes [244].

**La métrique de Wasserstein.** La distance quadratique de Wasserstein apparaît alors naturellement comme solution au problème de transport optimal :

$$\mathcal{W}_2(\mu, \nu)^2 = \int_X |x - \nabla\varphi(x)|^2 \ \mu(x)dx = \min_T \int_X |x - T(x)|^2 \ \mu(x)dx \ .$$

Notons qu'elle est équivalente à la combinaison 'convergence faible contre les fonctions à croissance au plus quadratique', et en particulier les seconds moments [244]. La distance de Wasserstein permet entre autres de démontrer des estimations de convergence dans un sens plus faible que l'entropie relative.

En dimension un d'espace les choses sont plus simples car explicites. On introduit $F$ et $G$ les fonctions de répartition de $\mu$ et $\nu$ respectivement, puis $\Phi$ et $\Psi$ leurs pseudo-inverses. Avec ces notations,

$$\mathcal{W}_2(\mu,\nu)^2 = \int_0^1 |\Phi(\rho) - \Psi(\rho)|^2 \, d\rho \; .$$

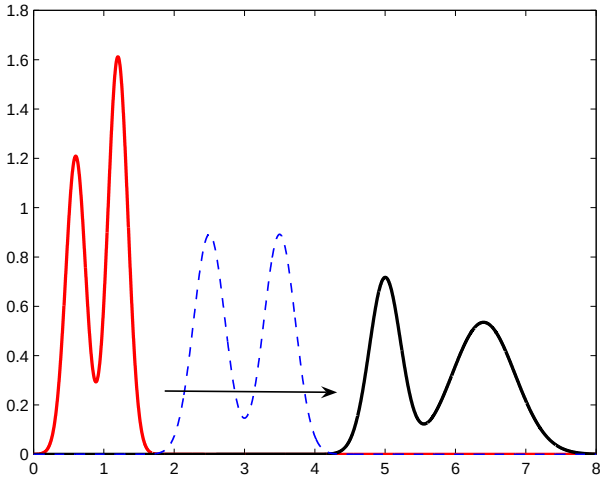


FIG. D.1 – Schéma pour l'interpolation par déplacement de deux densités de probabilité. On transporte la densité initiale en a densité finale (lignes pleines) par le transport de masse : la ligne hachée est un état intermédiaire $[u_0, u_1]_t$. Ceci est à opposer à l'interpolation 'classique' $(1-t)u_0 + tu_1$ pour laquelle la densité initiale s'évanouit pour laisser place à la densité finale qui 'sort de terre'.

**Convexité par déplacement.** L'équation de Fokker-Planck (D.3) possède une énergie libre, décroissante le long des trajectoires :

$$\mathcal{F}[u] = \int u \log u + \int uV \; , \quad \frac{d}{dt}\mathcal{F}[u(t)] \leq 0 \; . \tag{D.6}$$

Plus généralement on peut être amené à considérer (milieux poreux, particules en interaction) une fonctionnelle

$$\mathcal{F}[u] = \int \frac{u^m - mu}{m-1} \; + \int u(x)V(x) \; dx + \iint u(x)W(x-y)u(y) \; dxdy \; , \tag{D.7}$$

quoique nous assignons $W = 0$ dans cette annexe. Cette fonctionnelle n'est pas convexe au sens classique du terme le long du segment d'interpolation $(1-t)u_0 + tu_1$. En revanche elle est convexe au sens de la convexité par déplacement, pour l'interpolation

$$[u_0, u_1]_t = \Big((1-t)\mathrm{Id} + t\nabla\varphi\Big)\#u_0 \; ,$$

où $\nabla\varphi\#u_0 = u_1$ est la solution du problème de Monge (D.5).

**Théorème D.7** (McCann). *(i) Pour un exposant $m \geq 1 - 1/d$ la fonctionnelle d'énergie interne $\mathcal{F}_{\mathrm{int}} = \frac{1}{m-1}\int u^m$ est convexe par déplacement.*

*(ii) Si $V$ est convexe, la fonctionnelle d'énergie potentielle $\mathcal{F}_{\rm pot} = \int u(x)V(x)\,dx$ est également convexe par déplacement.*

*Démonstration.* Soient $u_0$ et $u_1$ deux densités de probabilité. On déplace $u_0$ en $u_1$ via l'interpolant $u_t = \Big((1-t)\mathrm{Id} + t\nabla\varphi\Big)\#u_0$. Après changement de variable $z = (1-t)x + t\nabla\varphi(x)$, l'énergie interne se réécrit

$$\begin{aligned}\mathcal{F}_{\rm int}[u_t] &= \frac{1}{m-1}\int u_t(z)^m\,dz \\ &= \frac{1}{m-1}\int u_t\big((1-t)x+\nabla\varphi(x)\big)^m \det((1-t)I + tD^2\varphi(x))\,dx \\ &= \frac{1}{m-1}\int \left(\frac{u_0(x)}{\det((1-t)I+tD^2\varphi(x))}\right)^m \det((1-t)I+tD^2\varphi(x))\,dy\ ,\end{aligned}$$

d'après l'équation de Monge-Ampère (D.4). L'inégalité arithmético-géométrique matricielle exprime que $\det^{1/d}$ est concave sur l'espace des matrices symétriques positives :

$$\forall A,B\in\mathcal{S}^+(\mathbb{R})\ \forall t\in(0,1)\quad \det\big((1-t)A+tB\big)^{1/d} \geq (1-t)(\det A)^{1/d} + t(\det B)^{1/d}\ .$$

Par conséquent la fonctionnelle $\frac{1}{m-1}\det^{(1-m)d/d}$ est convexe dès que $(1-m)d \leq 1$ (composition d'une fonction convexe décroissante avec une fonction concave). Par conséquent

$$\begin{aligned}\mathcal{F}_{\rm int}[u_t] &\leq \frac{1-t}{m-1}\int (u_0(x))^m \det(I)^{1-m}\,dx + \frac{t}{m-1}\int (u_0(x))^m\det(D^2\varphi(x))^{1-m}\,dx \\ &= (1-t)\mathcal{F}_{\rm int}[u_0] + t\mathcal{F}_{\rm int}[u_1]\ .\end{aligned}$$

Dans le cas où $m\to 1$, on obtient que la fonctionnelle d'entropie $\int u\log u$ est convexe par déplacement quelle que soit la dimension.

Il est à noter qu'en une dimension d'espace les choses sont plus simples, comme c'est toujours le cas (voir l'introduction à ce sujet). □

Le théorème D.7 fournit un cadre convexe pour l'étude de fonctionnelles telles que (D.7) et par là même pour l'équation de Fokker-Planck (entre autres). En particulier, le minimum d'une telle fonctionnelle, s'il existe, est unique.

**Flot gradient généralisé.** On attend en fait mieux des fonctions convexes 'au sens classique' (disons $V\in\mathbb{R}^d$) : le flot gradient

$$\dot{y} = -\nabla V(y)\ , \tag{D.8}$$

converge vers le minimum, avec une vitesse exponentielle si jamais $V$ est $\alpha-$convexe, c'est-à-dire $D^2V \geq \alpha\mathrm{Id}$. On est ainsi en mesure d'attendre une pareille dynamique du nouveau cadre de convexité par déplacement. C'est effectivement le cas tel que Jordan, Kinderlehrer et Otto l'ont mis en évidence [148, 200] (voir aussi [244, 7]).

Commençons une petite digression à ce propos. L'algorithme discret implicite en temps correspondant à (D.8) est

$$\frac{y(t+dt)-y(t)}{dt} = -\nabla V\big(y(t+dt)\big)\ ,$$

ce qui est rigoureusement équivalent à la formulation

$$y(t+dt) = \mathrm{argmin}_z\left\{V(z) + \frac{1}{2dt}\|y(t)-z\|^2\right\}\ . \tag{D.9}$$

La structure de gradient est cachée ici dans la métrique $L^2$. L'algorithme (D.9) se transpose à une métrique autre que $L^2$. En particulier la distance de Wasserstein fournit un schéma discret en temps/continu en espace :

$$u(t+dt) = \arg\,\min_w\left\{\mathcal{F}[w] + \frac{1}{2dt}\mathcal{W}(u(t),w)^2\right\}\ , \tag{D.10}$$

parfaitement adapté à l'équation de Fokker-Planck.

**Remarque D.8.** *Dans le cas 1D,* (D.10) *est tout simplement le flot $L^2$ implicite rapporté aux fonctions inverses de répartition, car $\mathcal{W}(u(t),w)^2 = \|\Phi(t)-\Omega\|_{L^2}^2$.*

Le schéma (D.10) préserve entre autres les estimations qui découlent de la décroissance de l'énergie libre (D.6), ce qui en fait un outil très appréciable pour les preuves de convergence basées sur les méthodes d'énergie.

**Algorithme de plus grande pente suivant la métrique de Wasserstein.** Félix Otto a interprété l'algorithme itératif de minimisation pénalisée par la distance de Wasserstein (D.10) selon un formalisme continu. Par là même il a construit formellement une structure riemannienne qui confère à (D.10) et à sa version continue le statut de flot gradient [200, 60] :

$$\partial_t u = -\nabla_{\mathcal{W}} \mathcal{F}[u] \ .$$

L'équation de Fokker-Planck est ainsi vue comme un flot gradient de l'énergie libre sur l'espace $\mathcal{P}_2$ des densités de probabilité dont le second moment est fini.

Dans le cas 1D à nouveau les choses sont faciles à expliciter. Le tenseur métrique riemannien est simplement le produit scalaire $L^2$ entre les fonctions inverses de répartition :

$$\langle \mu, \nu \rangle_g = \int_0^1 \Phi\Psi \ ,$$

ce qui n'est nullement surprenant au vu de ce qui précède.

Nous n'entrons pas dans les détails ici et renvoyons à [244, 7]. Mentionnons tout de même pour faire le lien entre ces différents paragraphes que l'interpolation par déplacement entre deux densités $\mu$ et $\nu$ s'effectue le long d'une géodésique dans l'interprétation d'Otto.

**Calcul d'Otto.** Où l'on retrouve que pour un potentiel $\alpha-$convexe $V$ la convergence vers la densité stationnaire est exponentielle en distance de Wasserstein.

Dans le but d'associer une structure riemannienne à la métrique de Wasserstein, Otto a introduit un formalisme qui permet de réaliser la convexité par déplacement de manière analytique plutôt que géométrique [200, 244]. Un travail analogue a été mené à bien dans [60]. Dans l'interprétation d'Otto, les géodésiques sur l'espace des mesures de probabilité à second moment fini $\mathcal{P}_2(\mathbb{R}^d)$ sont les interpolations par déplacement 'optimal' :

$$u_t = \Big((1-t)\mathrm{Id} + t\nabla\varphi\Big)\#u_0 \ .$$

D'après l'interpolation eulérienne du 'mouvement' des densités, les géodésiques sont les trajectoires du système

$$\begin{cases} \dfrac{\partial u_t}{\partial t} + \mathrm{div}\ (u_t v_t) = 0 \ , \\ \dfrac{\partial (u_t v_t)}{\partial t} + \mathrm{div}\ (u_t\ v_t \otimes v_t) = 0 \ , \end{cases}$$

où $v_t$ est la vitesse du fluide 'transporté' dont la densité est $u_t$. L'application de transport optimal apparaît dans la condition initiale : $v_0 = \nabla\varphi(x) - x$. Les quantités conservées par ce système sont : la masse du fluide $\int u_t(x)dx$, la vitesse moyenne $\int v_t u_t$ et l'énergie cinétique $\int |v_t|^2 u_t$ (absence de chocs).

Il est alors possible de calculer la dérivée seconde de la fonctionnelle d'énergie (D.7) le long de la géodésique :

$$\frac{d^2}{dt^2}\mathcal{F}[u_t] = (m-1)\int u_t^m (\mathrm{div}\ v_t)^2 + \int u_t^m\ \mathrm{trace}\left({}^tDv_t Dv_t\right) \qquad + \int \Big\langle D^2 V v_t, v_t \Big\rangle u_t \ . \tag{D.11}$$

La condition de McCann $m \geq 1 - 1/d$ se traduit dans ce contexte par la positivité de la première contribution (qui provient de l'énergie interne) dans (D.11). D'autre part on observe clairement qu'un

potentiel $\alpha-$convexe conduit dans ce formalisme à une fonctionnelle d'énergie elle-même $\alpha-$convexe pour la distance de Wasserstein :

$$\frac{d^2}{dt^2}\mathcal{F}[u_t] \geq 0 + \alpha \int |v_t|^2 u_t = \alpha \int |v_0|^2 u_0 = \alpha \int |\nabla\varphi(x) - x|^2 u_0(x)\ dx = \alpha \mathcal{W}(u_0, u_1)^2\ .$$

Pour une simple fonction $\alpha-$convexe $f : \mathbb{R} \to \mathbb{R}_+$, qui atteint son minimum en $a \in \mathbb{R}$, on a la relation suivante entre la fonction, sa dérivée et la distance euclidienne :

$$f(x) - f(a) - |x - a| \cdot |f'(x)| + \frac{\alpha}{2}|x - a|^2 \leq 0\ .$$

Ceci, une fois transposé à la fonctionnelle d'énergie susdite, donne une inégalité HWI [201] entre l'entropie relative $\mathbf{H}(u|u_\infty) = \mathcal{F}[u] - \mathcal{F}[u_\infty]$ ($u_\infty$ étant le minimiseur de $\mathcal{F}$), la distance de Wasserstein $\mathcal{W}(u, u_\infty)$, et puis l'information de Fisher $\mathbf{I}(u|u_\infty)$ :

$$\mathbf{H}(u|u_\infty) \leq \mathcal{W}(u, u_\infty)\sqrt{\mathbf{I}(u|u_\infty)} - \frac{\alpha}{2}\mathcal{W}(u, u_\infty)^2\ .$$

Cette inégalité entraîne, en optimisant le second membre pour éliminer la distance de Wasserstein, l'inégalité entropie/dissipation d'entropie de Bakry-Emery (théorème D.4) :

$$\mathbf{H}(u|u_\infty) \leq \frac{1}{2\alpha}\mathbf{I}(u|u_\infty)\ .$$

# Annexe E

# Instabilité dans le cerveau humain : un scénario à base de chimiotactisme

---

Cet article en collaboration avec Hossein Khonsari est la version courte et 'biologique' du chapitre 6. L'accent est mis sur les observations cliniques qui replacent la sclérose concentrique de Baló dans la perspective de la recherche médicale sur la sclérose en plaques. Le modèle de recrutement local des macrophages est discuté et les conclusions qualitatives (en particulier la corrélation positive entre aggressivité de la maladie et émergence d'une structure non homogène) sont soulignées. Ce travail est paru dans PLoS ONE sous le titre *The origins of concentric demyelination : self-organization in the human brain* [157].

---

Baló's concentric sclerosis has been a neuropathologic enigma since its description in 1927 (Baló 1927). Many hypotheses have been formulated to explain its striking, reproducible patterns. Early analogies with the phenomenon of Liesegang ring formation were proposed (Hallervorden et al. 1933). Our approach reconsiders these analogies and proposes a non-linear mechanism of self-organization involving a minimal number of assumptions on the course of the disease.

## Neuropathology of Baló's concentric sclerosis

The typical neuropathological lesion of multiple sclerosis (MS) is a spherical or cylindrical perivascular demyelinated zone in the hemispheric or medullar white matter. Myelin sheath depletion generally occurs within this sharply delimited area without major axonal injury. The final effectors of demyelination are the microglia, but the initial trigger that leads to abnormal microglial activation is unknown (Lumsden 1970). The demyelination pattern is seldom heterogeneous.

Concentric demyelination, also known as Baló's concentric sclerosis (Baló 1927), was initially described in acute, rapidly fatal, clinical MS forms. Due to the improvement of MRI resolution, concentric demyelination is now observed in chronic forms of MS, occurring along with classical homogeneous lesions (Stadelmann et al. 2004). Baló's lesions are perivascular bundles of concentric demyelinated zones in which areas where myelin is preserved regularly alternate with zones where myelin is destroyed (figure E.1). The external border of the lesion bands is sharp, but their internal limit with the normal white matter is not well defined. An MRI follow-up study of Baló patients has shown that the demyelinated layers form progressively in a centrifugal way (Chen et al. 1999). More recent results nevertheless indicate that the process of active demyelination takes place synchronously rather than successively, with a progressive evolution of the lesions towards homogeneous MS plaques (Kastrup et al. 2002). Furthermore, MR spectroscopic studies have confirmed the analogies between Baló's sclerosis and classical MS (Chen 2001). Baló's sclerosis may thus be a borderline form – or even an intermediate form – of typical MS.

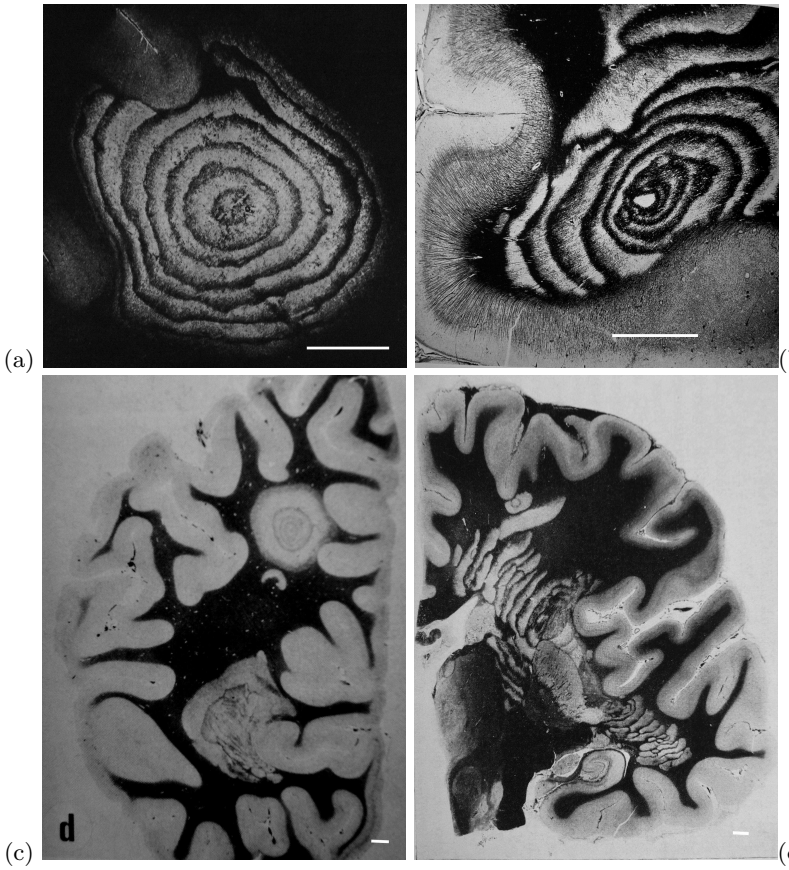


Figure E.1: Typical aspects of Baló's concentric sclerosis. (a) Original case of Baló. The width of the preserved bands increases radially; several anastomoses are located in the lower half of the lesion (from Baló 1928). (b) Lesion centered by a veinule showing ring fragmentation in a constrained area (from Hallervorden et al. 1933). (c) Lesions at the scale of the whole brain, reproduced from Castaigne et al. 1984. (d) Progress of the pathologic process from a center located in a constrained area, showing the transition from rings to bands (from Behr 1950). Scale bars have length $1cm$.

MS is now classified in four subtypes according to the supposed pathologic pathway leading to the microglial activation (Lassmann 2005). Baló's sclerosis belongs to subtype III, in which the oligodendrocytes are the disease's primary targets. Quantitative studies have in fact confirmed important oligodendrocyte depletion in Baló lesions, predominantly in the demyelinated bands (Yao et al. 1994). In MS type III lesions, the oligodendrocytes are the victims of a mitochondrial dysfunction creating local ischemic conditions (Aboul-Enein et al. 2005). Primary oligodendrocyte injury has also recently been proposed as the initial pathogenic event in MS lesion development, and early MS lesions sometimes show concentric patterns of demyelination (Barnett et al. 2004). Interestingly, concentric lesions in subjects who do not suffer from Baló's sclerosis are described in either ischemia, such as stroke (Courville 1970) and cyanide poisoning (in cats and rabbits, Ferraro 1933), or in cases where a specific oligodendrocyte destruction occurs, such as attacks by JC (Markiewicz et al. 1977) and HHV6 (Pohl et al. 2005) viruses. Concentric sclerosis and very early MS may thus both be the consequence of oxydative stress of oligodendrocytes.

The origins of concentric demyelination have puzzled generations of neuropathologists, and many interesting etiologic hypotheses have been formulated. Courville (1970) has argued that the lesions may be the direct result of microthrombosis in the brain capillary network. His vascular theory may not be valid as no concentric pattern in the blood vessel distribution exists in the human brain. Preserved myelin bands were then attributed to remyelination processes (Moore et al. 1985), but neuropathological arguments have proven this hypothesis incorrect (Moore et al. 2001). Recently, the periodic preservation of myelin in a radially expanding myelinoclastic process has been attributed to a preconditioning phenomenon (Stadelmann et al. 2005). According to these authors, a mitochondrial dysfunction triggers local protection mechanisms with a narrow efficiency range around the actively demyelinating zone. Proteins involved in ischemic preconditioning have in fact been found at the periphery of expanding Baló lesions.

Wiendl et al. (2005) have reported remarkable homogeneous diffusion abnormalities in MRI scans before any concentric contrast enhancement, in areas of acute lesion development. These abnormalities may correspond to an early cytotoxic oedema, and contradict the hypothesis of a strictly radially progressing pathological process. The diffusion abnormality is a very early event and it is not reported by all authors (Anschel 2006).

One model for testing the pathogenic hypothesis on Baló's sclerosis would be the experimental allergic encephalomyelitis of the common marmoset, where concentric lesions with high oligodendrocyte depletion and massive macrophage recruitment are reported (Genain et al. 1997).

## Baló's concentric sclerosis and Liesegang rings.

The interesting analogy between Baló's sclerosis and the Liesegang ring formation phenomenon was first underlined by Baló (1927) himself and has subsenquently been thoroughly studied (Hallervorden et al. 1933, Michalak 2004). Liesegang ring formation is a periodic precipitation process initially described in gels. Three chemical species are involved in the following order: $A + B \longrightarrow D$. Initially, $B$ (for example $AgNO_3$) is uniformly distributed in the gel and $A$ (for example HCl) propagates within a diffusion front. As the reaction goes on, consecutive bands of precipitate (AgCl in our example) form. Many theories have been proposed to explain this process. One of the earliest and most successful is Ostwald's supersaturation theory (Ostwald 1897), which is based on a spatially periodic nucleation phenomenon. Precipitation occurs whenever the concentration of compound $AB$ exceeds a *supersaturation threshold* $q^\star$ and takes place as long as $[AB] > q$, $q$ being the *saturation threshold*. Ostwald's theory postulates that each precipitated band of $D$ depletes the surrounding gel of $B$ by acting as a sink and thus creates a zone spared by the precipitation front by lowering $[AB]$ under $q^\star$ (Henisch 1986).

The position of the $n^{\text{th}}$ band, $x_n$, and the time $t_n$ elapsed before the precipitation of the $n^{\text{th}}$ band obey generic laws. The *time law* states that $x_n$ is proportional to $\sqrt{t_n}$ (diffusion scale). The *spacing law* indicates that the ratio between the position of two successive bands converges to a finite value 1+p, where $p > 0$. The width of the $n^{\text{th}}$ band increases with $n$ and obeys the *width law* $w_n \sim x_n^\alpha$, where $\alpha$ is close to one. The precipitation pattern also depends on geometry – bands are formed in test tubes and rings appear in Petri dishes (Droz 2000).

Many experimental facts cannot be explained by Ostwald's supersaturation theory, such as the *sec-*

*ondary banding* – one band breaks into narrower bands – and the *inversed spacing* – the spacing between the band decreases (Droz 2000). Other irregular patterns are observed in local diffusion barriers, such as gaps within the bands forming radial alleys free of precipitate, transition from bands to speckled patterns and links between the bands called *anastomoses* (Krug et al. 1996). Furthermore, a transient homogeneous colloid phase is observed before the formation of rings (Hatschek 1925).

The classical analogy between Baló's concentric sclerosis and Liesegang rings relies on the supersaturation theory. An unknown myelinotoxic molecule is supposed to diffuse from the center of the lesion and induce demyelination after periodic precipitation. More precisely, Hallervorden et al. (1933) suppose that the diffusing myelinotoxic substance induces a local formation of antibodies which inhibit myelin destruction. Protected regions, in which the toxin reacts with the antibodies, then behave as the precipitates in the Ostwald supersaturation theory by attracting the protective antibodies from the surrounding brain tissue. Demyelination thus occurs in the surrounding regions when they are reached by the toxin front, as they do not contain enough antibodies to remain protected. In this scenario, the preserved areas in the lesions correspond to the precipitation bands in Liesegang rings.

The hypothesis of Hallervorden et al. is a free interpretation of the supersaturation theory and has no biological basis. Furthermore, some Baló lesions display irregularities that bear some resemblance with the morphological characteristics of Liesegang rings that are not well explained by the supersaturation theory, such as branching patterns – close to the Liesegang anastomoses (figure E.1a,E.1d) – and speckled patterns – resembling the fragmentation of Liesegang rings when diffusion barriers occur (Zeman 1949). Baló's concentric lesions become bands in the brainstem and the medulla, where diffusion zones are narrower than in the brain (Itoyama et al. 1984). The initial non-periodic diffusion anomalies described in Baló's sclerosis (Wiendl et al. 2005) are also in line with the homogeneous colloid field found in the early phases of Liesegang ring formation. Finally, Baló's lesions do not respect any of the generic laws that characterize Liesegang rings (figure E.2). The analogy between Baló's concentric sclerosis and Liesegang rings thus requires a revision (see table E.1).

| Baló's concentric sclerosis | Liesegang rings | mathematical description |
|---|---|---|
| front of macrophage activation (e.g. antibody, oxydative stress) | leading reaction front | $\partial_t m = D\Delta m + \lambda m(\bar{m} - m)$ |
| MRI diffusion abnormalities before concentric demyelination | homogeneous colloidal field before periodic precipitation | diffusion of a homogeneous activating front |
| destruction of the oligodendrocytes | precipitation or nucleation | $\partial_t d = Fm(\bar{d} - d)$ |
| local recruitment of macrophages | rearrangements at the back of the front in post–nucleation theories and colloidal growth | $\partial_t m = -\nabla \cdot \big(\chi m(\bar{m} - m)\nabla c\big)$ |
| links between adjacent rings and ring fragmentation | anastomosis, speckled patterns and morphological instabilities | local breaking of symmetry close to the border and under perturbations. |

Table E.1: Analogies between Baló's sclerosis, Liesegang rings and mathematical description as proposed with model (E.3)-(E.4)-(E.5).

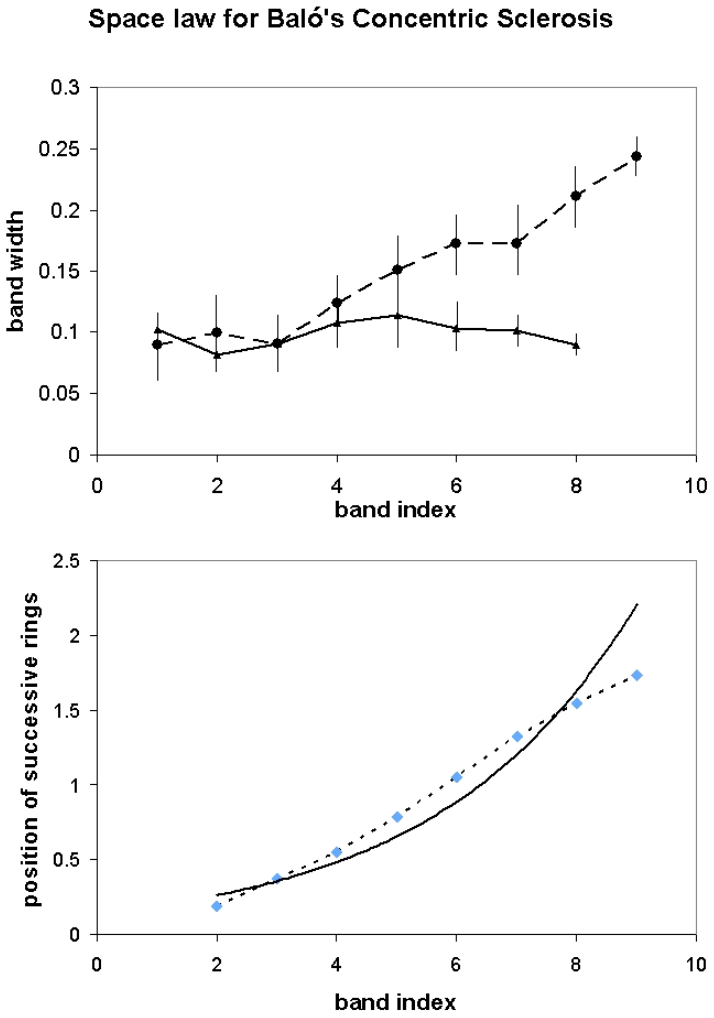


Figure E.2: Space laws from 12 measures made on the cases of Baló (1928) and Hallervorden et al. (1933). *(a)* Damaged (dashed line) and preserved (solid line) myelin. *(b)* Averaged successive positions of destroyed myelin bands (dashed), compared to the classical exponential space law for the Liesegang rings (solid line) obtained from a logarithmic regression; y-axis label in cms. The space law for concentric sclerosis is linear (correlation coefficient $r^2 = 0.996$). In all our mathematical models, the space law strongly depends on the shape of the activating front. As the biological nature of this front is unknown, selection between different scenarios (e.g. preconditioning model vs. local macrophage recruitment model) cannot be based on the space law. However the linear law for concentric sclerosis tends to indicate that an outer diffusing signal is unlikely.

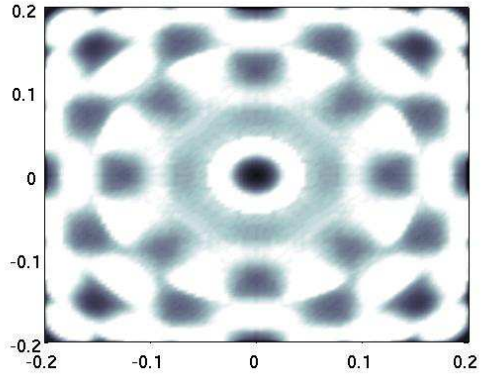


(a)

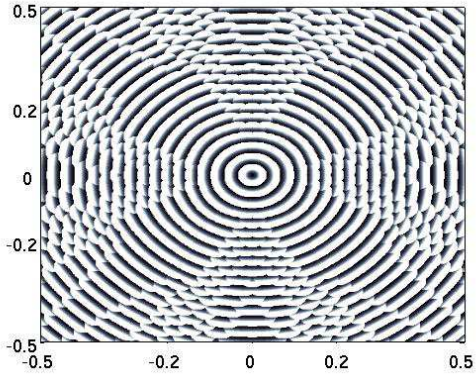


(b)

Figure E.3: Apparition of concentric patterns under the preconditioning model (E.1)–(E.2). The protection factor is given by Heaviside function $P(\phi) = (q - \phi)_+$, with a given threshold $q$. (a) We have replaced the preconditioning equation (E.2) with $\phi = K * d$, the kernel $K$ being a stiff Hill function with a $\sqrt{\varepsilon}$ range of action, $K(z) = \mathbf{1}_{|z| \leq \sqrt{\varepsilon}}$. Other parameters are $\varepsilon = 0.4$ and $q = 0.1$. Interestingly the range of action of the potential $\phi$ is larger than in figure E.5 whereas the size of the domain is considerably smaller. In fact, this range fully determines the width of the bands. (b) Same illustration with a degenerated potential $\phi(x) = \max_{|z| \leq \sqrt{\varepsilon}} d(x+z)$, $q = 0.8$, $\varepsilon = 0.1$. The size of the domain is four times smaller than in figure E.4, whereas the range of action is of the same order.

## Mathematical reconsideration of the preconditioning theory

The preconditioning theory makes the hypothesis that a protective substance, secreted by the attacked oligodendrocytes, prevents demyelination at the borders of the radially expanding lesion. From the scenario sketched by Stadelman et al. (2005), we extract the following continuous model for (E.1) the destroyed oligodendrocytes and (E.2) the preconditioning potential.

$$\frac{\partial d}{\partial t} = \underbrace{A(u)P(\phi)\ (\bar{d} - d)}_{\substack{\text{balance between destruction} \\ \text{and protection of oligodendrocytes}}} \quad , \tag{E.1}$$

$$\underbrace{-\varepsilon\Delta\phi + \alpha\phi = \mu d}_{\text{preconditioning potential}} \quad , \tag{E.2}$$

the outer variable $u$ being an auto-immune damaging front and $A$ (*activation*) and $P$ (*protection*) being typical Heaviside functions associated with given thresholds. Subsequently $\partial_t d$ is zero unless $u$ and $\phi$ are respectively above and below some given thresholds. The elliptic equation (E.2) results from a quasi steady state approximation in the classical reaction diffusion equation $\delta\partial_t\phi = \varepsilon\Delta\phi + \mu d - \alpha\phi$. Other laws than brownian diffusion can be considered (see figure E.3). As suggested by the authors, this model also exhibits concentric ring formation. However, numerical analysis indicates that the range of the potential $\phi$ – a very strong hypothesis in the preconditioning theory – determines entirely the width of the protected areas. This leads to the confusing hypothesis of a long-range action for $\phi$ (about 100 cells of amplitude) which is not in accordance with the reported diffusion lengths of signaling molecules. In frog embryos, TGF$\beta$1 freely diffuses in a range of seven cell diameters (about 150 to 200$\mu m$) and *activin* attains a diffusion distance of approximatively twelve cell diameters ($\simeq 350\mu m$) (Gurdon et al. 1994, Stringini et al. 2000). It seems improbable that the molecules involved in ischaemic preconditioning attain diffusion ranges more than ten times larger than the ones attained by key developmental factors. In the following model (E.3)-(E.4)-(E.5) the width of preserved areas is characterized by a non-linear process driven by chemotaxis and closely matches the quantitative aspects observed in human lesions (compare figures E.3 and E.4)

Furthermore, it is particularly difficult to render numerically the apparition of rings using the preconditioning model (E.1)–(E.2), which only leads to the progression of a balanced moving boundary between

the zero- and the homogeneous- state of destroyed myelin. The key mechanism that may be lacking in preconditioning is the presence of two thresholds, as in Ostwald's scenario for Liesegang rings. As a matter of fact, in Ostwald's model, precipitation initiates when $[AB] > q^\star$ and persists because the second threshold $q$ is strictly lower than $q^\star$. For periodic precipitation to occur in the preconditioning model E.2, it would be nevertheless possible to increase the efficiency of the protection potential by using for instance $\phi = K * d$, where the convolution kernel $K$ has a plateau-shape (figure E.3). In this case, however, $\phi$ has no clear biological significance. Another situation where preconditioning could lead to banding would involve temporal discontinuities in front progression during the period necessary for the formation of a lesion. Nevertheless, successive multiple sclerosis attacks are never clinically observed in such a short period of time.

## Concentric demyelination: a chemotactic approach

The so-called *post-nucleation* theories of Liesegang ring formation – Ostwald's supersaturation being a *pre-nucleation* theory – are based on the hypothesis that a diffusing intermediate colloidal compound $C$ interacts with $B$ and aggregates to form the precipitate. Post-nucleation theories consider that the first step of ring formation is the appearance of a homogeneous colloidal field subjected subsequently to competitive growth or coarsening between the colloidal particles (Venzl et al. 1982). These theories allow a more accurate description of the diversity of Liesegang ring patterns (Droz 2000, Krug et al. 1999) and take into account the existence of the initial transient homogeneous colloidal state.

The following scenario for two-dimensional ring formation in Baló's sclerosis is based on the analogy with post-nucleation Liesegang ring formation theories (table E.1). Namely it considers secondary rearrangement processes at the back of the structural front. It requires no hypothesis on concentric demyelination and makes very few assumptions about the molecular processes involved in the pathogeny of MS.

Inactive macrophages are initially spread in the white matter. Their density is about 330 cells/mm$^2$ (Nimmerjahn et al. 2005). An activation front travels in the white matter from a lesional center, which can be a blood vessel, and drives the macrophages into an auto-immune active state. This front can be an activating molecule like an antibody, or a wave of oxydative stress (Aboul-Enein et al. 2005). The activated macrophages attack the oligodendrocytes, which are evenly distributed at a density of 400 cells/mm$^2$ (Lucchinetti et al. 1999). Moreover, damaged cells and phagocyting macrophages produce a signal that attracts surrounding activated macrophages. This chemoattractant can be a pro-inflammatory cytokine, such as TNF$\alpha$, IL-1 and IFN$\gamma$ (Brosnan et al. 1996). Concentric lesions can develop in the first hours following a MS attack (Barnett et al. 2004), and the MRI of patients one week after the clinical onset of the disease shows fully concentric lesions (Chen et al. 1999). This indicates that a characteristic time scale of the order of one hour is relevant in the modelling (see table 2 for the whole set of parameters).

These observations lead us to describe the dynamics of (E.3) the density $m$ of activated macrophages, (E.4) the concentration $c$ of the attraction signal and (E.5) the density $d$ of destroyed oligodendrocytes.

$$\frac{\partial m}{\partial t} = \underbrace{D\Delta m + \lambda m(\bar{m} - m)}_{\substack{\text{front of macrophages} \\ \text{activation}}} - \underbrace{\nabla \cdot \Big(\chi m(\bar{m} - m)\nabla c\Big)}_{\substack{\text{local macrophage} \\ \text{recruitment}}} \tag{E.3}$$

$$\underbrace{-\varepsilon\Delta c + \alpha c = \mu d}_{\substack{\text{production of a fast} \\ \text{diffusing signal}}} \tag{E.4}$$

$$\frac{\partial d}{\partial t} = \underbrace{F(m)m(\bar{d} - d)}_{\text{destruction of oligodendrocytes}} , \tag{E.5}$$

with $\bar{m}$, $\bar{d}$ being characteristic densities of macrophages and oligodendrocytes respectively, involved into saturation phenomena in the activation and the recruitment of the macrophages (E.3) and in the de-

| | |
|---|---|
| characteristic density of oligodendrocytes | $\bar{d} = 400$ c/mm$^2$ (Lucchinetti et al. 1999) |
| characteristic density of macrophages | $\bar{m} = 350$ c/mm$^2$ (Nimmerjahn et al. 2005) |
| characteristic length (one band) | $L = \sqrt{D/\lambda\bar{m}} = 1$ mm (Courville 1970) |
| characteristic time | $T = 1$ h (Barnett et al. 2004, Chen et al. 1999) |
| approximative range of the signal | $\sqrt{\varepsilon/\alpha} = 0.3$ mm (Gurdon et al. 1994, Stringini et al. 2000) |
| damaging intensity | $(\kappa\bar{m})^{-1} = 1/2$ h |
| chemosensitivity | $\chi$ plays the role of an unknown bifurcation parameter |

Table E.2: Biomedical data for the Baló's concentric sclerosis. Mean values of the reduced parameters chosen for the numerical simulations are derived from these space/time scales (see appendix). Only $\chi$ remains as a free parameter because of the lack of biological knowledge about its interpretation or measurement. Within this panel, numerical experiments fit the real space laws (see also figures E.2 and E.4 ) up to this free parameter $\chi$. In particular the pattern wavelength is decorrelated from the signal's range of action, contrasting with the preconditioning model.

struction of the oligodendrocytes (E.5). Initial value is a small bump of activated macrophages ($m > 0$) centered at the origin, accounting for the porosity of the blood vessel at some time. Boundary conditions are zero-flux for both $m$ and $c$, but this is in fact of minor importance because there is no interaction with the boundary until the front reaches it. Apart from the activation front, the cell flux in (E.3) decomposes into a small diffusion part ($\partial_t m - \delta\Delta m$) and a drift enhanced by the gradient of the diffusing signal ($\partial_t m + \nabla\cdot(\chi(m)m\nabla c)$). The elliptic equation (E.4) again results from a quasi steady state approximation.

The front propagation in (E.3) follows a Fisher-type equation, but the final pattern is independent of this particular choice. The front can in fact be a diffusing molecule which does not interact with white matter cells, or a molecule involved in more complex interactions with macrophages, like an antibody. Both cases lead to the same behaviour, except for the spacing laws: a traveling front with constant speed induces a linear position increase, whereas a diffusing front generates quadratic increasing (see also figure E.2). Baló's sclerosis seems to follow a linear spacing law and may thus not be accurately described by a mechanism involving diffusion alone. The damaging function $F$ can be chosen almost arbitrarily as long as it is both positive and increasing. We set $F(m) = \kappa\ m/(\bar{m} + m)$.

Chemotaxis is the collective motion of cells induced by a chemical gradient. Aggregation may occur when the cells themselves produce attractive substances, creating a non-linear coupling and leading to a blow-up of the cell density. We have opted for the well-studied Patlak, Keller & Segel model (Patlak 1953, Keller et al. 1971). If $M$, $D$, $\chi$ denote respectively the total number of cells, the diffusion of cells and the chemosensitivity in this system, the reduced structural parameter $\chi M/D$ controls bifurcation and determines the appearance of bundles, as was first conjectured by Nanjundiah (1973), then proved rigorously by Jäger et al. (1992) and Nagai (1995). Recent advances have focused on the precise threshold value between spread of cells and formation of clusters (Gajewski et al. 1998, Dolbeault et al. 2004) and on the qualitative description of the system including nonlinear coefficients (Calvez et al. 2006). The volume-filling approach (Painter et al. 2002, Dolak et al. 2005), which can be viewed as an extreme

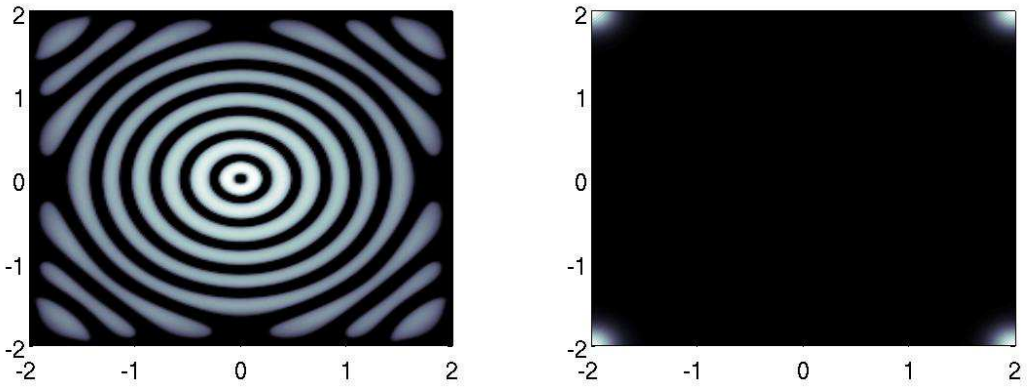


Figure E.4: Transition between concentric patterns and plaques is driven by the structural parameter $\chi$. Reduced parameters (see appendix) are $\tilde{\varepsilon} = 0.2$, $\kappa/\lambda = 4$, $\tilde{\chi} = 25$ (*left*) and $\tilde{\chi} = 8$ (*right*). The whole diameter is approximatively 4cm, and the final time is 24h. Destroyed oligodendrocytes are figured in black. Note that the white corners on the right are boundary artifacts.

saturation effect, plays a major role in our model (in equation (E.3)).

According to the basic Patlak, Keller & Segel model, structure formation in (E.3)-(E.4)-(E.5) is driven by the reduced parameter $\tilde{\chi} = \chi \bar{m} \mu \bar{d} / D\alpha$: a bifurcation occurs between a plaque state – for small values of $\tilde{\chi}$ – and a concentric pattern – for larger values of $\tilde{\chi}$ (figure E.4). High values of $\tilde{\chi}$ reflect the aggressivity of the demyelinating process and are obtained when $\bar{m}$ is large. In fact, the destruction of oligodendrocytes is correlated with the number of macrophages (Lucchinetti et al. 1999). Increasing levels of $\tilde{\chi}$ can also be interpreted as a more efficient inflammatory response. Again aggressivity is positively linked with pattern emergence. Interestingly, when there is a major oligodendroglial destruction (that is when the reduced parameter $r = \kappa/\lambda$ is large), patterning is favoured (see figure E.5a). The fact that the oligodendroglial destruction rate in Baló's sclerosis is generally larger than in classical forms of multiple sclerosis (Yao et al. 1994) is in line with the structurating role of cellular aggressivity.

Highly robust concentric patterning is supported by numerical evidence. The model only produces heterogeneous concentric damaged areas and homogeneous demyelinated plaques (figure E.5a). It is in addition absolutely insensitive to initial conditions: even an asymmetric source of activated macrophages leads to a perfect round-shaped pattern, because it is structured by the activation front. Furthermore, concentric symmetry is very well conserved by different types of random perturbation. White noise perturbation of chemical diffusion and randomization of the damaging function conserve the rings and induces the appearance of patterns close to the anastomoses and the peripheral fragmentation of the real lesions (see figure E.5b,c).

The concentric pattern is maintained as long as the destroyed oligodendrocytes produce the attractive potential $c$. This is justified because the characteristic time of our model is shorter than the relaxation time of the macrophages. The secondary dispersion of macrophages when oligodendrocytes do not produce $c$ anymore could explain that concentric lesions disappear in some MRI follow-up cases (Stadelmann et al. 2004).

## Conclusion

The non-linear approach involving a chemotactic mechanism for the lesional process allows a realistic description of Baló's sclerosis lesions without making any assumptions about specific cellular process. The variation range of the parameter $\tilde{\chi}$ shows a transition from a homogeneous plaque state characteristic of the classical MS lesions to a concentric, Baló-type, pattern. As our set of hypotheses only involves cellular events common to most subtypes of MS, our results are compatible with the hypothesis that Baló's sclerosis is a borderline form of MS. The high prevalence of this disease in South-Eastern Asian countries (Itoyama et al. 1984, Chen et al. 1999) may then be the result of extreme behaviours – for instance when the (reduced) chemotactic parameter $\tilde{\chi}$ is beyond the bifurcation threshold, and may reflect

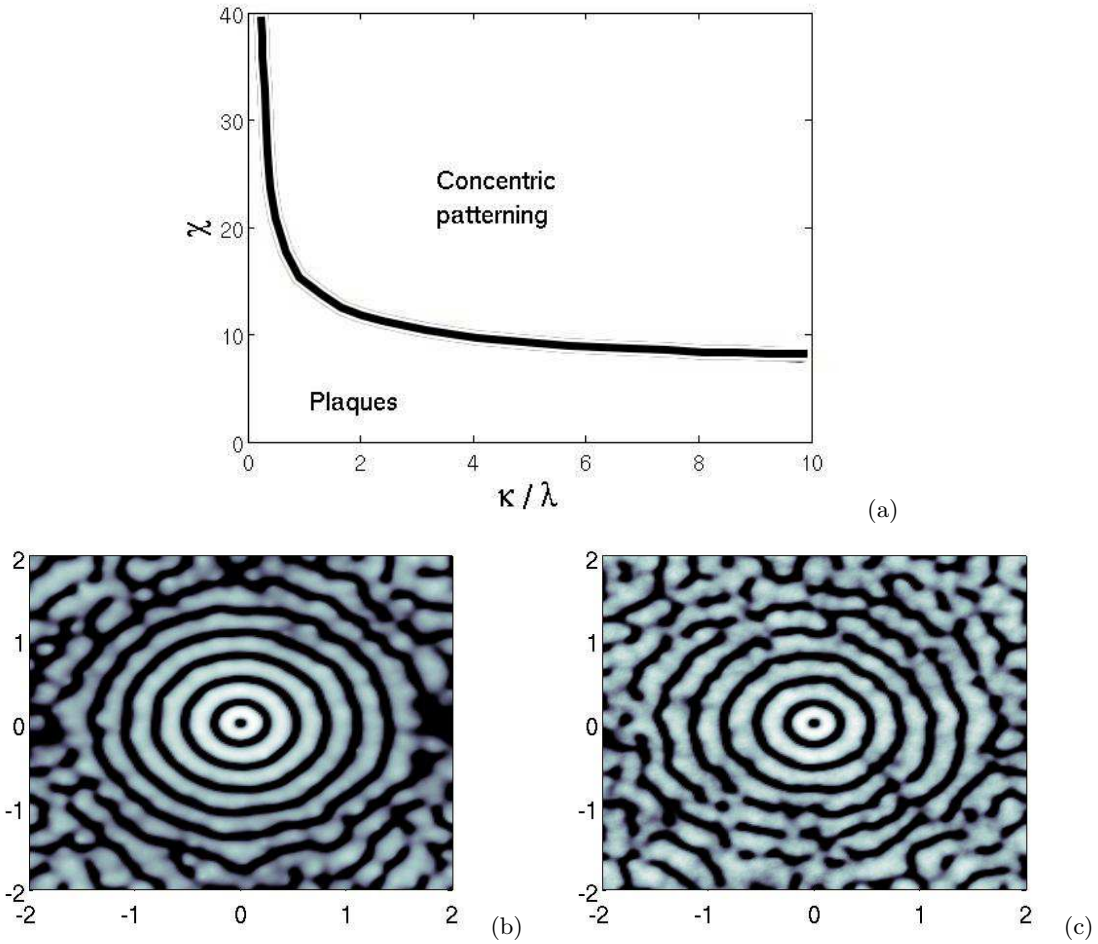


Figure E.5: (a) Bifurcation diagram for fixed reduced parameter $\tilde{\varepsilon} = 0.1$. Only two alternative patterns arise: concentric rings or plaques. (b) Imposed white noise perturbation with relative standard deviation $\sigma = 0.2$ to the chemical diffusion coefficient $\tilde{\varepsilon} = 0.2$. Other parameters are $\tilde{\chi} = 25$ and $\kappa/\lambda = 5$. (c) White noise perturbation with relative standard deviation $\sigma = 0.1$ to the damaging factor $\kappa/\lambda = 5$. We set $\tilde{\varepsilon} = 0.2$ and $\tilde{\chi} = 25$. Destroyed oligodendrocytes are figured in black. The damaging factor is more sensitive to perturbation, and increasing the standard deviation breaks the symmetry of the pattern, except around the origin.

the crucial role of cellular aggressivity in pattern formation.

## Appendix: adimensionalized parameters and equations

We set the reduced variables and parameters as follows:

$$\tilde{m} = \frac{m}{\bar{m}}, \quad \tilde{d} = \frac{d}{\bar{d}}, \quad \tilde{c} = \frac{\alpha}{\mu \bar{d}}, \quad \tau = \lambda \bar{m} t, \quad y = \sqrt{\frac{\lambda \bar{m}}{D}} x, \quad \tilde{\chi} = \frac{\chi \bar{m} \mu \bar{d}}{D\alpha}, \quad \tilde{F}(\tilde{m}) = \frac{\kappa}{\lambda} \frac{\tilde{m}}{1+\tilde{m}}, \quad \tilde{\varepsilon} = \frac{\varepsilon \lambda \bar{m}}{D\alpha}.$$

In particular the ratio $r = \kappa/\lambda$ balances the speed of the front and the intensity of the macrophages in damaging the myelin. We obtain the following non-dimensionalized system,

$$\begin{cases} \dfrac{\partial \tilde{m}}{\partial \tau} = \Delta \tilde{m} + \tilde{m}(1-\tilde{m}) - \nabla \cdot \Big( \tilde{\chi} \tilde{m}(1-\tilde{m}) \nabla \tilde{c} \Big), \\ -\tilde{\varepsilon} \Delta \tilde{c} + \tilde{c} = \tilde{d}, \\ \dfrac{\partial \tilde{d}}{\partial \tau} = \tilde{F}(\tilde{m}) \tilde{m}(1-\tilde{d}). \end{cases} \tag{E.6}$$

Only three structural parameters remain, namely the reduced chemosensitivity $\tilde{\chi}$, the reduced chemical diffusivity $\tilde{\varepsilon}$ and the ratio $r = \kappa/\lambda$.

# Annexe F

# Mécanismes d'immunité croisée

Ce travail plus ancien, effectué lors d'un stage au Centre for Mathematical Biology (Oxford), en collaboration avec Andrei Korobeinikov et Philip Maini, contribue à l'étude de certains modèles d'immuologie, dits d'immunité croisée, qui complexifient l'image usuelle des modèles SIR [194, 185]. Si le groupe des virus infectieux est divisé en éléments 'proches' quoique distincts, l'infection par un type de virus peut conférer une immunité 'partielle' à un individu infecté puis guéri, le protégeant ainsi des attaques ultérieures des autres virus de la même famille. Cette dynamique conduit à l'émergence de structures (clusters) dans la population des virus [124]. Nous étendons ici le modèle de Gupta et al. [123] à un petit nombre de variants (4, 8 ou 16) avec différents degrés d'immunité croisée. Nous donnons quelques règles simples, géométriques et intuitives pour prévoir et comprendre la synchronisation dans les groupes de virus infectieux. Ces résultats sont corroborés par des simulations numériques robustes. Cet article est paru dans Journal of Theoretical Biology sous le titre *Cluster formation for multi-strain infections with cross-immunity* [53].

## F.1 Introduction

Many pathogens have several different antigenic variants, or strains, present in a host population simultaneously. The classic example is influenza [10, 170, 210, 117, 72], where there are several circulating subtypes, with many minor variants within each subtype. Other important examples are meningitis [124, 122], dengue [117] and malaria [125].

Because of similarities in, for example, their mechanisms of infection, strains may interact with each other [124]. Infection with one strain may partially protect the host against infection with other strains. Cross-immunity is included in different ways in different models, but the general idea is the same: infection with one strain of the disease produces a lasting immune memory in the host which acts to protect against subsequent infection by other strains. That is, for two sufficiently close strains $A$ and $B$, infection by strain $A$ reduces the chance of a secondary infection by strain $B$. For instance, in the case of influenza, the surface protein hemagglutinin seems to be under strong positive selection because it is the target of the immune response, and therefore it presents high antigenic diversity in the virus population [10, 170, 210, 117]. This immune response may be enhanced because of a previous infection with a close variant.

There are different approaches to the cross-immunity problem [118]. For instance, we can assume that a fraction, say $\gamma_{BA}$, of individuals infected with strain $A$ gain complete immunity to strain $B$; alternatively, all the individuals infected with strain $A$ may be assumed to acquire partial immunity against $B$ (with a consequence that the force of secondary $B$-infection is reduced by a factor $\gamma_{BA}$). Another possible hypothesis is that the secondary infection is weaker and thus less transmissible by the infective host. These differences in the approaches to cross-immunity lead to variety of models providing

sometimes controversial outcomes. Under such circumstances it is reasonable to look for such features of the multi-strain system which are intrinsic to this system and are robust irrespective of model choice.

A system of multiple strains interacting via host cross-immunity tends to self-organise into groups, or clusters. The tendency for strains to occur in clusters reflects the observed influenza dynamics [117, 210]. Cluster formation was observed and discussed by [124, 123]. The phenomenon of clustering appears to be typical for many systems with internal order and may occur in such systems as multi-species predator-prey systems. For example, it was observed in neuronal networks [232, 231, 218, 217].

In this paper we consider formation of clusters in ordered multi-strain systems. We show that for complex systems several different types of cluster structure may arise. We also demonstrate that cluster structures are not specific to a particular model – on the contrary, they appear to be intrinsic to the given strain system. In general, cluster formation is a self-organisation phenomenon bearing many similarities to pattern formation. A remarkable feature of clusters is that they exhibit exceptional regularity even when dynamics of every strain is chaotic.

## F.2 Model

Due to different approaches to cross-immunity, a variety of models of multi-strain infections has been developed. These models sometimes lead to different outcomes. It is important, therefore, to find such indicators which are characteristic to the system itself and robust to choice of model.

We start from a comparatively simple model of a multi-strain infection suggested by [123]. This model is composed of only three compartments (and respectively three differential equations) for each strain. If $z_i(t)$ is the fraction of individuals who have been or are infected with the strain $i$ (either they are infectious or not), $y_i(t)$ is the fraction of the infectious with the strain, and $w_i(t)$ is the fraction of individuals who have been infected (or are infected) by any strain sufficiently close to the strain $i$ including $i$ itself (that is $w_i = \cup_{j\sim i} z_j$), then the model equations are

$$\begin{aligned} \frac{d\,z_i}{dt} &= \beta_i y_i (1 - z_i) - \mu z_i, \\ \frac{d\,w_i}{dt} &= \sum_{j\sim i} \beta_j y_j (1 - w_i) - \mu w_i, \\ \frac{d\,y_i}{dt} &= \beta_i y_i \left[(1 - w_i) + (1 - \gamma)(w_i - z_i)\right] - (\mu + \sigma_i) y_i. \end{aligned} \tag{F.1}$$

For this model, cross-protection does not affect susceptibility but reduces transmissibility by a factor $1 - \gamma$ (where the parameter $\gamma$ measures the degree of cross-protection between two strains). Here $j \sim i$ means that the $j$th strain is related to the $i$th strain and can induce cross-protection (that is if $j \sim i$ then $\gamma_{ij} \neq 0$). The parameters $1/\mu$ and $1/\sigma$ are, respectively, host life expectancy and average period of infectiousness, $\beta$ is transmission rate. We refer to this model as Gupta's model. This simple model has been analysed in [123] and provided important insights into pathogenes formation and strains genetic organisation.

To study the phenomenon of clustering we need to consider several levels of cross-protection. Whereas the original model implies only one level of cross-protection ($\gamma$ if two strains are related, or zero if they are not), and neglects possible multiple infections by strains related to $i$. We relax these assumptions below to make the model more generally applicable, while striving to keep the model simple. We assume that the probability of cross-protection between strains $i$ and $j$ is $\gamma_{ij}$ (that is, infection by the strain $j$ reduces the probability that the host will be infected by the strain $i$ by a factor $\gamma_{ij}$), and consider the barycenter of $\gamma_{ij}$, defined as

$$\Gamma_i = \left( \sum_{j\sim i, j\neq i} \gamma_{ij} \beta_j y_j \right) \Big/ \left( \sum_{j\sim i, j\neq i} \beta_j y_j \right). \tag{F.2}$$

We replace the coefficient $\gamma$ in the system (F.1) with the barycenter $\Gamma_i$. Substituting the barycenter $\Gamma_i$

into (F.1) and using variables $V_i = 1 - z_i$, $X_i = 1 - w_i$, $Y_i = \frac{\beta_i}{\mu} y_i$ and $\tau = \mu t$, we obtain the system

$$\begin{aligned} \frac{dV_i}{d\tau} &= 1 - \Big(1 + Y_i\Big)V_i, \\ \frac{dX_i}{d\tau} &= 1 - \Big(1 + \sum_{j\sim i} Y_j\Big)X_i, \\ \varepsilon_i \frac{dY_i}{d\tau} &= \Big((1-\Gamma_i)V_i + \Gamma_i X_i - r_i\Big)Y_i. \end{aligned} \tag{F.3}$$

Here $\varepsilon_i = \mu/\beta_i$ and $r_i = (\mu + \sigma_i)/\beta_i$. Obviously, $\Gamma_i \equiv \gamma$ for Gupta's model (when $\gamma_{ij}$ is either $\gamma$, or zero). Furthermore, computations show that for this model the function $\Gamma_i(t)$ most of the time remains taking one of a few constant values, with rapid shifting between these values (see Fig. F.3 (b)); this justifies the use of the function $\Gamma_i(t)$.

## F.3 Structure of a strain set

Systems of strains were formed as a result of a genetic process, and they generally inherited some internal order associated with this process. Having this intrinsic order, a system of strains may be organised in an ordered set, or a discrete strain space every point of which represents a strain. The idea of the strain space allows us to use the concept of "immunological distance". The immunological distance between two strains may be assumed to depend inversely on their mutual level of cross-protection.

The structure of the strain space depends on underlying immunological and genetic processes. For instance, [117] considered the simplest possible strain space: a linear strain space. In this case strains are arranged in a line, and they postulated $\gamma_{ij} = \exp(-(\frac{i-j}{d})^2)$, where $d$ is a constant. A multi-dimensional strain space may be organised in the same way, with immunological distance defined, for example, as the sum of horizontal and vertical distances. [81, 118] considered a system of four strains arranged in a circle. In this case each strain is assumed to interact more strongly with its adjacent neighbours than with the strain opposite.

Studying the maintenance of strain structure in a recombining virus population, [124] have introduced a simple framework where strains are organised as follows: each strain is characterised by a combination of alleles at loci which are of immunological interest. Strains induce cross-immunity if they share at least one allele. For example, in the case of two loci and two possible alleles at each locus (say $a$ or $b$ for the first locus, and $x$ or $y$ for the second one respectively) there are four different strains: the original strains $ax$ and $by$, and the recombinant strains $ay$ and $bx$. To visualise such a strain structure we will use a multi-dimensional graph where a dimension corresponds to a locus, and vertices represent strains. Figure F.1(a) illustrates the structure of the above mentioned four-strain system (two loci and two possible alleles at each locus). Figure F.1(b) shows the strain space of an eight-strain system organised on three loci with two alleles at each locus.

## F.4 Results

Cross-immunity may structure a set of strains into groups, or clusters. These groups can behave at least in three ways: remain in homogeneous equilibrium when no structure is observed (Fig. F.2 a), oscillate when the clusters alternate recurrently in succession (Fig. F.2 b), or one group may dominate with the others driven below survival level (Fig. F.2 c) [124, 123]. The phenomenon of clustering is conserved for all sufficiently large levels of cross-protection. Of course, when $\gamma \to 0$, the equations are decoupled, and the clustering disappears.

In the case of the four-strain system shown in Fig. F.1(a) it is natural to expect the formation of two clusters of non-overlapping (or discordant) strains, namely $ax$ groups with $by$, and $ay$ groups with $bx$ (in Fig. F.1(a) we respectively mark the strains by squares and cycles). Indeed, such clustering has been observed [118, 81, 124, 123]. Figure F.2 illustrates the strain dynamics: it is easy to see the formation of two clusters.

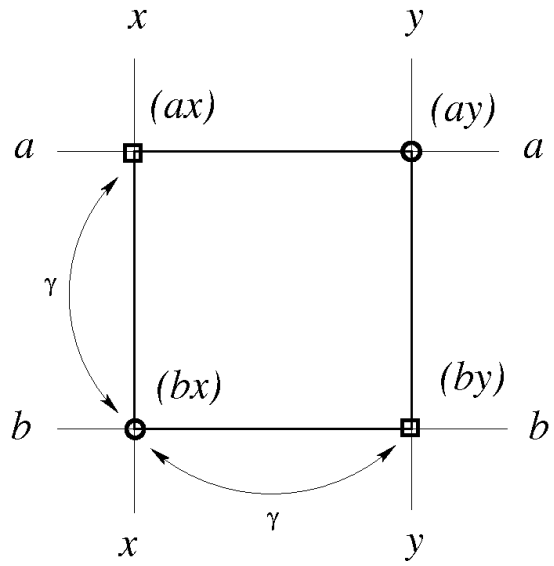


(a) Strain space of a four-strain system: two loci and two possible alleles at each locus (see text for details).

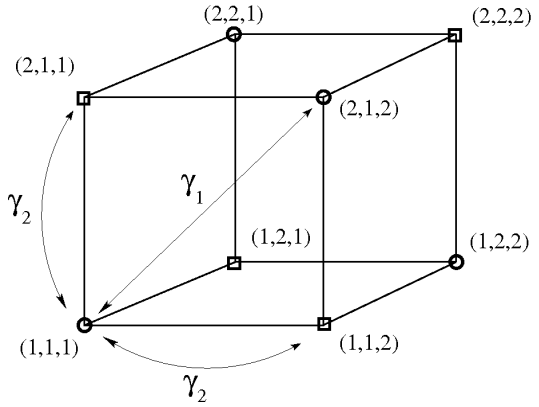


(b) Strain space of an eight-strain system: three loci with two alleles possible at each locus. Here, for instance, $(2, 2, 1)$ means that the second, the second and the first alleles are respectively at the first, the second and the third locus.

Figure F.1: Geometry of the strain spaces [124].

However, a multi-strain system with only one level of cross-protection, which is the same for all related strains, is hardly realistic. As the number of strains grows, and especially if there are several different levels of cross-protection, the self-organisation of the system may be more complicated. Furthermore, it may be different for different levels of cross-protection. For instance, for the eight-strain system shown in Fig. F.1(b) at least two different types of clustering are possible. From now on we will use the terms *cluster structure* and *type of cluster structure*. The difference between these objects is that different cluster structures may be of the same type. Below we will show this using an example.

For a system of eight strains organised in three loci with two alleles each (Fig. F.1(b)) we assume two levels of cross-protection: namely $\gamma_1$ if the strains share one allele, or $\gamma_2$ if they share two alleles. Naturally, $\gamma_1 \leq \gamma_2$. For this system one can expect formation of a structure of four clusters with two discordant strains each [123]. Every cluster of such structure corresponds to one of the four main diagonals of the cube in Fig. F.1(b). However, this type of cluster structure was observed only when $\gamma_1$ and $\gamma_2$ are sufficiently close. As the difference between $\gamma_1$ and $\gamma_2$ grows, a new type of cluster structure appears: now there are two clusters, $\alpha$ and $\beta$, with four strains each ($\alpha$ is composed of the strains (1,1,1), (1,2,2), (2,1,2) and (2,2,1), and $\beta$ of (2,2,2), (2,1,1), (1,2,1) and (1,1,2)). In Fig. F.1(b) the strains of these "tetrahedral" clusters are marked respectively by cycles and squares. This second type of clustering can hardly be expected *a priori*. However, this cluster structure exists for a much wider range of $\gamma_1$ and $\gamma_2$ than the first type (see Fig. F.5). Fig. F.3 illustrates the dynamics of the second type of clustering. Here, the logarithm of the forces of infection $\log Y_i(t)$ (Fig. F.3(top)) and the effective cross-protection $\Gamma_\alpha(t)$ (Fig. F.3(bottom)) are shown for $\varepsilon = 5 \cdot 10^{-3}$ (left column) and $5 \cdot 10^{-4}$ (right column). Note that the function $\Gamma_\alpha(t)$ most of the time remains constant, with rapid shifting between two constant values. Also note remarkable regularity of the function $\Gamma_\alpha(t)$ contrasting to chaotic behaviour of the forces of infection. The function $\Gamma_\beta(t)$ is qualitatively the same.

Figure F.4 shows the results of the stochastic perturbation of the system. Here we assume that $1/\varepsilon = 200 + \delta(t)$, where $\delta(t)$ is a Gaussian-distributed noise of magnitudes 1 (Fig. a), 10 (Fig. b) and 20 (Fig. c). It is easy to see that the cluster structure is robust to such stochastic perturbations.

A cluster structure may be qualitatively defined by the *clustering matrix* $M$: we set $m_{ij}$ equal to 1 if

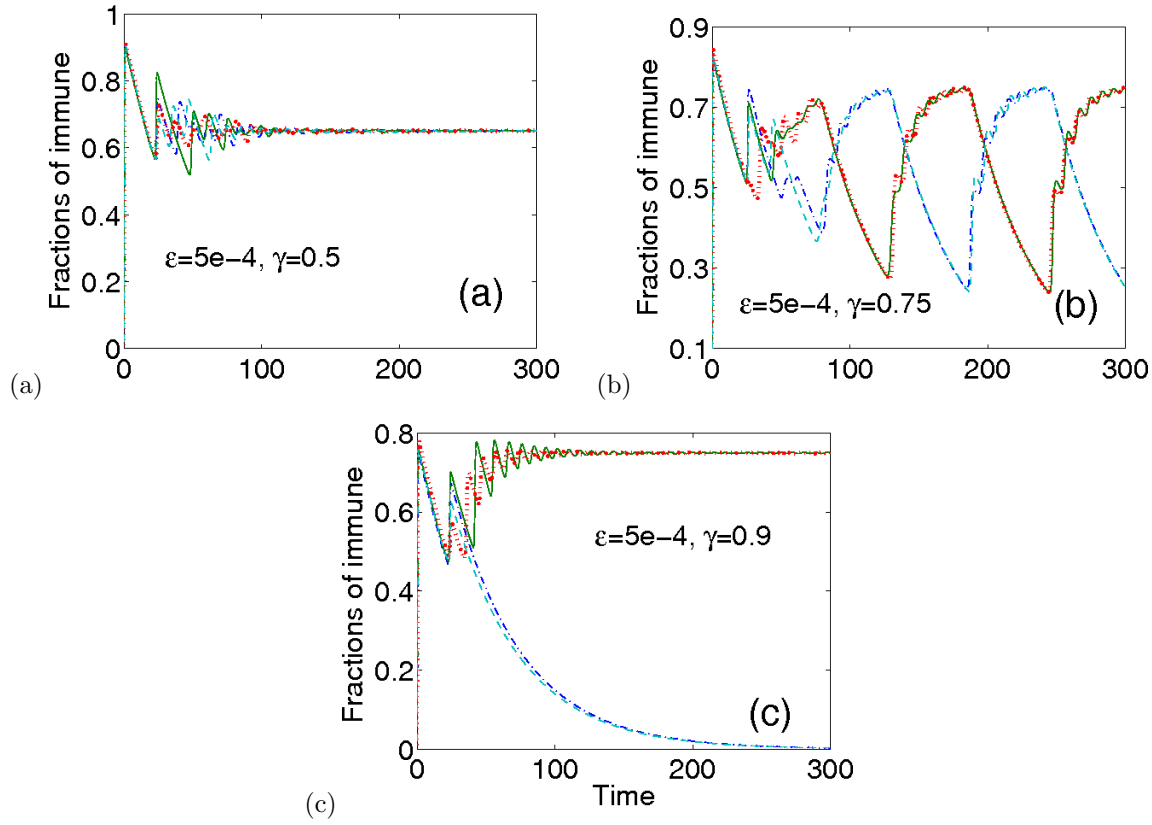


Figure F.2: Dynamics of the four-strain system shown in Fig. F.1(a). Here (b) and (c) illustrate formation of two clusters each consisting of two strains; in (a) the system is in homogeneous equilibrium, and no definite clustering can be observed.

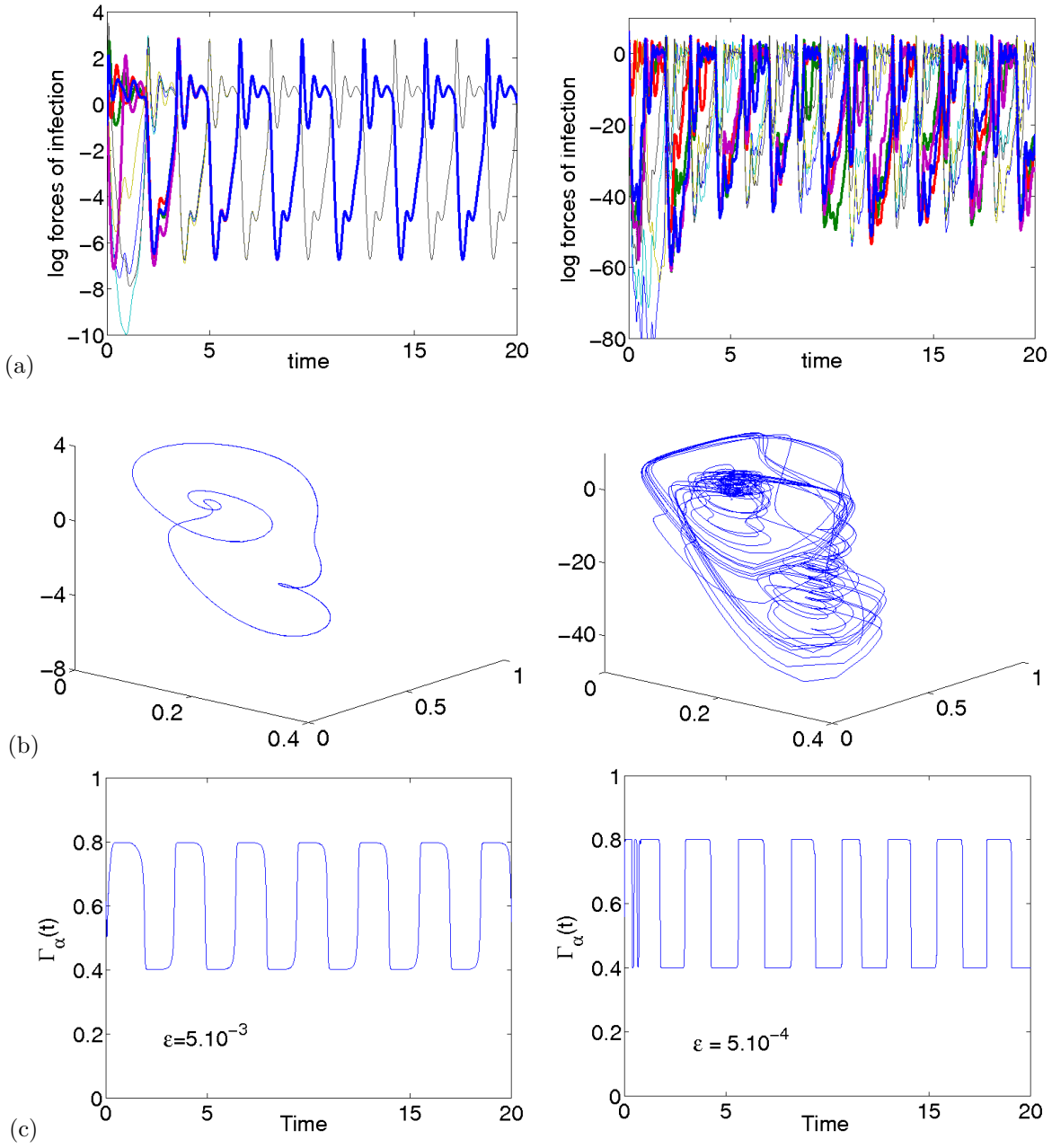


Figure F.3: (*top*) Dynamics of the logarithm of the forces of infection $Y_i(t)$; (*middle*) trajectories of the first strain in the $(V_1, X_1, \log Y_1)-$phase plane; (*bottom*) and the effective cross-protection $\Gamma_\alpha(t)$ for the "tetrahedric" cluster structure (two clusters with four strains each). The bold lines in (*top*) are the forces of infection of the four strains belonging to the first cluster. Here $\varepsilon = 5 \cdot 10^{-3}$ (left column) and $5 \cdot 10^{-4}$ (right column); $\gamma_1 = 0.4$ and $\gamma_2 = 0.8$. Note the remarkable synchronisation of the forces of infection for each cluster for $\varepsilon = 5 \cdot 10^{-3}$ and regularity of the function $\Gamma_\alpha(t)$ contrasting to chaotic behaviour of the forces of infection for $\varepsilon = 5 \cdot 10^{-4}$.

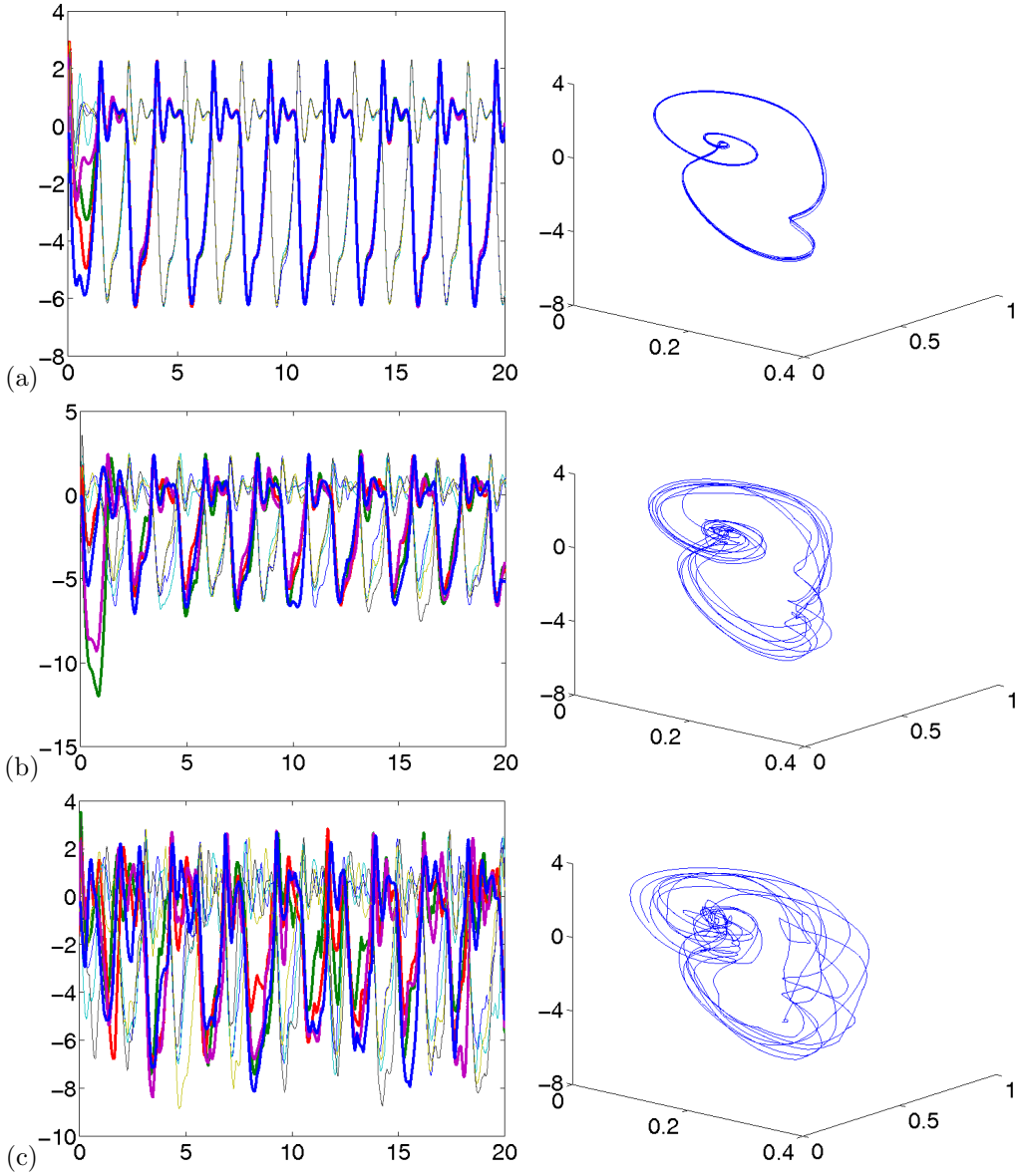


Figure F.4: The logarithm of the forces of infection $Y_i(t)$ for the "tetrahedric" cluster structure with stochastic perturbations. Here $1/\varepsilon = 200+\delta(t)$, where $\delta(t)$ is the Gaussian-distributed noise of magnitudes 1 (Fig. a), 10 (Fig. b) and 20 (Fig. c); $r = 0.25$, $\gamma_1 = 0.5$ and $\gamma_2 = 0.8$. The bold lines correspond to the strains of the first cluster.

the strains $i$ and $j$ belong to the same cluster, and $m_{ij} = 0$ otherwise. Naturally, the matrix is symmetric and $m_{ii} = 1$. For instance, if the vertices of the cube Fig. F.1(b) are ordered as follows

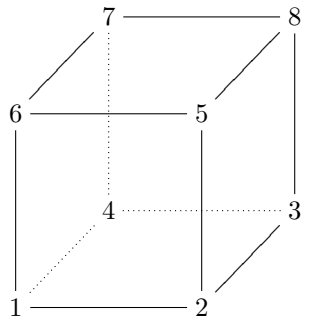


then the clustering matrices for the first and second types of clustering are

$$M_I = \begin{pmatrix} 1 & 0 & 0 & 0 & 0 & 0 & 0 & 1 \\ 0 & 1 & 0 & 0 & 0 & 0 & 1 & 0 \\ 0 & 0 & 1 & 0 & 0 & 1 & 0 & 0 \\ 0 & 0 & 0 & 1 & 1 & 0 & 0 & 0 \\ 0 & 0 & 0 & 1 & 1 & 0 & 0 & 0 \\ 0 & 0 & 1 & 0 & 0 & 1 & 0 & 0 \\ 0 & 1 & 0 & 0 & 0 & 0 & 1 & 0 \\ 1 & 0 & 0 & 0 & 0 & 0 & 0 & 1 \end{pmatrix} \quad \text{and} \quad M_{II} = \begin{pmatrix} 1 & 0 & 1 & 0 & 1 & 0 & 1 & 0 \\ 0 & 1 & 0 & 1 & 0 & 1 & 0 & 1 \\ 1 & 0 & 1 & 0 & 1 & 0 & 1 & 0 \\ 0 & 1 & 0 & 1 & 0 & 1 & 0 & 1 \\ 1 & 0 & 1 & 0 & 1 & 0 & 1 & 0 \\ 0 & 1 & 0 & 1 & 0 & 1 & 0 & 1 \\ 1 & 0 & 1 & 0 & 1 & 0 & 1 & 0 \\ 0 & 1 & 0 & 1 & 0 & 1 & 0 & 1 \end{pmatrix},$$

respectively. The idea of clustering matrix allows us to define the concepts of *cluster structure* and *type of cluster structure* rigorously. The cluster structures are of the same type if their clustering matrices can be transformed one into another by row and column permutations. We also define the effective correlation matrix $R$ with the coefficients [12]

$$R_{ij} = \frac{\big\langle Y_i(t), Y_j(t)\big\rangle_T - \big\langle Y_i(t)\big\rangle_T \big\langle Y_j(t)\big\rangle_T}{\sqrt{\Big(\big\langle Y_i(t)^2\big\rangle_T - \big\langle Y_i(t)\big\rangle_T^2\Big)\Big(\big\langle Y_j(t)^2\big\rangle_T - \big\langle Y_j(t)\big\rangle_T^2\Big)}}.$$

Here $\big\langle Y(t)\big\rangle_T$ is the mean average

$$\big\langle Y(t)\big\rangle_T = \frac{1}{T}\int_{\mathcal{I}} Y(\tau)d\tau.$$

The time interval $\mathcal{I}$ should be sufficiently long and exclude the transient regime. The correlation coefficient $R_{ij}$ is a measure of synchronisation of the time series for the forces of infection; $R_{ij} = 1$ when complete synchronisation occurs, and $R_{ij} = -1$ when the strains are in antiphase. Naturally, $R_{ii} = 1$. For example, for the case shown in Fig. F.3, $R_{ij}$ is equal to 1 for the strains of the same cluster and to $-0.6$ otherwise when $\varepsilon = 5 \cdot 10^{-3}$ (left column), and $R_{ij}$ is between 0.75 and 1 for the strains in the same cluster and between $-0.45$ and $-0.19$ otherwise when $\varepsilon = 5 \cdot 10^{-4}$ (right column).

It is thereby a fairly straightforward procedure to relate the coefficients $R_{ij}$ to the coefficients of clustering $m_{ij}$. For instance, a threshold function of the form $H(r) = \dfrac{\exp(\alpha(r-a))}{1+\exp(\alpha(r-a))}$, where $\alpha > 0$ is sufficiently large and $0 \le a < 1$, can be applied to the elements of the matrix $R$. Fig. F.5 illustrates the Euclidean distance between the effective correlation matrix $H(R)$ and the second type clustering matrix $M_{II}$,

$$\Delta = \big\|H(R) - M_{II}\big\|_2 = \left(\sum_{i,j}(R_{ij} - M_{ij})^2\right)^{\frac{1}{2}},$$

for different values of $\gamma_1$ and $\gamma_2$. (Here $\alpha = 20$ and $a = 0.7$.) It is easy to see that when $\gamma_1 \approx \gamma_2$, the rapid shift between the two types of clustering occurs.

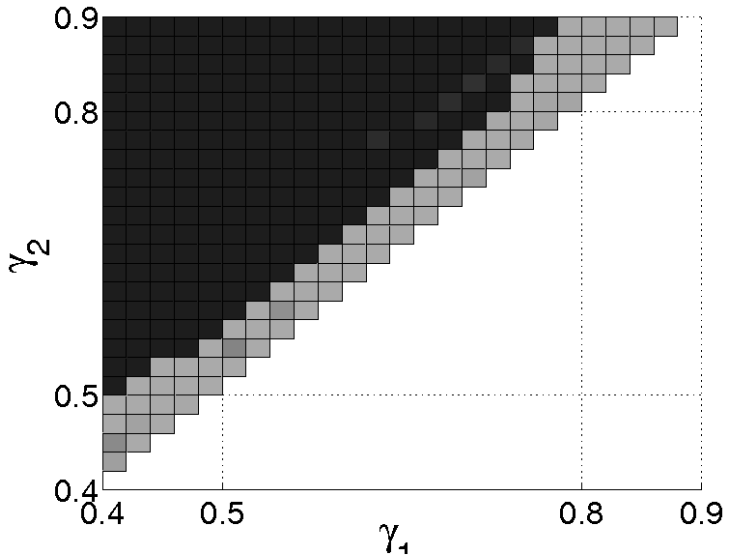


Figure F.5: Euclidean distance $\Delta$ between the effective correlation matrix $H(R)$ and the clustering matrix $M_{II}$ as a function of $\gamma_1$ and $\gamma_2$. In the black area $\Delta = 1$, that is the matrix $H(R)$ coincides with $M_{II}$. In the gray area $\Delta = 0$; the first type of clustering occurs in this area. The white area corresponds to the biologically unfeasible case $\gamma_1 > \gamma_2$ (the third type of clustering, mentioned in the text, occurs in this area).

In some cases, for instance when the system is near an equilibrium state, calculation of the coefficients $R_{ij}$ may be difficult. Then a similarity matrix with the coefficients

$$S_{ij}^2 = \frac{\left\langle \left(Y_i(t) - Y_j(t)\right)^2 \right\rangle_T}{\sqrt{\left\langle Y_i(t)^2 \right\rangle_T \left\langle Y_j(t)^2 \right\rangle_T}}$$

may be calculated.

New types of clustering may be obtained by breaking the natural constraint $\gamma_1 \leq \gamma_2$ or by introducing a nonzero level of cross-protection $\gamma_0$ between the discordant strains. For instance, the extremal case $\gamma_2 \ll \gamma_1$ generates a new type of cluster structure: four clusters of two neighbouring strains. Three different cluster structures,

$$\begin{pmatrix} 1&1&0&0&0&0&0&0\\ 1&1&0&0&0&0&0&0\\ 0&0&1&1&0&0&0&0\\ 0&0&1&1&0&0&0&0\\ 0&0&0&0&1&1&0&0\\ 0&0&0&0&1&1&0&0\\ 0&0&0&0&0&0&1&1\\ 0&0&0&0&0&0&1&1 \end{pmatrix}, \quad \begin{pmatrix} 1&0&0&1&0&0&0&0\\ 0&1&1&0&0&0&0&0\\ 0&1&1&0&0&0&0&0\\ 1&0&0&1&0&0&0&0\\ 0&0&0&0&1&0&0&1\\ 0&0&0&0&0&1&1&0\\ 0&0&0&0&0&1&1&0\\ 0&0&0&0&1&0&0&1 \end{pmatrix} \quad \text{and} \quad \begin{pmatrix} 1&0&0&0&0&1&0&0\\ 0&1&0&0&1&0&0&0\\ 0&0&1&0&0&0&0&1\\ 0&0&0&1&0&0&1&0\\ 0&1&0&0&1&0&0&0\\ 1&0&0&0&0&1&0&0\\ 0&0&0&1&0&0&1&0\\ 0&0&1&0&0&0&0&1 \end{pmatrix},$$

are possible for this type. (It is noteworthy that these cluster structures are in the same orbit under the action of cube rotations.)

For a multi-strain system, the dynamics of a single strain is sometimes chaotic[12] [123]. However, under the same conditions which cause chaotic strain dynamics, clusters usually behave in a surprisingly

[12]Here and through this paper, by the term "chaos" we imply deterministic chaos.

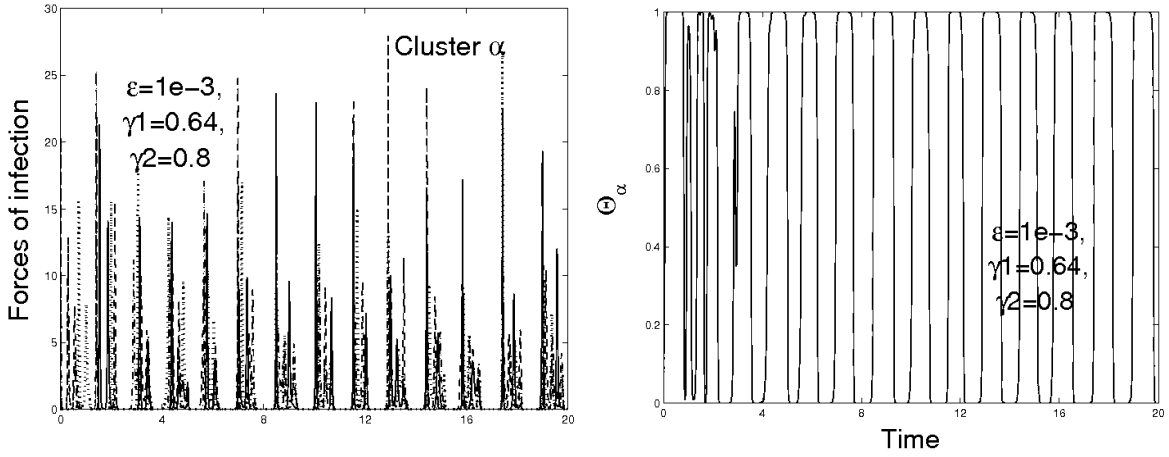


Figure F.6: Dynamics of forces of infection and relative force of infection $\Theta_\alpha(t)$ of the cluster $\alpha$ of the eight-strain system (Fig. F.1(b)) for the second type of clustering. (Here $\varepsilon = 1 \cdot 10^{-3}, \gamma_1 = 0.64$ and $\gamma_2 = 0.8$.) Note that while the dynamics of each single strain is chaotic, the cluster as a whole behaves remarkably regularly.

regular fashion. This regularity is hardly to be expected *apriori*. To describe the cluster dynamics, for each cluster, e.g. $\alpha$, we define the *relative force of infection* $\Theta_\alpha(t)$ of the cluster as

$$\Theta_\alpha(t) = \sum_{j \in \alpha} Y_j \Big/ \sum_{i=1}^{n} Y_i \ .$$

Naturally, $0 \leq \Theta_\alpha \leq 1$; $\Theta_\alpha \to 1$ when the cluster $\alpha$ dominates, and it tends to zero when one of the other clusters dominates. Fig. F.6 illustrates the dynamics of the cluster $\alpha$ of the eight-strain system: it is easy to see that the evolution of the relative force of infection of the cluster $\Theta_\alpha(t)$ is notably regular, while the dynamics of single strains is chaotic. The behaviour of the cluster $\beta$ is qualitatively the same.

The tendency of the strains to self-organise into clusters, and the remarkable regularity of the dynamics of these clusters, contrasting to the chaotic behaviour of a single strain, remain as the number of strains grows. With an increasing number of strains, the number of possible cluster structures grows as well, and new types of cluster structures appear.

The sixteen-strain system, such that for each strain there are four loci with two alleles possible at each locus, may be visualised as a four-dimensional cube. We assume three levels of cross-protection for this system: $\gamma_1$ if the strains share one allele, $\gamma_2$ if the strains share two alleles and $\gamma_3$ for the strains sharing three alleles (naturally, $\gamma_1 \leq \gamma_2 \leq \gamma_3$). At least six cluster structures of three different types are possible for this system. Particularly, if $\gamma_3$, $\gamma_2$ and $\gamma_1$ are approximately equal, a structure of eight clusters with two discordant strains each appears (each cluster corresponds to a main diagonal of the four-dimensional cube; strains of a cluster are the ends of the diagonal). If $\gamma_3$ is sufficiently large compared with $\gamma_1$ and $\gamma_2$, then the system self-organises into two clusters of eight strains each. In this case the strains of a cluster share either no allele at all, or two alleles; there is no cluster with strains sharing one allele in this case. If both $\gamma_3$ and $\gamma_2$ are large compared with $\gamma_1$, then a new stable type of cluster structure appears. In this case eight clusters with two strains each form. A structure of this type differs from the above mentioned structure of the first type (eight clusters with two discordant strains each) as follows: in this case the strains of each cluster share one allele which is at the same locus for every cluster of the structure. That is for this cluster structure, the strains belong to the diagonal of the three-dimensional sides of the four dimensional cube whereas for the cluster structure of the first type the strains are those on the main diagonal of the four-dimensional cube. Since there are four loci for this system, four different structures of this type are possible.

For this system one may also expect formation of a cluster structure of four clusters with four strains

each. However, such a cluster structure was not found for biologically feasible coefficients $\gamma$ (that is for $\gamma_1 \leq \gamma_2 \leq \gamma_3$). We have been able to generate this cluster structure only for $\gamma_2$ larger than $\gamma_1$ and $\gamma_3$.

Self-organisation of strains into clusters is not a particular feature of the model considered. Computations show that, for an ordered strain system given, the same cluster structures arise for other models, even if the dynamics of these clusters differ. It appears that a cluster structure is intrinsic to an ordered strain system.

For comparison purposes, we considered the models suggested by [117], and [118]. The Gog and Grenfell model is a comparatively simple $SIR$ model composed for $2n$ classes and purposed to investigate the role of cross-immunity in antigenic drift with a large number of strains. The model equations are

$$\begin{aligned} \frac{d\,S_i}{dt} &= \mu - S_i \sum_{j=1}^{n} \gamma_{ij}\beta_j I_j - \mu S_i, \\ \frac{d\,I_i}{dt} &= \beta_i I_i S_i - r_i I_i, \end{aligned} \tag{F.4}$$

where $S_i$ and $I_i$ are respectively the fractions of susceptibles and infectives for the $i$th strain, and $\gamma_{ii}$ is postulated to be equal to one. In contrast, the Gog and Swinton model is a very complex model comprising $n + 2^n$ classes. If $Z_J$ denotes the individuals who are immune to all the strains of the set $J \subset \{1, \ldots, n\}$ (thus they are susceptibles to ${}^cJ$) then the system equations are

$$\begin{aligned} \dot{I}_i &= \beta_i I_i \sum_{J: i \notin J} Z_J - (\mu + \sigma_i) I_i \\ \dot{Z}_J &= \sum_{i,K} C(K, J, i)\beta_i I_i Z_K - \sum_{i \notin J} \beta_i I_i Z_J - \mu Z_J + \mu \delta_{J,\emptyset} \end{aligned} \tag{F.5}$$

The term $C(K, J, i)$ represent the effect of cross-immunity. In fact, it is the rate of transfer from compartment $K$ to compartment $J$ after infection by the strain $i$.

Despite the huge difference in model complexity, both models demonstrate similarities in cluster formation. The behaviour of both these systems is somewhat simpler than that of Gupta's model. Particularly, no alternation of clusters was observed for these models: depending on the system parameters, the phase trajectories of the system converge towards one of the system equilibria with damped oscillations. Nevertheless, the same cluster structures were formed for both of these models. These cluster structures coincide with those for the modified Gupta's model (F.3), and the values of the cross-protection parameters at which the system shifts from one type of structure to another vary insignificantly from one model to the others. For instance, for the eight-strain system Fig. F.1(b), the type of cluster structure formed depends on the comparative values of $\gamma_{ij}$. As in the case of the system (F.3), a structure of four clusters with two discordant strains each appears when $\gamma_1$ and $\gamma_2$ are comparatively close and, as the difference between $\gamma_2$ and $\gamma_1$ grows, a shift to the structure of the second type (two clusters with four strains each) occurs. However, in contrast to the model (F.3), no regular oscillation of the clusters was observed: for both types of cluster structures solutions of the models tend to an equilibrium state.

## F.5 Conclusion

Strains of a multi-strain infection tend to self-organise into groups, or clusters. For a complex strain system several different types of cluster structures are possible and may arise. Which cluster structure occurs in reality depends mostly on levels of cross-protection and, in some cases, on initial conditions. It is important to note the distinction between the terms "cluster structure" and "type of cluster structure", as several structures of the same type are possible for complex strain systems. Cluster structures which are possible for a strain system do not depend on the particular model used. In fact, the structures are fairly robust to different models. It appears that cluster structures of a particular strain system depend on the structure of the strain space and on levels of cross-protection.

It is not clear why some cluster structures arise while others do not. While clustering in the four-strain system is transparent enough, it is already not so clear why in the eight-strain system the cluster structure

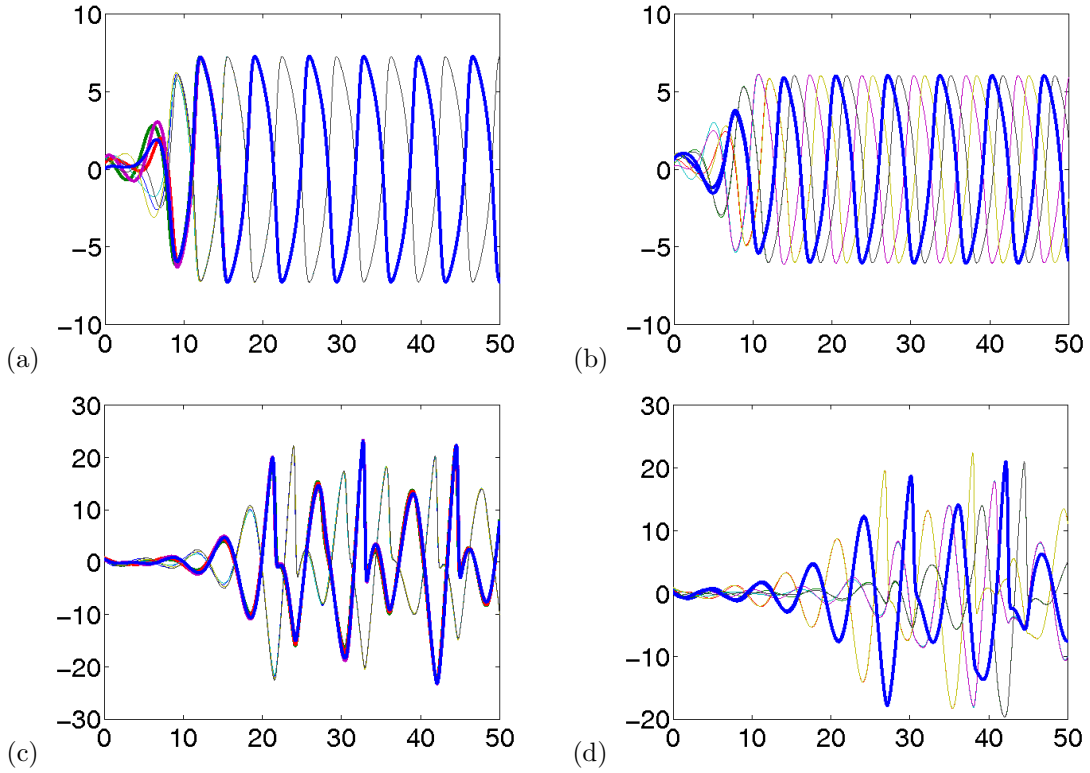


Figure F.7: (*top*) Clustering for the Van der Pol-based system : $\omega = 1$, $\varepsilon = 0.1$ and (a) $\gamma_1 = 0$, $\gamma_2 = 0.4$ : two clusters of tetraedric strains ; (b) $\gamma_1 = 0.4$, $\gamma_2 = 0.4$ : four clusters of opposite strains. (*bottom*) Clustering for the Rössler-based system : $\omega = 1$, $\alpha = -0.1$ and (c) $\gamma_1 = 0$, $\gamma_2 = 0.2$: two clusters of tetraedric strains ; (c) $\gamma_1 = 0.2$, $\gamma_2 = 0.2$ : four clusters of opposite strains. Once more time we have choosen one cluster and bolded strains inside (either two or four).

of second type (two clusters of four strains) appears. More complex systems, such as the sixteen-strain system, raise even more questions. For instance, it is not clear why no structure of four clusters with four strains each is possible for biologically feasible coefficients of cross-protection. It is a challenge to provide an exhaustive list of type of clustering which may occur for a given set of strain.

One possible interpretation of the phenomenon is that cross-immunity, suppressing some strains, forms negative feedback between the corresponding vertices of the graph (such as in Fig. F.1(a) and F.1(b)). This, in turn, induces a positive feedback on other vertices. The phenomenon of self-organisation of elements of an ordered system into clusters does not only occur in epidemiology: for instance, similar examples are observed in neural networks, and we believe that it may occur in other applications. In fact, it appears to be general for coupled dynamical systems. Clustering is a type of self-organisation similar to pattern formation. To compare with, we present two simple dynamical systems which, at once they are suitably coupled, present self-organisation in clusters (see Fig. F.7 and also [12]).

**The Van der Pol oscillator.**

$$\frac{d^2x_i}{dt^2} - \varepsilon\big(1 - x_i^2\big)\frac{dx_i}{dt} + \omega^2 x_i + \sum_{j\sim i} \gamma_{ij}\frac{dx_j}{dt} = 0.$$

**The Rössler oscillator.**

$$\begin{aligned}\frac{dx_i}{dt} &= -\omega y_i - z_i - \textstyle\sum_{j\sim i}\gamma_{ij}x_j \\ \frac{dy_i}{dt} &= \omega x_i + \alpha y_i \\ \frac{dz_i}{dt} &= 0.2 + (x_i - 10)z_i \ .\end{aligned}$$

Note that in the case of the Rössler oscillator, for the set of parameters we have chosen, the dynamic "at rest" (*i.e.* without coupling) is at equilibrium. This situation is similar to cross-immunity which makes oscillate a system *a priori* at equilibrium.

The most remarkable feature of the clusters is that they behave remarkably regularly (at least for ordered strain sets), in contrast to the generally chaotic behaviour of isolated strains. Furthermore, a cluster structure, once formed, appears to be exceptionally stable. This stability implies that in many cases we can (and even should) consider the dynamics of a few clusters, instead of the dynamics of multiple separate strains, reducing in this way the system size.

# Bibliographie


[1] F. Aboul-Enein and H. Lassmann. Mitochondrial damage and histotoxic hypoxia: a pathway of tissue injury in inflammatory brain disease? *Acta Neuropathol.*, 109:49–55, 2005.

[2] M. Agueh. Existence of solutions to degenerate parabolic equations via the Monge-Kantorovich theory. *Adv. Differential Equations*, 10:309–360, 2005.

[3] M. Agueh, N. Ghoussoub, and X. Kang. Geometric inequalities via a general comparison principle for interacting gases. *Geom. Funct. Anal.*, 14:215–244, 2004.

[4] N.D. Alikakos. $L^p$ bounds of solutions of reaction-diffusion equations. *Comm. Partial Differential Equations*, 4:827–868, 1979.

[5] W. Alt. Biased random walk models for chemotaxis and related diffusion approximations. *J. Math. Biol.*, 9:147–177, 1980.

[6] W. Alt and M. Dembo. Cytoplasm dynamics and cell motion: two-phase flow models. *Math. Biosciences*, 156:207–228, 1999.

[7] L.A. Ambrosio, N. Gigli, and G. Savaré. *Gradient flows in metric spaces and in the space of probability measures*. Lectures in Mathematics. Birkhäuser, 2005.

[8] A.R.A. Anderson and M.A.J. Chaplain. Continuous and discrete mathematical models of tumor-induced angiogenesis. *Bull. Math. Biol.*, 60:857–900, 1998.

[9] A.R.A. Anderson and M.A.J. Chaplain. A mathematical model for capillary network formation in the absence of endothelial cell proliferation. *Appl. Math. Lett.*, 11:109–114, 1998.

[10] V. Andreasen, J. Lin, and S.A. Levin. The dynamics of cocirculating influenza strains conferring partial cross-immunity. *J. Math. Biol.*, 35:825–842, 1997.

[11] C. Ané, S. Blachère, D. Chafaï, P. Fougères, I. Gentil, F. Malrieu, C. Roberto, and G. Scheffer. *Sur les inégalités de Sobolev logarithmiques*, volume 10 of *Panoramas et Synthèses*. Société Mathématique de France, Paris, 2000.

[12] V.S. Anishchenko, V.V. Astakhov, A.B. Neiman, T.E. Vadivasova, and L. Schimansky-Geier. *Nonlinear dynamics of chaotic and stochastic systems*. Springer, Berlin, 2002.

[13] D.J. Anschel. Reply to the paper by Wiendl et al.: Diffusion abnormality in Baló's concentric sclerosis: Clues for the pathogenesis. *Eur. Neurol.*, 55:111–112, 2006.

[14] J.P. Aubin. Un théorème de compacité. *C. R. Math. Acad. Sci. Paris*, 256:5042–5044, 1963.

[15] D. Bakry and M. Emery. Diffusions hypercontractives. In *Séminaire de probabilités, XIX, 1983/84*, volume 1123 of *Lecture Notes in Math.*, pages 177–206. Springer, Berlin, 1985.

[16] J. Baló. Leucoencephalitis periaxialis concentrica. *Magy Orvosi Arch.*, 28:108–124, 1927.

[17] J. Baló. Encephalitis periaxialis concentrica. *Arch. Neurol. Psychiatr.*, 19:242–264, 1928.

[18] C. Bardos and P. Degond. Global existence for the Vlasov-Poisson equation in 3 space variables with small initial data. *Ann. Inst. H. Poincaré Anal. Non Linéaire*, 2:101–118, 1985.

[19] M.H. Barnett and J.W. Prineas. Relapsing and remitting multiple sclerosis: pathology of the newly forming lesion. *Ann. Neurol.*, 55:458–468, 2004.

[20] F. Barthe. Inégalités de Brascamp-Lieb et convexité. *C. R. Math. Acad. Sci. Paris*, 324:885–888, 1997.

[21] F. Barthe. On a reverse form of the Brascamp-Lieb inequality. *Invent. Math.*, 310:685–693, 1998.

[22] F. Barthe. Autour de l'inégalité de Brunn-Minkowski. *Ann. Fac. Sci. Toulouse Math.*, 12:127–178, 2003.

[23] W. Beckner. Sharp Sobolev inequalities on the sphere and the Moser-Trudinger inequality. *Ann. of Math.*, 138:213–242, 1993.

[24] W. Behr. Über konzentrische sklerose. *Dtsch. Z. Nervenheilk.*, 164:480–489, 1950.

[25] E. Ben-Jacob, I. Cohen, O. Shochet, A. Tenenbaum, A. Czirók, and T. Vicsek. Cooperative formation of chiral patterns during growth of bacterial colonies. *Phys. Rev. Lett.*, 75:2899–2902, 1995.

[26] D. Benedetto, E. Caglioti, J.A. Carrillo, and M. Pulvirenti. A non-Maxwellian steady distribution for one-dimensional granular media. *J. Stat. Phys.*, 91:979–990, 1998.

[27] D. Benedetto, E. Caglioti, and M. Pulvirenti. A kinetic equation for granular media. *RAIRO Modél. Math. Anal. Numér.*, 31:615–641, 1997.

[28] P. Biler. Local and global solvability of some parabolic systems modelling chemotaxis. *Adv. Math. Sci. Appl.*, 8:715–743, 1998.

[29] P. Biler. Global solutions to some parabolic-elliptic systems of chemotaxis. *Adv. Math. Sci. Appl.*, 9:347–359, 1999.

[30] P. Biler, G. Karch, P. Laurençot, and T. Nadzieja. The $8\pi$ problem for radially symmetric solutions of a chemotaxis model in a disc. *Topol. Methods Nonlinear Anal.*, 27:133–147, 2006.

[31] P. Biler, G. Karch, P. Laurençot, and T. Nadzieja. The $8\pi$-problem for radially symmetric solutions of a chemotaxis model in the plane. *Math. Methods Appl. Sci.*, 29:1563–1583, 2006.

[32] P. Biler and T. Nadzieja. Existence and nonexistence of solutions for a model of gravitational interaction of particles. *Colloq. Math.*, 66:319–334, 1994.

[33] A. Blanchet, V. Calvez, and J.A. Carrillo. Convergence of the mass-transport steepest descent scheme for the sub-critical Patlak-Keller-Segel model. *to appear in SIAM J. Numer. Anal.*, 2007.

[34] A. Blanchet, J.A. Carrillo, and N. Masmoudi. Infinite time aggregation for the critical Patlak-Keller-Segel model in $\mathbb{R}^2$. *to appear in Comm. Pure Appl. Math.*, 2007.

[35] A. Blanchet, J. Dolbeault, and B. Perthame. Two dimensional Keller-Segel model in $\mathbb{R}^2$: optimal critical mass and qualitative properties of the solution. *Electron. J. Differential Equations*, 2006(44):1–33 (electronic), 2006.

[36] M. Bodnar and J.J.L. Velázquez. An integro-differential equation arising as a limit of individual cell-based models. *J. Differential Equations*, 222:341–380, 2006.

[37] N. Bournaveas, V. Calvez, S. Gutiérrez, and B. Perthame. Global existence for a kinetic model of chemotaxis via dispersion and Strichartz estimates. *to appear in Comm. Partial Differential Equations*, 2007.

[38] Y. Brenier. Polar factorization and monotone rearrangement of vector-valued functions. *Comm. Pure Appl. Math.*, 44:375–417, 1991.

[39] M.P. Brenner, P. Constantin, L.P. Kadanoff, A. Schenkel, and S.C. Venkataramani. Diffusion, attraction and collapse. *Nonlinearity*, 12:1071–1098, 1999.

[40] M.P. Brenner, L.S. Levitov, and E.O. Budrene. Physical mechanisms for chemotactic pattern formation by bacteria. *Biophys. J.*, 74:1677–1693, 1998.

[41] Didier Bresch, Thierry Colin, Emmanuel Grenier, Benjamin Ribba, and Olivier Saut. Computational modeling of solid tumor growth: the avascular stage. *Preprint*, 2007.

[42] C.F. Brosnan and C.S. Raine. Mechanisms of immune injury in multiple sclerosis. *Brain Pathol.*, 6:243–257, 1996.

[43] C.J. Budd, R. Carretero-González, and R.D. Russell. Precise computations of chemotactic collapse using moving mesh methods. *J. Comput. Phys.*, 202:463–487, 2005.

[44] E.O. Budrene and H.C. Berg. Dynamics of formation of symmetrical patterns by chemotactic bacteria. *Nature*, 376:49–53, 1995.

[45] M. Burger, Y. Dolak-Struß, and C. Schmeiser. Asymptotic analyis of an advection-dominated chemotaxis model in multiple spatial dimensions. *Preprint*, 2007.

[46] M. Burger and M. Di Francesco. Large time behavior of nonlocal aggregation models with non-linear diffusion. *Preprint*, 2007.

[47] H.M. Byrne and L. Preziosi. Modeling solid tumour growth using the theory of mixtures. *Math. Med. Biol.*, 20:341–366, 2004.

[48] E. Caglioti, P.L. Lions, C. Marchioro, and M. Pulvirenti. A special class of stationary flows for two-dimensional Euler equations: a statistical mechanics description. *Comm. Math. Phys.*, 143:501–525, 1992.

[49] A.P. Calderón and A. Zygmund. On the existence of certain singular integrals. *Acta Math.*, 88:85–139, 1952.

[50] V. Calvez and J.A. Carrillo. Volume effects in the Keller-Segel model: energy estimates preventing blow-up. *J. Math. Pures Appl.*, 86:155–175, 2006.

[51] V. Calvez and Y. Dolak-Struß. Asymptotic behavior of the Keller–Segel model with and without density control. In *Proceedings of the sixth ECMTB, Dresden*, 2005.

[52] V. Calvez and H. Khonsari. Mathematical description of concentric demyelination in the human brain: self-organization models, from Liesegang rings to chemotaxis. *To appear in Math. Comp. Model.*, 2007.

[53] V. Calvez, A. Korobeinikov, and P.K. Maini. Cluster formation for multi-strain infections with cross-immunity. *J. Theor. Biol.*, 233:75–83, 2005.

[54] V. Calvez and B. Perthame. A Lyapunov function for a two-chemical version of the chemotaxis model. *BIT Num. Math.*, 46(suppl.):S85–S97, 2006.

[55] V. Calvez, B. Perthame, and M. Sharifi tabar. Modified Keller-Segel system and critical mass for the log interaction kernel. In *Stochastic analysis and partial differential equations*, volume 429 of *Contemp. Math.* Amer. Math. Soc., Providence, RI, 2007.

[56] E. Carlen and M. Loss. Competing symmetries, the logarithmic HLS inequality and Onofri's inequality on $\mathbb{S}^n$. *Geom. Funct. Anal.*, 2:90–104, 1992.

[57] J.A. Carrillo, M.P. Gualdani, and G. Toscani. Finite speed of propagation for the porous medium equation by mass transportation methods. *C. R. Math. Acad. Sci. Paris*, 338:815–818, 2004.

[58] J.A. Carrillo, A. Jüngel, P.A. Markowich, G. Toscani, and A. Unterreiter. Entropy dissipation methods for degenerate parabolic problems and generalized Sobolev inequalities. *Monatsh. Math.*, 133:1–82, 2001.

[59] J.A. Carrillo, R.J. McCann, and C. Villani. Kinetic equilibration rates for granular media and related equations: entropy dissipation and mass transportation estimates. *Rev. Mat. Iberoamericana*, 19:1–48, 2003.

[60] J.A. Carrillo, R.J. McCann, and C. Villani. Contractions in the 2-Wasserstein length space and thermalization of granular media. *Arch. Ration. Mech. Anal.*, 179:217–263, 2006.

[61] J.A. Carrillo and G. Toscani. New trends in mathematical physics. In *Wasserstein metric and large–time asymptotics of non-linear diffusion equations*, pages 234–244. World Sci. Publ., Hackensack, NJ, 2004.

[62] J.A. Carrillo and G. Toscani. Contractive probability metrics and asymptotic behavior of dissipative kinetic equations. In *Porto Ercole 2006 Summer School Notes*. Riv. Mat. Parma, 2007.

[63] P. Castaigne, R. Escourolle, F. Chain, J.F. Foncin, F. Gray, V. Sauron, and C. Duyckaerts. La sclérose concentrique de Baló. *Rev. Neurol.*, 140:479–487, 1984.

[64] F. Castella and B. Perthame. Estimations de Strichartz pour les équations de transport cinétique. *C. R. Math. Acad. Sci. Paris*, 322:535–540, 1996.

[65] F.A.C.C. Chalub, Y. Dolak-Struß, P.A. Markowich, D. Ölz, C. Schmeiser, and A. Soreff. Model hierarchies for cell aggregation by chemotaxis. *Math. Mod. Meth. Appl. Sci.*, 16:1173–1197, 2006.

[66] F.A.C.C. Chalub, P.A. Markowich, B. Perthame, and C. Schmeiser. Kinetic models for chemotaxis and their drift-diffusion limits. *Monatsh. Math.*, 142:123–141, 2004.

[67] F.A.C.C. Chalub and J.F. Rodrigues. A class of kinetic models for chemotaxis with threshold to prevent overcrowding. *Port. Math.*, 63:1–24, 2006.

[68] S-Y.A. Chang and P.C. Yang. Conformal deformation of metrics on $\mathbb{S}^2$. *J. Differential Geom.*, 27:259–296, 1988.

[69] C.J. Chen. Serial proton magnetic resonance spectroscopy in lesions of Baló concentric sclerosis. *J. Comput. Assist. Tomogr.*, 25:713–718, 2001.

[70] C.J. Chen, N.S. Chu, C.S. Lu, and C.Y. Sung. Serial magnetic resonance imaging in patients with Baló's concentric sclerosis: natural history of lesion development. *Ann. Neurol.*, 46:651–656, 1999.

[71] S. Childress and J.K. Percus. Nonlinear aspects of chemotaxis. *Math. Biosciences*, 56:217–237, 1981.

[72] A.D. Cliff, P. Haggett, and J.K. Ord. *Spatial aspects of Influenza epidemics*. Pion, London, 1986.

[73] D. Cordero-Erausquin, W. Gangbo, and C. Houdre. *Inequalities for generalized entropy and optimal transportation*, volume 353 of *Contemp. Math.* Amer. Math. Soc., Providence, RI, 2004.

[74] L. Corrias and B. Perthame. Critical space for the parabolic-parabolic keller-segel model in $\mathbb{R}^d$. *C. R. Math. Acad. Sci. Paris*, 342:745–750, 2006.

[75] L. Corrias and B. Perthame. Asymptotic decay for the solutions of the parabolic-parabolic keller-segel chemotaxis system in critical spaces. *To appear in Math. Comp. Model.*, 2007.

[76] L. Corrias, B. Perthame, and H. Zaag. A chemotaxis model motivated by angiogenesis. *C. R. Math. Acad. Sci. Paris*, 336:141–146, 2003.

[77] L. Corrias, B. Perthame, and H. Zaag. Global solutions of some chemotaxis and angiogenesis systems in high space dimensions. *Milan J. Math.*, 72:1–28, 2004.

[78] C.B. Courville. Concentric sclerosis. In P.J. Vinken and G.W. Bruyn, editors, *Multiple sclerosis and other demyelinating diseases*, pages 437–451. Amsterdam: North-Holland, 1970.

[79] C.M. Dafermos. *Hyperbolic conservation laws in continuum physics*, volume 325 of *Grundlehren der Mathematischen Wissenschaften*. Springer-Verlag, Berlin, 2000.

[80] P.D. Dale, P.K. Maini, and J.A. Sherratt. Mathematical modelling of corneal epithelium wound healing. *Math. Biosciences*, 124:127–147, 1994.

[81] J.H.P. Dawes and J.R. Gog. The onset of oscillatory dynamics in models of multiple disease strains. *J. Math. Biol.*, 45:471–510, 2002.

[82] G.T. Dee. Patterns produced by precipitation at a moving reaction front. *Phys. Rev. Lett.*, 57:275–278, 1986.

[83] J. Denzler and R.J. McCann. Fast diffusion to self-similarity: Complete spectrum, long-time asymtotics and numerology. *Arch. Ration. Mech. Anal.*, 175:301–342, 2004.

[84] E. DiBenedetto, B. Perthame, and A. Stevens. Mathematical biology. In *Oberwolfach Reports*, volume 3, pages 1385–1462. Mathematisches Forschungsinstitut Oberwolfach, 2006.

[85] Y. Dolak and C. Schmeiser. The Keller-Segel model with logistic sensitivity function and small diffusivity. *SIAM J. Appl. Math.*, 66:286–308, 2005.

[86] J. Dolbeault and B. Perthame. Optimal critical mass in the two dimensional Keller-Segel model in $\mathbb{R}^2$. *C. R. Math. Acad. Sci. Paris*, 339:611–616, 2004.

[87] J. Dolbeault and C. Schmeiser. The two-dimensional Keller-Segel model after blow-up. *Preprint*, 2007.

[88] W.F. Donoghue. *Distributions and Fourier transforms*. Academic Press, 1969.

[89] D. Dormann and C.J. Weijer. Chemotactic cell movement during *Dictyostelium* development and gastrulation. *Curr. Opin. Genet. Dev.*, 16:367–373, 2006.

[90] D. Drasdo and S. Höhme. A single-cell-based model of tumor growth in vitro: monolayers and spheroids. *Phys. Biol.*, 2:133–147, 2005.

[91] D. Drasdo, S. Höhme, and M. Block. On the role of physics in the growth and pattern formation of multi-cellular systems: What can we learn from individual-cell based models? *J. Stat. Phys.*, 128:287–345, 2007.

[92] M. Droz. Recent theoretical developments on the formation of Liesegang patterns. *J. Stat. Phys.*, 101:509–519, 2000.

[93] J. Duoandikoetxea. *Fourier Analysis*, volume 29 of *Graduate Studies in Mathematics*. Amer. Math. Soc., Providence, RI, 2001.

[94] J. Duoandikoetxea and E. Zuazua. Moments, masses de Dirac et décomposition de fonctions. *C. R. Math. Acad. Sci. Paris*, 315:693–698, 1992.

[95] R. Erban and H.J. Hwang. Global existence results for complex hyperbolic models of bacterial chemotaxis. *Discrete Contin. Dyn. Syst. Ser. B*, 6:1239–1260, 2006.

[96] R. Erban and H.G. Othmer. Taxis equations for amoeboid cells. *J. Math. Biol.*, 54:847–885, 2007.

[97] C. Escudero. The fractional Keller-Segel model. *Nonlinearity*, 19:2909–2918, 2006.

[98] L.C. Evans. Partial differential equations and Monge-Kantorovich mass transfer. In *Current developments in mathematics, Cambridge, MA*. Int. Press, Boston, MA, available at `http://math.berkeley.edu/~evans/`, 1997.

[99] L.C. Evans. *Partial differential equations*, volume 19 of *Graduate Studies in Mathematics*. Amer. Math. Soc., Providence, RI, 1998.

[100] L.C. Evans, O. Savin, and W.E. Gangbo. Diffeomorphisms and nonlinear heat flows. *SIAM J. Math. Anal.*, 37:737–751, 2005.

[101] D. Feinn, P. Ortoleva, W. Scalf, S. Schmidt, and M. Wolff. Spontaneous pattern formation in precipitating systems. *J. Chem. Phys.*, 69:27–39, 1978.

[102] A. Ferraro. Experimental toxic encephalopathy. Diffuse sclerosis following subcutaneous injection of potassium-cyanide. *Psychiat. Q.*, 7:267–283, 1933.

[103] F. Filbet. A finite volume scheme for the Patlak-Keller-Segel chemotaxis model. *Numerische Math.*, 104:457–488, 2006.

[104] F. Filbet, P. Laurençot, and B. Perthame. Derivation of hyperbolic models for chemosensitive movement. *J. Math. Biology*, 50:189–207, 2004.

[105] M. Flicker and J. Ross. Mechanism of chemical instability for periodic precipitation phenomena. *J. Chem. Phys.*, 60:3458–3465, 1974.

[106] E. Gagliardo. Ulteriori proprietà di alcune classi di funzioni in più variabili. *Ricerche Mat.*, 8:24–51, 1959.

[107] H. Gajewski and K. Zacharias. Global behavior of a reaction-diffusion system modelling chemotaxis. *Math. Nachr.*, 195:77–114, 1998.

[108] A. Gamba, D. Ambrosi, A. Coniglio, A. de Candia, S. Di Talia, E. Giraudo, G. Serini, L. Preziosi, and F. Bussolino. Percolation, morphogenesis, and Burgers dynamics in blood vessels formation. *Phys. Rev. Lett.*, 90(11):118101, 2003.

[109] R.J. Gardner. The Brunn-Minkowski inequality. *Bull. Amer. Math. Soc.*, 39:355–405, 2002.

[110] A. Garfinkel, Y. Tintut, D. Petrasek, K. Boström, and L.L. Demer. Pattern formation by vascular mesenchymal cells. *Proc. Nat. Acad. Sci. USA*, 101:9247–9250, 2004.

[111] R.A. Gatenby and E.T. Gawlinski. A reaction-diffusion model of cancer invasion. *Cancer Res.*, 56:5745–5753, 1996.

[112] R.A. Gatenby and E.T. Gawlinski. The glycolytic phenotype in carcinogenesis and tumor invasion. *Cancer Res.*, 63:3847–3854, 2003.

[113] C.P. Genain and S.L. Hauser. Creation of a model for multiple sclerosis in *Callithrix jacchus* marmosets. *J. Mol. Med.*, 75:187–197, 1997.

[114] P. Gérard. Description du défaut de compacité de l'injection de Sobolev. *ESAIM Control Optim. Calc. Var.*, 3:213–233, 1998.

[115] D. Gilbarg and N.S. Trudinger. *Elliptic partial differential equations of second order*. Springer, third edition, 1998.

[116] R.T. Glassey. *The Cauchy problem in kinetic theory*. SIAM publications, Philadelphia, 1996.

[117] J.R. Gog and B.T. Grenfell. Dynamics and selection of many-strain pathogens. *Proc. Nat. Acad. Sci. USA*, 99:17209–17214, 2002.

[118] J.R. Gog and J. Swinton. A status-based approach to multiple strain dynamics. *J. Math. Biol.*, 44:169–184, 2002.

[119] L. Gosse and G. Toscani. Identification of asymptotic decay to self-similarity for one-dimensional filtration equations. *SIAM J. Numer. Anal.*, 43:2590–2606, 2006.

[120] L. Gosse and G. Toscani. Lagrangian numerical approximations to one-dimensional convolution-diffusion equations. *SIAM J. Sci. Comput.*, 28:1203–1227, 2006.

[121] L. Gross. Logarithmic Sobolev inequalities. *Amer. J. Math.*, 97:1061–1083, 1975.

[122] S. Gupta and R.M. Anderson. Population structure of pathogens: the role of immune selection. *Parasitol. Today*, 15:497–501, 1999.

[123] S. Gupta, N. Ferguson, and R.M. Anderson. Chaos, persistence, and evolution of strain structure in antigenically diverse infectious agents. *Science*, 280:912–915, 1998.

[124] S. Gupta, M.C.J. Maiden, I.M. Feavers, S. Nee, R.M. May, and R.M. Anderson. The maintenance of strain structure in populations of recombining infectious agents. *Nature Med.*, 2:437–442, 1996.

[125] S. Gupta, K. Trenholme, R.M. Anderson, and K.P. Day. Antigenic diversity and the transmission dynamics of *Plasmodium falciparum*. *Science*, 263:961–963, 1994.

[126] J.B. Gurdon, P. Harger, A. Mitchell, and P. Lemaire. Activin signalling and response to a morphogen gradient. *Nature*, 371:487–492, 1994.

[127] J. Hallervorden and H. Spatz. Über die konzentrische sklerose und die physicalisch-chemischen faktoren bei der ausbreitung von entmarkungsprozessen. *Arch. Psychiat. Nervenkr.*, 98:641–701, 1933.

[128] E. Hatschek. Der einfluss des lichtes auf bleichromat-schichtungen. *Kolloid Z.*, 37:297–298, 1925.

[129] H.K. Henisch. *Crystals in gels and Liesegang rings*. Cambridge University Press, Cambridge, 1986.

[130] M.A. Herrero, E. Medina, and J.L.L. Velázquez. Finite-time aggregation into a single point in a reaction-diffusion system. *Nonlinearity*, 10:1739–1754, 1997.

[131] M.A. Herrero and J.L.L. Velázquez. Chemotactic collapse for the Keller-Segel model. *J. Math. Biol.*, 35:177–194, 1996.

[132] M.A. Herrero and J.L.L. Velázquez. A blow-up mechanism for a chemotaxis model. *Ann. Scuola Norm. Sup. Pisa*, 24:633–683, 1997.

[133] D. Hilhorst, R. Van der Hout, M. Mimura, and I. Ohnishi. Fast reaction limits and liesegang bands. In *Free boundary problems*. Birkhäuser, Basel, 2007. Personal communication.

[134] T. Hillen and H.G. Othmer. The diffusion limit of transport equations derived from velocity-jump processes. *SIAM J. Appl. Math.*, 61:751–775, 2000.

[135] T. Hillen and K.J. Painter. Global existence for a parabolic chemotaxis model with prevention of overcrowding. *Adv. in Appl. Math.*, 26:280–301, 2001.

[136] T. Hillen, K.J. Painter, and C. Schmeiser. Global existence for chemotaxis with finite sampling radius. *Discrete Contin. Dyn. Syst. Ser. B*, 7:125–144, 2007.

[137] T. Hillen and A. Potapov. The one-dimensional chemotaxis model: global existence and asymptotic profile. *Math. Meth. Appl. Sci.*, 27:1783–1801, 2004.

[138] T. Höfer, J.A. Sherratt, and P.K. Maini. Cellular pattern formation in a model of *Dictyostelium* aggregation. *Physica D*, 85:425–444, 1995.

[139] T. Höfer, J.A. Sherratt, and P.K. Maini. *Dictyostelium discoideum*: cellular self-organization in an excitable biological medium. *Proc. Roy. Soc. Lond. B*, 259:249–257, 1995.

[140] D. Horstmann. The nonsymmetric case of the Keller-Segel model in chemotaxis: some recent results. *Nonlinear differ. equ. appl.*, 8:399–423, 2001.

[141] D. Horstmann. From 1970 until present: the Keller-Segel model in chemotaxis and its consequences. I. *Jahresber. Deutsch. Math.-Verein.*, 105:103–165, 2003.

[142] D. Horstmann and M. Winkler. Boundedness vs. blow-up in a chemotaxis system. *J. Differential Equations*, 215:52–107, 2005.

[143] H.J. Hwang, K. Kang, and A. Stevens. Drift-diffusion limits of kinetic models for chemotaxis: a generalization. *Discrete Contin. Dyn. Syst. Ser. B*, 5:319–334, 2005.

[144] H.J. Hwang, K. Kang, and A. Stevens. Global solutions of nonlinear transport equations for chemosensitive movement. *SIAM J. Math. Anal.*, 36:1177–1199, 2005.

[145] H.J. Hwang, K. Kang, and A. Stevens. Global existence of classical solutions for a hyperbolic chemotaxis model and its parabolic limit. *Indiana Univ. Math. J.*, 55:289–316, 2006.

[146] Y. Itoyama, J. Tateishi, and Y. Kuroiwa. A typical multiple sclerosis with concentric or lamellar demyelination lesions: two japanese patients studied post-mortem. *Ann. Neurol.*, 17:481–487, 1984.

[147] W. Jäger and S. Luckhaus. On explosions of solutions to a system of partial differential equations modelling chemotaxis. *Trans. Amer. Math. Soc.*, 329:819–824, 1992.

[148] R. Jordan, D. Kinderlehrer, and F. Otto. The variational formulation of the Fokker-Planck equation. *SIAM J. Math. Anal.*, 29:1–17, 1998.

[149] J. Jost. *Mathematical Methods in Biology and Neurobiology.* Available at `http://www.mis.mpg.de/jjost/publications.html`, 2007.

[150] D. Julkowska, M. Obuchowski, I.B. Holland, and S.J. Séror. Comparative analysis of the development of swarming communities of *Bacillus subtilis* 168 and a natural wild type: critical effects of surfactin and the composition of the medium. *J. Bacteriol.*, 187:65–76, 2005.

[151] O. Kastrup, P. Stude, and V. Limmroth. Baló's concentric sclerosis. Evolution of active demyelination demonstrated by serial contrast-enhanced MRI. *J. Neurol.*, 249:811–814, 2002.

[152] E.F. Keller and L.A. Segel. Initiation of slime mold aggregation viewed as an instability. *J. Theor. Biol.*, 26:399–415, 1970.

[153] E.F. Keller and L.A. Segel. Model for chemotaxis. *J. Theor. Biol.*, 30:225–234, 1971.

[154] E.F. Keller and L.A. Segel. Traveling bands of chemotactic bacteria: a theoretical analysis. *J. Theor. Biol.*, 30:235–248, 1971.

[155] J.B. Keller and S.I. Rubinow. Recurrent precipitation and Liesegang rings. *J. Chem. Phys.*, 74(9):5000–5007, 1981.

[156] R. Keller. Cell migration during gastrulation. *Curr. Opin. Cell. Biol.*, 17:533–541, 2005.

[157] H. Khonsari and V. Calvez. The origins of concentric demyelination: self-organization in the human brain. *Plos ONE*, doi:10.1371/journal.pone.0000150, 2007.

[158] S. Kondo and R. Asai. A reaction-diffusion wave on the skin of the marine angelfish *Pomacanthus*. *Nature*, 376:765–768, 1995.

[159] R. Kowalczyk. Preventing blow-up in a chemotaxis model. *J. Math. Anal. Appl.*, 305:566–588, 2005.

[160] H.J. Krug and H. Brandtstädter. Morphological characteristics of Liesegang rings and their simulations. *J. Phys. Chem. A*, 103:7811–7820, 1999.

[161] H.J. Krug, H. Brandtstädter, and K.H. Jacob. Morphological instabilities in pattern formation by precipitation and crystallization processes. *Geol. Rundsch.*, 85:19–28, 1996.

[162] H. Lassmann. Recent neuropathological findings in MS–implications for diagnosis and therapy. *J. Neurol.*, 251(S4):2–5, 2004.

[163] H. Lassmann. Multiple sclerosis pathology: evolution of pathogenic concepts. *Brain Pathol.*, 15:217–222, 2005.

[164] P. Laurençot and D. Wrzosek. A chemotaxis model with threshold density and degenerate diffusion. In *Nonlinear elliptic and parabolic problems*, volume 64 of *Progr. Nonlinear Differential Equations Appl.*, pages 273–290. Birkhäuser, Basel, 2005.

[165] H.A. Levine, S. Pamuk, B.D. Sleeman, and M. Nilsen-Hamilton. Mathematical modeling of capillary formation and development in tumor angiogenesis: penetration into the stroma. *Bull. Math. Biol.*, 63:801–863, 2001.

[166] H. Li and G. Toscani. Long–time asymptotics of kinetic models of granular flows. *Arch. Ration. Mech. Anal.*, 172:407–428, 2004.

[167] E.H. Lieb. Sharp constants in the Hardy-Littlewood-Sobolev and related inequalities. *Ann. of Math.*, 118:349–374, 1983.

[168] E.H. Lieb and M. Loss. *Analysis*, volume 14 of *Graduate Studies in Math.* Amer. Math. Soc., Providence, RI, second edition, 2001.

[169] R.E. Liesegang. *Photgr. Archiv.*, 21:221–, 1896.

[170] J. Lin, V. Andreasen, and S.A. Levin. Dynamics of influenza A drift: the linear three-strain model. *Math. Biosciences*, 162:33–51, 1999.

[171] C. Lucchinetti, W. Brück, J. Parisi, B. Scheithauer, M. Rodriguez, and H. Lassmann. A quantitative analysis of oligodendrocytes in multiple sclerosis lesions – a study of 113 cases. *Brain*, 122:2279–2295, 1999.

[172] C.E. Lumsden. The neuropathology of multiple sclerosis. In P.J. Vinken and G.W. Bruyn, editors, *Handbook of clinical neurology*, volume 9, pages 217–319. North Holland Publishing Co., Amsterdam, 1970.

[173] N.V. Mantzaris, S. Webb, and H.G. Othmer. Mathematical modeling of tumor-induced angiogenesis. *J. Math. Biol.*, 49:111–187, 2004.

[174] D. Markiewicz, Z. Adamczewska-Goncerzewicz, J. Dymecki, and A. Goncerzewicz. A case of primary form of progressive multifocal leukoencephalopathy with concentric demyelination of Baló type. *Neuropatol. Pol.*, 15:491–500, 1977.

[175] P.A. Markowich. *Applied partial differential equations: a visual approach.* Springer, Berlin, 2007.

[176] P.A. Markowich, C.A. Ringhofer, and C. Schmeiser. *Semiconductor equations.* Springer-Verlag, Vienna, 1990.

[177] A. Marrocco. 2D simulation of chemotactic bacteria aggregation. *M2AN Math. Model. Numer. Anal.*, 37:617–630, 2003.

[178] R.J. McCann. Existence and uniqueness of monotone measure-preserving maps. *Duke Math. J.*, 80:309–323, 1995.

[179] R.J. McCann. A convexity principle for interacting gases. *Adv. Math.*, 128:153–179, 1997.

[180] R.J. McCann. Polar factorization of maps on Riemannian manifolds. *Geom. Funct. Anal.*, 11:589–608, 2001.

[181] S. Michalak. Concentric patterns in the brain: a thermodynamic aspect of disease. *Studia Philosophica Tartu*, IV:139–155, 2004.

[182] G.R.W. Moore, K. Berry, J.J.F. Oger, A.J.E. Prout, D.A. Graeb, and R.A. Nugent. Baló's concentric sclerosis: surviving myelin in a patient with a relapsing remitting course. *Mult. Scl.*, 7:375–382, 2001.

[183] G.R.W. Moore, P.E. Neumann, K. Suzuki, H.N. Lijtmaer, U. Traugott, and C.S. Raine. Baló's concentric sclerosis: new observations on lesion development. *Ann. Neurol.*, 17:604–611, 1985.

[184] J. Moser. A sharp form of an inequality by N. Trudinger. *Indiana Univ. Math. J.*, 20:1077–1092, 1971.

[185] J.D. Murray. *Mathematical Biology.* Springer, third edition, 2003.

[186] G. Nadin, B. Perthame, and L. Ryzhik. Traveling waves for the Keller-Segel system with Fisher birth terms. *Preprint*, 2007.

[187] T. Nagai. Blow-up of radially symmetric solutions to a chemotaxis system. *Adv. Math. Sci. Appl.*, 5:581–601, 1995.

[188] T. Nagai. Blowup of nonradial solutions to parabolic-elliptic systems modeling chemotaxis in two-dimensional domains. *J. Inequal. Appl.*, 6:37–55, 2001.

[189] T. Nagai, T. Senba, and T. Suzuki. Chemotactic collapse in a parabolic system of mathematical biology. *Hiroshima Math. J.*, 30:463–497, 2000.

[190] T. Nagai, T. Senba, and K. Yoshida. Application of the trudinger-moser inequality to a parabolic system of chemotaxis. *Funk. Ekv.*, 40:411–433, 1997.

[191] V. Nanjundiah. Chemotaxis, signal relaying and aggregation morphology. *J. Theor. Biol.*, 42:63–105, 1973.

[192] A. Nimmerjahn, F. Kirchhoff, and F. Helmchen. Resting microglial cells are highly dynamic surveillants of brain parenchyma in vivo. *Science*, 308:1314–1318, 2005.

[193] L. Nirenberg. On elliptic partial differential equations. *Ann. Scuola Norm. Sup. Pisa*, 13:115–162, 1959.

[194] M.A. Nowak and R.M. May. *Virus dynamics. Mathematical principles of immunology and virology.* Oxford University Press, Oxford, 2000.

[195] D. Ölz. *Asymptotic nonlinear models in Mathematical Physics and Biology.* PhD thesis, Fakultät für Mathematik, Universität Wien, 2007.

[196] E. Onofri. On the positivity of the effective action in a theory of random surfaces. *Comm. Math. Phys.*, 86:321–326, 1982.

[197] W. Ostwald. *Lehrburch der allgemeinen chemie.* Engelman, Leipzig, 1897.

[198] H.G. Othmer, S.R. Dunbar, and W. Alt. Models of dispersal in biological systems. *J. Math. Biol.*, 26:263–298, 1988.

[199] H.G. Othmer and A. Stevens. Aggregation, blowup and collapse : the ABC's of taxis in reinforced random walks. *SIAM J. Appl. Math.*, 57:1044–1081, 1997.

[200] F. Otto. The geometry of dissipative evolution equations: the porous medium equation. *Comm. Partial Differential Equations*, 26:101–174, 2001.

[201] F. Otto and C. Villani. Generalization of an inequality by Talagrand, and links with the logarithmic Sobolev inequality. *J. Funct. Anal.*, 173:361–400, 2000.

[202] K.J. Painter and T. Hillen. Volume-filling and quorum-sensing in models for chemosensitive movement. *Can. Appl. Math. Q.*, 10:501–543, 2002.

[203] K.J. Painter, P.K. Maini, and H.G. Othmer. Stripe formation in juvenile *Pomacanthus* explained by a generalised Turing mechanism with chemotaxis. *Proc. Nat. Acad. Sci. USA*, 96:5549–5554, 1999.

[204] K.J. Painter, P.K. Maini, and H.G. Othmer. A chemotactic model for the advance and retreat of the primitive streak in avian development. *Bull. Math. Biol.*, 62:501–525, 2000.

[205] K.J. Painter, P.K. Maini, and H.G. Othmer. Chemotactic response to multiple signalling cues. *J. Math. Biol.*, 41:285–314, 2000.

[206] C.S. Patlak. Random walk with persistence and external bias. *Bull. Math. Biophys.*, 15:311–338, 1953.

[207] B. Perthame. Mathematical tools for kinetic equations. *Bull. Amer. Math. Soc.*, 41:205–244, 2004.

[208] B. Perthame. PDE models for chemotactic movements. Parabolic, hyperbolic and kinetic. *Appl. Math.*, 49:539–564, 2004.

[209] B. Perthame. *Transport equations in biology.* Frontiers in mathematics. Birkhäuser, 2006.

[210] J.B. Plotkin, J. Dushoff, and S.A. Levin. Hemagglutinin sequence clusters and the antigenic evolution of influenza A virus. *Proc. Nat. Acad. Sci. USA*, 99:6263–6268, 2002.

[211] D. Pohl, K. Rostasy, B. Krone, and F. Hanefeld. Baló's concentric sclerosis associated with primary human herpes virus 6 infection. *J. Neurol. Neurosurg. Psychiatry*, 76:1723–1725, 2005.

[212] F. Poupaud. Diagonal defect measures, adhesion dynamics and Euler equation. *Methods Appl. Anal.*, 9:533–561, 2002.

[213] L. Preziosi, editor. *Cancer modelling and simulation.* Math. Biol. Med. Ser. Chapman Hall/CRC Press, 2003.

[214] M. Primicerio and B. Zaltzman. Continuation of the solution to the chemotaxis problem beyond its blow-up. In *Free boundary problems (Trento, 2002)*, volume 147 of *Internat. Ser. Numer. Math.* Birkhäuser, Basel, 2004.

[215] T. Roose, J. Chapman, and P.K. Maini. Mathematical models of avascular tumor growth. *SIAM Rev.*, 49:179–208, 2007.

[216] S.M. Ross. *Introduction to probability models.* Academic Press, Inc., Boston, MA, fifth edition, 1993.

[217] J. Rubin and D. Terman. Analysis of clustered firing patterns in synaptically coupled networks of oscillators. *J. Math. Biol.*, 41:513–545, 2000.

[218] J. Rubin and D. Terman. Geometric analysis of population rythms in synaptically coupled neuronal networks. *Neural Comput.*, 12:597–645, 2000.

[219] R. Schaaf. Stationary solutions of chemotaxis systems. *Trans. Amer. Math. Soc.*, 292:531–556, 1985.

[220] D. Scharfetter and H. Gummel. Large signal analysis of a Silicon Read diode oscillator. *IEEE Trans. Electron Devices*, 16:64–77, 1969.

[221] T. Senba and T. Suzuki. Chemotactic collapse in parabolic-elliptic systems of mathematical biology. *Adv. Differential Equations*, 6:21–50, 2001.

[222] T. Senba and T. Suzuki. Weak solutions to a parabolic-elliptic system of chemotaxis. *J. Funct. Anal.*, 191:17–51, 2002.

[223] G. Serini, D. Ambrosi, E. Giraudo, A. Gamba, L. Preziosi, and F. Bussolino. Modeling the early stages of vascular network assembly. *The EMBO Journal*, 22:1771–1779, 2003.

[224] D. Serre. *Systems of conservation laws.* University Press, Cambridge, 1999.

[225] C. Stadelmann and W. Brück. Lessons from the neuropathology of atypical forms of multiple sclerosis. *Neurol. Sci.*, 25(suppl.):319–322, 2004.

[226] C. Stadelmann, S. Ludwinand T. Tabira, A. Guseo, C.F. Lucchinetti, L. Leel-Ossy, A.T. Ordinario, W. Brück, and H. Lassmann. Tissue preconditioning may explain concentric lesions in Baló's type of multiple sclerosis. *Brain*, 128:979–987, 2005.

[227] E.M. Stein. *Singular integrals and differentiability properties of functions.* Princeton University Press, Princeton, New Jersey, 1970.

[228] A. Stevens. Derivation of chemotaxis-equations as limit dynamics of moderately interacting stochastic many-particle systems. *SIAM J. Appl. Math.*, 61:183–212, 2000.

[229] M. Stringini and S.M. Cohen. Wingless gradient formation in the *Drosophila* wing. *Curr. Biol.*, 10:293–300, 2000.

[230] T. Tao. *Nonlinear dispersive equations: local and global analysis*, volume 106 of *CBMS Regional Conference Series in Mathematics.* Amer. Math. Soc., Providence, RI, 2006.

[231] D. Terman, N. Kopell, and A. Bose. Dynamics of two mutually coupled slow inhibitory neurons. *Physica D*, 117:241–275, 1998.

[232] D. Terman and E. Lee. Partial synchronization in a network of neural oscillators. *SIAM J. Appl. Math.*, 57:252–293, 1997.

[233] M. Tessier-Lavigne and C.S. Goodman. The molecular biology of axon guidance. *Science*, 274:1123–1133, 1996.

[234] C.M. Topaz, A.L. Bertozzi, and M.A. Lewis. A nonlocal continuum model for biological aggregation. *Bull. Math. Biol.*, 68:1601–1623, 2006.

[235] G. Toscani. One-dimensional kinetic models of granular flows. *RAIRO Modél. Math. Anal. Numér.*, 34:1277–1291, 2000.

[236] A. Turing. The chemical basis of morphogenesis. *Phil. Trans. R. Soc. Lond. B*, 237:37–72, 1982.

[237] R. Tyson, S.R. Lubkin, and J.D. Murray. A minimal mechanism for bacterial pattern formation. *Proc. R. Soc. Lond. B*, 266:299–304, 1999.

[238] R. Tyson, S.R. Lubkin, and J.D. Murray. Model and analysis of chemotactic bacterial patterns in a liquid medium. *J. Math. Biol.*, 38:359–375, 1999.

[239] J.J.L. Velázquez. Stability of some mechanisms of chemotactic aggregation. *SIAM J. Appl. Math.*, 62:1581–1633, 2002.

[240] J.J.L. Velázquez. Point dynamics in a singular limit of the Keller-Segel model. I. Motion of the concentration regions. *SIAM J. Appl. Math.*, 64:1198–1223, 2004.

[241] J.J.L. Velázquez. Point dynamics in a singular limit of the Keller-Segel model. II. Formation of the concentration regions. *SIAM J. Appl. Math.*, 64:1224–1248, 2004.

[242] G. Venzl and J. Ross. Nucleation and colloidal growth in concentration gradients (Liesegang rings). *J. Chem. Phys.*, 77(3):1302–1307, 1982.

[243] C. Villani. A review of mathematical topics in collisional kinetic theory. In *Handbook of mathematical fluid dynamics*. North-Holland, Amsterdam, 2002.

[244] C. Villani. *Topics in optimal transportation*, volume 58 of *Graduate Studies in Math.* Amer. Math. Soc, Providence, 2003.

[245] C. Villani. Mathematics of granular materials. *J. Statist. Phys.*, 124:781–822, 2006.

[246] C. Villani. *Optimal transport, old and new*. Lecture Notes for the 2005 Saint-Flour summer school. Springer, 2007.

[247] M.J. Ward, D. McInerney, P. Houston, D. Gavaghan, and P.K. Maini. The dynamics and pinning of a spike for a reaction-diffusion system. *SIAM J. Appl. Math.*, 62:1297–1328, 2002.

[248] C.J. Weijer. *Dictyostelium* morphogenesis. *Curr. Opin. Genet. Dev.*, 14:392–398, 2004.

[249] H. Wiendl, R. Weissert, U. Herrlinger, H. Krapf, and W. Kuker. Diffusion abnormality in Baló's concentric sclerosis: clues for the pathogenesis. *Eur. Neurol.*, 53:42–44, 2005.

[250] D. Wrzosek. Long-time behaviour of solutions to a chemotaxis model with volume-filling effect. *Proc. Roy. Soc. Edinburgh A*, 136:431–444, 2006.

[251] X. Yang, D. Dormann, A.E. Munsterberg, and C.J. Weijer. Cell movement patterns during gastrulation in the chick are controlled by positive and negative chemotaxis mediated by FGF4 and FGF8. *Dev. Cell*, 3:425–437, 2002.

[252] D.L. Yao, H.D. Webster, L.D. Hudson, M. Brenner, D.S. Liu, A.I. Escobar, and S. Komoly. Concentric sclerosis (Baló): morphometric and in situ hybridization study of lesions in six patients. *Ann. Neurol.*, 35:18–30, 1994.

[253] W. Zeman. Konzentrische sklerose. *Arch. Psychiatr. Nervenkr.*, 181:187–197, 1949.

# Résumé

## Modèles et analyses mathématiques pour les mouvements collectifs de cellules.

Cette thèse est consacrée à certains modèles mathématiques décrivant le mouvement d'une population de cellules, qui interagissent via un signal chimique. L'accent est mis sur le modèle parabolique de Patlak-Keller-Segel (PKS), et dans une moindre mesure, sur le modèle cinétique d'Othmer-Dunbar-Alt (ODA).

Dans une première partie nous étudions plusieurs variantes du modèle PKS classique, incluant notamment une diffusion non-linéaire des cellules, ou bien une loi de diffusion chimique à noyau de Green logarithmique. Puis nous montrons l'existence globale pour une masse sous-critique du modèle PKS classique dans tout l'espace $\mathbb{R}^2$, grâce à une bonne compréhension des deux ingalités fonctionnelles sous-jacentes : l'inégalité de Trudinger-Moser-Onofri et l'inégalité de Hardy-Littlewood-Sobolev logarithmique. On complexifie ensuite le modèle de base en ajoutant un intermédiaire chimique réactionnel, ce qui modifie l'homogénéité du système. Enfin les conditions d'existence globale pour le modèle cinétique ODA sont affaiblies par rapport aux travaux précédents, grâce à l'utilisation des estimations de dispersion et de Strichartz.

Dans une deuxième partie nous appliquons le modèle phénoménologique de PKS, et son principe de masse critique, à un processus d'auto-organisation remarquable dans le cerveau : la sclérose concentrique de Baló. Un couplage adéquat entre un front de propagation et une instabilité de PKS décrit raisonnablement les motifs en anneaux de la maladie. Comme conclusion partielle de notre étude, nous mettons en évidence que l'émergence d'une structure hétérogène est favorisée par l'agressivité de la maladie.

La troisième partie adopte le point de vue du transport optimal de masse pour analyser le modèle de PKS unidimensionnel modifié auparavant (afin de partager les caractéristiques de PKS 2D). Bien que la fonctionnelle d'énergie ne soit pas convexe par déplacement en raison du potentiel d'interaction logarithmique, nous démontrons la convergence vers un unique état d'équilibre, lorsqu'il existe. Ces nouvelles idées sont mises en œuvre numériquement : un flot gradient discret pour la distance de Wasserstein est analysé, puis simulé en dimension un d'espace.

Plusieurs annexes viennent compléter ce travail, dont une annexe qui regroupe tous les aspects numériques de la thèse. La dernière annexe, indépendante du reste, fait l'étude qualitative d'un système complexe en immunologie, dans lequel la population de virus se structure par compétition interne, via un mécanisme indirect d'immunité croisée.



# Abstract

## Mathematical models and analysis for the collective motion of cells.

We investigate some mathematical models describing the collective motion of a population of cells, interacting through a chemical signal. We highlight the parabolic model of Patlak-Keller-Segel, and also the kinetic model of Othmer-Dunbar-Alt.

The first part consists in studying several variants of the classical PKS model, including for instance nonlinear diffusion of the cells, or a chemical diffusion law based on a logarithmic Green kernel. Next we tackle the global existence problem for the full parabolic-parabolic PKS system in the whole space $\mathbb{R}^2$. Independently we complexify the basic model by adding a second reactant, modifying henceforth the system's homogeneity. Finally we are able to weaken the previous global existence assumptions for the kinetic ODA model with delocalization effects.

In the second part we apply the critical mass instability to model phenomenologically a remarkable pattern formation issue in the human brain, namely the Baló's Concentric Sclerosis. A suitable coupling between a front propagation and the PKS model exhibits the concentric rings appearing in this disease in a reasonable way.

In the third part we adopt the recent optimal transportation viewpoint to analyse the one dimensional PKS model obtained previously (which captures the key features of the 2D PKS). Although the energy functional is not displacement convex, we prove that solutions converge to a unique stationary state, as soon as it exists. This interpretation is performed numerically : a discrete gradient flow adapted to the Wasserstein distance is analysed and simulated in one dimension of space.

Several appendices complete this work, among which one gathers all numerical aspects of this thesis.